TRANSPORTATION POOLED FUND PROGRAM
QUARTERLY PROGRESS REPORT

Lead Agency (FHWA or State DOT): INDOT - Indiana Department of Transportation

INSTRUCTIONS:
Project Managers and/or research project investigators should complete a quarterly progress report for each calendar quarter during which the projects are active. Please provide a project schedule status of the research activities tied to each task that is defined in the proposal; a percentage completion of each task; a concise discussion (2 or 3 sentences) of the current status, including accomplishments and problems encountered, if any. List all tasks, even if no work was done during this period.

Transportation Pooled Fund Program Project # *(i.e, SPR-2(XXX), SPR-3(XXX) or TPF-5(XXX)* TPF-5(179) SPR 3280	**Transportation Pooled Fund Program - Report Period:** ☐Quarter 1 (January 1 – March 31) ☐Quarter 2 (April 1 – June 30) ☑Quarter 3 (July 1 – September 30) ☐Quarter 4 (October 1 – December 31)	
Project Title: Evaluation of Test Methods for Permeability (Transport) and Development of Performance Guidelines for Durability		
Name of Project Manager(s): Tommy Nantung	**Phone Number:** (765) 463-1521 ext. 248	**E-Mail** tnantung@indot.in.gov
Lead Agency Project ID: INDOT	**Other Project ID (i.e., contract #):**	**Project Start Date:** 07/01/2008
Original Project End Date: 06/30/2012	**Current Project End Date:** 06/30/2012	**Number of Extensions:**

Project schedule status:

☑ On schedule ☐ On revised schedule ☐ Ahead of schedule ☐ Behind schedule

Overall Project Statistics:

Total Project Budget	Total Cost to Date for Project	Percentage of Work Completed to Date
$883,000.00	$534,702.50	65%

Quarterly Project Statistics:

Total Project Expenses and Percentage This Quarter	Total Amount of Funds Expended This Quarter	Total Percentage of Time Used to Date
$31,991.00 - 3.6% of the total budget	4.5%	81%

Project Description:

The primary purpose of this project is to develop a test procedure that directly evaluates the permeability (transport properties) of concrete and relates these to anticipated field performance with the use of exposure conditions. This consists of the following distinct objectives:

• Evaluation of existing permeability (transport) test procedures.
• Development of new, or improvement of existing test, procedures to evaluate permeability (transport) properties of concrete.
• Correlation between permeability (transport) properties and measured material response to existing 'durability' tests.
• Develop guidelines to relate permeability, exposure conditions, and field performance for use in specifications and quality control processes.

Progress this Quarter (includes meetings, work plan status, contract status, significant progress, etc.):

Please see the report attached. It will be divided in the following sessions:
Session 1: NRMCA National Ready Mixed Concrete Association
Session 2: Purdue University
Session 3: Draft Papers

Anticipated work next quarter:

Continued testing on samples that have been conditioning

Rapid conditioning

The complete calculation of the time of equilibrium for different samples will be performed for samples that are being dried Additionally a rapid conditioning is being evaluated for use with the electrical testing.

Gas permeability measurements – comparison with Switzerland

The samples tested for oxygen permeability and diffusivity will be sent in a Swiss laboratory where the same tests will be repeated in order to check the proper setting of our instrument and the repeatability of the results.

Chloride Profile and Binding

Chloride profiling testing has been developed and will be summarized in the next report. It has been determined that additional information is needed to assess binding. A methodology proposed by Tang and Nilsson will be tested, in order to evaluate its effectiveness and a possible application.

Significant Results:

During the last quarter four important results were obtained.

First, the round robin study was completed using the bulk resistivity test. The results of this study are attached and the method should be able to be developed into an AASHTO standard. The data has also been provided to researchers working on a new ASTM standard and a draft standard will be drafted. This is the attached paper Spragg et al.

Second, it was observed that improvements for sample conditioning are needed for the ASTM C 1585 procedure. The improvements are needed for application to low w/c concrete, field concrete and concrete containing salts. A request for standard revision to reflect this needed has been sent to ASTM and these findings are discussed in the attached paper by Spragg et al.

Third, a procedure has been developed in earlier work (Pour Ghaz et al attached) however this procedure can be adopted here to better understand sample conditioning. The research team has begun to evaluate material properties for use in this model and has begun to compare them with theoretical expectations.

Fourth, OPI and gas diffusion test apparatus setups have been completed and these tests are now being compared with one another. This completes the setup of all the testing devices.

Circumstance affecting project or budget. (Please describe any challenges encountered or anticipated that might affect the completion of the project within the time, scope and fiscal constraints set forth in the agreement, along with recommended solutions to those problems).

Potential Implementation:

TRANSPORTATION POOLED FUND PROGRAM
QUARTERLY PROGRESS REPORT

Lead Agency (FHWA or State DOT): INDOT - Indiana Department of Transportation

INSTRUCTIONS:
Project Managers and/or research project investigators should complete a quarterly progress report for each calendar quarter during which the projects are active. Please provide a project schedule status of the research activities tied to each task that is defined in the proposal; a percentage completion of each task; a concise discussion (2 or 3 sentences) of the current status, including accomplishments and problems encountered, if any. List all tasks, even if no work was done during this period.

Transportation Pooled Fund Program Project # *(i.e, SPR-2(XXX), SPR-3(XXX) or TPF-5(XXX)* TPF-5(179) SPR 3280	**Transportation Pooled Fund Program - Report Period:** ☐Quarter 1 (January 1 – March 31) ☐Quarter 2 (April 1 – June 30) ☑Quarter 3 (July 1 – September 30) ☐Quarter 4 (October 1 – December 31)	
Project Title: Evaluation of Test Methods for Permeability (Transport) and Development of Performance Guidelines for Durability		
Name of Project Manager(s): Tommy Nantung	**Phone Number:** (765) 463-1521 ext. 248	**E-Mail** tnantung@indot.in.gov
Lead Agency Project ID: INDOT	**Other Project ID (i.e., contract #):**	**Project Start Date:** 07/01/2008
Original Project End Date: 06/30/2012	**Current Project End Date:** 06/30/2012	**Number of Extensions:** -

Project schedule status:

☑ On schedule ☐ On revised schedule ☐ Ahead of schedule ☐ Behind schedule

Overall Project Statistics:

Total Project Budget	Total Cost to Date for Project	Percentage of Work Completed to Date
$883,000.00	$53,4702.50	65%

Quarterly Project Statistics:

Total Project Expenses and Percentage This Quarter	Total Amount of Funds Expended This Quarter	Total Percentage of Time Used to Date
$31,991.00 - 3.6% of the total budget	4.5%	81%

Project Description:

The primary purpose of this project is to develop a test procedure that directly evaluates the permeability (transport properties) of concrete and relates these to anticipated field performance with the use of exposure conditions. This consists of the following distinct objectives:

• Evaluation of existing permeability (transport) test procedures.
• Development of new, or improvement of existing test, procedures to evaluate permeability (transport) properties of concrete.
• Correlation between permeability (transport) properties and measured material response to existing 'durability' tests.
• Develop guidelines to relate permeability, exposure conditions, and field performance for use in specifications and quality control processes.

Progress this Quarter (includes meetings, work plan status, contract status, significant progress, etc.):

Please see the report attached. It will be divided in the following sessions:

Session 1: NRMCA National Ready Mixed Concrete Association
Session 2: Purdue University
Session 3: Draft Papers

Anticipated work next quarter:

Continued testing on samples that have been conditioning

Rapid conditioning
The complete calculation of the time of equilibrium for different samples will be performed for samples that are being dried Additionally a rapid conditioning is being evaluated for use with the electrical testing.

Gas permeability measurements – comparison with Switzerland
The samples tested for oxygen permeability and diffusivity will be sent in a Swiss laboratory where the same tests will be repeated in order to check the proper setting of our instrument and the repeatability of the results.

Chloride Profile and Binding
Chloride profiling testing has been developed and will be summarized in the next report. It has been determined that additional information is needed to assess binding. A methodology proposed by Tang and Nilsson will be tested, in order to evaluate its effectiveness and a possible application.

Significant Results:

During the last quarter three important results were obtained.

First, the round robin study was completed using the bulk resistivity test. The results of this study are attached and the method should be able to be developed into an AASHTO standard. The data has also been provided to researchers working on a new ASTM standard and a draft standard will be drafted. This is the attached paper Spragg et al.

Second, it was observed that improvements for sample conditioning are needed for the ASTM C 1585 procedure. The improvements are needed for application to low w/c concrete, field concrete and concrete containing salts. A request for standard revision to reflect this needed has been sent to ASTM and these findings are discussed in the attached paper by Spragg et al.

Third, a procedure has been developed in earlier work (Pour Ghaz et al attached) however this procedure can be adopted here to better understand sample conditioning. The research team has begun to evaluate material properties for use in this model and has begun to compare them with theoretical expectations.

Fourth, OPI and gas diffusion test apparatus setups have been completed and these tests are now being compared with one another. This completes the setup of all the testing devices.

Circumstance affecting project or budget. (Please describe any challenges encountered or anticipated that might affect the completion of the project within the time, scope and fiscal constraints set forth in the agreement, along with recommended solutions to those problems).

None so far

Potential Implementation:

Still in development.

SESSION 1: NRMCA National Ready Mixed Concrete Association

This report is divided into three sections. The first section reports results from NRMCA (Page 1). The second section reports results from the last quarter performed at Purdue (Page 56). The third section provides chapters/papers of completed work (Page 72).

1.0: NRMCA National Ready Mixed Concrete Association

Concrete can fail due to chloride induced corrosion, sulfate attack, freeze thaw attack and ASR. NRMCA is using rapid index test criteria suitable for specifications will be developed that correlate well with slower performance tests for concrete exposed to chlorides, sulfates, and freeze thaw.

Chloride Ingress - Test Methods, Curing Conditions and Test Ages

Chloride ingress can occur from deicing salts applied in bridge decks in Northern regions as well as concrete exposed to marine conditions. It is well known that when the chloride concentration at the steel rebar exceeds the chloride threshold corrosion can initiate. The chloride diffusion test (ASTM C1556) is understood to be a good performance test. However, that is a very slow test and applicable only for sophisticated laboratories. So rapid index tests were evaluated as follows:

Mixture Proportions and Variables

w/cm	PC	15%FA	30%FA	25%SL	50%SL	7%SF	40%SL+5%SF
0.29	Yes - l						
0.34							Yes - n
0.39	Yes - m	Yes - l	Yes - vl	Yes - l	Yes - vl	Yes - vl	
0.49	Yes - h	Yes - m		Yes - m			
0.62			Yes - h		Yes - h		

where

H – High chloride permeability (>5 x 10^{-12} m^2/s) – 3 mixtures

M – moderate chloride permeability (3 to 5 x 10^{-12} m^2/s) – 3 mixtures

L – low chloride permeability (2 to 3 x 10^{-12} m^2/s) – 3 mixtures

VL – very low chloride permeability (0.7 to 2 x 10^{-12} m^2/s) – 3 mixtures

N – negligible chloride permeability (<0.7 x 10^{-12} m^2/s) – 1 mixture

The above mixtures were selected keeping the following in mind:

1. Cover a predicted (based on Life 365 computer program) 2 year chloride diffusion coefficient range that is broad – 6.8x10^{-12} to 0.62x10^{-12} m^2/s
2. To be able to use rapid index test criteria to choose mixtures with desired classification as indicated above and at the very least rapid index test criteria should help eliminate mixtures with high diffusion coefficients (>5 x 10^{-12} m^2/s)
3. Look at common SCMs like fly ash, slag, silica fume to see if correlation between the rapid index tests criteria and diffusion coefficients are independent of SCM types and dosages
4. w/cm, SCM dosages chosen must cover the ranges normally used in HPC
5. Also some mixtures that would yield high chloride diffusion coefficients (containing high w/cm, high pozzolan) should be made and the rapid index tests should yield high values so that such mixtures will not be selected. Also some mixtures that would yield low chloride diffusion coefficients (containing low w/cm, low or no pozzolan or conductive aggregates) should be made and the rapid index tests should yield low values so that such mixtures will be selected.

Mixture Prepared and Tested Thus Far

All the 13 concrete mixtures have now been cast in 2 phases. Phase I looked at 6 mixtures and the test results are provided in Table 1 whereas Phase II looked at 7 mixtures and the test results are provided in Table 2. The common elements of the two phases are:

Crushed coarse aggregate (1.0 in. nominal maximum size) ASTM C33 No. 57, natural sand FM=2.88

Adjusted water reducer or high range water reducer (if any) for desired slump = 5 to 7 in.

Non air entrained concrete mixtures – even though most of these mixtures in practice will contain air our aim here is to determine the validity of the rapid index tests and criteria in classifying mixtures based on their chloride diffusion coefficients. This validation will also hold for air entrained concrete mixtures. Also the use of air entrainment will make the comparisons between mixtures more challenging

Planned Test Methods, Curing Conditions and Test Ages

Normal Curing – Standard moist room curing starts immediately after making the specimens

Accelerated Curing – 7 days of normal curing followed by 21 days of curing in 100F water

For all mixtures measure the following:

Slump, temperature, air content, density, Strength (28 days), Shrinkage (7 days moist curing followed by 90 days of air drying). Shrinkage test is for reference and may be discontinued for future mixtures.

The following durability tests will be conducted for all the mixtures

Durability Tests

- **Rapid Chloride Permeability test – RCPT (ASTM C1202)**

i) 28 day accelerated
ii) 56 day normal curing
iii) 26 week (182 d) normal curing
iv) 78 week (546 d) normal curing

- **5 minute Conductivity Test (ASTM C1202 based)**

i) 28 day accelerated
ii) 56 day normal curing
iii) 26 week (182 d) normal curing
iv) 78 week (546 d) normal curing

- **Rapid Migration Test - RMT (AASHTO TP 64)**

i) 28 day accelerated
ii) 56 day normal curing
iii) 26 week (182 d) normal curing
iv) 78 week (546 d) normal curing

- **Chloride Diffusion Test (ASTM C1556)**

i) 59d week normal curing + 186d in solution. For Phase II this condition was replaced by 56d normal curing + cyclic exposure (75 week using 3d in solution/4d at 73F-50%rh cycle) in solution - 2
ii) 59d normal curing + 490d in solution till 78 weeks. For Phase II this condition was replaced by 6months normal curing + 15 months in solution - 1
iii) 59d normal curing + cyclic exposure (18 week using 4d in solution/3d at 100F-20%rh cycle) in solution. For Phase II this condition was replaced by 56d normal curing + cyclic exposure (21 week using 3d in solution/4d at 73F-50%rh cycle) in solution - 2
iv) 59d normal curing + 59d in solution. For Phase II it was 56d normal curing + 35d in solution
v) 26 weeks normal cure +35 days in solution

- **Sorptivity Test (ASTM C1585)**

i) 28 day accelerated + 18 d specimen conditioning (C1585)
ii) 56 day normal curing + 18 d specimen conditioning (C1585)
iii) 26 week (182 d) normal curing + 18 d specimen conditioning (C1585)

- **Absorption test BS 1881:122 (ASTM Draft)**

i) 10 day normal curing + 3 d in oven
ii) 28 day accelerated + 3 d in oven
iii) 26 week (182 d) normal curing + 3 d in oven

For Phase I the oven temperature was maintained at 105C where as for Phase II it was 60C. The difference followed the development of the ASTM drafts. It was felt that the high oven temperatures will lead to internal micro-cracking of concrete leading to misleading high results that are not reflective of the absorption characteristics of the concrete specimen being tested.

Rapid index tests need to correlate with chloride penetration levels for two real life situations:

a. when the structures are in a complete or near complete saturation state such as in a submerged marine exposure or possibly bridge decks in high humidity regions where chloride ingress is primarily diffusion controlled. The ASTM C1556 would be the correct comparison test here and the aim would be to observe which of the rapid index tests correlates well with diffusion coefficient (at oldest age). Ideally suitable rapid index test criteria (s) can be chosen so that mixtures can be selected based on the desired level of chloride diffusion coefficient.
b. when the structures are not completely saturated such as bridge decks in low humidity regions where the chloride ingress could be due to sorption and diffusion. ASTM C1556 conducted in a wet/dry scenario would be the closest comparison test here and the aim would be to observe which of the rapid index tests correlates well with the ingress coefficient (at oldest age). Ideally suitable rapid index test criteria (s) can be chosen so that mixtures can be selected based on the desired level of chloride diffusion coefficient.

Table 1. Yield Adjusted Mixture Proportions and Test Results

Calculated Batch Quantities						
	0.49Ctrl	**0.49SL25**	**0.39SL50**	**0.49FA15**	**0.39FA30**	**0.34SL40SF5**
Type I/II cement, lb/yd^3	554	416	306	472	431	382
Slag, lb/yd^3		139	306			277
Fly ash, lb/yd^3				83	185	
Silica Fume, lb/yd^3						35
SCM, %	0	25	50	15	30	45
Coarse Agg. (No.57), lb/yd^3	2075	2074	2070	2081	2081	2086
Fine Aggregate, lb/yd^3	1303	1293	1314	1273	1267	1264
Mixing Water, lb/yd^3	272	272	239	273	240	236
w/cm	0.49	0.49	0.39	0.49	0.39	0.34
ASTM C494 Type A, oz/cwt	4.0	4.0	4.0	4.0	4.0	4.0
ASTM C494 Type F, oz/cwt	2.5	2.9	4.3	2.4	5.0	7.8
Fresh Concrete Properties						
ASTM C143, Slump, in.	7 1/2	4 1/2	8	7	6 3/4	9
ASTM C231, Air, %	1.4	1.7	1.3	1.5	1.6	1
ASTM C138, Density, lb/ft^3	156.5	156.1	157.7	155.7	156.5	159.3

ASTM C1064, Temperature, °F	76	76	75	76	75	75
Hardened Concrete Properties						
ASTM C39, Compressive Strength, psi						
28 days	6,830	7,550	10,520	6,640	7,970	12,440
Draft ASTM Standard, Water Absorption Test at 105 °C, %						
10d normal cure	2.89	2.24	1.69	3.25	2.33	1.43
28d accelerated cure	2.52	1.77	1.34	2.44	1.63	1.26
196d normal cure	2.30	1.80	1.29	2.29	1.44	1.49
ASTM C1202, Rapid Chloride Permeability, Coulombs						
28d accelerated cure	4657	1992	561	2414	723	166
56d normal cure	4674	1912	581	3013	1417	270
196d normal cure	3356	1581	496	1551	340	147
550d normal cure	3891^{-}	1465^{-}	394^{-}	1070^{-}	174^{-}	166^{-}
Draft ASTM Standard, 5 minute Conductivity, Sm^{-1}						
28d accelerated cure	0.0189	0.0083	0.0030	0.0091	0.0030	0.0009
56 normal cure	0.0154	0.0072	0.0034	0.0129	0.0058	0.0013
196d normal cure	0.0099	0.0055	0.0021	0.0057	0.0018	0.0008
550d normal cure	0.0076^{-}	0.0054^{-}	0.0018^{-}	0.0054^{-}	0.0008^{-}	0.0009^{-}
AASHTO TP64, Rate of Penetration (RMT), mm/(V-hr)						
28d accelerated cure	0.065	0.030	0.004	0.046	0.015	0.003
56d normal cure	0.044	0.025	0.006	0.043	0.024	0.002
196d normal cure	0.047	0.016	0.006	0.025	0.006	0.002
550d normal cure	0.048^{-}	0.017^{-}	0.003^{-}	0.017^{-}	0.005^{-}	0.001^{-}
ASTM C157, Length Change (Drying Shrinkage), %						
28 days^{+}	0.035	0.039	0.031	0.029	0.028	0.028
56 days^{+}	0.046	0.048	0.037	0.039	0.036	0.032
90 days^{+}	0.055	0.054	0.044	0.048	0.043	0.039

180 days[+]	0.062	0.060	0.049	0.054	0.049	0.044
ASTM C 1585, Rate of Water Absorption (Sorptivity), x10^{-4} mm/s$^{1/2}$						
28d accel. cure (Initial/Secondary)	10.0 / 7.5	3.1[*] / 2.8	1.8[*] / 1.7	7.5 / 4.6	4.8[*] / 2.1	2.6[*] / 0.86
56d normal cure (Initial/Secondary)	9.9 / 6.9	6.8 / 2.4[*]	2.6[*] / 1.4	20.0 / 13.0	7.1[*] / 3.3	4.1[*] / 1.9[*]
196d normal cure (Initial/Secondary)	6.8[*] / 6.8	4.1[*] / 1.3	4.9[*] / 1.3	4.1 / 2.4	3.6[*] / 1.8	1.2[*] / 0.82[*]
28d accel. cure (Initial/Secondary), g	1.77 / 6.85	0.82 / 2.59	0.66 / 1.75	1.48 / 4.93	1.20 / 2.71	0.51 / 1.13
56d normal cure (Initial/Secondary), g	1.78 / 6.74	1.06 / 2.94	0.67 / 1.62	2.62 / 12.2	1.4 / 3.76	0.87 / 2.17
196d normal cure (Initial/Secondary), g	1.34 / 5.74	0.96 / 1.81	1.13 / 1.94	1.09 / 2.73	0.95 / 2.12	0.64 / 1.14
ASTM C 1556, Chloride Diffusion, x 10^{-12} m^2/s						
Case 4	5.28	2.24	0.84	8.64	4.81	0.36
Case 3	11.8	3.20	1.02	6.45	4.01	0.64
Case 1	2.28	1.37	0.47	1.74	0.14	0.26
Case 5	2.36	1.32	0.68	3.91	2.02	0.30
Case 2	11.29	3.34	0.55	4.75	1.12	0.35
ASTM C 1556, Surface Chloride, % by weight of concrete						
Case 4	1.12	1.77	1.03	0.96	0.75	3.02
Case 3	1.02	1.37	1.93	1.23	1.39	2.65
Case 1	1.01	1.90	2.11	1.26	5.62	1.90
Case 5	0.78	1.29	1.87	1.19	2.41	2.14
Case 2	1.03	1.05	1.84	1.23	1.40	1.90

[+] Curing period in 70°F, 50% RH environment NOT included 7 days initial wet curing period in water bath

[*] a correlation coefficient less than 0.98 indicating that the rate cannot be determined according to ASTM C1585

[-] Result of only one specimen

Rapid index tests results were compared with chloride diffusion test data. Research results were presented at the 2009 Concrete Technology Forum in Cincinnatti, OH as “Early Age Tests and Criteria for Predicting Long Term Chloride Penetration into Concrete”. Preliminary observations show promising correlations between the early age RCPT results and chloride diffusion coefficients for scenarios Case 1, and Case 3. For Cases 4, and 5 fly ash mixes

appear to be more prone to show higher Da's than what the early age RCPT results would have suggested.

Detailed analysis of the correlation between the measured diffusion coefficients and rapid index test results are being conducted. Future QPRs will feature those discussions. Some of the results were presented at the ACI Spring Convention in April.

Table 2. Yield Adjusted Mixture Proportions and Preliminary Test Results

Calculated Batch Quantities								
	0.39PC	**0.39FA15**	**0.39SL25**	**0.39SF7**	**0.62FA30**	**0.62SL50**	**0.29PC**	**0.39PC**-R**
Type I/II cement, lb/yd^3	612	520	462	565	349	249	803	612
Slag, lb/yd^3	-	-	154	-	-	249	-	-
Fly ash, lb/yd^3	-	92	-	-	149	-	-	-
Silica Fume, lb/yd^3	-	-	-	43	-	-	-	-
SCM, %	0%	15%	25%	7%	30%	50%	0%	0%
Coarse Agg. (No.57), lb/yd^3	2066	2068	2081	2052	2094	2093	2069	2066
Fine Aggregate, lb/yd^3	1331	1296	1331	1307	1216	1258	1183	1331
Mixing Water, lb/yd^3	238	239	240	237	287	290	236	238
w/cm	0.39	0.39	0.39	0.39	0.58	0.58	0.29	0.39
ASTM C494 Type A, oz/cwt	4	4	4	4	3	3	5	4
ASTM C494 Type F, oz/cwt	8.8	8.3	6.9	8.2	-	-	11.7	8.4
Fresh Concrete Properties								
ASTM C143, Slump, in.	5	6 1/2	7 3/4	6	6 1/2	7	8 3/4	7
ASTM C231, Air, %	1.8	1.6	1.2	1.8	1.6	1.4	1.1	1.7
ASTM C138, Density, lb/ft^3	158.1	156.9	158.9	156.5	152.5	154.1	159.7	158.1
ASTM C1064, Temperature, °F	75	75	75	75	75	75	76	76
Hardened Concrete Properties								
ASTM C39, Compressive Strength, psi								
28 days	10,460	9,590	10,300	10,740	3,880	5,380	13,480	9,890
Draft ASTM Standard, Water Absorption Test at 60 °C, %								
56d normal cure	1.03	1.02	1.00	0.82	1.88	1.75	0.91	-
213d normal cure	0.85	0.79	0.91	0.76	1.55	1.40	0.70	-
ASTM C1202, Rapid Chloride Permeability, Coulombs								

28d accelerated cure	2180^{-}	1031	1186	276	2495	661	1078	1980
56d normal cure	1722	1557	1272	299	4012	832	1209	-
213d normal cure	1607	563	873	252	1177	572	936	-
Draft ASTM Standard, 5 minute Conductivity, Sm^{-1}								
28d accelerated cure	0.0101^{-}	0.0054	0.0061	0.0014	0.0089	0.0037	0.0061	0.0102
56 normal cure	0.0089	0.0070	0.0058	0.0014	0.0119	0.0034	0.0056	-
213d normal cure	0.0062	0.0026	0.0037	0.0014	0.0042	0.0020	0.0040	-
AASHTO TP64, Rate of Penetration (RMT), mm/(V-hr)								
28d accelerated cure	0.034^{-}	0.017	0.013	0.004	0.047	0.007	0.012	0.029
56d normal cure	0.027	0.017	0.011	0.004	0.046	0.012	0.011	-
213d normal cure	0.021	0.009	0.009	0.002	0.033	0.006	0.007	-
ASTM C157, Length Change (Drying Shrinkage), %								
28 days^{+}	0.032	0.037	0.032	0.028	0.041	0.044	0.024	-
56 days^{+}	0.039	0.047	0.038	0.034	0.054	0.052	0.029	-
90 days^{+}	0.042	0.054	0.047	0.043	0.064	0.053	0.030	-
180 days^{+}	0.049	0.056	0.052	0.045	0.066	0.061	0.038	-
ASTM C 1585, Rate of Water Absorption (Sorptivity), $x10^{-4}$ $mm/s^{1/2}$								
28d accel. cure (Initial/Secondary)	-	3.1 / 2.1	4.7 / 2.0*	3.3 / 2.1	9.6 / 3.8	7.6 / 2.8	3.1 / 2.6	9.5 / 5.2
56d normal cure (Initial/Secondary)	5.9 / 3.3*	6.1 / 4.1	3.1* / 1.5*	3.1 / 1.9*	9.9 / 7.0	7.1* /2.8*	2.1*/ 2.9	-
213d normal cure (Initial/Secondary)	4.7* / 3.0	3.2* / 2.2	3.6* / 1.9	2.6* / 0.7*	4.6 / 3.7	5.6* / 1.6*	1.6*/1.3*	-
28d accel. cure (Initial/Secondary), g	-	0.5 /1.9	0.9 / 2.2	0.6 / 1.9	1.8 / 4.4	1.9 / 3.7	0.5 / 2.2	1.6 / 5.1
56d normal cure (Initial/Secondary), g	1.1 / 3.2	0.9 /3.8	0.8 / 1.7	0.6 / 1.7	2.3 / 6.9	2.1 / 3.9	0.5 / 2.4	-
213d normal cure (Initial/Secondary), g	0.8 / 2.5	0.5 / 2.0	0.7 / 1.8	0.5 / 1.0	1.3 / 4.0	1.4 / 2.7	0.3 / 1.2	-
ASTM C 1556, Chloride Diffusion, x 10^{-12} m^2/s								
56d nc + 35d in solution	4.58	2.89	2.21	1.18	6.99	2.90	1.32	-
6m nc + 35d in solution	2.72	1.34	1.12	0.67	7.10	2.31	1.04	-

6m nc + 15m in solution	1.35	0.48	0.61	0.22	1.10	0.45	0.48	-
56d nc + 21w cyclic exposure (3d solution+ 4d air)	1.59	1.24	0.87	0.66	8.33	2.33	0.67	-
56d nc + 75w cyclic exposure (3d solution+ 4d air)	1.57	0.35	0.40	0.33	4.72	1.39	0.23	-
ASTM C 1556, Surface Chloride, % by weight of concrete								
56d nc + 35d in solution	0.96	1.17	1.50	1.23	1.11	1.40	1.10	-
6m nc + 35d in solution	0.94	1.46	1.60	1.27	1.00	1.20	1.46	-
6m nc + 15m in solution	0.90	0.95	1.45	1.20	1.00	1.35	1.30	-
56d nc + 21w cyclic exposure (3d solution+ 4d air)	1.01	1.29	1.57	1.32	1.54	1.71	1.42	-
56d nc + 75w cyclic exposure (3d solution+ 4d air)	1.05	1.30	1.60	1.35	1.54	2.00	1.42	-

[-] Tested at 21d instead of 28d

[+] Curing period in 70°F, 50% RH environment NOT included 7 days initial wet curing period in water bath

[*] A correlation coefficient less than 0.98 indicating that the rate cannot be determined according to ASTM C1585

[**] Exact repeat of designated mixture

Preliminary Observations

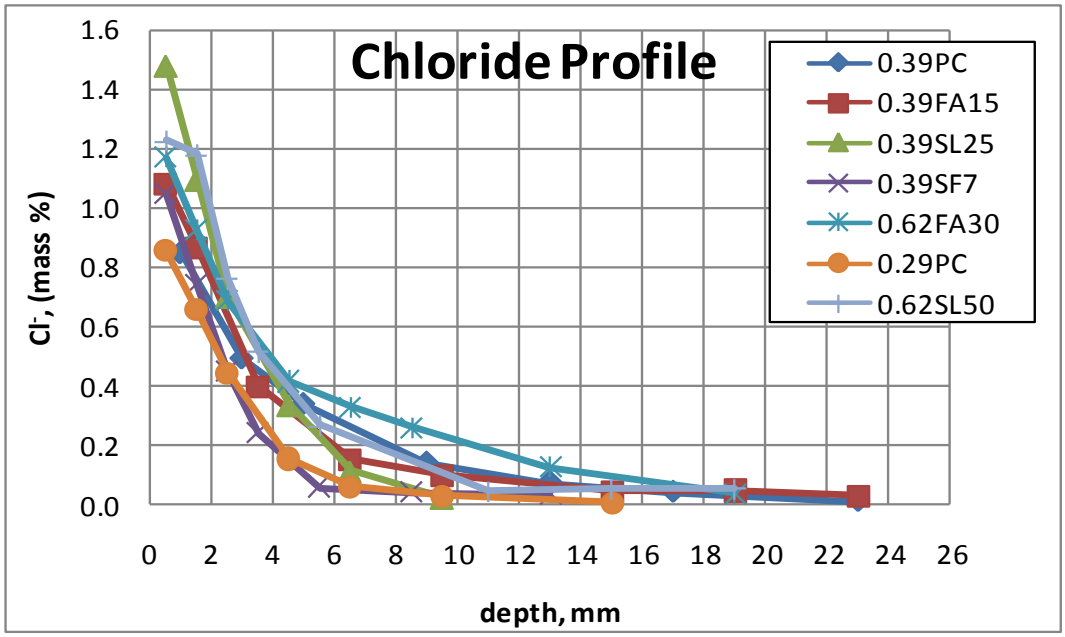

Figure 1. Chloride profile for 56d normal curing followed by 35d in solution

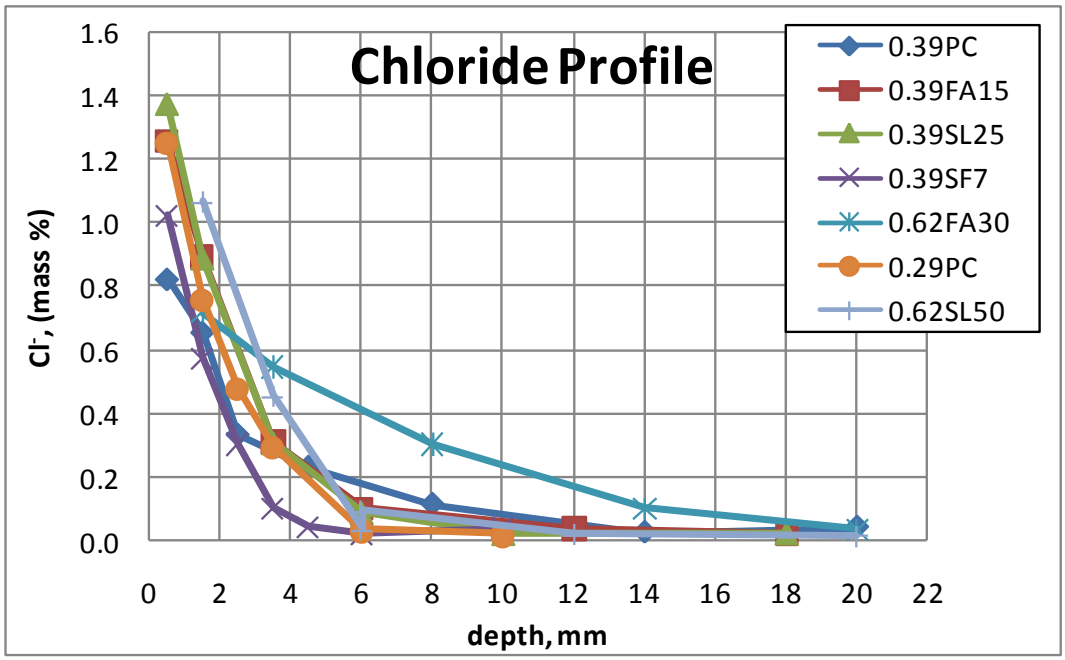

Figure 2. Chloride Profile (ASTM C1556) for 180d (6 month) normal curing followed by 35d in solution

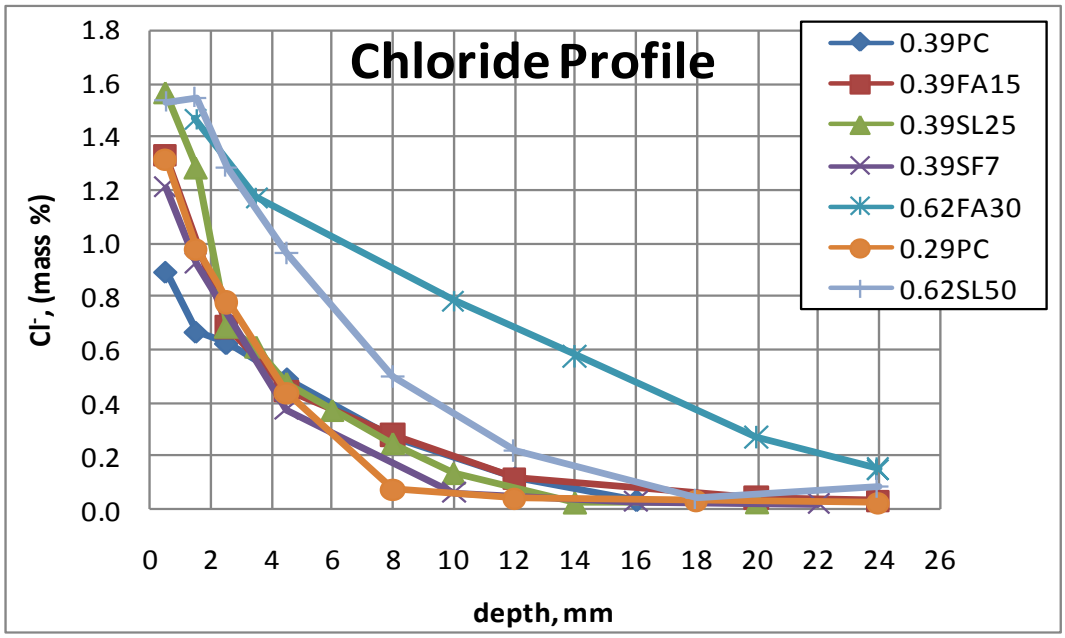

Figure 3. Chloride Profile (ASTM C1556) for 56d normal curing followed by 21 week in cyclic exposure

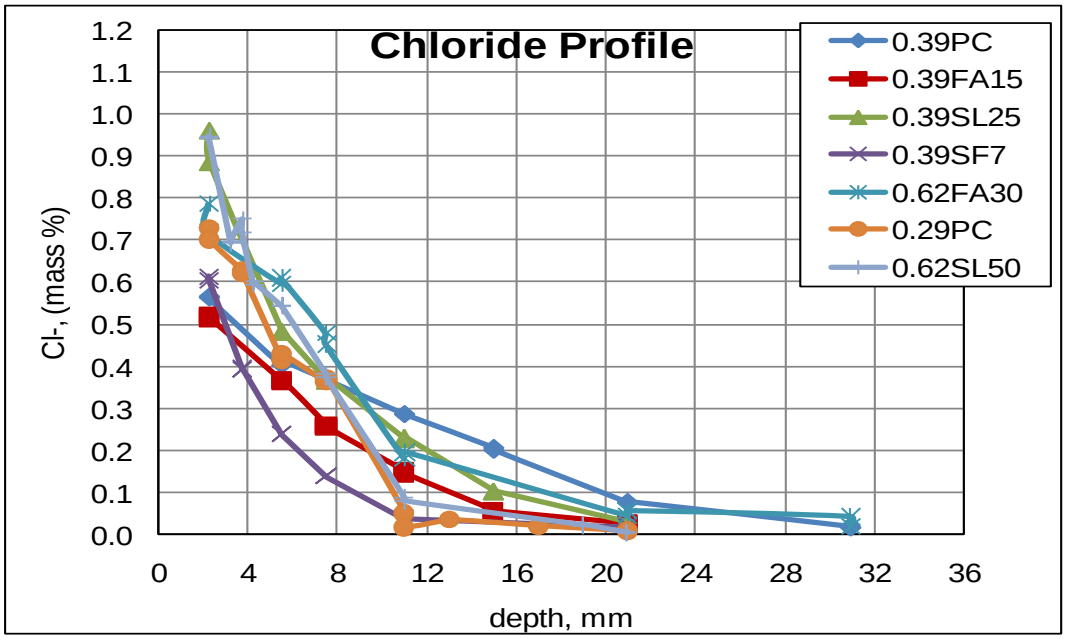

Figure 4. Chloride Profile (ASTM C1556) for 180d (6m) normal curing followed by 450d (15m) in solution

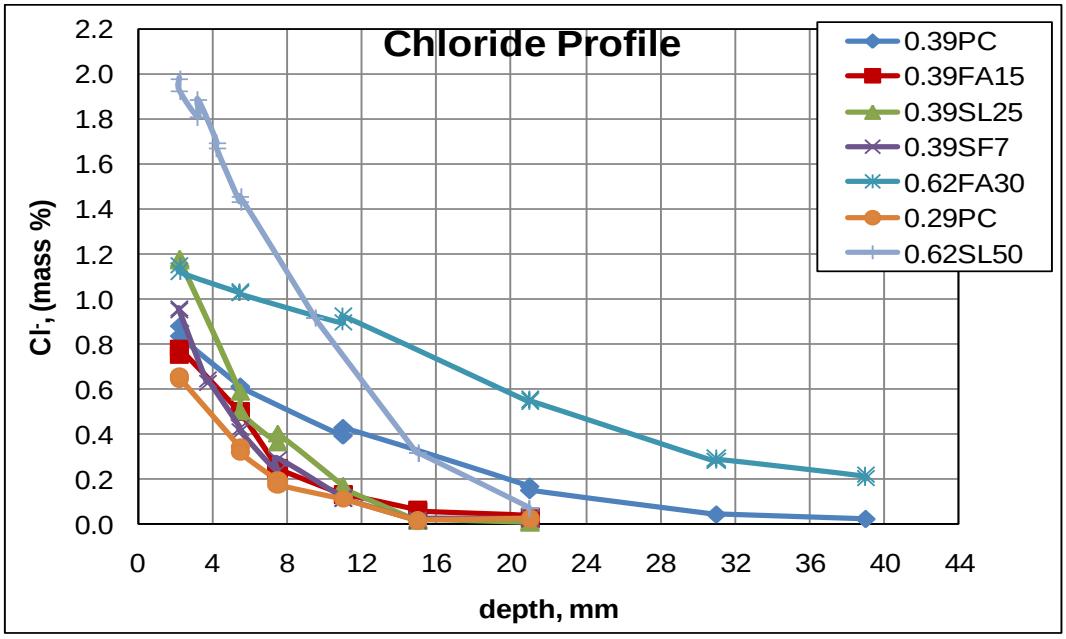

Figure 5. Chloride Profile (ASTM C1556) for 56d normal curing followed by 75 week in cyclic exposure

Preliminary Discussions on Chloride Diffusion Coefficient Test Results

1. Since the cases depicted in Figures4, and 5 show the longest exposure attention is paid to those. Judging by the chloride profiles shown in Figure 4 (6m normal curing+15 m in solution) the best performing mixes (showing low chloride ingress) in order were 0.39SF7<0.29PC=0.62SL50<039FA15<0.39SL25=0.62FA30<0.39PC. Judging by the chloride profiles shown in Figure 5 (56d normal curing+75 week cyclic) the best performing mixes (showing low chloride ingress) in order were 0.29PC<0.39SF7=0.39SL25=0.39FA15<0.39PC=0.62SL50<0.62FA30. The 0.39PC mixture had lower chloride ingress as compared to both the 0.62SL50 and 0.62FA30 mixtures. The two 0.62 w/cm mixtures had noticeably more chloride ingress when compared to all other mixtures. The 0.29PC mixture had the same chloride ingress as the best performing 0.39SF7 mixture. The cyclic condition is a little different as it involves chloride ingress into a partially saturated concrete surface. From the difference in performance between the 3 conditions it appears that a lower w/cm is more favorable for a cyclic case possibly due to the tighter pore structure it entails at the concrete surface and also difference in drying rates.
2. Judging by the chloride diffusion coefficient values reported in Table 2 for the mixtures in Fig. 4(6m normal curing+15 m in solution) the best performing mixes (lowest diffusion coefficient) in order were 0.39SF7<0.29PC=0.62SL50=039FA15<0.39SL25<0.62FA30<0.39PC. Judging by the chloride diffusion coefficient values reported in Table 2 for the mixtures in Fig. 5 (56d normal curing+75 week cyclic) the best performing mixes (lowest diffusion coefficient) in order were 0.29PC<0.39SF7=0.39SL25=0.39FA15<0.39PC=0.62SL50<0.62FA30. The ranking differences between visual observation based on chloride profile and diffusion coefficient estimation is identical for the cyclic case (Fig. 5). For the immersion case (Fig. 4) the difference is negligible and can be explained by the differences in the surface chloride content. The surface chloride contents did not vary substantially between the mixtures. It is the chloride diffusion coefficient value that is used for service life estimation and hence attention would be paid to that. However it is useful to look at the raw chloride profiles to make sure the order of mixtures is generally similar.
3. The chloride diffusion coefficient values vary as follows:
    1. 56d nc + 35d in solution - between 1.18 to 6.99 $x10^{-12}$ m^2/s
    2. 6m nc + 35d in solution - between 0.67 to 7.10 $x10^{-12}$ m^2/s
    3. 6m nc + 15m in solution - between 0.22 to 1.35 $x10^{-12}$ m^2/s
    4. 56d nc + 21w cyclic – between 0.66 to 8.33 $x10^{-12}$ m^2/s
    5. 56d nc + 21w cyclic - between 0.33 to 4.72 $x10^{-12}$ m^2/s

There is nearly an order of magnitude between the lowest and highest values in each condition and it encompasses the broad range of chloride diffusion coefficients.

Work Completed in this Quarter

Specimens exposed to the last two chloride exposure levels for Table 2 were tested the surface chloride contents and diffusion coefficients have been reported. All the diffusion results will be finalized in the next quarter and detailed analysis of the correlation between the measured

diffusion coefficients and rapid index test results will be conducted in subsequent quarters. The next QPR will feature those discussions. Some of the results were presented at the ACI Spring Convention in April.

The correlation between the diffusion coefficient results and various rapid index test results (conducted at various ages) are provided in the figures below.

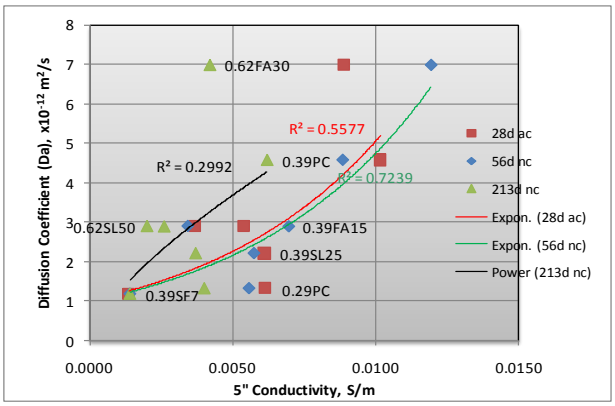

(a)

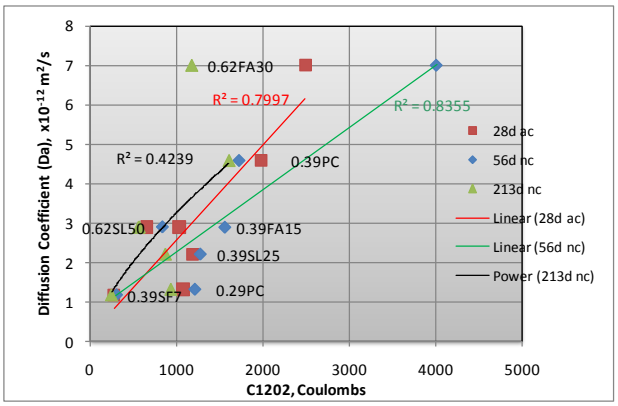

(b)

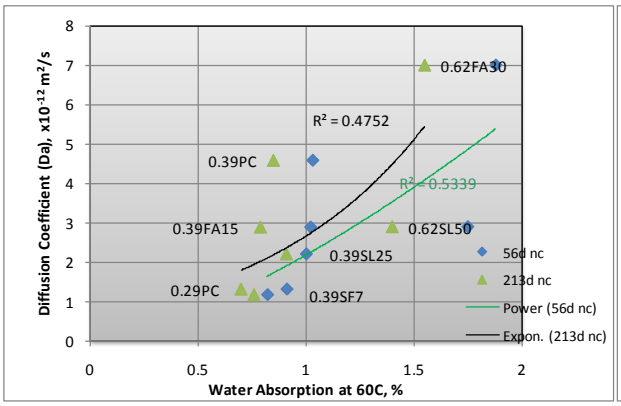

(c)

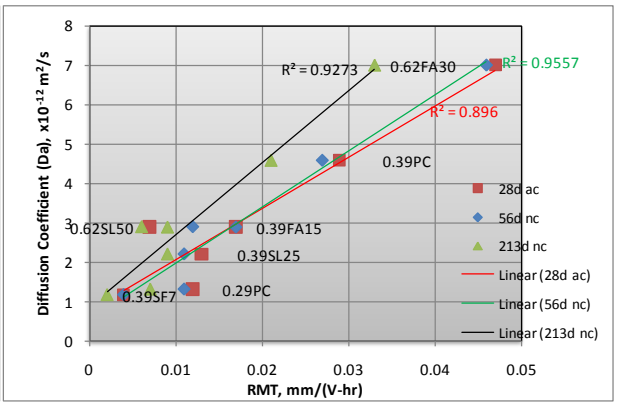

(d)

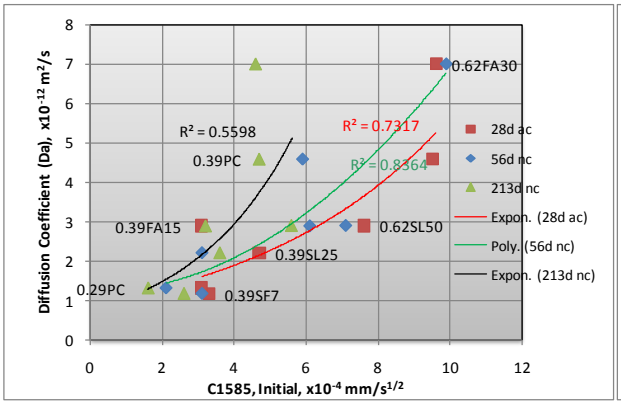

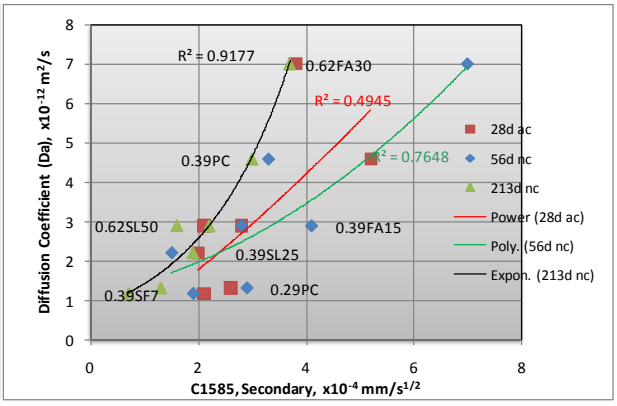

(e) (f)

Figure 4. (a) – (f) for 56d normal curing followed by 35d in solution

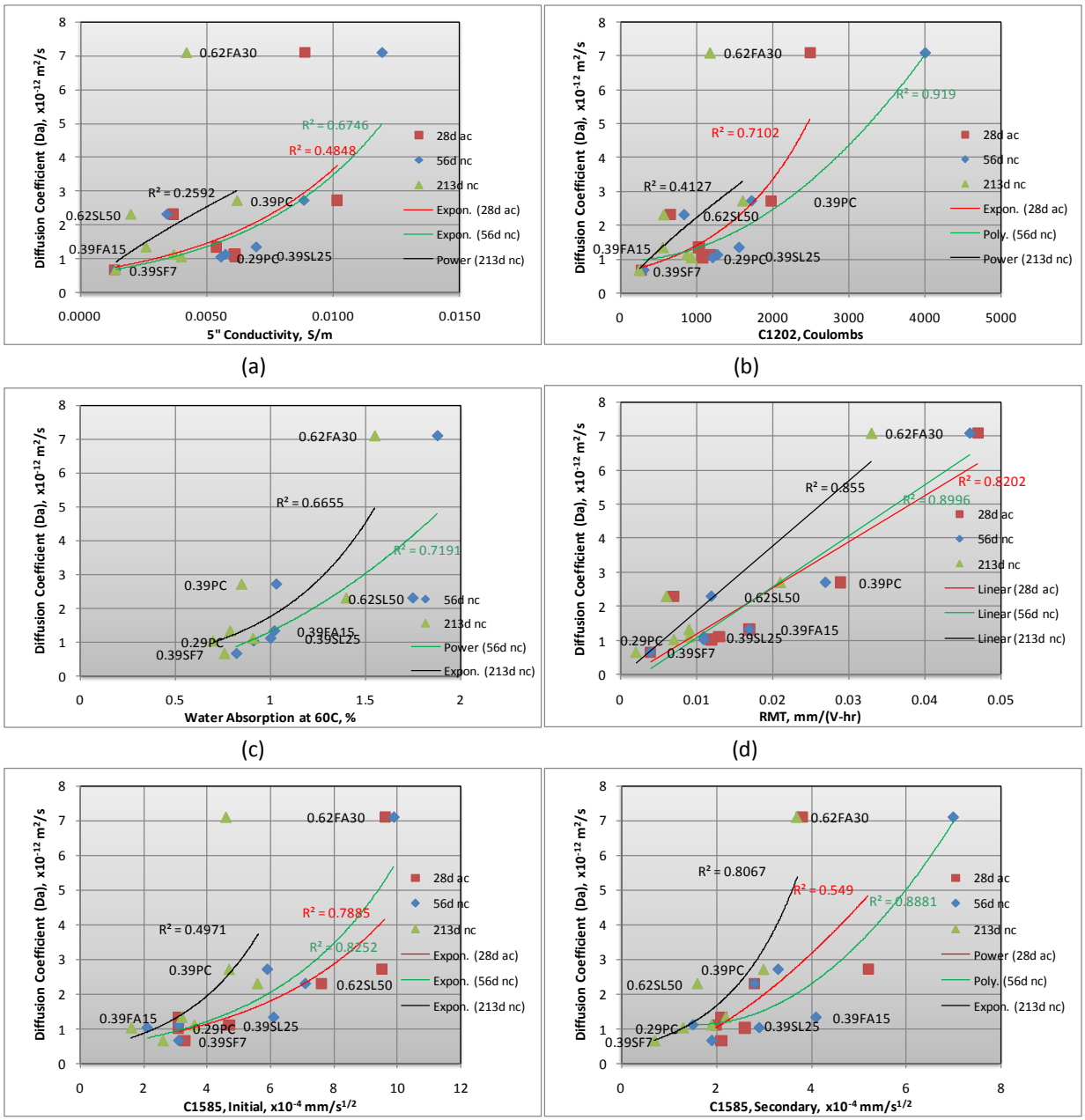

Figure 5. (a) – (f) for 180d normal curing followed by 35d in solution

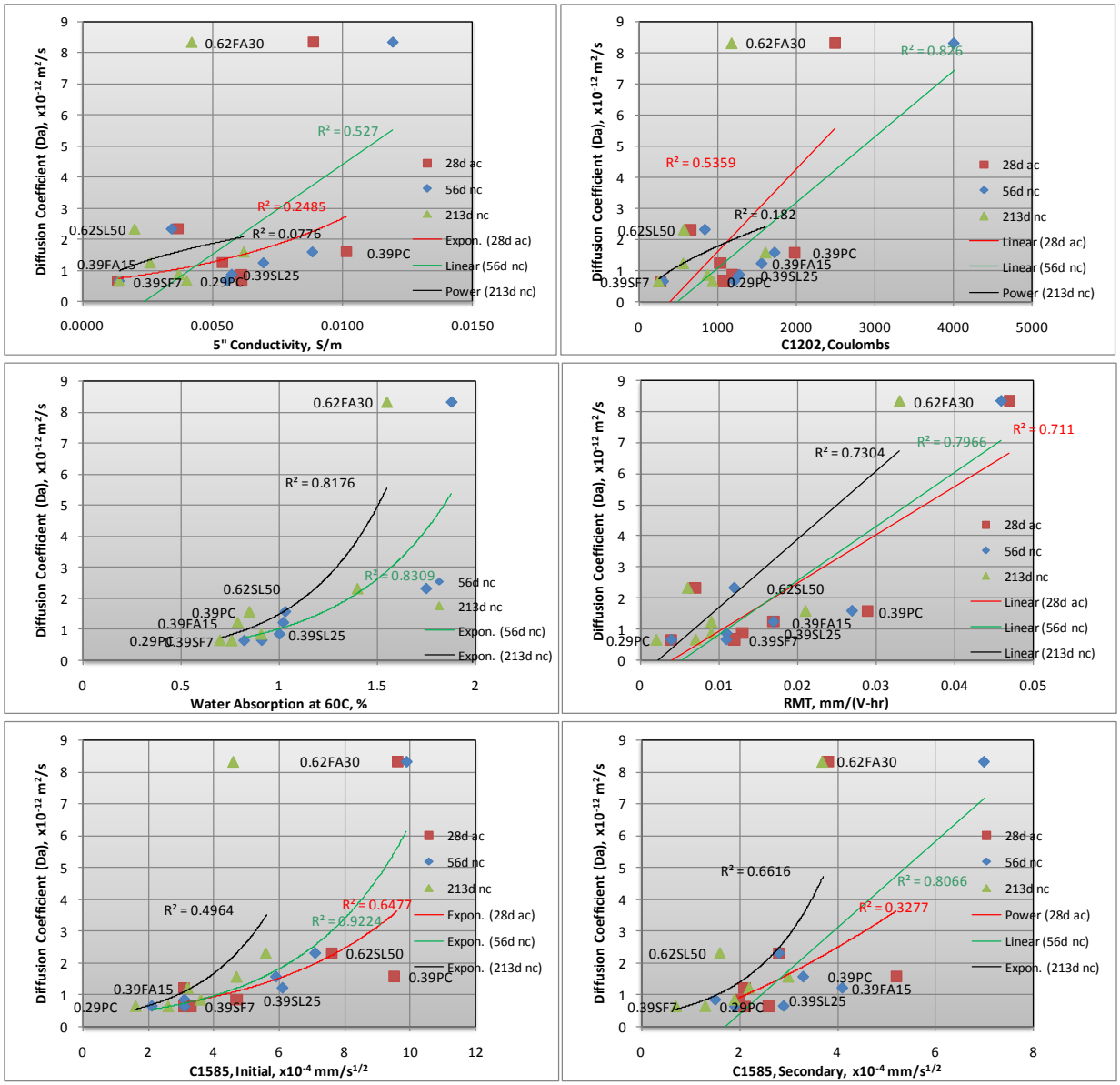

Figure 6. (a) – (f) for 56d normal curing followed by 21 week in cyclic exposure

Chloride Diffusion Coefficient and Rapid Index Test Results Comparisons

A quick look at the Figures 4-6 shows that the 56 day rapid index test results have the highest coefficient of correlation with the chloride diffusion coefficient in almost all cases. So the 56 day coefficient of correlations between each of the rapid index test and the chloride diffusion coefficients for the tree exposure classes has been summarized in the following Table.

Rapid Index Test	Coefficient of Correlations with Diffusion Coefficients, %			
	56d normal curing + 35d in solution	180d normal curing + 35d in solution	56d normal curing + 21w cyclic exposure	Average
5 minute Conductivity	0.72	0.67	0.52	0.64
ASTM C1202	0.84	0.92	0.83	0.86
Absorption	0.53	0.72	0.83	0.69
RMT, AASHTO TP64	0.96	0.90	0.80	0.89
Sorptivity, Initial	0.84	0.83	0.92	0.86
Sorptivity, Final	0.77*	0.89	0.81	0.82

The Rapid Migration Test (AASHTO TP64) has the best correlation of 0.89 followed by the ASTM C1202 and the initial sorptivity. If the cylic exposure is excluded then the RMT has an average correlation coefficient of 0.93 which is impressive. It is interesting to see that the 5 minute conductivity results have substantially poorer correlations. Similarly the absorption test has a poorer correlation as compared to the initial sorptivity test.

The 0.62SL50 mixture gave significantly low rapid index test results even at an early age of 56 days. The 56 day RCPT results for the 0.62SL50 mixture and the 0.29PC mixture were 832 and 1200 coulombs respectively but yet the chloride diffusion coefficients of the 0.29PC mixture was 2.2 to 3.5 times lower when the chloride exposures are for a shorter duration! However for the long term chloride exposure condition (6m nc + 15m in solution) the 0.62SL50 mixture and the 0.29PC mixture had similar chloride diffusion coefficients. For the long term cyclic exposure (56d nc + 75w cyclic exposure) the chloride diffusion coefficients of the 0.62SL50 mixture was 6 times higher than that of the 0.29PC mixture. Also the 0.62SL50 mixture had lower rapid index test result as compared to the 0.39FA15 and 0.39SL25 mixtures even though the diffusion coefficients of the 0.62SL50 mixture for the long term cyclic case was much higher (for the immersed case though the predictions from the rapid index test results are accurate). A job specification of 1000 coulombs would have allowed the 0.62SL50 mixture and rejected the 0.29PC mixture! While the 5 minute conductivity test is equally bad in concluding that the 0.62SL50 is a better mixture the RMT fairs slightly better. The 56 day RMT results for the 0.62SL50 mixture and the 0.29PC mixture were 0.012 and 0.011 respectively. The 56 day RMT results would lead one to conclude that both of these mixtures are similar. But it is evident that even the RMT is influenced by the effect of the pore solution conductivity albeit to a lesser extent than the RCPT and the 5 minute

conductivity tests. The clearest conclusion though comes from the absorption and sorptivity test results. The 56 day absorption and sorptivity test results were much higher for the 0.62SL50 as compared to the 0.29PC mixture.

The 0.62FA30 mixture has a different story. Fly ash tends to react slowly and therefore the early age rapid index test results of the 0.62FA30 mixture are still high and so they do not lead to incorrect conclusions as the 0.62SL50 mixture. But interestingly for the immersed case even the 0,.62FA30 mixture is catching up with the 0.29PC mixture.

Further the 56 day RCPT results for the 0.39SF7 mixture and the 0.29PC mixture were 299 and 1200 coulombs respectively. For the long term immersed case the measured chloride diffusion coefficients match the expected rapid index test results. However for the long term cyclic case the 0.39SF7 mixture had 50% higher chloride diffusion coefficients. Similar observations can be made when one looked at the 5 minute conductivity and RMT test results.

For the four w/c=0.39 mixtures the rapid index test results rank the 4 mixtures in the same order as the chloride diffusion coefficients. So the effect of pore solution conductivity is less evident when similar w/cm mixtures are compared. The biggest danger with the conductivity based tests is that high w/cm mixtures containing slag or silica fume (high w/cm silica fume mixtures performed similar to high w/cm slag mixtures) can show low early age values leading to the mistaken conclusion that they would help attain low diffusion coefficients. It should be pointed out that low values are being attained for the long term immersed case but not for the long term cyclic case. One possible way to address this is by the judicious use of the absorption or sorptivity test results to exclude the high w/cm mixtures. In that test the high w/cm mixtures always appear to give a high value so by requiring a maximum sorptivity criteria the high w/cm mixtures can be excluded. This may be appropriate in environments where chloride ingress by sorptivity can be a significant factor such as in bridge decks in low humidity regions where deicing salts are applied. Alternately, it would be simpler to use the very low 28day strengths to reject the two 0.62 w/cm mixes, then the other mixes could be ranked using one of the rapid index tests.

When the two 0.60 w/cm mixtures are removed as shown in Figure 7 the coefficient of correlations between the 56 day RMT and the chloride diffusion coefficients for the three exposure cases were 0.94, 0.99 and 0.92 or an average of 0.95.

On the basis of the chloride diffusion test results the mixtures can be classified as follows

Classification based on Chloride Diffusion Coefficient	180d normal curing followed by 35d in solution	56d normal curing followed by 21 week in cyclic exposure
Level 1 (≤1.0x10^{-12} m^2/s)	0.39SF7	0.39SF7, 0.29PC, 0.39SL25
Level 2 (1 to 3x10^{-12} m^2/s)	0.29PC, 0.39SL25, 0.39FA15, 0.39PC, 0.62SL50	0.39PC, 0.39FA15, 0.62SL50
Level 3 (≥3.0x10^{-12} m^2/s)	0.62FA30	0.62FA30

It will be interesting to observe if the rapid index test results can classify mixtures based on the different levels. When the last two chloride diffusion coefficient results become available the analysis will be completed. This will be completed for all mixtures in Table 1 and Table 2. Ideally suitable rapid index test criteria (s) can be chosen so that mixtures can be selected based on the desired level of chloride diffusion coefficient. Given that the different conditioning requirements lead to different mixtures it is clear that more than one rapid index test result may be required.

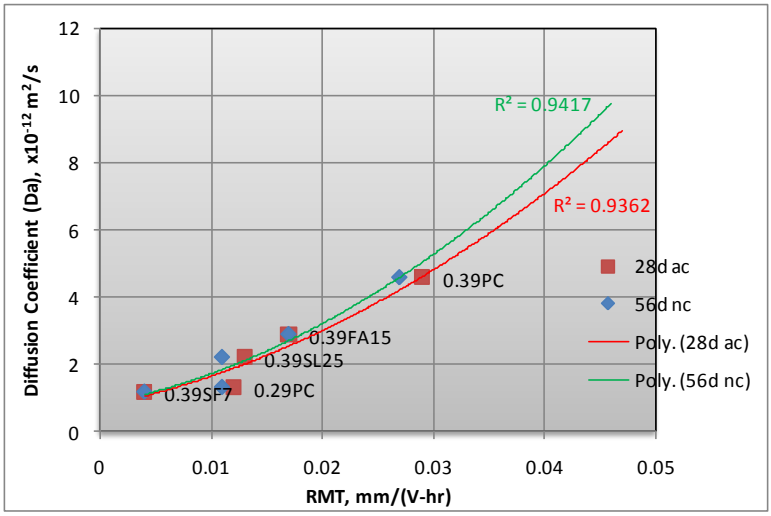

(a) 56d normal curing followed by 35d in solution

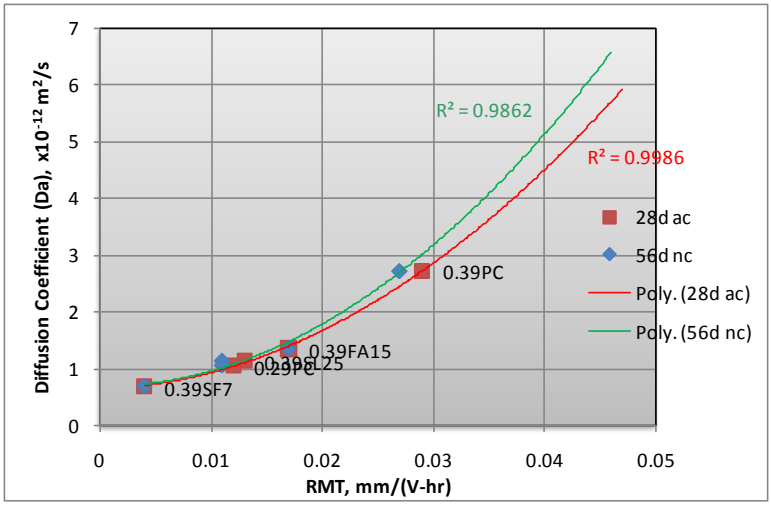

(b) 180d normal curing followed by 35d in solution

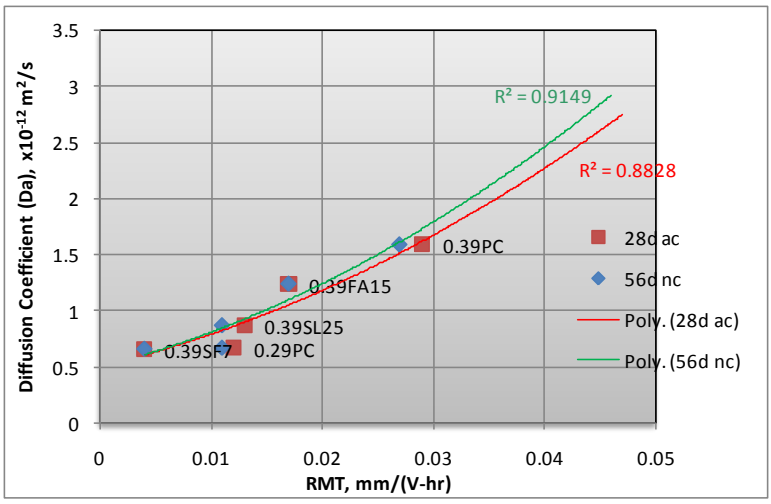

(c) 56d normal curing followed by 21 week in cyclic exposure

Figure 7. (a) – (c) Diffusion Coefficients vs RMT without High *w/cm* ratio Mixes

2.5 Field Core Testing Program (PROPOSED NO COST ADDITIONAL WORK BY NRMCA)

In addition to that lab experimental program it would be useful to get concrete cores from un-cracked areas from 10-30 years old structures in bridge deck (low relative humidity), bridge deck (high relative humidity), marine - submerged, tidal, spray zones. These samples would be used by NRMCA to measure sorptivity, chloride profile on top 2 in., discard the next 1 inch and conduct ASTM C1556 chloride diffusion test on next 2 inches. Do 2 rapid index test results

(RCPT, gas permeability) from sample just below that. So a 7 to 10 in. core thickness of 4 in. diameter may be required for this program. The aim would be to see if there is a unique relation between measured rapid index test result and calculated chloride diffusion coefficient from the chloride profiles. Also it would be worthwhile to compare those diffusion coefficients with mixture proportions and the 56 day rapid index results attained during quality assurance or mix qualification stage (if such is available). The core test program can account for a wide range of field conditions such as moist curing durations, wet/dry chloride exposures, chloride loadings and temperature exposures and is therefore an useful extension of this lab based experimental program.

Freeze Thaw - Test Methods, Curing Conditions and Test Ages

Freeze thaw (F-T) attack is another major concrete deterioration mechanism. Capillary sorption and water vapor diffusion are the two principal transport mechanisms that cause critical saturation of capillary pores which is necessary for freeze thaw damage. An air content of 5% to 7% with an air voids spacing factor less than 0.2 μm is typically necessary to maintain adequate freeze thaw resistance. While the air entrainment requirement is acceptable an attempt will be made to develop test and performance criteria as an alternative to the maximum w/cm requirement. ACI 318 states that for F1, F2, F3 categories max w/cm=0.45, min strength=4500 psi, and air content limits. It is clear that a low w/cm is required to ensure low water penetration and potential for critical saturation. By conducting mixes with different w/cm and various SCM dose and contents we will examine if F-T performance (as measured by no. of cycles for 15% mass loss or relative dynamic modulus of elasticity after 300 cycles) is better correlated with a rapid index test such as sorption or gas permeability criteria than w/cm. If at each w/cm, F-T performance varies widely depending on the test criteria the importance of the test criteria as opposed to w/cm is established. Also it would be determined whether some mixes with low w/cm and higher sorptivity/gas perm can have poorer F-T performance as compared to mixes with higher w/cm and lower sorptivity/gas perm which can again establish the importance of the test criteria as opposed to w/cm.

ACI 318-08 F classes

Moderate F1: Concrete exposed to freezing-and thawing cycles and occasional exposure to moisture

Severe F2: Concrete exposed to freezing-and thawing cycles and in continuous contact with moisture

Very severe F3: Concrete exposed to freezing-and thawing and in continuous contact with moisture and exposed to deicing chemicals

From the test results plots Concrete class F2 can be suggested to have RDM of 60-80% while F3 can have RDM>80% after 300 F-T cycles. It is hoped that these RDM and mass loss

correlates with rapid index test criteria such as sorptivity and we can use those test criteria rather than RDM.

For C672 Y axis will be mass loss or visual rating

Mixture Proportions Planned

w/cm	PC	20%FA	30%SL	25%SL+5%SF
0.40	Yes-m			Yes-vl
0.45	~~Yes-m~~	Yes-m	~~Yes-m~~	Yes-vl
0.50	~~Yes-h~~	~~Yes-m~~	~~Yes-m~~	~~Yes-l~~
0.60	~~Yes-h~~			~~Yes-m~~

The mixtures that have been struck off have been cast as of now and are shown in Table 3.

Crushed coarse aggregate (1.0" max) no. 57, natural sand FM=2.88

Adjust water reducer or high range water reducer (if any) for desired slump = 5 to 7 in.

Air entrained concrete mixtures – Target 5 to 6% air. Use AEA from same admix manufacturer

Normal Curing – Standard moist room curing starts immediately after making the specimens

Accelerated Curing – 7 days of normal curing followed by 21 days of curing in 100F water

For all mixtures measure the following: Slump, temperature, air content, density, Strength (28 days of moist curing followed by 28 days of air drying), Shrinkage (7 days moist curing followed by 90 days of air drying).

Durability Tests

For all tests at all ages, make 2 cylinders unless otherwise stated. Make 6 extra cylinders for each mix, moist cure for 28 days and then ship 4 to Purdue/UT for gas permeability testing and keep the other 2.

- Rapid Chloride Permeability test (ASTM C1202)

i) 28 day accelerated
ii) 56 day normal curing
iii) 26 week (182 d) normal curing

- ASTM C666. Test 2 replicate specimens as recommended by C666 standard. 28 day moist curing followed by 28 day air drying in 50% RH and 70F and then start C666. Do dynamic modulus, mass change tests as required by C666. Do test until 1000 cycles or visible differences between mixtures which-ever occurs first. Also mixtures should not be tested for >25% mass reduction or 50% relative dynamic modulus of elasticity.

- ASTM C672. Test 2 replicate specimens as recommended by C672 standard. 28 day moist curing followed by 28 day air drying in 50% RH and 70F and then start C672. Do test until 150 cycles or visible differences between mixtures which-ever occurs first. Determine visual rating every 5 cycles.

- Sorptivity Test (ASTM C1585) after:

i) 28 day accelerated + 18 d specimen conditioning (C1585)
ii) 38 day normal curing + 18 d specimen conditioning (C1585)
iii) 26 week (182 d) normal curing + 18 d specimen conditioning (C1585)

- Absorption test BS 1881:122 – use latest ASTM draft which states 50C.

i) 28 day accelerated + 3 d in oven
ii) 56 day normal curing + 3 d in oven
iii) 26 week (182 d) normal curing + 3 d in oven

Table 3. Yield Adjusted Mixture Proportions and Preliminary Test Results

Calculated Batch Quantities											
	0.57 PC	0.50 PC	0.50 FA20	0.50 SL30	0.50 SL25SF5	0.60 SL25SF5	0.45 PC	0.45 SL30	0.57 PC**-R	0.50 PC**-R	0.50 SL30**-R
Type I/II cement, lb/yd^3	506	539	442	385	385	353	592	414	505	541	382
Slag, lb/yd^3				165	137	126		177			164

Fly ash, lb/yd^3			111								
Silica Fume, lb/yd^3					27	25					
SCM, %	0	0	20	30	30	30	0	30	0	0	30
Coarse Agg. (No.57), lb/yd^3	2087	2021	2071	2060	2058	2077	2035	2029	2082	2026	2043
Fine Aggregate, lb/yd^3	1094	1083	1066	1093	1084	1072	1062	1048	1118	1086	1084
Mixing Water, lb/yd^3	290	270	276	275	275	302	267	266	293	270	273
w/cm	0.57	0.50	0.50	0.50	0.50	0.60	0.45	0.45	0.58	0.50	0.50
ASTM C494 AEA, oz/cwt	3.8	4.4	23.5	6.3	4.4	7.0	4.4	6.9	3.8	4.4	4.8
ASTM C494 Type F, oz/cwt		3.1	2.2	3.2	5.5	2.6	8.1	11		6.7	12.8
Fresh Concrete Properties											
ASTM C143, Slump, in.	7	6	6	5	5	6.5	5.25	6	5.5	4.75	7
ASTM C231, Air, %	6	7.2	6	6.2	6.5	6.2	7	7.6	5.8	7.2	7.2
ASTM C138, Density, lb/ft^3	148.1	145.7	147.7	148.1	147.7	147.3	147.3	146.5	148.9	146.1	146.9
ASTM C1064, Temperature, °F	75	75	73	70	72	70	70	70	70	70	68
Hardened Concrete Properties											
ASTM C39, Compressive Strength, psi											
28 days	4,918	4,895	4,101	5,376	6,249	4,844	5,427	5,182	4,738	4,454	5,312
Draft ASTM Standard, Water Absorption Test at 50 °C, %											
28d accelerated cure	-	-	1.41	-	1.24	1.56	1.61	1.2	2.28	1.81	1.47
56d normal cure	1.85	1.65	1.81	1.36	1.44	1.74	1.76	1.39	-	-	-
182d (26w) normal cure	1.67	1.47	1.19	1.45	1.29	1.51	1.49	1.20	-	-	-
ASTM C1202, Rapid Chloride Permeability, Coulombs											
28d accelerated cure	-	-	2014	-	332	516	2630	851	5015	3578	1077
56d normal cure	4876	3633	4287	1554	469	848	2957	1143	-	-	-
182d (26w) normal cure	5297	3879	2193	1340	532	622	2722	1094	-	-	-
ASTM C157, Length Change (Drying Shrinkage), %											

28 days[+]	0.045	0.039	0.041	0.049	0.053	0.063	0.036	0.039	-	-	-
56 days[+]	0.061	0.046	0.050	0.052	0.056	0.069	0.049	0.049	-	-	-
90 days[+]	0.069	0.054	0.057	0.058	0.065	0.075	0.055	0.055	-	-	-
180 days[+]	0.076	0.059	0.057	0.063	0.065	0.077	0.058	0.058	-	-	-
ASTM C 1585, Rate of Water Absorption (Sorptivity), x10^{-4} mm/s$^{1/2}$											
28d accelerated cure (Initial/Secondary)	-	-	8.7[*]/ 3.0	-	5.6[*]/ 2.8	7.1[*]/ 3.3	5.9[*]/ 4.1	6.7[*]/ 2.0[*]	17.6[*]/6.7[*]	10.8[*]/4.7[*]	5.7[*]/ 1.5
56d normal cure (Initial/Secondary)	13.7 /3.7[*]	8.2[*]/ 3.4	14.1/9.8	13.1[*]/ 4.3	6.0/ 3.2	6.3/ 3.5	9.4/ 5.9	5.1/ 3.0[*]	-	-	-
196d normal cure (Initial/Secondary)	4.3[*] /1.6[*]	3.0[*] / 2.1[*]	6.5[*] / 2.6[*]	5.0[*] / 1.2[*]	8.5 / 2.0[*]	5.0[*] / 1.7	5.6 / 3.3	3.5[*] / 2.4	-	-	-
28d accel. cure (Initial/Secondary), g	-	-	2.0/ 3.7	-	1.8/ 3.7	1.4/ 3.8	1.4/ 4.0	1.8/ 2.6	3.1/ 7.6	2.3/ 5.0	2.0/ 2.7
56d normal cure (Initial/Secondary), g	2.5/ 5.3	1.6/ 3.8	2.4/ 8.9	2.8/ 5.9	1.6/ 4.1	1.6/ 4.1	2.0/ 6.0	1.5/ 3.5	-	-	-
196d normal cure (Initial/Secondary), g	0.9 / 2.4	0.8 / 2.4	1.2 / 2.9	1.2 / 2.2	1.5 / 3.1	1.2 / 2.5	1.0 / 3.3	0.7 / 2.3	-	-	-
ASTM C 666, Freezing and Thawing Resistance, %											
Durability Factor @ 2,500 c	97	98	95	72	96	96	98	97	-	-	-
Mass Loss @ 2,500 c	5.0	2.8	5.9	5.9	4.3	6.8	3.7	5.4	-	-	-
ASTM C 672, Salt Scaling Resistance											
Visual Rating (0 – 5) @ 50 cyc	5	3.0	3.0	3.0	2.3	3.8	2.0	0.5	-	-	-
Visual Rating (0 – 5) @ 180 cyc	5[++]	3.5	4.5	3.0	3.6	4.3	2.8	1.5	-	-	-

[**] Exact repeat of designated mixture

[*] A correlation coefficient less than 0.98 indicating that the rate cannot be determined according to ASTM C1585

[+] Curing period in 70°F, 50% RH environment NOT included 7 days initial wet curing period in water bath

[-] Result of only one specimen

[++] Terminated at 75 cycles

After about 2500 cycles the freeze thaw performance of all mixtures are excellent given that most specifications will accept a concrete mixture with a durability factor (DF) greater than 80% after 300 cycles as excellent freeze thaw behavior. The test data is very consistent with both

freeze thaw specimens from a given mixture showing similar results in terms of durability factor and mass loss as seen from the table below.

FT#	Mix ID	Air%	# of Cyc	DF01	DF02	Avg. DF	ML01	ML02	Avg. ML
FT1	0.57PC	6.0	2741	97%	98%	97%	5.0%	5.0%	5.0%
FT2	0.5PC	7.2	2675	96%	99%	98%	2.7%	2.9%	2.8%
FT3	0.5FA20	6.0	2357	96%	93%	95%	6.2%	5.7%	5.9%
FT4	**0.5SL30**	**6.2**	**2672**	72%	72%	72%	5.9%	5.9%	5.9%
FT5	0.5SL25SF5	6.5	2652	97%	95%	96%	4.5%	4.2%	4.3%
FT6	0.6SL25SF5	6.2	2520	95%	96%	96%	6.6%	6.9%	6.8%
FT7	0.45PC	7.0	2497	100%	97%	98%	3.3%	4.1%	3.7%
FT8	0.45SL30	7.6	2482	97%	97%	97%	5.8%	4.9%	5.4%

The C666 mass loss is shown plotted against increasing number of cycles in Figure 8.

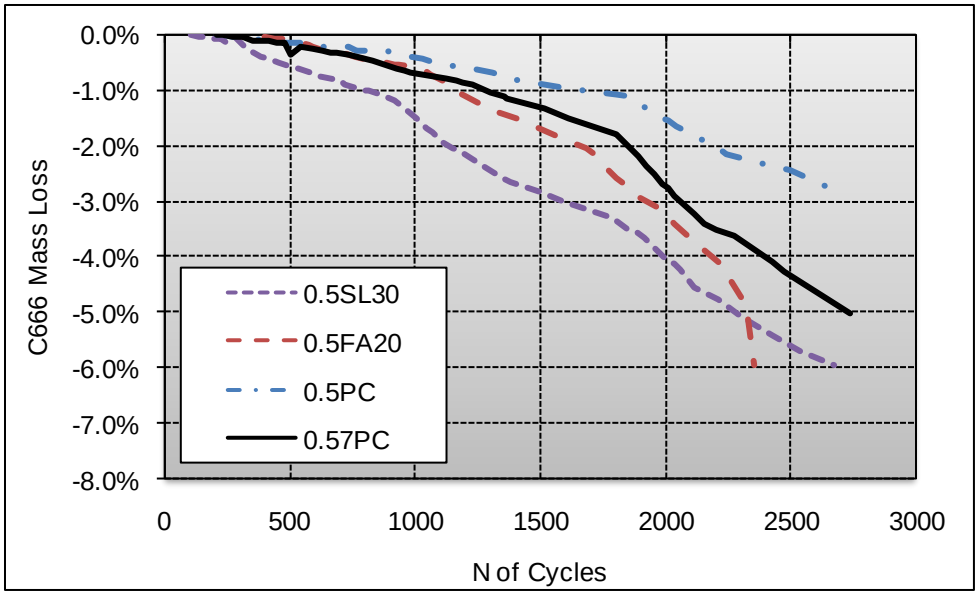

(a)

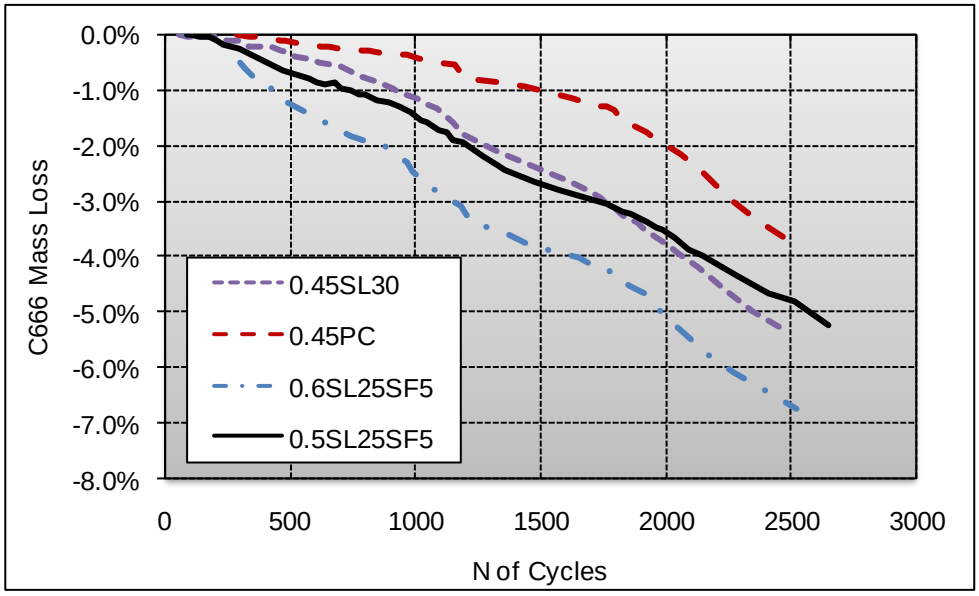

(b)

Figure 8. C666 mass loss vs N of cycles

Mixture 0.50SL30 does show a slightly lower durability factor of 72% where as all other mixtures have values exceeding 95%. Only light scaling on surfaces is observed from the F-T samples after 2500 cycles. F-T mass loss data is still low because the deterioration is low. This goes to show that even though mixtures tested varied a great deal in the 56 day rapid index test results

(RCPT, sorptivity and absorption) their freeze thaw performance is not compromised. In other words even though the transport properties may not be very good the air void system is a primary factor ensuring good freeze thaw behavior of these mixtures. At this point it does not appear productive to even try to do the remaining 4 concrete mixtures as they will have even better rapid index test results. At the end of about 2700 cycles the specimens will be taken out of the F-T machine. They will be surface dried, weighed and then subjected to 28 days of moist room curing. The specimens will be weighed again and then subject to 300 F-T cycles. This will be completed by the next quarter.

Figure 9 shows that C666 mass loss does not correlate well against w/cm.

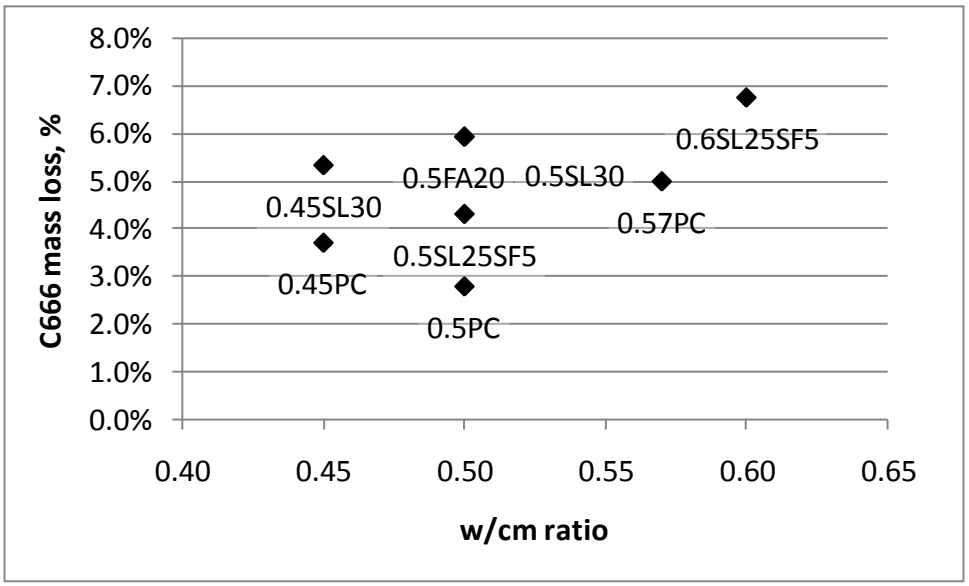

Note: MixID was noted at right below the data point

Figure 9. C666 mass loss vs. w/cm

Figure 10 shows that C666 mass loss does not correlate against initial sorptivity expressed as percent water absorbed at the end of the testing period corresponding to the primary rate of sorption.

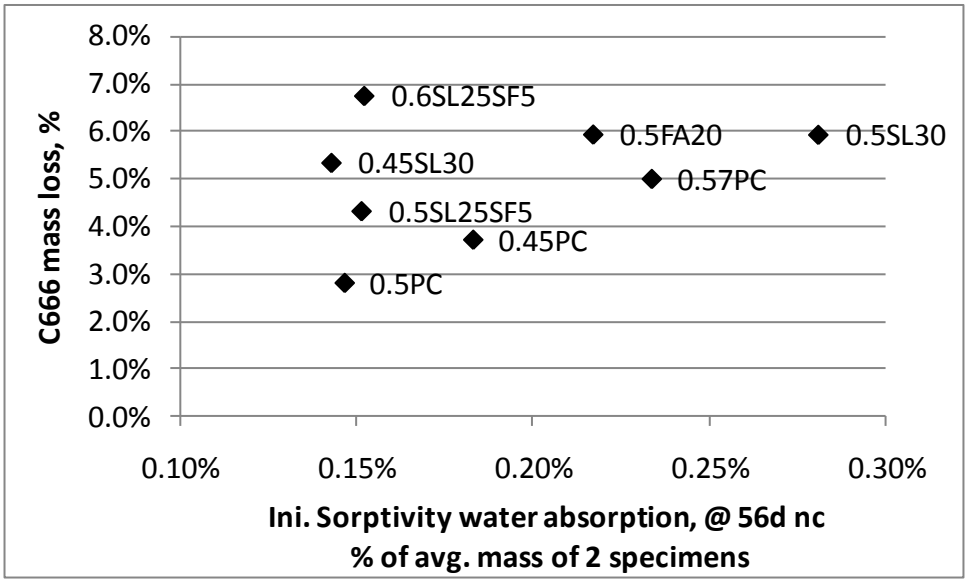

Note: MixID was noted at the right side of the data point

Figure 10. C666 mass vs Initial Sorptivity (expressed as S1 water absorption of avg. mass of 2 specimens) at 56d normal curing condition

Scaling tests have been completed and the visual ratings are given based on the following table from C672.

Rating	Condition of Surface
0	No scaling
1	Very slight scaling (1/8 in. depth max, no coarse aggregate visible)
2	Slight to moderate scaling
3	Moderate scaling (some coarse agg visible)
4	Moderate to severe scaling
5	Severe scaling (coarse agg visible over entire surface)

Since visual ratings are somewhat subjective they were given by 4 Engineering staff members and the ratings averaged for each mixture. It was interesting to note that the ratings between the staff members were fairly consistent. Ratings after 180 freeze thaw cycles are provided in

Table 3, except for Mixture 0.57PC for which the scaling after 75 cycles was so severe that the mix had to be terminated.

Mixture performance varied widely from a rating of 1.5 to a high in excess of 5. The Figure 11 shows the actual surface appearance of the various mixtures and the corresponding visual ratings of scaling.

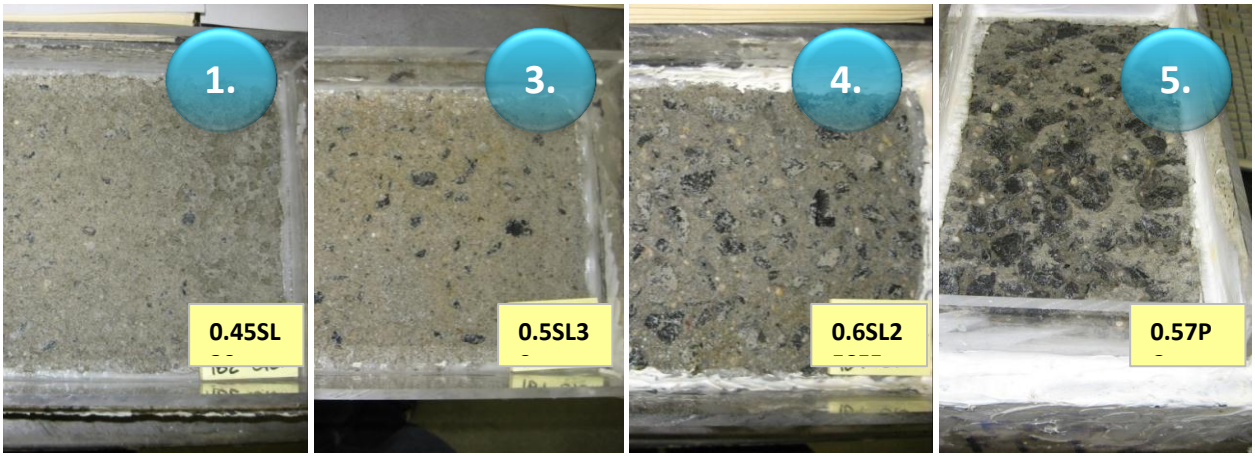

Figure 11. Salt scaling slabs with final visual ratings

Correlation between salt scaling test visual ratings and rapid index test results

Correlations between the visual ratings after 180 cycles and fresh air content and between the visual ratings after 180 cycles and the various rapid index tests such as absorption, sorptivity and rapid chloride permeability are drawn in Figure 12 a-d. Air content seemed to have the best coefficient of correlation at 0.69 with the visual rating of scaling after 180 cycles. Among the rapid index tests absorption test results had the best correlation where as correlation for the sorptivity and RCPT were very poor. This seems to confirm that deicing scaling resistance may not have a good correlation with any of the rapid index test evaluated in this report.

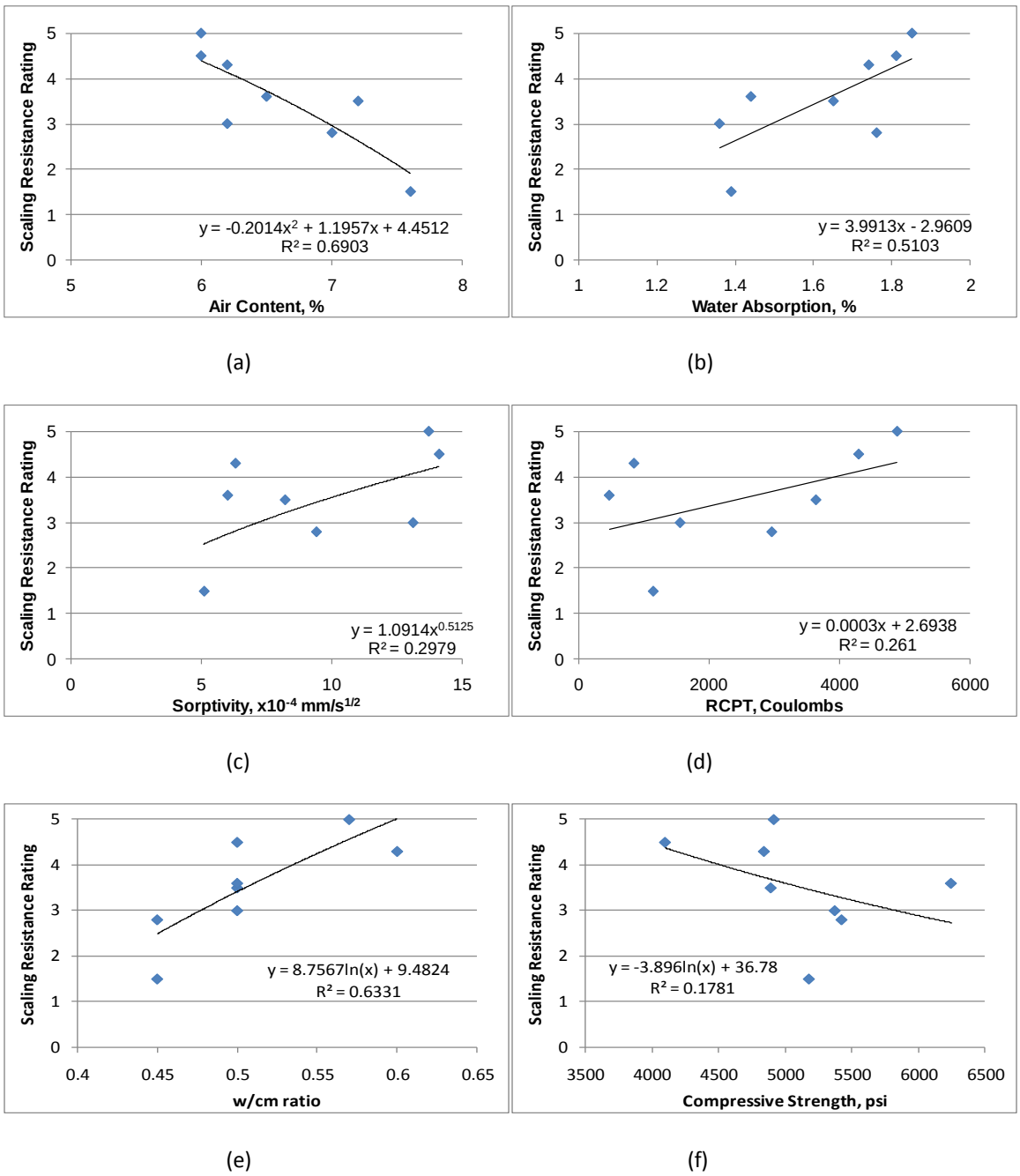

Figure 12. (a) – (f) Correlation between the visual ratings after 180 cycles and fresh air content, various rapid index tests

It should be kept in mind that the scaling resistance is evaluated after 50 cycles. Goodspeed et al. in their article HPC Defined have stated that a visual rating after 50 cycles of:

0,1 corresponded to the HPC performance Grade 3

2,3 corresponded to the HPC performance Grade 2

4,5 corresponded to the HPC performance Grade 1

Correlations between the visual ratings after 50 cycles and fresh air content and between the visual ratings after 50 cycles and the various rapid index tests such as absorption, sorptivity and rapid chloride permeability are drawn in Figure 13 a-d. In general these correlations are even poorer than Figure 12. It does not appear possible to select rapid index test criteria as an alternative to ASTM C672 to select mixtures with good scaling resistance.

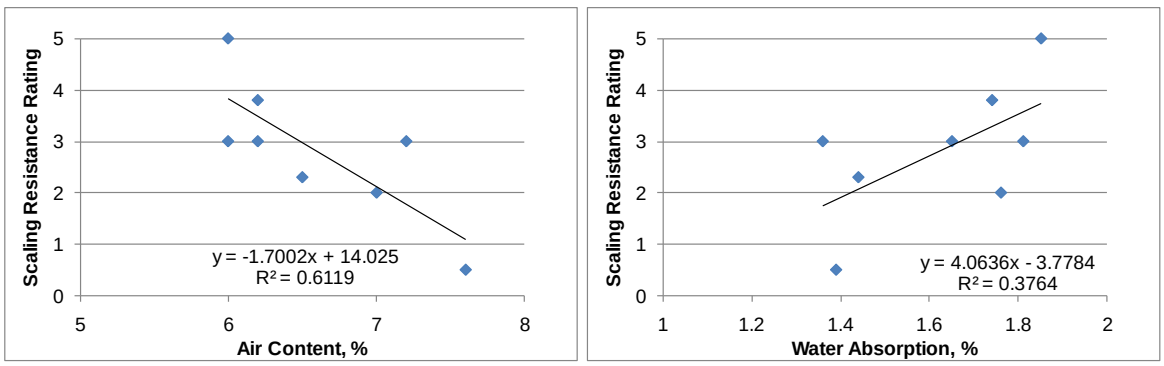

(a)

(b)

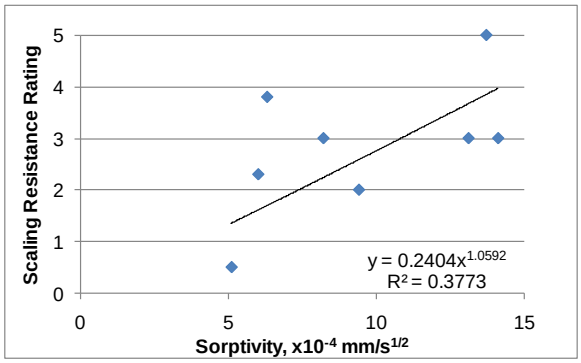

(c)

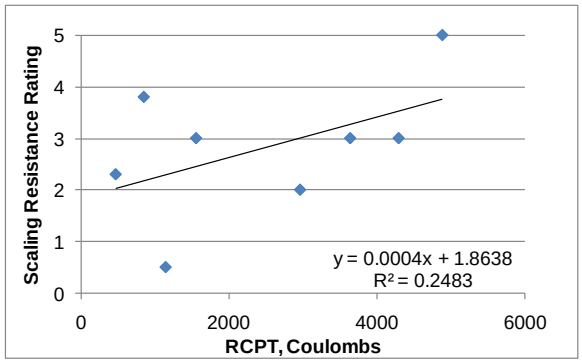

(d)

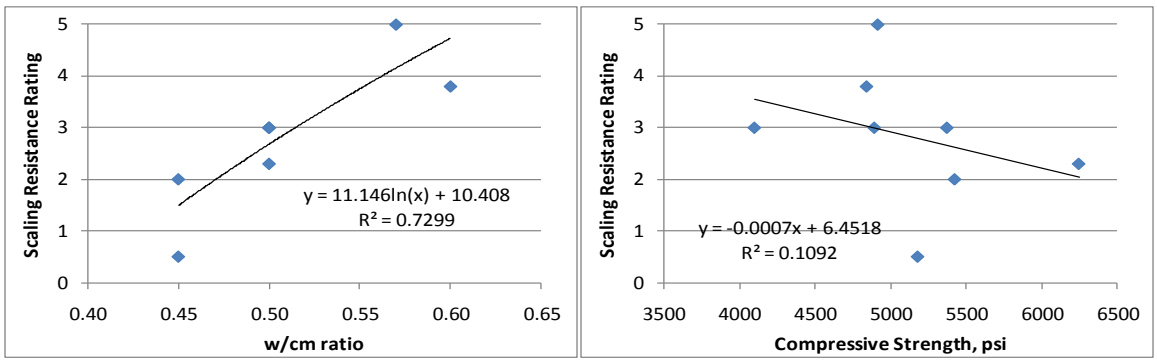

(e) (f)

Figure 13. (a) – (f) Correlation between the visual ratings after 50 cycles and fresh air content, various rapid index tests

Sulfate Resistance - Test Methods, Curing Conditions and Test Ages

Sulfate attack is another major concrete deterioration mechanism. Water soluble sulfates penetrate concrete by a combination of capillary sorption and diffusion. Three mechanisms are recognized:

1 Physical sulfate attack – generally by salt crystallization of certain sulfate salts

2 Chemical attack of aluminate phases in to form calcium sulfo-aluminate hydrates and gypsum.

3. Chemical attack on the calcium silicate hydrate matrix at cooler temperatures (thaumasite formation)

Note: The thaumasite sulfate attack mechanism is less common and is not addressed in this test program.

Concrete resistance to sulfate attack is governed by 2 factors:

1. Cementitious type – Increasing C3A in portland cement portion in concrete decreases its sulfate resistance. Aluminate phases from SCMs can also sometimes contribute to this effect – more likely in some Class C fly ashes or some higher alumina content slags from off shore.

2. Low permeability – that reduces the rate of penetration of sulfates into the concrete. The ACI 318 building Code recognizes 3 exposure classes of sulfate exposure in increasing severity based on concentration of water soluble sulfates in soil or water – S1, S2, and S3 and establishes the following (Table A) minimum requirements for concrete mixtures for adequate sulfate resistance:

Table A. ACI 318 Building code Requirements for Concrete Exposed to Sulfate

Category	CM type or Performance Equivalent	w/cm, strength
S0	None	None
S1	Type II or ASTM C1012 <0.1% at 6 mos	0.50, 4000 psi
S2	Type V or ASTM C1012 <0.1% at 12 mos	0.45, 4500 psi
S3	Type V+pozz or slag or ASTM C<1012 < 0.1% at 18 mos	0.45, 4500 psi

In ACI 318-08, ASTM C1012 expansion criteria are recognized as an alternative to the prescriptive requirements for the allowable types of cementitious materials.

The maximum w/cm limit is invoked to control the permeability of concrete. Besides w/cm, however, the permeability of concrete is also impacted by the composition of the cementitious materials. The aim of this task to develop rapid index test and performance criteria as an alternative to the maximum w/cm requirements. It is clear that a low w/cm is required to ensure low sulfate ingress by sorption and diffusion. Low permeability of concrete is an important factor to control both the physical and chemical forms of sulfate attack.

By testing concrete mixtures with different w/cm and cementitious types (including SCM types and contents) we will examine if concrete performance against sulfate attack (as measured by USBR 4908 method B) is better correlated with ASTM C1012 and a rapid index test alternative to w/cm criteria. Rapid index tests that will be evaluated include rapid chloride permeability (and conductivity), sorption or gas permeability.

USBR4908 is a test that was used by the US Bureau of Reclamation on historical research on sulfate resistance. It is a long term test on concrete and is not suited for inclusion in code or specification criteria. The evaluation of rapid index test results relative to performance in the USBR4908 will allow establishment of such required performance criteria. The test involves immersing 3x6 in. cylindrical concrete specimens in 10% sodium sulfate solutions for an extended period and measuring expansions periodically. An expansion of 0.5% is considered as failure and the test is expected to last at least 12-18 mos.

It is proposed that all concrete mixtures be subjected to an immersion period of 18 mos with the expansions recorded. Mixtures that show higher resistance to sulfate attack will result in lower expansions in the USBR test. By separating out mixtures into 3 categories based on their USBR expansion levels it will be possible to select mixtures that will perform in the different

sulfate exposure classes S1, S2, and S3 – mixtures with the lowest USBR expansion levels could be used for S3 exposure category and so on.

Additionally, partially submerged specimens in test solutions will be performed at the same sulfate concentration. This is intended to simulate sorption and wicking of sulfates in structures and the condition of physical sulfate attack.

The results will be interpreted as follows:

It is expected that two mixtures with different composition of cementitious materials could have the same performance in the USBR test due to different levels of sulfate ingress (permeability) into the concrete. It is proposed to tie the rapid index test criteria that measures a permeability property to the C1012 expansion levels (see Table B).

The process of developing these rapid index criteria is proposed to be accomplished by the following 3 plots.

Plot 1 will have 12 mo or 18 mo USBR expansions on the Y axis and rapid index test results on X axis. Plot only those mixtures (from the 20+ mixtures tested as per Table C) that satisfy the ASTM C1012 expansion criteria for the S1 exposure class but that fail that for exposure classes S2, and S3. Three different USBR expansion levels as suggested in column 2 of Table b will be used to delineate expansions in the USBR test on concrete specimens for the 3 exposure classes (these may need to be revised later based on the test results). Record the corresponding rapid index test criteria.

Plot 2 should have mixtures that satisfy the ASTM C1012 expansion criteria for the S2 exposure class but that fail that for exposure class S3. The same three expansion criteria for the USBR expansions will be used. Record the corresponding rapid index test criteria.

Plot 3 should have mixtures that satisfy the ASTM C1012 expansion criteria for S3 exposure class. The same three expansion criteria for the USBR expansions will be used. Record the corresponding rapid index test criteria.

The final outcome is expected to be along the following lines

This allows the two criteria to offset each other and can be established based on the USBR concrete performance testing – a more conservative result in the C1012 might permit a less conservative criteria in the rapid index for permeability and vice versa.

Table B. Interpretation of USBR expansion Results and Development of Rapid Index test Criteria

Category	USBR expansion	C1012	Rapid index (assume RCPT coulombs)
S1	0.4 to 0.6%	<0.1% at 6 mos	3000
		<0.1% at 12 mos	4000
		<0.1% at 18 mos	4000
S2	0.2 to 0.4%	<0.1% at 6 mos	2000
		<0.1% at 12 mos	3000
		<0.1% at 18 mos	4000
S3	<0.2%	<0.1% at 6 mos	NA
		<0.1% at 12 mos	1500
		<0.1% at 18 mos	2000

Table C. Mixture Proportions Planned

Category	w/cm	Cement	No SCM	15%FA	20%FA	30%FA	25%SL	35%SL	50%SL
S0	0.50	Type I	~~1 cement~~						
S1	0.50	Type II	~~1 cement~~						
	0.40	*Type I*		~~*Yes*~~			~~*Yes*~~		
	0.50	*Type I*		~~*Yes*~~			~~*Yes*~~		
	0.60	*Type I*		~~*Yes*~~			~~*Yes*~~		
S2	0.45	Type V	~~2 cements~~						
	0.40	Type II			~~Yes~~			~~Yes~~	
	0.50	Type II			~~Yes~~			~~Yes~~	

	0.60	Type II			~~Yes~~			~~Yes~~	
S3	0.40	Type V				~~Yes~~			~~Yes~~
	0.50	Type V				~~Yes~~			~~Yes~~
	0.60	Type V				~~Yes~~			~~Yes~~

For S1, 0.50, test 1 Type II control mix

For S2, 0.45, test 2 Type V control mixes

So there are a total of 22 mixtures – 18 with SCMs and 4 without. Some of these mixtures may be optimized if possible without losing research objective.

The mixtures that have been struck off have been cast as of now and are shown in Table 4.

Crushed coarse aggregate (1.0" max) no. 57, natural sand FM=2.88

FA will be Class F fly ash.

Adjust water reducer or high range water reducer (if any) for desired slump = 5 to 7 in.

Non air entrained concrete.

Need a Type I with relatively high C3A so its not too similar to the Type II

Planned Test Methods, Curing Conditions and Test Ages (Lab)

Mortar

ASTM C1012. Conduct C1012 tests. C1012 is normally done on mortar at a constant w/cm = 0.485. Therefore there will be a total of 10 mixtures - 6 SCM mixtures (2 with Type I, 2 with Type II, 2 with Type V) and 4 PC only mixtures. Consider 2 for replication at high and low expansion level. Conduct C1012 for 18 mos – some of mixtures with lower SCMs may be stopped earlier. Take periodic expansion readings as per C1012.

Concrete

Normal Curing – Standard moist room curing starts immediately after making the specimens

Accelerated Curing – 7 days of normal curing followed by 21 days of curing in 100F water

For all concrete mixtures measure the following: Slump, temperature, air content, density, Strength (4x8 cyl at 28 days of moist curing).

Durability Tests

For all tests at all ages, make 2 cylinders unless otherwise stated. Make 6 extra cylinders for each mix, moist cure for 28 days and then ship 4 to Purdue/UT for gas permeability testing and keep the other 2.

- Rapid Chloride Permeability test (ASTM C1202)

i) 28 day accelerated
ii) 56 day normal curing
iii) 52 week normal curing

- USBR4908 fully immersed method B. Test 3 prisms per mix. Start after 28 days of moist curing and 28 days of air drying (everything else similar to USBR 4908 requirements). Conduct test for 36 mos or as instructed. Take periodic expansion readings. Follow USBR test method for other requirements.

- USBR4908 partially immersed (same 10% solution as above). Test 3 prisms per mix. Start after 28 days of moist curing and 28 days of air drying (everything else similar to USBR 4908 requirements). Conduct test for 36 mos or as instructed. Take periodic expansion readings. The specimens are immersed half way following the procedure in the NIST report. Figure 14 shows the test set up. The partially immersed specimens were made for the high and low w/cm and PC only mixes. Mass change will also be measured to determine if there is surface spalling at the wet zone.

- Sorptivity Test (ASTM C1585) after :

i) 28 day accelerated + 18 d specimen conditioning (C1585)
ii) 56 day normal curing + 18 d specimen conditioning (C1585)
iii) 52 week normal curing + 18 d specimen conditioning (C1585)

- Absorption test BS 1881:122 – use latest ASTM draft

i) 28 day accelerated + 3 d in oven
ii) 56 day normal curing + 3 d in oven

iii) 52 week normal curing + 3 d in oven

Figure 14 USBR half immersed specimens in the container

If at each w/cm, sulfate performance varies depending on the test criteria the importance of the test criteria as opposed to w/cm is established. Also it would be determined whether some mixes with low w/cm and higher sorptivity/gas perm can have poorer sulfate performance as compared to mixes with higher w/cm and lower sorptivity/gas perm which can again establish the importance of the test criteria as opposed to w/cm.

This task does not consider the development of a more rapid test for C1012. Options include smaller specimen size/paste or higher temperature soln. exposure.

Some of the initial concrete mixtures are being cast at the moment.

Table 4 and Table 5 shows the results from all 22 concrete mixtures cast. At the moment all the early age rapid index test results are available. One year rapid index test results are available only for the mixtures in Table 4. For the USBR fully immersed and partially immersed

conditions 6 to 12 mo test data is available at this point and 12 mo data for all mixtures should become available by January 2012. For the fully immersed case the following are being measured – 1. Length change; 2. Mass change; 3. Visual rating/pictures. For the partially immersed case the following are being measured – 1. Scaling length; 2. Mass change; 3. Visual rating/pictures. Ambient RH will continue to be measured at 2 locations – one at 1 in. above the solution and the other near the top of the specimen. Only the 12 mo USBR data in Table 4 is available and is discussed below.

For the fully immersed case the length change vs age is plotted in Figure 15. There is expansion with increasing age with the higher w/cm mixtures having higher expansions both in the case of slag and fly ash mixtures. The expansion levels are still very low. For the 0.5 w/cm PC mixtures the mixture with the lower C_3A (0.5PC2) content had a lower expansion level as expected. The mass age vs age is plotted in Figure 16. Thus far there has been a mass increase as a result of absorption. The higher w/cm mixtures have had higher mass increases as a result of their absorption. Both the 0.6 w/cm slag and fly ash mixtures have shown a sharp mass decrease at a later age. This is primarily due to the corners of the prisms breaking off. Pictures taken at 12 mos for all the fully immersed specimens shown in Figure 17 confirm this.

For the partially immersed case mass loss has not been found to give good results thus far and is not reported. However scaling length has been measured. This is the length of scaling from the surface of the solution upwards. Scaling occurs because the sulfate solution is absorbed by the concrete migrates upwards evaporates from the top surface leaving behind salt crystals which can expand when they absorb moisture causing scaling and cracking. This is described as physical sulfate attack and does not require the chemical sulfate attack reaction. The measures scaling lengths are plotted for the different mixtures in Figure 18. Once again the low w/cm (0.40) mixtures had lower scaling lengths when compared to the higher w/cm mixtures (0.60) for both the fly ash and slag cement cases. The other interesting finding is that the two 0.50 PC mixtures had the similar scaling lengths even though the C_3A contents where quite different (8% vs 12%). This confirms that the failure is not due to chemical sulfate attack. Figure 19 shows the scaling details for the partially immersed specimens. For the portion of the specimens that has been immersed in the sulfate solutions the two 0.60 w/cm mixtures and the PC mixture with the higher C3A showed more significant mass loss.

Correlations between the rapid index test results and USBR expansion results would prove interesting. However such an exercise can be done only after at least 24 mo of USBR testing. For the fully immersed case length change might be the most promising way of classifying the mixtures. For the partially immersed case scaling length might be the most promising way of classifying the mixtures. At the end of the 18 months the following destructive testing can be conducted – 1. At least 2 cubes/specimen (3 in.) will be sawn off and tested for compressive

strength for the immersed case; For the partially immersed case at lest 1 cube will be sawn off and tested from the immersed part. Higher strength loss will be indicative of poorer sulfate resistance. 2. Sulfate ingress can be measured for both cases. Also to accelerate the deterioration process of the partially immersed case 2 week cycling may be considered starting later this Fall. It will consist of alternate periods in 73F and 100F conditions.

Table 6 shows the ASTM C1012 mortar test results for the 10 mixtures that have been cast. 6 month C1012 expansions and the originally expected sulfate exposure classes are also listed.

Table 4. Yield Adjusted Mixture Proportions and Preliminary Test Results

Calculated Batch Quantities	**1**	**2**	**3**	**4**	**5**	**6**	**7**	**8**
	0.4SL25	0.5SL25	0.6SL25	0.5PC-1	0.4FA15	0.5FA15	0.6FA15	0.5PC-2
Cement Type	I	I	I	I	I	I	I	I/II
Type I/II cement, lb/yd^3	457	419	378	559	519	476	413	557
Slag, lb/yd^3	152	140	126					
Fly ash, lb/yd^3					92	84	73	
SCM, %	25	25	25	0	15	15	15	0
Coarse Agg. (No.57), lb/yd^3	2060	2055	2079	2056	2062	2061	2068	2050
Fine Aggregate, lb/yd^3	1302	1247	1260	1256	1277	1277	1272	1253
Mixing Water, lb/yd^3	244	279	283	279	244	280	291	279
w/cm	0.40	0.50	0.56	0.50	0.40	0.50	0.60	0.50
ASTM C494 Type A, oz/cwt	3	3	3	3	3	3	3	3
ASTM C494 Type F, oz/cwt	9.15	5.64	0	3	10.29	3.3	2	2.41
Fresh Concrete Properties								
ASTM C143, Slump, in.	5.50	6.50	6.50	7.00	4.00	4.00	7.00	5.25
ASTM C231, Air, %	1.6	1.7	1.2	1.4	1.6	1.4	1.2	2.0
ASTM C138, Density, lb/ft^3	156.9	154.1	153.7	154.5	156.1	153.7	153.3	154.1

ASTM C1064, Temperature, °F	72	72	72	73	72	72	72	72
Hardened Concrete Properties								
ASTM C39, Compressive Strength, psi								
28 days	9,540	7,700	5,710	5,690	8,400	5,980	4,630	6,440
Draft ASTM Standard, Water Absorption Test at 50 °C, %								
28d accelerated cure	0.62	0.79	1.34	1.33	0.61	0.88	1.13	1.31
56d normal cure	0.63	0.75	1.17	1.04	0.61	0.83	1.01	1.23
52w normal cure	0.55	0.65	0.87	0.72	0.38	0.64	0.86	0.73
ASTM C1202, Rapid Chloride Permeability, Coulombs								
28d accelerated cure	728	1104	1842	3132	509	968	1849	3459
56d normal cure	704	1161	1947	2947	913	1593	2627	3610
52w normal cure	649	1004	1253	2365	353	526	963	3132
ASTM C 1585, Rate of Water Absorption (Sorptivity), x10^{-4} mm/s$^{1/2}$								
28d accelerated cure (Initial/Secondary)	2.7*/1.5*	2.8*/1.7*	3.4*/2.1*	6.8*/4.1	2.9*/1.4*	1.9*/1.6*	5.2*/3.1*	5.5/3.6*
56d normal cure (Initial/Secondary)	3.2*/2.2*	5.0/2.6*	8.1/3.0*	5.5*/3.4	4.0*/2.3*	5.7/2.8*	7.4/4.2*	6.3/3.8
52w normal cure (Initial/Secondary)	On-going	On-going	On-going	On-going	On-going	On-going	On-going	On-going
28d accel. cure (Initial/Secondary), g	0.6/ 1.6	0.7/ 1.8	1.3/ 2.6	1.4/ 4.4	0.8/ 1.8	0.7/ 1.8	1.3/ 3.5	0.9/ 3.5
56d normal cure (Initial/Secondary), g	0.7/2.1	0.9/2.9	2.2/4.3	1.4/3.8	0.9/2.6	1.4/3.5	1.8/5.0	1.2/3.9
52w normal cure (Initial/Secondary), g	On-going	On-going	On-going	On-going	On-going	On-going	On-going	On-going
USBR 4908 Fully Immersed Method B (10% solution), %								
Length Change @ 12 months	0.032	0.041	0.040	0.096	0.028	0.038	0.043	0.044
Length Change @ 18 months	On-going	On-going	On-going	On-going	On-going	On-going	On-going	On-going
Mass Change @ 12 months	0.60	1.03	0.74+	1.38	0.81	1.28	1.33+	1.64
Mass Change @ 18 months	On-going	On-going	On-going	On-going	On-going	On-going	On-going	On-going
USBR 4908 Partially Immersed (10% solution), inch								
Scaling Distance @ 12 months	0.00	-	1.38	1.29	1.33	-	1.71	1.33
Scaling Distance @ 18 months	On-going	-	On-going	On-going	On-going	-	On-going	On-going

* A correlation coefficient less than 0.98 indicating that the rate cannot be determined according to ASTM C1585

+ Both ends' corners of the specimen crumbled and fell off resulted in mass reduction instead of mass gain due to physical sulfate attack

Note. Type I cement had C_3A content of 12% whereas Type I/II cement had C_3A content of 8%.

Table 5. Yield Adjusted Mixture Proportions and Preliminary Test Results

Calculated Batch Quantities	**9**	**10**	**11**	**12**	**13**	**14**	**15**	**16**	**17**	**18**	**19**	**20**	**21**	**22**
	0.4FA20	0.5FA20	0.6FA20	0.4SL35	0.5SL35	0.6SL35	0.4FA30	0.5FA30	0.6FA30	0.4SL50	0.5SL50	0.6SL50	0.45PC-V1	0.45PC-V2
Cement Type	I/II	I/II	I/II	I/II	I/II	I/II	V-1	V-1	V-1	V-1	V-1	V-1	V-1	V-2
Type I/II cement, lb/yd^3	487	448	387	391	361	316								
Type V cement, lb/yd^3							429	392	343	300	281	245	577	581
Slag, lb/yd^3				210	195	170				300	281	245		
Fly ash, lb/yd^3	122	112	97				184	168	147					
SCM, %	20	20	20	35	35	35	30	30	30	50	50	50	0	0
Coarse Agg. (No.57), lb/yd^3	2057	2061	2062	2030	2046	2073	2069	2062	2088	2028	2070	2086	2049	2065
Fine Aggregate, lb/yd^3	1262	1216	1259	1279	1238	1267	1245	1194	1256	1271	1247	1270	1286	1296
Mixing Water, lb/yd^3	244	280	290	240	278	302	245	280	294	240	281	304	260	262
w/cm	0.40	0.50	0.60	0.40	0.50	0.62	0.40	0.50	0.60	0.40	0.50	0.62	0.45	0.45
ASTM C494 Type A, oz/cwt	3	3	3	3	3	3	3	3	3	3	3	3	3	3
ASTM C494 Type F, oz/cwt	4.67	1.8	0	5.84	2.16	0	4.58	0	0	1.17	0.72	0	2.5	2.5
Fresh Concrete Properties														
ASTM C143, Slump, in.	4.5	6.75	5	7	5	4.5	4.75	6.75	7	7	5.5	6	4.5	6.5

ASTM C231, Air, %	1.6	1.8	1.7	3.2	2.1	1.7	2	1.5	1	1.7	1.8	1.3	1.9	1.6
ASTM C138, Density, lb/ft^3	155.3	153.3	152.5	154.5	153.3	153.7	155.3	152.5	153.7	154.1	154.9	154.5	155.3	156.5
ASTM C1064, Temperature, °F	74	75	75	72	72	72	70	70	70	71	70	70	72	74
Hardened Concrete Properties														
ASTM C39, Compressive Strength, psi														
28 days	7,490	5,310	3,990	10,020	6,740	5,730	7,610	4,870	3,590	7,500	7,500	6,200	8,800	7,720
Draft ASTM Standard, Water Absorption Test at 50 °C, %														
28d accelerated cure	0.96	1.45	1.81	0.69	1.02	1.14	0.91	1.46	1.98	1.08	1.09	1.30	1.12	1.30
56d normal cure	0.92	1.38	1.65	0.78	1.08	1.29	0.93	1.47	1.86	1.07	1.12	1.52	1.14	0.96
364d normal cure	On-going	On-going	On-going	On-going	On-going	On-going	On-going	On-going	On-going	On-going	On-going	On-going	On-going	On-going
ASTM C1202, Rapid Chloride Permeability, Coulombs														
28d accelerated cure	1147	1776	3081	576	789	1143	592	1434	2618	470	487	586	2845	3437
56d normal cure	1848	2662	3856	705	943	1790	1543	3731	4772	593	887	1077	3456	3905
364d normal cure	On-going	On-going	On-going	On-going	On-going	On-going	On-going	On-going	On-going	On-going	On-going	On-going	On-going	On-going
ASTM C 1585, Rate of Water Absorption (Sorptivity), x10^{-4} mm/s$^{1/2}$														
28d accelerated cure (Initial/Secondary)	1.8*/1.6	2.1*/2.9	3.3*/3.3	5.9*/1.7*	4.1*/2.0	5.3*/2.2*	4.3*/1.6	5.6*/2.0	18.3*/4.9	6.9/2.0	5.3*/1.5*	6.2*/1.6*	5.4*/2.0	8.6*/3.3*
56d normal cure (Initial/Secondary)	6.1/2.8*	7.0/4.2	22.0/11.1*	5.4*/1.7*	7.1*/2.2*	12.9/2.2*	6.8/3.2	6.9*/2.0*	8.4/3.5	5.5*/1.6	4.3/1.4*	6.9/1.8*	6.5*/2.9	10.3/4.9
364d normal cure (Initial/Secondary)	On-going	On-going	On-going	On-going	On-going	On-going	On-going	On-going	On-going	On-going	On-going	On-going	On-going	On-going
28d accel. cure (Initial/Secondary), g	0.7/1.9	1.0/3.1	1.1/3.6	1.5/2.6	1.1/2.3	1.2/2.7	1.1/2.1	1.4/2.9	3.0/6.8	1.7/3.1	1.4/2.4	1.7/2.8	1.2/2.7	1.6/4.3

56d normal cure (Initial/Secondary), g	1.2/ 3.1	1.7/ 4.4	4.0/ 12.3	1.2/ 2.3	1.7/ 3.2	2.4/ 4.1	1.5/ 3.8	2.0/ 3.4	1.9/ 4.8	1.7/ 3.0	1.3/ 2.5	1.8/ 3.1	1.3/ 3.4	1.6. 5.1
364d normal cure (Initial/Secondary), g	On-going	On-going	On-going	On-going	On-going	On-going	On-going	On-going	On-going	On-going	On-going	On-going	On-going	On-going
USBR 4908 Fully Immersed Method B														
Length Change @ 12 months	On-going	On-going	On-going	On-going	On-going	On-going	On-going	On-going	On-going	On-going	On-going	On-going	On-going	On-going
Length Change @ 18 months														
Mass Change @ 12 months														
Mass Change @ 18 months														
USBR 4908 Partially Immersed														
Scaling Distance @ 12 months	On-going	-	On-going	On-going	-	On-going	On-going	-	On-going	On-going	-	On-going	On-going	On-going
Scaling Distance @ 18 months														

* A correlation coefficient less than 0.98 indicating that the rate cannot be determined according to ASTM C158

Note. Type I/II, V-1, and V-2 cements had C_3A content of 8%, 3%, and 5%, respectively.

Table 6. ASTM C1012 Mortar Mixture Proportions and Preliminary Test Results

Mix No.	**1**	**2**	**3**	**4**	**5**	**6**	**7**	**8**	**9**	**10**
Cement Type	I	I/II	V	V	I	I/II	V	I	I/II	V
C_3A (Cement mill cert.), %	12	8	3	5	12	8	3	12	8	3
Slag, %					25	35	50			
Fly ash, %								15	20	30
Batch Quantities										
Cement, g	500	500	500	500	375	325	250	425	400	350
Slag cement, g					125	175	250			
Fly ash, g								75	100	150
Graded Standard Sand, g	1375	1375	1375	1375	1375	1375	1375	1375	1375	1375
Water, g	243	243	243	243	243	243	243	243	243	243
w/cm	0.49	0.49	0.49	0.49	0.49	0.49	0.49	0.49	0.49	0.49
Fresh Mortar Properties										
ASTM C1064, Temperature, °F	74	75	75	75	75	75	72	77	74	73
ASTM C1437, Flow, %	92	111	122	116	108	108	118	89	107	121
ASTM C109, At Immersion into Sulfate Solution										
Age, days	1.9	1.8	1.3	1.9	1.8	2.0	5.8	6.8	3.8	6.0
Compressive strength, psi	2,850	3,381	2,925	3,169	2,894	2,931	4,019	2,850	2,850	2,856
ASTM C1012, Sulfate Expansions										
6 month, %	0.451	0.064	0.024	0.035	0.034	0.035	0.022	0.032	0.037	0.023
12 month, %	ongoing	ongoing	ongoing	ongoing	ongoing	ongoing	ongoing	ongoing	ongoing	ongoing
18 month, %	ongoing	ongoing	ongoing	ongoing	ongoing	ongoing	ongoing	ongoing	ongoing	ongoing
Coeff. Var.- 6 month, %	53	6	21	4	2	17	13	32	15	19

Coeff. Var.- 12 month, %	ongoing	ongoing	ongoing	ongoing	ongoing	ongoing	ongoing	ongoing	ongoing	ongoing
Coeff. Var.- 18 month, %	ongoing	ongoing	ongoing	ongoing	ongoing	ongoing	ongoing	ongoing	ongoing	Ongoing
Expected sulfate class	S0	S1	S2	S2	S1	S2	S3	S1	S2	S3

Note. Type I cement had C_3A content of 12% whereas Type I/II cement had C_3A content of 8%.

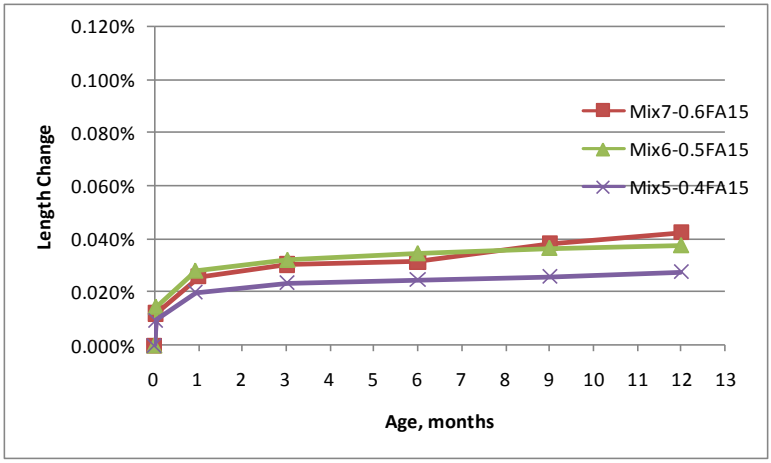
0.120%
0.100%
0.080%
0.060%
0.040%
0.020%
0.000%
Length Change
0 1 2 3 4 5 6 7 8 9 10 11 12 13
Age, months
Mix7-0.6FA15
Mix6-0.5FA15
Mix5-0.4FA15

(a)

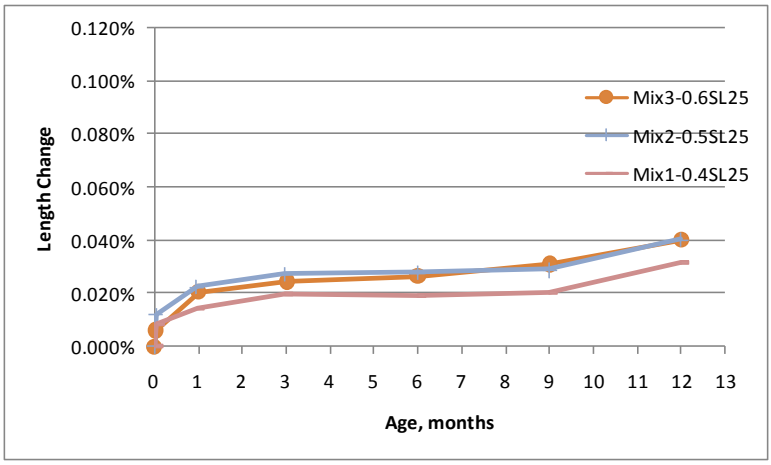
0.120%
0.100%
0.080%
0.060%
0.040%
0.020%
0.000%
Length Change
0 1 2 3 4 5 6 7 8 9 10 11 12 13
Age, months
Mix3-0.6SL25
Mix2-0.5SL25
Mix1-0.4SL25

(b)

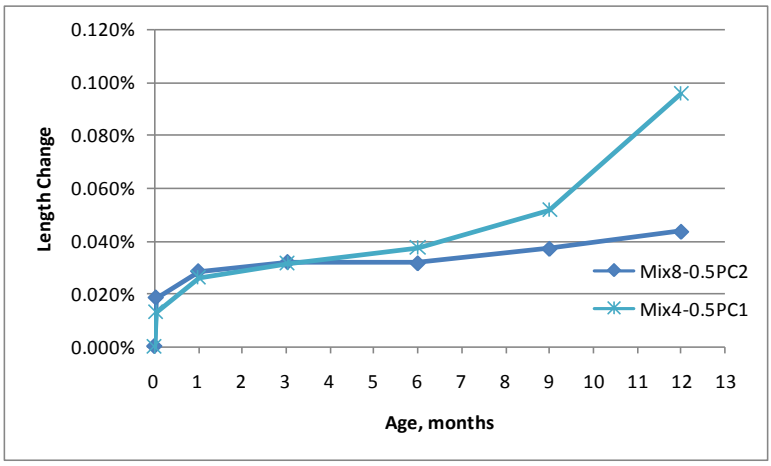
0.120%
0.100%
0.080%
0.060%
0.040%
0.020%
0.000%
Length Change
0 1 2 3 4 5 6 7 8 9 10 11 12 13
Age, months
Mix8-0.5PC2
Mix4-0.5PC1

(c)

Figure 15 USBR Fully Immersed Condition Length Change (Mixtures 1-8)

(a) 15% fly ash mixtures at various w/cm ratios, (b) 25% slag cement mixtures at various w/cm ratios, and (c) portland cement mixtures (PC1-C_3A=12% vs PC2-C_3A=8%)

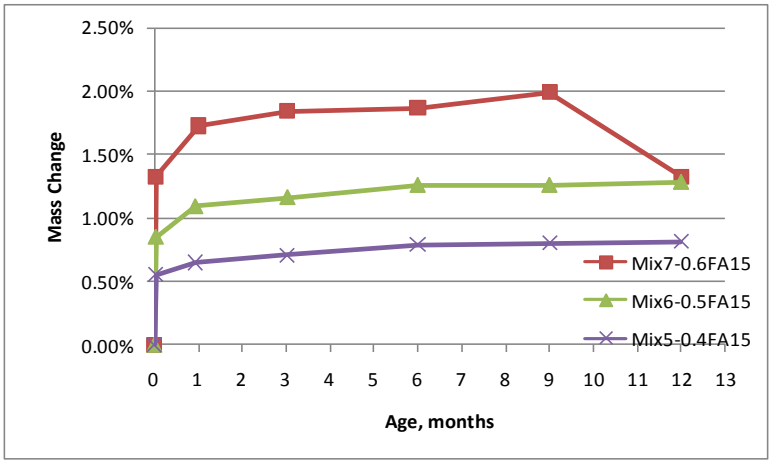

(a)

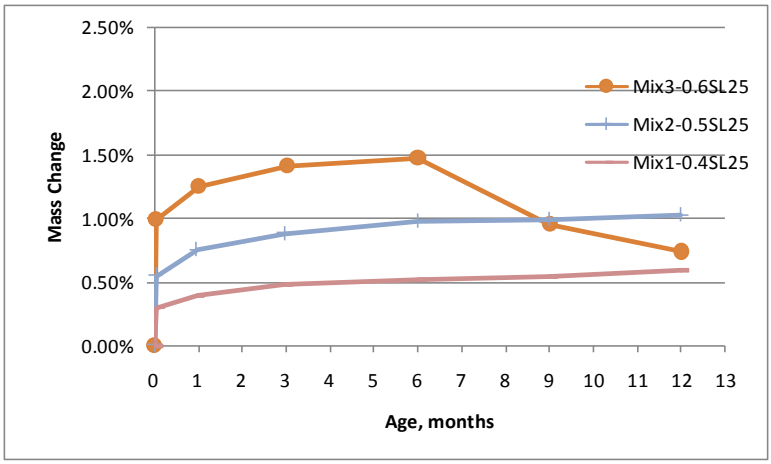

(b)

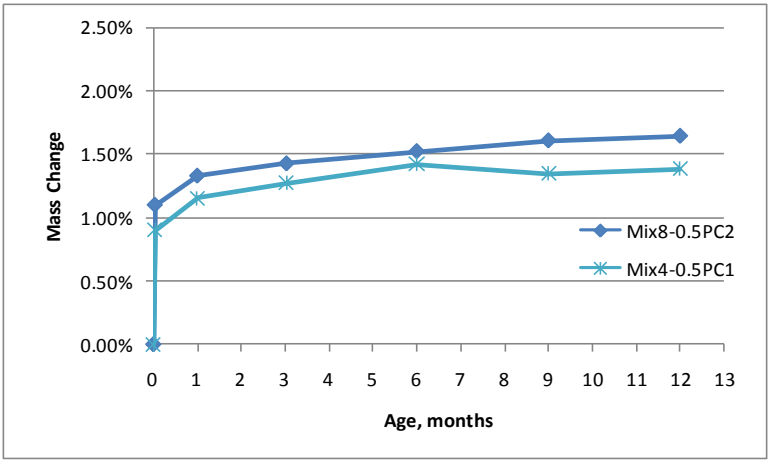

(c)

Figure 16 USBR Fully Immersed Condition Mass Change (Mixtures 1-8)

(a) 15% fly ash mixtures at various w/cm ratios, (b) 25% slag cement mixtures at various w/cm ratios, and (c) portland cement mixtures (PC1-C_3A=12% vs PC1-C_3A=8%)

(a)

(b)

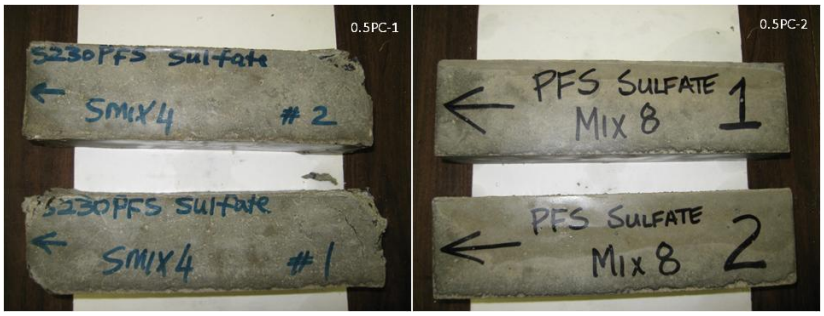

(c)

Figure 17 USBR Fully Immersed Sample Pictures after 12 months

(a) 15% fly ash mixtures at various w/cm ratios, (b) 25% slag cement mixtures at various w/cm ratios, and (c) portland cement mixtures (PC1-C_3A=12% vs PC1-C_3A=8%)

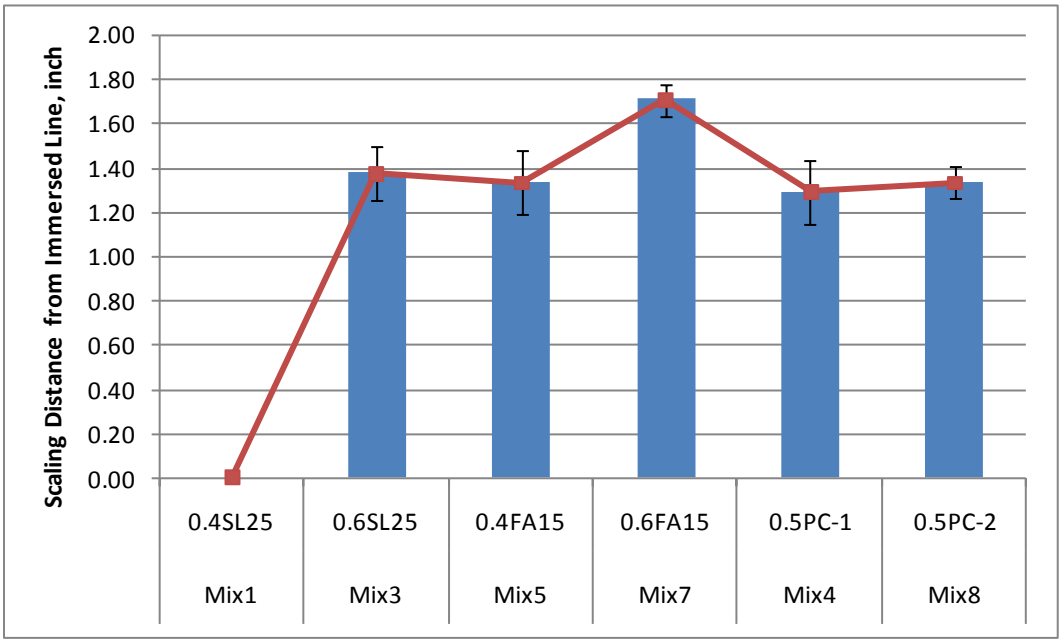

Figure 18 USBR Half Immersed Condition Scaling Distance from Immersion Line

Error Bars indicates ±1 standard deviation for the testing of three specimens,

PC-1, PC-2 had C_3A content of 12%, 8%, respectively

(a)

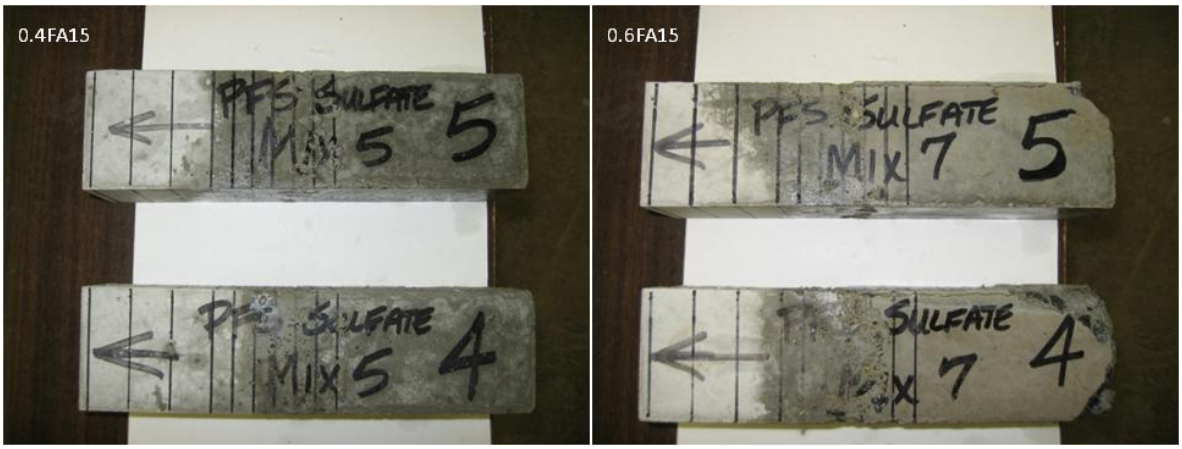

(b)

(c)

Figure 19 USBR Half Immersed Sample Pictures after 12 months

(a) 25% slag cement mixtures, (b) 15% fly ash mixtures, and (c) portland cement mixtures (PC1-C_3A=12% vs PC1-C_3A=8%)

SESSION 2 : Purdue University

Progress this Quarter (includes meetings, work plan status, contract status, significant progress, etc.):

The work performed this Quarter at Purdue has been divided in six sections. In addition, previously completed work that is ready in chapter form is provided in the final section of this document.

- 1.0 Swiss Oxygen Diffusivity
- 2.0 Comparing the Swiss Oxygen Diffusivity and the South African Gas Permeability (OPI), Influence of Sample Conditioning
- 3.0 Electrical Bulk Resistivity Round Robin Draft
- 4.0 Water Absorption and Comparison with Freeze Thaw Performance
- 5.0 The influence of salt on gas permeability
- 6.0 Theoretical calculations for rapid sample conditioning

1.0 Swiss Oxygen Diffusivity

Instrument setting

In previous quarters the basic elements of this technique have been discussed. The current design has been based on experiments by X and Y. Figure 1 shows a photo of the instrument which is now complete. A cut concrete core is conditioned and placed in the diffusivity cell. The test measures gas permeability and is based on the concept that oxygen is placed on one side of the sample, while nitrogen is placed on the other. The time it takes for the nitrogen to be detected in the oxygen cell is used to determine the diffusion coefficient.

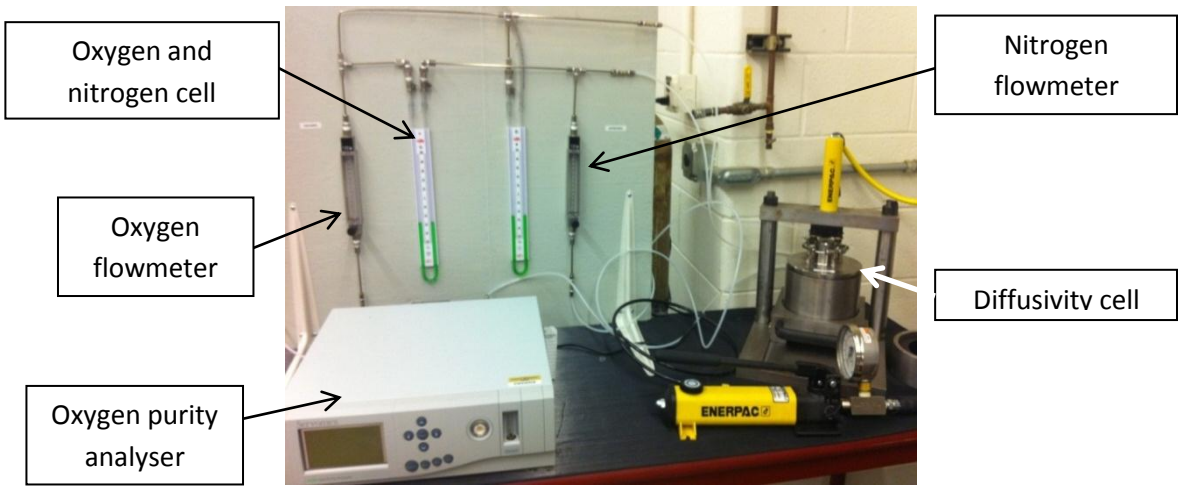

Figure 20: Oxygen diffusivity instrument

The calibration of the instrument has been done using a two calibration gases: Nitrogen with 1000 ppm of oxygen; and Oxygen 99.5% purity.

Details on the Testing and Calculation of Results from Testing

The instrument previously described is designed for two kinds of samples:

- 30 mm thick samples, 100 mm of diameter, used in the case of mortar samples;
- 50 mm thick samples, 100 mm of diameter, used for concrete.

The specimens can be obtained from the common 4 by 8 in cylinders, subsequently cut in slice 30 mm or 50 mm thick with a wet saw.
Afterwards, the samples need to be conditioned in a specific temperature- and humidity-controlled chamber, in order to make sure they have reached the equilibrium, in terms of mass change.

The test is conducted by exposing one flat face of the sample to a stream of oxygen and the opposite face to a stream of nitrogen at equal pressure and temperature. The rate of diffusion of oxygen is determined by measuring the oxygen concentration in the nitrogen stream.

The sample is fitted into a silicon rubber ring in the diffusion cell; the curved surface was sealed by loading the top plate and silicone rubber ring, which expands laterally, providing an air-tight grip onto the sample.

The gas flow rates need to be adjusted in order to minimize the pressure between the two streams. At steady state condition, the oxygen concentration in the nitrogen stream was measured using an oxygen analyzer: the analyzer consists of a zirconium oxide tube heated to 700 C, through which the gas stream to be analyzed is passed.

The measured oxygen concentration value, together with the gas flow rates, the pressure differential and the samples dimension were used to calculate the oxygen diffusion coefficient, D (m^2/s):

$$D_N = \frac{RT}{P}\frac{Q_{mol/s} \cdot L}{A \cdot \Delta C} = \frac{Q_{m3/s} \cdot L}{A \cdot \Delta C}$$

Where:

- $Q_{m3/s} = \frac{R_1}{60 \cdot 10^6} \cdot \frac{(G_1 - G_0)}{100}$
- $C_2 = \left[100 - \left(\frac{R_1}{R_2} \cdot \frac{(G_1 - G_0)}{2} \cdot \sqrt{\frac{32}{28}}\right)\right]$
- $C_1 = \frac{(G_1 + G_0)}{2}$
- $\Delta C = C_2 \cdot \frac{P_1}{100} - C_1 \cdot \frac{(P_1 - U_1)}{100} = \left[100 - \left(\frac{R_1}{R_2} \cdot \frac{(G_1 - G_0)}{2} \cdot \sqrt{\frac{32}{28}}\right)\right] \cdot \frac{P_1}{100} - \frac{(G_1 + G_0)}{2} \cdot \frac{(P_1 - U_1)}{100}$

The symbolism used above represents:

- D_N average diffusion constant based on simple diffusion – Fick's Law [m^2/s];
- $Q_{m3/s}$ is the rate of oxygen diffusion [m^3 of O_2 at 1 atm/s];
- R_1 is the flow rate of the nitrogen stream [cm^3/min];
- R_2 is the flow rate of the oxygen stream [cm^3/min];
- G_1 is the percentage of oxygen in the nitrogen stream at the end of the test [%];
- G_0 is the percentage of oxygen in the nitrogen stream initially [%];
- P_1 is the pressure of the oxygen stream [atm];
- U_1 is the difference between the oxygen stream pressure and the nitrogen stream pressure [atm];
- C_1 is the mean concentration of oxygen in the nitrogen stream [%];
- C_2 is the mean concentration of oxygen in the oxygen stream in contact with the specimen [%];
- ΔC is the change in concentration through the specimen [%];
- A is the area of the cross section of the sample [m^2];
- L is the thickness of the sample [m];
- R is the gas constant [j/(mol sec)];
- T is the temperature [°K]

It has been observed that the calculation procedures use in the literature and following studies that followed the original paper [1] are not consistent. We have rederived the equqations and will proceed with the calculation proposed above, that is according to Lawrence's paper [1] since we believe it is the correct one. We have also arranged for round robin testing with EMPA to obtain repeatability information between the different devices.

References

[1] C. D. Lawrence, "Transport of oxygen through concrete", Basic Materials Group Cement and Concrete Association, 1984

[2] C. Peretti , "Influence of conditioning on the transport properties of concrete", MS Thesis, 2011

[3] H. S. Wong, N. R. Buenfeld, J. Hill, A. W. Harris, "Mass transport properties of mature wasteform grouts", Advances in Cement Research, 19, p. 35-46, 2007

2.0 Comparing the Swiss Oxygen Diffusivity and the South African Gas Permeability measurements (oxygen permeability vs diffusivity)(OPI), Influence of Sample Conditioning

From previous studies it has been seen a consistent influence of samples conditioning on gas permeability; specifically the samples should be dried to a level where all pores relevant to transport are emptied. According to Parrot [3] the air permeability was very sensitive to moisture content, especially above 60% RH.

It has been found, moreover, that oxygen permeability and diffusivity are somehow related even though differences have been noticed. In particular it seems that permeability is a strong function of the pore size, while diffusivity seems function of the total porosity [4]. As a consequence, different parameters will be affecting permeability and diffusivity differently; for instance micro-cracking has a greater influence on permeability than diffusivity.

In this study, the investigation of the conditioning relative humidity and of the testing system used have been analyzed.

Materials

A series of experiments has been performed on mortar samples 0.30, 0.40, 0.42 and 0.50 w/c, to evaluate both the influence of the mixture proportions and the influence of sample conditioning. The mixture proportions are summarized in Table 1.

Table 1: Mixture proportions

	0.3 w/c	**0.4 w/c**	**0.42 w/c**	**0.5 w/c**
Cement [kg/m3]	631.25	547.37	534.13	481.16
Fly Ash [kg/m3]	1240.42	1240.42	1240.42	1240.42
Water [kg/m3]	211.89	242.79	247.20	264.86
WRA [g/m3]	3809.55	-	-	-
w/c	0.3	0.4	0.42	0.5

Testing and Results

The samples were cast, demolded 24 hours after and sealed in plastic bags for 28 days. Subsequently they were conditioned in a temperature- and humidity -controlled chamber at 23+/-1° C and at two different relative humidities: one set of samples at 65+/-2% and another set at 50+/-2% RH.

Oxygen permeability and oxygen diffusivity was measured for each sample when they were 19 months old and after a conditioning process of 18 months.

The oxygen diffusivity results are presented in Figure 21 and Table 2. Oxygen permeability results are shown in Figure 22 and Table 3. From the error bars it is evident that the possible variability range of oxygen permeability is much higher, so then an higher number of samples need to be tested in order to have representative results. The variability instead for oxygen diffusivity is consistently lower.

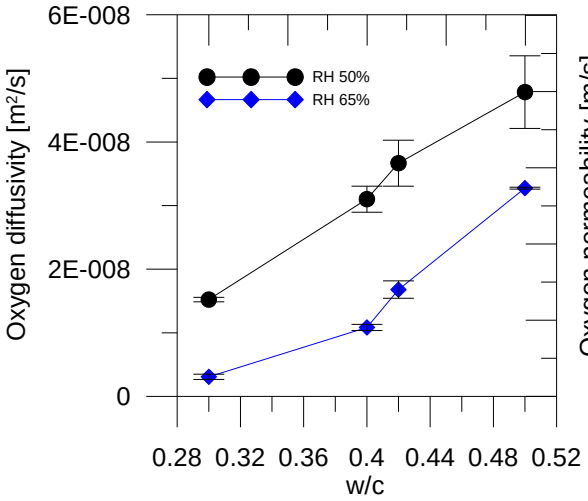

***Figure 21*: Oxygen diffusivity vs. w/c ratio**

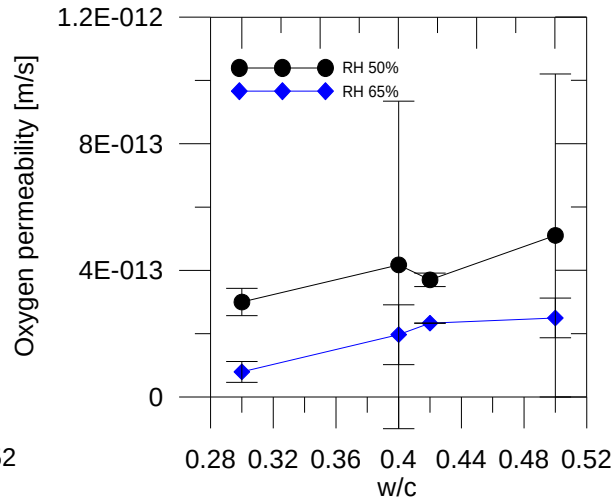

Figure 22: Oxygen permeability vs. w/c ratio

Oxygen diffusivity coefficients have been evaluated according to reference [1]. Oxygen permeability values have been calculated with reference to [2].

Table 2: Oxygen Diffusivity values, Samples geometry and tests parameters

SAMPLE ID	D1 [mm]	D2 [mm]	H1 [mm]	H2 [mm]	Mass before test [g]	Mass after test [g]	O2 flow [mm]	N2 flow [mm]	Absolute pressure	Initial O_2 content [%]	Final O_2 content [%]	Diff coeff. [m2/s]
0.5 - 65% - 1	102.4	102	29.76	30.84	520.75	520.54	117	10	24	0.010	0.479	3.59E-08
0.5 - 65% - 2	101.42	101.56	30.24	30.38	534.77	534.57	115	8	23	0.005	0.472	3.31E-08
0.42 - 65% - 1	101.27	101.67	30.38	30.55	540.68	540.42	114	9	23	0.008	0.212	1.52E-08
0.42 - 65% - 2	102.29	102.15	30.7	30.31	533.98	533.85	114	8	23	0.003	0.253	1.75E-08
0.42 - 65% - 3	101.67	101.93	30.88	31.16	553.11	552.95	114	8	24	0.005	0.247	1.74E-08
0.40 - 65% - 1	101.52	101.46	30.46	30.36	538.53	538.35	110	7	23	0.003	0.158	1.05E-08
0.40 - 65% - 2	101.42	101.75	29.93	29.98	529.13	528.98	115	9	23	0.008	0.163	1.13E-08
0.40 - 65% - 3	101.5	101.91	31.89	31.85	569.9	569.7	114	8	23	0.006	0.152	1.08E-08
0.30 - 65% - 1	101.18	101.28	30.4	30.31	555.32	552.15	115	9	23	0.009	0.047	2.83E-09
0.30 - 65% - 2	101.5	101.76	29.25	29.4	537.33	537.25	114	8	23	0.006	0.049	2.93E-09
0.30 - 65% - 3	101.4	101.29	31.16	30.69	562.55	562.41	115	9	23	0.007	0.053	3.48E-09
0.5 - 50% - 1	101.72	102.19	33.9	32.8	583.12	582.99	115	9	23	0.008	0.630	5.03E-08
0.5 - 50% - 2	101.7	101.13	32.53	33.5	575.15	575.08	119	10	24	0.002	0.499	4.21E-08
0.5 - 50% - 3	102.44	102.39	33.2	32.86	578.73	578.68	119	10	24	0.002	0.616	5.11E-08
0.42 - 50% - 1	102.6	102	31.96	31.98	557.55	557.48	114	9	23	0.004	0.527	4.03E-08
0.42 - 50% - 2	101.16	101.9	33.27	32.82	577.69	577.61	113	8	23	0.007	0.449	3.407E-08
0.42 - 50% - 3	101.97	102.09	32.8	33.19	574.94	574.85	116	10	23	0.006	0.431	3.557E-08
0.40 - 50% - 1	101.93	102.06	32.85	33.84	582.32	582.22	118	10	24	0.008	0.381	3.149E-08
0.40 - 50% - 2	102.01	101.99	32.5	32.86	576.61	576.59	115	9	23	0.009	0.374	2.90E-08
0.40 - 50% - 3	102.13	102.3	32.07	32.78	572.57	572.43	114	9	23	0.001	0.416	3.25E-08
0.30 - 50% - 1	101.8	101.93	32.54	32.52	584.45	584.4	118	10	24	0.009	0.194	1.526E-08
0.30 - 50% - 2	102.46	102.37	33.24	32.3	592.75	592.7	117	10	24	0.004	0.184	1.488E-08
0.30 - 50% - 3	102.4	102.6	32.28	33.17	590.26	590.15	115	9	23	0.002	0.199	1.552E-08

Table 3: Oxygen permeability results and samples geometry

SAMPLE ID	H1 [mm]	H2 [mm]	D1 [mm]	D2 [mm]	Oxygen Permeability [m/s]
0.5 - 65% - A	30.88	30.41	68.04	68.06	2.50E-13
0.5 - 65% - B	32.08	31.66	67.99	68.03	
0.5 - 65% - C	32.23	31.56	68.03	68.08	
0.5 - 65% - D	31.68	32.03	68.06	67.88	
0.42 - 65% - A	31.74	31.34	68	68.03	2.33E-13
0.42 - 65% - B	30.43	31.89	67.93	67.99	
0.42 - 65% - C	31.28	31.47	68.04	68.02	
0.42 - 65% - D	31.56	32.33	67.95	68.04	
0.40 - 65% - A	31.36	31.23	67.97	68	1.97E-13
0.40 - 65% - B	31.37	31.05	68.04	68.04	
0.40 - 65% - C	30.78	30.65	68.07	68.01	
0.40 - 65% - D	31.44	30.76	68.04	68.01	
0.30 - 65% - A	31.14	31.37	68.07	68.01	7.93E-14
0.30 - 65% - B	31.72	32.56	68	68.03	
0.30 - 65% - C	32.2	30.91	68.01	67.93	
0.30 - 65% - D	31.53	30.81	67.91	68	
0.5 - 50% - A	32.67	32.74	67.9	67.89	5.10E-13
0.5 - 50% - B	31.07	31.47	67.87	67.97	
0.5 - 50% - C	31.43	31.93	67.92	67.96	
0.5 - 50% - D	31.43	31.83	67.88	68.01	
0.42 - 50% - A	30.9	30.28	67.95	67.95	4.17E-13
0.42 - 50% - B	31.59	32.22	67.99	67.97	
0.42 - 50% - C	30.22	29.99	67.85	67.92	
0.42 - 50% - D	31.28	31.14	67.92	67.75	
0.40 - 50% - A	30.29	31.26	67.98	68.09	3.70E-13
0.40 - 50% - B	30.95	32.66	68.02	68.05	
0.40 - 50% - C	32.03	31.43	68.01	68.07	
0.40 - 50% - D	30.64	31.11	67.95	68.04	
0.30 - 50% - A	31.59	31.09	68.03	67.99	3.00E-13
0.30 - 50% - B	31.2	31.34	68.08	67.95	
0.30 - 50% - C	32.12	31.12	68	68.04	
0.30 - 50% - D	32.28	31.82	67.97	68.09	

Conclusion

From the results a direct correspondence between the tests can be noticed (Figure 23). In addition it has been confirmed the influence of w/c ratio and of RH on gas permeability and diffusivity measurements.

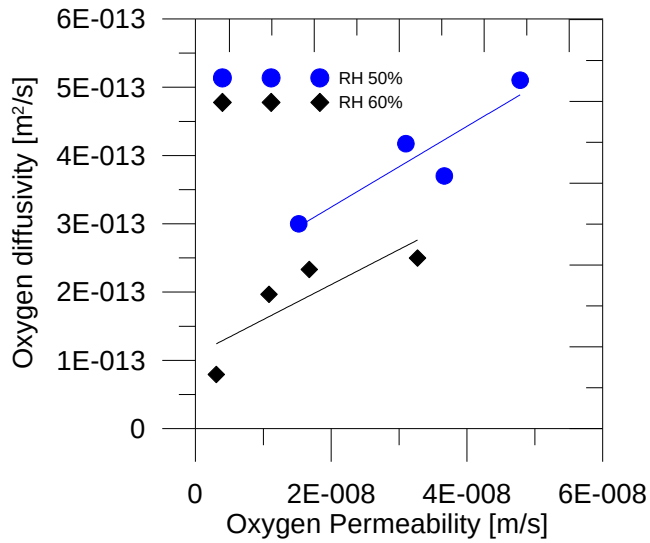

Figure 23: Oxygen diffusivity instrument

References

[1] C. D. Lawrence, "Transport of oxygen through concrete", Basic Materials Group Cement and Concrete Association, 1984

[2] M.G. Alexander, J. R. Mackechnie, Y. Ballim, "Guide to the use of durability indexes for achieving durability in concrete structures", Research Monograph. No. 2, UCT, Wits, 1999

[3] L.J. Parrot, Moisture conditioning and transport properties of concrete test specimens. Materials and Structures, 1994, 27, No. 8, 460-468

[4] H. S. Wong, M. Zobel, N. R. Buenfeld and R. W. Zimmerman, Influence of the ITZ and microcracking on the diffusivity, permeability and sorptivity of cement based materials after drying, Magazine of Concrete Research, 2009, 61, n. 8

3.0 Electrical Bulk Resistivity Round Robin Draft

A report is attached that outlines the results of an experimental study that evalued the use of the bulk resistivity test (along with the proposed testing approach). The statistical analysis is currently being completed however that will soon be sumitted for journal review.

4.0 Water Absorption and Comparison with Freeze Thaw Performance

Introduction

Companion samples from previous freeze and thaw mixtures (from previous NRMCA progress reports) have been further analyzed: three cylinders from each mixture have been used in order to evaluate the response of materials to water absorption, ion diffusion and moisture transport tests (STADIUM testing) and quantify their degree of saturation.

Mixture proportions

The samples tested belong to two groups of mixes and they are summarized in the following table: (Table 4).

Table 4: Mixture proportions of NRMCA Freeze-Thaw Samples

Date cast	10/13/2009	10/13/2009	11/12/2009	10/20/2009	10/27/2009	11/4/2009	11/10/2009	11/10/2009
Calculated Batch Quantities	**FT1**	**FT2**	**FT3**	**FT4**	**FT5**	**FT6**	**FT7**	**FT8**
	0.57PC	**0.50PC**	**0.50FA20**	**0.50SL30**	**0.5SL25SF5**	**0.6SL25SF5**	**0.45PC**	**0.45SL30**
Type I/II cement, lb/yd^3	506	539	442	385	385	353	592	414
Slag, lb/yd^3				165	137	126		177
Fly ash, lb/yd^3			111					
Silica Fume, lb/yd^3					27	25		
SCM, %	0	0	20	30	30	30	0	30
Coarse Agg. (No.57), lb/yd^3	2087	2021	2071	2060	2058	2077	2035	2029
Fine Aggregate, lb/yd^3	1094	1083	1066	1093	1084	1072	1062	1048
Mixing Water, lb/yd^3	290	270	276	275	275	302	267	266
w/cm	0.57	0.50	0.50	0.50	0.50	0.60	0.45	0.45
ASTM C494 AEA, oz/cwt	0.76	0.81	4.26	1.15	0.86	1.39	0.74	1.16
ASTM C494 Type F, oz/cwt		0.57	0.40	0.58	2.59	0.51	1.37	1.87
Fresh Concrete Properties								
ASTM C143, Slump, in.	7	6	6	5	5	6.5	5.25	6
ASTM C231, Air, %	6	7.2	6	6.2	6.5	6.2	7	7.6
ASTM C138, Density, lb/ft^3	148.1	145.7	147.7	148.1	147.7	147.3	147.3	146.5
ASTM C1064, Temperature, F	75	75	73	70	72	70	70	70

Samples preparation and testing

The three cylinders 4x8 inches used for each mixture, previously sealed, have been cut in order to have:

- Two samples 50 mm thick for absorption test;
- Two samples 50 mm thick for STADIUM migration test;
- Two samples 50 mm thick and two samples 10 mm thick for STADIUM drying test;
- One sample 50 mm thick for porosity and DOS evaluation.

Absorption Test

Absorption test has been done according to the procedure described in ASTM C 1585. However, a modification has been done to the conditioning procedure: samples were kept in the oven at 80% until they have reached mass equilibrium (Δm <0.5%) and not only for three days as suggested in the standard.

STADIUM migration and drying tests

Migration test consists in monitoring the intensity of electrical current passing through a cylindrical test specimen over a 14-days period. A constant DC potential is maintained constant across the specimen by an electrical power supply. The upstream cell is filled with a chloride-containing electrolytic solution and connected to the negative electrode, while the downstream cell is filled with a base solution and connected to the positive electrode.

A picture of the migration test setup is presented in Figure 24.

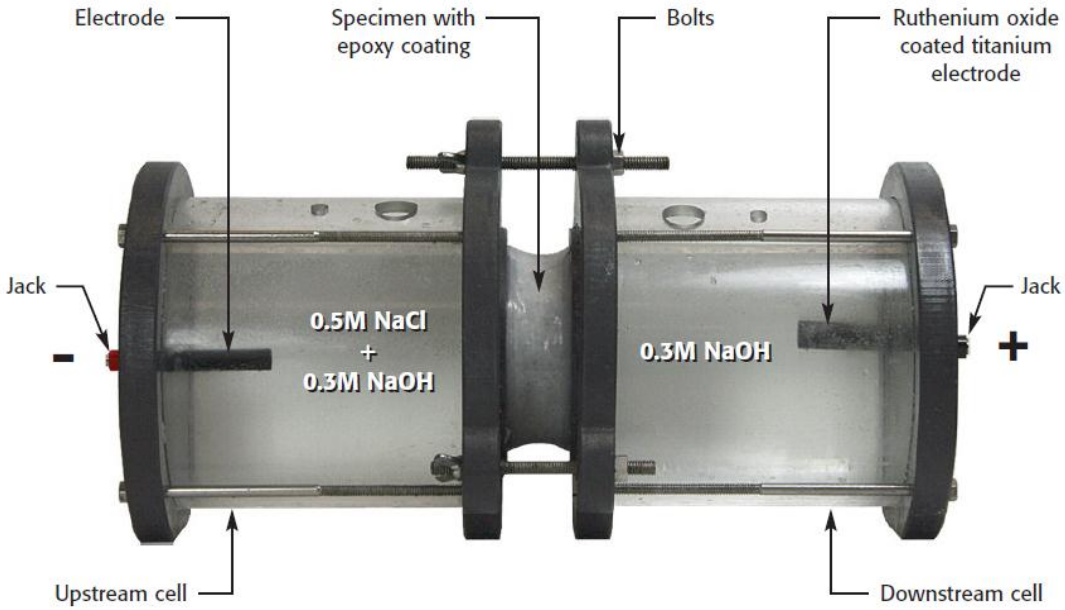

Figure 24: Migration test setup *(STADIUM Lab User Guide v3)*

Before the test, cylindrical samples 50 mm thick were cut from the original cylinders, then they were covered with epoxy on the edge and finally kept in lime water until they have reached mass equilibrium (Δm<0.5%). Afterwards, they were vacuum saturated with 0.3M NaOH solution for 18 hours following the procedure described in ASTM C1202. The test was then started and the current and potential were monitored through a continuous monitoring system for 14 days.

Drying test determines the drying rate of concrete by measuring the mass loss due to evaporation and moisture transport in specimens exposed to constant temperature and relative humidity.

The samples, two cylinders 50mm thick and two 10 mm thick with diameter of ~100 mm, were kept in lime water before the test started, until the moment they have reached mass equilibrium ($\Delta m<0.5\%$). Subsequently the samples were moved in an environmentally controlled chamber (23° C and 50% RH) and the mass was monitored in the following days: 1,2,3,4,5,6,7,9,11,13,15,22,29,etc. until the mass measurement show less than 0.5% variation.

Density, absorption and porosity test

Density, absorption and voids were determined using one cylinder 50 mm thick and with 100 mm diameter for each mixture and following the procedure described in ASTM C 642.

Results and preliminary discussion

The results from the ASTM C 1585 absorption test are presented in Table 5.

Table 5: Sorptivity results

	Initial Absorption [-]	**Secondary Absorption** [-]
FT Mix 1	0.00685	-
FT Mix 2	0.00426	-
FT Mix 3	0.00150	0.00060
FT Mix 4	0.00401	0.00075
FT Mix 5	0.00265	0.00062
FT Mix 6	0.00498	0.00080
FT Mix 7	0.00240	0.00148
FT Mix 8	0.00113	0.00043

In order to evaluate also the degree of saturation of the samples during the test, porosity measurements are being performed and are currently being analyzed. Electrical resistance testing is also being performed and the results are provided in Table 6. Additional testing is being performed, results of which will be available in the next quarterly progress report including results from the SIMCO cells, comparison with resistivity, and comparisions with drying and water absorption..

The results from resistivity measurements are presented in Table 6.

Table 6: Resistivity values

	Direct measure [kΩ cm]
FT mix 1	7.85
FT mix 2	9.97
FT mix 3	32.72
FT mix 4	28.19
FT mix 5	61.04
FT mix 6	49.61
FT mix 7	10.91
FT mix 8	27.93

Conclusions

From the results presented above some considerations can be deducted:

- Resistivity and ions diffusion are inversely related;
- it looks like the addition of SCM is positive in terms of resistivity, SCM seems to decrease the ions and moisture diffusion.
- Increasing the w/c ratio, we have always noticed a decreasing of performance;
- It appears not easy to connect the results presented above with previous freeze/thaw tests.

5.0 The influence of salt on gas permeability

Previous research has shown that salts can alter the rate of fluid absorption and can alter the drying process [1]. A request has been sent to ASTM to include information regarding previous findings in ASTM C1585 as it applies to sample conditioning, field samples and samples containing salt. This research is seeking to evaluate the role of salts on water retention and its influence on gas permeability.

Influence of salt solution on diffusion processes

The influence of salt solution presence on drying process and ions diffusion has been evaluated.
The samples used for this experiment have been casted with 0.42 w/c mortar: the mixture proportions are presented in Table 7:

Table 7: Mixture proportions 0.42 w/c mortar

Material	***Quantity***
sand [lb/yd^3]	2390.7
cement [lb/yd^3]	1026.7
water [lb/yd^3]	432.2
w/c	0.42

Figure 25 and 26 illustrate the influence of salt on the mass loss and drying time for samples. This indicates that samples containing salt will be more saturated than water filled samples for the same drying level. Samples are being prepared for OPI testing.

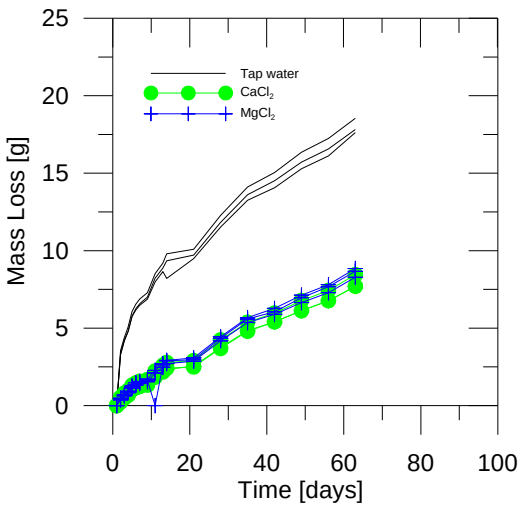

Figure 25: Mass Loss versus time for 2 in thick samples

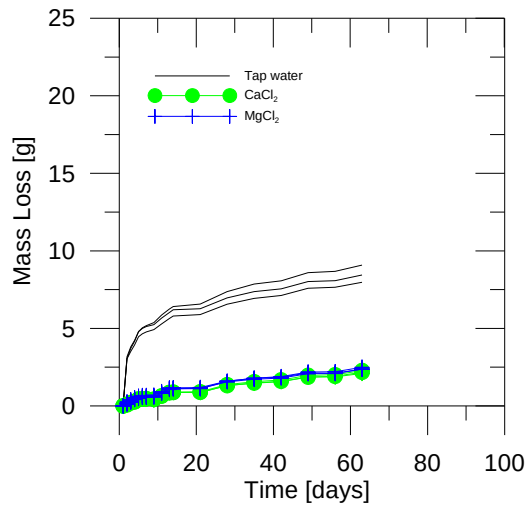

Figure 26: Mass Loss versus time for ½ in thick samples

[1] R. Spragg, J. Castro, W. Li, M.Pour-Ghaz P.Huang, J. Weiss, *Wetting and Drying Concrete Using Aqueous Solutions Containing Deicing Salts (Draft attached)*

6.0 Theoretical calculations for rapid sample conditioning

One question that has come up repeatedly is how fast samples can be conditioned for water absorption tests. This study is examining the estimated times and conditions that can be used for rapid conditioning. The approach that is being used is to use diffusional analysis to determine the times that are required for the samples to attain equilibrium and then to make a recommendation on the procedure that should be used. A sorption-desorption approach has been used to obain the moisture vapor diffusion coefficient which will be used for performing the calculations as described in the following section.

Mixture proportions

The mixture proportions of the mortar were presented in Table 7.

Samples preparation and testing

For the desorption-absorption mesaurements used to obtain the diffusion coeffficient, mortar samples have been saturated in deionized water for 24 hours. The desorption isotherms have been obtained in three conditions:

- 50° C with 20% RH steps from 97.5% to oven dry condition;
- 23° C with 20% RH steps from 97.5% to oven dry condition;
- 5° C with 20% RH steps from 97.5% to oven dry condition.

According to [2], it is possible to evaluate the diffusivity from the desorption curve. Indeed, each step in RH gives an initial mass change that is linear when plot on a square root of time scale and the linear part can be used to evaluate the diffusivity *D* or the diffusion coefficient with water vapor content as potential D_v:

$$D = \frac{L^2\pi}{16}\left(\frac{dE}{d\sqrt{t}}\right) \quad (1) \qquad\qquad D_v = D\frac{dc}{dv} \quad (2)$$

being *L* the thickness of the specimen, *E* the mass, *t* time, *dc/dv* is the change in moisture concentration in the specimen per change in water vapor content in ambient air.

The drying process can be described by the following equation:

$$\frac{\partial H}{\partial t} = div(D_H gradH) - \frac{\partial H_s}{\partial t}$$

where H is the relative humidity, D_H is the moisture diffusivity as a function of relative humidity and H_s is the variation of relative humidity due to self-desiccation.

So then, knowing the diffusivity in each relative humidity step, it is possible to evaluate the humidity profiles in the specific sample during time.
The partial differential equation has been solved using a Crank-Nicolson (central difference) scheme, using a Matlab program previously developed in the laboratory [2] (the paper mentioned is also attached to this report).

Results and preliminary discussion

The data from desorption isotherm are presented in Figure 27.

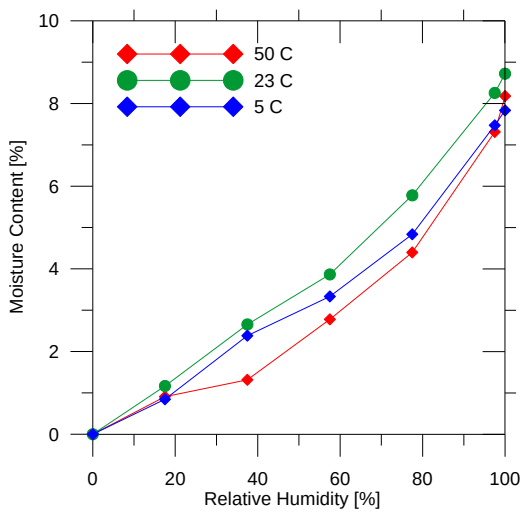

Figure 27: Desorption curve at 5, 23 and 50 C for 0.42 mortar

Typical diffusivity values are provided below.

Table 8: Diffusivity values at 50 C

Relative Humidity (%)	Diffusivity [mm²/s]	Effective Diffusivity [mm²/s]
87.5	2.06E-05	3.02E-08
67.5	1.04E-05	8.54E-09
47.5	1.02E-05	7.53E-09
27.5	3.67E-05	7.56E-09
8.75	4.65E-06	2.43E-09

Table 9: Diffusivity values at 23 C

Relative Humidity (%)	Diffusivity [mm²/s]	Effective Diffusivity [mm²/s]
87.5	2.05E-05	2.55E-08
67.5	1.29E-05	1.24E-08
47.5	5.49E-06	3.34E-09
27.5	9.67E-06	7.24E-09
8.75	1.95E-06	1.30E-09

Table 10: Diffusivity values at 5 C

Relative Humidity (%)	Diffusivity [mm^2/s]	Effective Diffusivity [mm^2/s]
87.5	1.01E-05	1.34E-08
67.5	6.73E-06	5.08E-09
47.5	6.28E-06	2.99E-09
27.5	3.67E-06	2.84E-09
8.75	2.54E-06	1.23E-09

A function has been fitted to the data to determine the non-linear moisture diffusion coefficient following the approach described by Bazant.

$$D(H) = D_1\left(\alpha_0 + \frac{1-\alpha_0}{1+\left(\frac{1-H}{1-H_c}\right)^n}\right)$$

The fitting has been done considering only RH between 100% and 50%.

Solving the differential equation for drying process (Fick's second law), it was possible to evaluate the time of equilibrium when the sample was having the same relative humidity along all its height.

This information will be used to study the drying time.

References

[1] Anderberg A., Wadso L., 'Method for simultaneous determination of sorption isotherms and diffusivity of cement-based materials', Cement and Concrete Research 38 (2008) 89-94

[2] Pou-Ghaz M., Spragg R., Weiss J. 'Moisture profiles and diffusion coefficients in mortars containing shrinkage reducing admixtures', International RILEM Conference on Use of Superabsorbent Polymers and Other New Additives in Concrete

[3] Bazant Z. P., Najjar L. J., Nonlinear water diffusion in nonsaturated concrete, Materiaux et Constructions, Vol. 5 n. 25 (1972)

SESSION 3: DRAFT PAPERS

The following draft papers will be attached:

- Castro, J., Spragg, R., and Weiss, W. J., *"Internal Curing for W/C Systems Between 0.30 and 0.45: Impact on Water Absorption and Electrical Conductivity*," ASCE Journal of Civil Engineering Materials

- Li, W., Pour-Ghaz, M., Castro, J., and Weiss, W. J., (accepted) "*Water Absorption and the Critical Degree of Saturation as it relates to Freeze-Thaw Damage in Concrete Pavement Joints*," ASCE Journal of Civil Engineering Materials

- Castro, J. Bentz, D., and Weiss, W. J., (2011) "*Effect of Sample Conditioning on the Water Absorption of Concrete*," Cement & Concrete Composites 33 (2011) 805–813

- Poursaee, A., and Weiss, W. J., (2010) "*An Automated Electrical Monitoring System (AEMS) to Assess Concrete Property Development'*, Journal of Automation in Construction, Volume 19, Issue 4, July 2010, Pages 485-490

- Sant, G., Rajabipour, F., and Weiss, W.J., (2008) '*The Influence of Temperature on Electrical Conductivity Measurements and Maturity Predictions in Cementitious Materials during Hydration*', Indian Concrete Journal, April 2008, pp. 10

- R.P. Spragg, J. Castro, T Nantung, M. Paredes, and J. Weiss, '*Variability Analysis of the Bulk Resistivity Measured Using Cylinders'*, Report.

- R. Spragg, J. Castro, W. Li, M.Pour-Ghaz P.Huang, J. Weiss*, Wetting and Drying Concrete Using Aqueous Solutions Containing Deicing Salts, Draft Paper*

- M. pour-Ghaz, R. Spragg, J. Weiss, '*Moisture profiles and diffusion coefficient in mortars containing shrinkage reducing admixtures'*, International RILEM Conference on Use of Superabsorbent Polymers, 2011, Denmark

Water Absorption and Electrical Conductivity for Internally Cured Mortars with a *W/C* between 0.30 and 0.45

Javier Castro[1], Robert Spragg[2], and Jason Weiss[3]

Abstract: Internal curing has emerged over the last decade as an approach to counteract the negative effects associated with self-desiccation in low water to cement ratio (*w/c*) mixtures. Specifically much of the early research on internal curing focused on the reduction of autogenous shrinkage. Recent work has however demonstrated that internal curing can also be beneficial in reducing drying shrinkage cracking, reducing the propensity for thermal cracking, reducing fluid absorption and reducing ion diffusion in concrete. However several aspects of internal curing still require closer examination. One of these aspects is the application of internal curing for mixtures with a wider range of water to cement ratios. This paper describes results from experiments that investigated the potential use of internal curing in mortar systems with *w/c* of 0.30, 0.36, 0.42 and 0.45 in terms of water absorption and electrical conductivity. Test results show that internal curing reduces the water absorption in all the systems. Similarly, results obtained on electrical conductivity at late ages (1 year) also show a benefit. It was also found that care needs to be taken to analyze electrical conductivity results at early ages due to the increased amount of fluid because the inclusion of the prewetted lightweight aggregate.

CE Database subject heading: Absorption, Concrete, Curing

Author keywords: Internal curing, Lightweight aggregate, Water absorption, Electrical conductivity

[1] PhD Candidate, School of Civil Engineering, Purdue University, 550 Stadium Mall Drive, West Lafayette, Indiana, USA, Phone: (765) 494 – 7999, jcastro@purdue.edu. Corresponding author

[2] Undergraduate Research Assistant, School of Civil Engineering, Purdue University, 550 Stadium Mall Drive, West Lafayette, Indiana, USA, Phone: (765) 494 – 7999, rspragg@purdue.edu

[3] Professor, Director of Pankow Materials Laboratory, Purdue University, 550 Stadium Mall Drive, Indiana, USA, Phone: (765) 496 – 2215, Fax: (765) 496 – 1364, wjweiss@ecn.purdue.edu.

BACKGROUND ON INTERNAL CURING

Internal curing has emerged over the last decade as a method to improve the performance of low water to cement ratio (*w/c*) mixtures [Rilem 2007, ACI SP-256 2008, ACI Committee 231 2010, INDOT 2010, Bentz and Weiss 2011]. Specifically, internal curing refers to the use of prewetted lightweight aggregate or other water filled inclusions such as Super Absorbent Polymers (SAP) or cellular fibers that can provide curing water throughout the cross section of the concrete. This differs from conventional water curing where water is provided after placement and where the water is applied only at the surface of the concrete. Internal curing was originally promoted to reduce autogenous shrinkage and autogenous shrinkage cracking [Bentz and Snyder 1999, Jensen and Hansen 2001a, Jensen and Hansen 2001b, Jensen 2005, Cusson and Hoogeveen 2008, Lopez et al. 2009]. However its potential benefits include reducing drying shrinkage cracking [Henkensiefken et al. 2008, Henkensiefken et al. 2009a], reducing the likelihood of thermal cracking [Schlitter et al. 2010, Byard et al. 2010] and reducing the likelihood of plastic shrinkage cracking [Henkensiefken et al. 2010]. Internal curing can also improve the freeze-thaw resistance [INDOT 2010], increase the resistance to fluid absorption [Bentz and Snyder 1999, Henkensiefken et al. 2009b, Peled et al. 2010] and reduce ion diffusion [Bentz 2009] in concrete. Internal curing has great potential for the concrete industry to create a longer lasting, more sustainable product. Several aspects of internal curing still require closer examination. One of these aspects is the use of internal curing for mixtures containing over a wider range of water to cement ratios (w/c) (e.g., mixtures with a *w/c* between 0.30 and 0.45).

To fully understand how internal curing works we need to first realize that the hydration of cement paste causes a volume reduction which is known as chemical shrinkage [Le Chatelier 1900, Powers 1935, L'Hermite 1960]. While chemical shrinkage starts at the time the water comes in contact with the cement, it has a different impact on the system before and after the paste sets. Before set, the chemical shrinkage causes bulk shrinkage of the cement paste that is equal to the total external volume change. After set, however, the cement paste becomes stiff enough to resist a portion of the volume change caused by chemical shrinkage [Barcelo et al. 1999, Sant et al. 2006]. Contact between the cement particles does not permit this volume reduction to occur. As a result, vapor-filled pockets form inside the cement paste in the largest

pores [Jensen and Hansen 2001b, Couch et al. 2006, Lura et al. 2009]. This is known as self-desiccation.

Chemical shrinkage occurs in all cementitious materials, irrespective of the *w/c* [Geiker 1983]. In low *w/c* mixtures, these vapor filled cavities can result in substantial relative humidity reduction and shrinkage since the vapor filled cavities form in relatively small pores with a small radius of curvature [Bentz and Jensen 2006, Radlinska et al. 2008, Lura et al. 2009]. In higher *w/c* mixtures those vapor filled spaces also develop however they occur in much larger pores with less impact on volume change. As a result, it has been thought that many of the higher *w/c* system would not see as much benefit from internal curing.

Lightweight aggregate are used as a water reservoir that can provide water to replenish the empty pore volume that is created by the chemical shrinkage occurring during hydration. Since water is removed from large pores to small pores, the ideal lightweight aggregate would have pore sizes larger that the pore size that develops the cement paste due to chemical shrinkage [Bentz 2009, Castro et al. 2010a]. This is the case for many commercially available expanded clays, slates or shales [Castro et al. 2010a].

APPROACHES FOR MIXTURE PROPORTIONING INTERNALLY CURED CONCRETE

The design of concrete for internal curing requires that a sufficient amount of water is placed in the concrete to aid in hydration and to overcome the effects of self-desiccation. Different approaches had been used during the recent years to determine and quantify the amount water needed for internal curing. Two of the most widely used approaches are discussed here.

Bentz and Snyder Approach

Bentz and Snyder [1999] developed an approach to determine the volume of prewetted LWA that should be use to “ensure adequate water for complete curing of concrete, which means that the cement reaches the maximum degree of hydration that is possible, given the space limitation

for forming hydration products in low *w/c* systems". It is based on the concept of filling the volume reduction of chemical shrinkage with water from the lightweight aggreagate. [Bentz et al. 2005]. This approach was first published by Bentz and Snyder [1999] as shown in Equation 1:

$$M_{LWA} = \frac{C_f \times CS \times \alpha_{\max}}{S \times \phi_{LWA}} \qquad \text{(Equation 1)}$$

where M_{LWA} (kg/m^3) is the mass of LWA (in a dry state) that needs to be water filled to provide water to fill in the voids created by chemical shrinkage, C_f (kg/m^3) is the cement content of the mixture, CS (ml of water per g of cement) is the chemical shrinkage of the cement, α_{max} (unitless) is the expected maximum degree of hydration: [(*w/c*)/0.36] for *w/c* below 0.36 and 1 for *w/c* higher than 0.36, Φ_{LWA} (kg of water/kg of dry LWA) is the absorption capacity of the LWA (taken here as the 24 h absorption value), and S (unitless) is the expected degree of saturation of the LWA, expressed as a function of the taken absorption value (Φ_{LWA}). Water absorption and S values from the most used LWA in America were previously reported by Castro et al. [2010a].

In theory, this approach may over estimate the amount of water required for internal curing, because it does consider the volume change that occurs before set [Henkensiefken 2009], however this approach is preferred due to its simplicity.

Jensen and Hansen approach

Jensen and Hansen [2001a] developed an approach to proportion internally cured mixtures with the intention of limiting the negative effects of self desiccation in cementitious systems by maximizing the volume of cement that can react. The equations were developed based on the Powers' model to calculate the minimum amount of water that needs to be stored (entrained) to enable the maximum degree of hydration. It has been published by Jensen and Hansen [2001a] and is shown in Equation 2:

$$(w/c)_e = \begin{cases} 0.18(w/c) & ;\ for\ \ w/c \leq 0.36 \\ 0.42-(w/c) & ;\ for\ \ 0.36 \leq w/c \leq 0.42 \\ 0 & ;\ for\ \ w/c \geq 0.42 \end{cases} \qquad \text{(Equation 2)}$$

where $(w/c)_e$ is the amount of additional water for internal curing, expressed as gram of water by gram of cement, and the (w/c) is the original water to cement ratio of the system.

EXTENSION OF INTERNAL CURING TO HIGH W/C SYSTEMS

Figure 1 (after Bentz et al. 2005) illustrates both approaches as a function of the *w/c*. It can be seen that below a w/c of 0.36 both approaches are identical. The Bentz approach adds water to fill all the chemical shrinkage volume which causes it to stay constant above *w/c* of 0.36 while the Jensen approach considers only adding the water needed for full hydration which results in the water recommended decreasing above a *w/c* of 0.36.

It should be noted that both approaches assume that all the mixing water will be accessible to react with the un-hydrated cement. Issues associated with the distance that the water needs to travel or a lack of adequate mixing are not considered. These two issues may decrease the amount of hydration that occurs and may increase the porosity of the system and its connectivity.

RESEARCH OBJECTIVES

The objective of this research is to examine the potential benefits of internal curing in mortar systems with *w*/c from 0.30 to 0.45. In particular this research will evaluate the benefits in terms of water absorption and electrical conductivity on systems with *w/c* of 0.30, 0.36, 0.42 and 0.45.

MATERIALS

An ASTM C150 Type I ordinary portland cement (OPC) was used in this study, with a Blaine fineness of 370 m^2/kg and an estimated Bogue composition of 56 % C_3S, 16 % C_2S, 12 % C_3A, 7 % C_4AF and a Na_2O equivalent of 0.68 % by mass.

The sand used was natural river sand with a fineness modulus of 2.71, an apparent specific gravity of 2.58, and water absorption of 1.0 % by mass. Portions of the normal weight sand were replaced with expanded shale with a fineness modulus of 3.10 and a specific gravity of 1.45 (LWA). The 24 hour absorption of the LWA was determined to be 17.5 % according to the paper towel method [NYDOT 2008, Castro et al. 2010].

Mixture proportioning

Twenty different mixtures were prepared. The mortars had a single volume fraction of fine aggregate (55% of the total volume) and different *w/c* (0.30, 0.36, 0.42, and 0.45). For each system LWA was used as a replacement of NWA at five different levels of normal weight sand (NWA): 0 %, 25 %, 50 %, 75 % and 100 % of the values calculated using Equation 1. It is important to note that replacement is on a total volume basis, the volume of aggregate (LWA and sand) remained constant at 55 % since only the sand was replaced with LWA. A list of the mixture proportions can be found in Table 1.

Mixing procedure

The mixing procedure used for the mortar was in accordance with ASTM C305 [ASTM 2006]. The LWA was oven dried, air cooled, and then submerged in water for 24 ± 1 h prior to mixing. The volume of water used to submerge the LWA included both mixing water and the water the LWA would absorb in 24 h. The excess water (water not absorbed in 24 h) was then decanted and used as the mixing water. The normal weight sand was oven dried and cooled for 24 h before mixing. For the plain mortar mixtures and the pastes, the water and cement were conditioned for 24 h at room temperature.

EXPERIMENTAL METHOD PROCEDURES

Water absorption

Six 100 mm × 200 mm cylinders were cast for water absorption testing for each mixture. After one day of curing, the samples were demolded and then sealed in a double layer of plastic bags for sealed curing. Bags were stored at 23 ± 1 °C until samples reached an age of 90 d. At that point the cylinders were removed from the bags and three 50 mm ± 2 mm thick samples were cut from the central portion of each cylinder using a wet saw.

After cutting, samples were conditioned by placing them in environmental chambers at 23 ± 0.5 °C and at two different relative humidities (65 ± 1 % and 80 ± 1 %). Samples were conditioned in the environmental chamber for a period of 9 months.

Once the samples were removed from the chambers the side surface (i.e. outer circumference) was sealed with aluminum tape and the top surface was covered with plastic to avoid evaporation from the sample during testing. After the samples were prepared, absorption testing was conducted in accordance with ASTM C1585 [ASTM 2004], with the exception of the conditioning method described above.

It should be noted, the effect of internal curing can be increased under sealed conditions employed in this study as compared with other curing conditions (unsealed curing or curing under lime water). In sealed curing, the internally cured specimens will have a greater amount of water available for hydration and will likely hydrate further. This will lead to a denser microstructure with lower transport coefficients. The authors considered that the sealed curing condition can represent appropriately the field conditions, and can also isolate the effect of internal curing on the specimens. However, the authors also consider that differences in the curing conditions for both internally and not internally cured specimens can affect the performance of the specimens.

Electrical impedance

Electrical conductivity of mortar samples was measured using cylindrical specimens (70 mm height and 35 mm diameter). Two 2.5 mm diameter rods spaced 20 mm were embedded longitudinally inside each mold (Figure 2).

A Solartron 1260™ Impedance Gain-Phase analyzer measured the impedance response of each specimen. The measurements were made over a frequency range from 1 MHz to 1 Hz, using a 100 mV AC signal. Measurements were performed at 3 d, 7 d, 90 d and 365 d.

The electrical conductivity was obtained from the measured bulk resistance according to Equation 3.

$$\sigma = \frac{k}{R} \qquad \text{(Equation 3)}$$

where σ is the conductivity (S/m), k is the geometry factor (1/m), and R is the bulk resistance (ohm). A geometry factor of k = 22.15/m was determined in this research for the used molds.

A modified parallel model is normally used to describe the electrical conductivity of the concrete [McCarter and Brousseau 1990, Rajabipour 2006]. Since the conductivity of liquid phase is several orders of magnitude higher that the conductivity of solid and vapor phases, concrete is normally considered as a composite material with a single conductive component and the modified parallel model can be simplified to Equation 4. It should be noted that this typically assumes only the fluid phase is conductive. For internally cured concrete mixtures however the water in the LWA may also be conductive and the implications of this will be discussed later in the paper.

$$\sigma = \sigma_o \phi_o \beta_o \qquad \text{(Equation 4)}$$

where:

σ_o = Conductivity of the pore solution, sigma notch (S/m)

ϕ_o = Volume fraction of pore solution (unitless)

β_o = Connectivity of pores structure (unitless)

EXPERIMENTAL RESULTS AND DISCUSSION

Water absorption

Figure 3 shows the cumulative absorbed water in the samples that were 1 year old (3 months of sealed curing and 9 months of conditioning) after 8 d of testing for samples conditioned at 65 % and 80 % relative humidity. Figure 4 show the initial sorptivity (i.e., related to the rate of water absorption) for samples conditioned at 65 % and 80 % relative humidity calculated as the slope of the absorption vs. the square root of time during the first six hours of test. Figure 5 show the secondary sorptivity for samples conditioned at 65 % and 80 % relative humidity calculated as the slope of the absorption vs. the square root of time from the second to the eight day of test.

From Figures 3 to 5 it can be noticed that the water absorption is very sensitive to both the relative humidity at which the specimens were pre-conditioned before testing [Castro et al. 2011] and the *w/c* of the systems. Samples conditioned at 65 % relative humidity show higher values than similar samples conditioned at 80 % relative humidity. Samples from the mixtures with a higher *w/c* show higher absorption values compared with samples with lower *w/c*, both conditioned at the same relative humidity.

These trends can be explained by the fact that water ingress in unsaturated concrete is dominated by capillary suction upon initial contact with water [Hall 1989]. Capillary absorption can be related to the volume of the pores as well as the size of empty capillary pores. Then, system with higher *w/c* will have a greater proportion of capillary pores. The relation between the equilibrated relative humidity and the radius of the smallest empty pore is given by the Kelvin-

Laplace equation. Using this equation it is possible to calculate that these capillary pores are filled with water vapor at relative humidities above 80 %.

As such, the relative humidity used to condition the sample prior to the sorption test and the *w/c* of the system can have a significant impact on the results. The higher the *w/c* of the system, the greater the total volume of capillary pores. The lower the relative humidity, the greater the total volume of pores that are empty and available to be filled with water during the sorption test. Further, the lower humidity will empty smaller pores, creating a higher suction force in the materials and resulting in a greater sorption rate and a larger overall total absorption.

From Figures 3 to 5 it can also be seen that the total volume of water and the rate of absorbed water decrease when a higher amount of LWA is used. This observation is independent of both the relative humidity used for conditioning and the *w/c* of the system. Even more, it can be observed that proportionally a greater benefit is obtained in those mixtures containing the highest *w/c*.

When water leaves the pores of the LWA it is available in the cement paste to enable additional hydration. This additional hydration results in a paste microstructure that is more dense which has a large impact on the cement paste matrix [Henkensiefken et al. 2009b]. Internal curing water can also increase the hydration of the areas surrounding the LWA [Henkensiefken et al. 2009b] producing a more dense ITZ [Zhang and Gjørv 1990, Elsharief et al. 2005]. Considering that the Interfacial Transition Zone (ITZ) of the normal weight aggregate (NWA) could be percolated across the 3D microstructure, the inclusion of the LWA could depercolate these ITZ pathways [Winslow et al. 1994, Bentz 2009, Peled et al. 2010]. If LWA, with the denser ITZ it creates, were added to the system, the NWA ITZ may not be as percolated, resulting in a lower absorption. As more LWA is used, the potential for percolation of the normal weight aggregate ITZ also decreases. If enough LWA is used, the ITZ of the NWA would depercolate [Bentz 2009]. For this reason, it could be expected that the absorption of mortars with LWA could be lower, even in system with a high *w/c*.

The benefits of internal curing are most dramatic for specimens in the sealed condition used in the study (as compared with curing under lime water). Under sealed conditions the internally cured specimens have a greater amount of water available for hydration than the plain samples. This increased hydration produces a more dense microstructure with lower transport coefficients (Bentz and Stutzman). The sealed curing condition is likely however a good representation for field concrete that uses a curing compound.

Electrical impedance

Figure 6 shows the electrical conductivity of sealed samples at the age of 3, 7, 90 and 365 days after casting. The systems with higher *w/c* have a higher conductivity due mainly to the higher volume of pore fluid as described by equation 4. The conductivity decreases with the time due to continued hydration which reduces the volume of conductive pore fluid by hydration which also makes the conduction path more tortuous.

The mixture with a *w/c* of 0.30 shows that internal curing results in a reduction of the measured conductivity which can be explained by the effect of the water provided for internal curing which helps to increase the hydration of the areas surrounding the LWA [Henkensiefken et al. 2009b]. However, in the systems with higher *w/c* an increase in the LWA content increases the electrical conductivity at early ages. This may be explained by the fact that these systems have water contained in the LWA particles that remains for a longer time in the LWA pores without reacting with the un-hydrated cement. As a result, the total amount of fluid in the system will be increased with additional LWA, thereby increasing the measured electrical conductivity of the samples.

As the samples hydrate (e.g. at 90 days), the system with *w/c* = 0.36 starts to show the benefits of internal curing, decreasing the conductivity. At this time, the systems with higher w/c still show higher conductivity with the use of LWA (again due to the additional water in the system). Finally at the age of 365 days, all the systems show the benefits of the use of internal curing. At this age a considerable reduction of the measured electrical conductivity can be observed.

The water for internal curing requires longer times to leave the LWA pores in the higher *w/c* systems due to the lack of a driving force (which is the under pressure build up due to self desiccation in the case of a low *w/c* system). However, at some point, the smaller pores of the cement paste will develop a meniscus which will make the water move from the LWA pores to the cement paste. Eventually, this water will react with the un-hydrated cement to increase the amount of hydration products reducing both the total porosity and the fluid filling the pores of the system. This will produce a reduction on the measured electrical conductivity.

A direct comparison of electrical conductivity of the system containing different *w/c* presents some difficulties, mainly because the complications associated with determining the volume fraction of pore solution at different ages. For this reason, after the electrical conductivity of the samples was measured in a sealed condition at the age of 365 d, samples were vacuum saturated for 24 hours using tap water. After saturation, electrical conductivity was measured again and results are shown in Figure 7.

The conductivities presented in Figure 7 are proportional to the total volume of accessible pores and their connectivity through the samples. These are parameters that can be used to describe the transport of fluid in concrete [Rajabipour and Weiss 1997]. Then, Figure 7 shows that using internal curing on systems with high *w/c* help to reduce the connectivity of the porosity, which helps to reduce the fluid transport in concrete.

Comparing Figures 6d) and 7 it can be observed that the electrical conductivity increases when samples were re-saturated. It can be explained by the fact that resaturation results in a higher volume of pore fluid as described by equation 4. However it is important to note that sample re-saturation does not seem to fill the LWA pores, because an increment of conductivity with the percentage of LWA is not observed.

Empirical relations for water absorption and electrical conductivity

Analyzing the data from Figures 3, 4 and 5 it is possible to obtain an empirical relationship for the cumulative absorption, the initial and secondary sorptivity which is presented in Equation 5.

From Figure 7 it is possible to obtain an empirical relationship for the saturated electrical conductivity, which is presented in Equation 6.

$$Absorption\ equations = C_1 \cdot (w/c)^{C_2} \cdot \exp\ (-C_3 \cdot IC) \qquad \text{(Equation 5)}$$

$$Conductivity = [C_4 \cdot (w/c) - C_5] \cdot \exp\ [(-C_6 \cdot (w/c) + C_7) \cdot IC] \qquad \text{(Equation 6)}$$

where "*w/c*" is the water to cement ratio (e.g. 0.36), "*IC*" is the internal curing percentage from Equation 1 (e.g. IC = 50 is 50% of the IC water predicted from equation 1), and C_1, C_2, C_3, C_4, C_5, C_6 and C_7 are the regression constants the values of which are included in Table 2.

Figure 8 illustrates the proportional reduction of water absorption, initial sorptivity and secondary sorptivity on the internally cured samples. Figure 9 illustrates the proportional reduction on electrical conductivity of 1-year old saturated internally cured samples.

From Figure 8 it can be seen that when LWA is added according to the Bentz and Snyder approach (equation 1), the internally cured system shows an average reduction of 55 % in the initial sorptivity and the 8-days cumulated absorption, and 70 % in the secondary sorptivity, independently of the relative humidity at which the samples were conditioned prior testing. From Figure 9 it can be seen that internal curing is more efficient to reduce the electrical conductivity in high *w/c* systems that in low *w/c* systems. A reduction of 40 % in conductivity is observed on the system with *w/c* of 0.30, but a reduction of 75 % is observed on the system with *w/c* of 0.45.

CONCLUSIONS

A series of twenty mortars were prepared to evaluate the effect of internal curing on the fluid transport properties of mortars over a range of *w/c*'s. The effect of internal curing was evaluated using water absorption and electrical conductivity measurements.

The total absorbed water was reduced when the level of internal curing was increased. This reduction in water absorption was known for the system with the low *w/c*, but the results show

that the benefits are extendible to systems with higher *w/c*. These benefits were also observed in reducing the rate of water absorption showing a lower initial and secondary sorptivity. An average maximum reduction of 55 % was observed in both the initial sorptivity and cumulated absorption and a maximum reduction of 70 % was observed in the secondary sorptivity.

Electrical conductivity tests, performed in sealed samples a year after casting, show a benefit in the use of internal curing in mortar systems containing low *w/c* as expected, but also in systems with higher *w/c*. The effect of internal curing is proportionally larger in samples prepared with the highest *w/c*. A reduction of 40 % is observed on the system with *w/c* of 0.30, this reduction was observed to increase to 75 % on the system with *w/c* of 0.45.

The benefits of internal curing are most dramatic for specimens in the sealed condition used in the study as compared with curing under lime water. Under sealed conditions the internally cured specimens have a greater amount of water available for hydration than the plain samples. This increased hydration produces a more dense microstructure with lower transport coefficients.

Precaution are needed for interpreting the electrical properties of IC concrete at an early age due to the higher amount of fluid present in system when prewetted LWA is added.

ACKNOWLEDGMENTS

This work was supported in part by the Expanded Shale, Clay and Slate Institute (ESCSI) and by the Joint Transportation Research Program administered by the Indiana Department of Transportation and Purdue University (Project SPR 3211) and the authors gratefully acknowledge that support. The contents of this paper reflect the views of the authors, who are responsible for the facts and the accuracy of the data presented herein, and do not necessarily reflect the official views or policies of the Indiana Department of Transportation, nor do the contents constitute a standard, specification, or regulation. The experiments reported in this paper were conducted in the Pankow Materials Laboratories at Purdue University. The authors acknowledge the support that has made this laboratory and its operation possible.

REFERENCES

ACI Committee 231 (2010). "Report on early-age cracking: causes, measurement and mitigation." American Concrete Institute - Committee 231, Farmington Hills, MI, p. 48.

ACI SP-256 (2008). "Internal curing of high performance concrete: laboratory and field experiences." American Concrete Institute, Farmington Hills, MI, p. 110.

ASTM Standard C1585 (2004). "Standard test method for measurement of rate of absorption of water by hydraulic-cement concretes." ASTM International, West Conshohocken, PA.

ASTM Standard C305 (2006). "Standard practice for mechanical mixing of hydraulic cement pastes and mortars of plastic consistency." ASTM International, West Conshohocken, PA.

ASTM Standard C128 (2007). "Standard test method for density, relative density (specific gravity), and absorption of fine aggregate." ASTM International, West Conshohocken, PA.

Barcelo, L., Boivin, S., Rigaud, S., Acker, P., Clauvaud, B. (1999). "Linear vs volumetric autogenous shrinkage measurements: material behavior or experimental artefact." In: Persson B, Fagerlund G, editors. Proceedings of the second international seminar on self-desiccation and its importance in concrete technology, Lund University, Sweden; p. 109–125.

Bentz, D.P. and Snyder, K.A. (1999). "Protected paste volume in concrete: Extension to internal curing using saturated lightweight fine aggregate." *Cem. Concr. Res*., 29(11), 1863-1867.

Bentz, D.P., Lura, P. and Roberts, J.W. (2005). "Mixture proportioning for internal curing." *Concr. Inter.*, 27(2), 35-40.

Bentz, D.P. and Jensen, O.M (2006). "Mitigation strategies for autogenous shrinkage cracking." *Cem. Concr. Compos*., 26(6), 677-685.

Bentz, D.P. (2009). "Influence of internal curing using lightweight aggregates on interfacial transition zone percolation and chloride ingress in mortars." *Cem. Concr. Compos.*, 31(5), 285-289.

Bentz, D.P. and Weiss, J. (2011). "Internal curing: A 2010 state of the art review." National NISTIR 7765. Institute of Standards and Technology, U.S. Department of Commerce. Gaithersburg, MD.

Byard, B.E, Schindler, A.K. and Barnes, R.W (2010). "Cracking tendency of lightweight concrete in bridge deck applications." Proceedings of the concrete bridge conference, Phoenix, Arizona.

Castro, J., Keiser, L. Golias, M., Weiss, J. (2010a). "Absorption and desorption properties of fine lightweight aggregate for application to internally cured concrete mixtures". Submitted to *Cem. Concr. Compos*.

Castro, J., Bentz, D., Weiss, J. (2010b). "Effect of sample conditioning on the water absorption of concrete." Submitted to *Cem. Concr. Compos*.

Couch, J., Lura, P., Jensen, O. and Weiss, J. (2006). "Use of acoustic emission to detect cavitation and solidification (time zero) in cement pastes." In: International RILEM conference on volume changes of hardening concrete: testing and mitigation. Jensen O, Lura P, Kovler K, editors; 2006. Denmark, pp. 393-400.

Cusson, D. and Hoogeveen, T. (2008). "Internal curing of high-performance concrete with pre-soaked lightweight aggregate sand for prevention of autogenous shrinkage cracking." *Cem. Concr. Res*., 38(6), 757-765.

Elsharief, A., Cohen, M. and Olek, J. (2005). "Influence of lightweight aggregate on the microstructure and durability of mortar." *Cem. Concr. Res*., 35(7), 1368-1376.

Geiker, M. (1983). "Studies of Portland cement hydration by measurements of chemical shrinkage and a systematic evaluation oh hydration curves by means of the dispersion model." PhD Dissertation, Technical University of Denmark.

Hall, C. (1989). "Water sorptivity of mortars and concretes: a review." Mag. Concr. Res., 41(146), 51-61.

Henkensiefken, R., Nantung, T. and Weiss, W. (2008). "Reducing restrained shrinkage cracking in concrete: examining the behavior of self-curing concrete made using different volumes of saturated lightweight aggregate." In: National concrete bridge conference, St. Louis, MO.

Henkensiefken, R., Bentz, D., Nantung, T., Weiss, J. (2009a). "Volume change and cracking in internally cured mixtures made with saturated lightweight aggregate under sealed and unsealed conditions." *Cem. Concr. Compos*., 31(7), 427-437.

Henkensiefken, R., Castro, J., Bentz, D., Nantung, T. and Weiss, J. (2009b). "Water absorption in internally cured mortar made with water-filled lightweight aggregate." *Cem. Concr. Res*., 39(10), 883-892.

Henkensiefken, R., Briatka, P., Nantung, T., Bentz, D. and Weiss, J. (2010). "Plastic shrinkage cracking in internally cured mixtures made with pre-wetted lightweight aggregate." Concr. Inter., 32(2), 49-54.

Jensen, O.M. and Hansen, P.F. (2001a). "Water-entrained cement-based materials: I. Principles and theoretical background. Cem Concr Res 2001a; 31(4): 647-654.

Jensen, O.M, and Hansen, P.F. (2001b). "Autogenous deformation and rh-change in perspective. *Cem. Concr. Res*., 31(12), 1859-1865.

Jensen, O.M. (2005). "Autogenous Phenomena in Cement-Based Materials." PhD Thesis. Aalborg University, 2005.

Le Chatelier, H., (1900). “Sur les changements de volume qui accompagent le durcissement des ciments.” In Bulletin Societe de l'encouragement pour l'industrie nationale. Paris, France.

L’Hermite, R.G. (1960). “Volume changes of concrete.” In 4th International symposium on the chemistry of cement. Washington DC.

Lopez, M., Kahn, L.F. and Kurtis, K.E. (2009). “Characterization of elastic and time-dependent deformations in high performance lightweight concrete by image analysis.” *Cem. Concr. Res*., 39(7), 610-619.

Lura, P., Couch, J., Jensen, O.M. and Weiss, J. (2009). “Early age acoustic emission measurement in hydrating cement paste: Evidence for cavitation during solidification due to self-desiccation.” *Cem. Concr. Res*., 39 (10): 861-867.

McCarter, W. and Brousseau, R. (1990). “The A.C. response of hardened cement paste.” *Cem. Concr. Res*., 20(6): 891-900.

NYDOT. (2008). “Test Method No.: NY 703-19 E: Moisture content of lightweight fine aggregate.” New York State Department of Transportation, Materials Bureau, Albany, NY.

Peled, A., Castro, J. and Weiss, J. (2010). “Atomic force microscopy examinations of mortar made by using water-filled lightweight aggregates.” *Transp. Res. Rec*., 2141: 92-101.

Powers, T. (1935). “Absorption of water by portland cement paste during the hardening process.” *Ind. Eng Chem*., 27(7), 790–4.

Radlinska, A., Rajabipour, F., Bucher, B., Henkensiefken, R., Sant, G., Weiss, J. (2008). “Shrinkage mitigation strategies in cementitious systems: a closer look at sealed and unsealed material behavior.” *Transp. Res. Rec*., 2070: 58–67.

Rajabipour, F. (2006), "In Situ Electrical Sensing and Material Health Monitoring in Concrete Structures", PhD Dissertation, Purdue University p. 173.

Rajabipour, F. and Weiss, J. (2007). "Electrical conductivity of drying cement paste." *Mater. Struct.* 2007(40),1143-1160.

RILEM Report 41 (2007). "Internal curing of concrete – state of the art." Kovler, K. And Jensen, O.M. editors. RILEM Publications S.A.R.L; 2007, p. 161.

Sant, G., Lura, P. and Weiss, J. (2006). "Measurement of volume change in cementitious materials at early ages: review of testing protocols and interpretation of results." *Transp. Res. Rec*., 1979, 21-29.

Schlitter, J., Henkensiefken, R., Castro, J., Raoufi, K., Weiss, J. and Nantung, T. (2010). "Development of internally cured concrete for increase service life." JTRP Report SPR-3211, p. 252.

Winslow, D.N., Cohen, M., Bentz, D., Snyder, K. and Garboczi, E. (1994). "Percolation and pore structure in mortars and concrete." *Cem. Concr. Res*., 24(1), 25-37.

Zhang, M.-H. and Gjørv, O.E. (1990). "Microstructure of the interfacial zone between lightweight aggregate and cement paste." *Cem. Concr. Res*., 20(4), 610-618.

Table headings

Table 1. Mixture Proportions for the Internally Cured Mixtures.

Table 2. Parameters for Equation 5 and 6

Table 1. Mixture Proportions for the Internally Cured Mixtures.

w/c	% LWA from Eq. 1	Cement (kg/m^3)	Mixing Water (kg/m^3)	NWA, SSD (kg/m^3)	LWA, Dry (kg/m^3)	IC Water (kg/m^3)	Aggregate Volume (%) NWA	LWA	Total
0.30	0%	727.0	218.1	1429.7	0.0	0.0	55.0	0.0	55.0
	25%	727.0	218.1	1330.2	55.4	9.7	51.2	3.8	55.0
	50%	727.0	218.1	1230.6	110.8	19.4	47.3	7.7	55.0
	75%	727.0	218.1	1131.1	166.2	29.1	43.5	11.5	55.0
	100%	727.0	218.1	1031.5	221.6	38.8	39.7	15.3	55.0
0.36	0%	662.6	238.6	1419.7	0.0	0.0	55.0	0.0	55.0
	25%	662.6	238.6	1320.9	60.6	10.6	50.8	4.2	55.0
	50%	662.6	238.6	1212.0	121.2	21.2	46.6	8.4	55.0
	75%	662.6	238.6	1103.1	181.8	31.8	42.4	12.6	55.0
	100%	662.6	238.6	994.2	242.4	42.4	38.2	16.8	55.0
0.42	0%	608.7	255.7	1429.7	0.0	0.0	55.0	0.0	55.0
	25%	608.7	255.7	1329.7	55.7	9.7	51.2	3.8	55.0
	50%	608.7	255.7	1229.7	111.4	19.4	47.3	7.7	55.0
	75%	608.7	255.7	1129.7	167.1	29.1	43.5	11.5	55.0
	100%	608.7	255.7	1029.7	222.8	38.8	39.6	15.4	55.0
0.45	0%	584.9	263.2	1429.7	0.0	0.0	55.0	0.0	55.0
	25%	584.9	263.2	1333.6	53.5	9.4	51.3	3.7	55.0
	50%	584.9	263.2	1237.5	107.0	18.8	47.6	7.4	55.0
	75%	584.9	263.2	1141.4	160.5	28.2	43.9	11.1	55.0
	100%	584.9	263.2	1045.3	214.0	37.6	40.2	14.8	55.0

Table 2. Parameters for Equation 5 and 6

Parameters	Water Absorption at 8 days		Initial Sorptivity		Secondary Sorptivity		1-year Electrical Conductivity
	65% RH	80% RH	65% RH	80% RH	65% RH	80% RH	Saturated
C_1	72.776	19.391	0.084	0.045	0.113	0.019	-
C_2	3.93	3.35	3.30	4.06	4.57	3.20	-
C_3	0.0093	0.0084	0.0080	0.0083	0.0127	0.0106	-
C_4	-	-	-	-	-	-	184.59
C_5	-	-	-	-	-	-	46.915
C_6	-	-	-	-	-	-	0.0558
C_7	-	-	-	-	-	-	0.0108

Figure captions

Fig 1 Water for internal curing needed to maintain saturated condition in cement paste (after Bentz et al. 2005)

Fig 2 Picture of the mold used for continuous electrical conductivity measurements

Fig 3 Cumulative amount of water absorbed after 8 days of testing for samples conditioned at: a) 65% RH and b) 80% RH. Error bars represent the standard deviation on the average of 3 samples. Continues lines represent empirical equations described at the end of the paper

Fig 4: Initial sorptivity as a function of the w/c and the amount of LWA for samples conditioned at: a) 65% RH and b) 80% RH. Error bars represent the standard deviation on the average of 3 samples. Continues lines represent empirical equations described at the end of the paper

Fig 5 Secondary sorptivity as a function of the w/c and the amount of LWA for samples conditioned at: a) 65% RH and b) 80% RH. Error bars represent the standard deviation on the average of 3 samples. Continues lines represent empirical equations described at the end of the paper

Fig 6 Electrical conductivity of sealed samples as a function of the amount of LWA at the age of: a) 3 days, b) 7 days, c) 90 days, and d) 365 days. Error bars represent the standard deviation on the average of 3 samples.

Fig 7 Electrical conductivity of vacuum saturated samples at the age of 365 days. Error bars represent the standard deviation on the average of 3 samples. Continues lines represent empirical relations described in a further section.

Fig 8 Proportional reduction on the absorption, initial sorptivity and secondary sorptivity of internally cured samples

Fig 9 Proportional reduction on the electrical conductivity of 1-year old saturated internally cured samples

Figures:

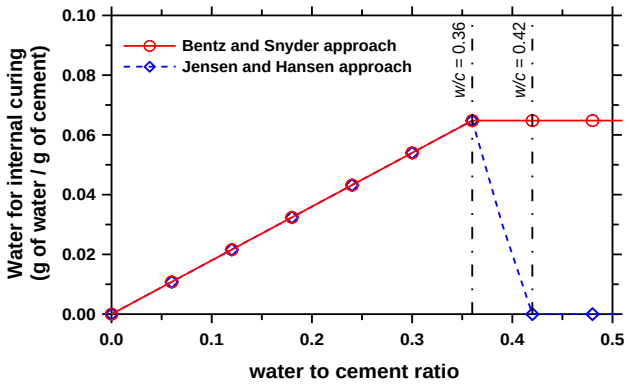

Fig 1 Water for internal curing needed to maintain saturated condition in cement paste (after Bentz et al. 2005)

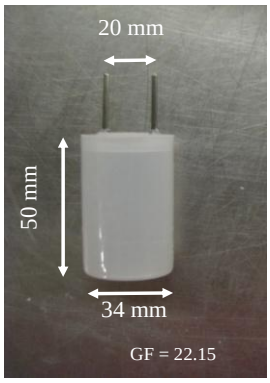

Fig 2 Picture of the mold used for continuous electrical conductivity measurements

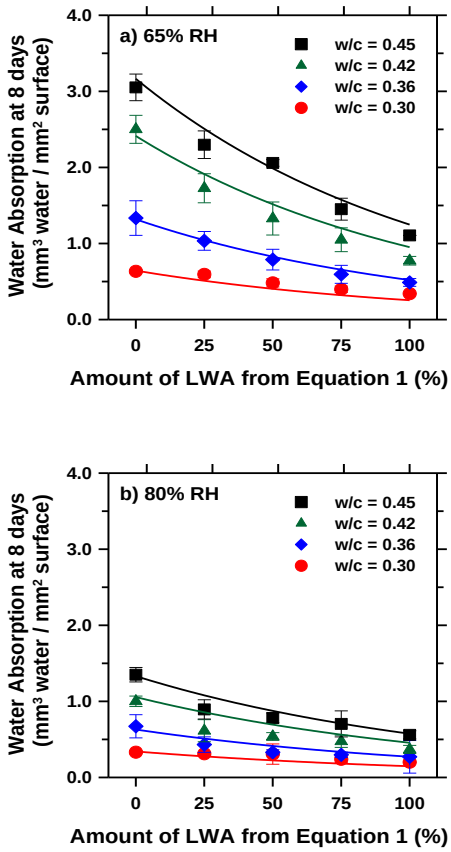

Fig 3 Cumulative amount of water absorbed after 8 days of testing for samples conditioned at: a) 65% RH and b) 80% RH. Error bars represent the standard deviation on the average of 3 samples. Continues lines represent empirical equations described at the end of the paper

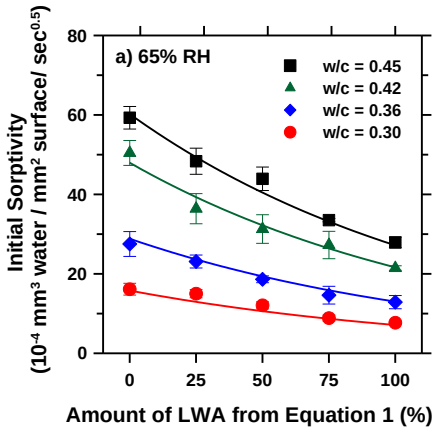

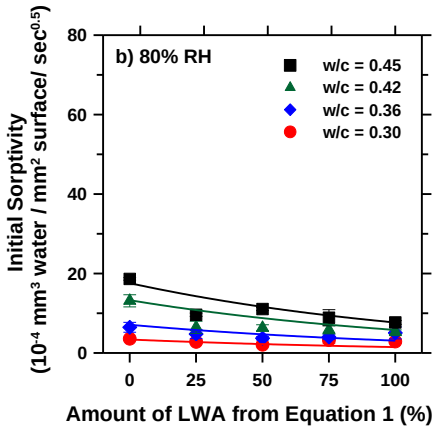

Fig 4: Initial sorptivity as a function of the w/c and the amount of LWA for samples conditioned at: a) 65% RH and b) 80% RH. Error bars represent the standard deviation on the average of 3 samples. Continues lines represent empirical equations described at the end of the paper

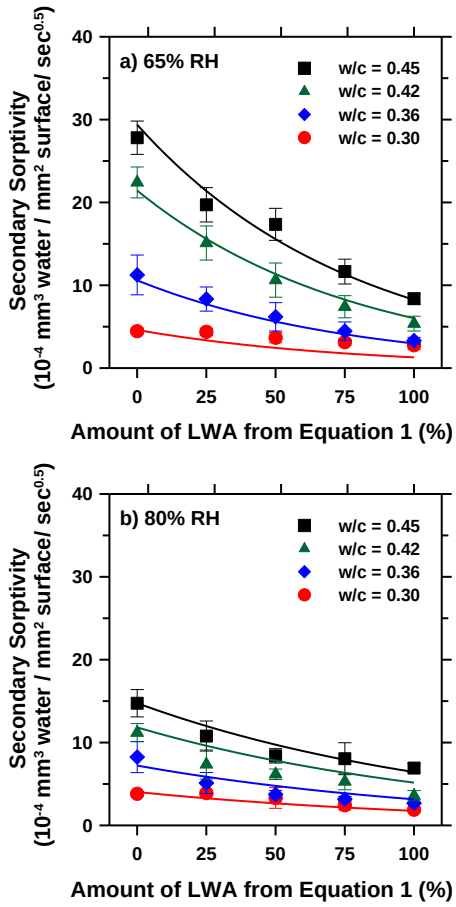

Fig 5 Secondary sorptivity as a function of the w/c and the amount of LWA for samples conditioned at: a) 65% RH and b) 80% RH. Error bars represent the standard deviation on the average of 3 samples. Continues lines represent empirical equations described at the end of the paper

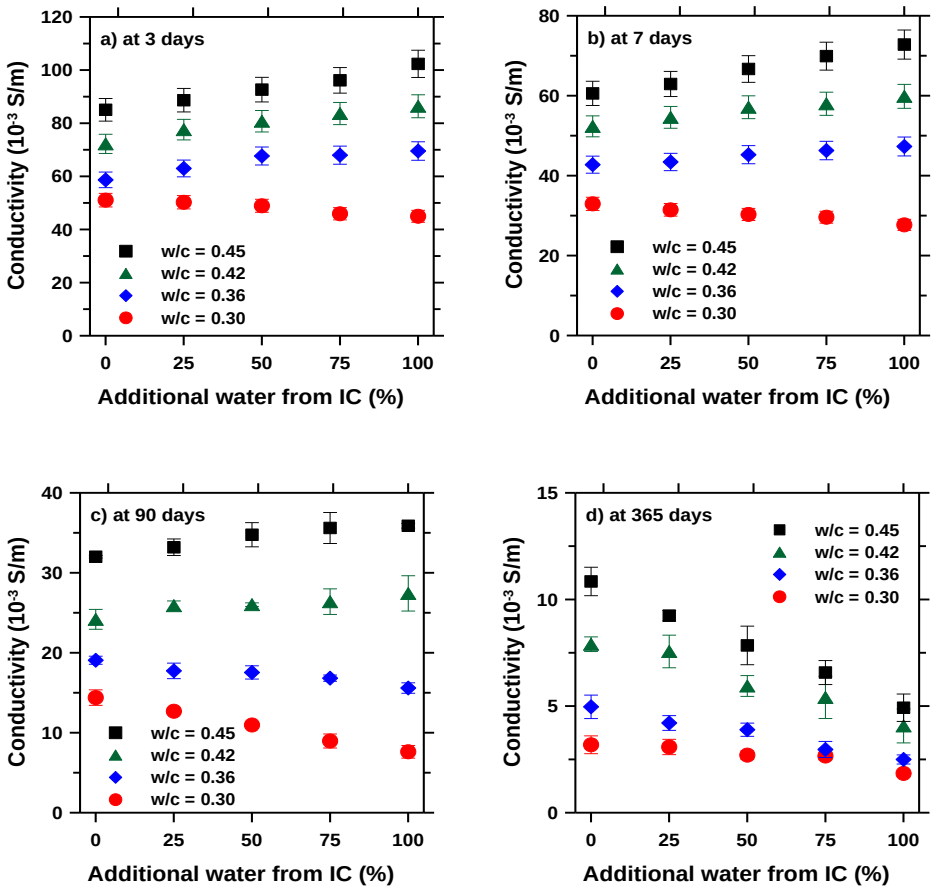

Fig 6 Electrical conductivity of sealed samples as a function of the amount of LWA at the age of: a) 3 days, b) 7 days, c) 90 days, and d) 365 days. Error bars represent the standard deviation on the average of 3 samples.

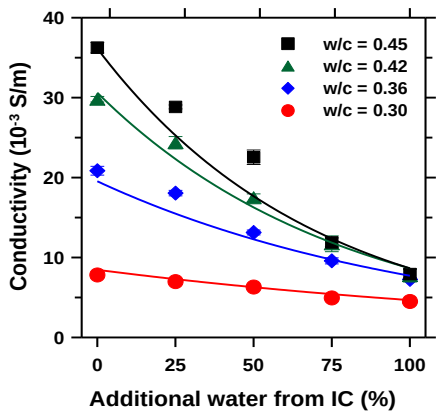

Fig 7 Electrical conductivity of vacuum saturated samples at the age of 365 days. Error bars represent the standard deviation on the average of 3 samples. Continues lines represent empirical relations described in a further section.

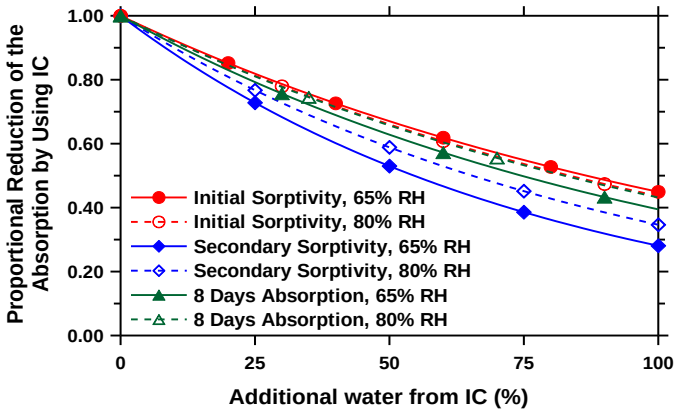

Fig 8 Proportional reduction on the absorption, initial sorptivity and secondary sorptivity of internally cured samples

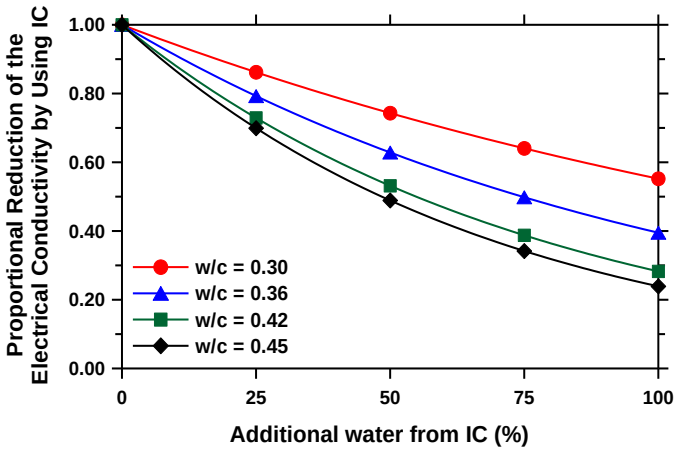

Fig 9 Proportional reduction on the electrical conductivity of 1-year old saturated internally cured samples

Water Absorption and Critical Degree of Saturation as it Relates to Freeze-Thaw Damage in Concrete Pavement Joints

Wenting Li[1], Mohammad Pour-Ghaz[2], Javier Castro[3], and Jason Weiss[4] (Corresponding author)

ABSTRACT: Fluid ingress is a primary factor that influences freeze-thaw damage in concrete. This paper discusses the influence of fluid ingress on freeze-thaw damage development. Specifically, this paper examines the influence of entrained air content on the rate of water absorption, the degree of saturation, and the relationship between the saturation level and freeze-thaw damage. The results indicate that while air content delays the time it takes for concrete to reach a critical degree of saturation it will not prevent the freeze-thaw damage from occurring. The results of the experiments show that when the degree of saturation exceeds 86 to 88% freeze-thaw damage is inevitable with or without entrained air, even with very few freeze-thaw cycles.

CE Database subject headings: Absorption, Acoustic techniques, Air entrainment, Concrete, Concrete pavement, Saturation, Deterioration, Freeze and thaw, Pavements, Joints.

Author keywords: Absorption, Acoustic emission, Air content, concrete, Concrete pavement, Degree of saturation, Deterioration, Freeze-thaw, Pavement joint, Water absorption

[1] Graduate Research Assistant, School of Materials Science, Southeast University, Nanjing 211189, China, and Graduate Research Assistant, School of Civil Engineering, Purdue University, 550 Stadium Mall Drive, West Lafayette, Indiana, USA, Phone: (765) 494 – 7999, li448@purdue.edu.

[2] Graduate Research Assistant, School of Civil Engineering, Purdue University, 550 Stadium Mall Drive, West Lafayette, Indiana, USA, Phone: (765) 494 – 7999, pourghaz@purdue.edu.

[3] PhD Candidate, School of Civil Engineering, Purdue University, 550 Stadium Mall Drive, West Lafayette, Indiana, USA, Phone: (765) 494 – 7999, jcastro@purdue.edu.

[4] Professor, director of Pankow Materials Laboratory, Purdue University, 550 Stadium Mall Drive, Indiana, USA, Phone: (765) 496 – 2215, Fax: (765) 496 – 1364, wjweiss@ecn.purdue.edu.

Background on the Problem of Joint Deterioration in Concrete Pavements

Concrete pavements represent a large portion of the transportation infrastructure. While many of these pavements provide excellent long-term performance, a portion of these pavements have recently shown premature joint deterioration throughout the Midwestern states (Weiss et al. 2007; Sutter et al. 2006; Leech et al. 2008; Rangaraju et al. 2006). This joint deterioration is problematic since it compromises the performance and potential service life of an otherwise healthy pavement. Figure 1 shows photographs of a typical damaged pavement joint. This type of damage is frequently seen as either the development of cracking parallel to the joint or spalling and cracking at the joint from the bottom of the saw cut to the surface of pavement approximately 4 to 6 inches from the joint. Unfortunately damage is not frequently observed at the surface of the pavement until a significant amount of damage has occurred inside the joint. During field inspections it has been observed that where the joints are damaged the sealant is damaged and the joint contained standing water. Research is needed to better understand how this standing water may lead to freeze-thaw damage. Further, this damage occurs in both poorly air entrained and properly air entrained concrete. As a result the role of air content needed to be quantified which is the reason for this study.

Background on Water Absorption and the Critical Degree of Saturation

Concrete is susceptible to freeze and thaw damage when it is saturated (Sutter et al. 2006; Leech et al. 2008; Rangaraju et al. 2006; Fagerlund 1972, 1975, 1977, 1979, 1981, 2004; Bentz et al. 2001; Litvan 1988; Litvan and Sereda 1980; Shimada et al. 1991, Beaudoin and Cameron 1972; Feldman 1987; Scherer 1993; Scherer and Valenza 2005; Sun et al. 2007). While the water content in concrete can be quantified in several different ways, this paper defines the degree of saturation (S) as the ratio of the absolute volume of absorbed water to the total volume of pores (i.e., the total volume of water that can be absorbed by concrete).

It has been suggested that there is a critical degree of saturation (S_{cr}) beyond which freeze and thaw damage can begin to initiate (Fagerlund 1972, 1975, 1977, 1979, 1981, 2004; Bentz et al. 2001; Litvan 1988; Litvan and Sereda 1980; Shimada et al. 1991, Beaudoin and Cameron 1972). For degrees of saturation below the critical degree of saturation freeze-thaw damage is not observed to occur even after a large number of freeze-thaw cycles (Fagerlund 1972, 1975, 1977, 1979, 1981, 2004; Bentz et al. 2001; Litvan 1988; Litvan and Sereda 1980; Shimada et al. 1991, Beaudoin and Cameron 1972).

Figure 2 schematically illustrates the concept of water absorption and the critical degree of saturation (Fagerlund 2004; Barde et al. 2009). We can begin by assuming that the representative volume element shown in Figure 2 is filled with pores with different sizes at a given spacing. It

is assumed that there are two critical values that describe the freeze-thaw performance. The first parameter is related to the degree of saturation as described above. The second parameter is related to a "critical flow distance" (i.e., D_{cr}), which is the maximum distance that water can flow from freezing site to the surrounding nearest air-filled space. Damage doesn't occur when the flow distance (D) is below the critical distance (D_{cr}) and the degree of saturation (S) is less than the critical degree of saturation (S_{cr}) as shown in Fig. 2(*a*). However, the flow distance increases with the amount of absorbed water (or poor quality air void system), as does the degree of saturation. If either the critical flow distance or the critical degree of saturation is exceeded, frost damage initiates upon the next freezing cycle. The degree of damage can be quantified by the reduction in the dynamic elastic modulus of concrete as shown schematically in Fig. 2(*d*).

In Fig. 2(*d*) for all the values of degree of saturation below the critical degree of saturation the amount of damage (reduction is the elastic modulus) is very small. As soon as the degree of saturation exceeds the critical degree of saturation damage initiates in the material (Fagerlund 1972, 1975, 1977, 2004; Bentz et al. 2001).

It should be noted that the quality of air distribution and the volume of the air are two important parameters affecting the freeze-thaw resistance of the system. The quality of the air system is related to the critical flow distance while the quantity of the air voids (volume of air) is related to the critical degree of saturation. A fully saturated system, however, regardless of the

quantity and quality of the air cannot even sustain a single freezing cycle without accumulating a significant amount of damage (Litvan 1988).

Background on Use of Acoustic Emission to Quantify Freeze and Thaw Damage

Acoustic emission (AE) is a nondestructive test method that is based on measuring the release of energy in concrete (e.g. the release of energy that occurs at the time of cracking). It should also be noted that AE can be performed in either a passive (i.e., capturing the acoustic wave generated due to formation of permanent defect such as crack) or active (i.e., using one transducer to generate a pulse and another transducer to capture the same pulse (in the simplest arrangement)). Classically AE is typically performed in passive mode in cement/concrete studies (Ohtsu 1999, 1993; Bentz et al. 2008; Hossain et al. 2003; Shah and Weiss 2006; Kim and Weiss 2003; Moon and Weiss 2006; Ouyang et al. 1991a, 1991b; Suari and Van Mier 1995, 1993; Pour-Ghaz et al. 2010; Puri and Weiss 2003; Yang et al. 2006; Yoon et al. 1999). AE has been used in concrete to assess damage due to restrained shrinkage (Bentz et al. 2008; Hossain et al. 2003; Shah and Weiss 2006; Kim and Weiss 2003; Moon and Weiss 2006) and mechanical loading (Ouyang et al. 1991a, 1991b; Suari and Van Mier 1995, 1993; Pour-Ghaz et al. 2010; Puri and Weiss 2003; Yang et al. 2006; Yoon et al. 1999). AE has also been used to monitor freezing and thawing of mortar and it was observed that activity during both freezing and

thawing (Shimada et al. 1991; Krishnan 2002).

In the present work, the evolution of damage in concrete during freeze–thaw cycles was monitored using both active and passive AE. The reduced relative dynamic elastic modulus was calculated for each cycle according to the transmitting time of waves using active AE. Passive AE was recorded to better understand the damage that develops during the freeze-thaw cycle.

Hypothesis and Outline for Experimental Investigation

There has been a great deal of debate on possible causes of joint deterioration in concrete pavements. It is the hypothesis of this work that the presence of water (or solution containing deicing salt solutions) in the joints plays a significant role in the deterioration of concrete pavement joints. First, it is hypothesized that joints can hold water or deicing fluids substantially longer than other parts of the pavement. This would enable the concrete at the joint to become preferentially saturated. The potential for a joint to hold water increases when the joint sealant is damaged or missing, at low spots in the pavement, and when the joint does not crack and open as designed (as has been noticed in the field). It is hypothesized that this propensity for saturation could make the concrete more susceptible to local freeze-thaw damage. Second, it is hypothesized that the use of air entrainment can increase the resistance to joint deterioration however it also believed that the use of air entrainment will not eliminate the potential for damage to occur. The addition of air entrainment is believed to extend the time required for the

concrete to reach to the critical degree of saturation.

While other factors can contribute to joint deterioration (e.g., the use of specific deicers, curing conditions, mixture proportions, construction details), they are not specifically considered in this paper. The scope of this paper is to examine the role of air entrainment on the rate of water ingress and degree of saturation increase in concrete. Second, this paper provides data to relate the degree of saturation to freeze-thaw damage in air entrained and non-air entrained concrete.

Experimental Plan

This section describes mixture proportioning, specimen conditioning and the procedures of the testing in detail.

Mixture Proportions

Three mortar mixtures were prepared with different air contents (6, 10, 14% air by volume as measured in mortar). The air volume was calculated for an equivalent paste and concrete system respectively with the assumptions shown in Table 1. All specimens were made with ordinary Portland cement (Type I) and had a water to cement ratio (w/c) of 0.42 which is typical of concrete pavements in the state of Indiana. Table 1 presents the proportions of the materials that were used.

Mixing was performed in accordance with ASTM C192-06 (ASTM 2006). Two specimen geometries were used in this study: cylinders (25 mm height by 100 mm diameter) and prisms

(25 mm by 25 mm by 125 mm). Cylindrical specimens were used the water absorption test. The prisms specimens were used to evaluate the freeze-thaw damage development using AE. These specimens were cut from larger specimens.

Specimen Conditioning

The method of the specimen conditioning prior to water absorption testing can substantially influence the results of the test (Castro et al. 2010a, 2010b, 2010c; Spragg et al. 2011). If the specimen is not properly conditioned it can lead to a misunderstanding of the actual absorption behavior (Castro et al. 2010a, 2010b, 2010c; Spragg et al. 2011). Due to the significance of conditioning and necessity for the specimens to reach equilibrium the standard curing procedures was not used (Scherer and Valenza 2005). The procedure that was used in this study allowed the specimens to equilibrate for a longer period.

The cylindrical specimens were cut 24 hours after casting from a larger cylindrical sample and sealed in two layers of plastic. The specimens were stored at 23 +/- 1°C for 28 days. After 28 days the specimens were removed from the plastic bag and placed in 50 +/- 1, 65 +/-1 and 80 +/-1% relative humidity (RH) environments where they were kept for more than a year to equilibrate. Table 2 lists the air content and relative humidity of each specimen.

Water Absorption

A procedure similar to ASTM C1585-04 (ASTM 2004) was used however the specimens

were not conditioned following the accelerated ASTM testing procedure (described above). After conditioning, the outer circumference of the specimen was sealed with two layers of epoxy resin. After the epoxy hardened, the specimens were placed under water. Two small spacers were placed under the sample to provide a small gap between the bottom of the container and the lower surface of the sample. This allowed water absorption from both circular surfaces (Fig. 3).

Freeze-Thaw Testing

This section describes specimen preparation and procedures used in freeze-thaw testing.

Specimen Saturation

The prismatic specimens were prepared to have different degrees of saturation before freeze-thaw testing was performed. The specimens were oven dried in steps to 105°C where they were maintained for 2 days. The specimens were then placed in a desiccator and evacuated to a residual pressure of 30mm Hg (4000 Pa) for 3 hours. After evacuation and while still under vacuum, water was introduced into the desiccators to cover the specimens. The specimens were left in the desiccators for 24 hours. This condition was considered as saturated (i.e., 100% degree of saturation). The degree of saturation was reduced for some specimens (i.e. 0.96, 0.92, 0.90, 0.86, 0.82, and 0.78) by short periods of drying at 23°C and 50% relative humidity. During the drying period the mass of the specimens was closely monitored. After drying all the specimens were sealed in plastic bags for a minimum of 3 days to allow moisture to re-distribute before

freezing and thawing testing.

Preparation of the Specimen for Freezing and Thawing

Figure 4 shows the procedure used for preparing the specimens for AE testing during freeze-thaw cycles. The specimens were first preconditioned to different degrees of saturation as described in section 5.4.1. After preconditioning the specimens were wrapped with a thin plastic sheet as shown in Fig. 4(*a*). The thin plastic sheet was used to protect the sample from further drying during the handling. The specimens were then sealed with a "heat shrink wrap" to further protect the specimens against moisture exchange with surroundings (prevent them from absorbing or releasing water during the freeze-thaw process) as shown in Fig. 4(*b*). It is important to note that the "heat shrink wrap" was in loose contact with sample (with the exception of the specimen ends) so that the specimen can expand freely during the test while minimizing any restraint.

The AE sensors (transducers) were attached on the two ends with a thin layer of vacuum grease as shown in Fig. 4(*c*). Figure 5 shows that all the specimens were placed on a suspended base in testing to minimize noise/vibration transmission from surrounding environment. The threshold was set at 60 dB and 34 dB for active and passive AE, respectively. Testing was also performed on dry specimens to ensure that sounds were not being recorded from the environment, freezing unit, or coupling agent (Pour-Ghaz and Weiss 2010).

Temperature Cycle used for Freeze-Thaw Testing

Figure 6 shows the temperature cycle (in air) which allows one cycle per day. Temperature was controlled to vary from 10 +/- 1°C to -18 +/- 1°C. The rate of the temperature change was 14°C/hour resulting in a 2-hour transition period and two 10–hour periods at 10 +/-1 °C and -18 +/-1 °C respectively.

Experimental Results and Discussion

Water Absorption

Sorptivity

The amount of absorbed water (I) is normalized by the cross-sectional area exposed to water as outlined in ASTM C1585 (ASTM 2004):

$$I = m_t / (a.d) \quad (1)$$

where: m_t is the change in specimen mass at time t in grams; a is the area of the both sides exposed to water, in mm^2; d is the density of water in g/mm^3.

Sorptivity is defined as the slope of the water absorption versus square root of time curve (ASTM 2004). The initial sorptivity is the slope of this curve within the first 6 hours, while the secondary sorptivity is the slope of the curve between 1 to 8 days.

Figure 7(*a*) illustrates the sorption results for the specimens conditioned at 50% RH with 13% and 31% air contents by volume of paste. The specimens show a similar sorptivity (slope of

the curves) and amount of absorbed water initially; however, over time the specimens with higher volumes of air absorb more water. This occurs since the air voids provide space for water (Helmuth 1961; Warris 1964), however, the diffusion of air and the over-pressure in the air-bubbles delays water absorption which corresponds for the long time to saturation (Fagerlund 1993, 1995, 2004). It should be noted that although the secondary sorptivity for sample with higher air content is higher, this sample requires to absorb more water to reach to the critical degree of saturation.

Figure 7(*b*) shows the water absorption results for specimens conditioned at 65% RH. Comparing this result with Fig. 7(*a*) suggests that the amount of absorbed water for the specimens conditioned at 65% RH is lower than that of specimens conditioned at 50% RH with the same air content. Figure 7(*c*) shows the absorption for specimens conditioned at 80% RH. The specimens at 65% RH and 50% RH show a nick-point at the end of the 6 hours on a water absorption square-root of time curve however, the nick-point can not be seen on the results of 80% RH and a more graduate rate of absorption can be seen.

The relative humidity in which the specimens were conditioned in has a significant impact on the results (Castro et al. 2010a, 2010b, 2010c; Spragg et al. 2011). The driving force of unsaturated fluid transport is the capillary suction (Hall and Hoff 2002; Martys and Ferraris 1997; Hanžič et al. 2010). When samples are in equilibrium with a lower relative humidity a larger

volume of pores are empty and available to be filled with water during the water sorption. Furthermore, at lower humidity, the maximum size of the pores that is filled with water is smaller, creating a higher suction force. The overall effect will be higher rate of water absorption and high volume of absorbed water.

Degree of Saturation

Figure 8(*a*) shows that the degree of saturation (*S*) of the specimens conditioned at 50% RH with two air contents (13 and 31% by volume of paste). Note that the degree of saturation is plotted as a function of square-root of time on the lower x-axis while actual time is shown on the upper x-axis.

The most striking feature of the graphs in Fig. 8 is the fact that the degree of saturation decreases with air content. At the end of the initial 6-hour sorption period samples with lower air content show higher degree of saturation. For samples equilibrated at 50% RH the degree of saturation is 39% less when the air content increases 10%, the decrease in degree of saturation for samples equilibrated at 65% and 80% RH is 23% and 26% respectively.

Note that the secondary rate of absorption (Fig. 7) is different for samples with different air content; however, in Fig.8 the secondary rate of increase in degree of saturation is approximately the same for materials with different air content. This suggests that for an equal time of exposure to water, the specimen with the higher air content has a lower degree of saturation (Fagerlund

1993, 1995, 2004).

The secondary rate of increase in degree of saturation can be fitted with a linear function to estimate the amount of absorbed water over a long period of time. The linear fit used in Fig. 8 is shown with a solid line. Since the objective here is to estimate the degree of saturation over a long period of time only the date between 100 to 240 days is used in fitting this straight line. Using this linear function the time to reach to critical degree of saturation is calculated for each specimen with different air content and initial equilibrium condition and reported in Table 3.

Freeze-Thaw Testing

Monitoring the Damage Development Using Active Acoustic Emission

The relative dynamic elastic modulus is frequently used as an index to evaluate the extent of damage (Fagerlund 1972, 1975, 1977, 1979, 1981, 2004; Bentz et al. 2001; Litvan 1988; Litvan and Sereda 1980; Shimada et al. 1991). Using active AE the transmission time of a single pulse was measured along the sample. The transmission time along the length of the sample was measured in both directions (i.e., from sensor 1 to 2 and from sensor 2 to 1). The transmission time was measured three times in each direction and the average transmission time is reported here (average of 6 values). The transmitting time was measured after each cycle when the temperature was stable at 10°C for a minimum of 2 hours.

The relative elastic modulus, i.e. E_t/E_o is square proportional to the velocity of wave

transmitting through materials, which is inversely square proportional to the ratio of the wave transmission times (ASTM 2008) as shown in Eq. 2. Damage parameter (D) can also be estimated using Eq. 2.

$$D = 1 - E_t / E_o = 1 - (T_o / T_t)^2 \quad (2)$$

where E_o, T_o are the dynamic elastic modulus before freeze-thaw testing began and corresponding transmitting time; E_t, T_t are the dynamic elastic modulus during testing at any time t and corresponding transmitting time.

It should be noted that the main cracks were along the direction of wave propagation and as such the wave is least sensitive to these cracks however the damage was still easily recorded.

Figure 9 illustrates the damage index (Eq. 2) with increasing cycles of freezing and thawing. The damage initiates during the first cycle when the degree of saturation is above 86~88%. The specimens with lower degree of saturation do not show damage while specimens with a higher degree of saturation show a rapid deterioration. It can be seen that the saturated specimens (S=100%) can not sustain more than 3 cycles before complete failure occurs.

Figure 10 shows the rate of damage (dD) development per freeze-thaw cycle (dN) (as determined by the slope of Fig. 9) for specimens with different degrees of saturation. A critical degree of saturation appears to occur at approximately 86 - 88%. The critical degree of saturation appears to be independent of the air content.

Acoustic Energy Measured Using Passive Acoustic Emission

Figure 11 shows the amplitude of the acoustic events as a function time for a specimen with 96% degree of saturation and 13% air content during freezing cycle. The temperature is the temperature measured in the center of the mortar specimen. Figure 11(*a*) illustrates the amplitude distribution for the first freeze-thaw cycle and Fig. 11(*b*) illustrates the amplitude distribution during the second freeze-thaw cycle for the same specimen.

In Fig. 11(*a*) the acoustic events begin to occur as the temperature of the specimen decreases. A cluster of acoustic event is shown in Fig. 11(*a*) as highlighted by the ellipsoid. This cluster of data is not seen in Fig. 11(*b*). These events can be attributed to micro-cracking of the specimen due to thermal loading which may be a result of temperature gradient or a result of thermal expansion coefficient mismatch between the paste and aggregate. Since the thermal loading is not changed during the second cycle, the damage due to thermal loading does not exceed the previous level of damage in materials and additional cracking would not be expected (Kaiser 1950; Kline and Egle 1987).

In Figure 11 the acoustic events begin to increase dramatically after the temperature drops below -8°C in both cycles. The number of events is higher in the first cycle compared to the second cycle as more cracking would be expected in the first freeze-thaw cycle while these cracks would be expected to extend in the following cycles. The damage at the point (below -8°C)

is likely attributed to formation of ice and cracking inside the specimen. This is consisted with the observation that pore solution freezes below 0°C due to pore confinement and dissolved ions in pore solution (Fagerlund 1973; Helmuth 1960).

Desorption Isotherm

Figure 12 shows the desorption isotherm for the specimens with 13% and 31% air content by volume of paste. The desorption curve demonstrates the mass of water lost from the specimen at each relative humidity step (i.e., different pore sizes begin to empty out at different relative humidities starting with large pores at high relative humidities and smaller pores at lower humidities). The profile of the desorption curve is similar for both specimens until high relative humidities, i.e. 97.5% RH. At relative humidities higher than 97.5%, a larger difference of the porosity can be seen. This difference corresponds to the air entrained porosity.

The critical degree of saturation (88%) corresponds to relative humidity of 98.4% for specimen with 13% air content and 98.96% RH for specimen with 31% air content, respectively. This implies that some of the air entrained pores are water filled when the specimen is at or above critical degree of saturation. The difference in mass loss between the 13 and 31% air content at 2.5% RH is currently unknown however this is repeatable between specimens.

Calculated Time to Reach the Critical Degree of Saturation

In section 6.1 the rate of absorption of water and its relation to the degree of saturation was

discussed and in section 6.2 the influence of the degree of saturation on freeze-thaw damage was discussed. To better understand how these findings can be related to one another to predict the time to freeze-thaw damage a linear function was fit to the plot of degree of saturation verses square root of time data (using the secondary absorption).

Table 3 shows the time required for each specimen equilibrated at different initial condition to reach the critical degree of saturation (i.e., 88% in this study). Specimens without air entrainment can reach to the critical degree of saturation within days (4~6 days). The use of air entrainment raised the air content, and decreases the degree of saturation. This increases the time to reach a critical degree of saturation to 3~6 years. The rate of water absorption is substantially different in the systems with entrained air compared to non-air entrained systems.

Conclusions

The water absorption of mortar containing different volumes of entrained air was examined in this study. While tests like ASTM C 1585-04 (ASTM 2004) can be used to provide an index of water absorption, the differences between non air entrained and air entrained systems were small when only mass gain was investigated. While the absorption rates in plain and air entrained systems were similar initially the air entrained system showed a higher rate of ingress at later ages. By normalizing the results of water absorption in terms of the degree of saturation a clear distinction between the non air entrained and air entrained mixtures can be made. While the non

air entrained system took 4 to 6 days to reach 88 % saturation, the air entrained system is estimated to require approximately 3 to 6 years. This shows that entrained air will substantially increase the time to failure.

The damage due to freeze-thaw was monitored using both passive and active AE. A critical degree of saturation was observed with specimens that have a degree of saturation greater than the 86 to 88% exhibiting damage during the few freeze-thaw cycles.

The critical degree of saturation appears to be independent of the air content as materials with a degree of saturation above the critical degree undergoing damage after a few of freeze-thaw cycles irrespective of the air content. The volume of air and quality of the air void system however likely has a strong relation to the critical flow distance.

Increasing the air content resulted in a longer time for the mortar to reach to the critical degree of saturation. While increasing the air content can delay the time freeze-thaw damage initiates in practice; it appears that increasing of the air content can not eliminate the potential for freeze-thaw damage.

Acknowledgements

The experiments reported in this paper were conducted in the Pankow Materials Laboratories at Purdue University. This work was supported in part by Compass Minerals and the Joint Transportation Research Program administered by the Indiana Department of

Transportation and Purdue University. The contents of this paper reflect the views of the authors, who are responsible for the facts and the accuracy of the data presented herein, and do not necessarily reflect the official views or policies of the Indiana Department of Transportation, nor do the contents constitute a standard, specification, or regulation. The authors appreciate the assistance of Gaurav Sant for his work in casting/cutting the specimens while he was a graduate assistant working on this project. The authors also acknowledge many useful discussions with Dick Newell, John Poncher, Mike Byers, Tommy Nantung, Dave Andrewski, and Jan Olek.

References

ASTM Standard C192 (2006). "Standard practice for making and curing concrete test specimens in the laboratory." ASTM International, West Conshohocken, PA.

ASTM Standard C1585-04 (2004). "Standard test method for measurement of rate of absorption of water by hydraulic-cement concretes." ASTM International, West Conshohocken, PA.

ASTM Standard C666 (2008). "Test method for resistance of concrete to rapid freezing and thawing." ASTM International, West Conshohocken, PA.

Barde, V. Radlinska, A., Cohen, M. and Weiss, W.J. (2009). "Relating material properties to exposure conditions for predicting service life in concrete bridge decks in Indiana." *The Joint Transportation Research Program of the Indiana Department of Transportation*, Purdue University, West Lafayette, IN.

Beaudoin, J.J. and Cameron, M., (1972). "Dimentional changes of hydrated Portland cement paste during slow cooling and warming." *Cem. Concr. Res.*, 2(2), 225-240.

Bentz, D.P., Ehlen, M.A., Ferraris, C.F., and Garboczi, E.J. (2001). "Sorptivity-based service life predictions for concrete pavements." *7th Int. Conf. on Concrete Pavements*, NIST, Orlando, Florida, U.S., 181-193.

Bentz, D.P. Sant, G. and Weiss, J. (2008). "Early-age properties of cement-based materials I: influence of cement fineness." *J. Mater. Civ. Eng.*, 20(7), 502-508.

Castro, J., Bentz, D., and Weiss, J. (2010). "Effect of specimen conditioning on the water absorption of concrete." Submitted to *Cem. Concr. Compos.*

Castro, J., Kompare, P., Poursaee, P., Nantung, T. and Weiss, J. (2010). "Portland cement concrete pavement performance relative to permeability." *JTRP Report SPR-3093*, Indiana Department of Transportation, West Lafayette, IN.

Fagerlund, G. (1972). "Critical degrees of saturation at freezing of porous and brittle materials." *Report 34*, Division of Building Technology, Lund Institute of Technology, Lund, Sweden, 408.

Fagerlund, G. (1973). “Determination of pore-size distribution from freezing-point depression.” *Mater. Struct.*, 6(3), 215-225.

Fagerlund, G. (1975). “The significance of critical degrees of saturation at freezing of porous and brittle materials.” *Conf. on Durability of concrete*, ACI STP, Atlantic, New Jersey and Ottawa, Ontario, 47, 13-65.

Fagerlund, G. (1977). “The critical degree of saturation method of assessing the freeze/thaw resistance of concrete and the international cooperative test of the critical degree of saturation method of assessing the freeze/thaw resistance of concrete.” *Mater. Struct.*, 1977(10), 217-229 and 231-253.

Fagerlund, G. (1979). “Prediction of the service life of concrete exposed to frost action, studies on concrete technology.” *Studies on Concrete Technology*, Swedish Cement and Concrete Research Institute, Stockholm, 249-276.

Fagerlund, G. (1981). “The principles of frost resistance of concrete.” *Nordisk Betong*, 1981(2), 5-13, In Swedish.

Fagerlund, G. (1993). “The long-time water absorption in the air-pore structure of concrete.” Report TVBM-3051, Division of Building Technology, Lund Institute of Technology, Lund, Sweden.

Fagerlund, G. (1995). “The required air content of concrete.” *Proc., In. Workshop on Mass-Energy Transfer and Determination of Building Components*, BRI-Japan and CSTB-France, Paris, France, 591-609.

Fagerlund, G. (2004). “A service life model for international frost damage in concrete.” Report TVBM-3119, Division of Building Technology, Lund Institute of Technology, Lund, Sweden.

Feldman, R.F. (1987). “Diffusion measurements in cement paste by water replacement using propan-2-OL.” *Cem. Concr. Res.*, 17(4), 602-612.

Hall, C., and Hoff, W.D. (2002). “Water in porous materials.” *Water-Transport in Brick, Stone and Concrete*, Taylor&Francis, Abingdon, Oxon, 29-41.

Hanžič, L., Kosec, L., and Anžel, I. (2010). “Capillary absorption in concrete and the lucas–washburn equation.” *Cem. Concr. Compos.*, 32, 84–91.

Helmuth, R.A. (1960). “Capillary size restrictions on ice formation in hardened Portland cement pastes.” *Proc., 4th Int. Symp. on Chemistry of Cement*, Paper VI-S2, 855–869.

Helmuth, R.A. (1961). “Dimensional changes of hardened Portland cement pastes caused by temperature changes.” *Proc., Highway Research Board*, 40, 315–336.

Hossain, A.B., Pease, B. and Weiss, J. (2003). “Quantifying early-age stress development and cracking in low water-to-cement concrete - restrained-ring test with acoustic emission.” *Transp. Res. Rec.*, 1834, 24-32.

Kaiser, J., (1950). “A study of acoustic phenomena in tensile tests.” Dr.-Ing. dissertation, Technical University of Munich, Bayern, Germany.

Kim, B. and Weiss, J. (2003). “Using acoustic emission to quantify damage in restrained fiber-reinforced cement mortars.” *Cem. Concr. Compos.*, 33, 207–214.

Kline, R.A., and Egle, D.M. (1987). “A brief note on the Kaiser and Felicity effects.” *J. Acoust. Emiss.*, 6, 205.

Krishnan, A. (2002). “Durability of concrete containing fly ash or slag exposed to low temperatures at early ages.” M.S. Thesis, Purdue University, West Lafayette, IN.

Leech, C., Lockington, D., Hooton, R.D., Galloway, G., Cowin, G. and Dux, P. (2008). “Validation of mualem's conductivity model and prediction of saturated permeability from sorptivity.” *J. ACI Mater.*, 105(1), 44-51.

Litvan, G.G. and Sereda, P.J. (1980). “Freeze-thaw durability of porous building materials.” *Durability of Building Materials and Components*, ASTM STP 691, Sereda, P.J. and Litvan, G.G., eds., ASTM International, 455-463.

Litvan, G.G. (1988). “The mechanism of frost action in concrete-theory and practical implications.” *Proc., of Workshop on Low Temperature Effects on Concrete*, National Research Council of Canada, Montreal, Canada, 115-134.

Martys, N.S., and Ferraris, C.E. (1997). "Capillary transport in mortars and concrete." *Cem. Concr. Res*, 27(5), 747-760.

Moon, J.H., and Weiss, J. (2006). "Estimating residual stress in the restrained ring test under circumferential drying." *Cem. Concr. Compos.*, 28, 486–496.

Ohtsu, M. and Shigeishi, M. (1993). "Experimental crack identification of mixed mode by acoustic emission." *Int. Conf. on Fracture and Damage of Concrete and Rock (FDCR-2)*, Rossmanith, H. P. eds., E&FN Spon., London, 186-195.

Ohtsu, M. (1999). "Estimation of crack and damage progression in concrete by quantitative acoustic emission analysis." *Mater. Eval.*, 57(5), 521-525.

Ouyang, C., Landis, E. and Shah, S.P. (1991). "Detection of microcracking in concrete by acoustic emission." *Exp. Tech.*, 15(3), 24-28.

Ouyang, C., Landis, E. and Shah, S.P. (1991). "Damage assessment in concrete using quantitative acoustic emission." *J. Eng. Mech.*, 117(11), 2681-2698.

Pour-Ghaz, M., Nadukuru, S., O'Connor, S., Kim, J., Michalowski, R., Bradshaw, A., Green, R.A., Lynch, J.P., Poursaee, A. and Weiss, W.J. (2010). "Using electrical, magnetic and acoustic sensors to detect damage in segmental concrete pipes subjected to permanent ground deformation." Purdue University, School of Civil Engineering, West Lafayette, IN.

Pour-Ghaz, M. and Weiss, J. (2010). "Quantifying damage due to aggregate expansion in cement matrix." *Advances in the Material Science of Concrete*, ACI SP-270-9, 101-113.

Puri, S. and Weiss, J. (2003). "Assessment of localized damage in concrete under compression using acoustic emission." *ASCE J. Mater. Civ. Eng.*, 18(3), 325-333.

Rangaraju, P.R., Sompura, K.R. and Olek, J. (2006). "Investigation into potential of alkali-acetate-based deicers to cause alkali-silica reaction in concrete." *Transp. Res. Rec.*, 1979, 69-78.

Scherer, G.W. (1993). "Freezing gels." *J. Non-Cryst Solids*, 155, 1-25.

Scherer, G.W. and Valenza, J.J. (2005). “Mechanisms of frost damage.” *Mater. Sci. Concr.*, 7, 209-246.

Shah, H.R., and Weiss, J. (2006). “Quantifying shrinkage cracking in fiber reinforced concrete using the ring test.” *Mater. Struct.*, 39(9), 887-899.

Shimada, H., Sakai, K., and Litvan, G.G. (1991). “Acoustic emissions of mortar subjected to freezing and thawing.” *J. ACI Mater.*, 126, 263-278.

Spragg, R., Castro,J., Li, W., Pour-Ghaz, M., Huang, P., and Weiss, J. (2011). “Wetting and drying of concrete in the presence of deicing salt solutions.” Submitted to *Cem. Concr. Compos.*

Suaris, W. and van Mier, J. G. M. (1993). “Acoustic emission and source location in concrete subjected to mixed mode loading.” *Int. Conf. on Fracture and Damage of Concrete and Rock (FDCR-2)*, Rossmanith, H. P., eds., E&FN Spon, London, 157-165.

Suaris, W., and Van Mier, J.G.M. (1995). “Acoustic emission source characterization in concrete under biaxial loading.” *Mater. Struct.*, 28(8), 444-449.

Sun, Z., Kumpf,D. and Scherer, G.W. (2007). “Kinetics of ice growth in concrete.” *Proc., 12th Int. Cong. Cement Chemistry*, paper W4-07.1, Beaudoin, J.J., Makar, J.M., Raki, L. eds., National Research Council of Canada, Montreal, Canada.

Sutter, L., Van Dam, T., Peterson, K. R. and Johnston, D. P. (2006). “Long-term effects of magnesium chloride and other concentrated salt solutions on pavement and structural Portland cement concrete phase I results.” *Transp. Res. Rec.*, 1979, 60-68.

Warris, B. (1964). “The influence of air-entrainment on the frost-resistance of concrete, part B, hypothesis and freezing experiments.” *Proc., No. 36 Swedish Cement and Concrete Research Institute*, Stockholm, 130.

Weiss, W.J., Abraham, D., and Nantung, T. (2007). “SPR3200—A proposal for a research study on saw-cutting and curing of concrete pavements.” *The Joint Transportation Research Program of the Indiana Department of Transportation*, Purdue University, West Lafayette, IN.

Yang, Z.F. Weiss, W.J. and Olek, J. (2006). “Water transport in concrete damaged by tensile loading and freeze-thaw cycling. ” *J. Mater. Civ. Eng.*, 18(3), 424-434.

Yoon, D.J. Weiss, W.J. Prine, D.W. and Shah, S.P. (1999). “Assessing corrosion damage in reinforced concrete beams using acoustic emission.” *Non-Destr. Eval. Bridg. Highw.*, 3587, 254-263.

Table headings

Table 1. Mixture proportions and constituent materials

Table 2. Initial condition, air content and namely scheme for specimens used in the present study

Table 3. Time to reach to the critical level of saturation (88%) for the specimens with different air content

Table 1. Mixture proportions and constituent materials

Air content of paste (% by volume of mortar [a]/ concrete [b])	Cement (Type I) (kg/m^3)	Water (kg/m^3)	Sand (kg/m^3)
13 (6/4)	573.3	240.8	1333.3
22 (10/7)	548.9	230.6	1276.5
31 (14/9)	524.5	220.3	1219.8

Note: [a] In calculating the equivalent air content in mortar it was assumed 45% paste by volume of the mortar; [b] In calculating the equivalent air content in concrete it was assumed 30% paste by volume of the concrete.

Table 2. Initial condition, air content and namely scheme for specimens used in the present study

Specimen name	Air content of the Paste (%)	Relative humidity (%)
50-13 [a]	13	50
65-13	13	65
80-13	13	80
50-22	22	50
65-22	22	65
80-22	22	80
50-31	31	50
65-31	31	65
80-31	31	80

Note: [a] The first number shows the initial humidity of the specimen (e.g.50-13 is 50% RH);
The second number shows the air content of mortar of the specimen (e.g. 50-13 is 13% air by volume of paste).

Table 3. Time to reach to the critical level of saturation (88%) for the specimens with different air content

Initial relative humidity (%)	Air content by volume of paste (%)	Secondary sorptivity ($mm^3/mm^2.d^{0.5}$)	Time to reach the critical degree of saturation (88%) (S_{cr}) in years (+/-1.7%)
50	13	0.485	0.011 (4d)
	22	0.691	5.08
	31	0.750	6.10
65	13	0.368	0.016 (6d)
	22	0.513	5.63
	31	0.785	5.90
80	13	0.563	0.015 (5d)
	22	0.606	4.00
	31	1.009	5.82

Figure captions

Fig. 1 Photography of field observation showing damage in pavement joints

Fig. 2 Schematic illustration of relation between degree of saturation with freeze-thaw damage [10, 19]

Fig. 3 Double sided sorption test of specimen with 1-inch thickness

Fig. 4 Specimens prepared for acoustic emission testing during freeze-thaw cycle: (*a*) thin plastic sheet to avoid evaporation during specimen preparation and handling (*b*) specimen covered by heat shrinkable wrap to avoid evaporation during specimen preparation and handling

Fig. 5 Specimens placed on a suspended base to eliminate vibration and noise from surrounding environment (inside of freeze-thaw chamber)

Fig. 6 Temperature cycle used in freeze-thaw experiment (air temperature)

Fig. 7 Effect of air content and initial moisture on water absorbed: (*a*) 50% RH (*b*) 65% RH (*c*) 80% RH

Fig. 8 Results of sorption test provided as increase in the degree of saturation: (*a*) 50% RH (*b*) 65% RH (*c*) 80% RH

Fig. 9 Decrease of the relative dynamic elastic modulus with freeze-thaw cycles

Fig. 10 Rate of decrease of relative dynamic elastic modulus with degree of saturation

Fig. 11 Amplitude in the transition time of freezing (96*S*): (*a*) first cycle (*b*) second cycle

Fig. 12 Mass change at decreasing RH containing de-ionized water

Figures:

Fig. 1 Photograph of field observation showing damage in pavement joints

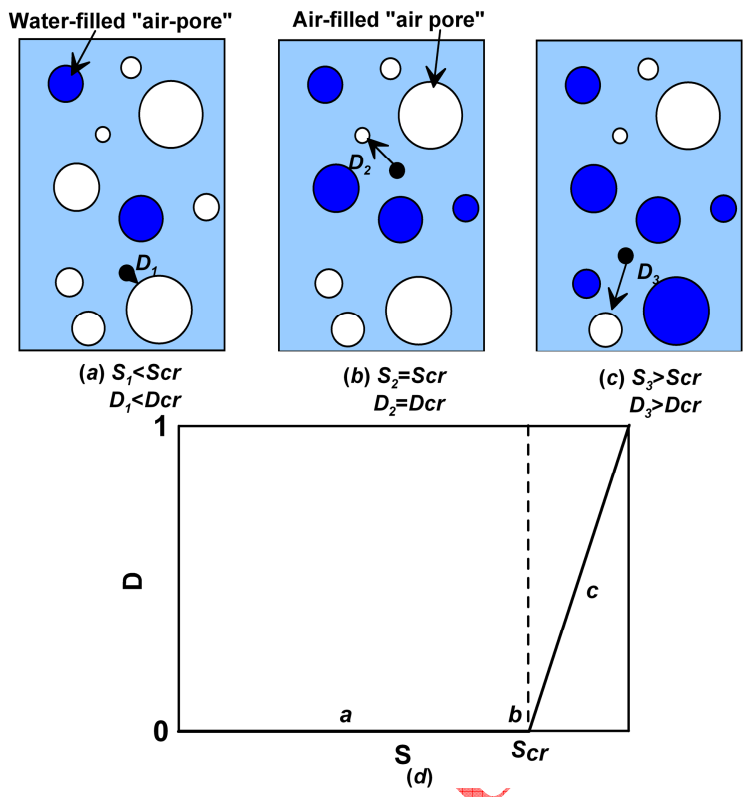

Fig. 2 Schematic illustration of relation between degree of saturation with freeze-thaw damage [10, 19]

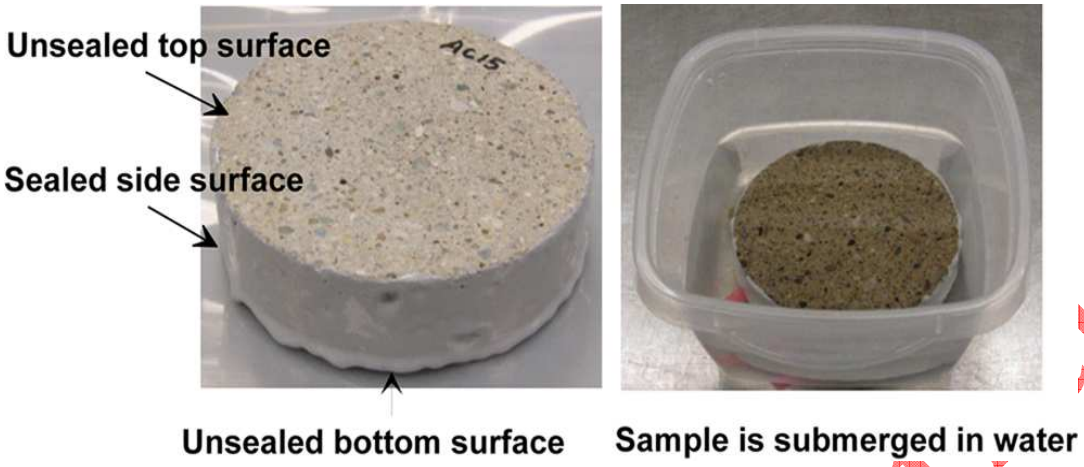

Fig. 3 Double sided sorption test of specimen with 1-inch thickness

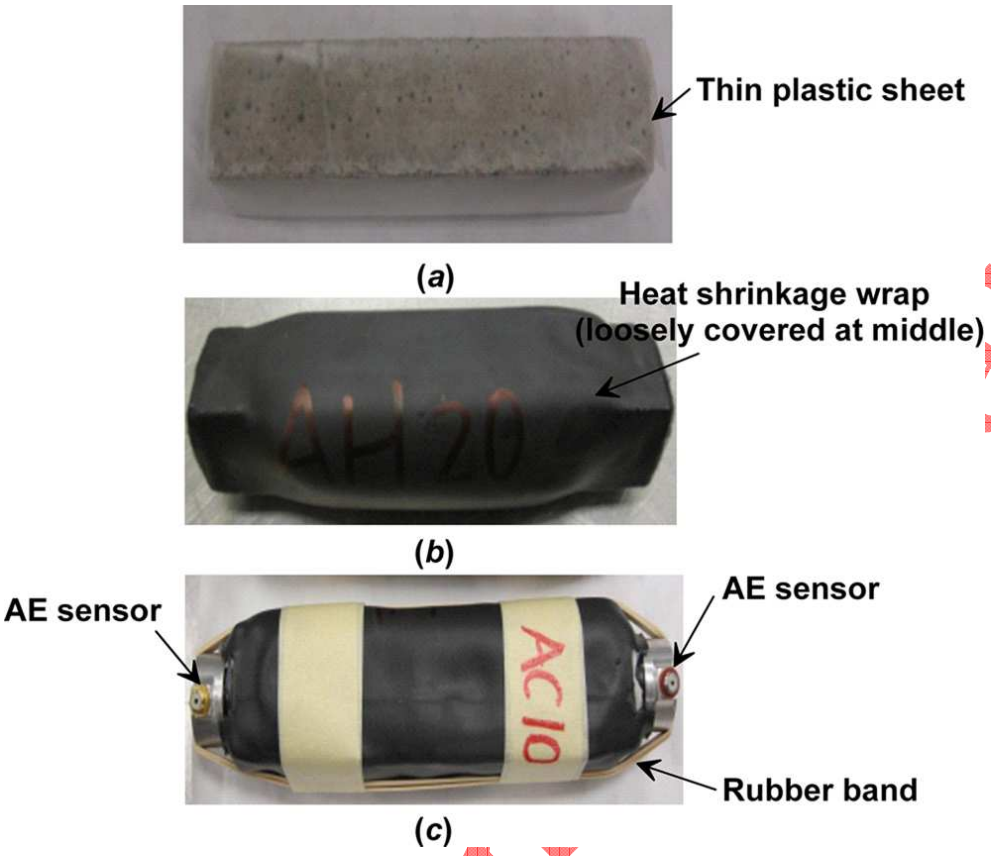

Fig. 4 Specimens prepared for acoustic emission testing during freeze-thaw cycle: (*a*) thin plastic sheet to avoid evaporation during specimen preparation and handling (*b*) specimen covered by heat shrinkable wrap to avoid evaporation during specimen preparation and handling

Suspended plate to eliminate vibration and noise from environment

Fig. 5 Specimens placed on a suspended base to eliminate vibration and noise from surrounding environment (inside of freeze-thaw chamber)

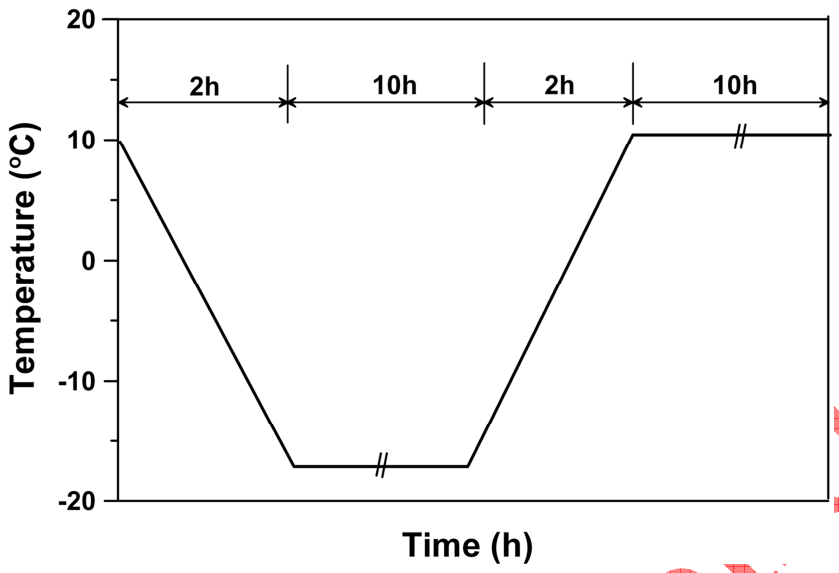

Fig. 6 Temperature cycle used in freeze-thaw experiment (air temperature)

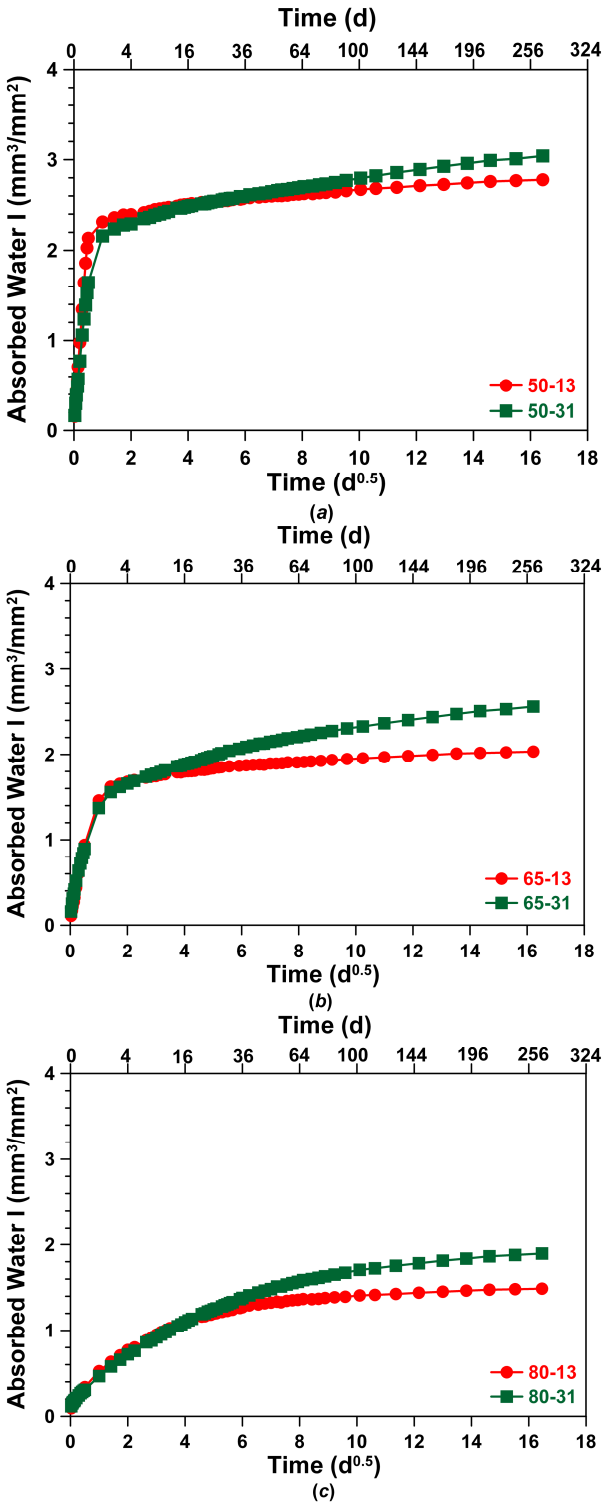

Fig. 7 Effect of air content and initial moisture on water absorbed: (*a*) 50% RH (*b*) 65% RH (*c*) 80% RH

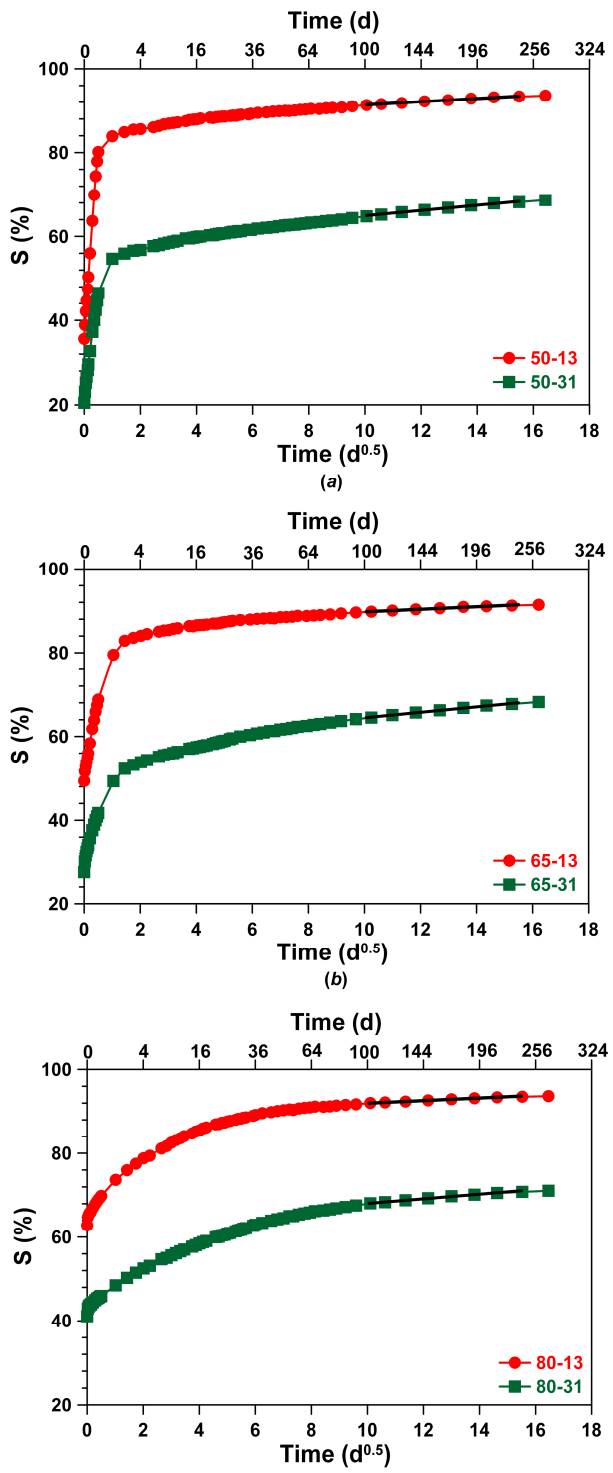

Fig. 8 Results of sorption test provided as increase in the degree of saturation: (*a*) 50% RH (*b*) 65% RH (*c*) 80% RH

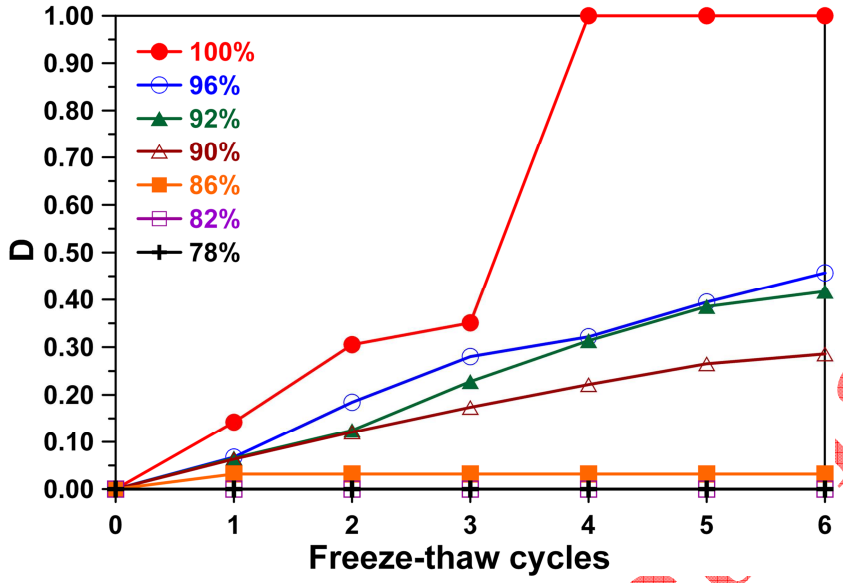

Fig. 9 Decrease of the relative dynamic elastic modulus with freeze-thaw cycles

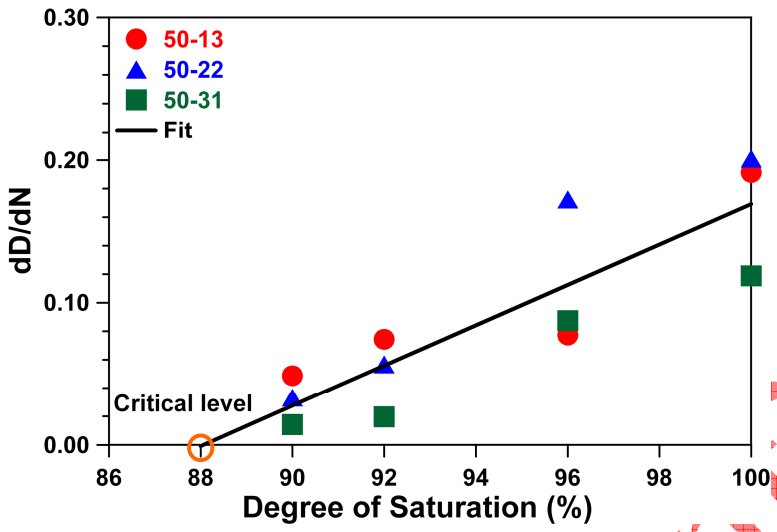

Fig. 10 Rate of decrease of relative dynamic elastic modulus with degree of saturation

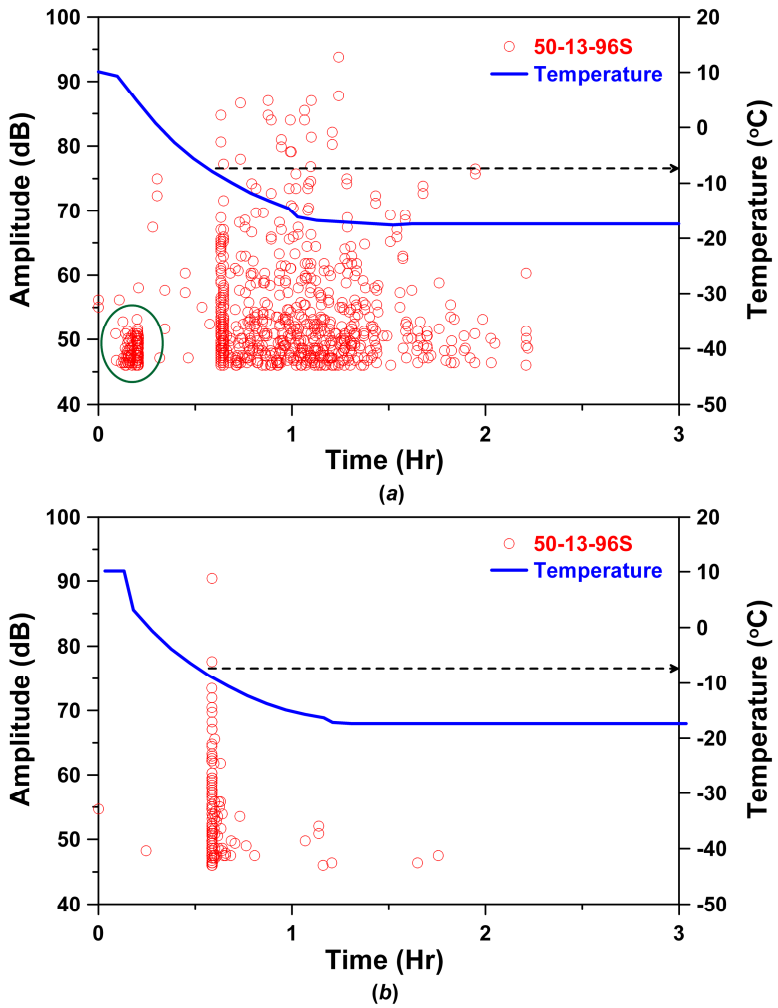

Fig. 11 Amplitude in the transition time of freezing (96*S*): (*a*) first cycle (*b*) second cycle

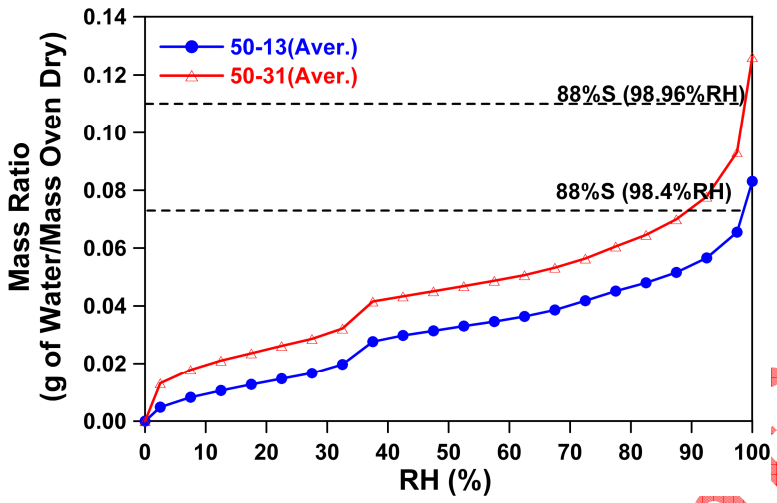

Fig. 12 Mass change at decreasing RH containing de-ionized water

Elsevier Editorial System(tm) for Cement and Concrete Composites
Manuscript Draft

Manuscript Number: CCC-D-10-00479

Title: Effect of sample conditioning on the water absorption of concrete

Article Type: Research Paper

Keywords: Water absorption; Sample conditioning; Moisture effect; Relative humidity

Corresponding Author: Mr. Javier Castro,

Corresponding Author's Institution: Purdue University

First Author: Javier Castro

Order of Authors: Javier Castro; Dale Bentz; Jason Weiss

Abstract: ASTM C1585 is commonly used to determine the absorption and rate of absorption of water in unsaturated hydraulic cement concretes. ASTM C1585 preconditions the samples for a total of 18 days. Unfortunately, the range of relative humidities that can exist in the samples after this relatively short conditioning period may provide a wide enough variation to considerably influence the results of the test. Three main variables were studied in this program to assess the effect of preconditioning. First, the role of water to cement ratio was investigated by testing mortar samples with 55 % aggregate by volume with four different water-to-cement ratios (w/c of 0.35, 0.40, 0.45 and 0.50). Second, the role of paste volume was investigated by considering samples with 55 %, 45 %, and 35 % aggregate by volume with a w/c = 0.50. Finally, the effect of conditioning was assessed by exposing all the samples in three different relative humidities (50 %, 65 % and 80 %) until they reached mass equilibrium (defined as a change of mass less than 0.02 % over 15 days), taking approximately 14 months. Oven dry samples were also prepared and tested for comparison. The results confirm that water absorption testing is considerably influenced by sample preparation. Samples conditioned at 50 % relative humidity can show up to six times greater total absorption than similar samples conditioned at 80 % relative humidity. Samples that were conditioned in the oven at 105 °C do not appear to follow a similar trend when compared with specimens conditioned in chambers for the longer duration. The absorption is also influenced by the volume of paste in the samples. The experiments show that a lack of control on moisture content or lack of consideration of the material composition may lead to a misunderstanding of the actual absorption behavior.

Javier Castro
Purdue University
School of Civil Engineering
550 Stadium Mall
West Lafayette, IN, 47907
765-494-7999
Email: jcastro@purdue.edu

Dear Editor:

Enclosed for your consideration in an original research article, entitled "**Effect of sample conditioning on the water absorption of concrete**". A brief description of this paper is provided below.

Best regards,

Javier Castro

Brief description of the present work:

ASTM C1585 is commonly used to determine the absorption of water in unsaturated hydraulic cement concretes. Unfortunately, the initial moisture content that can exist in the samples after the samples preparation may provide a wide enough variation to considerably influence the results of the test. This paper provides a series of measurements to evaluate the role of the relative humidity of the samples prior the test. The role of the w/c and the cement paste volume were also evaluated. The results of this research confirm that water absorption testing is considerably influenced by sample preparation, the w/c and by the volume of paste in the samples. The experiments show that a lack of control on moisture content or lack of consideration of the material composition may lead to a misunderstanding of the actual absorption behavior.

Effect of sample conditioning on the water absorption of concrete

Javier Castro
Graduate Research Assistant and Ph.D. Candidate
School of Civil Engineering
Purdue University
School of Civil Engineering
550 Stadium Mall, West Lafayette, IN 47907-2051, USA
E-mail: jcastro@purdue.edu
Phone: (765) 494-7999

Dale Bentz
Chemical Engineer
National Institute of Standards and Technology
Materials and Construction Research Division
Building and Fire Research Laboratory
100 Bureau Drive, Stop 8615, Gaithersburg, MD 20899-8615, USA
E-mail: dale.bentz@nist.gov
Phone: (301) 975-5865

Jason Weiss
Professor and Director of Pankow Materials Laboratory
Associate Director of the Center for Advanced Cement Based Materials
School of Civil Engineering
Purdue University
School of Civil Engineering
550 Stadium Mall, West Lafayette, IN 47907-2051, USA
E-mail: wjweiss@purdue.edu
Phone: (765) 494-2215

1. Introduction

The durability of concrete subjected to aggressive environments depends largely on transport properties, which are influenced by the pore system [1-7]. Three main mechanisms can be used to describe transport in cementitious systems: permeability, diffusion and absorption. Permeability is the measure of the flow of water under a pressure gradient, while diffusion is the movement of ions due to a concentration gradient. Absorption can be described as the ability to take in water by means of capillary suction. All three mechanisms are heavily influenced by the volume of pores as well as the connectivity of the pore network. A large fraction of concrete in service is only partly saturated and the initial ingress of water and dissolved salts is influenced, at least in part, by capillary absorption [7]. As such, water absorption has been used as an important factor for quantifying the durability of cementitious systems [4-11]. Water absorption is the primary focus of this study since it is being increasingly used by specifiers and in forensic studies to provide a parameter that can describe an aspect of concrete durability. It is also important that these properties be adequately described for use in service life models [6, 11].

1.1 Water absorption test

ASTM C1585 [1] is commonly used to determine the absorption and rate of absorption (commonly referred to as sorptivity) of water in unsaturated hydraulic cement concretes. This test method, based on work reviewed by Hall [12], consists of preconditioning samples to a known moisture content, then exposing the bottom surface of the sample to liquid water and measuring the increase in mass resulting from water absorption. According to the standard conditioning procedure, samples are conditioned for 18 days. This conditioning period begins by first placing the sample in a 50˚C and 80 % relative humidity (RH) environment for three days. The samples are then removed from this environment and placed in individually sealed containers where they remain for a minimum 15 days at 23 °C, to allow internal moisture to redistribute throughout the specimens before the test begins.

The absorption test involves recording incremental mass change measurements at relatively frequent intervals during the first six hours after the sample comes in contact with water and subsequently taking one measurement every day for the next eight days. The amount of absorbed water is normalized by the cross-section area of the specimen exposed to the fluid using Equation 1:

$$i = \frac{m_t}{(a \cdot \rho)} \qquad (1)$$

where: i is the normalized absorbed fluid volume, m_t is the change in specimen mass at time t; a is the area of the specimen exposed to the fluid (i.e., that of the bottom face), and ρ is the density of the absorbed fluid (taken to be 1000 kg/m^3 at 23 °C for water).

These absorbed fluid volumes are then plotted as a function of the square root of time. The initial sorptivity is determined as the slope of the curve during the first six hours, while secondary sorptivity is determined using the slope of the same measurements between one and eight days, as outlined in ASTM C1585 (1). It should be noted that these times work well for

water though they may not work as well for other fluids with different surface tension and/or viscosity [13].

The initial and secondary sorptivities can be used to evaluate the connectivity of the pore network [9]. Additionally, the secondary sorptivity, combined with exposure conditions, has been used for performing service life predictions [11].

1.2 The role of the relative humidity

Water ingress in unsaturated concrete is dominated by capillary suction upon initial contact with water [7, 12-18]. Capillary absorption can be related to the volume of the pores as well as the size (i.e. radius) of the partially empty capillary pores (Figure 1a). The relation between the equilibrated relative humidity and the radius of the smallest empty pore is given by the Kelvin-Laplace equation (Equation 2).

$$\mathrm{Ln}\,(RH) = \frac{2\,\sigma\,\mathrm{V_m}}{r_m\,R\,T} \qquad (2)$$

where: RH is the relative humidity, σ is the surface tension of water (pore solution), V_m is the molar volume of water, r_m is the average radius of curvature, R is the universal gas constant, and T is the absolute temperature.

It should be noted that this expression is simplified as it does not consider the effect of water that is absorbed on the walls of the pores. Largely the concrete community has considered two sizes of pores as introduced by Powers [19]. The gel pores are considered to be small pores (< 10 nm diameter) that are a part of the hydration products. Capillary pores are larger pores that occur due to excess water. Capillary porosity is particularly of concern in transport, as is the interconnectivity of the capillary pores.

Figure 1b) shows a conceptual illustration based on Powers [19] that uses a desorption isotherm to illustrate the volume of water located in the different size pores at different relative humidities.

The relative humidity used to condition the sample prior to the sorption test can have a significant impact on the results [1]. Previous test results by Parrot [20, 21] indicated that the water absorption rate was very sensitive to the moisture content of the concrete, particularly at relative humidities above 60 % which were common for field exposure. Water leaves the largest accessible pores first. It can be seen from Figure 1b that capillary pores occupy the range of humidity from approximately 80% to 100% RH. As such, initially upon drying water leaves the capillary pores. The lower the relative humidity, the greater the total volume of pores that are empty and available to be filled with water during the sorption test. Further, the lower humidity will empty smaller pores, creating a higher suction force in the materials and resulting in a greater sorption rate and a larger overall total absorption.

According to ASTM C1585, the standardized test conditioning will generally provide an internal relative humidity similar to relative humidities found near the surface in some field concrete

structures [1, 22, 23]. This range of relative humidities can represent what is found in samples in the field; however, it is wide enough to considerably affect the test results.

Castro et al. [24] shows that the relative humidity of samples that were kept in the field under different exposure conditions was in the range of 80 % to 100 % depending on the type of exposure, which is somewhat higher than what is mentioned in ASTM C1585.

1.3 Research objectives

The objectives of this research are threefold. First, this research will examine the influence of conditioning relative humidity (oven dry, 50%, 65% and 80% RH) on the results of sorption tests performed on mortars with different *w/c*, containing a fixed volume of aggregate. Second, this research will examine the influence of the volume of aggregate (or equivalently the paste content) on the results of sorption testing. Third, this research will examine the effect of the conditioning method specified in ASTM C1585-04.

2. Materials

An ASTM C150 Type I ordinary portland cement (OPC) was used in this study, with a Blaine fineness of 370 m^2/kg and an estimated Bogue composition of 56 % C_3S, 16 % C_2S, 12 % C_3A, 7 % C_4AF and a Na_2O equivalent of 0.68 % by mass.

A polycarboxylate-based high-range water-reducing admixture (HRWRA) was added in varying rates as indicated in Table 1, depending on the mixture proportions, to maintain similar consistencies (i.e., workability). The sand used was natural river sand with a fineness modulus of 2.71, an apparent specific gravity of 2.58, and a water absorption of 1.8 % by mass.

2.1 Mixture proportioning

Six different mixtures were prepared in total. Four of the mixtures were mortars with a single volume fraction of fine aggregate (55% of the total volume) and different *w/c* (0.35, 0.40, 0.45, and 0.50). These mixtures were designated as 55/0.35, 55/0.40, 55/0.45 and 55/0.50, with the number on the left representing the volume fraction of fine aggregate and the number on the right representing *w/c*. Additionally, two other mortars were prepared with *w/c* of 0.50, but with different volume fractions of fine aggregate (35 % and 45 % of the total volume). They were designated as 35/0.50, 45/0.50. A list of the mixture proportions can be found in Table 1.

2.2 Mixing procedure

The mixing procedure used for the mortar was in accordance with ASTM C192-06 [25]. The aggregate was oven dried and cooled for 24 h before mixing. The volume of water was corrected by the absorption of the aggregate. The water and cement were conditioned for 24 h at room temperature prior to mixing.

3. Experimental method

Six 100 mm × 200 mm cylinders were cast for each mixture. After one day of curing, the samples were demolded and then sealed in double plastic bags for sealed curing. Bags were stored in a room at 23 ± 1 °C until samples reached an age of 28 d. After that, cylinders were removed from bags and three 50 mm ± 2 mm thick samples were cut from the central portion of each cylinder with a wet saw using water as the cooling fluid.

After cutting, samples were conditioned by placing them in environmental chambers at 23 ± 0.5 °C. Specimens from mixtures 55/0.35, 55/0.40, 55/0.45 and 55/0.50 were placed in environmental chambers at three different relative humidities (50 ± 1 %, 65 ± 1 % and 80 ± 1 %). Specimens from mixtures 35/0.50 and 45/0.50 were placed in an environmental chamber at 50 ± 1 % relative humidity. Samples were kept in the environmental chamber until they reached mass equilibrium, defined as a mass change of less than 0.02 % over a 15 day period. Mixture 55/0.35 placed at 50 ± 1 % relative humidity required the longest period of time (14 months) to reach mass equilibrium. However, all samples were maintained in the chambers for 14 months to test them all at the same age.

Additional specimens from mixtures 55/0.35, 55/0.40, 55/0.45 and 55/0.50 were placed at 50 ± 1 % RH. After the 14 months, these specimens were dried in an oven at 105 ± 2 °C until they reached mass equilibrium.

Once the samples were removed from the chambers or from the oven, the side surface (i.e. outer circumference) was sealed with epoxy and the top surface was covered with plastic to avoid evaporation from the sample during testing. After the samples were prepared, testing occurred in accordance with ASTM C1585-04 [1]. Specimens from mixtures 55/0.35, 55/0.40, 55/0.45 and 55/0.50 were tested over a period of 90 days. Specimens from mixtures 35/0.50 and 45/0.50 were tested over a period of 8 days.

Two additional 100 mm × 200 mm cylinders were cast for each mortar mixture. After one day of curing, the samples were demolded and then sealed in double plastic bags for sealed curing. Bags were stored in a room at 23 ± 1 °C until samples reached an age of 28 d. After that, cylinders were removed from bags and 10 mm ± 2 mm thick samples were cut from the central portion of each cylinder with a wet saw. After cutting, mortar samples were vacuum saturated for 24 h. After that, specimens were placed in environmental chambers at six different relative humidities (93 ± 1 %, 87 ± 1 %, 80 ± 1 %, 75 ± 1 %, 65 ± 1 % and 50 ± 1 %) to determine their desorption isotherms.

4. Experimental results and discussion

4.1 Desorption isotherms

Figure 2 shows the desorption isotherm curves measured using 10 mm thick samples. Mass change was monitored at regular intervals until it reached equilibrium, defined as a mass change

of less than 0.02 % over a 15 day period. At the end, all samples were oven dried to express water absorption in terms of the dry mass of the sample.

It can be noticed that while the values of the moisture content are similar at 50% and lower RH (lower RH results not shown in Figure 2), as it refers to the small gel pore system [19], the capillary pores at high RH are strongly influenced by the *w/c*.

4.2 Effect of initial conditioning on water absorption tests

4.2.1 Effects of relative humidity on sorption test

Figure 3 shows the absorbed water during the 90 days of testing performed on mortars conditioned at different relative humidities (mixtures 55/0.35, 55/0.40, 55/0.45 and 55/0.50). It can be noticed that the water absorption is very sensitive to the relative humidity at which the specimens were pre-conditioned before testing. In each case, as the conditioning relative humidity increases, more water is retained in the pore system and thus the absorption decreases.

These results can be viewed in a slightly different manner if they include the initial amount of water held in the pores before the test. In order to do this, samples were oven dried at the end of the sorption test to calculate the amount of water they held before starting the test. Additional specimens that were kept at 50 ± 1 % RH during the 14 months were oven dried and then saturated by the procedure described in ASTM C642-07 [26] to measure the total amount of interconnected porosity in the systems. Results from Figure 3 were then normalized by the total amount of pores in the system, which can be viewed as the degree of saturation of the sample as a function of time. This is presented in Figure 4. Figure 5 shows the total degree of saturation for the samples after 90 days.

Figures 4 and 5 show that samples prepared at different relative humidities with a low *w/c* (e.g. *w/c* = 0.35) do not reach values near to saturation even after 90 days of being in contact with water. It may be attributed to the refined pore network of this low *w/c* system which makes it difficult for water to move through the sample to fill all the pores. This is commonly referred to as depercolation, which occurs after different hydration times for different *w/c* [27].

In contrast after 90 days, samples prepared with a higher *w/c* (e.g. *w/c* = 0.50) reach much higher levels of saturation. It can be noted from Figure 4 that samples conditioned at 50 % RH reach values near saturation after about 40 days of testing, similar to what is obtained with oven dry samples. Again this may be attributed to the connectivity of the pore network and the size of these pores. In this case, a more interconnected pore network will facilitate the movement of water to the interior of the specimens and the diffusion of water vapor out of the sample. However, when these samples were conditioned at higher relative humilities (65 and 80 % RH), the amount of initially retained water is high enough to reduce the diffusion of vapor out of the sample. As a result, this may explain why the level of saturation of these specimens is lower.

4.2.2 Effects of relative humidity on the amount of absorbed water after 8 days

Figure 6 shows the cumulative water that was absorbed after 8 days of testing performed on mortars conditioned at different relative humidities, expressed as a function of *w/c* (Figure 6a) and as a function of the relative humidity (Figure 6b).

Figure 6a) shows that mixture 55/0.50 can exhibit six times higher absorption when the samples are conditioned at 50 % RH compared with similar samples conditioned at 80 % RH.

Figure 7 shows a normalization of the data presented in Figure 6. In Figure 7a) the normalization is made with respect to the absorption of samples with *w/c* = 0.35 (mixture 55/0.35). In Figure 7b) the normalization is made with respect to the absorption of samples conditioned at 50 % relative humidity. It can be seen that the values follow a consistent trend in each case, except for the oven dry samples. This is in general agreement with the parallel nature of the desorption isotherms for the mortars provided in Figure 2.

4.2.3 Effects of relative humidity on initial sorptivity

Figure 8 shows the initial sorptivity calculated as the slope of the absorption vs. the square root of time during the first six hours of test [1].

Figure 8a) shows that mixture 55/0.50 can exhibit a ten times higher initial sorptivity when the samples are conditioned at 50 % RH compared with similar samples conditioned at 80 % RH.

It needs to be noted that the oven dry samples show a much higher initial sorptivity, due to the fact that the gel's capillary pores are empty and possibly to microcracking. While the increase in sorptivity is observed to be linear for the specimens conditioned at 50%, 65% and 80% relative humidity, this trend appears to break down for the oven dry samples which may be attributed to micro-cracking generated during the sample preparation [28-32].

4.2.4 Effects of relative humidity on secondary sorptivity

Figure 9 shows the secondary sorptivity calculated as the slope of the absorption vs. the square root of time between 1 d and 8 d of testing. Trends are similar to those observed for the initial sorptivity. However, it needs to be noted that samples that were oven dry prior to the test present a considerably lower secondary absorption with respect to the samples conditioned in environmental chambers. This may be explained by the high initial absorption of the oven dry samples shown in Figure 8. During this initial absorption it can be noticed that since a majority of the water was already absorbed in the first hours of the test, the secondary rate of absorption will be much lower. It can also be expected that microcracking enabled a more rapid ingress of water [33].

Figure 9 shows a similar trend to what was noted in the case of total absorption and initial sorptivity, namely that the secondary sorptivity of samples conditioned in chambers exhibits a consistent trend when the results are plotted against the w/c or the relative humidity at which

samples were conditioned. However, samples that are conditioned by drying them in an oven at 105 °C do not follow the same tendency.

4.3 Effects of initial moisture of samples on ASTM C1585 conditioning method

At the age of 24 months, samples from each mixture conditioned at the three different relative humidities were removed from the chambers. The side surface was sealed with epoxy to be then "re-conditioned" using the 18 day procedure described in ASTM C1585. In addition, three other samples from each mixture were saturated following the procedure described in ASTM C642 [26], to then be "re-conditioned" following the same 18 day procedure. While such a resaturation procedure was employed in the initial sorption testing upon which the ASTM C1585 standard was based [34], it was subsequently omitted from the standard. After samples were fully prepared, testing was performed in accordance with ASTM C1585 over a period of 8 days, with results provided in Figure 10. In addition, Figure 11 shows the calculated initial and secondary sorptivities from these tests. Secondary sorptivity values are not reported when the correlation coefficient is lower than 0.98.

Figures 10 and 11 show that the 3 days of controlled drying at 50 ± 2 °C and 80 % RH followed by the 15 days for internal moisture equilibration is not capable of eliminating the effects of the "moisture history". These results suggest that the ASTM C1585 preparation method does not prepare all the samples to the same water content before a water absorption test. As such this accelerated method can make a substantial difference in how the data is interpreted. This may be due to a moisture hysteresis effect [35]. It should be noted that this can be a concern for field samples evaluated using this method, as their as-received relative humidities may easily vary between the extremes examined in this study.

4.4 Effects of volume of aggregate on sorption test

Figure 12 shows the absorbed water during 8 days of testing performed on mortars containing different volumes of aggregate (mixtures 55/0.50, 45/0.50 and 35/0.50) conditioned at 50 % relative humidity. In Figure 12 a) the effect of a higher volume of paste is observed as the mixture containing the lower volume of aggregate has the higher absorption. However, when the results are normalized by the volume of paste (volume of the main absorbent material), a reversal in the order of the samples is observed (Figure 12 b). The samples with the higher volume of aggregates have a higher absorption.

Water absorption is typically reported without considering the effect of the absorption of the aggregate in the samples. To better understand its effect, Figure 13 was calculated assuming five different sand absorptions (0.0 %, 0.6 %, 1.2 %, 1.8 %, and 2.4 %) to then subtract these values from the absorption in Figure 12 b). When the sand absorption is assumed to be 0.0 %, the resulting absorption at 8 days will be the same as the absorption presented in Figure 12 b). From Figure 13, it can be noticed that for the assumed 1.8 % sand absorption, the normalized water absorbed for the sample is the same after 8 days, independent of the amount of aggregate in the sample.

Figure 14 shows a desorption isotherm for the sand used in these mixtures. It can be noted that at 50 % RH (humidity at which the samples were conditioned), the amount of water on the sand is about 0.2%. Considering that the aggregate used in this study has a 24 h absorption of 1.8%, the difference on water absorption of samples containing different amounts of aggregate can be explained mainly by the amount of water absorbed by the aggregates.

5. Conclusions

This paper has described the absorption behavior of mortars conditioned at different relative humidities. As was shown in previous works by Hall [12], Hooton et al. [4, 7] and Martys and Ferraris [16, 34], the water absorption test is considerably affected by the relative humidity of the samples before starting the test, which if not properly accounted for can lead to a misunderstanding of the actual absorption behavior. Samples conditioned at a 50 % relative humidity can show a total absorption that is approximately six times greater than similar samples conditioned at 80 % relative humidity. This is consistent with expectations based on the mortars' desorption curves.

Initial sorptivity, secondary sorptivity and total absorption at 8 days for samples conditioned in chambers show a linear trend related to the *w/c* and the relative humidity at which samples were conditioned. Samples that are conditioned by drying in an oven at 105 °C do not follow the same trend as samples conditioned in other approaches. This is attributed to two factors: 1) emptying of a wider range of pores, and 2) the potential for microcracking. The conditioning procedure described in ASTM C1585-04 is not able to eliminate the "moisture history" of the samples, and thus can lead to a misunderstanding of the water absorption test results, especially in field samples which have obtained a lower relative humidity. It is recommended that field samples be pre-saturated prior to being exposed to the conditioning regimen of ASTM C1585.

Comparing samples containing different volumes of aggregate can also lead to a misunderstanding of the actual absorption behavior. Samples containing higher volumes of cement paste will absorb more water. When the results are normalized by the volume of cement paste, the sample containing lower volumes of cement paste will absorb more water. However, for the materials examined in this study, this difference can be mainly explained by the amount of water absorbed by the aggregates in the sample.

Acknowledgments

This work was supported in part by the Joint Transportation Research Program administered by the Indiana Department of Transportation and Purdue University (Project SPR 3093). The contents of this paper reflect the views of the authors, who are responsible for the facts and the accuracy of the data presented herein, and do not necessarily reflect the official views or policies of the Federal Highway Administration and the Indiana Department of Transportation, nor do the contents constitute a standard, specification, or regulation. The authors gratefully acknowledge support received from the Center for Advanced Cement Based Materials.

References

[1] ASTM International, ASTM C1585. Standard test method for measurement of rate of absorption of water by hydraulic-cement concretes; 2004.

[2] Sabir B, Wild S, O'Farrell M. A water sorptivity test for mortar and concrete. Mater Struct 1998; 31(8): 568-574.

[3] Maltais Y, Samson E, Marchand J. Predicting the durability of Portland cement systems in aggressive environments - laboratory validation. Cement Concrete Res 2004, 34(9); 1579-1589.

[4] Hooton RD, Mesisc T, Beal DL. (1993). Sorptivity testing of concrete as an indicator of concrete durability and curing efficiency. Proceedings of the Third Canadian Symposium on Cement and Concrete, Ottawa, Ontario, 1993; p. 264-275.

[5] Parrot LJ. Water absorption in cover concrete. Mater Struct 1992; 25(5): 284-292.

[6] Fagerlund G. Predicting the service-life of concrete exposed to frost action through a modeling of the water absorption process in the air pore system. The Modeling of Microstructure and its Potential for Studying transport Properties and Durability, Jennings H, Kropp J, Scrivener K, editors. The Netherlands, 1996; p. 503-539.

[7] Hearn N, Hooton D, Mills R. Pore structure and permeability. Significance of Tests and Properties of Concrete and Concrete-Making Materials, ASTM STP 169C. Klieger P, Lamond J, editors; 1994; 240-262.

[8] Henkensiefken R, Castro J, Bentz D, Nantung T, Weiss J. Water Absorption in Internally Cured Mortar Made with Water-Filled Lightweight Aggregate. Cement Concrete Res 2009; 39(10): 883-892.

[9] Neithalath N. Analysis of moisture transport in mortars and concrete using sorption-diffusion approach. ACI Mater J 2006; 103(3): 209-218.

[10] Yang Z. Assessing cumulative damage in concrete and quantifying its influence on life cycle performance modeling. PhD thesis, Purdue University, 2004.

[11] Bentz DP, Ehlen MA, Ferraris CF, Garboczi EJ. Sorptivity-based service life predictions for concrete pavements. Proceedings. 7th international conference on concrete pavements, Orlando FL, 2001; p. 181-193.

[12] Hall C. Water sorptivity of mortars and concretes: a review. Mag Concrete Res 1989; 41(146): 51-61.

[13] Spragg R. Castro J. Li W, Pour-Ghaz M, Huang P, Weiss J. Wetting and drying of concrete in the presence of deicing salt solutions. Submitted to Transportation Research Board 90th annual meeting, 2011.

[14] Yang Z, Weiss J, Olek J. Water absorption in partially saturated fracture concrete. RILEM workshop: transport mechanism in cracked concrete. Ghent, 2007.

[15] Martys NS. Diffusion in partially saturated porous materials. Mater Struct 1999, 32(8): 991-1004.

[16] Martys N. Ferraris CF. Capillary transport in mortar and concrete. Cement Concrete Res 1997; 27(5): 747-760

[17] Lockington D, Parlange JY, Dux P. Sorptivity and the estimation of water penetration into unsaturated concrete. Mater Struct 1999; 32(5): 342-347.

[18] Hall C. Anomalous diffusion in unsaturated flow: fact or fiction?, Cement Concrete Res 2007; 37(3): 378–385.

[19] Powers TC, Brownyard TL. Studies of the physical properties of hardened Portland cement paste. American Concrete Institute Proceedings 1946; 43: 469-482.
[20] Parrott LJ. Moisture conditioning and transport properties of concrete test specimens. Mater Struct 1994; 27(8): 460-468.
[21] Parrott LJ. Factor influencing relative humidity in concrete. Mag Concrete Res 1991; 43(154): 45-52.
[22] DeSouza SJ, Hooton RD, Bickley JA. Evaluation of laboratory drying procedures relevant to field conditions for concrete sorptivity measurements. Cem Concrete Agg 1997; 19(2): 59-63.
[23] DeSouza SJ, Hooton RD, Bickley JA. A field test for evaluating high performance concrete covercrete quality. Can J Civil Eng 1998; 25(3): 551-556.
[24] Castro J, Kompare P, Poursaee P, Nantung T, Weiss J. JTRP Report SPR-3093, Portland cement concrete pavement performance relative to permeability. Indiana Department of Transportation, 2010.
[25] ASTM International, ASTM C305. Standard practice for mechanical mixing of hydraulic cement pastes and mortars of plastic consistency, 2006.
[26] ASTM International ASTM C642. Standard test method for density, absorption, and voids in hardened concrete, 2006.
[27] Powers TC, Copeland LI, Mann HM. Capillary continuity or discontinuity in cement pastes. J. PCA Res. Dev. Lab 1959; 1(2): 38-48.
[28] Hwang C, Young J. Drying shrinkage of portland cement pastes. microcracking during drying. Cement Concrete Res 1984; 14(4): 585-594.
[29] Chatterji S. (1976). “Drying shrinkage of cement paste and concrete: a reappraisal of the measurement technique and its significance. Cement Concrete Res 1976; 6(1): 145-148.
[30] Bisschop J. Van Mier J. How to study drying shrinkage microcracking in cement-based materials using optical and scanning electron microscopy? Cement Concrete Res 2002; 32(2): 279-287.
[31] Samaha H. Hover K. Influence of microcracking on the mass transport properties of concrete. ACI Mater J 1992; 89(4): 416-424.
[32] Yang Z, Weiss J, Olek J. Water transport on concrete damaged by tensile loading and freeze-thaw cycling. J Mater Civil Eng 2006; 18(3): 424-434.
[33] Yang Z. Assessing cumulative damage in concrete and quantifying its influence on life cycle performance modeling. PhD thesis, Purdue University, West Lafayette, Indiana, 2004.
[34] Bentz DP, Ehlen CF, Ferraris CF, Winpigler JA. Service life prediction based on sorptivity for highway concrete exposed to sulfate attack and freeze-thaw conditions, FHWA-RD-01-162, U.S. Department of Transportation, 2002, 62 pp.
[35] Nilsson LO. Hygroscopic moisture in concrete – drying, measurements and related material properties. PhD thesis. Lund University, 1980.

Table

Table 1. Mixture proportions in saturated surface dry (SSD) conditions.

Material	55/0.35	55/0.40	55/0.45	55/0.50	45/0.50	35/0.50
Volume fraction of aggregate	55%	55%	55%	55%	45%	35%
w/c	0.35	0.40	0.45	0.50	0.50	0.50
Cement (kg/m^3)	673	626	585	549	671	793
Water (kg/m^3)	235	250	263	275	336	397
Fine Aggregate (kg/m^3), SSD	1442	1442	1442	1442	1180	918
HRWRA (g/ 100 g cement)	0.60	0.40	0.20	0.00	0.00	0.00

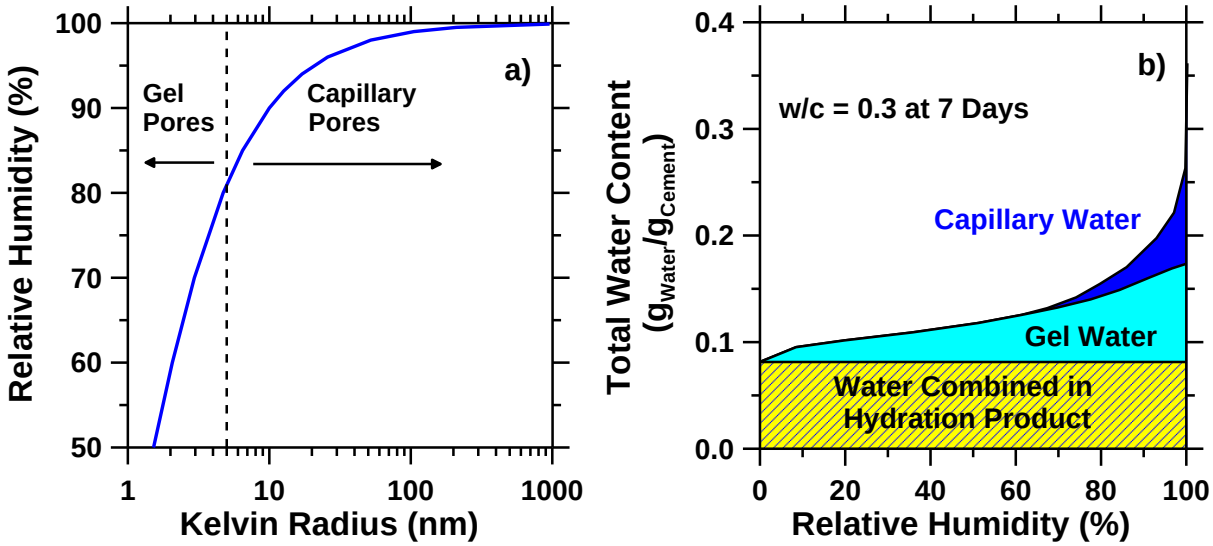

Fig. 1. Relation between relative humidity and partially empty pores in cement paste.

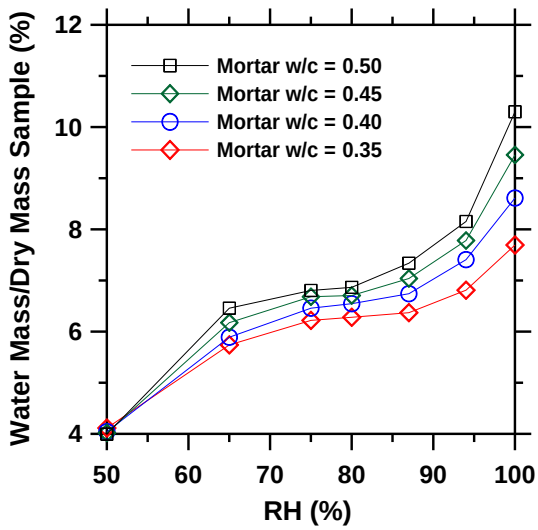

Fig. 2. Desorption curves for 14 m mortar samples (typical standard deviation in the average of 3 samples is lower than 0.2%).

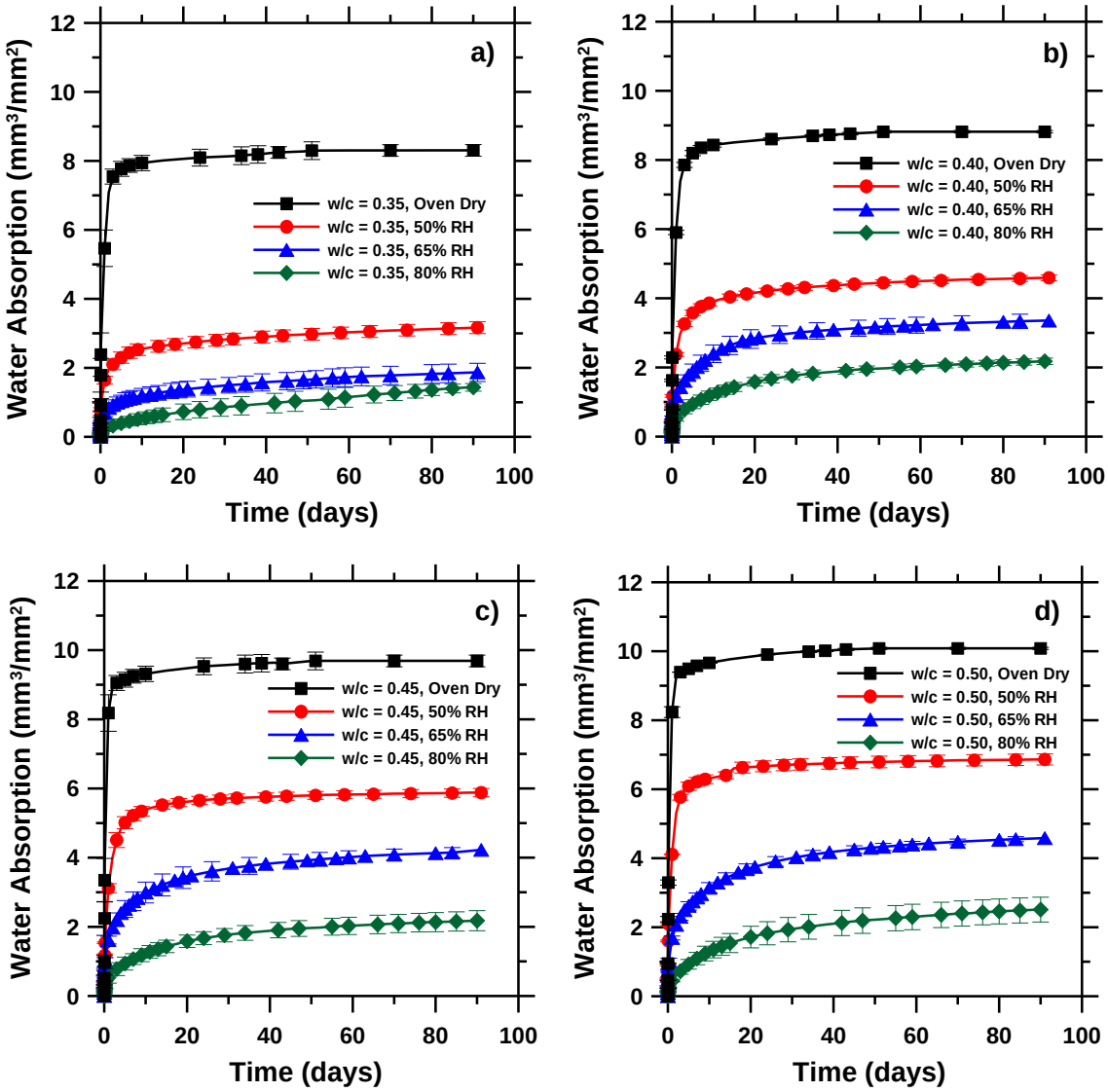

Fig. 3. Absorbed water in mortars as a function of relative humidity a) mixture 55/0.35, b) mixture 55/0.40, c) mixture 55/0.45, d) mixture 55/0.50. Error bars represent the standard deviation for the average of three samples.

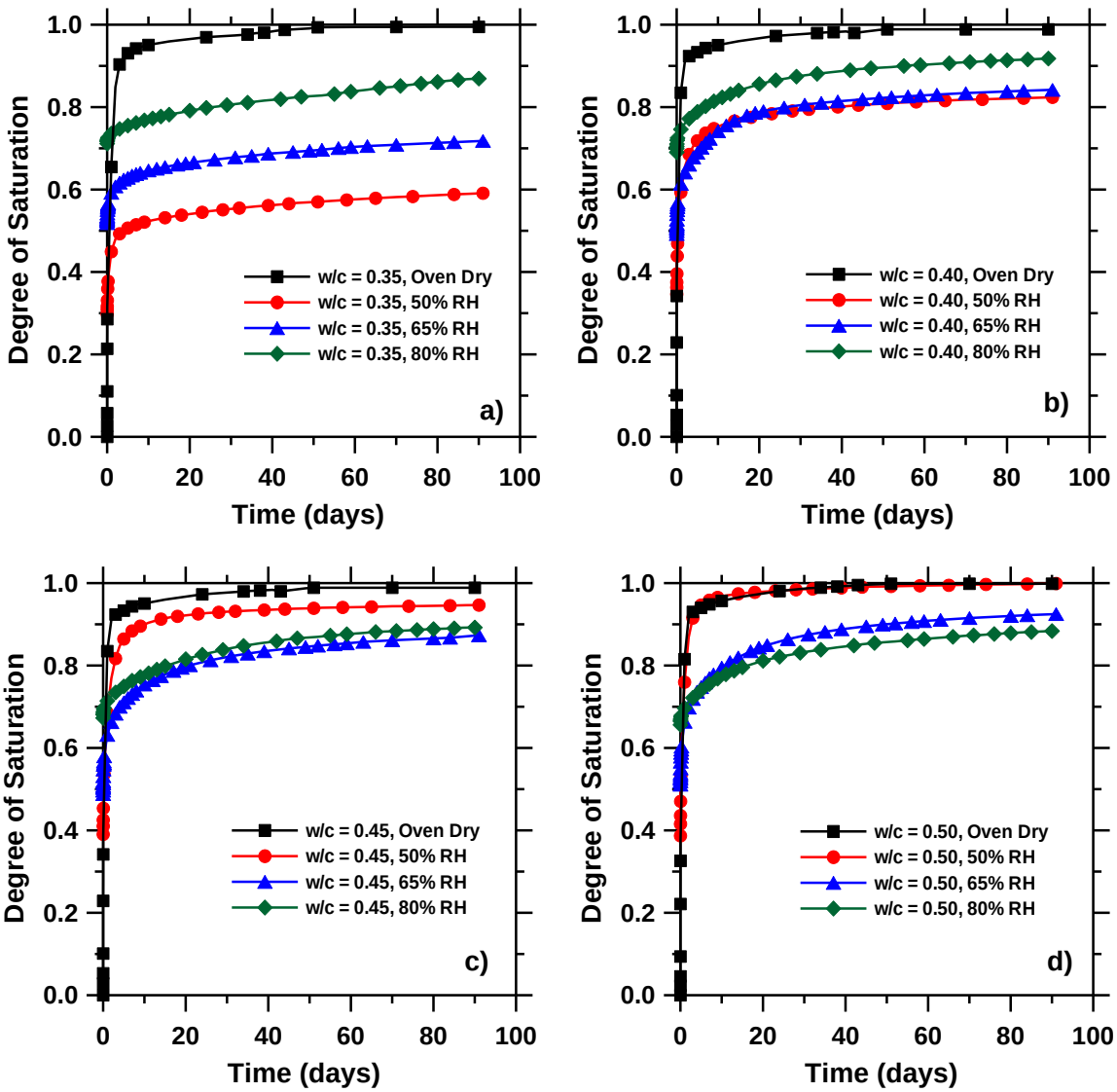

Fig. 4. Degree of saturation as a function of time during the water absorption test: a) mixture 55/0.35, b) mixture 55/0.40, c) mixture 55/0.45, d) mixture 55/0.50. Typical standard deviation of the average of three samples is lower than 0.02 points in the degree of saturation.

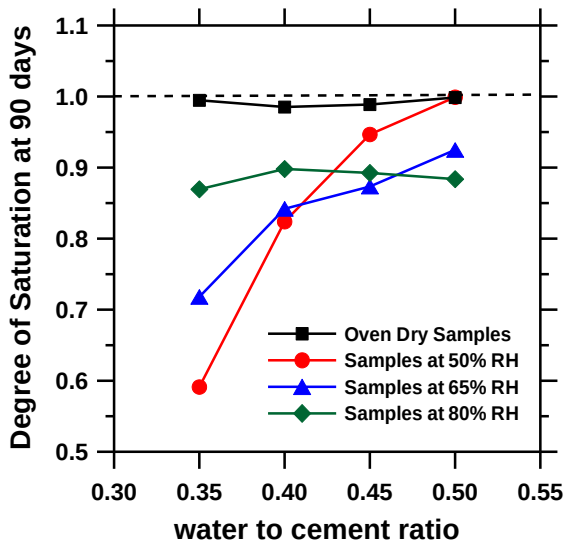

Fig. 5. Degree of saturation after 90 d in contact with water as a function of the *w/c*.

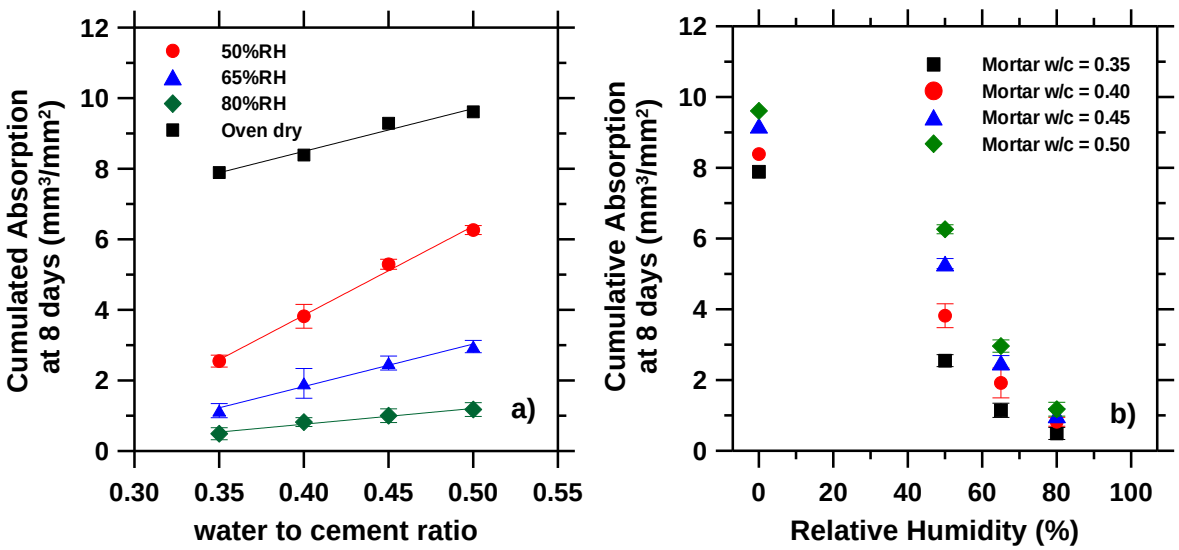

Fig. 6. Cumulative absorption at 8 d for mortars with 55 % aggregates versus: a) *w/c*, b) relative humidity. Solid lines are provided only to show a general tendency in the data. Error bars represent the standard deviation on the average of 3 samples.

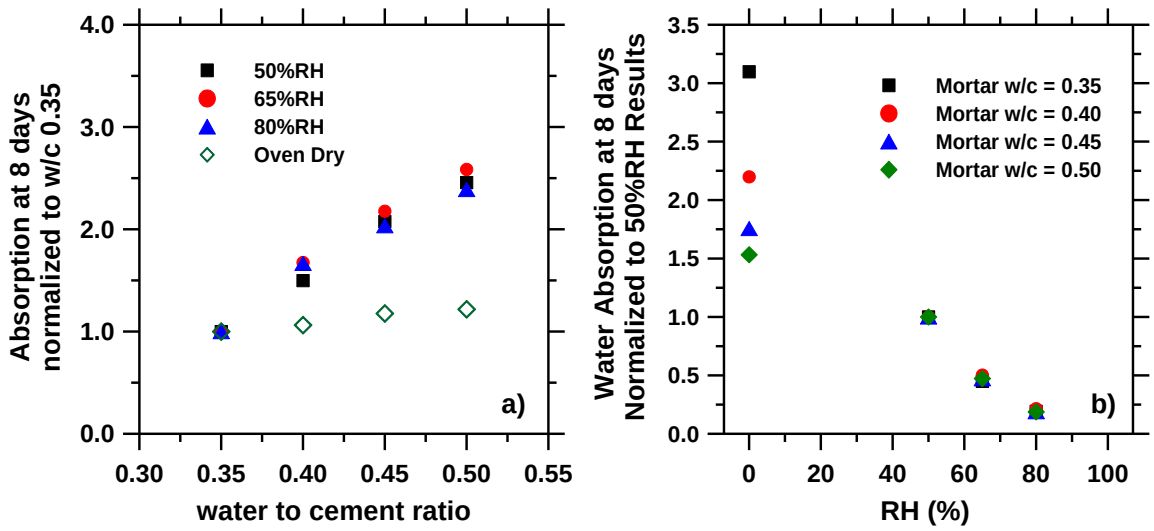

Fig. 7. Cumulative absorption at 8 days versus *w/c* and relative humidity: a) normalized to absorption of mixture 55/0.35, b) normalized to absorption at 50 %RH.

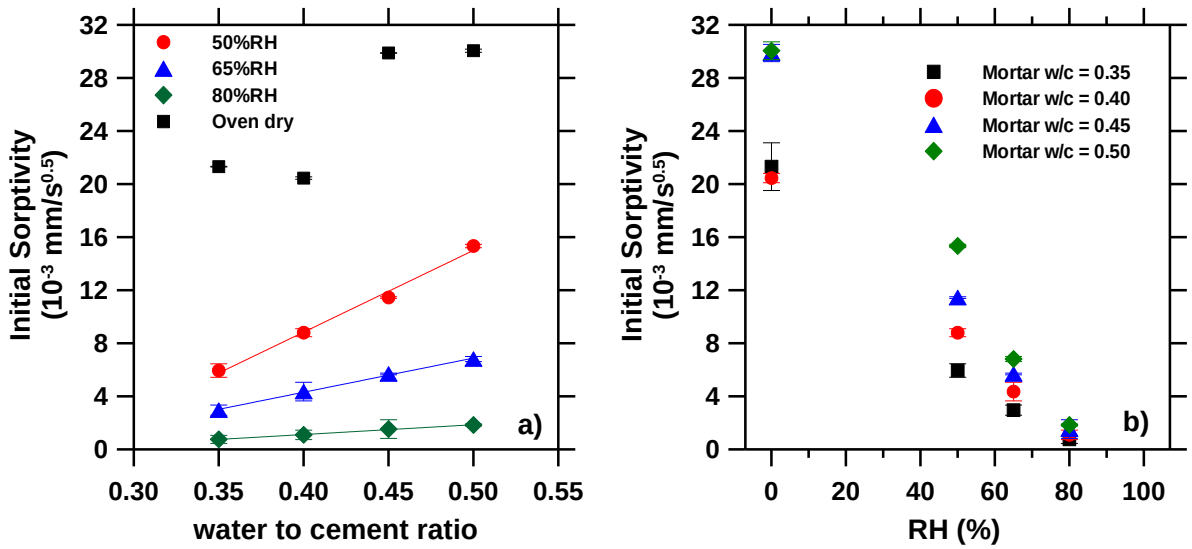

Fig. 8. Initial absorption of the 55 % aggregate mortars conditioned at different RH as a function of: a) *w/c*, b) relative humidity. Solid lines are provided to show a general tendency in the data. Error bars represent the standard deviation on the average of 3 samples.

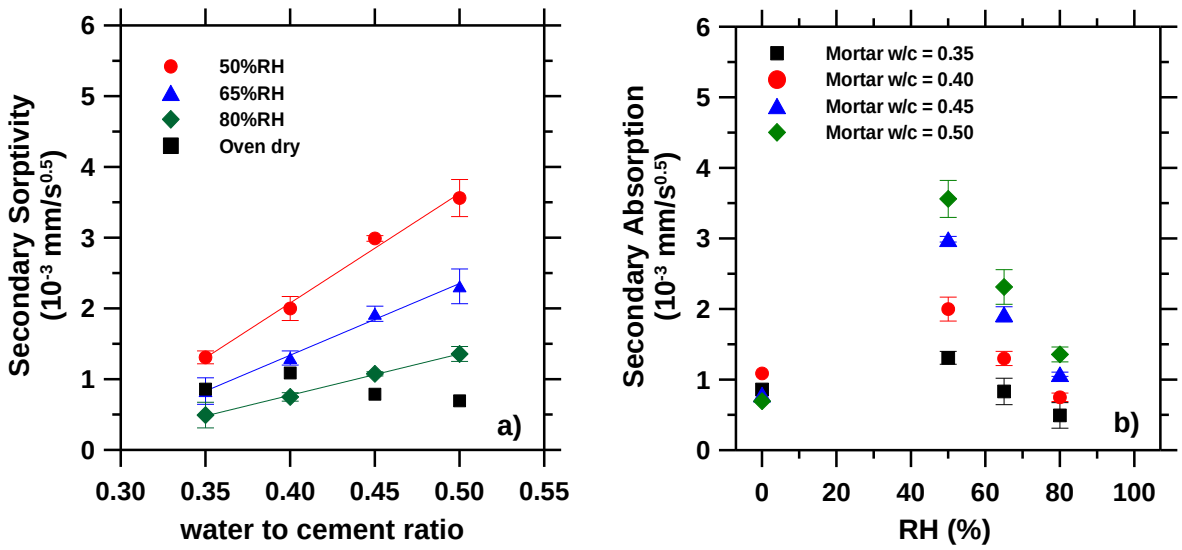

Fig. 9. Secondary absorption on mortars with 55 % aggregates conditioned at different RH as a function of: a) *w/c*, b) relative humidity. Solid lines are provided to show a general tendency in the data. Error bars represent the standard deviation on the average of 3 samples.

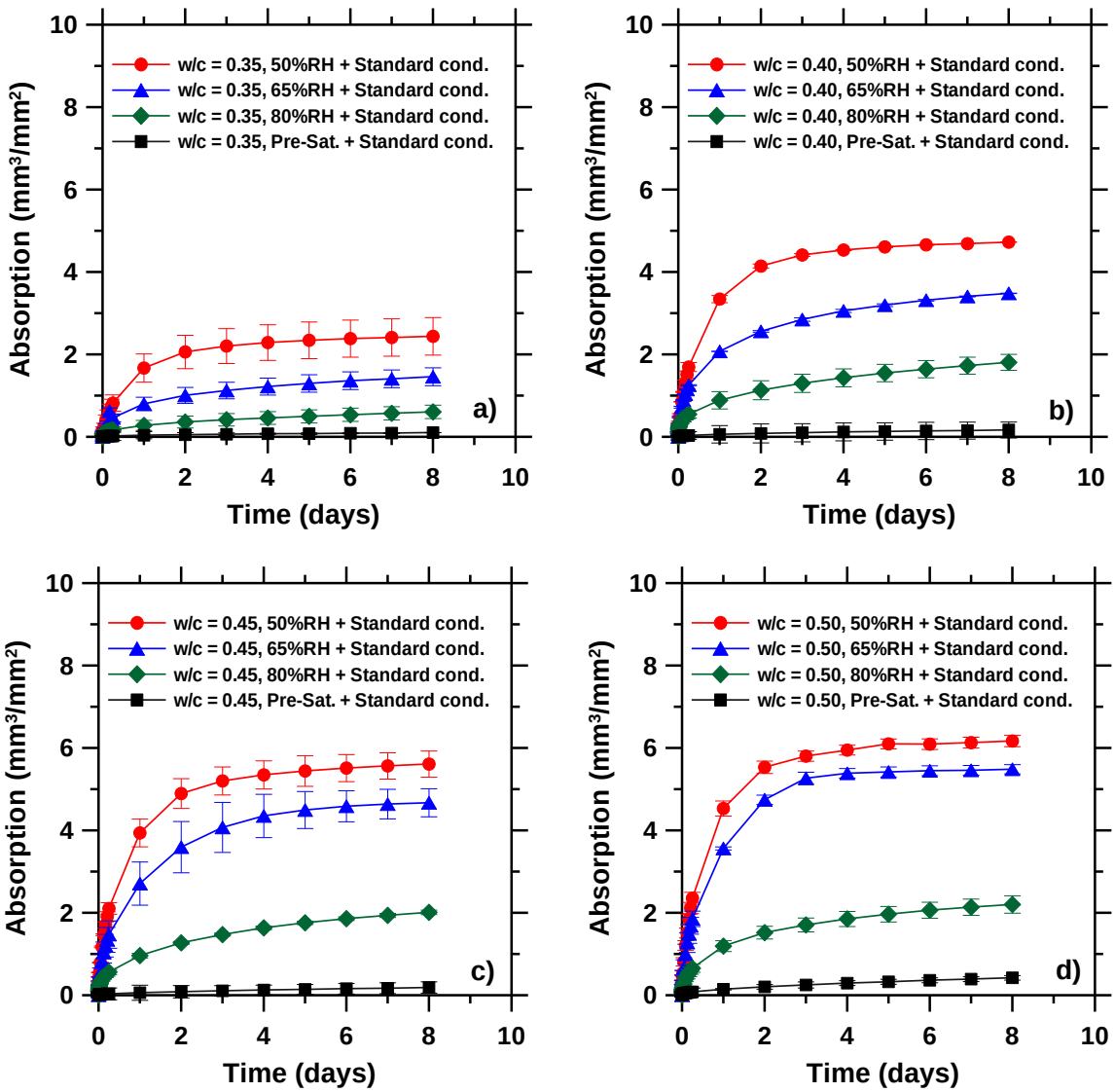

Fig. 10. Effect of initial moisture on the conditioning procedure established in ASTM C1585-04 a) mixture 55/0.35, b) mixture 55/0.40, c) mixture 55/0.45, d) mixture 55/0.50. Error bars represent the standard deviation for the average of three samples.

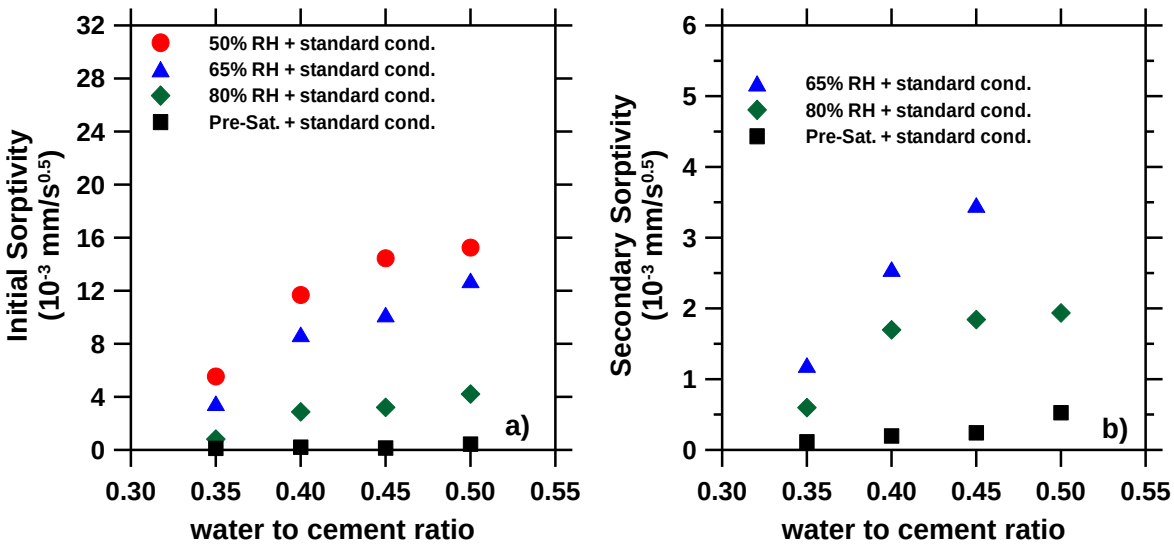

Fig. 11. Initial and secondary sorptivities on mortars with different initial moisture contents, conditioned with the procedure established in ASTM C1585-04.

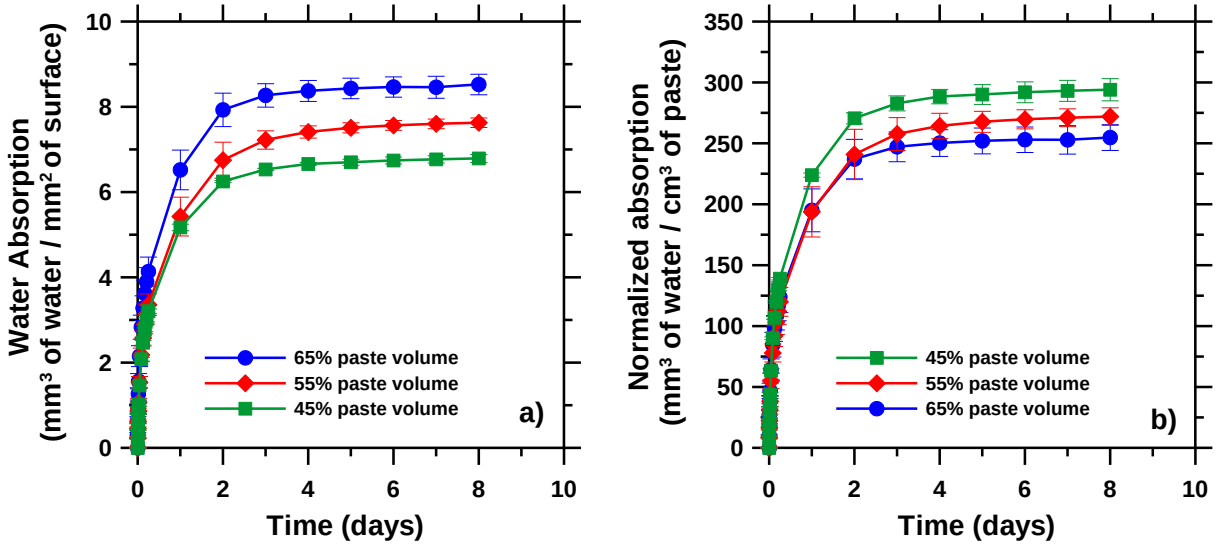

Fig. 12. Water absorption in mortars containing different volume of aggregates: a) normalized by surface in contact with water, (b) normalized by volume of paste.

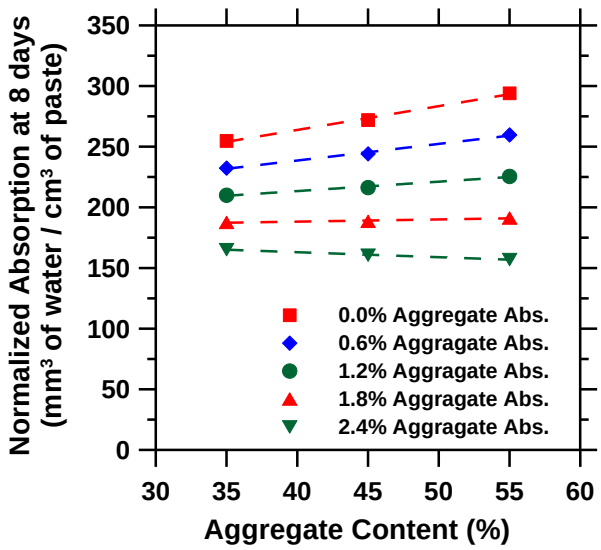

Fig 13. Water absorption at 8 d normalized by volume of paste, corrected by different values of aggregate absorption.

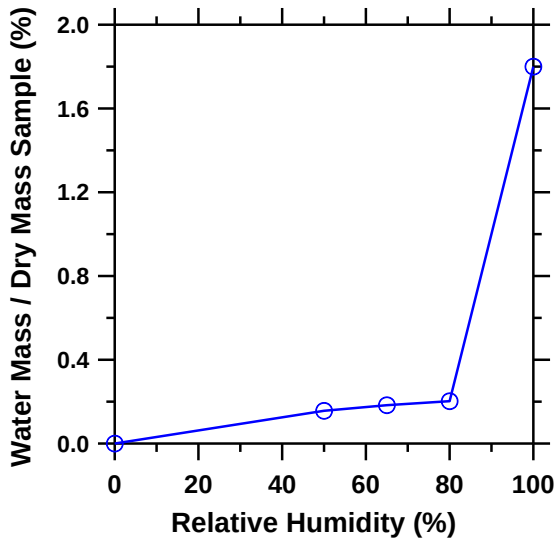

Fig. 14. Desorption isotherm for the sand used in this research.

Automation in Construction 19 (2010) 485–490

Contents lists available at ScienceDirect

Automation in Construction

journal homepage: www.elsevier.com/locate/autcon

An automated electrical monitoring system (AEMS) to assess property development in concrete

A. Poursaee *, W.J. Weiss

School of Civil Engineering, Purdue University, West Lafayette, IN, 47907, United States

ARTICLE INFO

Article history:
Accepted 29 December 2009

Keywords:
Electrical impedance
Automation
Concrete
Electrical properties
Imaging
LabVIEW

ABSTRACT

Electrical impedance measurement techniques are being increasingly used to measure material property development and permeability of concrete and other cement based materials. This paper describes the development of an automated electrical measurement system (AEMS) for measuring the properties of cementitious materials. The components of this system are an electrical impedance spectrometer, a digital multi-meter, a switching unit, and a customized software (AEMS) which communicates between different components of the system to control the testing and to collect data. This system enables electrical properties of multiple specimens to be measured in an automated fashion thereby making this approach very amenable for use in quality control applications. Further, an extension of this system is proposed which would enable its use to detect flaws in concrete using electrical imaging.

1. Introduction

Electrical impedance measurement techniques have been shown to provide useful information that can be used to characterize cementitious systems [1–3]. This technique studies the system response to the application of a small amplitude alternating potential signal at different frequencies. AC electrical impedance measurements have the advantages of being non-invasive and non-destructive, require little in term of preparation of the sample, and offer the possibility of continual measurements to describe the effect of hydration [4,5] drying [6], or permeability [7].

Electrical impedance techniques have been used in different research projects in concrete to study a wide range of concrete properties specifically this included studies on the microstructural development of cementitious materials [8,9], precipitation of calcium hydroxide on the surface of steel after the setting of the mortar [10], long-term effectiveness of concrete inhibitors for steel in concrete [11–15], the chloride diffusivity in concrete [16], chloride permeability of high performance concrete [17], detection of damage during tensile loading of cement composites [18], freezing of water in Portland cement paste [19], water penetration in concrete [20–22], setting time of concrete [23,24], measuring the concrete internal moisture content [25], and assessing the change in microstructure due to rapid chloride permeability test [26,27].

While numerous applications exit, they are frequently limited to the measurement of one sample at a time. It is regularly necessary to conduct experimental measurements at multiple locations in a sample or on multiple specimens. For example, Schmit [28] described the use of multiple sensors and quantified the influence of sensor position and number in uncertainty of the results. The ability to perform multiple measurements is very valuable for monitoring the hydration process, monitoring multiple specimens, or imaging the crack by electrical impedance measurements [29]. In addition, a single measurement cannot properly represent the behavior of a material. To improve measurements accuracy multiple measurements are needed. This paper describes the development of a user friendly Automatic Electrical Monitoring System (AEMS). By using this system, multiple electrical measurements can be performed on specimens and different properties of concrete materials can be monitored. The developed system is discussed and some applications of the AEMS were shown in this paper.

2. Objective

This paper describes the development of an Automated Electrical Monitoring System (AEMS). The data acquisition system consists of a computer, a Keithley digital multi-meter and switching unit [30], and Solartron 1260 impedance spectrometer[1] [31]. The role of the software is to communicate between all components of the system and to control data collection. This paper shows that the system is reliable for both short and long-term monitoring. Further, this paper points out that while in the past the use of electrical impedance

[1] Certain commercial products are identified in this paper to specify the materials used and procedures employed. In no case does such identification imply endorsement by the authors, nor does it indicate that the products are necessarily the best available for the purpose.

* Corresponding author.
E-mail address: poursaee@purdue.edu (A. Poursaee).

0926-5805/$ – see front matter © 2010 Elsevier B.V. All rights reserved.
doi:10.1016/j.autcon.2009.12.016

measurement techniques has been time consuming, automation enables these measurements to be performed efficiently. This enables new applications, like electrical imaging, to be performed effectively and enables EIS to be extended for use in daily quality control processes such as permeability measurements. Since electrical impedance requires less preparation and time, it can be a good replacement for the tests like rapid chloride permeability which is time consuming and can alter the microstructure of the concrete.

3. Component of the measurement system

The system developed for this investigation can be used to measure the AC electrical impedance response of the material. The components in the system consist of an impedance spectrometer, digital multi-meter, and a switching unit.

The electrical impedance spectrometer used in this study is capable of performing only one measurement at a time. There are multi-channel spectrometer units on the commercial market. However, in addition to their high cost most of the units are limited to only a few measurements (up to 16) at a time which also may be a limiting factor.

The digital multi-meter and switching unit chosen for this project included a Keithley model 2750 mainframe which has five slots and a model 2700 which has two slots for inserting the plug-in switch/control modules. Each slot can support a series of multiplexer, matrix, or control modules. For example the Module 7708 which was used in this project has 40 channels. The general features of this module are described in [32]. The role of the mainframe is to communicate between channels. Temperature can also be measured using this system as this is needed for temperature corrections [33].

For each impedance measurement (each sample), 2 channels are required, (i.e., the Keithley model 2750 mainframe with five 7708 modules can be used for 100 impedance measurements). If more than 100 measurements are necessary, several mainframes can be joined together to provide the appropriate number of channels.

To combine the mentioned components, the software (named AEMS) was developed, using LabVIEW. This software selects the sample that will be tested and then runs the impedance spectrometer on that sample. After the measurements are completed, the AEMS, stops the spectrometer, switches the sample and runs the test again. The measurements are performed one by one not simultaneously. In all the graphs shown in the paper, this time is considered. This time for AC measurements is a function of selected frequency and in all examples in this paper it was about 40 s. However, when the concrete is hardened, this time difference is not considerable. If some interval time is necessary between measurements, the AEMS can be programmed to place the necessary time interval between measurements. In addition, the AEMS can communicate with the mainframe to measure voltage, DC resistance and temperature independent from the spectrometer. Fig. 1 schematically shows the component of the system and the actual parts are shown in Fig. 2.

While an RS-232 serial port was used to control the multi-meter and switching system in this study, faster data transfer can be performed using a GPIB[2] [34] card. The role of the AEMS software is to control and switch the channels for each measurement, to control and run the spectrometer and save data to the computer for later analysis.

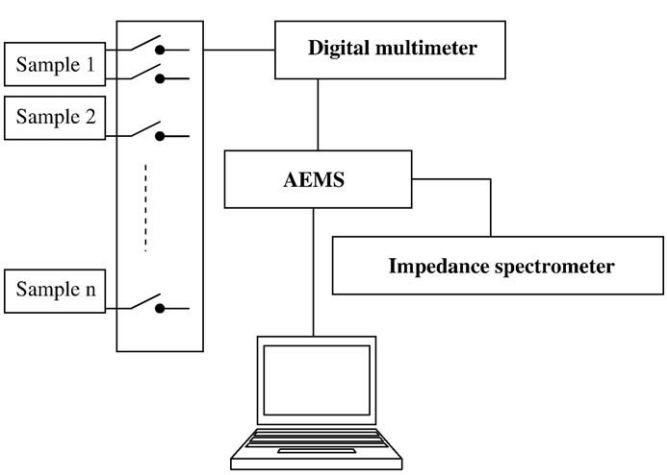

Fig. 1. Schematic relationship between the components of the system.

Fig. 2. Components of the system.

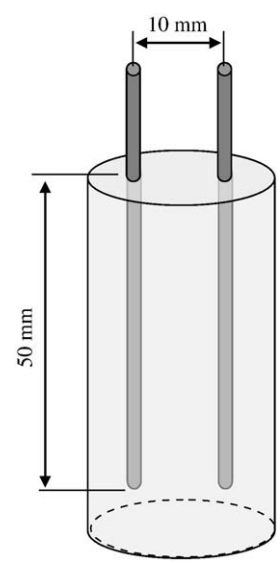

Fig. 3. Schematic view of the cylindrical paste specimens, used to measure variability in cement paste.

[2] The General Purpose Interface Bus (GPIB) is an industry standard published by the Institute of Electrical and Electronic Engineers (IEEE) as ANSI/IEEE Standard 488. GPIB defines the electrical, mechanical, functional, and software specifications of an interfacing system to connect PCs to programmable instrument.

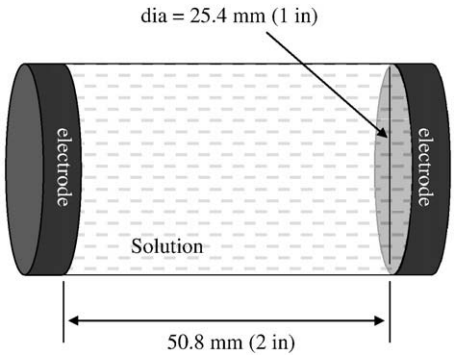

Fig. 4. Schematic view of the container with known geometry, to measure the conductivity of the solutions.

The software contains options which enable the user to set the number of samples, measurement frequency, and the time between each set of measurements. The saved data can be opened and analyzed in Excel®. Based on the number of measurements, one may end up with thousands of data files. Therefore, a macro was developed to automatically analyze individual data and place the summarized results in a worksheet.

4. Experimental results

To verify the performance of the switching units, two simple experiments were conducted. In the first test, a known resistor (10 Ω) was connected to all available channels and the resistance was measured. In the second test, a known potential was measured, using all channels. Results show that there is no significant difference between measured values with each channels and the relative standard deviation was less than 0.005%.

4.1. Electrical conductivity of cement paste sample during hydration

Electrical measurements can provide information about the change in pore structure due to hydration process [23,35]. It is important to use multiple specimens for these measurements due to the inhomogeneity and corresponding variability of cementitious materials. To determine the variation between different samples the electrical conductivity of cement paste samples was measured using cylindrical paste specimens as described in Fig. 3. Type I ordinary Portland cement was used with a Blaine fineness of 360 m^2/kg and a Bogue phase composition of 60% C_3S, 12% C_2S, 12% C_3A, 7% C_4AF and Na_2O equivalent of 0.72%. Fifteen samples were prepared with a *w*/*c* of 0.45 and 5 samples were prepared with a *w*/*c* of 0.50. The measurement frequency range that was used for the tests ranged from 1 MHz to 10 Hz with ten measurements per decade using the 500 mV AC stimulus. To determine the conductivity of the material, the bulk resistance (R_b) obtained from the impedance response normalized for the effects of specimen and electrode geometries, using the following equation:

$$\sigma_t = k / R_b \quad (1)$$

where, σ_t is the conductivity (S/m) of the paste, R_b is the measured bulk resistance (Ω) and *k* is a geometry factor. The geometry factor

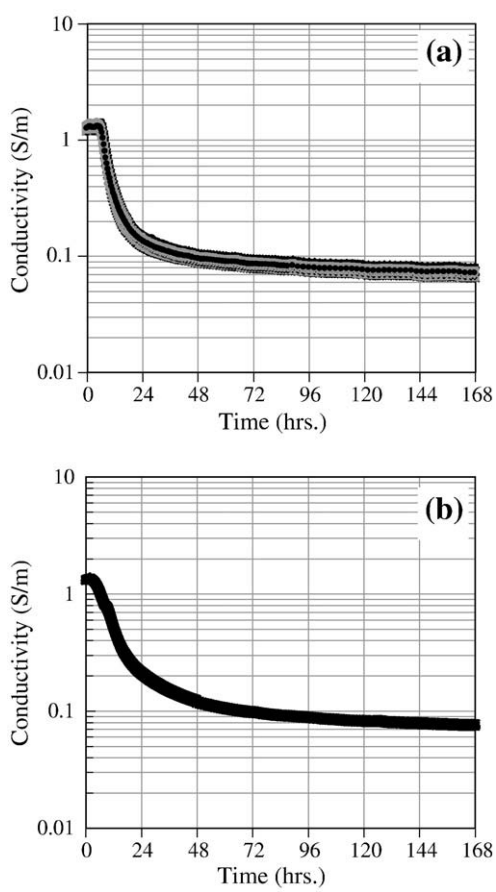

Fig. 5. Development of the conductivity of (a) 15 cement paste samples with *w*/*c* = 0.45 and, (b) 5 cement paste samples with *w*/*c* = 0.5.

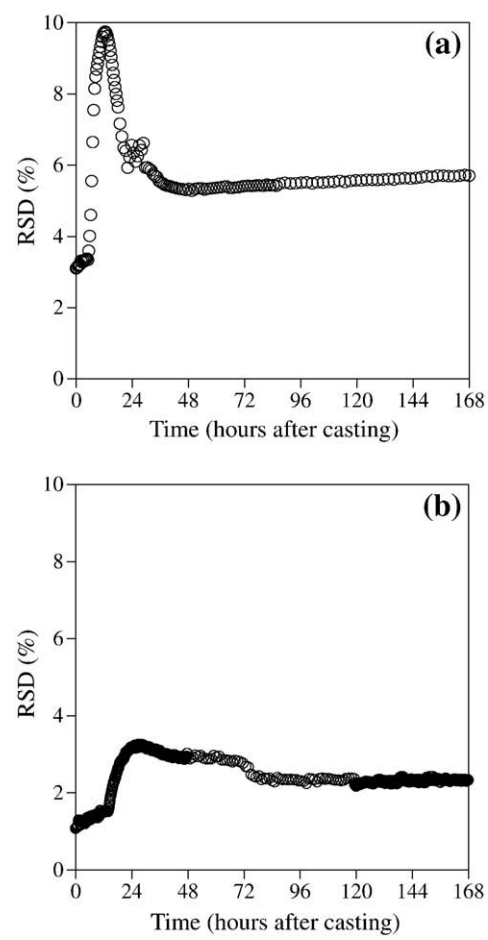

Fig. 6. Relative standard deviation between (a) 15 cement paste samples, with *w*/*c* = 0.45, at different ages and, (b) between 5 cement paste samples, with *w*/*c* = 0.50, at different ages.

was determined by filling the molds with solutions of known conductivity and measuring the bulk resistance between the electrodes. In this experiment two sodium chloride solutions were prepared with two different concentrations (0.1 M and 1 M). The conductivity of the two solutions was measured (7.72 and 1.01 S/m for 1 M and 0.1 M solutions, respectively), using a container with known geometry as shown in Fig. 4. By using this information, the value of the geometry factor, k, was calculated to be 15.5/m for the geometry shown in Fig. 3.

The electrical impedance of the samples was measured for 7 days, starting 30 min after casting. Fig. 5 shows the conductivity of the samples with w/c of 0.45 and 0.50, respectively. At the end of the test, all samples were inspected to ascertain the uniformity of specimen.

It can be seen that the conductivity of all samples follows the same pattern. As expected, the conductivity decreases as the system hydrates [36–38].

To better assess the variation, the relative standard deviation (RSD) can be used. The RSD is useful for comparing the uncertainty between different measurements of varying absolute magnitude. The RSD is the absolute value of the coefficient of variation calculated using Eq. (2):

$$\mathrm{RSD} = \frac{(\text{Standard devation of conductivity})}{\text{Average of conductivity}} \times 100 \tag{2}$$

Fig. 6 shows the RSD of the samples at different ages. Results show that, even when the samples are made from one mixture there is variability in the conductivity of the samples, especially at early ages when the properties change most dramatically. However, the RSD decreases over time as the measurements stabilize. This is shown in Fig. 7, which gives the histograms of conductivities for $w/c = 0.45$ (15 samples) at two different ages. The maximum difference is less than 10% for $w/c = 0.45$ and 3.5% for $w/c = 0.50$ at all ages.

Table 1
Mixture proportions of concrete samples.

Materials	Batch proportion for 100 kg (kg)		
	$w/c = 0.48$, no WR	$w/c = 0.53$, no WR	$w/c = 0.48$ with WR
Cement (Type I)	8.0	8.0	8.0
Water	3.9	4.3	3.9
Coarse aggregate	68.9	68.6	68.7
Fine aggregate	19.1	19.0	19.0
Water reducer (WR)	0.0	0.0	0.3

4.2. Electrical conductivity of concrete sample

To show the capability of the AEMS, the conductivity of concrete cylinders was measured with different mixture proportions (shown in Table 1). For this purpose, 200 mm (diameter) × 400 mm (length) concrete cylinders were prepared with two (1.9 mm diameter) stainless steel rods as the electrodes. The electrodes were spaced 100 mm apart from each other and fixed in the mold. For each mixture, five cylinders were cast and impedance tests were performed every 15 min. The impedance measurements began 30 min after casting and continued for 7 days. Results show that the conductivities of all five samples of each mixture have very similar results with the RSD between 1 and 2.5% as can be seen in Fig. 9. As can be seen in Fig. 8, at about 10 h, the conductivity of concrete samples is similar. It is obvious from the results that impedance spectroscopy technique is capable to evaluate and compare different samples with different mixture proportions.

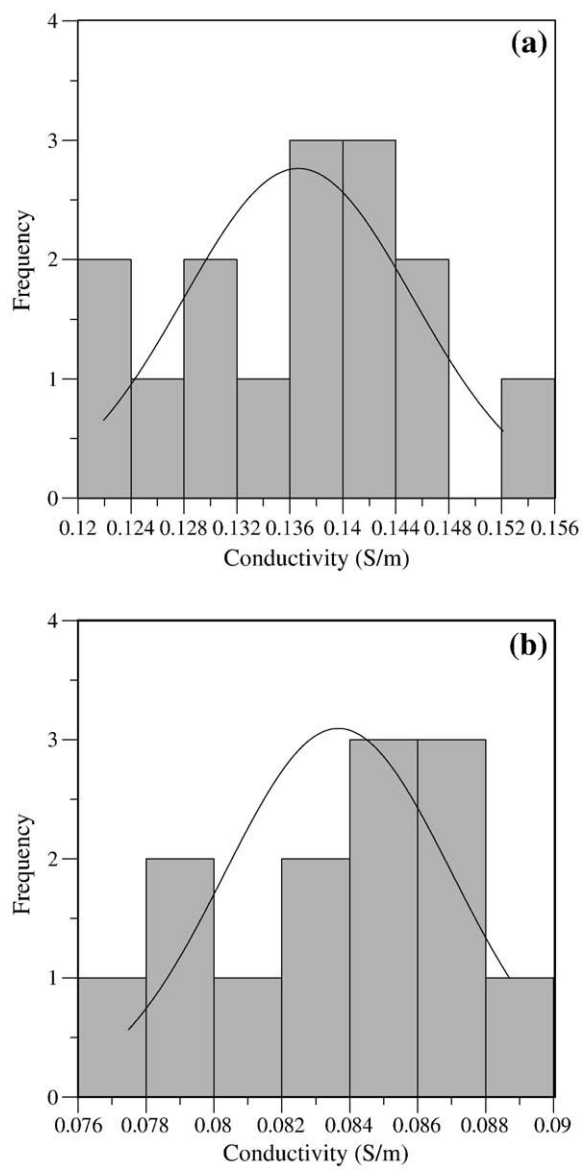

Fig. 7. Histogram of conductivity of paste samples with $w/c = 0.45$ (a) 24 h after casting, (b) 72 h after casting.

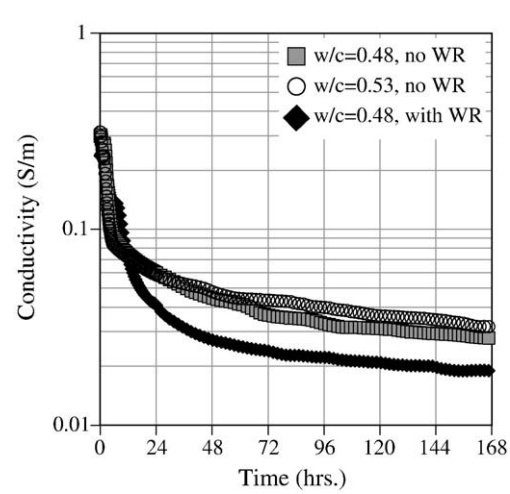

Fig. 8. Conductivity of concrete with three different mixture proportions, shown in Table 1.

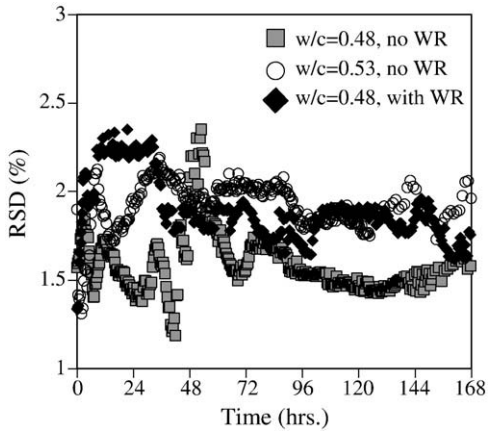

Fig. 9. Relative standard deviation between concrete samples with three different mixture proportions, shown in Table 1, at different ages.

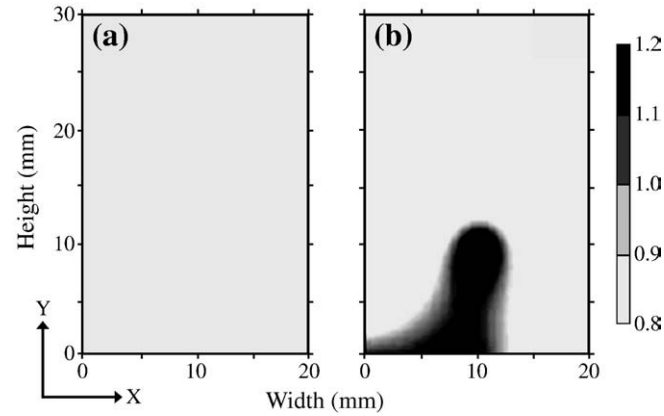

Fig. 11. Image of the concrete sample (a) without and (b) with saw cut, created by electrical impedance measurements.

4.3. Crack imaging in cement paste and concrete, using impedance spectroscopy

Electrical impedance imaging has been used by many researchers in the medical field to monitor various physiological variables [39–41]. Previous studies indicated that this technique can also be used in imaging the defects in cementitious materials [29,42]; however, studies in cement are somewhat limited. The approach consists of measuring the impedance at different locations on the surface of the concrete and constructing electrical conductivity (or resistivity) contour plot from the measured impedances. Since the presence of damage (e.g., a crack) changes the path of electrical flow in the concrete, any damage will appear on the plot. Electrical contour plots can be used to locate visible and invisible damage. In order to investigate this technique a small test unit developed consisting of twenty electrodes, as shown in Fig. 10. The impedance was measured between each pin, in *X* and *Y* directions. Then the measured values were used to construct electrical resistance contour plots. For this experiment, two concrete samples were prepared with water: cement:coarse aggregates:fine aggregates ratio of 0.4:1:3:2.85:2.37. The measurement frequency range was 1 MHz to 10 Hz, with the 500 mV AC stimulus. After performing the measurements, the resistances measured between each pin were normalized based on the maximum measured value in each case and then the normalized values were mapped. Fig. 11 shows the constructed image. The location of the saw cut is clearly visible in this image. A similar setup (with different size and spacing between electrodes) can be used to determine the location of the damaged area beneath the sealed saw cut or joints which is currently under investigation.

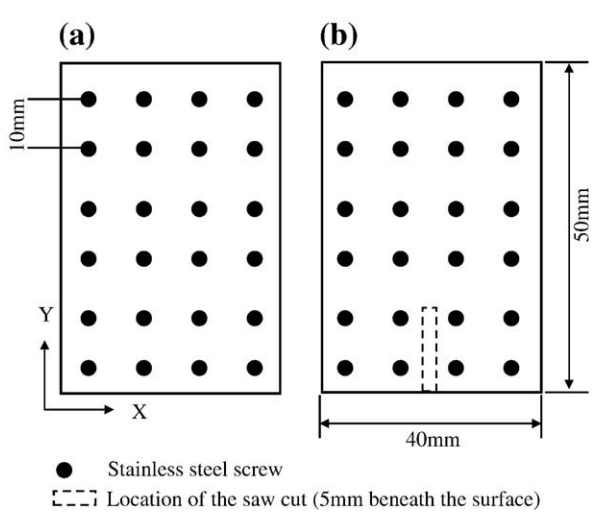

Fig. 10. The dimensions of the concrete samples and the measurement setup, used for imaging: (a) concrete sample with no cut, and (b) concrete sample with the saw cut.

5. Conclusion

This paper described an approach to automate electrical impedance measurements with an automated electrical monitoring system (AEMS) that enable multiple measurements to be made.

This switching system enables measurements to be performed on multiple specimens or where multiple locations are needed. This enables the aging processes be better quantified, allows variability to be qualified for quality control, and enables electrical imaging to be performed.

The system described in this paper was successfully used to investigate the behavior of concrete sample with different mixture proportions by continuously monitoring their conductivity. In addition, variability among different samples was studied and the results show that there is variability between samples even cast from one batch which needs to be considered, specifically in statistical analysis. Constructed electrical image maps can be used to locate the cracked and damaged area, even if it is beneath the surface.

Acknowledgements

This work was supported in part by the Joint Transportation Research Program administered by the Indiana Department of Transportation and Purdue University (study no. TPF-5(179)). The contents of this paper reflect the views of the authors, who are responsible for the facts and the accuracy of the data presented herein, and do not necessarily reflect the official views or policies of the Indiana Department of Transportation, nor do the contents constitute a standard, specification, or regulation.

References

[1] W.J. McCarter, et al., Characterization and monitoring of cement-based systems using intrinsic electrical property measurements, Cement and Concrete Research 33 (2003) 197–206.
[2] B.J. Christensen, et al., Impedance spectroscopy of hydrating cement-based materials: measurement, interpretation, and application, Journal of the American Ceramic Society 77 (1) (1994) 2789–2801.
[3] P. Gu, P. Xie, J.J. Beaudoin, Some applications of AC impedance spectroscopy in cement research, Cement, Concrete and Aggregates 17 (2) (1995) 113–118.
[4] F. Rajabipour, W.J. Weiss, Electrical conductivity of drying cement paste, Materials and Structures 40 (2007) 1143–1160.
[5] W.J. Weiss, J.D. Shane, A. Mieses, T.O. Mason, S.P. Shah. Aspects of monitoring moisture changes using electrical impedance spectroscopy. In 2nd Symposium on Self-Desiccation and Its Importance in Concrete Technology. 1999. Lund, Sweden: Lund Institute of Technology, Division of Building Materials.

[6] A. Schiessl, et al., Assessing the moisture profile of drying concrete using impedance spectroscopy, Concrete Science and Engineering 2 (2) (2000) 106–116.
[7] Z. Liu, J.J. Beaudoin, An assessment of the relative permeability of cement systems using A.C. impedance techniques, Cement and Concrete Research 29 (7) (1999) 1085–1090.
[8] P. Gu, P. Xie, J.J. Beaudoin, Microstructural characterization of the transition zone in cement systems by means of A. C. impedance spectroscopy, Cement and Concrete Research 23 (1993) 581–591.
[9] R.A. Olson, et al., 1995. Microstructure-electrical property relationships in cement-based materials. in Materials Research Society Symposium. Boston, MA, USA: Materials Research Society, Pittsburgh, PA, United States.
[10] L. Lemoine, F. Wenger, J. Galland, Study of the corrosion of concrete reinforcement by electrochemical impedance measurement, Corrosion Rates of Steel in Concrete ASTM STP 1065, American Society for Testing and Materials, 1990.
[11] L. Dhouibi, E. Triki, A. Raharinaivo, The application of electrochemical impedance spectroscopy to determine the long-term effectiveness of corrosion inhibitors for steel in concrete, Cement & Concrete Composites 24 (2002) 35–43.
[12] C. Monticelli, A. Frignani, G. Trabanelli, A study on corrosion inhibitors for concrete application, Cement and Concrete Research 30 (2000) 635–642.
[13] G. Trabanelli, et al., Electrochemical study on inhibitors of rebar corrosion in carbonated concrete, Cement and Concrete Research 35 (2005) 1804–1813.
[14] P. Gu, et al., A study of corrosion inhibitor performance in chloride contaminated concrete by electrochemical impedance spectroscopy, ACI Materials Journal 94 (5) (1997) 385–395.
[15] B.B. Hope, A.K.C. Ip, Corrosion inhibitors for use in concrete, ACI Materials Journal 86 (6) (1989) 602–608.
[16] M. Shi, Z. Chen, J. Sun, Determination of chloride diffusivity in concrete by AC impedance spectroscopy, Cement and Concrete Research 29 (7) (1999) 1111–1115.
[17] M.R. Hansen, et al., 1993. Chloride permeability and AC impedance of high performance concrete. ACI–SP140-06. 140: p. 121–146.
[18] A. Peled, et al., Electrical impedance spectra to monitor damage during tensile loading of cement composites, ACI Materials Journal 98 (4) (2001) 313–322.
[19] S. Perron, J.J. Beaudoin, Freezing of water in Portland cement paste—an AC impedance spectroscopy study, Cement & Concrete Composites 24 (5) (2002).
[20] W.J. McCarter, H. Ezirim, M. Emerson, Properties of concrete in the cover zone: water penetration, sorptivity, and ionic ingress, Magazine of Concrete Research 48 (1996) 149–156.
[21] A. Schieβl, et al., Assessing the moisture profile of drying concrete using impedance spectroscopy, Concrete Science and Engineering 2 (2) (2000) 106–116.
[22] F. Rajabipour, et al., Procedure to interpret electrical conductivity measurements in cover concrete during rewetting, ASCE Journal of Materials in Civil Engineering 17 (5) (2005) 586–594.
[23] Z. Li, L. Xiao, X. Wei, Determination of concrete setting time using electrical resistivity measurement, Journal of Materials Science in Civil Engineering 19 (5) (2007) 423–427.
[24] G. Sant, F. Rajabipour, P. Fishman, P. Lura, W.J. Weiss. Electrical conductivity measurements in cement paste at early ages. in International RILEM Workshop on Advanced Testing of Fresh Cementitious Materials, 2006, Stuttgart, Germany: RILEM.
[25] G.D. Davis, M.J. Rich, L.T. Drzal, Monitoring moisture uptake and delamination in CFRP-reinforced concrete structures with electrochemical impedance sensors, Journal of Nondestructive Evaluation 23 (1) (2004) 1–9.
[26] J.D. Shane, et al., Microstructural and pore solution changes induced by rapid chloride permeability test measured by impedance spectroscopy, Concrete Science and Engineering 1 (2) (1999) 110–119.
[27] C. Shi, Effect of mixing proportions of concrete on its electrical conductivity and the rapid chloride permeability test (ASTM C1202 or ASSHTO T277) results, Cement and Concrete Research 34 (2004) 537–545.
[28] T.J. Schmit, A fundamental investigation on utilizing error propagation, Monte Carlo simulation, and measurement interpretation technique to design efficient in situ covercrete sensing systems MS thesis in Civil Engineering, Purdue University, 2005.
[29] M. Niemuth, Using Impedance Spectroscopy to Detect Flaws in Concrete, Purdue University, MS thesis in Civil Engineering, 2004.
[30] Keithley Instruments Inc., 2700, 2701 and 2750 Multimeter/Data Acquisition/Switch Systems, Keithley Instruments Inc., 2009 http://www.keithley.com/products/dmm/integrasystems/?path=2700/Documents#4.
[31] Solartron Group, 2009. *www.solartronanalytical.com/downloads/datasheets/1260.pdf*.
[32] Keithley Instruments Inc., Integra Series Technical Data Sheet, 2003.
[33] G. Sant, F. Rajabipour, W.J. Weiss, The influence of temperature on electrical conductivity measurements and maturity predictions in cementitious materials during hydration, The Indian Concrete Journal (April 2008) 1–10.
[34] National Instruments, What is NI GPIB?, 2009.
[35] P. Gu, et al., Study of the hydration and setting behavior of OPC-HAC pastes, Cement and Concrete Research 24 (4) (1994) 682–694.
[36] C.A. Scuderi, T.O. Mason, H.M. Jennings, Impedance spectra of hydrating cement pastes, Journal of Materials Science 26 (1991) 349–353.
[37] J.M. Torrents, R. Pallas-Areny, 1997. Measurement of cement setting by impedance monitoring. in IEEE Instrumentation and Measurement, Technology Conference. May 19–21. Ottawa, Canada.
[38] A. Poursaee, C.M. Hansson, Reinforcing steel passivation in mortar and pore solution, Cement and Concrete Research 37 (2007) 1127–1133.
[39] D. Murphy, et al., Impedance imaging in the newborn, Clinical Physics and Physiological Measurement 8 (Suppl. A) (1987) 131–140.
[40] M. Weindling, et al., Electrical impedance to study cerebral haemodynamics in the newborn: which index is best? Biology of the Neonate 45 (1984) 300.
[41] L. Tarassenko, P. Rolfe, Imaging spatial distribution of resistivity—an alternative approach, Electronics letters 20 (1984) 574–576.
[42] T. Hou, J.P. Lynch, Electrical impedance tomographic methods for sensing strain fields and crack damage in cementitious structures, Journal of Intelligent Material Systems and Structures, , 2008, pp. 1–18.

The influence of temperature on electrical conductivity measurements and maturity predictions in cementitious materials during hydration

Gaurav Sant, Farshad Rajabipour and Jason Weiss

Electrical property measurements are being increasingly used to assess the transport properties of building materials. While conductivity measurements have been extensively used, the combined dependence of electrical conductivity on measurement temperature and microstructural development (cement hydration) is often overlooked. In this paper the influence of temperature and microstructural development (i.e. hydration) are separated. Two cement paste mixtures are assessed at 283K, 296K, and 309K, and the conductivity response is analysed to differentiate the contribution of maturity (pore structure refinement due to hydration) and temperature (due to changing ionic mobility). The conductivity measurements are used to determine the activation energy of electrical conduction (i.e. temperature dependence of ion mobility) and hydration (i.e. temperature dependence of reaction rates). This work provides an improved understanding of how temperature influences electrical measurements in cementitious systems at early ages, and can provide for an accurate interpretation of the electrical properties of the system. This information will enable improvements in the use of electrical measurements for quality control and quality assurance (QC/QA) testing.

Keywords: *Electrical conductivity, hydration, maturity, temperature, quality control.*

Electrical measurements are powerful non-destructive testing techniques that are capable of providing information about hydration reactions, microstructural features and the transport properties of cement based materials. However, electrical measurements (e.g., conductivity or resistivity) exhibit temperature dependence due to changing ionic mobility with temperature. In an electrolyte, electrical conduction occurs due to the migration of ions through the solution under an applied potential gradient[1]. Consequently, conduction in aqueous electrolytes is dependent on ionic mobility and the solution's concentration. In cementitious materials, temperature change influences ionic mobility and salt solubility resulting in a change in the electrical conduction response as a function of temperature[2]. These considerations highlight the need to account for the temperature dependent conductivity response of cementitious materials. Further, chemical reactions (such as cement hydration) are influenced by temperature[3]. This topic has received significant treatment in the literature with the objective of determining how temperature influences the rate of material property development[4,5,6,7]. Maturity transformations have been extensively used to correlate material properties to the extent of reaction that occurs in the system[8,9].

Due to the influence of temperature on the rate of hydration and ionic mobility it would be reasonable to consider that the electrical properties (conductivity or

resistivity) of cement systems are a function of maturity and temperature effects as shown in Equation 1.

$$\sigma(t,T) = f(M) \bullet f(T) \qquad .....(1)$$

where, $\sigma(t,T)$ is the time and temperature dependent electrical property (in this case the conductivity (S/m)) of the sample, $f(M)$ is a function which defines the influence of time and temperature on the sample maturity (microstructure development), and $f(T)$ is a function that defines the influence of sample temperature and accounts for effects such as the ionic mobility and solution concentration.

The temperature dependence of electrical properties in cement based systems was studied several decades ago by Hammond and Robson who used the Hinrichson-Rasch law to describe the conductivity of concrete over a range of temperatures (Equation 2).[10,11]

$$ln\left(\frac{\sigma(T)}{\sigma(T_{REF})}\right) = A\left(\frac{1}{T} - \frac{1}{T_{REF}}\right) \qquad .....(2)$$

where, $\sigma(T)$ is the concrete conductivity (S/m) at temperature T (K), $\sigma(T_{REF})$ is the conductivity (S/m) at a reference temperature T_{REF} (296K for this work) and 'A' is an empirical constant (K). Hammond and Robson indicated 'A' to be equal to 5500K based on work by Spencer[10,12]. Later, Elkey and Sellevold extended the scope of this investigation and determined 'A' to vary between 2000 and 5000K depending on the mixture composition[13].

Whittington et al. used a similar approach to investigate concrete using electrical resistivity[14]. Using a slightly different form of relationship (Equation 3) described by Hammond and Robson they determined concrete to have a negative temperature coefficient of resistivity, equal to 0.022/°C.

$$\frac{\rho(T)}{\rho(T_{REF})} = \frac{1}{1 + \alpha(T - T_{REF})} \qquad .....(3)$$

where, $\rho(T) = 1/\sigma(T)$ is the resistivity (ohms.m) at temperature T (K), $\rho(T_{REF})$ is the resistivity (ohms.m) at a reference temperature T_{REF} (K) and α is temperature coefficient of resistivity of the material. The work of Whittington et al translates to an empirical constant 'A' of 2130 K for the concretes tested.

In the 1990s, McCarter determined the temperature coefficient of resistivity of concrete as 0.026/°C.[15] More recently, McCarter proposed a formulation to determine the activation energy of electrical conduction based on the Arrhenius Law (Equation 4)[16,17].

$$\sigma_{Bulk} = A \bullet exp\left[\frac{-E_{aC}}{R \bullet T}\right] \qquad .....(4)$$

where, σ_{Bulk} is the bulk sample conductivity (S/m) at an absolute temperature T (K), R is the universal gas constant (8.314 J/K mol), E_{aC} is the activation energy for the conduction process (J/mol) and A (S/m) is a material constant (theoretically equivalent to the conductivity at infinite temperature; $\sigma(T = \infty)$). The activation energies of electrical conduction were determined to be in the range of 16-30 KJ/mole for the mixtures evaluated in this project.

Research objective

This paper proposes an approach to simultaneously assess the influence of temperature and microstructural changes (i.e. maturity) on the measured electrical conductivity in cementitious systems. The results of this work are aimed at understanding the influence of temperature on early-age conductivity measurements. This understanding would permit the reliable use of electrical measurements in early-age quality control and quality assurance (QC/QA) testing and for specification compliance of cement-based materials.

Materials and mixing procedures

Two different cement paste mixtures were prepared according to the mixture proportions shown in Table 1. Type I ordinary portland cement was used with a Blaine fineness of 360 m^2/kg and a Bogue phase composition of 60% C_3S, 12% C_2S, 12% C_3A, 7% C_4AF and a Na_2O equivalent of 0.72%. To enhance the workability of the mixtures, a high range water reducing admixture was added. A commercially available shrinkage reducing admixture (SRA) was added at a 5% concentration of the initial water content by replacement (by mass) of the initial mixing water. For the measurement of electrical conductivity de-aired, neat cement pastes were prepared using de-ionised water. The water was de-aired by boiling then cooled to room temperature before mixing. The dry constituent materials were placed inside a special mixing chamber[18]. The chamber was then sealed, air was evacuated from the chamber using a vacuum pump, and the solution of water and the chemical admixtures was introduced into the chamber

under the same evacuated condition. The chamber was then placed in a commercial paint shaker and shaken for five minutes to uniformly mix the constituents and obtain a consistent cement paste mixture. After mixing, the chamber was opened and the cement paste slurry was placed in the moulds using external vibration.

Table 1. Mixture proportions (mass)

	W/C = 0.30	W/C = 0.30 + 5% SRA
Water	0.300	0.285
Cement	1.000	1.000
HRWRA	0.005	0.005
SRA	~	0.015

Experimental procedures

Electrical conductivity of fresh and mature cement pastes

The electrical conductivity of cement paste samples was measured using cylindrical paste specimens (22 mm diameter, 50 mm height). The specimens were cast and stored in an airtight plastic vial. Two stainless steel electrodes (2.5 mm diameter rods spaced 10 mm centre to centre) were embedded longitudinally inside each vial (Figure 1b). A impedance gain-phase analyser measured the impedance response of each specimen. The measurements were made over a wide frequency range; i.e. 10 MHz to 1 Hz (10 steps/frequency decade) using a 100 mV AC stimulus. The bulk resistance (R_b) obtained from the impedance response was used to determine the material's conductivity after normalising for the effects of specimen and electrode geometry (Equation 5).

$$\sigma_t = \frac{k}{R_b} \qquad .....(5)$$

where, σt is the paste conductivity (S/m), R_b is the bulk resistance (ohms; Ω) and k is a geometry factor (15.76/m) that was determined experimentally for this specific geometry[19]. During measurements, the specimens remained sealed inside plastic vials. Electrical impedance measurements were performed for a duration of 7 days (at a reference temperature of 296K) after casting on

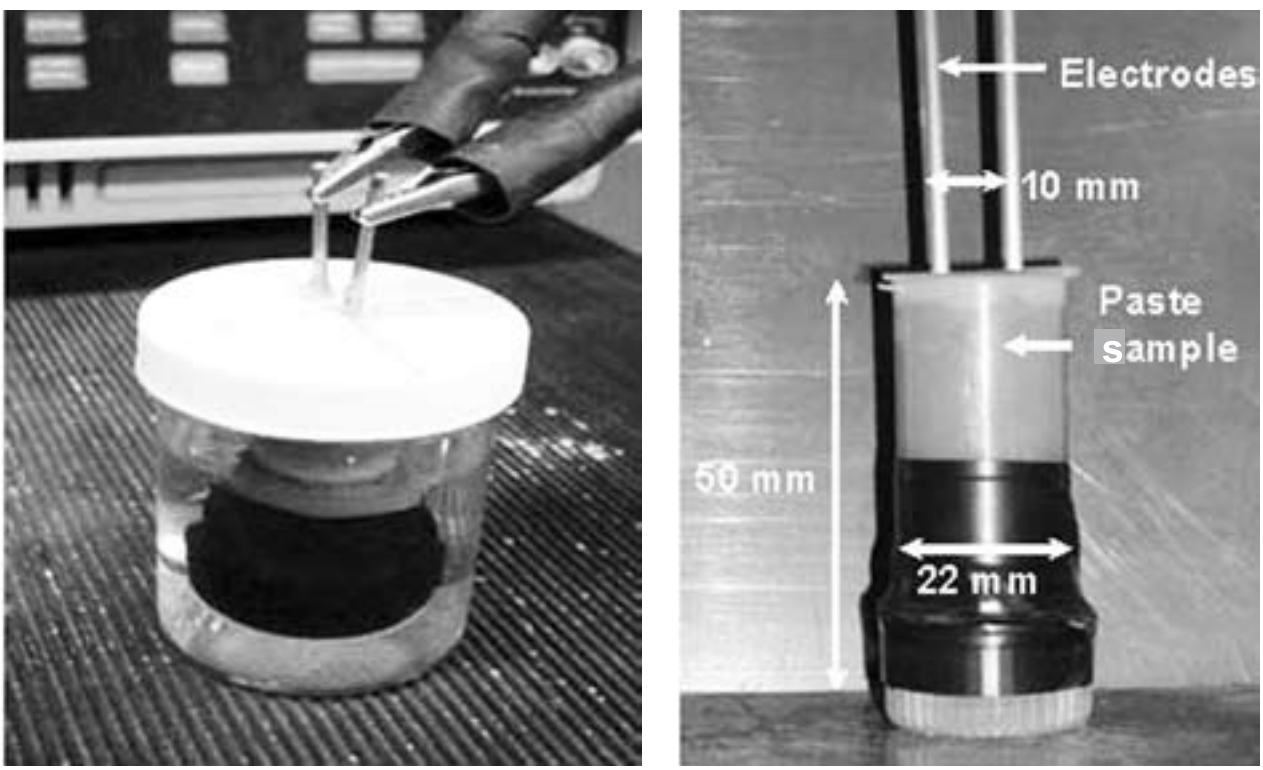

(a) (b)

Figure 1. An illustration of the apparatus used for the measurement of electrical conductivity of cement pastes (a) The conductivity cell for cement pastes immersed in a water bath (b) The vial with embedded electrodes for paste and pore solution conductivity assessment

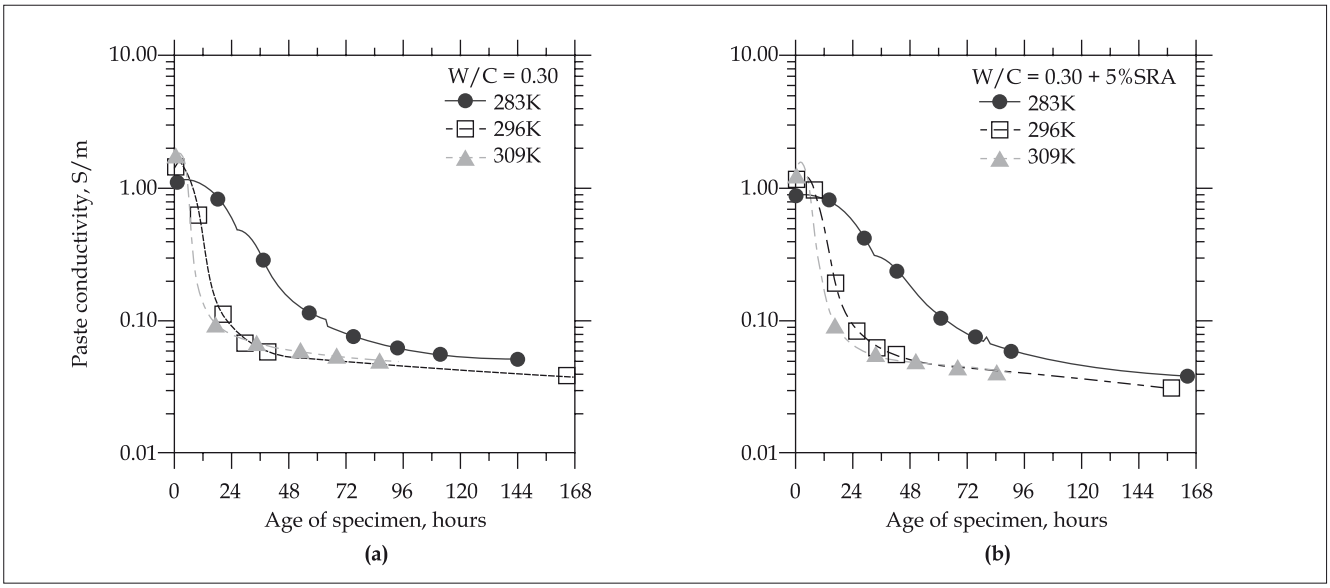

Figure 2. The electrical conductivity of the cement pastes as function of specimen age (a) W/C = 0.30 and (b) W/C = 0.30 + 5% SRA

specimens which were kept in a water bath to minimise temperature variations (Figure 1a). Measurements were performed on samples cured at 283K (14 days), 296K (7 days) and 309K (4 days). Prior to mixing, the raw materials were temperature conditioned to ensure an appropriate mixture temperature (equivalent to the measuring temperature) at the end of the mixing cycle. For consistency, conductivity measurements until an age of 168 hours (real and equivalent age) are presented in this paper. The measurements were used to determine the activation energy of cement hydration, after a correction to account for the influence of temperature (ionic mobility) on electrical conductivity.

To determine the influence of temperature on the conductivity of the pore solution (i.e. activation energy of electrical conduction; E_{aC} (J/mol)) in cement pastes, conductivity measurements were performed on cement paste samples (cured for 7 days at 296K; ~70% hydration – which corresponds to the maximum degree of hydration for the mixture as computed using Powers model[20] that were conditioned to 283K, 296K and 309K (± 0.5K) in an environmental chamber. Further, companion specimens were cast with thermocouples embedded to monitor the temperature profile of the cement paste mixtures.

Electrical conductivity of synthetic pore solutions

To determine the activation energy of electrical conduction in an electrolyte, synthetic pore solutions of varying concentrations were prepared (0.35 KOH + 0.05 NaOH, 0.70 KOH + 0.10 NaOH, 1.40 KOH + 0.20 NaOH). The solutions were then conditioned to 283K, 296K and 309K (± 0.5K) in an environmental chamber. When the solutions had achieved an equilibrium temperature (measured using thermocouples immersed in the solution), the conductivity of the solutions was measured using a conductivity cell (Figure 1b) connected to a impedance gain-phase analyser[20].

Experimental results

Influence of the rate of reaction on the electrical conductivity

Figure 2 shows the electrical conductivity of cement paste mixtures cured at temperatures of 283K, 296K and 309K. An initial increase in the conductivity is noted for ~1.5 hours for all the cement paste mixtures. This may be explained by the rapid initial dissolution of alkalis and sulphates into the mixing water. After this time (1.5 hours), a reduction in conductivity is noted for all mixtures. A significantly different trend is observed in the rate of measured conductivity (Figure 2) for specimens cured at different temperatures. The samples cured at low temperatures show a gradual decrease in the conductivity, while mixtures cured at higher temperatures exhibit a more rapid decrease. This observation may be explained by the temperature dependence of the rate of hydration in these cement paste mixtures (i.e. the rate of pore structure refinement as a function of the reaction temperature).

Influence of temperature on the electrical conductivity of cement pastes

Figure 3 shows the measured electrical conductivity of two cement paste specimens (cured for 7 days), which have been subjected to thermal cycles. After being cured for 7 days at 296K, the samples were placed at temperatures of 283K and 309K (alternate heating and cooling was performed for 12 hours to ensure equivalent maturity). The results are shown in Figure 3(b). As expected, the measured conductivity is lower at lower temperatures. The lower conductivity of the SRA mixture as compared to the plain mixture is attributed to the non-conductive nature of the SRA in cement paste and pore solution[20,21]. The measured value of conductivity was then used to determine the activation energy of the conduction process in cement pastes. This is further discussed later.

Influence of temperature on the electrical conductivity of pore solution

Figure 4 shows the measured electrical conductivity of synthetic pore solutions (0.35 KOH + 0.05 NaOH, 0.70 KOH + 0.10 NaOH, 1.40 KOH + 0.20 NaOH) conditioned to temperatures of 283K, 296K and 309K. The electrical conductivity is observed to increase linearly over the temperature range from 283K to 309K. This is consistent with the increase in ionic mobility and the extent of dissociation of the dissolved ionic species as a function of temperature. The measured value of conductivity was then used to determine the activation energy of the conduction process in the electrolytes. This is further discussed later.

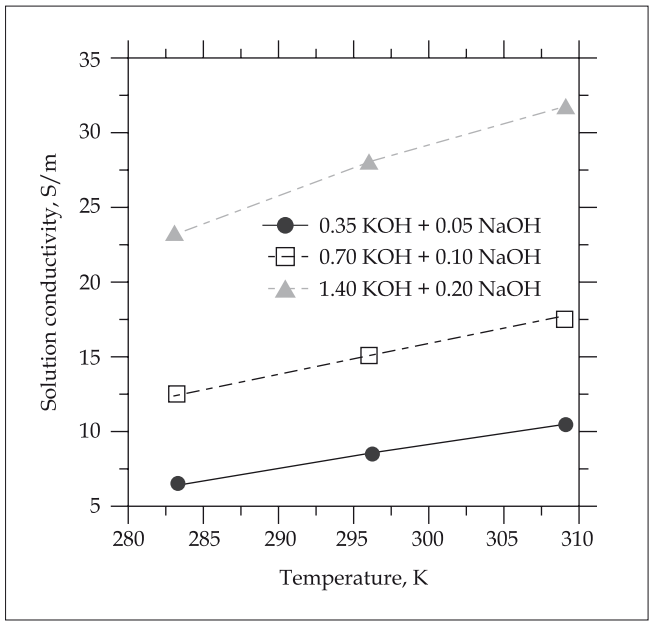

Figure 4. The temperature dependent response of electrical conductivity of synthetic pore solutions investigated in this project

Discussion of experimental results

The electrical conductivity of cementitious materials has been described extensively using a modified parallel

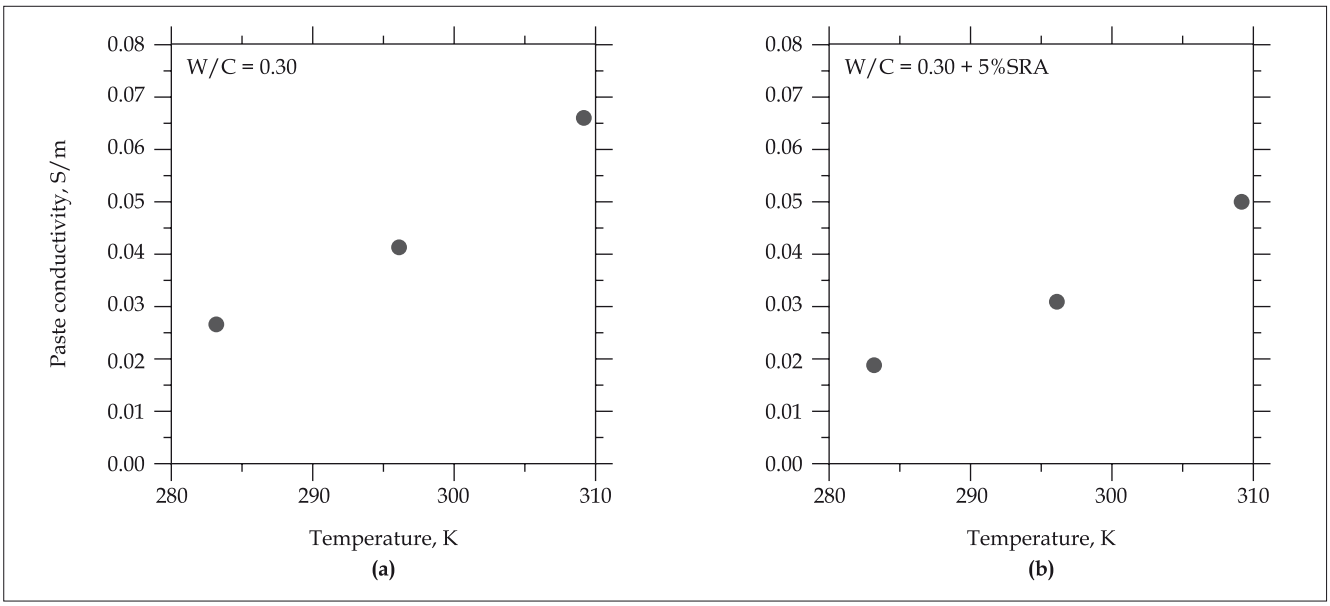

Figure 3. The temperature dependent electrical conductivity of the cement pastes (a) W/C = 0.30 and (b) W/C = 0.30 + 5% SRA

law[22,23,24]. This relationship can be described using Equation 6.

$$\sigma_t = \sigma_0 \phi \beta \qquad .....(6)$$

where, σ_t is the bulk cement paste conductivity (S/m), σ_0 is the pore solution conductivity (S/m), φ is the volume fraction of the solution contained in the pores and β is the pore connectivity. The modified parallel law can be used to determine which parameters are impacted by a change in temperature. The first component which would contribute to the bulk conductivity would be the pore solution conductivity. Considering hydrated products and cement particles to be non-conductive (their conductivity is several orders of magnitude lower than the ionic pore solution), electrical conduction in cementitious materials can be modelled to occur primararily through the ionic pore fluid (in the gel and capillary porosity)[20,23]. This is significant, as temperature influences chemical equilibrium states; impacting ionic mobility (primary effect) and solubility (secondary effect)[25,26]. Ionic mobility (or equivalent conductivity) is noted to increase with increasing temperature due to the decreasing viscosity of the fluid (water), and an increase in the extent of dissociation of the dissolved ionic species, which increases the conductivity of the system[1]. An inverse effect (decreasing conductivity) would be noted with decreasing temperature.

The second component which contributes to the overall conductivity would be the pore fluid volume. For a sealed system, at a given degree of hydration ignoring changes in fluid volume due to changes in density with temperature, the pore fluid volume would be fixed; as solution is not removed from or added to the system. This should however be distinguished from a change in the pore fluid volume due to the consumption of water during hydration.

The third component is the pore fluid connectivity (equivalent to the inverse tortuosity), which decreases due to pore structure refinement with increasing maturity; a function of time and the reaction temperature.

Activation energy of electrical conduction in cement paste and pore solution

Cement paste specimens subjected to thermal cycling were used to determine the influence of temperature on the cement paste conductivity, Figure 3. The results were used to determine the activation energy of electrical conduction (E_{aC}) in cement pastes, Figure 5. The activation energy of conduction was determined to be 25.6 kJ/mol for the plain mixture and 27.6 kJ/mol for the SRA mixture. A higher activation energy of conduction

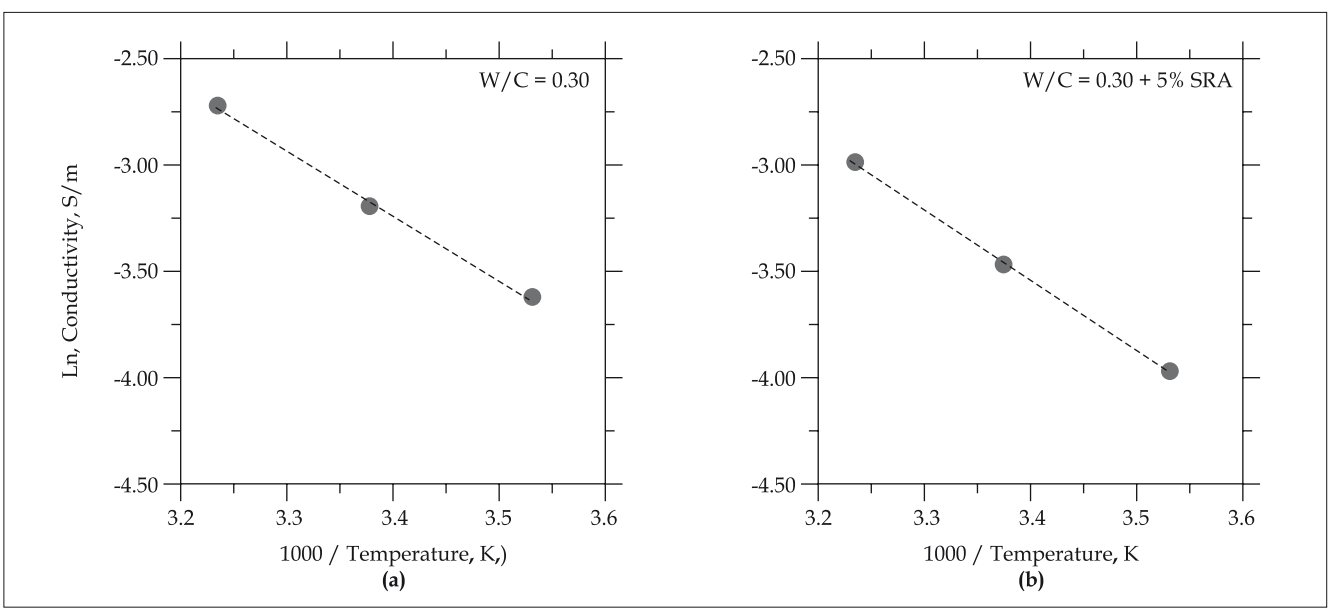

Figure 5. The activation energy of electrical conduction for cement pastes investigate (a) W/C = 0.30 and (b) W/C = 0.30 + 5% SRA

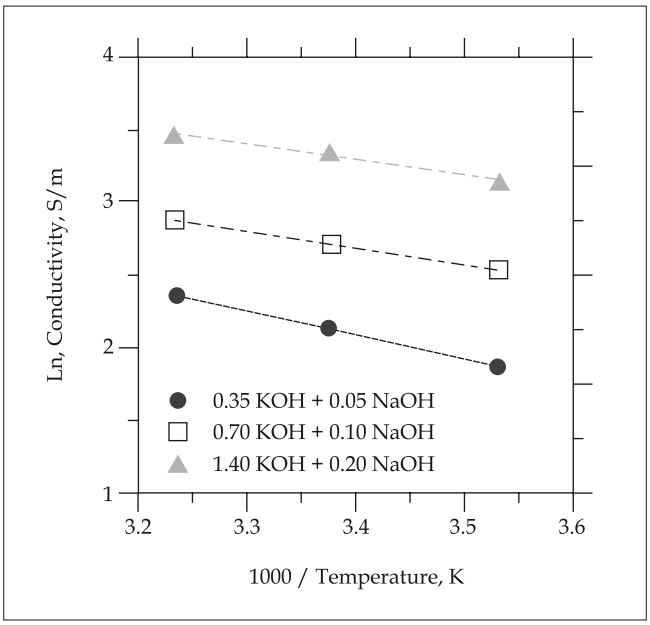

Figure 6. The activation energy of the conduction process for synthetic pore solutions

in mixtures containing a SRA may be explained by the non-conductive nature of the SRA which impedes ion migration in the system. Further, the SRA may bind ions reducing electrical conduction in the system[21].

To fully understand the influence of temperature on the conductivity of an aqueous electrolyte a brief background on electrolytic conductivity is needed. The conductivity of an aqueous electrolyte can be expressed using Equation 7 where, z is the species valence (unitless), c is the molar concentration of the electrolyte (mol/L) and λ is the equivalent conductivity (cm^2 S/mole) of each species at infinite dilution (which is a function of temperature) and is proportional to the ionic mobility[26]. At low concentrations (< 0.01 mol/l), that is, in dilute solutions the equivalent conductivity is a constant for a specific species. However, at high concentrations the equivalent conductivity is observed to decrease inversely (but non-linearly), due to ion-ion interactions in the solution[19,27].

$$\sigma_{Solution} = \sum z_i c_i \lambda_i \qquad .....(7)$$

Conductivity measurements were performed on synthetic pore solutions subjected to thermal cycling. The solutions were selected to correspond to the concentration of the pore fluid of an early-age cement paste (~ 2 hours), a later age cement paste (48 hours), and a pore fluid with a very high molar (ionic) strength. The results of these tests were used to determine the activation energy of the conduction process (E_{aC}) (Figure 6; 13.55 kJ/mole, 9.65 kJ/mole and 8.98 kJ/mole, respectively, in order of increasing solution concentration) in the ionic solutions. It is noticed that the activation energy decreases with increasing concentration, indicating concentrated solutions are less sensitive to temperature change as compared to dilute solutions. This observation can be explained by the large degree of inter-ionic interactions in concentrated solutions, which significantly alter the conductivity behaviour[27].

Temperature correction for electrical conductivity

The activation energy of conduction in an electrolyte can be used to correct the influence of temperature, by transforming the conductivity at any temperature (in this case 283K or 309K) to a reference temperature (in this case 296K) using the expression shown in Equation 8.

$$\sigma(T_{REF}) = \frac{\sigma(T)}{exp\left(-\frac{E_{ac}}{R}\left(\frac{1}{T} - \frac{1}{T_{REF}}\right)\right)} \qquad .....(8)$$

where, $\sigma(T)$ is the sample conductivity (S/m) at any temperature T (K), $\sigma(T_{REF})$ is the conductivity (S/m) at a reference temperature, T_{REF} (296K), E_{aC} is the activation energy of electrical conduction in an electrolyte (or cement paste) (J/mole) and R is the universal gas constant (J/K.mole). The temperature correction is performed using the activation energy of conduction of the pore solution, having the lowest concentration (conductivity). This solution was selected as it is noted to correspond to the pore solution chemistry (conductivity) of a 2 hour old cement paste (0.35 KOH + 0.05 NaOH), which contains a large fluid volume; whose electrical conductivity behaviour is most sensitive to changes in temperature (Figure 6 – highest E_{aC}).

Determination of the activation energy of the hydration reaction

Electrical conductivity can be corrected to account for the influence of temperature on the rate of hydration and, consequently microstructural development (pore structure refinement). This component may be accounted for using a temperature transformation such as an equivalent age (i.e. maturity) function proposed by Hansen and Pedersen[28]; Equation 9. In this paper, the equivalent age function (Equation 9) is used to

determine the activation energy of cement hydration (E_{aR}), after normalising conductivity at any temperature to a reference temperature T(K); using Equation 8.

$$M(t,T) = \int_0^t exp\left(-\frac{E_{aR}}{R}\left(\frac{1}{T} - \frac{1}{T_{REF}}\right)\right) \bullet dt \qquad .....(9)$$

where, M (hours) is the maturity (or equivalent age) of the specimen at a reference temperature T_{REF} (K), E_{aR} (KJ/mol) is the apparent activation energy of the hydration reaction, R (J/(mol · K)) is the gas constant (8.314 J/mol-K), T (K) is the average temperature of the concrete, and dt (hours) is the time interval[28]. The apparent activation energy determined from 10% to 35% hydration; (39.50 kJ/mol) is similar to values determined by other methods (e.g. chemical shrinkage) for the cement systems investigated[20].

Correction for the influence of temperature on hydration and electrical conductivity

As illustrated in Equation 1, the conductivity behaviour of a cementitious material can be expressed as a function of maturity and the measurement temperature. This section will describe a procedure which can be used to simultaneously account for the influence of temperature on cement hydration and electrical conductivity. Due to space considerations, this paper will describe the procedure only for the plain cement mixture (W/C = 0.30).

A function can be fit to describe the experimental conductivity measurement (W/C = 0.30) at the reference temperature (in this case 296K). This function is shown in Equation 10 (R2 = 0.9996).

$$\sigma(t,296K) = \frac{1.38 - 0.82t + 0.19t^2 - 0.01t^3 + 0.0002t^4}{1.00 - 0.66t + 0.19t^2 - 0.02t^3 + 0.001t^4 + 0.00002t^5} \qquad .....(10)$$

where, $\sigma(t,296K)$ is the measured conductivity at time t (hours) at a measurement temperature of 296K (the reference temperature). The type of fit used to describe the conductivity response is not important. To extend the applicability of this function to describe the electrical conductivity behaviour at any temperature requires the incorporation of a reaction rate constant k_R (unitless) which accounts for the influence of temperature on the rate of cement hydration and an electrical conduction constant k_T (unitless) which accounts for the influence of temperature on electrical conductivity. This approach is described in Equations 11, 12 and 13.

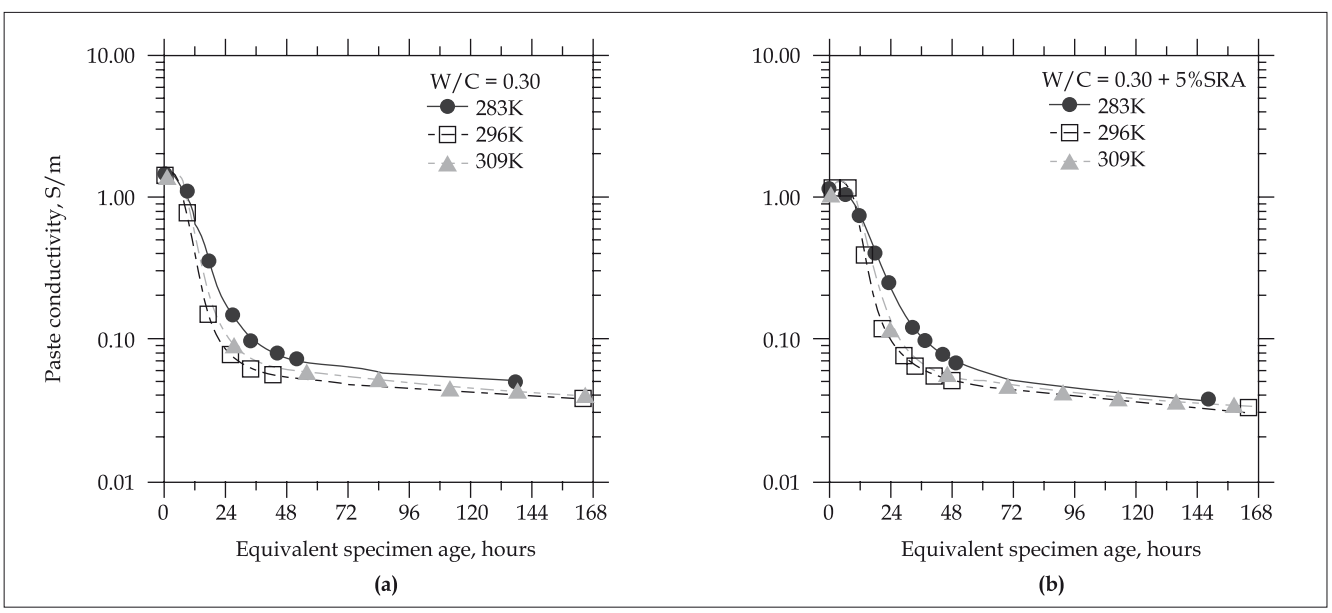

Figure 7. The reaction and solution temperature corrected electrical conductivity of the cement pastes as a function of equivalent specimen age (a) W/C = 0.30 and (b) W/C = 0.30 + 5% SRA

$$\sigma(t,T) = \left(\frac{1.38 - 0.82(t \bullet k_R) + 0.19(t \bullet k_R)^2 - 0.01(t \bullet k_R)^3 + 0.0002(t \bullet k_R)^4}{1.00 - 0.66(t \bullet k_R) + 0.19(t \bullet k_R)^2 - 0.02(t \bullet k_R)^3 + 0.001(t \bullet k_R)^4 + 0.00002(t \bullet k_R)^5} \right) \bullet (k_T) \quad .....(11)$$

where,

$$k_R = exp\left[-\frac{E_{aR}}{R}\left(\frac{1}{T} - \frac{1}{T_{REF}}\right)\right] \quad .....(12)$$

$$k_T = exp\left[-\frac{E_{aC}}{R}\left(\frac{1}{T} - \frac{1}{T_{REF}}\right)\right] \quad .....(13)$$

where, k_R (unitless) is the reaction rate constant which accounts for the influence of temperature on the rate of cement hydration, k_T (unitless) is the electrical conduction constant which accounts for the influence of temperature on electrical conductivity and T (K) is the average temperature of the concrete.

Figure 7 shows the electrical conductivity response of the two cement paste mixtures evaluated using the approach described above, to account for the influence of temperature on cement hydration and electrical conductivity; using the activation energy of cement hydration (E_{aR} = 39.50 kJ/mole) and electrical conduction for the electrical conductivity response of an early pore fluid (0.35 KOH + 0.05 NaOH; EaC = 13.55 kJ/mole). It can be seen that (Figure 7), using the approach described in Equation 11, the influence of temperature on hydration and electrical conductivity can be comprehensively described for mixtures cured at any temperature.

An improved approach is proposed to perform the temperature correction for electrical conductivity if the pore solution chemistry (conductivity) at early-ages is well known. This would involve determining the activation energy of electrical conduction in electrolytes (pore fluids) having an age-dependent concentration (and conductivity). This information can be used to perform a comprehensive temperature correction for electrical conductivity. An example of such an approach is illustrated in Figure 8 which shows the activation energy of electrical conduction as a function of the solution's conductivity at the reference temperature (296K)[20,29].

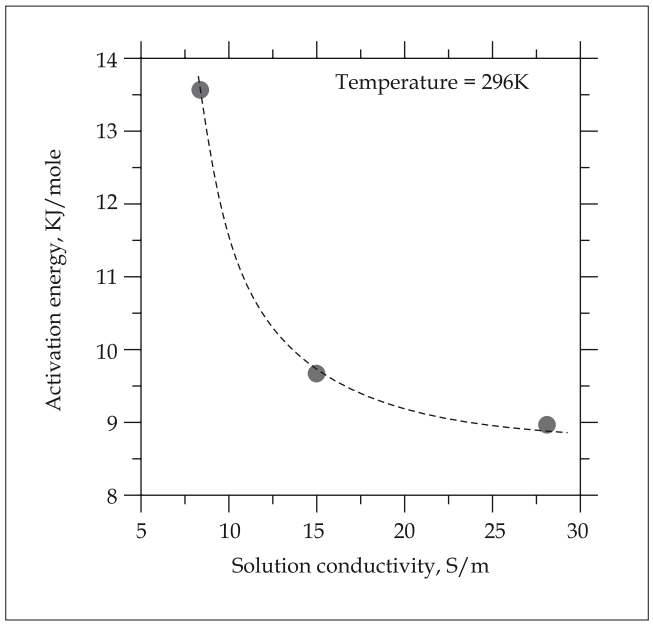

Figure 8. The non-linear relationship between the activation energy of electrical conduction(E_{aC}) and the solution conductivity at 296K

Conclusions

Measurements of electrical conductivity performed on paste, mortar and concrete require a two-part correction to accurately describe early-age behaviour. The first part of this approach accounts for the influence of temperature on cement hydration (pore refinement), and the second part accounts for the influence of temperature on electrical conductivity. This paper demonstrates the successful application of this correction for electrical conductivity measurements using the activation energy of electrical conduction and cement hydration. In this context, the activation energy of electrical conduction has been determined for electrolytes of varying concentrations and for cement pastes. In addition, the activation energy of cement hydration has been determined to be 39.50 kJ/mol (independent of w/c) and is noted to be similar to values determined using other techniques (e.g. chemical shrinkage or heat of hydration). The approach demonstrated in this paper would be crucial for forecasting the long-term durability performance of field concretes, based on the early-age electrical properties of the material using an approach similar to that presented by Lane[30]. An approach of this nature would provide fundamental information needed for quality control and quality assurance (QC/QA) applications and for ensuring the specification compliance of field concretes. This information would have an immense impact in determining how field concrete is specified, evaluated or purchased.

Acknowledgement

The authors gratefully acknowledge the support from the Center for Advanced Cement Based Materials (ACBM) and the National Science Foundation (NSF). This material is based in part on work supported by NSF Grant No. 0134272: a 'CAREER AWARD' granted to the last author. This work was conducted in the Material Characterisation and Sensing Laboratory at Purdue University and as such, the authors gratefully acknowledge the support that has made this laboratory and its operation possible. The contents of this paper reflect the views of the authors, who are responsible for the accuracy of the data presented herein.

References

1. Adamson, A.W., *A Text-book of Physical Chemistry*, Academic Press, USA, 1973.
2. Binder, R.C., *Fluid Mechanics*, Prentice-Hall Inc., Englewood Cliffs, NJ, 1973.
3. Activation Energy, *Encyclopedia Britannica*, 2007.
4. Carino, N.J., The maturity method, *CRC handbook on nondestructive testing of concrete* , Edited by V.M. Malhotra and N.J. Carino, CRC Press, Boca Rotan, Florida, 1991, pp. 101-146.
5. Weiss, W.J., Experimental determination of the 'Time-Zero', *Early age cracking in cementitious systems* – RILEM report TC-EAS, Edited by Arnon Bentur, 2002.
6. Pinto, R.C.A. and Hover, K.C., Application of maturity approach to setting time,' *ACI Materials Journal*, 1999, Vol. 96, No. 6, pp. 686-691.
7. Roy, D.M., Scheetz, B.E., Sabol, S., Brown, P.W., Shi, D., Licastro, P.H., Idorn, G.M., Andersen, P.J., and Johanson, V., Maturity model and curing technology, Strategic Highway Research Program, SHRP-C-625, (1993)
8. Nurse, R.W., Steam curing of concrete, *Magazine of Concrete Research*, 1949, Vol. l, No. 2, pp. 79-88.
9. Saul, A.G.A., Principles underlying the steam curing of concrete at atmospheric pressure, *Magazine of Concrete Research*, 1951, pp. 127-140.
10. Hammond, E., and Robson, T.D., Comparison of Electrical Properties of Various Cements and Concretes, *The Engineer*, 1955, Vol. 199, pp. 78-80.
11. Rasch, E. and Hinrichsen, F.W., Uber eine beziehung zwischen elektrischer leitfahigkeit und Temperatur, *Zeitschrift fur electrochemie*, 1908, Vol. 14, No. 41, pp. 41- 48.
12. Spencer, R.W., Measurement of the Moisture content of concrete, *Journal of the American Concrete Institute*, 1937, Vol. 9, No. 1, pp. 45-61.
13. Elkey, W. and Sellevold, E.J., *Electrical resistivity of concrete, Norwegian Road Research Laboratory*, Publication No. 80, 1995, Oslo.
14. Whittington, H.W., McCarter, W.J. and Forde, M.C., The conduction of electricity through concrete, *Magazine of Concrete Research*, 1981, Vol. 33, No. 114, pp. 48-60.
15. McCarter, W.J., Effects of temperature on conduction and polarization in portland cement mortar, *Journal of the American Ceramic Society*, 1995, Vol. 78, No. 2, pp. 411-415.
16. McCarter, W.J., Starrs, G. and Chrisp, T.M., Electrical conductivity, diffusion, and permeability of portland cement-based mortars, *Cement and Concrete Research*, 2000, Vol. 30, No. 9, pp. 1395-1400.
17. Arrhenius, S., On the reaction velocity of the inversion of cane sugar by acids, Zeitschrift für physikalische Chemie, 4, 226, (1889).
18. Sant, G., Lura, P. and Weiss, W.J., Measurement of volume change in cementitious materials at early ages: Review of testing protocols and interpretation of results, *The Transportation Research Record*, 2006, 1979.
19. Rajabipour, F., Weiss, W.J. and Abraham, D., Insitu electrical conductivity measurements to assess moisture and ionic transport in concrete, Advances in concrete through science and engineering, *Proceedings of the International RILEM Symposium*, Evanston, Illinois, 2004.
20. Sant, G., *Examining volume changes, stress development and cracking in cement-based systems*, MSCE Thesis, Purdue University, West Lafayette, Indiana, USA, 2007.
21. Rajabipour, F., Sant, G. and Weiss, W.J., Interactions between shrinkage reducing admixtures and cement paste's pore solution, *Cement and Concrete Research*, 2008, Vol. 38, pp. 606-615.
22. Garboczi, E.J., Permeability, diffusivity, and microstructural parameters : A critical review, *Cement and Concrete Research*, Vol. 20, No. 4, pp. 591-601.
23. Rajabipour, F., *Insitu electrical sensing and material health monitoring in concrete structures*, PhD Dissertation, Purdue University, West Lafayette, Indiana, USA, 2006.
24. Christensen, B.J., Coverdale, R.T., Olson, R.A., Ford, S.J., Garboczi, E.J., Jennings, H.M. and Mason, T.O., Impedance spectroscopy of hydrating cement-based materials: Measurement, interpretation, and application, The American Ceramic Society, 1994, Vol. 77, No. 11, pp. 2789-2802.
25. Taylor, H.F.W., *Cement Chemistry*, Academic Press, London, (1990)
26. Bockris, J.O.M., and Reddy, A.K.N., *Modern electrochemistry*, Vol. 1, Section 4.4, 1970, Plenum, New York City, NY, USA.
27. Snyder, K.A., Feng, X., Keen, B.D. and Mason, T.O., Estimating the electrical conductivity of cement paste pore solutions from OH-, K+ and Na+ concentrations, *Cement and Concrete Research*, 2003, Vol. 33, No. 6, pp. 793-798.
28. Hansen, F., and Pedersen, E. J., Maturity computer for controlled curing and hardening of concrete, *Nordisk Betong*, 1977, No. 1, pp. 21-25 (in Danish).
29. _____*Standard practice for estimating concrete strength by the maturity method*, ASTM C1074-04, ASTM International, West Conshohocken, Pennsylvania, USA, 2004.
30. Lane, D.S., Supplanting the rapid chloride permeability test with a quick measurement of concrete conductivity, Virginia Transportation Research Council, Charlottesville, Virginia, USA, 2005.

Mr. Gaurav Sant received his bachelor's (BSCE) and master's degrees (MSCE) in civil engineering from Purdue University with an emphasis in construction materials. Currently, he is pursuing his PhD at the School of Civil Engineering at Purdue University. His research interests include early-age shrinkage and cracking, non-destructive testing and moisture transport in cementitious materials.

Dr. Farshad Rajabipour received his BSc from Sharif University of Technology (Tehran) and his MS and PhD from Purdue University. Currently, he is an assistant professor of civil and environmental engineering at the University of Hawaii, Mānoa. His research interests include materials science of concrete, construction sustainability and use of recycled materials, and non-destructive testing and health monitoring.

Prof. Jason Weiss is associate head in the School of Civil Engineering at Purdue University and the associate director of the National Science Foundation, Center for Advanced Cement Based Materials at Northwestern University. His research interests include early-age shrinkage, cracking and its influence on durability, durability of environmentally friendly binders, moisture transport and service-life predictions of civil infrastructure.

Variability Analysis of the Bulk Resistivity Measured Using Cylinders

R.P. Spragg[(1)], J. Castro[(2)], T Nantung[(4)], M. Paredes[(3)], and J. Weiss[(5)]

[(1)] Graduate Research Assistant, Purdue University, School of Civil Engineering, 500 Stadium Mall Dr., West Lafayette, IN, 47907, rspragg@purdue.edu

[(2)] Assistant Professor, Pontificia Universidad Catolica de Chile, School of Civil Engineering, Casilla 306, Correo 22, Santiago, Chile, jecastro@ing.puc.cl

[(3)] Manger for Pavement Materials and Construction Research, Indiana Department of Transportation, Division of Research and Development P.O. Box 2279, West Lafayette, IN, 47906, tnantung@indot.in.gov

[(4)] State Corrosion Engineer, Florida Department of Transportation State Materials Office, Corrosion Research and Durability Laboratory, 6007 NE 39th Avenue, Gainesville, FL, 32609, mario.paredes@dot.state.fl.us

[(5)] Professor of Civil Engineering and Director of Pankow Materials Laboratory, Purdue University, School of Civil Engineering, 500 Stadium Mall Dr., West Lafayette, IN, 47907, wjwweiss@purdue.edu

ABSTRACT

Many agencies are interested in using a rapid test method for measuring the electrical properties of concrete (i.e., the resistivity or conductivity) since they are related to fluid transport (e.g., diffusion). The advantage of the electrical testing is that it is relatively easy to perform and the test method is relatively fast (on the order of 1 minute). Over the last century, many studies have investigated different approaches to measuring electrical properties. This paper describes the variability associated with the method of measuring the bulk resistivity along the longitudinal axis of a cylinder after placing electrodes on either end. A multi-laboratory study of ten participating laboratories provided variability data for twelve concrete mixtures at testing ages of 28, 56, and 91 days. The variability within the same laboratory was evaluated as the operator variability while the variability between laboratories was evaluated as the multi-laboratory variability. Information on the variability is important in the development of precision and bias statements for this test. In addition, this work discusses how the resistivity results obtained from this test can be correlated with surface resistivity measurements made using the Wenner probe. After correcting for geometry using the approach proposed by Morris et. al. (1996), a linear agreement was noticed between the Wenner test and the measurement through the cylinder. Additionally, the effect of the electrode resistance was discussed and for high resistivity concrete such as that used in much of the transportation infrastructure, this effect appears to be negligible, however it can be accounted for numerically.

1.0 INTRODUCTION

For at least a century, tests have been proposed to measure the electrical properties of concrete [1-7]. These methods have an advantage of being relatively fast to perform and the principle behind these tests is relatively straightforward. While concrete is a composite consisting of a vapor phase (vapor filled porosity or "air"), a solid phase (aggregate and cementitious solids) and a fluid phase (the pore solution) the conductivity of each of these individual phases are very different. The conductivity of the solid and vapor phases are extremely low, approximated as 10^{-9} and 10^{-15} S/m respectively, while the conductivity of the liquid phase is several orders of magnitude higher, ranging from 1 to 20 S/m [8, 9].

As such, it can be assumed that the majority of conduction occurs through the pore fluid. A number of composite models have been developed where this concept is used [10-13]. Two of the more popular equations that are used in the cement and concrete literature are Archies expression and the modified parallel expression [11, 14]. While several documents have reviewed these methods previously, the goal of this section is to describe that the overall conduction is dependent on three factors as illustrated with the modified parallel rule in Equation 1:

$$\sigma_c = \frac{\sigma_0 \cdot \phi \cdot \phi}{\tau} \qquad [1]$$

Where σ is the bulk conductivity, σ_0 represents the conductivity of the fluid phase, ϕ is the volume portion of the fluid phase, s is the degree of saturation and , τ is the tortuosity of the pore network. Collectively, the factor , τ/ϕ can be referred to as the formation factor for a given saturation. This implies that electrical testing is sensitive to concrete with a higher fluid volume (higher water content) and a more open pore network that leads to higher connectivity (higher w/c).

One of the more popular electrical test methods is the Rapid Chloride Permeability Test or RCP test [15, 16]. This test method involves placing a saturated concrete specimen, typically four-inch diameter and two inches thick, between electrodes in different solutions and integrating the charge that is passed over a six hour testing period [15]. While this test has gained wide use, there are a few drawbacks that have been pointed out [17-19]. First this test is destructive in nature. As a result each sample can only provide a single measurement at a single age. Second, saturating the specimen can take a relatively long preparation time. Third, the potential for heating effects due to the large voltage and long test period, and possible modification of the microstructure [20, 21]. There has been research regarding temperature correction for the RCP test [22, 23], but for many RCP test setups monitoring of temperature can be difficult or is frequently not done. Proposed changes to this test have been proposed include extrapolating the charge passed after a test duration of 30-minutes and extrapolating to the 6-hour value [24], increasing the size of the reservoirs to reduce the heating effects [25], and using a single resistance reading measured at an early age, often 1-minute or 5-minutes [18, 19].

Alternative testing methods have been proposed that require little to no sample preparation or enable the sample to be tested at different ages. One rapid test for electrical resistivity of concrete is the Wenner probe. As with any test, there are certain considerations that can impact the results. For example, the probe spacing, geometry of the sample, aggregate size and surface moisture conditions can all influence the measured electrical response. Since the moisture conditions at the surface of the test specimens are quite important, care should be taken to protect against drying or using on surface treated concretes [26-28]. Some work has been done to evaluate the effect of differing layer properties [29]. Additionally, some work has suggested the need for an additional non-linear geometry factor for this method that occurs from the constricted geometry, such as that of a standard test cylinder [30]. Further, when this method is used on real structures the location and proximity of the rebar needs to be considered [29, 31].

Several of these concerns can be addressed if a standard testing protocol is adopted. A draft test method has been developed to use a four-probe Wenner configuration on a 102 mm x 205 mm cylinder with probe spacing of 38.1 mm [32]. This surface resistivity (SR) test method places the probes directly on the surface of the test specimen. This test method has been accepted for use by the Florida Department of Transportation as a quality control test [26]. Additional departments of transportation have evaluated

the SR method as a possible quality control method as well [33]. Work has also been done to correlate RCP testing and diffusion testing with SR [26, 34, 35]. This method has a distinct advantage in that it is rapid to perform and easy to perform on the surface of a cylinder.

The resistance of a concrete cylinder can alternatively be evaluated by using plate electrodes that can be placed on the end of the sample [31, 36]. The resistance value obtained can be normalized by specimen geometry, simply the ratio of sample cross-sectional area to length, to obtain the sample resistivity, termed the bulk resistivity or BR. For this test, good electrical contact must be ensured between the plate electrodes and the test specimen [30, 36]. While this can be assisted through the use of a conductive medium, the surface finish of the cylinder ends should be flat. Some work was also done on evaluating the contact pressure between the plate and the specimen [36]. This test has the distinct advantage of rapid testing and a simple geometry factor. To the best of the authors knowledge, a multi-laboratory study of variability has not been performed on this geometry though some studies have reported exchanges of samples between two labs [36].

Three major factors that should be considered in any electrical resistivity testing are the effects of geometry and temperature. While the bulk resistivity of concrete can be considered a material property, the tests that are performed provide a measure of electrical resistance. The resistance measurement should be corrected for the geometry. This correction can be determined empirically or numerically, although some corrections are simpler. Different geometries have been considered where the geometry factor can be determined experimentally [8, 37]. Temperature is another important factor in the testing of concrete resistivity. This occurs as the primary conduction path is through the ionic pore solution; the increase of temperature increases the mobility of the ions decreasing the resistivity. There has been work that has investigated the possibility of a temperature correction for resistivity test s [6, 38-42]. In this work the samples are all performed in laboratory conditions, as such the sample should be 23+/-2C. Lastly, from Equation 1, saturation is a major component of the bulk conductivity of concrete. As such, knowledge of the moisture history and moisture content at testing are important considerations in the evaluation of resistivity data [43].

The main objectives of this study are fourfold:

- First, it provides some background on electrical property measurements for concrete and provides some of the physical principles behind these tests.
- Second, it presents the results of an inter-laboratory test of the electrical bulk resistivity of concrete. This information can be used in the development of precision and bias statements
- Third, it demonstrates the relationship between surface resistance test methods (e.g. wenner) and measurements performed on a cylindrical geometry.
- Fourth, it highlights important considerations in the development of testing standards and development of policies for the use of electrical methods as quality control/quality assurance tests.

2.0 EXPERIMENTAL DETAILS

2.1 Materials

A round robin test testing program was proposed in 2009 to evaluate the repeatability of the Wenner and bulk resistance tests on concrete cylinders. A series of twelve concrete mixtures were prepared at the laboratories who participated in this study. The mixtures are structural/bridge deck concretes used by state departments of transportation from around the country. A final report detailing a parallel series of wenner and bulk resistivity tests conducted by AASTHO TIG group are available [44, 45].

Table 1—Summary of mixture proportions used in this study, SSD masses

Mixture No.	w/cm	Water	Cement	Fly Ash	Micron Fly Ash	Slag	Silica Fume	Meta-Kaolin	Coarse Aggregate 1	Coarse Aggregate 2	Fine Aggregate
		kg/m^3	kg/m^3	kg/m^3	kg/m^3	kg/m^3	kg/m^3	kg/m^3	kg/m^3	kg/m^3	kg/m^3
1	0.34	163	237	119	-	119	-	-	1059	-	717
2	0.40	144	285	71	-	-	-	-	282	854	824
3	0.39	199	392	119	-	-	-	-	785	-	724
4	0.35	158	279	178	-	-	-	-	940	-	793
5	0.40	164	308	103	-	-	-	-	909	-	879
6	0.37	145	390	-	-	-	-	-	1068	-	712
7	0.40	160	297	80	-	-	24	-	532	528	686
8	0.39	131	251	84	-	-	-	-	555	-	1295
9	0.41	151	291	65	-	-	15	-	1032	-	697
10	0.30	151	297	153	44	-	-	-	1009	-	638
11	0.30	157	430	95	-	-	-	-	1033	-	577
12	0.35	156	402	-	-	-	-	44	1009	-	624

2.2 Sample Conditioning

The samples were demolded at an age of 48-hours and placed into a saturated lime-water bath kept at a constant room temperature until the age of testing (23+/- 2C). At an age of 14-days, the respective laboratories removed the samples and wrapped them in paper towels soaked in saturated lime-water. The samples were then double-bagged and prepared to be shipped via two-day shipping to the other participating laboratories. The goal is to ensure the samples remain wet during testing.

After the samples were received by other testing laboratories, they were removed from the bag and place into saturated lime water baths kept at room temperature (23+/- 2C). At ages of 28, 56, and 91-days, the samples were removed from saturated lime bath, the surface was wiped dry, and the samples were tested for SR and DR. After this testing the samples were placed back in the saturated lime water.

3.0 TESTING PROCEDURE

It should be noted that the test described herein (the plates placed on the end of the cylinder) was a part of a larger study conducted by the AASTHO TIG evaluating surface resistivity [44, 45]. Not all of the labs chose to participate in this portion of the study, so those laboratories have been excluded from the following data though to avoid confusion the original laboratory numbers were retained.

3.1 Equipment

The equipment involved in this test consisted of a CNS Farnell Mk II, U95 surface resistivity meter using an alternating current at 13 Hz, a set of 4-inch diameter stainless steel plate electrodes, and 16 gauge, two-conductor wire to connect the probe tips of the surface resistivity meter to the plate electrodes.

The cable was outfitted with alligator clips on one end to allow easy access to the probe tips of the resistivity meter. The other end of the cable was outfitted with a ring terminal to connect to the plate electrode. The plate electrode was drilled and tapped to allow easy and consistent attachment.

An important consideration is to ensure proper electrical contact between the cylinder and the plate electrodes [30, 36]. For this study, this was done using thin, lime-water saturated sponges.

3.2 Testing Procedure

The plate electrodes should be connected to the pins of the surface resistivity meter. The first two pins that generate the current and measure the potential were connected to one of the steel plate electrodes and likewise for the second set of pins, as shown in Figure 1.

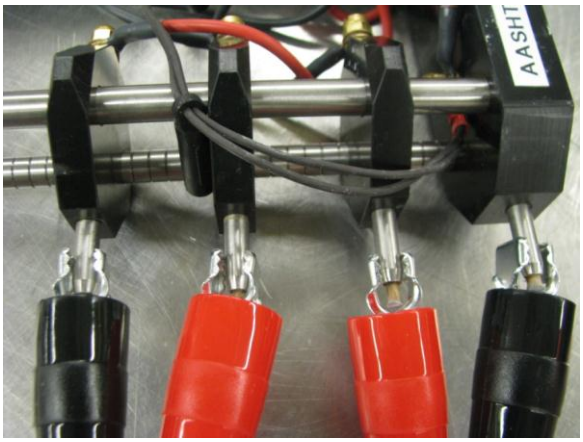

(a)

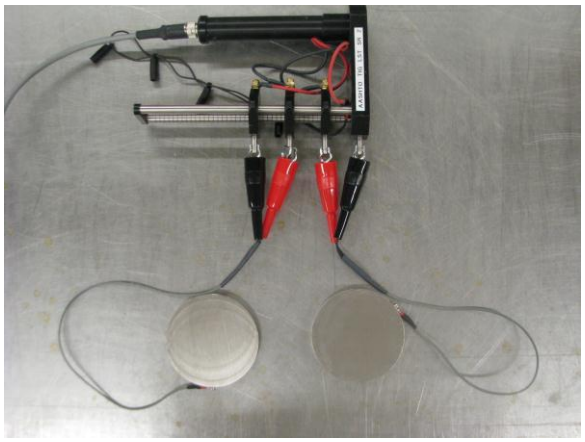

(b)

Figure 1—Attach the alligator clips to the Wenner probe tips. a.) close-up b.) at a distance

The resistances of the top and bottom sponges were then measured, as shown in Figure 2. As resistance of the sponges is largely dependent on moisture content, a test cylinder was used to ensure the pressure on the sponge was consistent for the test of sponge resistance and the measurement of the test cylinder. This was to ensure approximately the same moisture content. The goal of this was to provide a correction for sponge resistance, as discussed below.

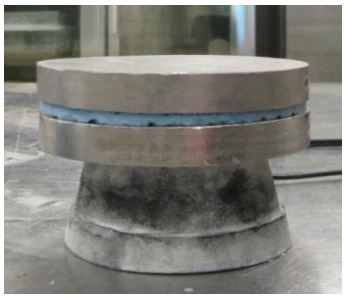

(a)

(b)

Figure 2—Measuring the sponge resistance for a.) the top and b.) the bottom sponges.

The concrete cylinder is then placed between the plate electrodes, with sponges being placed between the plates and the concrete cylinder, as shown in Figure 3.

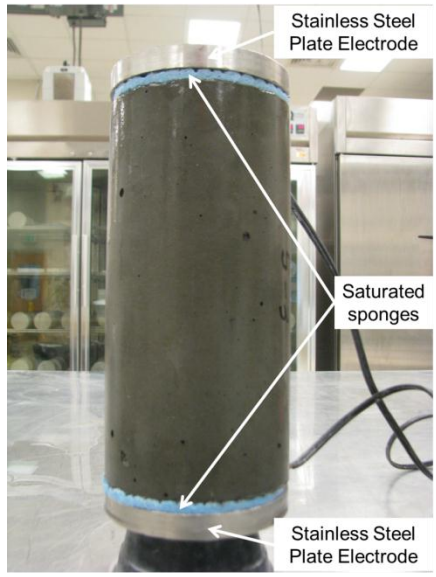

Figure 3—Measuring the resistance of the system.

3.3 Calculations

The resistances of the top and bottom of the top and bottom sponge are termed $R_{\text{top sponge}}$ and $R_{\text{bottom sponge}}$ respectively. The measured resistance of the system, as depicted in Figure 3, was termed R_{measured}. The measured resistance was corrected for the resistance of the sponges by treating the system as resistors in series, as shown in Equation 2. [36]. It was noticed for the sponges used in this study that their resistance values in each lab tended to remain relatively constant. Thus, for sponges that show this constant resistance it is proposed they only be measured periodically and their resistances can be assumed.

$$R_{\text{cylinder}} = R_{\text{measured}} - R_{\text{top sponge}} - R_{\text{bottom sponge}} \quad [2]$$

The bulk resistivity, denoted ρ, can be determined by using Equation 2. Where the geometry factor, K,for current flow through the bulk material is given by Equation 3.

$$\rho = \mathrm{K} \cdot R_{\text{cylinder}} \quad [3]$$

$$\mathrm{K} = \frac{\mathrm{A}}{\mathrm{L}} \quad [4]$$

where R_{cylinder} is the calculated resistance of the concrete test cylinder from Equation 1, A is the cross-sectional area, and L is the length of test specimen.

4.0 RESULTS AND DISCUSSION

4.1 Bulk Resistivity Data

The samples were tested at three ages: 28, 56, and 91-days. The average bulk resistivity (BR) and coefficient of variation (COV) of three test cylinders measured at each testing age is presented below. Cells marked with N/A represent no data reported.

Data measured at ages of 28-days is presented in Table 2. Mixtures 1 through 5 were not tested for 28-day BR as the equipment was in the process of being distributed. Data measured at ages of 56-days is

presented in Table 3. Mixture 1 was not tested for 56-day BR as the equipment had still not been received by one laboratory. Data measured at ages of 91-days is presented in Table 4.

Table 2—Average BR and COV obtained at a testing age of 28-days.

Lab	Test Statistic	Mix 1	Mix 2	Mix 3	Mix 4	Mix 5	Mix 6	Mix 7	Mix 8	Mix 9	Mix 10	Mix 11	Mix 12	Average
1	Average	N/A	N/A	N/A	N/A	N/A	5.29	13.41	14.97	8.84	12.67	6.46	14.89	
	COV	N/A	N/A	N/A	N/A	N/A	0.52	1.15	8.52	1.84	0.47	9.96	5.52	4.00
2	Average	N/A	N/A	N/A	N/A	N/A	5.27	14.12	16.98	8.36	13.49	6.73	18.84	
	COV	N/A	N/A	N/A	N/A	N/A	0.21	1.50	1.07	0.23	2.23	9.56	3.21	2.57
3	Average	N/A	N/A	N/A	N/A	N/A	5.19	13.54	14.03	7.69	11.53	5.43	16.04	
	COV	N/A	N/A	N/A	N/A	N/A	0.58	0.85	1.69	1.79	1.50	0.91	10.67	2.57
5	Average	N/A	N/A	N/A	N/A	N/A	5.65	15.19	16.73	8.31	16.93	7.36	N/A	
	COV	N/A	N/A	N/A	N/A	N/A	0.97	0.63	2.83	1.58	0.97	1.38	N/A	1.39
6	Average	N/A	N/A	N/A	N/A	N/A	5.55	15.24	15.69	9.60	13.72	6.68	20.24	
	COV	N/A	N/A	N/A	N/A	N/A	1.84	1.14	0.57	0.87	3.17	0.77	0.07	1.20
7	Average	N/A	N/A	N/A	N/A	N/A	5.03	13.59	15.01	8.91	12.87	6.88	16.90	
	COV	N/A	N/A	N/A	N/A	N/A	0.89	0.89	1.06	0.08	1.12	1.03	0.39	0.78
8	Average	N/A	N/A	N/A	N/A	N/A	5.84	14.36	16.58	8.63	14.59	6.81	18.21	
	COV	N/A	N/A	N/A	N/A	N/A	0.55	2.54	0.83	1.11	3.07	1.90	0.85	1.55
9	Average	N/A	N/A	N/A	N/A	N/A	5.31	14.39	16.37	8.91	13.15	7.00	16.48	
	COV	N/A	N/A	N/A	N/A	N/A	0.03	0.06	0.68	0.58	3.03	0.58	5.07	1.43
10	Average	N/A	N/A	N/A	N/A	N/A	5.12	14.20	15.60	8.62	14.22	6.77	18.55	
	COV	N/A	N/A	N/A	N/A	N/A	0.01	0.35	0.13	4.51	0.92	0.22	0.63	0.97
12	Average	N/A	N/A	N/A	N/A	N/A	5.68	14.02	15.11	8.30	12.30	6.40	16.76	
	COV	N/A	N/A	N/A	N/A	N/A	0.01	0.20	0.04	0.21	0.26	0.13	0.11	0.14
All Labs	Average	N/A	N/A	N/A	N/A	N/A	5.39	14.21	15.71	8.62	13.55	6.65	17.43	
	COV	N/A	N/A	N/A	N/A	N/A	5.00	4.45	6.03	5.89	11.01	7.62	9.46	

Table 3—Average BR and COV obtained at a testing age of 56-days.

Lab	Test Statistic	Mix 1	Mix 2	Mix 3	Mix 4	Mix 5	Mix 6	Mix 7	Mix 8	Mix 9	Mix 10	Mix 11	Mix 12	Average
1	Average	N/A	6.73	8.76	12.63	8.07	6.56	24.34	29.99	14.78	22.20	11.98	18.14	
	COV	N/A	3.86	3.23	3.35	1.51	2.46	0.87	0.73	2.65	2.62	2.50	1.02	2.25
2	Average	N/A	8.64	9.10	12.05	10.83	7.22	24.52	27.25	13.14	22.53	12.69	20.12	
	COV	N/A	2.68	2.55	2.65	7.47	4.17	4.61	1.20	1.67	3.95	6.31	3.21	3.68
3	Average	N/A	6.18	7.81	12.26	7.71	5.81	23.13	21.61	12.17	17.26	N/A	17.71	
	COV	N/A	7.82	2.81	0.82	0.60	0.79	3.70	2.87	2.68	2.55	N/A	6.87	3.15
5	Average	N/A	7.98	9.26	11.41	7.26	7.08	24.10	29.12	14.92	22.48	10.91	N/A	
	COV	N/A	0.00	7.48	1.52	4.69	2.13	2.58	1.67	7.09	1.65	0.76	N/A	2.96
6	Average	N/A	7.70	9.16	12.89	9.99	6.70	N/A	25.02	N/A	19.62	10.09	21.49	
	COV	N/A	3.24	7.42	1.12	1.01	6.86	N/A	3.74	N/A	4.50	2.77	1.62	3.59
7	Average	N/A	8.38	8.55	12.34	8.33	6.57	24.20	27.18	16.50	21.37	12.16	19.88	
	COV	N/A	9.52	3.50	2.29	2.77	3.06	2.15	4.45	1.48	0.66	8.34	3.96	3.83
8	Average	N/A	7.18	9.27	13.64	9.31	6.72	25.89	31.29	14.38	24.98	12.55	20.85	
	COV	N/A	5.85	3.66	1.75	3.01	2.68	5.07	2.63	3.47	2.42	2.55	3.24	3.30
9	Average	N/A	N/A	9.20	13.50	8.59	6.52	26.09	30.28	15.13	23.23	13.43	20.27	
	COV	N/A	N/A	3.61	6.27	1.17	3.48	1.00	2.98	2.05	4.15	3.52	2.47	3.07
10	Average	N/A	7.98	8.92	14.85	7.94	6.26	26.58	26.03	14.20	22.24	11.22	21.46	
	COV	N/A	0.00	5.33	5.28	4.52	1.91	2.20	1.09	6.33	1.83	1.60	2.32	2.95
12	Average	N/A	6.10	8.34	11.94	7.90	6.52	22.21	23.65	13.06	18.67	9.95	15.99	
	COV	N/A	3.00	1.44	1.35	5.13	2.55	5.98	3.48	5.57	4.57	2.21	5.79	3.73
All Labs	Average	N/A	7.43	8.84	12.75	8.59	6.59	24.56	27.14	14.25	21.46	11.66	19.55	
	COV	N/A	12.51	5.43	7.91	13.01	5.95	5.79	11.50	9.14	10.72	10.27	9.60	

Table 4—Average BR and COV obtained at a testing age of 91-days.

Lab	Test Statistic	Mix 1	Mix 2	Mix 3	Mix 4	Mix 5	Mix 6	Mix 7	Mix 8	Mix 9	Mix 10	Mix 11	Mix 12	Average
1	Average	10.24	8.07	12.14	18.71	11.36	7.58	38.05	42.08	19.44	34.98	17.90	18.80	
	COV	4.31	2.81	3.92	3.35	1.33	3.20	0.26	6.35	3.14	3.16	2.49	4.73	3.25
2	Average	12.16	10.43	15.12	18.83	16.81	8.31	32.40	39.19	17.58	29.78	16.17	24.58	
	COV	5.71	2.68	2.55	4.65	4.68	2.46	5.09	1.27	1.14	3.75	5.82	4.22	3.67
3	Average	10.43	7.85	10.61	16.58	9.46	6.65	28.87	31.78	14.63	22.71	13.10	17.18	
	COV	3.85	8.39	7.77	1.60	4.56	7.64	5.05	5.11	3.86	2.00	6.79	3.49	5.01
5	Average	11.01	8.36	12.12	16.21	10.20	8.48	33.45	37.14	20.19	28.66	15.45	N/A	
	COV	4.08	1.53	5.63	1.44	3.94	1.70	2.12	2.79	8.16	1.82	3.51	N/A	3.34
6	Average	13.91	10.11	14.34	23.58	N/A	7.65	30.97	30.81	15.60	29.92	15.80	20.96	
	COV	0.17	1.78	7.11	1.28	N/A	8.25	3.19	0.76	3.77	3.15	1.58	0.58	2.87
7	Average	10.67	10.05	14.11	19.27	12.58	7.94	35.83	40.06	20.81	29.55	17.18	21.03	
	COV	3.59	6.60	6.45	1.04	2.23	2.30	2.34	3.88	1.12	1.08	0.94	3.29	2.91
8	Average	12.22	8.92	13.25	20.47	13.29	7.67	38.06	45.59	19.19	35.36	18.49	20.29	
	COV	1.05	5.37	3.19	2.36	2.46	2.86	5.27	3.06	3.44	2.89	2.29	3.52	3.15
9	Average	11.16	14.35	14.35	19.54	12.06	8.60	37.74	43.37	N/A	34.48	22.41	19.55	
	COV	0.21	1.58	1.58	8.51	2.65	7.51	0.38	7.26	N/A	5.63	9.89	4.55	4.52
10	Average	12.39	9.75	13.71	22.44	12.65	6.74	37.54	38.41	18.26	30.51	16.50	21.15	
	COV	2.19	9.15	4.24	6.30	9.41	0.59	1.31	0.75	6.02	2.23	2.30	2.26	3.90
12	Average	10.07	7.82	11.12	15.96	10.40	7.26	31.21	33.11	14.93	22.67	12.69	18.01	
	COV	4.73	1.84	0.55	1.32	3.78	2.91	5.62	4.19	4.85	3.89	0.63	0.71	2.92
All Labs	Average	11.43	9.57	13.09	19.16	12.09	7.69	34.41	38.15	17.85	29.86	16.57	20.17	
	COV	10.66	20.39	11.56	13.25	18.07	8.77	10.03	13.06	12.95	15.08	16.71	10.75	

4.2 Operator Variability

The operator variability is described from the average COV from each mixture for each different laboratory. This is shown as the last column in Tables 2-5. The maximum of average within-laboratory COV for each testing age is presented in Table 6. Previous work evaluating the development of an automated resistivity testing system has reported similar within-laboratory variability [46].

Table 6—Maximum within-laboratory COV

Testing Age	Within-laboratory COV
28-days	4.00 %
56-days	3.83 %
91-days	5.01 %

4.3 Multi-laboratory Variability

The multi-laboratory variability can be described from the average COVs from each laboratory for the different mixtures. This is shown as the last row in Tables 2-5, termed All Lab COV. The maximum of average multi-laboratory COV for each testing age is presented in Table 7, and is used to develop the precision statement for multi-laboratory variability. It should be noted that the variation increases over time. It is believed that this may be due to slight variations in curing conditions which may have occurred at each lab which could amplify differences overtime.

Table 7—Maximum multi-laboratory COV

Testing Age	Multi-laboratory COV
28-days	11.01 %
56-days	13.01 %
91-days	20.39 %

4.4 Precision Statements

Precision estimates were calculated [47]. For this experiment, the fundamental statistic was determined to be the COV, represented as 1s% in ASTM C670-10. Therefore, the calculated precision indices will correspond to d2s% described in ASTM C670-10. This index represents the maximum difference between two individual test results, expressed as a percentage of their average. The precision indices for different testing ages are shown in Table 8.

Table 8—Precision indices for direct resistivity

Testing Age	Within-laboratory	Multi-laboratory
28-days	11.30	31.14
56-days	10.84	36.79
91-days	14.17	57.66

The maximum precision index for the within-laboratory and multi-laboratory variability will be used to form the precision statements.

The maximum pooled single-operator coefficient of variation was found to be 5.01 %. Therefore, the results of two properly conducted tests by the same operator on the same concrete material at the same age are not expected to differ by more than 14.2 % of their average. The maximum pooled multi-laboratory coefficient of variation was found to be 20.39. Therefore, the results of two properly conducted tests by different laboratories on the same concrete material at the same age are not expected to differ by more than 57.7 % of their average.

4.5 Correlation with Surface Resistivity Measurements

Surface resistivity measurements were conducted as a part of this study [44]. Figure 4 compares the measured SR and the calculated BR.

A linear correlation was noticed, except that SR measurements tended to be 1.86 times higher than BR. This large data of experimental results support previous work using finite element that showed additional geometry factors must be used to account for test geometry, such as probe spacing, cylinder length, and cylinder diameter [30]. The factor of 1.86 is in good agreement with the geometric correction proposed by Morris et. al. (1995) for a cylinder with a length of 205 mm, diameter of 102 mm, probe spacing of 38.1 mm and a MSA of 19 mm, which was approximately 1.9.

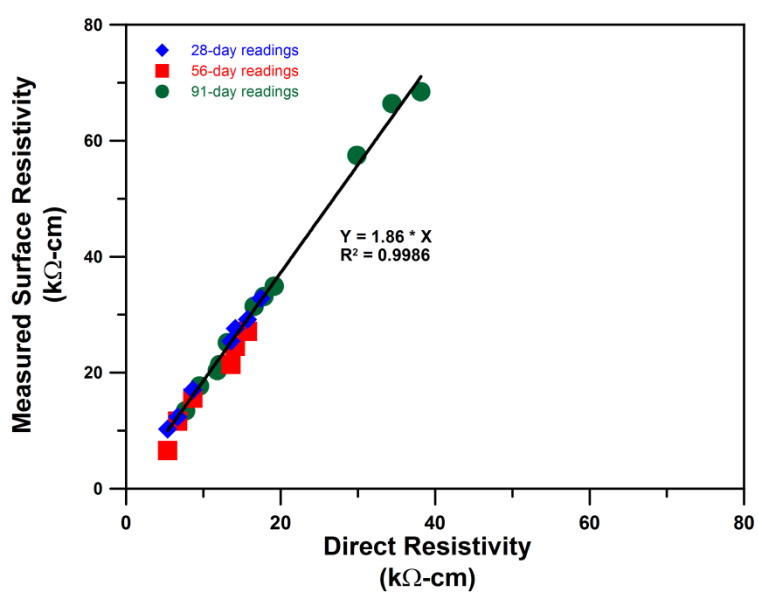

Figure 4—Correlation of measured SR and DR of samples from differing ages, each data point represents the average of three samples.

4.6 Effects of Electrode Resistance

Previous work has shown that electrode resistance (and other factors to insure connectivity between the electrode and sample) may influence the results as discussed in Equation 2.

The major contributor to electrode resistance is bad contact between the plate electrode and the surface of the test cylinder. Some work has suggested the possibility of using flexible electrodes [30]. However, a more practical solution is to use an aid that allows for good electrical contact. In the laboratory, this can be accomplished through the use of an electrically conductive jelly [48, 49]. The alternative is to use another soft, conductive medium. Popular solutions have included the use of saturated sponges, chamois cloth, and paper towels [21, 36].

An important issue becomes the associated resistance of the sponges. Previously, this associated resistance can be treated as a series of resistors in parallel with the test cylinder, which produces the correction shown and described by Equation 2.

The sponge resistance is largely dependent on the moisture content of the sponges and the conductivity of the solution in which they are saturated. For this study, the solution was saturated lime water, which was also used as the storage solution for the test cylinders. Furthermore, to ensure proper moisture content, the contact pressure for the sponge was kept constant between the sponge resistivity test and the cylinder test, as shown in Figures 2 and 3.

While this correction provides the truest value for resistivity, the results of this study show that this correction might not always be very large. For the sponges used in this study, the resistances of the two sponges were much less than the resistance of the cylinder. Figure 5a shows the measured resistance (i.e., sample, sponges and electrodes) as a function of the cylinder resistance (i.e., the sample alone), as defined in Equation 2.The best fit line shows only a small difference between the measured resistance and the cylinder resistance.

Additionally, the ratio of the measured resistance to the cylinder resistance, as defined in the preceding paragraph, can be shown against the concrete resistivity, depicted in Figure 5b. This ratio represents the correction from cylinder resistance. Figure 5b shows that for high resistivity concrete, the resistance correction become almost negligible, while for lower resistivity concrete the sponge resistance might play a larger role.

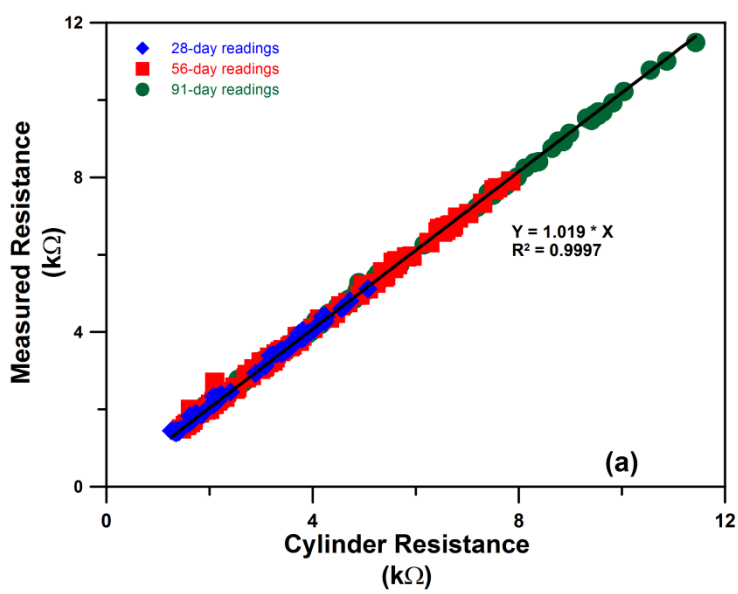

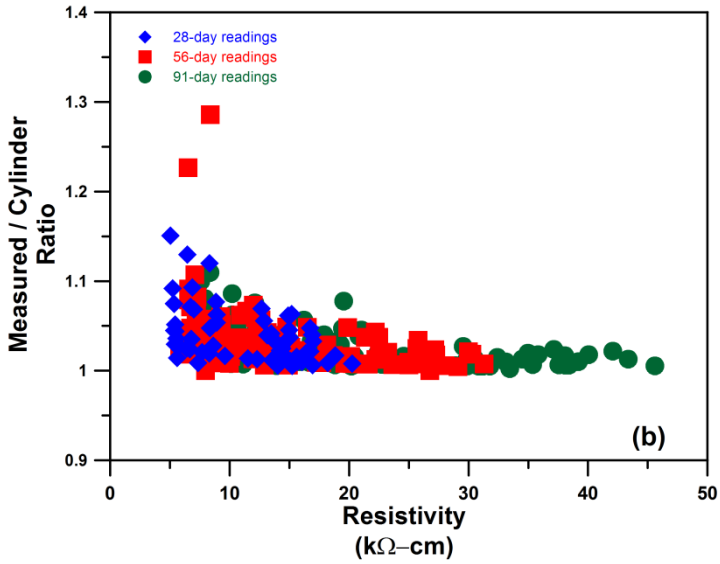

Figure 5—Influence of electrode resistance on a.) the measured resistance (sample and electrodes) as a function of the cylinder (sample) resistance and b.) the ratio of measured resistance (sample and electrodes) and cylinder (sample) resistance as a function of concrete resistivity.

5.0 SUMMARY AND CONCLUSIONS

This paper reports results from a multi-laboratory investigation of the variability associated with testing the electrical bulk resistivity of concrete cylinders by placing plate electrodes on the ends of the cylinder. An analysis of the data is presented. The following observations can be made regarding the variability of the resistivity test method. It should be noted that the samples used in this study were conditioned by storing in lime saturated water between test measurements. First, resistivity testing is a rapid test method that allows for rapid results. This rapid test drastically reduces the amount of time a technician needs to spend conditioning the sample and conducting the test. Therefore, this test is well suited for quality control testing. Second, resistivity testing can be considered a non-destructive test. This means that for each mixture being evaluated using resistivity, only a small number of samples need be prepared. This can be contrasted with other destructive electrical tests that require a larger series of samples for proper mixture evaluation. In fact, this testing can be performed on cylindrical samples before they are tested for compressive or splitting tensile strength. Third, the operator and multi-laboratory precision of this test method have been quantified using data from the maximum COV obtained from an inter-laboratory study consisting of ten laboratories and twelve differing mixtures. Fourth, specimen geometry can greatly influence the results of an electrical test. This often requires the use of a geometry correction factor. For the direct resistivity test, this geometry factor is simply the ratio of sample area to sample length. Finally, the effects of electrode resistance were addressed using a series model. While previous work described corrections for end plate resistance, the variability data from this investigation shows that for the materials used in this study, the correction that is needed is quite small. It is suggested that a resistivity test be developed that could include a variety of sample geometries including 1) the wenner probe geometry, 2) the direct bulk resistance described herein, and 3) alternative geometries provided the geometry factor can be quantified.

6.0 ACKNOWLEDGEMENTS

The experiments reported in this paper were conducted as part of a larger study sponsored by the Pooled Fund Program and the American Association of American Highway and Transportation Officials Technology Implementation Group and organized by the Florida Department of Transportation. This portion of the present study was conducted in conjunction with the Indiana Department of Transportation. The contents of this report reflect the views of the authors, who are responsible for the facts and the accuracy of the data presented herein. The contents do not necessarily reflect the official views or

policies of the Indiana Department of Transportation or the Federal Highway Administration at the time of publication. This report does not constitute a standard, specification, or regulation.

The authors would like to thank the participating laboratories and testing personnel for their time and efforts. This includes, but is not limited to, Rob Reis, Cipriano Manansala, and Joe Shanabrook, California Department of Transportation; Jagan Gudimettla, FHWA Mobile Concrete Laboratory; Celik Ozyildirim and Bill Ordel, Virginia Department of Transportation; Wilfredo Malpica and Javier Molinari, Grupo-Carmelo; Ed McGaffin and Dan Dennis, New York State Department of Transportation; Lieska Halsey, Jeremy Weigel, and Tim Krason, Nebraska Department of Transportation; Eric Prieve and Azis Khan, Colorado Department of Transportation; John Kern and Wayne DeMarco, CEMEX; Thomas Frank and Ronald Simmons, Florida Department of Transportation; Jeremiah Hersey and Professor Mike Jackson, University of North Florida.

Check up to 26

7.0 REFERENCES

[1] E. Hammond, T.D. Robson, Comparison of electrical properties of various cements and concretes. I-II, The Engineer, 199 (1955) 78-80.
[2] Y. Shimizu, An electrical method for measuring the setting time of portland cement, Concrete, 32 (1928) 111-113.
[3] J. Calleja, Effect of current frequency on measurement of electrical resistance of cement pastes, J Am Conc Inst, 24 (1952) 329-332.
[4] W.J. Weiss, J.D. Shane, A. Mieses, T.O. Mason, S.P. Shah, Aspects of monitoring moisture changes using electrical impedance spectroscopy, in: Second symposium on the importance of self desiccation in concrete technology, Lund, Sweden, 1999.
[5] G.E. Monfore, The electrical resistivity of concrete, Portland Cement Association, Research and Development Laboratories, Skokie, IL, 1968.
[6] H.W. Whittington, J. McCarter, M.C. Forde, The conduction of electricity through concrete, Mag Concr Res, 33 (1981) 48-60.
[7] B.J. Christensen, R.T. Coverdale, R.A. Olson, S.J. Ford, E.J. Garboczi, H.M. Jennings, T.O. Mason, Impedance spectroscopy of hydrating cement-based materials: measurement, interpretation, and application, J Am Ceram Soc, 77 (1994) 2789-2804.
[8] F. Rajabipour, Insitu electrical sensing and material health monitoring in concrete structures, Ph.D. Dissertation, Purdue University, West Lafayette, Indiana, 2006.
[9] F. Rajabipour, J. Weiss, Linking health monitoring in concrete structures with durability performance simulations, in: B. Cross, J. Finke (Eds.) ASCE Structures Congress, ASCE, St. Loius, MO, 2006.
[10] S. Torquato, Random heterogeneous materials: microstructure and macroscopic properties, Springer, New York, NY, 2002.
[11] G.E. Archie, The electrical resistivity log as an aid in determining some reservoir characteristics, SPE Reprint Series, (2003) 9-16.
[12] K.L. Aplin, Aspirated capacitor measurements of air conductivity and ion mobility spectra, Rev Sci Instrum, 76 (2005) 104501.
[13] D.S. McLachlan, M. Blaszkiewicz, R.E. Newnham, Electrical resistivity of composites, J Am Ceram Soc, 73 (1990) 2187-2203.
[14] E.J. Garboczi, Permeability, diffusivity, and microstructural parameters: A critical review, Cem Concr Res, 20 (1990) 591-601.
[15] ASTM C1202, 2010, Standard test method for electrical indication of concrete's ability to resist chloride ion penetration, ASTM International, West Conshohocken, PA.
[16] AASTHTO T277, 2007, Standard method of test for electrical indication of concrete's ability to resist chloride ion penetration, American Association of State Highway and Transportation Officials, Washington, D.C.
[17] J.D. Shane, C.D. Aldea, N.F. Bouxsein, T.O. Mason, H.M. Jennings, S.P. Shah, Microstrucutral and pore solution changes induced by the rapid chloride permeability test measured by impedance spectroscopy, Concr Sc Eng, 1 (1999) 110-119.
[18] K.A. Riding, J.L. Poole, A.K. Schindler, M.C.G. Juenger, K.J. Folliard, Simplified concrete resistivity and rapid chloride permeability test method, ACI Mater J, 105 (2008) 390-394.

[19] K.A. Snyder, C. Ferraris, N.S. Martys, E.J. Garboczi, Using impedance spectroscopy to assess the viability of the rapid chloride test for determining concrete conductivity, J NIST, 105 (2000) 497-509.
[20] D. Sohn, T.O. Mason, Electrically induced microstructural changes in portland cement pastes, Adv Cem Based Mater, 7 81-88.
[21] J.D. Shane, Electrical conductivity and transport properties of cement-based materials measured by impedance spectroscopy, Ph.D. Dissertation, Northwestern University, Evanston, IL, 2000.
[22] G.A. Julio-Betancourt, R.D. Hooton, Study of the Joule effect on rapid chloride permeability values and evaluation of related electrical properties of concretes, Cem Concr Res, 34 (2004) 1007-1015.
[23] B. Dale P, A virtual rapid chloride permeability test, Cem Concr Compos, 29 (2007) 723-731.
[24] P.F. McGrath, R.D. Hooton, Re-evaluation of the AASHTO T259 90-day salt ponding test, Cem Concr Res, 29 (1999) 1239-1248.
[25] C.C. Yang, S.W. Cho, R. Huang, The relationship between charge passed and the chloride-ion concentration in concrete using steady-state chloride migration test, Cem Concr Res, 32 (2002) 217-222.
[26] R.J. Kessler, R.G. Powers, M.A. Paredes, Resistivity Measurements of Water Saturated Concrete as an Indicator of Permeability, in, 2005.
[27] S.G. Millard, Reinforced concrete resistivity measurement techniques, Proceedings - Institution of Civil Engineers Part 2 Research and theory, 91 (1991) 71-88.
[28] F. Rajabipour, J. Weiss, J.D. Shane, T.O. Mason, S.P. Shah, Procedure to interpret electrical conductivity measurements in cover concrete during rewetting, J Mater Civ Eng, 17 (2005) 586-594.
[29] F. Presuel-Moreno, Y. Liu, M. Paredes, Concrete resistivity on the apparent surface resistivity measured via the four-point wenner method, in: Corrosion 2009, March 22, 2009 - March 26, 2009, National Assoc. of Corrosion Engineers International, Atlanta, GA, United states, 2009, pp. Carboline; Multi-chem; Corrpo; Champion Technologies; Loresco.
[30] W. Morris, E.I. Moreno, A.A. Sagues, Practical evaluation of resistivity of concrete in test cylinders using a Wenner array probe, Cem Concr Res, 26 (1996) 1779-1787.
[31] R.B. Polder, Test methods for on site measurement of resistivity of concrete — a RILEM TC-154 technical recommendation, Constr Build Mater, 15 125-131.
[32] FM 5-578, 2004, Florida Method of Test for Concrete Resistivity as an Electrical Indicator of its Permeability, Flordia Department of Transportation,
[33] T.D. Rupnow, P. Icenogle, Evaluation of Surface Resistivity Measurements as an Alternative to the Rapid Chloride Permeability Test for Quality Assurance and Acceptance, in, Louisiana Department of Transportation, Baton Rouge, LA, 2011, pp. 68.
[34] N.S. Berke, M.C. Hicks, Estimating the Life Cycle of Reinforced Concrete Decks and Marine Piles Using Laboratory Diffusion and Corrosion Data, in, 1992.
[35] E. Vivas, H.R.I. Hamilton, A.J. Boyd, Permeability of Concrete - Comparison of Conductivity and Diffusion Methods, in, Department of Civil and Coastal Engineering, University of Florida, Gainsville, FL, 2007, pp. 238.
[36] M.D. Newlands, M.R. Jones, S. Kandasami, T.A. Harrison, Sensitivity of electrode contact solutions and contact pressure in assessing electrical resistivity of concrete, Mater Struct, 41 (2008) 621-621-632.
[37] J. Castro, R. Spragg, P. Kompare, W.J. Weiss, Portland Cement Concrete Pavement Permeability Performance, in, Joint Transportation Research Program, Indiana Department of Transportation and Purdue University, West Lafayette, Indiana, 2010.
[38] M. Nokken, A. Boddy, X. Wu, R.D. Hooton, Effects of temperature, chemical, and mineral admixtures on the electrical conductivity of concrete, J ASTM Int, 5 (2008).
[39] M. Castellote, C. Andrade, C. Alonso, Temperature correction, from 3 to 25C of the electrical resistivity of mortars and concretes, Industria Italiana del Cemento, 71 (2001) 916-923+850-851.
[40] G. Sant, F. Rajabipour, J. Weiss, The influence of temperature on electrical conductivity measurements and maturity predictions in cementitious materials during hydration, Indian Concr J, 82 (2008) 7-16.
[41] Y.A. Villagran Zaccardi, J. Fullea Garcia, P. Huelamo, A.A. Di Maio, Influence of temperature and humidity on Portland cement mortar resistivity monitored with inner sensors, Mater Corros, 60 (2009) 294-299.
[42] W.J. McCarter, M.C. Forde, H.W. Whittington, RESISTIVITY CHARACTERISTICS OF CONCRETE, Proceedings of the Institution of Civil Engineers (London) Part 1 - Design & Construction, 71 (1981) 107-117.

[43] J. Castro, R. Spragg, J. Weiss, Water Absorption and Electrical Conductivity for Internally Cured Mortars with a W/C between 0.30 and 0.45, J Mater Civ Eng, In press (2011).
[44] N.M. Jackson, Results of Round-Robin Testing for the Development of Precision Statements for the Surface Resistivity of Water Saturated Concrete, in, Ponte Vedra Beach, Florida, 2011.
[45] Draft standard method of test for surface resistivity indication of concrete's ability to resist chloride ion penetration, American Association of State Highway and Transportation Officials, Washington, D.C.
[46] A. Poursaee, W.J. Weiss, An automated electrical monitoring system (AEMS) to assess property development in concrete, Autom Constr, 19 (2010) 485-490.
[47] ASTM C670, 2010, Standard practice for preparing precision and bias statements for test methods for construction materials, ASTM International, West Conshohocken, PA.
[48] R. Henkensiefken, J. Castro, D. Bentz, T. Nantung, J. Weiss, Water absorption in internally cured mortar made with water-filled lightweight aggregate, Cem Concr Res, 39 (2009) 883-892.
[49] M.D.A. Thomas, The use of conductive gel, personal communication, W.J. Weiss, 2008.

Wetting and Drying of Concrete Using Aqueous Solutions Containing Deicing Salts

Robert P. Spragg
Undergraduate Research Assistant
School of Civil Engineering
Purdue University
West Lafayette, IN 47907-2051
E-mail: rspragg@purdue.edu
Phone: 765.494.0358

Javier Castro
Graduate Research Assistant and Ph.D. Candidate
School of Civil Engineering
Purdue University
West Lafayette, IN 47907-2051
E-mail: jcastro@purdue.edu
Phone: 765.494.0358

Wenting Li
Graduate Research Assistant
School of Civil Engineering
Purdue University and Southeast University
West Lafayette, IN 47907-2051
Nanjing, China 211189
E-mail: li448@purdue.edu
Phone: 765.494.0358

Mohammad Pour-Ghaz
Graduate Research Assistant
School of Civil Engineering
Purdue University
West Lafayette, IN 47907-2051
E-mail: mpourghaz@purdue.edu
Phone: 765.494.0358

Pao-Tsung Huang
Graduate Research Assistant
School of Civil Engineering
Purdue University
West Lafayette, IN 47907-2051
E-mail: huang69@purdue.edu
Phone: 765.494.6242

Jason Weiss (Corresponding Author)
Professor and Director of Pankow Materials Laboratory
Associate Director of the Center for Advanced Cement Based Materials
School of Civil Engineering
Purdue University
West Lafayette, IN 47907-2051
E-mail: wjweiss@purdue.edu
Phone: 765.494.2215

Abstract

A series of wetting and drying tests were performed on concrete using different aqueous solutions containing deicing salts. The rate of fluid absorption was generally lower for aqueous solutions containing deicing salts than it was for water. In addition, less fluid was absorbed for samples exposed to aqueous solutions containing deicing salts than for samples exposed to water. The change in the rate of aqueous fluid absorption was proportional to the square root of the ratio of surface tension and viscosity of the absorbed fluid. Concrete that has been exposed to solutions containing deicing salts showed less mass loss during drying. Measures of equilibrium relative humidity over the salt solutions are used to interpret drying behavior. Experimental data indicates that concretes that had previously been exposed to deicing solutions can also exhibit reduced rate of absorption, even if water is the fluid being absorbed.

1. Research Need and Significance

Some jointed plain portland cement concrete pavements in freezing prone climates have shown premature deterioration at the longitudinal and transverse joints. While some have attributed this damage to a chemical attack, inadequate air entrainment, poor mixture design, inadequate constituent materials, or poor construction practices; it is the hypothesis of the authors of this paper that this joint deterioration may be attributed, at least in part, to preferential absorption of fluid at joints. This hypothesis was developed based on observations from the field that show these deteriorated locations frequently occurred at low spots in the pavement, where joint sealers were damaged, where water has collected, or where the joint does not appear to have opened thereby trapping water [1]. Preferential fluid ingress at joints could increase a variety of damage mechanisms including deleterious chemical reactions, crystallization pressure, or freeze thaw damage that may degrade the concrete. To fully evaluate fluid ingress at the joints it is essential that the wetting and drying behavior of concrete is evaluated using aqueous solutions containing deicing salts.

This work is limited in scope as it considers only the ingress of aqueous solutions over short time periods and does not explicitly consider any chemical reaction that occurs between the aqueous solution and the concrete. This information is intended to provide reference for those developing tests to evaluate potential deicer-concrete interactions [2], for developing tests on fluid absorption, for evaluating fluid absorption in concrete [3], for input parameters in computer simulation of fluid ingress at joints [4], and for potential approaches to limit joint deterioration like penetrating sealers for possible use in concrete pavements [5].

2. Fluid Absorption in Porous Materials

Fluid absorption is a frequently used test to provide an indication of the durability of concrete systems since it is simple to perform. Several standard tests exist for measuring water absorption including ASTM C 1585-04 [6], BS 1881-99 [7], and ASTM D6489-99 [8]. While the concept behind these tests is very similar, there are differences in how the samples are conditioned, treated, and tested. In each of these tests water is typically used as the fluid that is being absorbed. Hall [9] discusses that water can interact with the cement matrix adding complexity to the interpretation of results. To overcome some of these limitations or to indicate how absorption can be reduced by fluid composition other solutions have been tested [9-13].

MacInnis and Nathawad [14] assessed the absorption of an aqueous solution consisting of a NaCl deicing salt and reported a decrease in absorption. Sutter et al. [15] reported that sorptivity decreased from highest to lowest in the order of water, NaCl, $CaCl_2$ and $MgCl_2$. Similar data has recently been observed by Janusz [16]. As a result, it can be observed that concrete exposed to deicing salt solutions absorb fluid at a slower rate than they would absorb water; however the previous work has not related this behavior to the fluid properties or described the influence of salt concentration or properties of the aqueous solution.

The results of one-dimensional fluid absorption tests (assuming negligible gravitational effects) are typically reported as the cumulative water absorbed per surface area (surface from which water is absorbed) versus the square root of wetting time. Equation 1 is frequently used to

describe the water absorption (total volume of fluid absorbed) and the sorptivity (related to the rate of absorption) [17].

$$i = S\tau^{1/2} \qquad \text{Eq. 1}$$

where i [mm^3/mm^2] is the cumulative water absorption, S [mm/s$^{1/2}$] is the sorptivity, and τ [s] is the elapsed time. It should be noted that additional equation have been proposed to account for time dependent properties [18].

Hall [9] proposed that the diffusion would scale proportionately with the ratio of surface tension (γ) and viscosity (η) of the fluid. Hall further related this to sorptivity since sorptivity is related to the square root of diffusion. Kelham [19] derived an expression for fluid absorption (Equation 2) that shows the relationship between depth of penetration and the square root of the ratio of surface tension and viscosity.

$$x(\tau) = \sqrt{\frac{4k\gamma\cos(\theta)\tau}{p\eta r}} \qquad \text{Eq. 2}$$

where $x(\tau)$ [mm] is the penetration depth, γ [N/mm] is the surface tension, θ [rad] is the liquid-solid contact angle, p [Dimensionless] dis the porosity of the medium, r [mm] is the pore radius, k [mm^2] is the intrinsic permeability of the material, and η [Pa.s] is the viscosity of fluid. An expression similar to equation 2 was derived by Scherer and Wheeler [20] for stone consolidates.

Previous research using organic fluids has shown an absorption rate that scales proportionally with the square root of the ratio of surface tension and viscosity of the fluid ($(\gamma/\eta)^{1/2}$). This work will use this approach to attempt to interpret results from absorption tests that used aqueous solutions containing deicing salts.

3. Properties of Deicing Salt Solutions

Physical properties of pure solutions were gathered from literature and compared with measured values for the industrially available deicing solutions tested in this research, and they are provided here for convenience in one location. The properties of the deicing solutions will be used in interpreting the wetting and drying results, discussed later in this paper. This section is divided into four sections. The first three sections describe the influence of the deicing solutions in terms of surface tension, viscosity, and equilibrium relative humidity over the aqueous solution. The fourth section describes the specific gravity of the solution as a function of concentration as this is used to determine the volume of solution absorbed during the absorption test.

3.1 Surface Tension of Deicing Salt Solutions

Figure 1 (a) shows surface tension measurements at different concentrations for the three solutions used in this research: NaCl, $CaCl_2$, $MgCl_2$. The surface tension for NaCl was obtained from [10], $CaCl_2$ from [21] and $MgCl_2$ from [22]. A Du Noüy Ring Tensiometer KRÜSS was used with a resolution of 0.1 mN/m for the industrial deicers tested in this study. The tensiometer was cleaned between measurements following ASTM D971-04 [24]. The tensiometer was first calibrated using de-ionized water, which provided a value of 71.0 x 10^{-6} N/mm. A series of three measurements were performed for each solution, with the average reported.

The closed points in Figure 1 (a) are the values measured for the industrially available solutions. The lines represent values taken from literature for pure salt solutions at different mass concentrations. While the general trends are consistent, differences between the solutions containing industrial deicing salts and literature values may be due to impurities or other additves however further work is needed to examine this in greater detail.

3.2 Viscosity of Deicing Salt Solutions

Figure 1 (b) shows a comparison of the viscosities for the solutions used in this research between pure solutions taken from literature and measurements of the deicing solutions. Viscosity measurements for the industrial deicers were performed on the salt solutions using an Anton-Parr rheometer, model Physica MCR 301. The rheometer kept the solution being tested at 23.0 ± 0.02 ºC and from the torque applied to the fluid that causes a shear from which the viscosity can be found. Calibration of the device was performed using a reference standard.

The dashed lines presented are viscosities at different concentrations and are taken from literature [10, 21-23], while the points represent measured viscosities of the industrially available solutions. Again, differences between literature values and those of the solutions measured can be explained by differences in possible additions or chemistries of the industrial deicers.

3.3 Relative Humidity of Deicing Salt Solutions

Relative humidity measurements were performed on the salt solutions using Rotronic HygrClip2S sensors (± 0.8 % RH at 23 ± 0.1 °C). The relative humidity probes were mounted in a 75 mm x 68 mm stainless steel cylinder that was placed over a water jacketed sample cup holder. The water jacket was connected with a water bath at a constant temperature of 23.0 ± 0.1 ºC.

Figure 1 (c) shows the relative humidity measured over salt solutions for a wide range of solution concentrations. As the concentration increased the relative humidity over the solution decreased. The measured relative humidities of these unsaturated salt solutions are higher than that of the saturated solution of these salts which are 75.4 % RH for NaCl [25], 33.0 % RH for $MgCl_2$ [25] and 22 % for $CaCl_2$ [21].

3.4 Specific Gravity of Deicing Salt Solutions

Figure 1 (d) shows the specific gravity of different deicing solutions as a function of concentration. The specific gravity of the solution increases with concentration. The $CaCl_2$ and $MgCl_2$ increase at very similar rates with an increase in concentration, while the NaCl increases slightly less than the $CaCl_2$ and $MgCl_2$ (i.e., 25 % less increase with concentration). This may be attributed to the colligative properties of solutions.

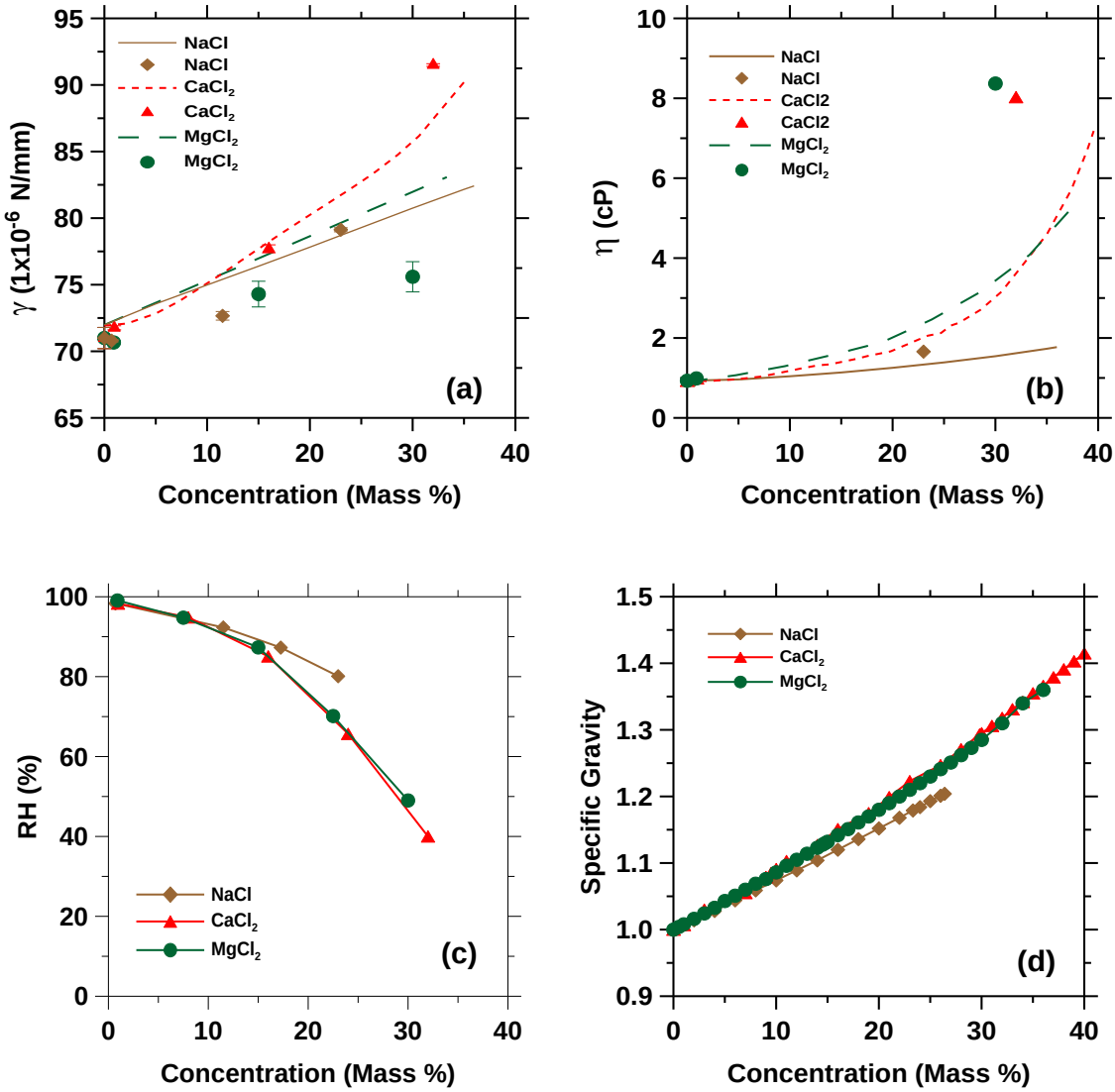

Fig .1. Properties of Deicing Salts at 23-25 ºC: (a) Surface Tension (b) Viscosity (c) Relative Humidty (d) Specific Gravity (Rosenburgh 2010, unpublished data)

4. Wetting and Drying for Concrete with Deicing Solutions

4.1 Experimental Program of Wetting and Drying of Concrete with Deicing Solutions

The concrete mixture that was used for these tests was a typical INDOT class C bridge deck concrete. The mixture proportions of this concrete are shown in Table 1. The fresh air content was 5.7 %, which was measured according to ASTM C231-09 [26]. The hardened air content of the concrete was 4.4 % as assessed using an automated optical scanning approach [18] based on the method proposed by Peterson et al. [28].

Table 1. Mixture Proportions of Concrete Assuming Saturated Surface Dry (SSD) Conditions

Material	Mass
Cement (kg/m^3)	316
Class C Fly Ash (kg/m^3)	60
Water (kg/m^3)	150
Fine Aggregate (kg/m^3)	736
Coarse Aggregate (kg/m^3)	1049
Air Entraining Admix. (ml/100 kg of cem. materials)	20
High Range Water Reducer Admix. (ml/100 kg of cem. materials)	456
Retarder Admixture (ml/100 kg of cem. materials)	98

The concrete was produced in a central mix plant and discharged from a ready mix concrete truck. A series of 100 mm × 200 mm cylinders were cast. After one day of curing, the cylinders were demolded and sealed in double plastic bags at 23 ± 0.5 °C until the samples reached an age of 28 d. After 28 days of curing the cylinders were removed from bags and three 50 mm ± 2 mm thick samples were cut from the central portion of each cylinder using a wet saw.

Two different sets of samples were used in this study. The first set of samples were used to evaluate the effect of sample conditioning on water absorption. In each condition, three samples were used. A total of five conditions were considered: ASTM C1585-04, oven-dry, 50 % RH, 65 % RH and 80 % RH. To ensure that these samples that were conditioned at 50 %, 65 %, and 80 % RH, reached equilibrium, a 12-month conditioning was period was considered. The second set of

samples that were used for aqueous salt solution absorption, drying, and de-ionized water re-absorption were conditioned at 50 ± 2 % RH, 23 ± 0.5 °C for 36 months and two samples were tested for each salt solution.

To prepare the specimens for fluid absorption testing, the sides of the samples were sealed with epoxy. After the epoxy had hardened, the top surface was covered with plastic to avoid evaporation from the sample during testing.

The absorption test involves recording incremental mass change measurements during the first six hours after the sample comes in contact with the fluid and subsequently taking one measurement every day for the next eight days. The amount of absorbed fluid is normalized by the cross-section area of the specimen exposed to the fluid using Equation 3.

$$i = \frac{m_t}{(a \cdot \rho)} \qquad \text{Eq. 3}$$

where: i (mm^3/mm^2) is the normalized absorbed fluid, m_t (g) is the change in specimen mass at time t; a (mm^2) is the area of the specimen exposed to the fluid (i.e., that of the bottom face), and ρ (g/mm^3) is the density of the absorbed fluid (this is provided in greater detail in 3.1). These absorption measurements are then plotted as a function of the square root of time, as provided by Equation 1. The sorptivity is the slope of this graph.

The second series of samples were tested using seven different fluids. Their composition was primarily based on one of three different industrially available deicing products, either NaCl, $MgCl_2$ or $CaCl_2$. A low concentration was used for each salt solution as well as a higher concentration that was selected to be near the eutectic composition for each salt. De-ionized water was also used as a reference fluid.

4.2 Experimental Results from Wetting with Water for Different Conditioning Methods

Figure 2 shows the results from water absorption tests performed on the first series of samples that were conditioned with different environmental conditions as mentioned earlier (ASTM C1585-04 accelerated conditioning, 80 % RH, 65 % RH, 50 % RH and oven drying). It should be remembered that these samples were conditioned for 12 months while the remainder of the samples discussed in this paper were conditioned at 50 % RH for a much longer time. Sample preparation has an enormous impact on the water absorption results as more severe drying enables a greater volume of water to be absorbed during the test.

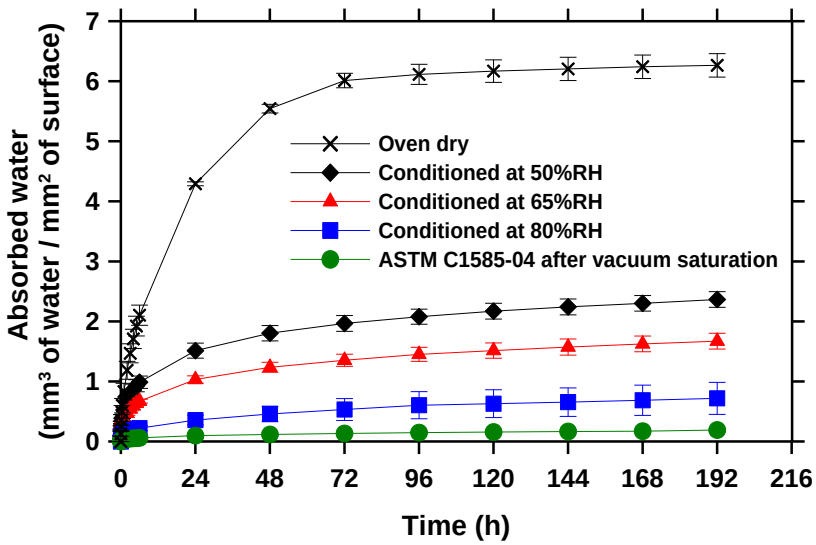

Fig. 2. Water absorption on samples subjected to different conditioning procedures.

4.3 Experimental Results from Wetting and Drying with Deicing Solutions

Figure 3 illustrates the results of the fluid absorption test as a function of time (for concrete at 50 % RH for a longer conditioning time than the samples in Figure 2). It can be seen that even though the concrete that is used for all the tests in Figure 3 has the same conditioning and exposure conditions, the volume of solution absorbed by each material is dependent on the deicing salt solution and the concentration of the deicing salt solution that was absorbed. The sample with the low concentration of NaCl showed a slight increase in the rate of absorption (as compared with water) as well as the amount of fluid absorbed. This is consistent with the data reported by

MacInnis and Nathawad [14]. The absorption of all the other fluids was reduced when compared with water. As a result, it can be concluded that in general as the salt concentration increased the rate of absorption reduced and and the total absorption was reduced. Further work is needed to examine lower concentrations for NaCl to ascertain why a slight increase is typically reported.

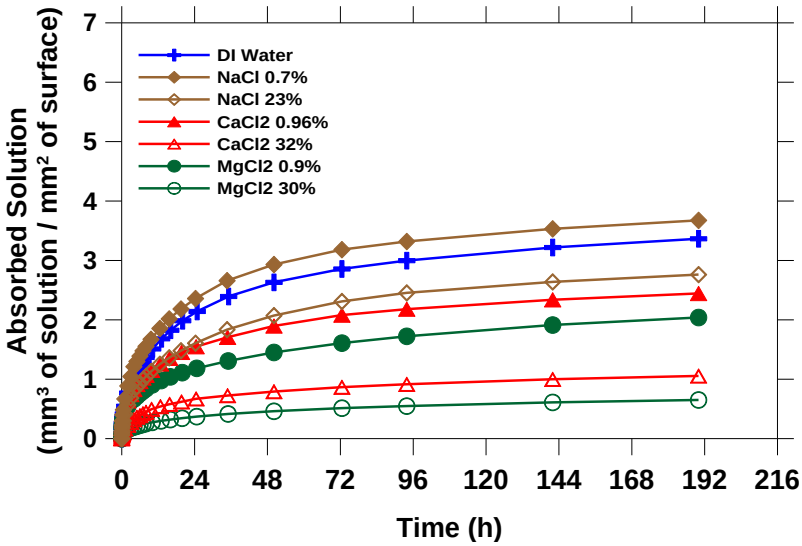

Fig. 3. Volume of deicing solutions absorbed by concrete as a function of time (typical standard deviation less than 0.1 mm^3/mm^2).

After the fluid absorption test was performed for 8 days the samples were dried at 50 ± 2 % RH, 23 ± 0.5 °C for seven days. The samples were kept in the same one-faced exposed condition for the drying test; however, the exposed surface that was facing down in the absorption testing was placed facing up to simulate drying from the top. During the drying test the mass of the samples was recorded at regular intervals.

Figure 4 shows the volume of water loss during the drying period. It is important to note that the drying test will result in only the water portion of the solution being evaporated from the system leaving the salt to become more concentrated in the solution before it eventually precipitates out. It can be noticed that as the concentration of deicing solution was increased the mass loss during drying decreased. This was particularly evident in the high concentration solutions, which showed nearly no mass loss or even a slight gain during drying.

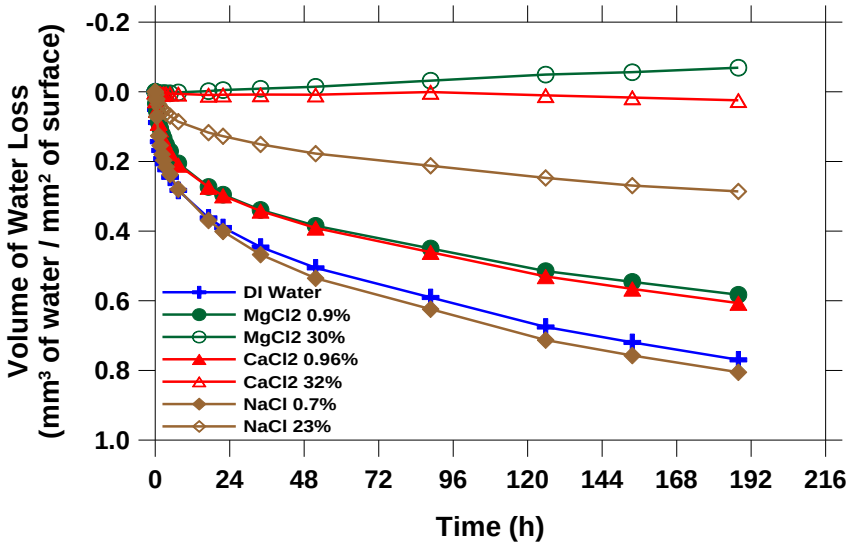

Fig. 4. Drying of concrete prewetted with different salt solutions as a function of time (typical standard deviation less than 0.03 mm^3 water/mm^2).

4.4 Experimental Results from Wetting Previously Exposed to Deicing Solutions

The same set of samples that were previously tested for absorption and drying were oven dried to be tested for second absorption test using de-ionized water. This was done to investigate the effects of previously absorbed salts on re-absorption of de-ionized water. However, in the case of the oven-dried samples, higher water absorption is expected. This can be due to the empty capillary pores and possibly to microcracking generated during oven drying [29-33].

To prepare the samples for the de-ionized water re-absorption test, the samples were placed in an oven at 105 ± 2 °C until they reached to equilibrium. The equilibrium condition was defined as a difference less than 0.5 % between two successive mass measurements (24 hours apart). It is important to note that this drying process will evaporate only the water portion of the solution pre-absorbed, leaving salt in the pores. Since these samples were oven dried, their absorption rates and absorbed water are not comparable with any previous tests.

Figure 5 shows the results for this second absorption test. It can be seen by comparing the results to the results in Figure 3 that the behavior of the samples was dependent on the deicing solutions and the concentrations of deicing solutions used in the first wetting test. These results are a clear indication that the history of the samples affects the results of fluid absorption. This suggests when sorption testing is preformed on field concretes, some understanding of the admixtures or salts that remain in the pore system is needed to fully interpret the results.

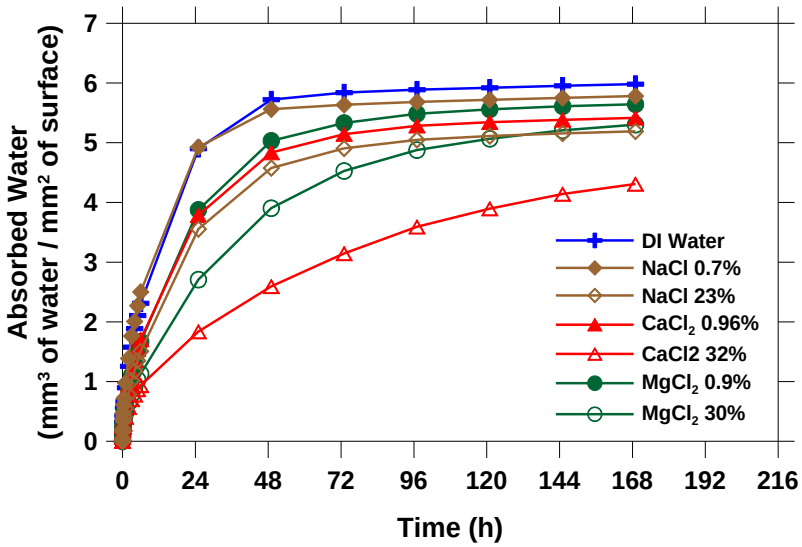

Fig 5. Volume of de-ionized water absorbed by concrete as a function of time in the second fluid absorption test (Fluid from the original test is shown in the caption).

4.5 Drying of Mortars Saturated with Different Deicing Salts

Moisture desorption is an established technique for evaluating the effect of moisture loss at a given humidity for a material. A TA Q5000 SA moisture sorption analyzer was used to carefully control temperature and humidity. Mortar samples were prepared (*w/c* = 0.42 and 55 % aggregate by volume) and cast in a cylindrical mold with a 34 mm diameter and 50 mm height. At an age of 28 days the specimens were demolded and 34 mm diameter 0.8 ± 0.05 mm thick slices were taken from the middle of the samples. The samples were dried under controlled conditions (at 23 ± 0.1 °C and 50 ± 1 % RH) in a CO_2 free chamber until they reach mass

equilibrium. Then, samples were submerged for a minimum of 5 days in aqueous solutions with 23 % NaCl, 32 % $CaCl_2$, and 30 % $MgCl_2$ by mass.

For the samples submerged in NaCl, $CaCl_2$, and $MgCl_2$ solutions a 50 mg to 70 mg piece of sample was placed in a tared quartz pan after a minimum of 5 days of submersion. The pan containing the sample was then suspended from the balance (± 0.001 mg accuracy) and placed in the relative humidity chamber to equilibrate at 23.0 ± 0.1 °C and 97.5 ± 0.1 % RH for up to 96 h or until the sample had achieved a stable mass (less than an 0.001 % mass change/15 minutes). Then, the relative humidity was reduced to reach 95 %. After the sample mass equilibrated, the relative humidity in the chamber was changed in 10 % RH steps to 55 % RH, allowing the sample to attempt to equilibrate (12 h or 0.01% change in mass over 15 minutes) at each new humidity. After equilibrating at 55 % RH the samples were dried to 0 % RH. For the sample submerged in de-ionized water the procedure was similar, but the relative humidity was reduced in 5 % steps from 97.5 % to 2.5 %, and then reduced to 0 % RH.

Figure 6 shows the plot of mass change as a function of time for the mortar saturated in de-ionized water. The sample soaked in water can be seen to lose mass with the decrease of RH. For this system, when the environment is below 100 % RH, water will move from the pores to outside of the sample and classical drying behavior is observed. The maximum mass of the sample is 8.5 % higher than the mass of the oven dry sample.

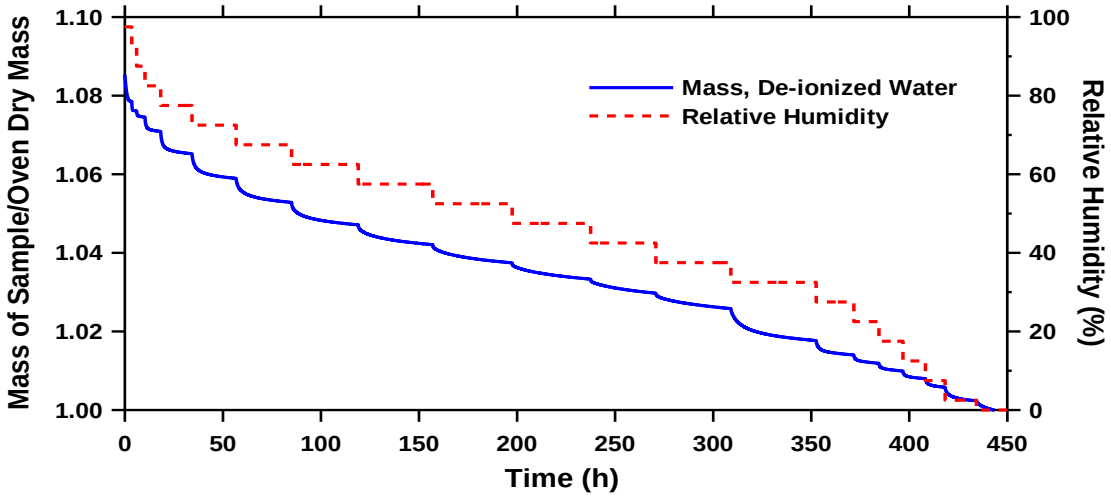

Fig. 6. Mass change at decreasing RH for samples containing de-ionized water

Figure 7 shows a plot of mass change for the mortar samples submerged in aqueous solutions of 23 % NaCl, 32 % $CaCl_2$, and 30 % $MgCl_2$. It can be observed that initially upon placement in the testing chamber at 97.5 % relative humidity the mass of the sample increases for the first 96 h until the relative humidity of the chamber is changed. The samples absorb water during this time of preconditioning, with values much higher than the 8.5 % increase in mass of the sample with de-ionized water as compared with the oven dry sample.

The sample loses weight as the relative humidity is decreased however it should be noted that the sample mass does not decrease to below the initial mass obtained from soaking the sample in the deicing solution until relative humidity was decreased below 85 %, 55 % and 55 % for NaCl, $CaCl_2$ and $MgCl_2$ respectively. This will be compared with the equilibrium relative humidity of the salt solution later in the paper.

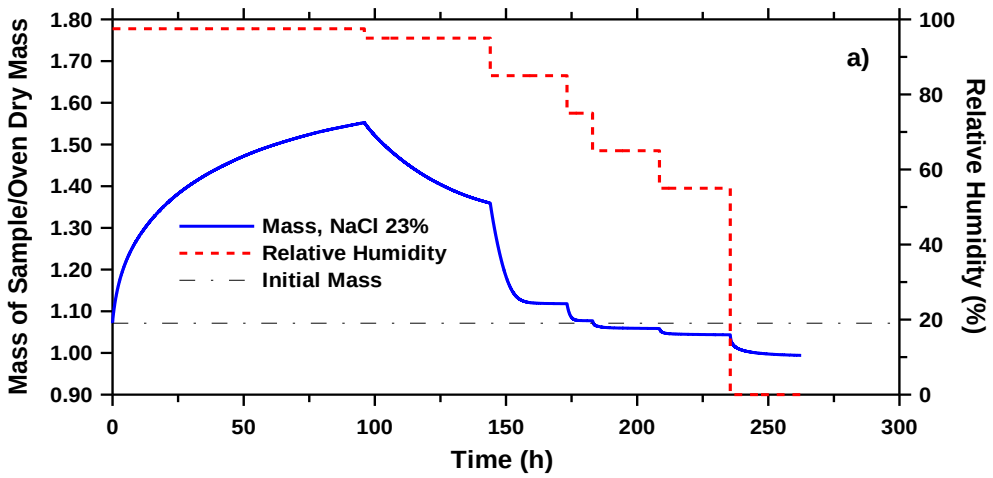
a)
Mass, NaCl 23%
Relative Humidity
Initial Mass
Mass of Sample/Oven Dry Mass
Relative Humidity (%)
Time (h)

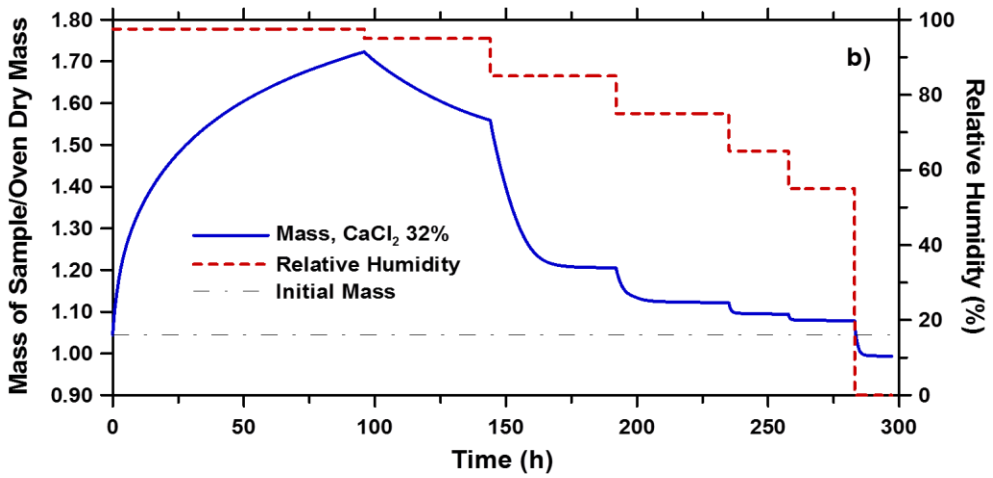
b)
Mass, CaCl2 32%
Relative Humidity
Initial Mass
Mass of Sample/Oven Dry Mass
Relative Humidity (%)
Time (h)

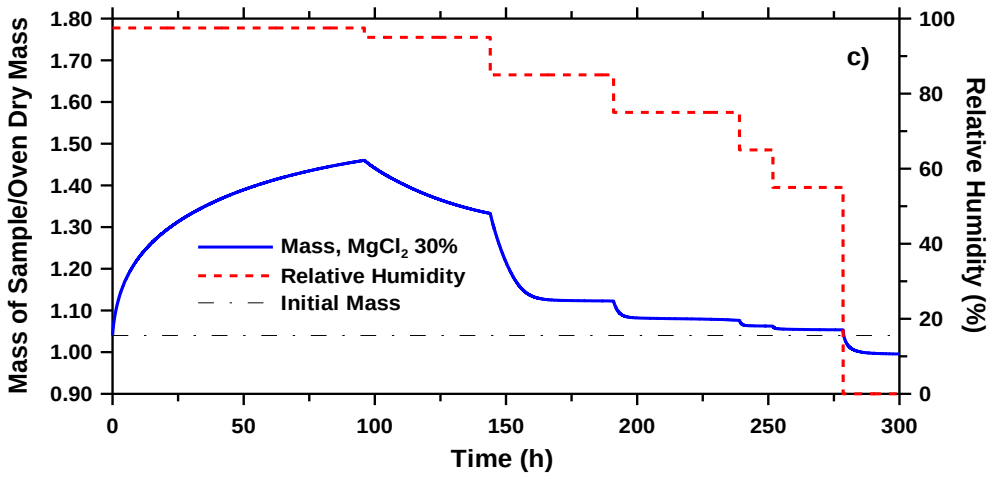
c)
Mass, MgCl2 30%
Relative Humidity
Initial Mass
Mass of Sample/Oven Dry Mass
Relative Humidity (%)
Time (h)

Fig. 7. Mass change for samples submerged in aqueous solutions containing deicing salts: (a) NaCl 23% (b) $CaCl_2$ 32 % and (c) $MgCl_2$ 30%.

5. Discussion of Results

5.1 Aqueous Solution Absorption Behavior as a Function of Surface Tension and Viscosity

Equation 3 showed that the rate of absorption was related to the square root of surface tension and viscosity. Figure 8 plots the square root of the ratio of surface tension and viscosity versus mass concentration of salt. Pure salt solutions are shown as lines while industrial deicing solutions are presented as solid points, and the open points represent the measured sorption response of concrete (i.e., salt sorptivity/water sorptivity) from Figure 3. Figure 8 confirms that as the solution concentration increases, the rate of fluid absorption (i.e., sorptivity) decreases. Further, while the properties of pure solutions may not exactly represent the response of industrially available deicing solutions they do provide a comparable trend. Reasonable agreement is seen between the measured sorption and square root of the ratio of surface tension and viscosity the measured properties. Additional work is currently being performed to extend these results to a wide range of temperatures.

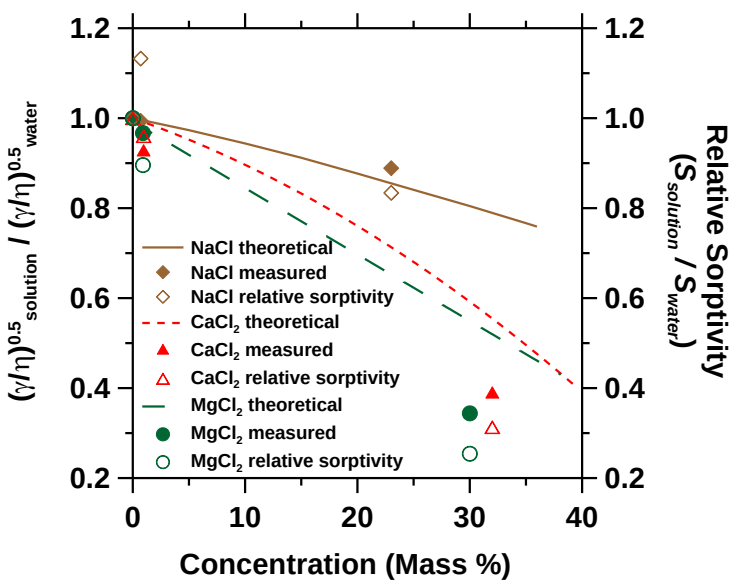

Fig 8. Relative sorptivity for deicing solutions.

5.2 Drying Time Versus Wetting Time

Comparing Figures 3 and 4 indicates that wetting happens much faster than drying. When de-ionized water was used as the absorbed fluid, the amount of fluid that was evaporated from the sample after eight days was 0.8 mm^3/mm^2. In contrast, it took just two hours for samples to absorb the same amount of fluid. These differences are even larger when salt solutions were used as the absorbed fluid. When $MgCl_2$ solution was used as the absorbed fluid, the amount of fluid that was evaporated from the sample after eight days was 0.07 mm^3/mm^2, but it took just ten minutes for the samples to absorb the same amount of fluid.

This is important as it suggests that field concrete may be more susceptible to increasing its level of saturation over time rather than drying out. Further, it shows that laboratory tests that use equal times for drying and wetting increase the saturation level of the concrete over time. Researchers [34] observed an increase in sample mass during wetting and drying cycling with deicers which was attributed to microcracking; however an increase in mass would be consistent with the wetting and behavior observed in this paper.

5.3 Reduced Drying with Salt Solutions – The Role of Solution Equilibrium Humidity

The relative humidity of different salt solutions presented in Figure 1 (b) help to understand the results from the drying tests. The equilibrium relative humidity for the 23% NaCl, 32% $CaCl_2$ and 30% $MgCl_2$ solutions are 80 %, 40 % and 50 % respectively. When the samples are placed in an environment with a relative humidity that is greater than or equivalent to the approximate equilibrium relative humidity over the aqueous solution in the pores water will not be lost to then environment. (Figure 4) and the sample can actually gain mass (Figure 4 and 7), most likely due to the water absorption on the surface of the sample. This can be seen by the thinner (dashed lines in Figure 7), which show the initial mass of the sample after it has been submerged in a

aqueous solution for over 5 days. At relative humidity higher than the equilibrium of the aqueous salt solution the samples will increase in mass. At relative humidities where the environment is less than the equilibrium humidity over the salt solution, the samples will be expected to decrease in mass. The drying behavior of systems containing concentrated aqueous solutions of deicing salts is complex and requires additional research.

5.4 Effect of Solution on Rewetting

When samples of concrete that were previously exposed to deicing solutions were rewet with water they had an absorption and rate of absorption that depended on the history of the specimens (Figure 5). The absorption of water can be 30 % to 50 % less in specimens that were exposed to deicing solutions at some point in their lives. This is an important, yet subtle, factor to understand. This is important since absorption tests of field concrete may be mistakenly interpreted by relating the reduction in sorption to pore filling or delayed sorption. Both of these observations (lower sorptivity and delayed sorption) are consistent with data here for samples that did not have reduced porosity or differences in sample damage.

6. Summary and Conclusions

This paper has reported experimental results of fluid absorption measurements and drying of concrete in the presence of deicing solutions. The following observations can be made. First, the absorption of fluid in concrete depends on the drying environment used to condition the samples. Samples stored at a lower RH absorbed a greater volume of fluid. Second, it was observed that the deicing solutions reduce the rate of fluid absorption. This reduction can be related to the square root of the ratio of surface tension and viscosity [10]. Third, the time scale between drying and wetting is different and concrete is more likely to become preferentially increasingly wet over time. Fourth, the drying of concrete containing aqueous solutions with deicers differs from that of water. The equilibrium relative humidity of the aqueous solution plays an important role on limiting drying. Finally, the presence of deicing salts in field samples

impacts the absorption when field samples are tested in the lab using water. This suggests that care must be taken in analyzing field concrete exposed to deicing salt solutions.

7. Acknowledgments

The experiments reported in this paper were conducted in the Pankow Materials Laboratories at Purdue University. This work was supported in part by the Joint Transportation Research Program administered by the Indiana Department of Transportation and Purdue University (SPR 3093 and 3200). The contents of this paper reflect the views of the authors, who are responsible for the facts and the accuracy of the data presented herein, and do not necessarily reflect the official views or policies of the Indiana Department of Transportation, nor do the contents constitute a standard, specification, or regulation.

8. References

1. Weiss J, Nantung T. INDOT Proposal on the Permeability of Concrete Pavement Performance Relative to Permeability, 2006.
2. Shi X, Fay L, Peterson MM, Yang Z. Freeze-Thaw damage and chemical change of a Portland cement concrete in the presence of diluted deicers. Mater Struct, 2010; 43(7): 933-946.
3. Hong K, Hooton RD. Effect of cyclic chloride exposure on penetration of concrete cover. Cement Concrete Res 1999, 29(9): 1379-1386.
4. Pour-Ghaz M, Rajabipour F, Couch J, Weiss J. Numerical and experimental assessment of unsaturated fluid transport in saw-cut (notched) concrete elements. SP-266 American Concrete Institute: Modeling as a solution to concrete problems, 2009.
5. Coates K, Mohtar S, Tao B, Weiss J. Can soy methyl esters reduce fluid transport and improve the durability of concrete? Transport Res Rec, 2009; 2113:.22-30.
6. ASTM International, ASTM C1585. Standard test method for measurement of rate of absorption of water by hydraulic cement concretes; 2004.

7. British Standard Institution, BS 1881. Methods of testing concrete part 5: Methods of testing hardened concrete for other than strength; 1990.
8. ASTM International, ASTM D6489. Standard test method for determining the water absorption of hardened concreted treated with a water repellent coating; 2006.
9. Hall C, Marchand J, Gerard G, Sosoro M. Chapter 2: Transport of fluids in homogenous isotropic cementitous composites. In: Reinhardt HW, editor. Penetration and permeability of concrete, RILEM report 16, 1997; pp. 5-79.
10. Hall C, Hoff WD. Water-transport in brick, stone and concrete. London: Spon Press, 2002.
11. Weiss WJ. Prediction of early-age shrinkage cracking in concrete. Ph.D. thesis. Evanston, IL Northwestern University, 1999.
12. Bentz DP, Peltz MA, Snyder KA, Davis JM. VERDiCT: Viscosity enhancers reducing diffusion in concrete technology. Concrete International, 2009; 31(1): 31-36.
13. Sant G, Eberhardt A, Bentz DP, Weiss J. Influence of shrinkage-reducing admixtures on moisture absorption in cementitious materials at early ages. J Mater Civil Eng, 2010; 22(3): 277-286.
14. MacInnis C, Nathawad YR. The effects of a deicing agent on the absorption and permeability of various concretes. In: Litvan GG, Sereda PJ, editors. Proceedings of the first international conference on durabaility of building materials and components, ASTM Special Technical Publication STP-691, 1980. pp 485-496.
15. Sutter L, Peterson K, Julio-Betancourt G, Hooton D, Van Dam T, Smith K. The deleterious chemical effects of concentrated deicing solutions on Portland cement concrete. South Dakota Department of Transportation, Final Report, 2008.
16. Janusz A. Investigation of Deicing Chemicals and Their Interactions with Concrete Materials. Master Thesis. West Lafayette, IN Purdue University, 2010.
17. Martys, NS. (1995). Survey of concrete transport properties and their measurments. NISTIR 5592, U.S. Departament of Commerce
18. Martys N, Ferraris CF. Capillary transport in mortar and concrete. Cement Concrete Res 1997; 27(5): 747-760
19. Kelham M. A Water absorption test for concrete. Mag Concrete Res, 1988; 40(143): 106-110.

20. Scherer G, Wheeler GS. Silicate consolidants for stone. Key Engineering Materials, 2009; 391: 1-25.
21. Conde M. Aqueous solutions of lithium and calcium chlorides: Property formulations for use in air conditioning equipment design. International Journal of Material Sciences, 2004; 43(4): 367-382.
22. Phang S, Stokes RH. Density, Viscosity, Conductance and transference numbers of concentrated aqueous magnesium chloride at 25C. J Solution Chem, 1980; 9(7): 497-505.
23. Afzai M, Saleem M, Mahmood MT. Temperature and concentration dependence of viscosity of aqueous electrolytes from 20 to 50C. Chlorides of Na+, K+, MG2+, Ca2+, Ba2+, SR2+ Co2+, Ni2+, Cu2+, and Cr3+. Journal of Chemical Engineering Data, 1989; 34(3): 339-346.
24. ASTM International, ASTM D971. Standard test method for interfacial of oil against water by the ring method; 2004.
25. Greenspan L. Humidity fixed points of binary saturated aqueous solutions. Journal of Research of the National Bureau of Standards – A, Physics and Chemistry, 1977; 81A(1): 89-96.
26. ASTM International, ASTM C231. Standard test method for air content of freshly mixed concrete by the pressure method; 2009.
27. Castro J, Kompare P, Poursaee A, Nantung T, Weiss J. JTRP Report SPR-3093, Portland cement concrete pavement performance relative to permeability. Indiana Department of Transportation, 2010.
28. Peterson KW, Swartz RA, Sutter LL, Van Dam TJ. Hardened concrete air void analysis with a flatbed scanner. Transport Res Rec 2001; 1775: 36-43.
29. Hwang C, Young J. Drying shrinkage of portland cement pastes. microcracking during drying. Cement Concrete Res 1984; 14(4): 585-594.
30. Chatterji S. (1976). Drying shrinkage of cement paste and concrete: a reappraisal of the measurement technique and its significance. Cement Concrete Res 1976; 6(1): 145-148.
31. Bisschop J, Van Mier J. How to study drying shrinkage microcracking in cement-based materials using optical and scanning electron microscopy? Cement Concrete Res 2002; 32(2): 279-287.
32. Samaha H, Hover K. Influence of microcracking on the mass transport properties of concrete. ACI Mater J 1992; 89(4): 416-424.

33. Yang Z, Weiss J, Olek J. Water transport on concrete damaged by tensile loading and freeze-thaw cycling. J Mater Civil Eng 2006; 18(3): 424-434.
34. Wang K, Nelsen D, Nixon W. Damaging effects of deicing chemicals on concrete materials. Cement and Concrete Composite, 2006; 28(2): 173-188.

International RILEM Conference on Use of Superabsorbent Polymers and Other New Additives in Concrete
15-18 August 2010, Technical University of Denmark, Lyngby, Denmark

MOISTURE PROFILES AND DIFFUSION COEFFICIENTS IN MORTARS CONTAINING SHRINKAGE REDUCING ADMIXTURES

Mohammad Pour-Ghaz[(1)], Robert Spragg [(1)] and Jason Weiss [(1)]

(1) Purdue University, School of Civil Engineering, West Lafayette, Indiana, USA

Abstract
Shrinkage reducing admixtures (SRAs) have been used over the last three decades to reduce the volume change (i.e., shrinkage) that occurs in cement paste, mortar, and concrete during drying. The goal of reducing shrinkage is to reduce the risk of shrinkage cracking in concrete elements. SRAs alter the properties of the pore solution, such as surface tension and viscosity, which result in a reduction in the magnitude of drying shrinkage, especially at humidities below 80-85%. In addition to altering the magnitude of shrinkage, SRAs appear to alter the rate of drying and diffusivity coefficient. This paper examines the role of SRAs in two ways. First, desorption spectra are measured to obtain the moisture diffusivity of plain mortar and mortar containing SRA. Second, the paper measures relative humidity in slabs to obtain moisture profiles. The relative humidity profile predicted from the non-linear diffusion coefficient is compared with the measured humidity profile.

1. Background

Shrinkage Reducing Admixtures (SRAs) were introduced to the concrete industry in the 1980's [1, 2]. Recent reviews have summarized three decades of research on SRA on concrete properties [3-6]. SRA's are generally observed to reduce shrinkage which can substantially reduce the propensity for restrained shrinkage cracking.

The majority of shrinkage measurements on concrete containing SRA are performed on concrete samples with a relatively large cross section, like those that one may use in standard shrinkage tests like ASTM C-157 [7]. While this type of test can provide information on the benefits of SRA, it has two primary limitations. First, it generally only describes the shrinkage of the concrete at one relative humidity (50% for example for ASTM C-157 [7]). Second, it measures the average length change of the prism and does not explicitly account for moisture gradients.

To overcome the limitation of measuring shrinkage at one relative humidity, a series of tests were performed measuring small paste and mortar samples with and without SRA at different relative humidities [8]. This response can be used to describe the shrinkage that may be expected over a wide range of relative humidities [9-11]. This does however indicate, not surprisingly, that shrinkage is not linearly related to relative humidity [8]. The shrinkage of the paste can be extended to mortar or concrete using the Pickett [12] or Hobbs [13] approaches.

Previous work has been performed to measure relative humidity profiles in concrete. This includes the work of Monfore [14] and Grasley et al. [15] who used resistance based gages to measure humidity in vapor filled cavities in concrete, the work of Molina [16] who measured relative humidity using chilled mirror technology, and work of Schieβl et al. [17] using electrical resistance measurements of concrete to assess the moisture distribution.

Relative humidity measurements in slabs can be complicated by the size of the probe that is used to measure the humidity. Measurements in small cavities with limited vapor volume can make it difficult to use techniques that require a substantial air flow rate like chilled mirrors. Previous measures of electrical resistance of concrete require two assumptions. First, that there are no hysteretic effects [18, 19] and second, that the resistance is measured at the depth of the electrodes. It can be noted that the first assumption is required since electrical measurements measure water content and not relative humidity directly and hysteretic effects due to drying and wetting can complicate the interpretation [19]. The second assumption is more nebulous as the shape of the electrical field that develops between the two electrodes is not symmetric at the plane of the electrodes since more charge will pass through the side containing more liquid [19]. As such it may be beneficial to measure the moisture diffusion coefficient directly rather than measuring relative humidity profiles and back calculating the diffusion coefficient.

One advantage of using desorption measurements to obtain a non-linear diffusion coefficient is the fact that the testing can be performed over a much shorter duration than drying of thick concrete slabs. For example, the non-linear diffusion coefficient measured in this paper took approximately 5 days to measure after casting and curing which is substantially shorter than allowing a concrete slab to dry and back-fitting the diffusion coefficient (which can take many many months). Second, this approach is not subjected so some of the issues that arise in attempting to ascertain the correct depth of the relative humidity measurement or the influence of a relatively large size cavity on the measured value.

2. Research Objective

This paper describes research that is attempting to measure a non-linear moisture diffusion coefficient in a mortar. Mortar was preferred to cement paste to minimize the potential impact of different pore size distributions that may occur between pastes and mortars. In addition the mortar was preferred to minimize potential issues that may occur with inconsistent mixing action that can be encountered in paste samples. This paper has three main objectives:

- First, the paper describes tests on mortar that is dried in a controlled fashion to evaluate the non-linear diffusion coefficient following the approach used by Anderberg and Wadso [20] and Garbalinska [21],
- Second, the paper provides data that illustrates the influence of shrinkage reducing admixture on the non-linear diffusion coefficient, and
- Third, the paper will provide a comparison of the relative humidity profile predicted using the non-linear diffusion coefficient with a measured relative humidity profile in a slab.

3. Relative Humidity Gradient and Cracking Potential

Previous work [9, 10, 22-24] has suggested that the humidity gradient in a slab can be used to predict the free shrinkage, stress development, slab cracking, and curling in a thick concrete element. The background for this type of approach can be found in [10, 25]. Figure 1 schematically illustrates the approach can be taken to utilize the relative humidity profile to compute the stress distribution and gradient. Strong dependence of diffusion coefficient on the shape and magnitude of the relative humidity profile can result in higher stress gradient and increase in cracking potential.

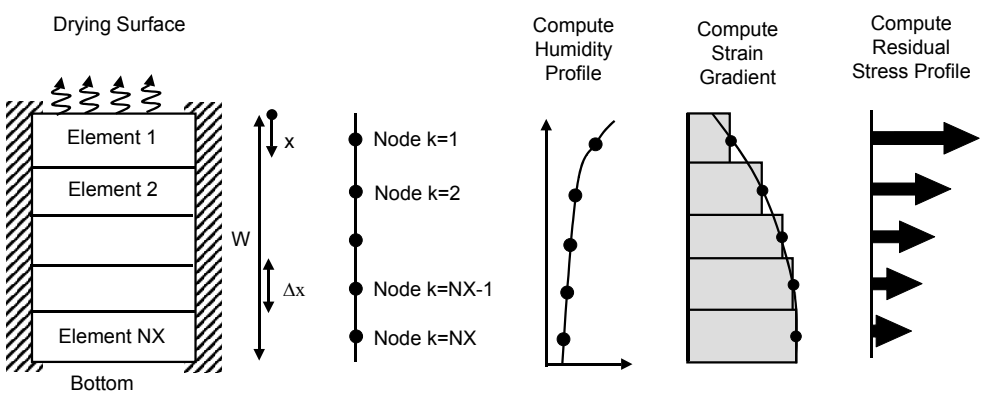

Figure 1: Schematically illustrates the approach can be taken to utilize the relative humidity and moisture content (W) profile to compute the stress distribution [10].

4. Materials and Methods

Three mortar mixtures were prepared for this study. The plain mortar had a water to cement ratio (w/c) of 0.50 and consisted of 55% aggregate by volume. The mortars containing shrinkage reducing admixture (SRA) had 1% and 5% of the mix water replaced with a SRA (denoted as 1% SRA and 5% SRA respectively). ASTM C150 [7] Type I ordinary portland cement (OPC) was used with a Blaine fineness of 370 m^2/kg and an estimated Bogue phase composition of 56 % C_3S, 16 % C_2S, 12 % C_3A, 7 % C_4AF and a Na_2O equivalent of 0.68 % by mass. The normal weight aggregate (NWA) was natural river sand with a fineness modulus of 2.71, an apparent specific gravity of 2.58, and an absorption of 1.8 % by mass.

The SRA was commercially available Tetragaurd AS20. All of the NWA was oven-dried and air-cooled for 24 hr before mixing. The mixing procedure used for the mortar was in accordance with ASTM C192-06 [7]. The samples were all tested in a sealed condition unless otherwise noted.

The experiments that were performed consist primarily of two specimen geometries. The first sample geometry was used for the diffusivity tests. This sample consisted of a 0.8 mm thick by 6 mm diameter mortar disk that was taken from a larger cylinder that was sealed from the time of casting before being exposed to progressive drying at an age of 7 days for determination of the moisture diffusivity. The second sample geometry consisted of slab specimens (177.8 mm x 254.0 mm x 508.0 mm) with relative humidity sensors embedded at four depths (12.7, 25.4, 38.1 and 92 mm) measured from the drying surface. The slabs were exposed to drying at 50 ± 1% at an age of 7 days. The slab geometry is shown in Figure 2.

Figure 2: Slab geometry with one-sided drying

5. Measurements of a Non-Linear Diffusion Coefficient

The samples used for determining the diffusion coefficient were cut from a small cylinder of mortar using a high precision wet saw. The test started approximately 5 minutes after cutting the sample. The samples were kept in water. At the start of the test the sample was removed from the water and was placed in a clean towel for a few seconds to remove the surface water. The sample was then placed in the desorption analyzer. The diffusivity test was performed in an automated absorption/desorption analyzer [26, 27] at 23°C in which samples were subjected to isothermal desorption at different relative humidities. The first step in the isothermal desorption was isothermal conditioning at 97.5 % relative humidity. The samples were allowed to equilibrate to 97.5%. After isothermal conditioning at 97.5% the relative humidity was decreased in 5% relative humidity increments. Samples at each step of the desorption were considered to be at equilibrium when the mass change was smaller than 0.001 mg for 15 minutes [26].

For a slab geometry with double-sided drying (where the contribution of mass transfer from the edges of the sample is negligible compared to mass transfer from the surface of the slab [20, 21, 28]) the mass change due to drying (M_t), at any time (t), can be related to the moisture diffusivity, (D), using Equation 1 [20, 21, 28]

$$\frac{M_t}{M_\infty} = \frac{4}{\pi}\left(\frac{Dt}{L^2}\right)^{1/2} \quad (1)$$

where M_∞ is the mass change at equilibrium and L is the thickness of the sample.

The diffusivity over each relative humidity step can be obtained from the linear portion of a plot of $(M_t / M_\infty)^2$ against $(16t/\pi^2 L^2)$. Generally the mortar samples tested exhibited the linear portion of their curve between 20 and 80% of the equilibrium mass. For materials for which the diffusivity is a function of relative humidity, Equation 1 can be used provided that the diffusivity can be assumed constant during each isothermal desorption step. In the present work since the samples were subjected to 5% change of relative humidity, the diffusivity can be assumed constant during each step of desorption. Better results can be obtained by decreasing the size of the steps, however the duration of the testing would increase but a sensitivity analysis would need to be determined.

Figure 3 illustrates the calculated diffusivity of the 0.8 mm thick specimens (exposed to 2 sided drying) of plain mortar, and mortar samples with 1 and 5% SRA. Note that the diffusivity at each step is expressed as diffusivity at average relative humidity of that step (e.g., the diffusivity of the samples that is equilibrated at 97.5% relative humidity and exposed to 92.5% relative humidity is reported as diffusivity at 95%). The samples with SRA demonstrate a lower diffusivity than the plain system at higher relative humidity. This lower relative humidity in the SRA system corresponds with a reduced rate of drying (at high relative humidity). This would suggest that plain mortar has a more non-linear moisture diffusivity while samples with SRA are more linear with respect to the diffusivity over a large range of moisture contents. This can have substantial implications on the moisture profile, shrinkage profile, reduction in curling, drying rate, and microcracking at the surface of the slab [29].

6. Relative Humidity Measurements in Slabs

The internal relative humidity and temperature of the slab was measured at four depths (12.7, 25.4, 38.1 and 92 mm) in a series of 250 mm hollow shafts (parallel to the surface) that contain I-button sensors [30] that measure temperature and relative humidity. The depth of the hollow shaft reported is measured from the exposed surface of the slab to the center of the shaft. Slabs were exposed to drying from the top surface.

The I-button data loggers measure the relative humidity with $\pm$1.0% and temperature $\pm$0.1^{o}C accuracy respectively. The advantage of this type of relative humidity sensor is the fact that it measures the relative humidity of the air inside the hollow shaft directly which is in equilibrium with surrounding materials. To ensure accuracy of the measurements all the sensors were compared to two salt solutions with 87 and 78% relative humidities. The sensors were within $\pm$1.0% of the expected relative humidity. In addition to calibration, data were corrected for saturation drift [30].

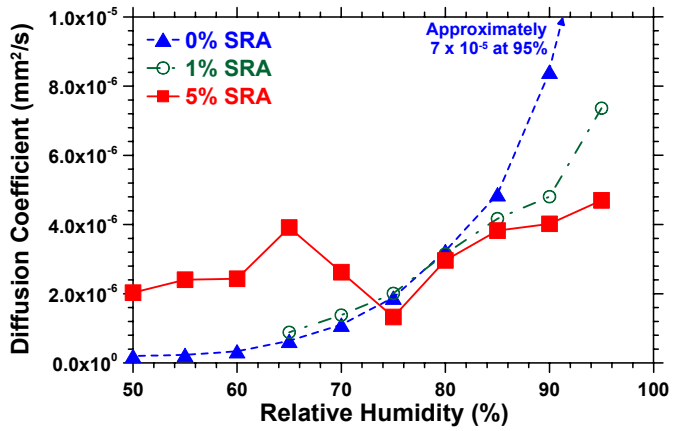

Figure 3: Moisture diffusivity of mortar samples with different loadings of shrinkage reducing admixture (SRA)

At the time of casting the slabs, cylindrical samples (with 2.54 cm diameter and 5.1 cm height) were cast from the same materials used to make the slabs and was kept sealed. These samples were used to measure the internal relative humidity at 7, 28 and 63 days (two samples at each age). The measurements were performed by crushing the samples and placing them in an air-tight container against a temperature and relative humidity sensor [26]. These measurements were performed to account for the self-desiccation effect which is needed in Equation 2.

Figure 4 illustrates the relative humidity of the slabs that have been exposed to drying at an age of 7 days (results are based on the average independent measurement in two slabs). It can be noticed that the relative humidity appears to remain higher in the samples containing SRA. The depth of the sensors is the distance to the center of the hollow shaft (in which sensor in placed in) from the surface of the slab. It is expected that the measured relative humidity with sensor may be more representative of the top of the hollow shaft.

7. Comparing Slab Measurements with Predictions Using the Diffusion Coefficient

Equation 2 describes the relative humidity as a function of time and position [31-35]

$$\frac{\partial H}{\partial t} = div\left(D_H \; grad \; H\right) - \frac{\partial H_s}{\partial t} \qquad (2)$$

where H is the relative humidity, D_H is the moisture diffusivity as a function of relative humidity and H_s is the variation of relative humidity due to self-desiccation.

Equation 2 assumes that the contribution of thermal gradients and aging are negligible [33]. The second term on the right-hand-side of Equation 2 is the contribution of self-desiccation [33]. The self-desiccation term in the present work is measured independently from crushed samples as described above. The boundary conditions at the sealed (bottom) surface of the

slab and top (exposed to drying) surface of the slab can be expressed by $\partial H / \partial x = 0$ and $H = 0.50$ respectively. The initial condition of the slab at drying (i.e., humidity at 7 days) is obtained by measuring the internal relative humidity of the crushed samples.

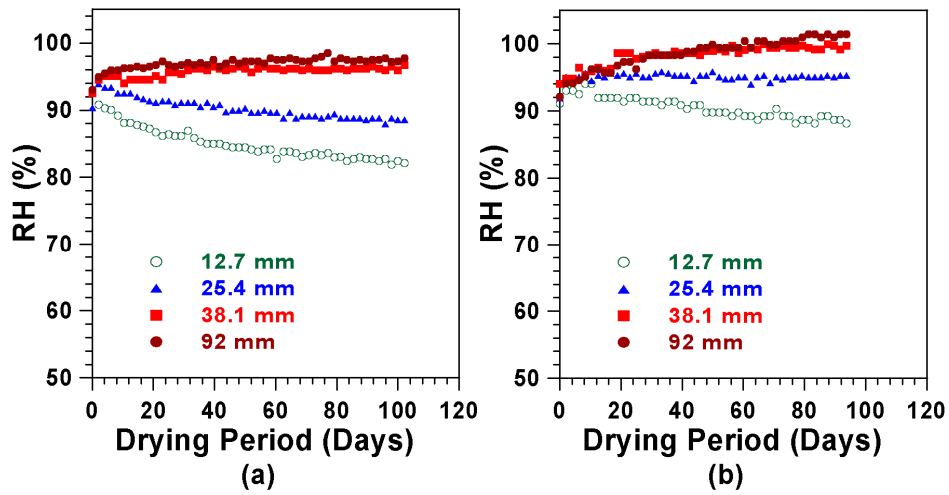

Figure 4: Change of internal relative humidity of slabs at different depth measured from exposed surface of the slab, (a) plain mortar, (b) mortar containing 5% shrinkage reducing admixture (SRA)

A non-linear finite difference scheme [33, 36, 37] was used. To effectively capture the non-linearity caused by the diffusivity, Crank-Nicolson (central difference) scheme was used. Crank-Nicolson scheme is stable [33, 36, 37] and effective in capturing non-linearities caused by strong dependence of diffusivity on relative humidity. In using this scheme any oscillations around the exact solution can be avoided by decreasing the time increments. In each time step the first solution was obtained by time lagging the diffusivity one time step and then improving the solution by subsequent iterations. In subsequent iterations, a weighted average diffusivity of the last two iterations was used. This method of averaging is known as modified Picard iterations [38] and requires less number of iterations in each time step.

Figure 5 illustrates the comparison of the experimentally obtained relative humidity at different locations and the numerically obtained profiles using the non-linear diffusivity coefficients.

8. Implications of Differences in Relative Humidity Profiles

Results of the non-linear diffusion coefficient can be used to describe moisture distribution at early ages and its potential impact on microcracking, curling and through cracking. The SRA's, especially at 5% show a reduced rate of drying. This is confirmed with less mass loss. This work may also provide insight on microcracking and damage localization that ultimately leads to through cracking in restrained elements. Acoustic emission has shown that the inclusion of SRA substantially reduces the acoustic activity due to microcracking in the specimens that contain 5% SRA as compared with the plain mixture.

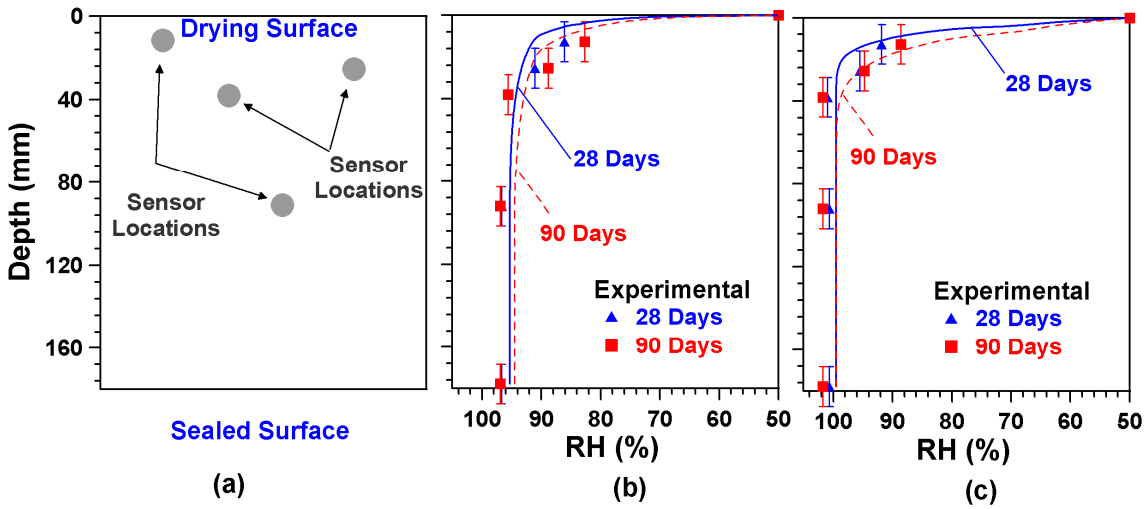

Figure 5: Comparison of the experimentally measured relative humidity and numerically obtained relative humidity profile, (a) illustration of location of the sensors and boundary conditions of the slab, (b) plain mortar, (c) mortar with 5% shrinkage reducing admixture (SRA)

9. Conclusions

This paper examined the role of SRAs on the relative humidity profile that develops in a drying mortar. The paper begins by describing the measurement of desorption spectra to obtain the moisture diffusivity of plain mortar and mortar containing SRA. The paper uses these non-linear diffusion coefficients to predict the moisture profiles that would be expected to occur in drying slabs. The results indicate that SRA dries more slowly at high relative humidities (liquid diffusion) however this trend may be reduced for lower relative humidities when the vapor diffusion prevails. The relative humidity profiles computed using the non-linear diffusion coefficient were directly compared with independently measured relative humidity in slabs. A reasonable comparison was observed given the issues associated with errors in relative humidity depth location and the shortcomings of using a non-aging coefficient. The implications of this approach could be more rapid indications of relative humidity profiles in concrete as well as explanations of shrinkage, stress and cracking distributions throughout the sample cross section.

10. Acknowledgements

The authors gratefully acknowledge the support of BASF, the Construction Chemical Company. This work was conducted in the Charles Pankow Concrete Materials Laboratory at Purdue University. As such, the authors gratefully acknowledge the support which has made this laboratory and its operation possible.

8. References

[1] Sato, T., Goto, T., and Sakai, K., 'Mechanism for Reducing Drying Shrinkage of Hardened Cement by Organic Additives,' *CAJ Review,* (1983) 52-54.

[2] Tomita, R., Simoyama, Y., and Inoue, K., 'Properties of hardened concrete impregnated with cement shrinkage reducing agent,' *CAJ Review,* (1986) 314-317.

[3] ACI.Committee.231, 'Report on Early-Age Cracking: Causes, Measurement, and Mitigation,' American Concrete Institute ACI 231R-10, 2010.

[4] Nmai, C., Tomita, R., Hondo, F., and Buffenbarger, J., 'Shrinkage reducing admixtures,' *Concr. Int.,* **20** (4)(1998) 31-37.

[5] Shah, S.P., Weiss, W.J., and Yang, W., 'Shrinkage cracking – can it be prevented?,' *Concr. Int.,* **20** (4)(1998) 51-55.

[6] Weiss, J. and Berke, N.S., 'Shrinkage reducing admixtures,' in *Early age cracking in cementitious systems, RILEM state-of-the-art report—Report 25*, A. Bentur, Ed., ed Bagneux, France: RILEM, 2002.

[7] *Annual Book of ASTM Standards*. West Conshohocken, PA: American Society for Testing and Materials, ASTM International, 2009.

[8] Weiss, J., Lura, P., Rajabipour, F., and Sant, G., 'Performance of shrinkage-reducing admixtures at different humidities and at early ages,' *ACI Mater. J.,* **105** (5) Sep-Oct (2008) 478-486.

[9] Bazant, Z.P., Ed., *Fourth RILEM International symposium on Creep and Shrinkage of Concrete: Mathematical Modeling* Northwestern University, 1986.

[10] Weiss, W.J., 'Prediction of early-age shrinkage cracking in concrete,' Ph.D., Civil Engineering, Northwestern University, Evanston, IL, 1999.

[11] Moon, J.H., 'Shrinkage, Residual Stress, and Cracking in Heterogeneous Materials,' Ph.D., Civil Engineering, Purdue University, West Lafayette, IN, 2006.

[12] Pickett, G., 'Shrinkage stresses in concrete,' *Mater. Struct.,* **42** (8)(1946) 165-204.

[13] Hobbs, D.W., 'Influence of aggregate restraint on the shrinkage of conrete,' *ACI Journal,* **71-30** (1974) 445-450.

[14] Monfore, G.E., 'A small probe-type gauge for measuring relative humidity,' *Journal of the PCA Research and Development Laboratories,* **5** (2)(1962).

[15] Grasley, Z.C., Lange, D.A., and D'Ambrosia, M.D., 'Internal relative humidity and drying stress gradients in concrete,' *Mater. Struct.,* **39** (9) Nov (2006) 901-909.

[16] Molina, L., 'Measurement of high humidity in cementitious material at an early age,' Swedish Cement and Concrete Research Institute, Stockholm, Sweden1990.

[17] Schielβl, A., Weiss, W.J., Shane, J.D., Berke, N.S., Mason, T.O., and Shah, S.P., 'Assessing the moisture profile of drying concrete using impedance spectroscopy,' *Concr. Sci. Eng.,* **2** (2000) 106-116.

[18] Elkey, W. and Sellevold, E.J., 'Electrical resistivity of concrete,' Norwegian Road Research Laboratory1995.

[19] Rajabipour, F., 'Insitu electrical sensing and materials health monitoring in conrete structures,' Ph.D., Civil Engineering, Purdue University, West Lafayette, IN, 2006.

[20] Anderberg, A. and Wadso, L., 'Method for simultaneous determination of sorption isotherms and diffusivity of cement-based materials,' *Cem. Concr. Res.,* **38** (1) Jan (2008) 89-94.

[21] Garbalinska, H., 'Application of root t-type, logarithmic and half-time methods in desorptive measurements of diffusivity in narrow humidity ranges,' *Cem. Concr. Res.,* **36** (7) Jul (2006) 1294-1303.

[22] Moon, J.H. and Weiss, J., 'Estimating residual stress in the restrained ring test under circumferential drying,' *Cem. Concr. Compos.,* **28** (5) May (2006) 486-496.

[23] Weiss, W.J., Yang, W., and Shah, S.P., 'Shrinkage cracking of restrained concrete slabs,' *J. Eng. Mech.,* **124** (7) Jul (1998) 765-774.

[24] Weiss, W.J., Yang, W., and Shah, S.P., 'Influence of specimen size/geometry on shrinkage cracking of rings,' *J. Eng. Mech.,* **126** (1) Jan (2000) 93-101.

[25] Bazant, Z.P., 'Material Models for Structural Creep Analysis,' in *Mathematical Modeling of Creep and Shrinkage of Concrete*, Z. P. Bazant, Ed., ed New York: John Wiley and Son Ltd, 1988.

[26] Castro, J., Lura, P., Rajabipour, F., and Weiss, J., 'Internal curing: discussion on the role of pore solution on relative humidity measurements and desorption of lightweight aggregate (LWA) ' in *Advances in the Material Science of Concrete*. vol. SP-270, J. H. Ideker and A. Radlinska, Eds., ed Chicago, IL: American Concrete Institute, 2010.

[27] Instruments, T., 'Dynamic Vapor Sorption Analysis: Q5000 SA,' http://www.tainstruments.com2010.

[28] Crank, J., *The Mathematics of Diffusion*, 2nd ed. New York: Oxford University Press, 1980.

[29] Neithalath, N., Pease, B.J., Moon, J.H., Rajabipour, F., Weiss, J., and Attiogbe, E., 'Considering moisture gradients and time-dependent crack growth in restrained concrete elements subjected to drying,' in *High Performance Cement Based Concrete Composites*, J. J. Bernacki*, et al.*, Eds., ed Chennnai, India: American Ceramics Society, 2005, pp. 279-290.

[30] Maxim, 'Data Logger, Temperature/Humidity Loggers, and Sensors,' Sunnyvale, CA, 2010.

[31] Bazant, Z.P. and Kim, J.K., 'Consequences of Diffusion-Theory for Shrinkage of Concrete,' *Mater. Struct.,* **24** (143) Sep (1991) 323-326.

[32] Bazant, Z.P., Kim, J.K., and Panula, L., 'Improved Prediction Model for Time-Dependent Deformations of Concrete .1. Shrinkage,' *Mater. Struct.,* **24** (143) Sep (1991) 327-345.

[33] Bazant, Z.P. and Najjar, L.J., 'Nonlinear water diffusion in nonsaturated concrete,' *Mater. Struct.,* **5** (25)(1972) 3-20.

[34] Xi, Y.P., Bazant, Z.P., and Jennings, H.M., 'Moisture Diffusion in Cementitious Materials - Adsorption-Isotherms,' *Adv. Cem. Based Mater,* **1** (6) Nov (1994) 248-257.

[35] Xi, Y.P., Bazant, Z.P., Molina, L., and Jennings, H.M., 'Moisture Diffusion in Cementitious Materials - Moisture Capacity and Diffusivity,' *Adv. Cem. Based Mater,* **1** (6) Nov (1994) 258-266.

[36] Crank, J. and Nicolson, P., 'A Practical Method for Numerical Evaluation of Solutions of Partial Differential Equations of the Heat-Conduction Type,' *Proceedings of the Cambridge Philosophical Society,* **43** (1)(1947) 50-67.

[37] Ozisik, M.N., *Finite Difference in Heat Transfer*. London: CRC Press, 1994.

[38] Pour-Ghaz, M., 'A novel approach for practical modelling of steel corrosion in concrete,' M.A.Sc, Civil Engineering, Carleton University, Ottawa, Canada, 2007.

Water Absorption and Electrical Conductivity for Internally Cured Mortars with a *W/C* between 0.30 and 0.45

Javier Castro[1], Robert Spragg[2], and Jason Weiss[3]

Abstract: Internal curing has emerged over the last decade as an approach to counteract the negative effects associated with self-desiccation in low water to cement ratio (*w/c*) mixtures. Specifically much of the early research on internal curing focused on the reduction of autogenous shrinkage. Recent work has however demonstrated that internal curing can also be beneficial in reducing drying shrinkage cracking, reducing the propensity for thermal cracking, reducing fluid absorption and reducing ion diffusion in concrete. However several aspects of internal curing still require closer examination. One of these aspects is the application of internal curing for mixtures with a wider range of water to cement ratios. This paper describes results from experiments that investigated the potential use of internal curing in mortar systems with *w/c* of 0.30, 0.36, 0.42 and 0.45 in terms of water absorption and electrical conductivity. Test results show that internal curing reduces the water absorption in all the systems. Similarly, results obtained on electrical conductivity at late ages (1 year) also show a benefit. It was also found that care needs to be taken to analyze electrical conductivity results at early ages due to the increased amount of fluid because the inclusion of the prewetted lightweight aggregate.

CE Database subject heading: Absorption, Concrete, Curing

Author keywords: Internal curing, Lightweight aggregate, Water absorption, Electrical conductivity

[1] PhD Candidate, School of Civil Engineering, Purdue University, 550 Stadium Mall Drive, West Lafayette, Indiana, USA, Phone: (765) 494 – 7999, jcastro@purdue.edu. Corresponding author

[2] Undergraduate Research Assistant, School of Civil Engineering, Purdue University, 550 Stadium Mall Drive, West Lafayette, Indiana, USA, Phone: (765) 494 – 7999, rspragg@purdue.edu

[3] Professor, Director of Pankow Materials Laboratory, Purdue University, 550 Stadium Mall Drive, Indiana, USA, Phone: (765) 496 – 2215, Fax: (765) 496 – 1364, wjweiss@ecn.purdue.edu.

BACKGROUND ON INTERNAL CURING

Internal curing has emerged over the last decade as a method to improve the performance of low water to cement ratio (*w/c*) mixtures [Rilem 2007, ACI SP-256 2008, ACI Committee 231 2010, INDOT 2010, Bentz and Weiss 2011]. Specifically, internal curing refers to the use of prewetted lightweight aggregate or other water filled inclusions such as Super Absorbent Polymers (SAP) or cellular fibers that can provide curing water throughout the cross section of the concrete. This differs from conventional water curing where water is provided after placement and where the water is applied only at the surface of the concrete. Internal curing was originally promoted to reduce autogenous shrinkage and autogenous shrinkage cracking [Bentz and Snyder 1999, Jensen and Hansen 2001a, Jensen and Hansen 2001b, Jensen 2005, Cusson and Hoogeveen 2008, Lopez et al. 2009]. However its potential benefits include reducing drying shrinkage cracking [Henkensiefken et al. 2008, Henkensiefken et al. 2009a], reducing the likelihood of thermal cracking [Schlitter et al. 2010, Byard et al. 2010] and reducing the likelihood of plastic shrinkage cracking [Henkensiefken et al. 2010]. Internal curing can also improve the freeze-thaw resistance [INDOT 2010], increase the resistance to fluid absorption [Bentz and Snyder 1999, Henkensiefken et al. 2009b, Peled et al. 2010] and reduce ion diffusion [Bentz 2009] in concrete. Internal curing has great potential for the concrete industry to create a longer lasting, more sustainable product. Several aspects of internal curing still require closer examination. One of these aspects is the use of internal curing for mixtures containing over a wider range of water to cement ratios (w/c) (e.g., mixtures with a *w/c* between 0.30 and 0.45).

To fully understand how internal curing works we need to first realize that the hydration of cement paste causes a volume reduction which is known as chemical shrinkage [Le Chatelier 1900, Powers 1935, L'Hermite 1960]. While chemical shrinkage starts at the time the water comes in contact with the cement, it has a different impact on the system before and after the paste sets. Before set, the chemical shrinkage causes bulk shrinkage of the cement paste that is equal to the total external volume change. After set, however, the cement paste becomes stiff enough to resist a portion of the volume change caused by chemical shrinkage [Barcelo et al. 1999, Sant et al. 2006]. Contact between the cement particles does not permit this volume reduction to occur. As a result, vapor-filled pockets form inside the cement paste in the largest

pores [Jensen and Hansen 2001b, Couch et al. 2006, Lura et al. 2009]. This is known as self-desiccation.

Chemical shrinkage occurs in all cementitious materials, irrespective of the *w/c* [Geiker 1983]. In low *w/c* mixtures, these vapor filled cavities can result in substantial relative humidity reduction and shrinkage since the vapor filled cavities form in relatively small pores with a small radius of curvature [Bentz and Jensen 2006, Radlinska et al. 2008, Lura et al. 2009]. In higher *w/c* mixtures those vapor filled spaces also develop however they occur in much larger pores with less impact on volume change. As a result, it has been thought that many of the higher *w/c* system would not see as much benefit from internal curing.

Lightweight aggregate are used as a water reservoir that can provide water to replenish the empty pore volume that is created by the chemical shrinkage occurring during hydration. Since water is removed from large pores to small pores, the ideal lightweight aggregate would have pore sizes larger that the pore size that develops the cement paste due to chemical shrinkage [Bentz 2009, Castro et al. 2010a]. This is the case for many commercially available expanded clays, slates or shales [Castro et al. 2010a].

APPROACHES FOR MIXTURE PROPORTIONING INTERNALLY CURED CONCRETE

The design of concrete for internal curing requires that a sufficient amount of water is placed in the concrete to aid in hydration and to overcome the effects of self-desiccation. Different approaches had been used during the recent years to determine and quantify the amount water needed for internal curing. Two of the most widely used approaches are discussed here.

Bentz and Snyder Approach

Bentz and Snyder [1999] developed an approach to determine the volume of prewetted LWA that should be use to “ensure adequate water for complete curing of concrete, which means that the cement reaches the maximum degree of hydration that is possible, given the space limitation

for forming hydration products in low *w/c* systems". It is based on the concept of filling the volume reduction of chemical shrinkage with water from the lightweight aggreagate. [Bentz et al. 2005]. This approach was first published by Bentz and Snyder [1999] as shown in Equation 1:

$$M_{LWA} = \frac{C_f \times CS \times \alpha_{\max}}{S \times \phi_{LWA}} \qquad \text{(Equation 1)}$$

where M_{LWA} (kg/m^3) is the mass of LWA (in a dry state) that needs to be water filled to provide water to fill in the voids created by chemical shrinkage, C_f (kg/m^3) is the cement content of the mixture, CS (ml of water per g of cement) is the chemical shrinkage of the cement, α_{max} (unitless) is the expected maximum degree of hydration: [(*w/c*)/0.36] for *w/c* below 0.36 and 1 for *w/c* higher than 0.36, Φ_{LWA} (kg of water/kg of dry LWA) is the absorption capacity of the LWA (taken here as the 24 h absorption value), and S (unitless) is the expected degree of saturation of the LWA, expressed as a function of the taken absorption value (Φ_{LWA}). Water absorption and S values from the most used LWA in America were previously reported by Castro et al. [2010a].

In theory, this approach may over estimate the amount of water required for internal curing, because it does consider the volume change that occurs before set [Henkensiefken 2009], however this approach is preferred due to its simplicity.

Jensen and Hansen approach

Jensen and Hansen [2001a] developed an approach to proportion internally cured mixtures with the intention of limiting the negative effects of self desiccation in cementitious systems by maximizing the volume of cement that can react. The equations were developed based on the Powers' model to calculate the minimum amount of water that needs to be stored (entrained) to enable the maximum degree of hydration. It has been published by Jensen and Hansen [2001a] and is shown in Equation 2:

$$(w/c)_e = \begin{cases} 0.18(w/c) & ;\ for\ \ w/c \leq 0.36 \\ 0.42-(w/c) & ;\ for\ \ 0.36 \leq w/c \leq 0.42 \\ 0 & ;\ for\ \ w/c \geq 0.42 \end{cases} \qquad \text{(Equation 2)}$$

where $(w/c)_e$ is the amount of additional water for internal curing, expressed as gram of water by gram of cement, and the (w/c) is the original water to cement ratio of the system.

EXTENSION OF INTERNAL CURING TO HIGH W/C SYSTEMS

Figure 1 (after Bentz et al. 2005) illustrates both approaches as a function of the *w/c*. It can be seen that below a w/c of 0.36 both approaches are identical. The Bentz approach adds water to fill all the chemical shrinkage volume which causes it to stay constant above *w/c* of 0.36 while the Jensen approach considers only adding the water needed for full hydration which results in the water recommended decreasing above a *w/c* of 0.36.

It should be noted that both approaches assume that all the mixing water will be accessible to react with the un-hydrated cement. Issues associated with the distance that the water needs to travel or a lack of adequate mixing are not considered. These two issues may decrease the amount of hydration that occurs and may increase the porosity of the system and its connectivity.

RESEARCH OBJECTIVES

The objective of this research is to examine the potential benefits of internal curing in mortar systems with *w*/c from 0.30 to 0.45. In particular this research will evaluate the benefits in terms of water absorption and electrical conductivity on systems with *w/c* of 0.30, 0.36, 0.42 and 0.45.

MATERIALS

An ASTM C150 Type I ordinary portland cement (OPC) was used in this study, with a Blaine fineness of 370 m^2/kg and an estimated Bogue composition of 56 % C_3S, 16 % C_2S, 12 % C_3A, 7 % C_4AF and a Na_2O equivalent of 0.68 % by mass.

The sand used was natural river sand with a fineness modulus of 2.71, an apparent specific gravity of 2.58, and water absorption of 1.0 % by mass. Portions of the normal weight sand were replaced with expanded shale with a fineness modulus of 3.10 and a specific gravity of 1.45 (LWA). The 24 hour absorption of the LWA was determined to be 17.5 % according to the paper towel method [NYDOT 2008, Castro et al. 2010].

Mixture proportioning

Twenty different mixtures were prepared. The mortars had a single volume fraction of fine aggregate (55% of the total volume) and different *w/c* (0.30, 0.36, 0.42, and 0.45). For each system LWA was used as a replacement of NWA at five different levels of normal weight sand (NWA): 0 %, 25 %, 50 %, 75 % and 100 % of the values calculated using Equation 1. It is important to note that replacement is on a total volume basis, the volume of aggregate (LWA and sand) remained constant at 55 % since only the sand was replaced with LWA. A list of the mixture proportions can be found in Table 1.

Mixing procedure

The mixing procedure used for the mortar was in accordance with ASTM C305 [ASTM 2006]. The LWA was oven dried, air cooled, and then submerged in water for 24 ± 1 h prior to mixing. The volume of water used to submerge the LWA included both mixing water and the water the LWA would absorb in 24 h. The excess water (water not absorbed in 24 h) was then decanted and used as the mixing water. The normal weight sand was oven dried and cooled for 24 h before mixing. For the plain mortar mixtures and the pastes, the water and cement were conditioned for 24 h at room temperature.

EXPERIMENTAL METHOD PROCEDURES

Water absorption

Six 100 mm × 200 mm cylinders were cast for water absorption testing for each mixture. After one day of curing, the samples were demolded and then sealed in a double layer of plastic bags for sealed curing. Bags were stored at 23 ± 1 °C until samples reached an age of 90 d. At that point the cylinders were removed from the bags and three 50 mm ± 2 mm thick samples were cut from the central portion of each cylinder using a wet saw.

After cutting, samples were conditioned by placing them in environmental chambers at 23 ± 0.5 °C and at two different relative humidities (65 ± 1 % and 80 ± 1 %). Samples were conditioned in the environmental chamber for a period of 9 months.

Once the samples were removed from the chambers the side surface (i.e. outer circumference) was sealed with aluminum tape and the top surface was covered with plastic to avoid evaporation from the sample during testing. After the samples were prepared, absorption testing was conducted in accordance with ASTM C1585 [ASTM 2004], with the exception of the conditioning method described above.

It should be noted, the effect of internal curing can be increased under sealed conditions employed in this study as compared with other curing conditions (unsealed curing or curing under lime water). In sealed curing, the internally cured specimens will have a greater amount of water available for hydration and will likely hydrate further. This will lead to a denser microstructure with lower transport coefficients. The authors considered that the sealed curing condition can represent appropriately the field conditions, and can also isolate the effect of internal curing on the specimens. However, the authors also consider that differences in the curing conditions for both internally and not internally cured specimens can affect the performance of the specimens.

Electrical impedance

Electrical conductivity of mortar samples was measured using cylindrical specimens (70 mm height and 35 mm diameter). Two 2.5 mm diameter rods spaced 20 mm were embedded longitudinally inside each mold (Figure 2).

A Solartron 1260™ Impedance Gain-Phase analyzer measured the impedance response of each specimen. The measurements were made over a frequency range from 1 MHz to 1 Hz, using a 100 mV AC signal. Measurements were performed at 3 d, 7 d, 90 d and 365 d.

The electrical conductivity was obtained from the measured bulk resistance according to Equation 3.

$$\sigma = \frac{k}{R} \qquad \text{(Equation 3)}$$

where σ is the conductivity (S/m), k is the geometry factor (1/m), and R is the bulk resistance (ohm). A geometry factor of k = 22.15/m was determined in this research for the used molds.

A modified parallel model is normally used to describe the electrical conductivity of the concrete [McCarter and Brousseau 1990, Rajabipour 2006]. Since the conductivity of liquid phase is several orders of magnitude higher that the conductivity of solid and vapor phases, concrete is normally considered as a composite material with a single conductive component and the modified parallel model can be simplified to Equation 4. It should be noted that this typically assumes only the fluid phase is conductive. For internally cured concrete mixtures however the water in the LWA may also be conductive and the implications of this will be discussed later in the paper.

$$\sigma = \sigma_o \phi_o \beta_o \qquad \text{(Equation 4)}$$

where:

σ_o = Conductivity of the pore solution, sigma notch (S/m)

ϕ_o = Volume fraction of pore solution (unitless)

β_o = Connectivity of pores structure (unitless)

EXPERIMENTAL RESULTS AND DISCUSSION

Water absorption

Figure 3 shows the cumulative absorbed water in the samples that were 1 year old (3 months of sealed curing and 9 months of conditioning) after 8 d of testing for samples conditioned at 65 % and 80 % relative humidity. Figure 4 show the initial sorptivity (i.e., related to the rate of water absorption) for samples conditioned at 65 % and 80 % relative humidity calculated as the slope of the absorption vs. the square root of time during the first six hours of test. Figure 5 show the secondary sorptivity for samples conditioned at 65 % and 80 % relative humidity calculated as the slope of the absorption vs. the square root of time from the second to the eight day of test.

From Figures 3 to 5 it can be noticed that the water absorption is very sensitive to both the relative humidity at which the specimens were pre-conditioned before testing [Castro et al. 2011] and the *w/c* of the systems. Samples conditioned at 65 % relative humidity show higher values than similar samples conditioned at 80 % relative humidity. Samples from the mixtures with a higher *w/c* show higher absorption values compared with samples with lower *w/c*, both conditioned at the same relative humidity.

These trends can be explained by the fact that water ingress in unsaturated concrete is dominated by capillary suction upon initial contact with water [Hall 1989]. Capillary absorption can be related to the volume of the pores as well as the size of empty capillary pores. Then, system with higher *w/c* will have a greater proportion of capillary pores. The relation between the equilibrated relative humidity and the radius of the smallest empty pore is given by the Kelvin-

Laplace equation. Using this equation it is possible to calculate that these capillary pores are filled with water vapor at relative humidities above 80 %.

As such, the relative humidity used to condition the sample prior to the sorption test and the *w/c* of the system can have a significant impact on the results. The higher the *w/c* of the system, the greater the total volume of capillary pores. The lower the relative humidity, the greater the total volume of pores that are empty and available to be filled with water during the sorption test. Further, the lower humidity will empty smaller pores, creating a higher suction force in the materials and resulting in a greater sorption rate and a larger overall total absorption.

From Figures 3 to 5 it can also be seen that the total volume of water and the rate of absorbed water decrease when a higher amount of LWA is used. This observation is independent of both the relative humidity used for conditioning and the *w/c* of the system. Even more, it can be observed that proportionally a greater benefit is obtained in those mixtures containing the highest *w/c*.

When water leaves the pores of the LWA it is available in the cement paste to enable additional hydration. This additional hydration results in a paste microstructure that is more dense which has a large impact on the cement paste matrix [Henkensiefken et al. 2009b]. Internal curing water can also increase the hydration of the areas surrounding the LWA [Henkensiefken et al. 2009b] producing a more dense ITZ [Zhang and Gjørv 1990, Elsharief et al. 2005]. Considering that the Interfacial Transition Zone (ITZ) of the normal weight aggregate (NWA) could be percolated across the 3D microstructure, the inclusion of the LWA could depercolate these ITZ pathways [Winslow et al. 1994, Bentz 2009, Peled et al. 2010]. If LWA, with the denser ITZ it creates, were added to the system, the NWA ITZ may not be as percolated, resulting in a lower absorption. As more LWA is used, the potential for percolation of the normal weight aggregate ITZ also decreases. If enough LWA is used, the ITZ of the NWA would depercolate [Bentz 2009]. For this reason, it could be expected that the absorption of mortars with LWA could be lower, even in system with a high *w/c*.

The benefits of internal curing are most dramatic for specimens in the sealed condition used in the study (as compared with curing under lime water). Under sealed conditions the internally cured specimens have a greater amount of water available for hydration than the plain samples. This increased hydration produces a more dense microstructure with lower transport coefficients (Bentz and Stutzman). The sealed curing condition is likely however a good representation for field concrete that uses a curing compound.

Electrical impedance

Figure 6 shows the electrical conductivity of sealed samples at the age of 3, 7, 90 and 365 days after casting. The systems with higher *w/c* have a higher conductivity due mainly to the higher volume of pore fluid as described by equation 4. The conductivity decreases with the time due to continued hydration which reduces the volume of conductive pore fluid by hydration which also makes the conduction path more tortuous.

The mixture with a *w/c* of 0.30 shows that internal curing results in a reduction of the measured conductivity which can be explained by the effect of the water provided for internal curing which helps to increase the hydration of the areas surrounding the LWA [Henkensiefken et al. 2009b]. However, in the systems with higher *w/c* an increase in the LWA content increases the electrical conductivity at early ages. This may be explained by the fact that these systems have water contained in the LWA particles that remains for a longer time in the LWA pores without reacting with the un-hydrated cement. As a result, the total amount of fluid in the system will be increased with additional LWA, thereby increasing the measured electrical conductivity of the samples.

As the samples hydrate (e.g. at 90 days), the system with *w/c* = 0.36 starts to show the benefits of internal curing, decreasing the conductivity. At this time, the systems with higher w/c still show higher conductivity with the use of LWA (again due to the additional water in the system). Finally at the age of 365 days, all the systems show the benefits of the use of internal curing. At this age a considerable reduction of the measured electrical conductivity can be observed.

The water for internal curing requires longer times to leave the LWA pores in the higher *w/c* systems due to the lack of a driving force (which is the under pressure build up due to self desiccation in the case of a low *w/c* system). However, at some point, the smaller pores of the cement paste will develop a meniscus which will make the water move from the LWA pores to the cement paste. Eventually, this water will react with the un-hydrated cement to increase the amount of hydration products reducing both the total porosity and the fluid filling the pores of the system. This will produce a reduction on the measured electrical conductivity.

A direct comparison of electrical conductivity of the system containing different *w/c* presents some difficulties, mainly because the complications associated with determining the volume fraction of pore solution at different ages. For this reason, after the electrical conductivity of the samples was measured in a sealed condition at the age of 365 d, samples were vacuum saturated for 24 hours using tap water. After saturation, electrical conductivity was measured again and results are shown in Figure 7.

The conductivities presented in Figure 7 are proportional to the total volume of accessible pores and their connectivity through the samples. These are parameters that can be used to describe the transport of fluid in concrete [Rajabipour and Weiss 1997]. Then, Figure 7 shows that using internal curing on systems with high *w/c* help to reduce the connectivity of the porosity, which helps to reduce the fluid transport in concrete.

Comparing Figures 6d) and 7 it can be observed that the electrical conductivity increases when samples were re-saturated. It can be explained by the fact that resaturation results in a higher volume of pore fluid as described by equation 4. However it is important to note that sample re-saturation does not seem to fill the LWA pores, because an increment of conductivity with the percentage of LWA is not observed.

Empirical relations for water absorption and electrical conductivity

Analyzing the data from Figures 3, 4 and 5 it is possible to obtain an empirical relationship for the cumulative absorption, the initial and secondary sorptivity which is presented in Equation 5.

From Figure 7 it is possible to obtain an empirical relationship for the saturated electrical conductivity, which is presented in Equation 6.

$$Absorption\ equations = C_1 \cdot (w/c)^{C_2} \cdot \exp\ (-C_3 \cdot IC) \qquad \text{(Equation 5)}$$

$$Conductivity = [C_4 \cdot (w/c) - C_5] \cdot \exp\ [(-C_6 \cdot (w/c) + C_7) \cdot IC] \qquad \text{(Equation 6)}$$

where "*w/c*" is the water to cement ratio (e.g. 0.36), "*IC*" is the internal curing percentage from Equation 1 (e.g. IC = 50 is 50% of the IC water predicted from equation 1), and C_1, C_2, C_3, C_4, C_5, C_6 and C_7 are the regression constants the values of which are included in Table 2.

Figure 8 illustrates the proportional reduction of water absorption, initial sorptivity and secondary sorptivity on the internally cured samples. Figure 9 illustrates the proportional reduction on electrical conductivity of 1-year old saturated internally cured samples.

From Figure 8 it can be seen that when LWA is added according to the Bentz and Snyder approach (equation 1), the internally cured system shows an average reduction of 55 % in the initial sorptivity and the 8-days cumulated absorption, and 70 % in the secondary sorptivity, independently of the relative humidity at which the samples were conditioned prior testing. From Figure 9 it can be seen that internal curing is more efficient to reduce the electrical conductivity in high *w/c* systems that in low *w/c* systems. A reduction of 40 % in conductivity is observed on the system with *w/c* of 0.30, but a reduction of 75 % is observed on the system with *w/c* of 0.45.

CONCLUSIONS

A series of twenty mortars were prepared to evaluate the effect of internal curing on the fluid transport properties of mortars over a range of *w/c*'s. The effect of internal curing was evaluated using water absorption and electrical conductivity measurements.

The total absorbed water was reduced when the level of internal curing was increased. This reduction in water absorption was known for the system with the low *w/c*, but the results show

that the benefits are extendible to systems with higher *w/c*. These benefits were also observed in reducing the rate of water absorption showing a lower initial and secondary sorptivity. An average maximum reduction of 55 % was observed in both the initial sorptivity and cumulated absorption and a maximum reduction of 70 % was observed in the secondary sorptivity.

Electrical conductivity tests, performed in sealed samples a year after casting, show a benefit in the use of internal curing in mortar systems containing low *w/c* as expected, but also in systems with higher *w/c*. The effect of internal curing is proportionally larger in samples prepared with the highest *w/c*. A reduction of 40 % is observed on the system with *w/c* of 0.30, this reduction was observed to increase to 75 % on the system with *w/c* of 0.45.

The benefits of internal curing are most dramatic for specimens in the sealed condition used in the study as compared with curing under lime water. Under sealed conditions the internally cured specimens have a greater amount of water available for hydration than the plain samples. This increased hydration produces a more dense microstructure with lower transport coefficients.

Precaution are needed for interpreting the electrical properties of IC concrete at an early age due to the higher amount of fluid present in system when prewetted LWA is added.

ACKNOWLEDGMENTS

This work was supported in part by the Expanded Shale, Clay and Slate Institute (ESCSI) and by the Joint Transportation Research Program administered by the Indiana Department of Transportation and Purdue University (Project SPR 3211) and the authors gratefully acknowledge that support. The contents of this paper reflect the views of the authors, who are responsible for the facts and the accuracy of the data presented herein, and do not necessarily reflect the official views or policies of the Indiana Department of Transportation, nor do the contents constitute a standard, specification, or regulation. The experiments reported in this paper were conducted in the Pankow Materials Laboratories at Purdue University. The authors acknowledge the support that has made this laboratory and its operation possible.

REFERENCES

ACI Committee 231 (2010). "Report on early-age cracking: causes, measurement and mitigation." American Concrete Institute - Committee 231, Farmington Hills, MI, p. 48.

ACI SP-256 (2008). "Internal curing of high performance concrete: laboratory and field experiences." American Concrete Institute, Farmington Hills, MI, p. 110.

ASTM Standard C1585 (2004). "Standard test method for measurement of rate of absorption of water by hydraulic-cement concretes." ASTM International, West Conshohocken, PA.

ASTM Standard C305 (2006). "Standard practice for mechanical mixing of hydraulic cement pastes and mortars of plastic consistency." ASTM International, West Conshohocken, PA.

ASTM Standard C128 (2007). "Standard test method for density, relative density (specific gravity), and absorption of fine aggregate." ASTM International, West Conshohocken, PA.

Barcelo, L., Boivin, S., Rigaud, S., Acker, P., Clauvaud, B. (1999). "Linear vs volumetric autogenous shrinkage measurements: material behavior or experimental artefact." In: Persson B, Fagerlund G, editors. Proceedings of the second international seminar on self-desiccation and its importance in concrete technology, Lund University, Sweden; p. 109–125.

Bentz, D.P. and Snyder, K.A. (1999). "Protected paste volume in concrete: Extension to internal curing using saturated lightweight fine aggregate." *Cem. Concr. Res*., 29(11), 1863-1867.

Bentz, D.P., Lura, P. and Roberts, J.W. (2005). "Mixture proportioning for internal curing." *Concr. Inter.*, 27(2), 35-40.

Bentz, D.P. and Jensen, O.M (2006). "Mitigation strategies for autogenous shrinkage cracking." *Cem. Concr. Compos*., 26(6), 677-685.

Bentz, D.P. (2009). "Influence of internal curing using lightweight aggregates on interfacial transition zone percolation and chloride ingress in mortars." *Cem. Concr. Compos.*, 31(5), 285-289.

Bentz, D.P. and Weiss, J. (2011). "Internal curing: A 2010 state of the art review." National NISTIR 7765. Institute of Standards and Technology, U.S. Department of Commerce. Gaithersburg, MD.

Byard, B.E, Schindler, A.K. and Barnes, R.W (2010). "Cracking tendency of lightweight concrete in bridge deck applications." Proceedings of the concrete bridge conference, Phoenix, Arizona.

Castro, J., Keiser, L. Golias, M., Weiss, J. (2010a). "Absorption and desorption properties of fine lightweight aggregate for application to internally cured concrete mixtures". Submitted to *Cem. Concr. Compos*.

Castro, J., Bentz, D., Weiss, J. (2010b). "Effect of sample conditioning on the water absorption of concrete." Submitted to *Cem. Concr. Compos*.

Couch, J., Lura, P., Jensen, O. and Weiss, J. (2006). "Use of acoustic emission to detect cavitation and solidification (time zero) in cement pastes." In: International RILEM conference on volume changes of hardening concrete: testing and mitigation. Jensen O, Lura P, Kovler K, editors; 2006. Denmark, pp. 393-400.

Cusson, D. and Hoogeveen, T. (2008). "Internal curing of high-performance concrete with pre-soaked lightweight aggregate sand for prevention of autogenous shrinkage cracking." *Cem. Concr. Res*., 38(6), 757-765.

Elsharief, A., Cohen, M. and Olek, J. (2005). "Influence of lightweight aggregate on the microstructure and durability of mortar." *Cem. Concr. Res*., 35(7), 1368-1376.

Geiker, M. (1983). "Studies of Portland cement hydration by measurements of chemical shrinkage and a systematic evaluation oh hydration curves by means of the dispersion model." PhD Dissertation, Technical University of Denmark.

Hall, C. (1989). "Water sorptivity of mortars and concretes: a review." Mag. Concr. Res., 41(146), 51-61.

Henkensiefken, R., Nantung, T. and Weiss, W. (2008). "Reducing restrained shrinkage cracking in concrete: examining the behavior of self-curing concrete made using different volumes of saturated lightweight aggregate." In: National concrete bridge conference, St. Louis, MO.

Henkensiefken, R., Bentz, D., Nantung, T., Weiss, J. (2009a). "Volume change and cracking in internally cured mixtures made with saturated lightweight aggregate under sealed and unsealed conditions." *Cem. Concr. Compos*., 31(7), 427-437.

Henkensiefken, R., Castro, J., Bentz, D., Nantung, T. and Weiss, J. (2009b). "Water absorption in internally cured mortar made with water-filled lightweight aggregate." *Cem. Concr. Res*., 39(10), 883-892.

Henkensiefken, R., Briatka, P., Nantung, T., Bentz, D. and Weiss, J. (2010). "Plastic shrinkage cracking in internally cured mixtures made with pre-wetted lightweight aggregate." Concr. Inter., 32(2), 49-54.

Jensen, O.M. and Hansen, P.F. (2001a). "Water-entrained cement-based materials: I. Principles and theoretical background. Cem Concr Res 2001a; 31(4): 647-654.

Jensen, O.M, and Hansen, P.F. (2001b). "Autogenous deformation and rh-change in perspective. *Cem. Concr. Res*., 31(12), 1859-1865.

Jensen, O.M. (2005). "Autogenous Phenomena in Cement-Based Materials." PhD Thesis. Aalborg University, 2005.

Le Chatelier, H., (1900). “Sur les changements de volume qui accompagent le durcissement des ciments.” In Bulletin Societe de l'encouragement pour l'industrie nationale. Paris, France.

L’Hermite, R.G. (1960). “Volume changes of concrete.” In 4th International symposium on the chemistry of cement. Washington DC.

Lopez, M., Kahn, L.F. and Kurtis, K.E. (2009). “Characterization of elastic and time-dependent deformations in high performance lightweight concrete by image analysis.” *Cem. Concr. Res*., 39(7), 610-619.

Lura, P., Couch, J., Jensen, O.M. and Weiss, J. (2009). “Early age acoustic emission measurement in hydrating cement paste: Evidence for cavitation during solidification due to self-desiccation.” *Cem. Concr. Res*., 39 (10): 861-867.

McCarter, W. and Brousseau, R. (1990). “The A.C. response of hardened cement paste.” *Cem. Concr. Res*., 20(6): 891-900.

NYDOT. (2008). “Test Method No.: NY 703-19 E: Moisture content of lightweight fine aggregate.” New York State Department of Transportation, Materials Bureau, Albany, NY.

Peled, A., Castro, J. and Weiss, J. (2010). “Atomic force microscopy examinations of mortar made by using water-filled lightweight aggregates.” *Transp. Res. Rec*., 2141: 92-101.

Powers, T. (1935). “Absorption of water by portland cement paste during the hardening process.” *Ind. Eng Chem*., 27(7), 790–4.

Radlinska, A., Rajabipour, F., Bucher, B., Henkensiefken, R., Sant, G., Weiss, J. (2008). “Shrinkage mitigation strategies in cementitious systems: a closer look at sealed and unsealed material behavior.” *Transp. Res. Rec*., 2070: 58–67.

Rajabipour, F. (2006), "In Situ Electrical Sensing and Material Health Monitoring in Concrete Structures", PhD Dissertation, Purdue University p. 173.

Rajabipour, F. and Weiss, J. (2007). "Electrical conductivity of drying cement paste." *Mater. Struct.* 2007(40),1143-1160.

RILEM Report 41 (2007). "Internal curing of concrete – state of the art." Kovler, K. And Jensen, O.M. editors. RILEM Publications S.A.R.L; 2007, p. 161.

Sant, G., Lura, P. and Weiss, J. (2006). "Measurement of volume change in cementitious materials at early ages: review of testing protocols and interpretation of results." *Transp. Res. Rec*., 1979, 21-29.

Schlitter, J., Henkensiefken, R., Castro, J., Raoufi, K., Weiss, J. and Nantung, T. (2010). "Development of internally cured concrete for increase service life." JTRP Report SPR-3211, p. 252.

Winslow, D.N., Cohen, M., Bentz, D., Snyder, K. and Garboczi, E. (1994). "Percolation and pore structure in mortars and concrete." *Cem. Concr. Res*., 24(1), 25-37.

Zhang, M.-H. and Gjørv, O.E. (1990). "Microstructure of the interfacial zone between lightweight aggregate and cement paste." *Cem. Concr. Res*., 20(4), 610-618.

Table headings

Table 1. Mixture Proportions for the Internally Cured Mixtures.

Table 2. Parameters for Equation 5 and 6

Table 1. Mixture Proportions for the Internally Cured Mixtures.

w/c	% LWA from Eq. 1	Cement (kg/m^3)	Mixing Water (kg/m^3)	NWA, SSD (kg/m^3)	LWA, Dry (kg/m^3)	IC Water (kg/m^3)	Aggregate Volume (%) NWA	LWA	Total
0.30	0%	727.0	218.1	1429.7	0.0	0.0	55.0	0.0	55.0
	25%	727.0	218.1	1330.2	55.4	9.7	51.2	3.8	55.0
	50%	727.0	218.1	1230.6	110.8	19.4	47.3	7.7	55.0
	75%	727.0	218.1	1131.1	166.2	29.1	43.5	11.5	55.0
	100%	727.0	218.1	1031.5	221.6	38.8	39.7	15.3	55.0
0.36	0%	662.6	238.6	1419.7	0.0	0.0	55.0	0.0	55.0
	25%	662.6	238.6	1320.9	60.6	10.6	50.8	4.2	55.0
	50%	662.6	238.6	1212.0	121.2	21.2	46.6	8.4	55.0
	75%	662.6	238.6	1103.1	181.8	31.8	42.4	12.6	55.0
	100%	662.6	238.6	994.2	242.4	42.4	38.2	16.8	55.0
0.42	0%	608.7	255.7	1429.7	0.0	0.0	55.0	0.0	55.0
	25%	608.7	255.7	1329.7	55.7	9.7	51.2	3.8	55.0
	50%	608.7	255.7	1229.7	111.4	19.4	47.3	7.7	55.0
	75%	608.7	255.7	1129.7	167.1	29.1	43.5	11.5	55.0
	100%	608.7	255.7	1029.7	222.8	38.8	39.6	15.4	55.0
0.45	0%	584.9	263.2	1429.7	0.0	0.0	55.0	0.0	55.0
	25%	584.9	263.2	1333.6	53.5	9.4	51.3	3.7	55.0
	50%	584.9	263.2	1237.5	107.0	18.8	47.6	7.4	55.0
	75%	584.9	263.2	1141.4	160.5	28.2	43.9	11.1	55.0
	100%	584.9	263.2	1045.3	214.0	37.6	40.2	14.8	55.0

Table 2. Parameters for Equation 5 and 6

Parameters	Water Absorption at 8 days		Initial Sorptivity		Secondary Sorptivity		1-year Electrical Conductivity
	65% RH	80% RH	65% RH	80% RH	65% RH	80% RH	Saturated
C_1	72.776	19.391	0.084	0.045	0.113	0.019	-
C_2	3.93	3.35	3.30	4.06	4.57	3.20	-
C_3	0.0093	0.0084	0.0080	0.0083	0.0127	0.0106	-
C_4	-	-	-	-	-	-	184.59
C_5	-	-	-	-	-	-	46.915
C_6	-	-	-	-	-	-	0.0558
C_7	-	-	-	-	-	-	0.0108

Figure captions

Fig 1 Water for internal curing needed to maintain saturated condition in cement paste (after Bentz et al. 2005)

Fig 2 Picture of the mold used for continuous electrical conductivity measurements

Fig 3 Cumulative amount of water absorbed after 8 days of testing for samples conditioned at: a) 65% RH and b) 80% RH. Error bars represent the standard deviation on the average of 3 samples. Continues lines represent empirical equations described at the end of the paper

Fig 4: Initial sorptivity as a function of the w/c and the amount of LWA for samples conditioned at: a) 65% RH and b) 80% RH. Error bars represent the standard deviation on the average of 3 samples. Continues lines represent empirical equations described at the end of the paper

Fig 5 Secondary sorptivity as a function of the w/c and the amount of LWA for samples conditioned at: a) 65% RH and b) 80% RH. Error bars represent the standard deviation on the average of 3 samples. Continues lines represent empirical equations described at the end of the paper

Fig 6 Electrical conductivity of sealed samples as a function of the amount of LWA at the age of: a) 3 days, b) 7 days, c) 90 days, and d) 365 days. Error bars represent the standard deviation on the average of 3 samples.

Fig 7 Electrical conductivity of vacuum saturated samples at the age of 365 days. Error bars represent the standard deviation on the average of 3 samples. Continues lines represent empirical relations described in a further section.

Fig 8 Proportional reduction on the absorption, initial sorptivity and secondary sorptivity of internally cured samples

Fig 9 Proportional reduction on the electrical conductivity of 1-year old saturated internally cured samples

Figures:

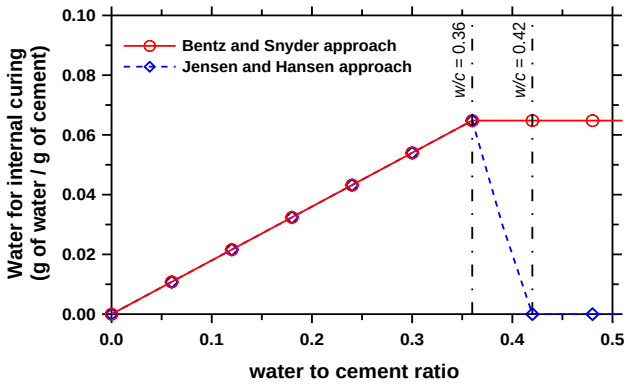

Fig 1 Water for internal curing needed to maintain saturated condition in cement paste (after Bentz et al. 2005)

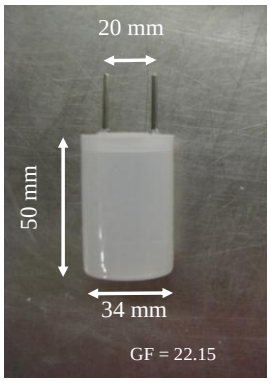

Fig 2 Picture of the mold used for continuous electrical conductivity measurements

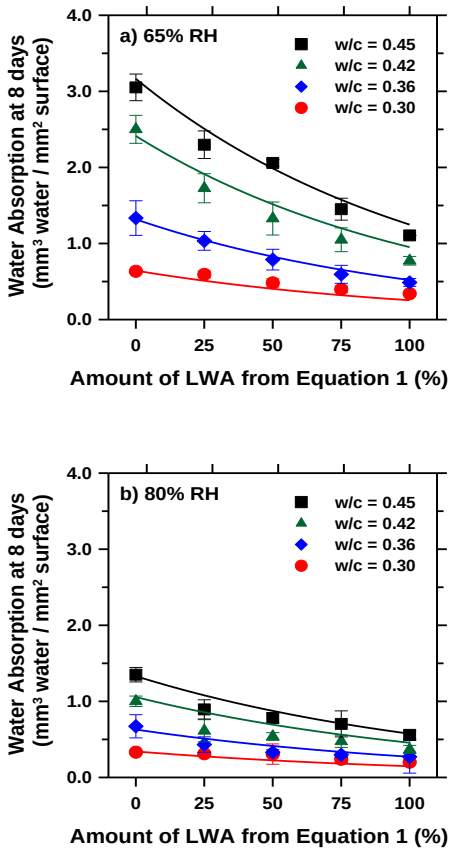

Fig 3 Cumulative amount of water absorbed after 8 days of testing for samples conditioned at: a) 65% RH and b) 80% RH. Error bars represent the standard deviation on the average of 3 samples. Continues lines represent empirical equations described at the end of the paper

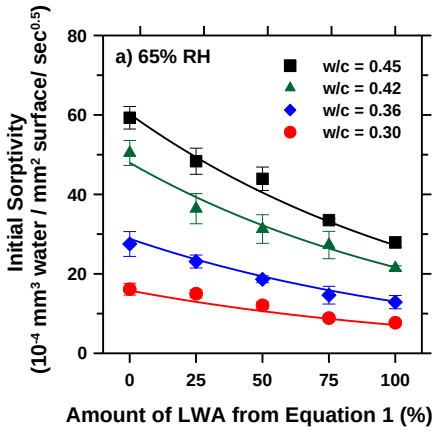

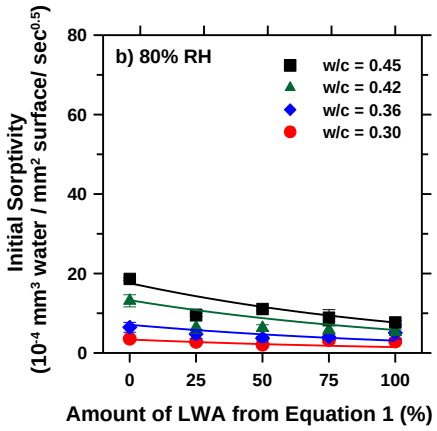

Fig 4: Initial sorptivity as a function of the w/c and the amount of LWA for samples conditioned at: a) 65% RH and b) 80% RH. Error bars represent the standard deviation on the average of 3 samples. Continues lines represent empirical equations described at the end of the paper

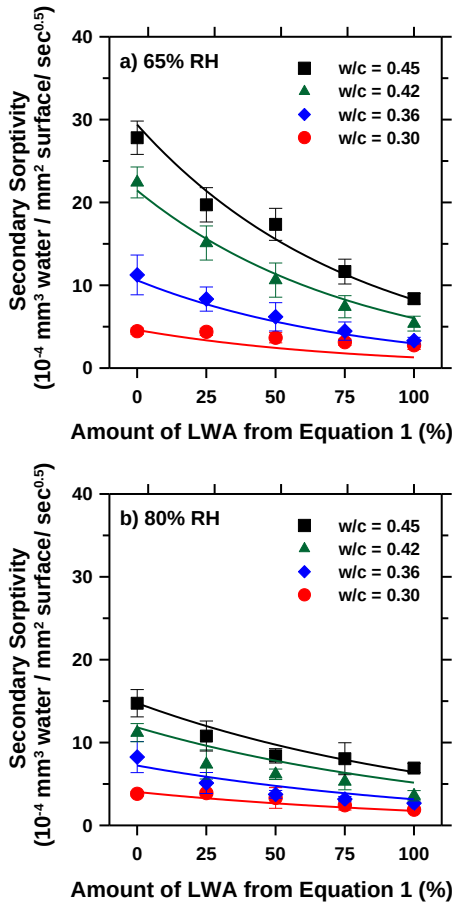

Fig 5 Secondary sorptivity as a function of the w/c and the amount of LWA for samples conditioned at: a) 65% RH and b) 80% RH. Error bars represent the standard deviation on the average of 3 samples. Continues lines represent empirical equations described at the end of the paper

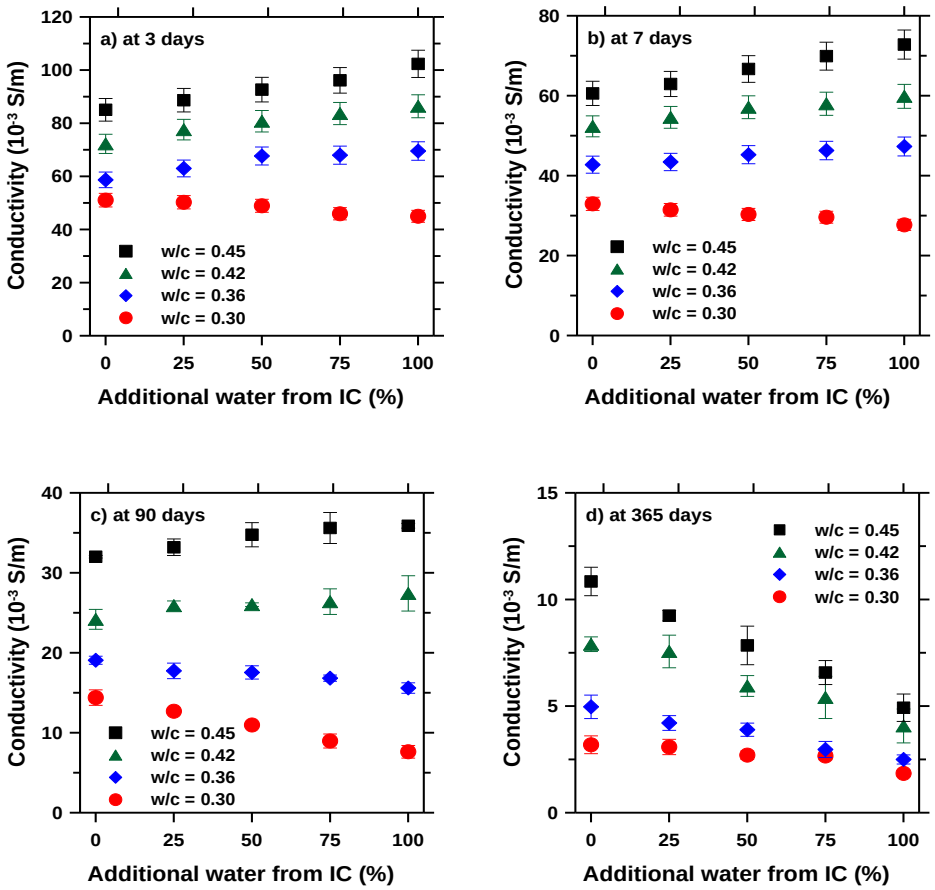

Fig 6 Electrical conductivity of sealed samples as a function of the amount of LWA at the age of: a) 3 days, b) 7 days, c) 90 days, and d) 365 days. Error bars represent the standard deviation on the average of 3 samples.

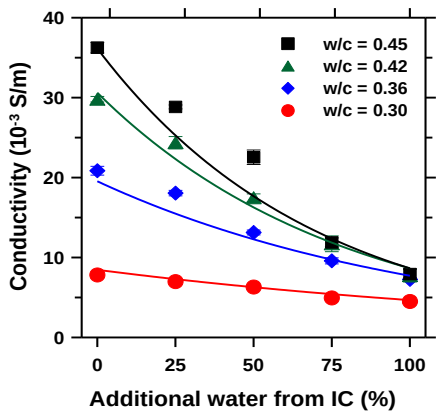

Fig 7 Electrical conductivity of vacuum saturated samples at the age of 365 days. Error bars represent the standard deviation on the average of 3 samples. Continues lines represent empirical relations described in a further section.

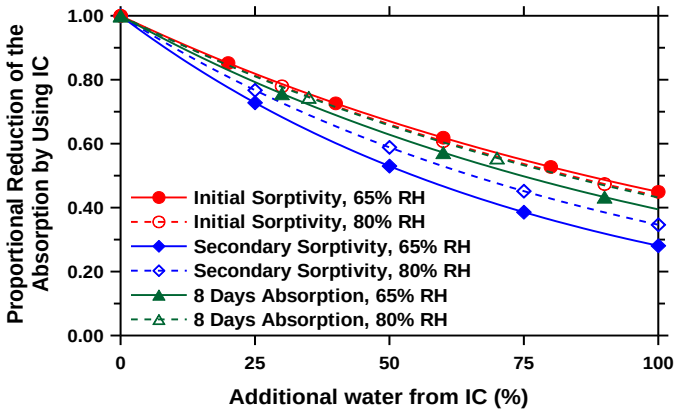

Fig 8 Proportional reduction on the absorption, initial sorptivity and secondary sorptivity of internally cured samples

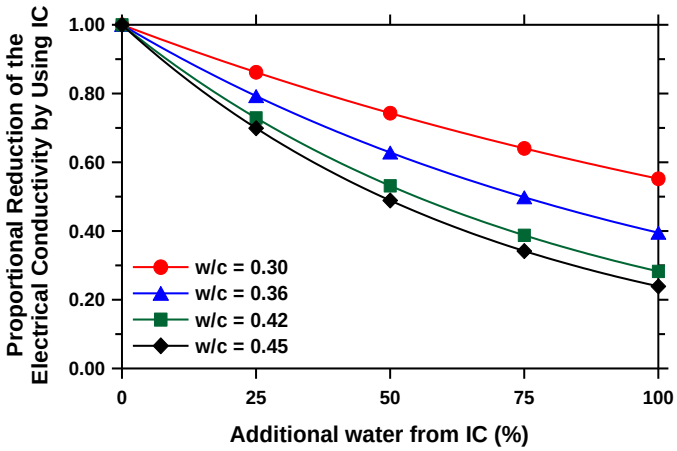

Fig 9 Proportional reduction on the electrical conductivity of 1-year old saturated internally cured samples

Water Absorption and Critical Degree of Saturation as it Relates to Freeze-Thaw Damage in Concrete Pavement Joints

Wenting Li[1], Mohammad Pour-Ghaz[2], Javier Castro[3], and Jason Weiss[4] (Corresponding author)

ABSTRACT: Fluid ingress is a primary factor that influences freeze-thaw damage in concrete. This paper discusses the influence of fluid ingress on freeze-thaw damage development. Specifically, this paper examines the influence of entrained air content on the rate of water absorption, the degree of saturation, and the relationship between the saturation level and freeze-thaw damage. The results indicate that while air content delays the time it takes for concrete to reach a critical degree of saturation it will not prevent the freeze-thaw damage from occurring. The results of the experiments show that when the degree of saturation exceeds 86 to 88% freeze-thaw damage is inevitable with or without entrained air, even with very few freeze-thaw cycles.

CE Database subject headings: Absorption, Acoustic techniques, Air entrainment, Concrete, Concrete pavement, Saturation, Deterioration, Freeze and thaw, Pavements, Joints.

Author keywords: Absorption, Acoustic emission, Air content, concrete, Concrete pavement, Degree of saturation, Deterioration, Freeze-thaw, Pavement joint, Water absorption

[1] Graduate Research Assistant, School of Materials Science, Southeast University, Nanjing 211189, China, and Graduate Research Assistant, School of Civil Engineering, Purdue University, 550 Stadium Mall Drive, West Lafayette, Indiana, USA, Phone: (765) 494 – 7999, li448@purdue.edu.

[2] Graduate Research Assistant, School of Civil Engineering, Purdue University, 550 Stadium Mall Drive, West Lafayette, Indiana, USA, Phone: (765) 494 – 7999, pourghaz@purdue.edu.

[3] PhD Candidate, School of Civil Engineering, Purdue University, 550 Stadium Mall Drive, West Lafayette, Indiana, USA, Phone: (765) 494 – 7999, jcastro@purdue.edu.

[4] Professor, director of Pankow Materials Laboratory, Purdue University, 550 Stadium Mall Drive, Indiana, USA, Phone: (765) 496 – 2215, Fax: (765) 496 – 1364, wjweiss@ecn.purdue.edu.

Background on the Problem of Joint Deterioration in Concrete Pavements

Concrete pavements represent a large portion of the transportation infrastructure. While many of these pavements provide excellent long-term performance, a portion of these pavements have recently shown premature joint deterioration throughout the Midwestern states (Weiss et al. 2007; Sutter et al. 2006; Leech et al. 2008; Rangaraju et al. 2006). This joint deterioration is problematic since it compromises the performance and potential service life of an otherwise healthy pavement. Figure 1 shows photographs of a typical damaged pavement joint. This type of damage is frequently seen as either the development of cracking parallel to the joint or spalling and cracking at the joint from the bottom of the saw cut to the surface of pavement approximately 4 to 6 inches from the joint. Unfortunately damage is not frequently observed at the surface of the pavement until a significant amount of damage has occurred inside the joint. During field inspections it has been observed that where the joints are damaged the sealant is damaged and the joint contained standing water. Research is needed to better understand how this standing water may lead to freeze-thaw damage. Further, this damage occurs in both poorly air entrained and properly air entrained concrete. As a result the role of air content needed to be quantified which is the reason for this study.

Background on Water Absorption and the Critical Degree of Saturation

Concrete is susceptible to freeze and thaw damage when it is saturated (Sutter et al. 2006; Leech et al. 2008; Rangaraju et al. 2006; Fagerlund 1972, 1975, 1977, 1979, 1981, 2004; Bentz et al. 2001; Litvan 1988; Litvan and Sereda 1980; Shimada et al. 1991, Beaudoin and Cameron 1972; Feldman 1987; Scherer 1993; Scherer and Valenza 2005; Sun et al. 2007). While the water content in concrete can be quantified in several different ways, this paper defines the degree of saturation (S) as the ratio of the absolute volume of absorbed water to the total volume of pores (i.e., the total volume of water that can be absorbed by concrete).

It has been suggested that there is a critical degree of saturation (S_{cr}) beyond which freeze and thaw damage can begin to initiate (Fagerlund 1972, 1975, 1977, 1979, 1981, 2004; Bentz et al. 2001; Litvan 1988; Litvan and Sereda 1980; Shimada et al. 1991, Beaudoin and Cameron 1972). For degrees of saturation below the critical degree of saturation freeze-thaw damage is not observed to occur even after a large number of freeze-thaw cycles (Fagerlund 1972, 1975, 1977, 1979, 1981, 2004; Bentz et al. 2001; Litvan 1988; Litvan and Sereda 1980; Shimada et al. 1991, Beaudoin and Cameron 1972).

Figure 2 schematically illustrates the concept of water absorption and the critical degree of saturation (Fagerlund 2004; Barde et al. 2009). We can begin by assuming that the representative volume element shown in Figure 2 is filled with pores with different sizes at a given spacing. It

is assumed that there are two critical values that describe the freeze-thaw performance. The first parameter is related to the degree of saturation as described above. The second parameter is related to a "critical flow distance" (i.e., D_{cr}), which is the maximum distance that water can flow from freezing site to the surrounding nearest air-filled space. Damage doesn't occur when the flow distance (D) is below the critical distance (D_{cr}) and the degree of saturation (S) is less than the critical degree of saturation (S_{cr}) as shown in Fig. 2(*a*). However, the flow distance increases with the amount of absorbed water (or poor quality air void system), as does the degree of saturation. If either the critical flow distance or the critical degree of saturation is exceeded, frost damage initiates upon the next freezing cycle. The degree of damage can be quantified by the reduction in the dynamic elastic modulus of concrete as shown schematically in Fig. 2(*d*).

In Fig. 2(*d*) for all the values of degree of saturation below the critical degree of saturation the amount of damage (reduction is the elastic modulus) is very small. As soon as the degree of saturation exceeds the critical degree of saturation damage initiates in the material (Fagerlund 1972, 1975, 1977, 2004; Bentz et al. 2001).

It should be noted that the quality of air distribution and the volume of the air are two important parameters affecting the freeze-thaw resistance of the system. The quality of the air system is related to the critical flow distance while the quantity of the air voids (volume of air) is related to the critical degree of saturation. A fully saturated system, however, regardless of the

quantity and quality of the air cannot even sustain a single freezing cycle without accumulating a significant amount of damage (Litvan 1988).

Background on Use of Acoustic Emission to Quantify Freeze and Thaw Damage

Acoustic emission (AE) is a nondestructive test method that is based on measuring the release of energy in concrete (e.g. the release of energy that occurs at the time of cracking). It should also be noted that AE can be performed in either a passive (i.e., capturing the acoustic wave generated due to formation of permanent defect such as crack) or active (i.e., using one transducer to generate a pulse and another transducer to capture the same pulse (in the simplest arrangement)). Classically AE is typically performed in passive mode in cement/concrete studies (Ohtsu 1999, 1993; Bentz et al. 2008; Hossain et al. 2003; Shah and Weiss 2006; Kim and Weiss 2003; Moon and Weiss 2006; Ouyang et al. 1991a, 1991b; Suari and Van Mier 1995, 1993; Pour-Ghaz et al. 2010; Puri and Weiss 2003; Yang et al. 2006; Yoon et al. 1999). AE has been used in concrete to assess damage due to restrained shrinkage (Bentz et al. 2008; Hossain et al. 2003; Shah and Weiss 2006; Kim and Weiss 2003; Moon and Weiss 2006) and mechanical loading (Ouyang et al. 1991a, 1991b; Suari and Van Mier 1995, 1993; Pour-Ghaz et al. 2010; Puri and Weiss 2003; Yang et al. 2006; Yoon et al. 1999). AE has also been used to monitor freezing and thawing of mortar and it was observed that activity during both freezing and

thawing (Shimada et al. 1991; Krishnan 2002).

In the present work, the evolution of damage in concrete during freeze–thaw cycles was monitored using both active and passive AE. The reduced relative dynamic elastic modulus was calculated for each cycle according to the transmitting time of waves using active AE. Passive AE was recorded to better understand the damage that develops during the freeze-thaw cycle.

Hypothesis and Outline for Experimental Investigation

There has been a great deal of debate on possible causes of joint deterioration in concrete pavements. It is the hypothesis of this work that the presence of water (or solution containing deicing salt solutions) in the joints plays a significant role in the deterioration of concrete pavement joints. First, it is hypothesized that joints can hold water or deicing fluids substantially longer than other parts of the pavement. This would enable the concrete at the joint to become preferentially saturated. The potential for a joint to hold water increases when the joint sealant is damaged or missing, at low spots in the pavement, and when the joint does not crack and open as designed (as has been noticed in the field). It is hypothesized that this propensity for saturation could make the concrete more susceptible to local freeze-thaw damage. Second, it is hypothesized that the use of air entrainment can increase the resistance to joint deterioration however it also believed that the use of air entrainment will not eliminate the potential for damage to occur. The addition of air entrainment is believed to extend the time required for the

concrete to reach to the critical degree of saturation.

While other factors can contribute to joint deterioration (e.g., the use of specific deicers, curing conditions, mixture proportions, construction details), they are not specifically considered in this paper. The scope of this paper is to examine the role of air entrainment on the rate of water ingress and degree of saturation increase in concrete. Second, this paper provides data to relate the degree of saturation to freeze-thaw damage in air entrained and non-air entrained concrete.

Experimental Plan

This section describes mixture proportioning, specimen conditioning and the procedures of the testing in detail.

Mixture Proportions

Three mortar mixtures were prepared with different air contents (6, 10, 14% air by volume as measured in mortar). The air volume was calculated for an equivalent paste and concrete system respectively with the assumptions shown in Table 1. All specimens were made with ordinary Portland cement (Type I) and had a water to cement ratio (w/c) of 0.42 which is typical of concrete pavements in the state of Indiana. Table 1 presents the proportions of the materials that were used.

Mixing was performed in accordance with ASTM C192-06 (ASTM 2006). Two specimen geometries were used in this study: cylinders (25 mm height by 100 mm diameter) and prisms

(25 mm by 25 mm by 125 mm). Cylindrical specimens were used the water absorption test. The prisms specimens were used to evaluate the freeze-thaw damage development using AE. These specimens were cut from larger specimens.

Specimen Conditioning

The method of the specimen conditioning prior to water absorption testing can substantially influence the results of the test (Castro et al. 2010a, 2010b, 2010c; Spragg et al. 2011). If the specimen is not properly conditioned it can lead to a misunderstanding of the actual absorption behavior (Castro et al. 2010a, 2010b, 2010c; Spragg et al. 2011). Due to the significance of conditioning and necessity for the specimens to reach equilibrium the standard curing procedures was not used (Scherer and Valenza 2005). The procedure that was used in this study allowed the specimens to equilibrate for a longer period.

The cylindrical specimens were cut 24 hours after casting from a larger cylindrical sample and sealed in two layers of plastic. The specimens were stored at 23 +/- 1°C for 28 days. After 28 days the specimens were removed from the plastic bag and placed in 50 +/- 1, 65 +/-1 and 80 +/-1% relative humidity (RH) environments where they were kept for more than a year to equilibrate. Table 2 lists the air content and relative humidity of each specimen.

Water Absorption

A procedure similar to ASTM C1585-04 (ASTM 2004) was used however the specimens

were not conditioned following the accelerated ASTM testing procedure (described above). After conditioning, the outer circumference of the specimen was sealed with two layers of epoxy resin. After the epoxy hardened, the specimens were placed under water. Two small spacers were placed under the sample to provide a small gap between the bottom of the container and the lower surface of the sample. This allowed water absorption from both circular surfaces (Fig. 3).

Freeze-Thaw Testing

This section describes specimen preparation and procedures used in freeze-thaw testing.

Specimen Saturation

The prismatic specimens were prepared to have different degrees of saturation before freeze-thaw testing was performed. The specimens were oven dried in steps to 105°C where they were maintained for 2 days. The specimens were then placed in a desiccator and evacuated to a residual pressure of 30mm Hg (4000 Pa) for 3 hours. After evacuation and while still under vacuum, water was introduced into the desiccators to cover the specimens. The specimens were left in the desiccators for 24 hours. This condition was considered as saturated (i.e., 100% degree of saturation). The degree of saturation was reduced for some specimens (i.e. 0.96, 0.92, 0.90, 0.86, 0.82, and 0.78) by short periods of drying at 23°C and 50% relative humidity. During the drying period the mass of the specimens was closely monitored. After drying all the specimens were sealed in plastic bags for a minimum of 3 days to allow moisture to re-distribute before

freezing and thawing testing.

Preparation of the Specimen for Freezing and Thawing

Figure 4 shows the procedure used for preparing the specimens for AE testing during freeze-thaw cycles. The specimens were first preconditioned to different degrees of saturation as described in section 5.4.1. After preconditioning the specimens were wrapped with a thin plastic sheet as shown in Fig. 4(*a*). The thin plastic sheet was used to protect the sample from further drying during the handling. The specimens were then sealed with a "heat shrink wrap" to further protect the specimens against moisture exchange with surroundings (prevent them from absorbing or releasing water during the freeze-thaw process) as shown in Fig. 4(*b*). It is important to note that the "heat shrink wrap" was in loose contact with sample (with the exception of the specimen ends) so that the specimen can expand freely during the test while minimizing any restraint.

The AE sensors (transducers) were attached on the two ends with a thin layer of vacuum grease as shown in Fig. 4(*c*). Figure 5 shows that all the specimens were placed on a suspended base in testing to minimize noise/vibration transmission from surrounding environment. The threshold was set at 60 dB and 34 dB for active and passive AE, respectively. Testing was also performed on dry specimens to ensure that sounds were not being recorded from the environment, freezing unit, or coupling agent (Pour-Ghaz and Weiss 2010).

Temperature Cycle used for Freeze-Thaw Testing

Figure 6 shows the temperature cycle (in air) which allows one cycle per day. Temperature was controlled to vary from 10 +/- 1°C to -18 +/- 1°C. The rate of the temperature change was 14°C/hour resulting in a 2-hour transition period and two 10–hour periods at 10 +/-1 °C and -18 +/-1 °C respectively.

Experimental Results and Discussion

Water Absorption

Sorptivity

The amount of absorbed water (I) is normalized by the cross-sectional area exposed to water as outlined in ASTM C1585 (ASTM 2004):

$$I = m_t / (a.d) \quad (1)$$

where: m_t is the change in specimen mass at time t in grams; a is the area of the both sides exposed to water, in mm^2; d is the density of water in g/mm^3.

Sorptivity is defined as the slope of the water absorption versus square root of time curve (ASTM 2004). The initial sorptivity is the slope of this curve within the first 6 hours, while the secondary sorptivity is the slope of the curve between 1 to 8 days.

Figure 7(*a*) illustrates the sorption results for the specimens conditioned at 50% RH with 13% and 31% air contents by volume of paste. The specimens show a similar sorptivity (slope of

the curves) and amount of absorbed water initially; however, over time the specimens with higher volumes of air absorb more water. This occurs since the air voids provide space for water (Helmuth 1961; Warris 1964), however, the diffusion of air and the over-pressure in the air-bubbles delays water absorption which corresponds for the long time to saturation (Fagerlund 1993, 1995, 2004). It should be noted that although the secondary sorptivity for sample with higher air content is higher, this sample requires to absorb more water to reach to the critical degree of saturation.

Figure 7(*b*) shows the water absorption results for specimens conditioned at 65% RH. Comparing this result with Fig. 7(*a*) suggests that the amount of absorbed water for the specimens conditioned at 65% RH is lower than that of specimens conditioned at 50% RH with the same air content. Figure 7(*c*) shows the absorption for specimens conditioned at 80% RH. The specimens at 65% RH and 50% RH show a nick-point at the end of the 6 hours on a water absorption square-root of time curve however, the nick-point can not be seen on the results of 80% RH and a more graduate rate of absorption can be seen.

The relative humidity in which the specimens were conditioned in has a significant impact on the results (Castro et al. 2010a, 2010b, 2010c; Spragg et al. 2011). The driving force of unsaturated fluid transport is the capillary suction (Hall and Hoff 2002; Martys and Ferraris 1997; Hanžič et al. 2010). When samples are in equilibrium with a lower relative humidity a larger

volume of pores are empty and available to be filled with water during the water sorption. Furthermore, at lower humidity, the maximum size of the pores that is filled with water is smaller, creating a higher suction force. The overall effect will be higher rate of water absorption and high volume of absorbed water.

Degree of Saturation

Figure 8(*a*) shows that the degree of saturation (*S*) of the specimens conditioned at 50% RH with two air contents (13 and 31% by volume of paste). Note that the degree of saturation is plotted as a function of square-root of time on the lower x-axis while actual time is shown on the upper x-axis.

The most striking feature of the graphs in Fig. 8 is the fact that the degree of saturation decreases with air content. At the end of the initial 6-hour sorption period samples with lower air content show higher degree of saturation. For samples equilibrated at 50% RH the degree of saturation is 39% less when the air content increases 10%, the decrease in degree of saturation for samples equilibrated at 65% and 80% RH is 23% and 26% respectively.

Note that the secondary rate of absorption (Fig. 7) is different for samples with different air content; however, in Fig.8 the secondary rate of increase in degree of saturation is approximately the same for materials with different air content. This suggests that for an equal time of exposure to water, the specimen with the higher air content has a lower degree of saturation (Fagerlund

1993, 1995, 2004).

The secondary rate of increase in degree of saturation can be fitted with a linear function to estimate the amount of absorbed water over a long period of time. The linear fit used in Fig. 8 is shown with a solid line. Since the objective here is to estimate the degree of saturation over a long period of time only the date between 100 to 240 days is used in fitting this straight line. Using this linear function the time to reach to critical degree of saturation is calculated for each specimen with different air content and initial equilibrium condition and reported in Table 3.

Freeze-Thaw Testing

Monitoring the Damage Development Using Active Acoustic Emission

The relative dynamic elastic modulus is frequently used as an index to evaluate the extent of damage (Fagerlund 1972, 1975, 1977, 1979, 1981, 2004; Bentz et al. 2001; Litvan 1988; Litvan and Sereda 1980; Shimada et al. 1991). Using active AE the transmission time of a single pulse was measured along the sample. The transmission time along the length of the sample was measured in both directions (i.e., from sensor 1 to 2 and from sensor 2 to 1). The transmission time was measured three times in each direction and the average transmission time is reported here (average of 6 values). The transmitting time was measured after each cycle when the temperature was stable at 10°C for a minimum of 2 hours.

The relative elastic modulus, i.e. E_t/E_o is square proportional to the velocity of wave

transmitting through materials, which is inversely square proportional to the ratio of the wave transmission times (ASTM 2008) as shown in Eq. 2. Damage parameter (D) can also be estimated using Eq. 2.

$$D = 1 - E_t / E_o = 1 - (T_o / T_t)^2 \quad (2)$$

where E_o, T_o are the dynamic elastic modulus before freeze-thaw testing began and corresponding transmitting time; E_t, T_t are the dynamic elastic modulus during testing at any time t and corresponding transmitting time.

It should be noted that the main cracks were along the direction of wave propagation and as such the wave is least sensitive to these cracks however the damage was still easily recorded.

Figure 9 illustrates the damage index (Eq. 2) with increasing cycles of freezing and thawing. The damage initiates during the first cycle when the degree of saturation is above 86~88%. The specimens with lower degree of saturation do not show damage while specimens with a higher degree of saturation show a rapid deterioration. It can be seen that the saturated specimens (S=100%) can not sustain more than 3 cycles before complete failure occurs.

Figure 10 shows the rate of damage (dD) development per freeze-thaw cycle (dN) (as determined by the slope of Fig. 9) for specimens with different degrees of saturation. A critical degree of saturation appears to occur at approximately 86 - 88%. The critical degree of saturation appears to be independent of the air content.

Acoustic Energy Measured Using Passive Acoustic Emission

Figure 11 shows the amplitude of the acoustic events as a function time for a specimen with 96% degree of saturation and 13% air content during freezing cycle. The temperature is the temperature measured in the center of the mortar specimen. Figure 11(*a*) illustrates the amplitude distribution for the first freeze-thaw cycle and Fig. 11(*b*) illustrates the amplitude distribution during the second freeze-thaw cycle for the same specimen.

In Fig. 11(*a*) the acoustic events begin to occur as the temperature of the specimen decreases. A cluster of acoustic event is shown in Fig. 11(*a*) as highlighted by the ellipsoid. This cluster of data is not seen in Fig. 11(*b*). These events can be attributed to micro-cracking of the specimen due to thermal loading which may be a result of temperature gradient or a result of thermal expansion coefficient mismatch between the paste and aggregate. Since the thermal loading is not changed during the second cycle, the damage due to thermal loading does not exceed the previous level of damage in materials and additional cracking would not be expected (Kaiser 1950; Kline and Egle 1987).

In Figure 11 the acoustic events begin to increase dramatically after the temperature drops below -8°C in both cycles. The number of events is higher in the first cycle compared to the second cycle as more cracking would be expected in the first freeze-thaw cycle while these cracks would be expected to extend in the following cycles. The damage at the point (below -8°C)

is likely attributed to formation of ice and cracking inside the specimen. This is consisted with the observation that pore solution freezes below 0°C due to pore confinement and dissolved ions in pore solution (Fagerlund 1973; Helmuth 1960).

Desorption Isotherm

Figure 12 shows the desorption isotherm for the specimens with 13% and 31% air content by volume of paste. The desorption curve demonstrates the mass of water lost from the specimen at each relative humidity step (i.e., different pore sizes begin to empty out at different relative humidities starting with large pores at high relative humidities and smaller pores at lower humidities). The profile of the desorption curve is similar for both specimens until high relative humidities, i.e. 97.5% RH. At relative humidities higher than 97.5%, a larger difference of the porosity can be seen. This difference corresponds to the air entrained porosity.

The critical degree of saturation (88%) corresponds to relative humidity of 98.4% for specimen with 13% air content and 98.96% RH for specimen with 31% air content, respectively. This implies that some of the air entrained pores are water filled when the specimen is at or above critical degree of saturation. The difference in mass loss between the 13 and 31% air content at 2.5% RH is currently unknown however this is repeatable between specimens.

Calculated Time to Reach the Critical Degree of Saturation

In section 6.1 the rate of absorption of water and its relation to the degree of saturation was

discussed and in section 6.2 the influence of the degree of saturation on freeze-thaw damage was discussed. To better understand how these findings can be related to one another to predict the time to freeze-thaw damage a linear function was fit to the plot of degree of saturation verses square root of time data (using the secondary absorption).

Table 3 shows the time required for each specimen equilibrated at different initial condition to reach the critical degree of saturation (i.e., 88% in this study). Specimens without air entrainment can reach to the critical degree of saturation within days (4~6 days). The use of air entrainment raised the air content, and decreases the degree of saturation. This increases the time to reach a critical degree of saturation to 3~6 years. The rate of water absorption is substantially different in the systems with entrained air compared to non-air entrained systems.

Conclusions

The water absorption of mortar containing different volumes of entrained air was examined in this study. While tests like ASTM C 1585-04 (ASTM 2004) can be used to provide an index of water absorption, the differences between non air entrained and air entrained systems were small when only mass gain was investigated. While the absorption rates in plain and air entrained systems were similar initially the air entrained system showed a higher rate of ingress at later ages. By normalizing the results of water absorption in terms of the degree of saturation a clear distinction between the non air entrained and air entrained mixtures can be made. While the non

air entrained system took 4 to 6 days to reach 88 % saturation, the air entrained system is estimated to require approximately 3 to 6 years. This shows that entrained air will substantially increase the time to failure.

The damage due to freeze-thaw was monitored using both passive and active AE. A critical degree of saturation was observed with specimens that have a degree of saturation greater than the 86 to 88% exhibiting damage during the few freeze-thaw cycles.

The critical degree of saturation appears to be independent of the air content as materials with a degree of saturation above the critical degree undergoing damage after a few of freeze-thaw cycles irrespective of the air content. The volume of air and quality of the air void system however likely has a strong relation to the critical flow distance.

Increasing the air content resulted in a longer time for the mortar to reach to the critical degree of saturation. While increasing the air content can delay the time freeze-thaw damage initiates in practice; it appears that increasing of the air content can not eliminate the potential for freeze-thaw damage.

Acknowledgements

The experiments reported in this paper were conducted in the Pankow Materials Laboratories at Purdue University. This work was supported in part by Compass Minerals and the Joint Transportation Research Program administered by the Indiana Department of

Transportation and Purdue University. The contents of this paper reflect the views of the authors, who are responsible for the facts and the accuracy of the data presented herein, and do not necessarily reflect the official views or policies of the Indiana Department of Transportation, nor do the contents constitute a standard, specification, or regulation. The authors appreciate the assistance of Gaurav Sant for his work in casting/cutting the specimens while he was a graduate assistant working on this project. The authors also acknowledge many useful discussions with Dick Newell, John Poncher, Mike Byers, Tommy Nantung, Dave Andrewski, and Jan Olek.

References

ASTM Standard C192 (2006). "Standard practice for making and curing concrete test specimens in the laboratory." ASTM International, West Conshohocken, PA.

ASTM Standard C1585-04 (2004). "Standard test method for measurement of rate of absorption of water by hydraulic-cement concretes." ASTM International, West Conshohocken, PA.

ASTM Standard C666 (2008). "Test method for resistance of concrete to rapid freezing and thawing." ASTM International, West Conshohocken, PA.

Barde, V. Radlinska, A., Cohen, M. and Weiss, W.J. (2009). "Relating material properties to exposure conditions for predicting service life in concrete bridge decks in Indiana." *The Joint Transportation Research Program of the Indiana Department of Transportation*, Purdue University, West Lafayette, IN.

Beaudoin, J.J. and Cameron, M., (1972). "Dimentional changes of hydrated Portland cement paste during slow cooling and warming." *Cem. Concr. Res.*, 2(2), 225-240.

Bentz, D.P., Ehlen, M.A., Ferraris, C.F., and Garboczi, E.J. (2001). "Sorptivity-based service life predictions for concrete pavements." *7th Int. Conf. on Concrete Pavements*, NIST, Orlando, Florida, U.S., 181-193.

Bentz, D.P. Sant, G. and Weiss, J. (2008). "Early-age properties of cement-based materials I: influence of cement fineness." *J. Mater. Civ. Eng.*, 20(7), 502-508.

Castro, J., Bentz, D., and Weiss, J. (2010). "Effect of specimen conditioning on the water absorption of concrete." Submitted to *Cem. Concr. Compos.*

Castro, J., Kompare, P., Poursaee, P., Nantung, T. and Weiss, J. (2010). "Portland cement concrete pavement performance relative to permeability." *JTRP Report SPR-3093*, Indiana Department of Transportation, West Lafayette, IN.

Fagerlund, G. (1972). "Critical degrees of saturation at freezing of porous and brittle materials." *Report 34*, Division of Building Technology, Lund Institute of Technology, Lund, Sweden, 408.

Fagerlund, G. (1973). “Determination of pore-size distribution from freezing-point depression.” *Mater. Struct.*, 6(3), 215-225.

Fagerlund, G. (1975). “The significance of critical degrees of saturation at freezing of porous and brittle materials.” *Conf. on Durability of concrete*, ACI STP, Atlantic, New Jersey and Ottawa, Ontario, 47, 13-65.

Fagerlund, G. (1977). “The critical degree of saturation method of assessing the freeze/thaw resistance of concrete and the international cooperative test of the critical degree of saturation method of assessing the freeze/thaw resistance of concrete.” *Mater. Struct.*, 1977(10), 217-229 and 231-253.

Fagerlund, G. (1979). “Prediction of the service life of concrete exposed to frost action, studies on concrete technology.” *Studies on Concrete Technology*, Swedish Cement and Concrete Research Institute, Stockholm, 249-276.

Fagerlund, G. (1981). “The principles of frost resistance of concrete.” *Nordisk Betong*, 1981(2), 5-13, In Swedish.

Fagerlund, G. (1993). “The long-time water absorption in the air-pore structure of concrete.” Report TVBM-3051, Division of Building Technology, Lund Institute of Technology, Lund, Sweden.

Fagerlund, G. (1995). “The required air content of concrete.” *Proc., In. Workshop on Mass-Energy Transfer and Determination of Building Components*, BRI-Japan and CSTB-France, Paris, France, 591-609.

Fagerlund, G. (2004). “A service life model for international frost damage in concrete.” Report TVBM-3119, Division of Building Technology, Lund Institute of Technology, Lund, Sweden.

Feldman, R.F. (1987). “Diffusion measurements in cement paste by water replacement using propan-2-OL.” *Cem. Concr. Res.*, 17(4), 602-612.

Hall, C., and Hoff, W.D. (2002). “Water in porous materials.” *Water-Transport in Brick, Stone and Concrete*, Taylor&Francis, Abingdon, Oxon, 29-41.

Hanžič, L., Kosec, L., and Anžel, I. (2010). “Capillary absorption in concrete and the lucas–washburn equation.” *Cem. Concr. Compos.*, 32, 84–91.

Helmuth, R.A. (1960). “Capillary size restrictions on ice formation in hardened Portland cement pastes.” *Proc., 4th Int. Symp. on Chemistry of Cement*, Paper VI-S2, 855–869.

Helmuth, R.A. (1961). “Dimensional changes of hardened Portland cement pastes caused by temperature changes.” *Proc., Highway Research Board*, 40, 315–336.

Hossain, A.B., Pease, B. and Weiss, J. (2003). “Quantifying early-age stress development and cracking in low water-to-cement concrete - restrained-ring test with acoustic emission.” *Transp. Res. Rec.*, 1834, 24-32.

Kaiser, J., (1950). “A study of acoustic phenomena in tensile tests.” Dr.-Ing. dissertation, Technical University of Munich, Bayern, Germany.

Kim, B. and Weiss, J. (2003). “Using acoustic emission to quantify damage in restrained fiber-reinforced cement mortars.” *Cem. Concr. Compos.*, 33, 207–214.

Kline, R.A., and Egle, D.M. (1987). “A brief note on the Kaiser and Felicity effects.” *J. Acoust. Emiss.*, 6, 205.

Krishnan, A. (2002). “Durability of concrete containing fly ash or slag exposed to low temperatures at early ages.” M.S. Thesis, Purdue University, West Lafayette, IN.

Leech, C., Lockington, D., Hooton, R.D., Galloway, G., Cowin, G. and Dux, P. (2008). “Validation of mualem's conductivity model and prediction of saturated permeability from sorptivity.” *J. ACI Mater.*, 105(1), 44-51.

Litvan, G.G. and Sereda, P.J. (1980). “Freeze-thaw durability of porous building materials.” *Durability of Building Materials and Components*, ASTM STP 691, Sereda, P.J. and Litvan, G.G., eds., ASTM International, 455-463.

Litvan, G.G. (1988). “The mechanism of frost action in concrete-theory and practical implications.” *Proc., of Workshop on Low Temperature Effects on Concrete*, National Research Council of Canada, Montreal, Canada, 115-134.

Martys, N.S., and Ferraris, C.E. (1997). "Capillary transport in mortars and concrete." *Cem. Concr. Res*, 27(5), 747-760.

Moon, J.H., and Weiss, J. (2006). "Estimating residual stress in the restrained ring test under circumferential drying." *Cem. Concr. Compos.*, 28, 486–496.

Ohtsu, M. and Shigeishi, M. (1993). "Experimental crack identification of mixed mode by acoustic emission." *Int. Conf. on Fracture and Damage of Concrete and Rock (FDCR-2)*, Rossmanith, H. P. eds., E&FN Spon., London, 186-195.

Ohtsu, M. (1999). "Estimation of crack and damage progression in concrete by quantitative acoustic emission analysis." *Mater. Eval.*, 57(5), 521-525.

Ouyang, C., Landis, E. and Shah, S.P. (1991). "Detection of microcracking in concrete by acoustic emission." *Exp. Tech.*, 15(3), 24-28.

Ouyang, C., Landis, E. and Shah, S.P. (1991). "Damage assessment in concrete using quantitative acoustic emission." *J. Eng. Mech.*, 117(11), 2681-2698.

Pour-Ghaz, M., Nadukuru, S., O'Connor, S., Kim, J., Michalowski, R., Bradshaw, A., Green, R.A., Lynch, J.P., Poursaee, A. and Weiss, W.J. (2010). "Using electrical, magnetic and acoustic sensors to detect damage in segmental concrete pipes subjected to permanent ground deformation." Purdue University, School of Civil Engineering, West Lafayette, IN.

Pour-Ghaz, M. and Weiss, J. (2010). "Quantifying damage due to aggregate expansion in cement matrix." *Advances in the Material Science of Concrete*, ACI SP-270-9, 101-113.

Puri, S. and Weiss, J. (2003). "Assessment of localized damage in concrete under compression using acoustic emission." *ASCE J. Mater. Civ. Eng.*, 18(3), 325-333.

Rangaraju, P.R., Sompura, K.R. and Olek, J. (2006). "Investigation into potential of alkali-acetate-based deicers to cause alkali-silica reaction in concrete." *Transp. Res. Rec.*, 1979, 69-78.

Scherer, G.W. (1993). "Freezing gels." *J. Non-Cryst Solids*, 155, 1-25.

Scherer, G.W. and Valenza, J.J. (2005). “Mechanisms of frost damage.” *Mater. Sci. Concr.*, 7, 209-246.

Shah, H.R., and Weiss, J. (2006). “Quantifying shrinkage cracking in fiber reinforced concrete using the ring test.” *Mater. Struct.*, 39(9), 887-899.

Shimada, H., Sakai, K., and Litvan, G.G. (1991). “Acoustic emissions of mortar subjected to freezing and thawing.” *J. ACI Mater.*, 126, 263-278.

Spragg, R., Castro,J., Li, W., Pour-Ghaz, M., Huang, P., and Weiss, J. (2011). “Wetting and drying of concrete in the presence of deicing salt solutions.” Submitted to *Cem. Concr. Compos.*

Suaris, W. and van Mier, J. G. M. (1993). “Acoustic emission and source location in concrete subjected to mixed mode loading.” *Int. Conf. on Fracture and Damage of Concrete and Rock (FDCR-2)*, Rossmanith, H. P., eds., E&FN Spon, London, 157-165.

Suaris, W., and Van Mier, J.G.M. (1995). “Acoustic emission source characterization in concrete under biaxial loading.” *Mater. Struct.*, 28(8), 444-449.

Sun, Z., Kumpf,D. and Scherer, G.W. (2007). “Kinetics of ice growth in concrete.” *Proc., 12th Int. Cong. Cement Chemistry*, paper W4-07.1, Beaudoin, J.J., Makar, J.M., Raki, L. eds., National Research Council of Canada, Montreal, Canada.

Sutter, L., Van Dam, T., Peterson, K. R. and Johnston, D. P. (2006). “Long-term effects of magnesium chloride and other concentrated salt solutions on pavement and structural Portland cement concrete phase I results.” *Transp. Res. Rec.*, 1979, 60-68.

Warris, B. (1964). “The influence of air-entrainment on the frost-resistance of concrete, part B, hypothesis and freezing experiments.” *Proc., No. 36 Swedish Cement and Concrete Research Institute*, Stockholm, 130.

Weiss, W.J., Abraham, D., and Nantung, T. (2007). “SPR3200—A proposal for a research study on saw-cutting and curing of concrete pavements.” *The Joint Transportation Research Program of the Indiana Department of Transportation*, Purdue University, West Lafayette, IN.

Yang, Z.F. Weiss, W.J. and Olek, J. (2006). “Water transport in concrete damaged by tensile loading and freeze-thaw cycling. ” *J. Mater. Civ. Eng.*, 18(3), 424-434.

Yoon, D.J. Weiss, W.J. Prine, D.W. and Shah, S.P. (1999). “Assessing corrosion damage in reinforced concrete beams using acoustic emission.” *Non-Destr. Eval. Bridg. Highw.*, 3587, 254-263.

Table headings

Table 1. Mixture proportions and constituent materials

Table 2. Initial condition, air content and namely scheme for specimens used in the present study

Table 3. Time to reach to the critical level of saturation (88%) for the specimens with different air content

Table 1. Mixture proportions and constituent materials

Air content of paste (% by volume of mortar [a]/ concrete [b])	Cement (Type I) (kg/m^3)	Water (kg/m^3)	Sand (kg/m^3)
13 (6/4)	573.3	240.8	1333.3
22 (10/7)	548.9	230.6	1276.5
31 (14/9)	524.5	220.3	1219.8

Note: [a] In calculating the equivalent air content in mortar it was assumed 45% paste by volume of the mortar; [b] In calculating the equivalent air content in concrete it was assumed 30% paste by volume of the concrete.

Table 2. Initial condition, air content and namely scheme for specimens used in the present study

Specimen name	Air content of the Paste (%)	Relative humidity (%)
50-13 [a]	13	50
65-13	13	65
80-13	13	80
50-22	22	50
65-22	22	65
80-22	22	80
50-31	31	50
65-31	31	65
80-31	31	80

Note: [a] The first number shows the initial humidity of the specimen (e.g.50-13 is 50% RH);
The second number shows the air content of mortar of the specimen (e.g. 50-13 is 13% air by volume of paste).

Table 3. Time to reach to the critical level of saturation (88%) for the specimens with different air content

Initial relative humidity (%)	Air content by volume of paste (%)	Secondary sorptivity ($mm^3/mm^2.d^{0.5}$)	Time to reach the critical degree of saturation (88%) (S_{cr}) in years (+/-1.7%)
50	13	0.485	0.011 (4d)
	22	0.691	5.08
	31	0.750	6.10
65	13	0.368	0.016 (6d)
	22	0.513	5.63
	31	0.785	5.90
80	13	0.563	0.015 (5d)
	22	0.606	4.00
	31	1.009	5.82

Figure captions

Fig. 1 Photography of field observation showing damage in pavement joints

Fig. 2 Schematic illustration of relation between degree of saturation with freeze-thaw damage [10, 19]

Fig. 3 Double sided sorption test of specimen with 1-inch thickness

Fig. 4 Specimens prepared for acoustic emission testing during freeze-thaw cycle: (*a*) thin plastic sheet to avoid evaporation during specimen preparation and handling (*b*) specimen covered by heat shrinkable wrap to avoid evaporation during specimen preparation and handling

Fig. 5 Specimens placed on a suspended base to eliminate vibration and noise from surrounding environment (inside of freeze-thaw chamber)

Fig. 6 Temperature cycle used in freeze-thaw experiment (air temperature)

Fig. 7 Effect of air content and initial moisture on water absorbed: (*a*) 50% RH (*b*) 65% RH (*c*) 80% RH

Fig. 8 Results of sorption test provided as increase in the degree of saturation: (*a*) 50% RH (*b*) 65% RH (*c*) 80% RH

Fig. 9 Decrease of the relative dynamic elastic modulus with freeze-thaw cycles

Fig. 10 Rate of decrease of relative dynamic elastic modulus with degree of saturation

Fig. 11 Amplitude in the transition time of freezing (96*S*): (*a*) first cycle (*b*) second cycle

Fig. 12 Mass change at decreasing RH containing de-ionized water

Figures:

Fig. 1 Photograph of field observation showing damage in pavement joints

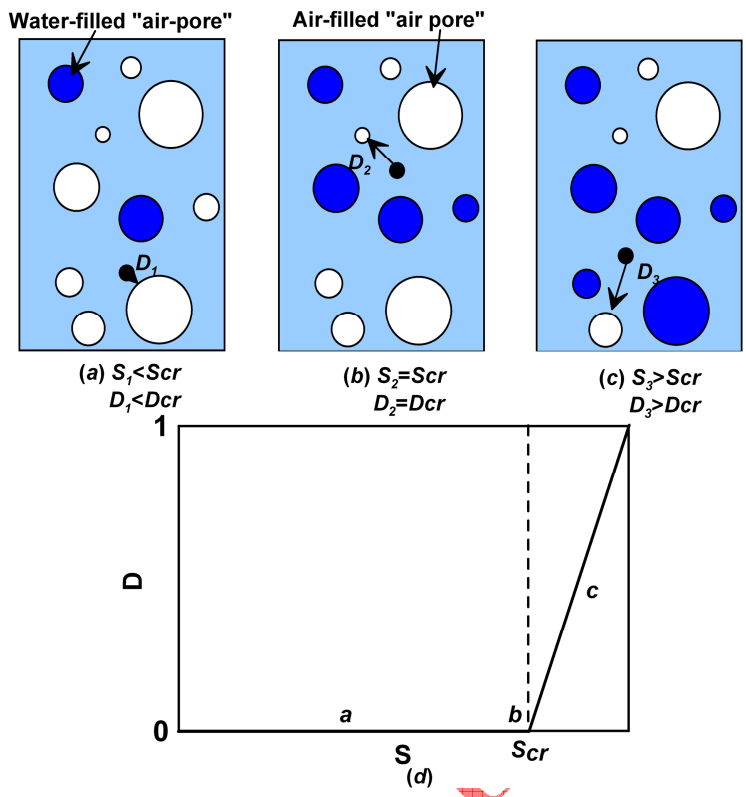

Fig. 2 Schematic illustration of relation between degree of saturation with freeze-thaw damage [10, 19]

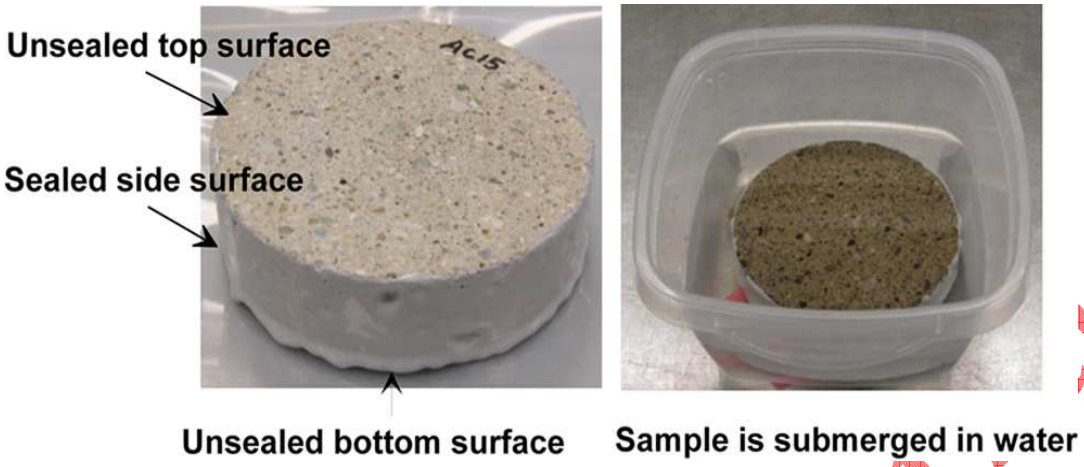

Fig. 3 Double sided sorption test of specimen with 1-inch thickness

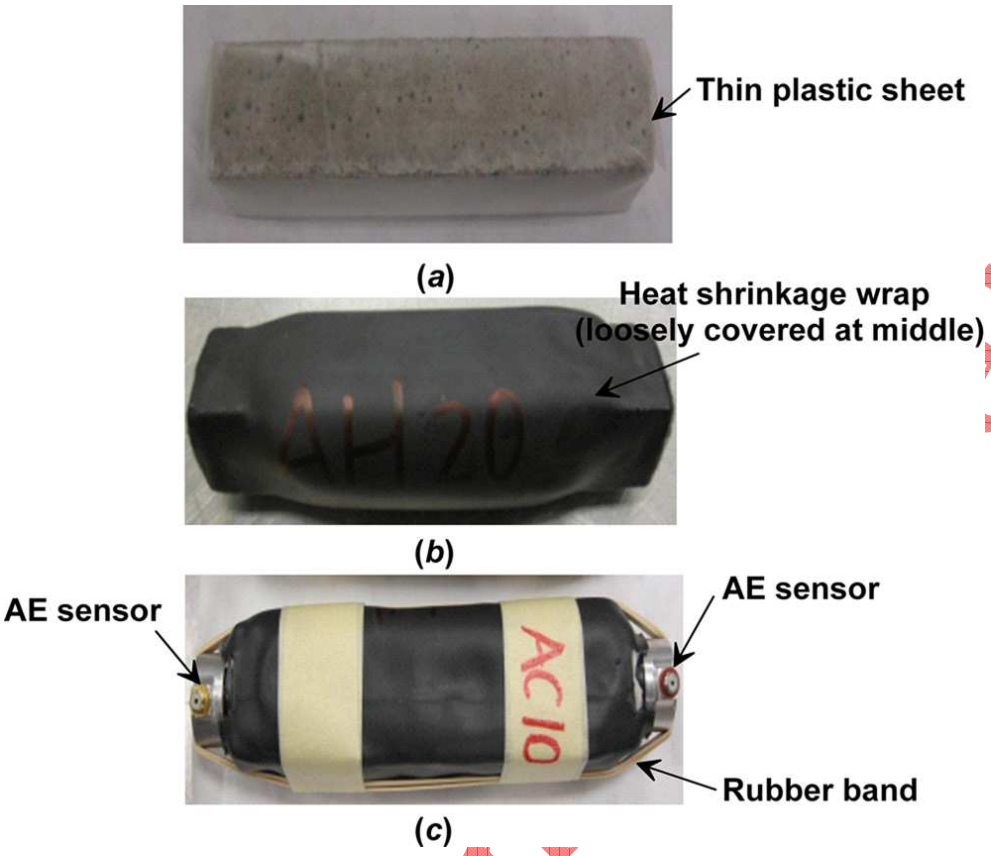

Fig. 4 Specimens prepared for acoustic emission testing during freeze-thaw cycle: (*a*) thin plastic sheet to avoid evaporation during specimen preparation and handling (*b*) specimen covered by heat shrinkable wrap to avoid evaporation during specimen preparation and handling

Suspended plate to eliminate vibration and noise from environment

Fig. 5 Specimens placed on a suspended base to eliminate vibration and noise from surrounding environment (inside of freeze-thaw chamber)

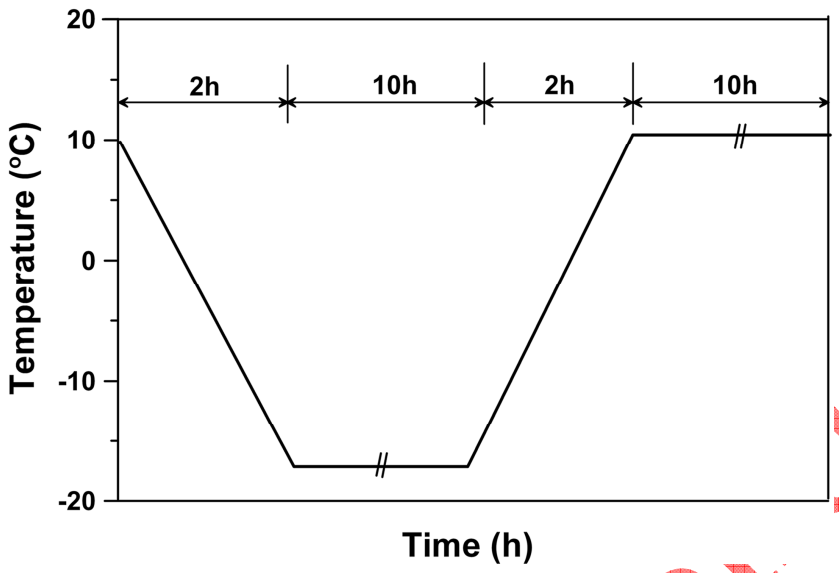

Fig. 6 Temperature cycle used in freeze-thaw experiment (air temperature)

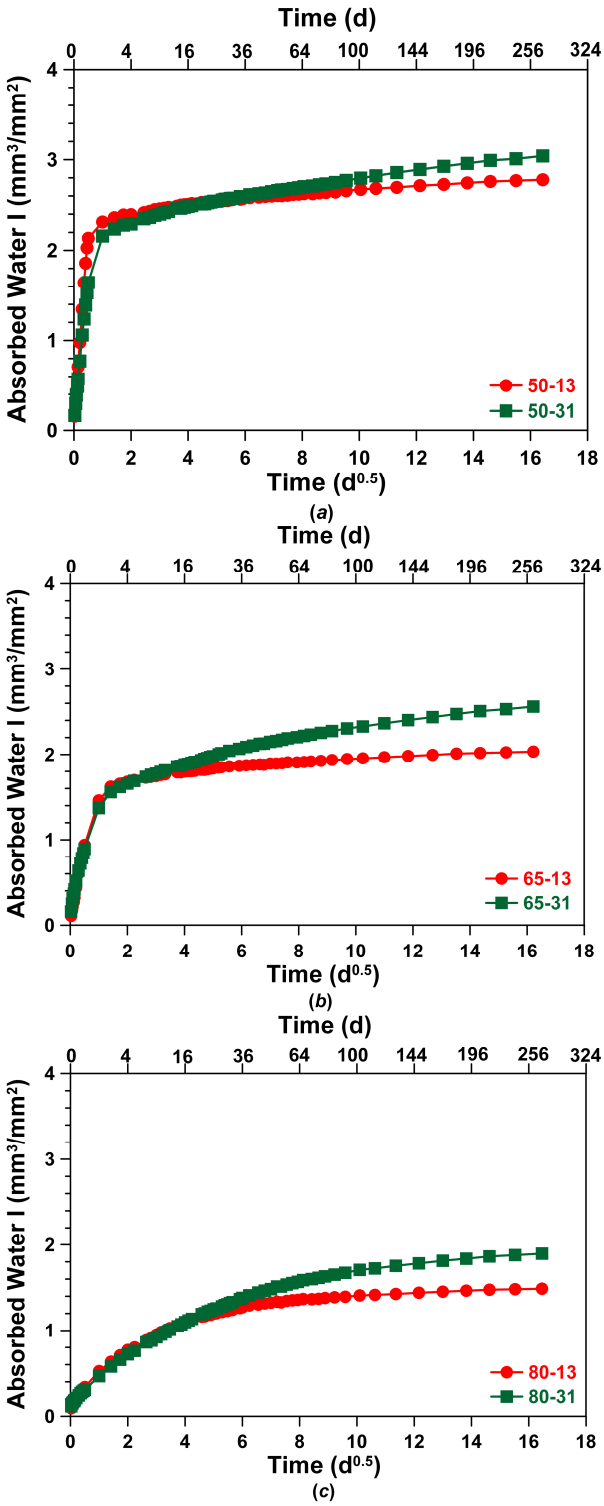

Fig. 7 Effect of air content and initial moisture on water absorbed: (*a*) 50% RH (*b*) 65% RH (*c*) 80% RH

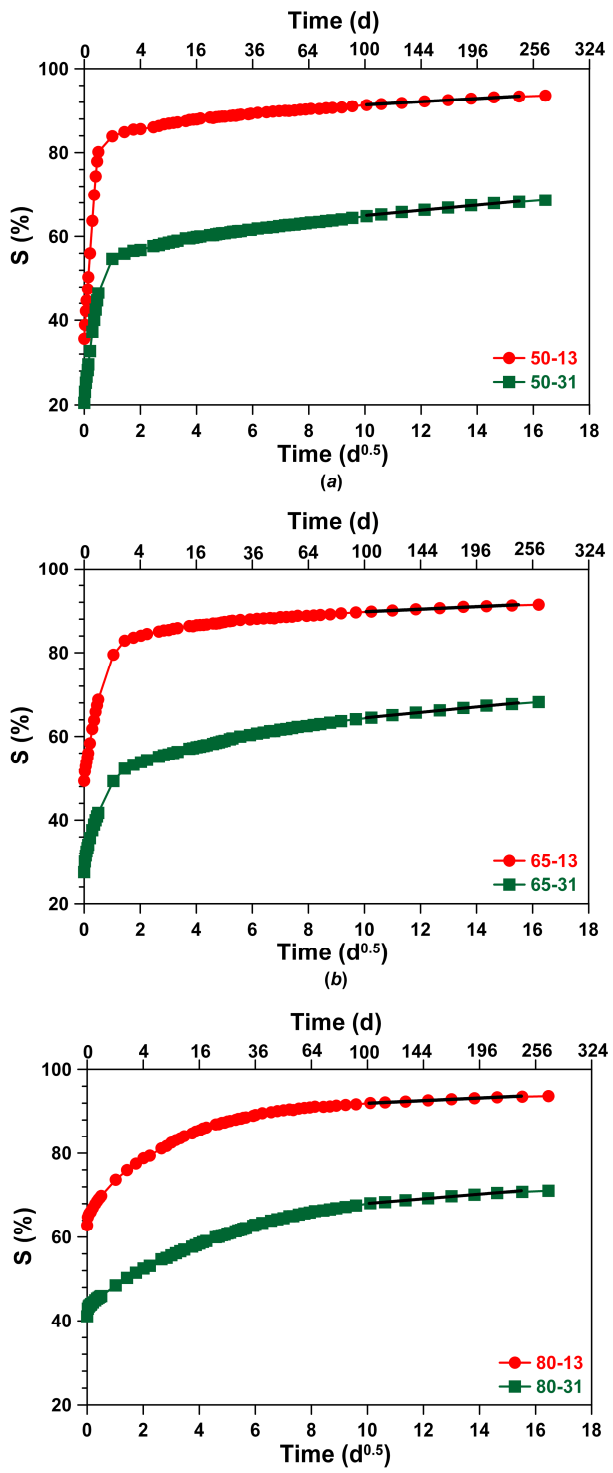

Fig. 8 Results of sorption test provided as increase in the degree of saturation: (*a*) 50% RH (*b*) 65% RH (*c*) 80% RH

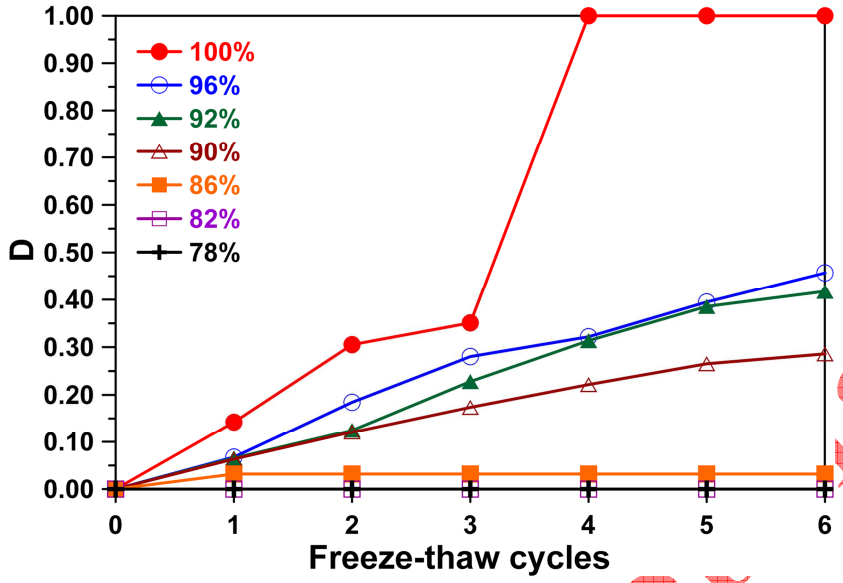

Fig. 9 Decrease of the relative dynamic elastic modulus with freeze-thaw cycles

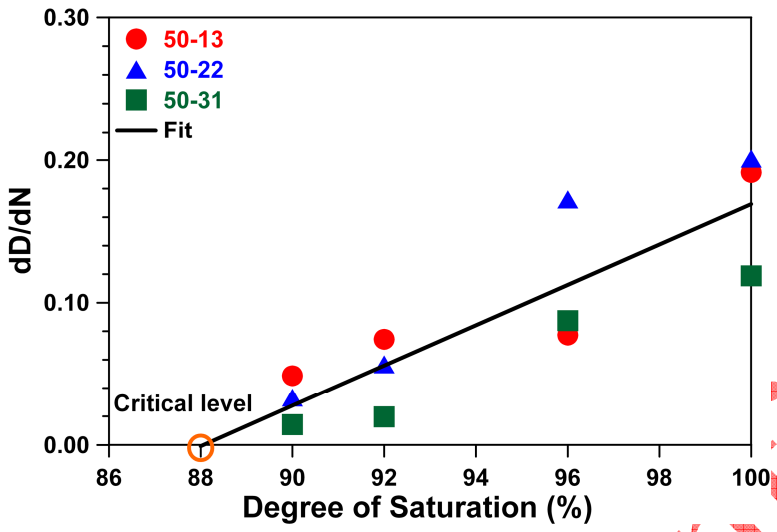

Fig. 10 Rate of decrease of relative dynamic elastic modulus with degree of saturation

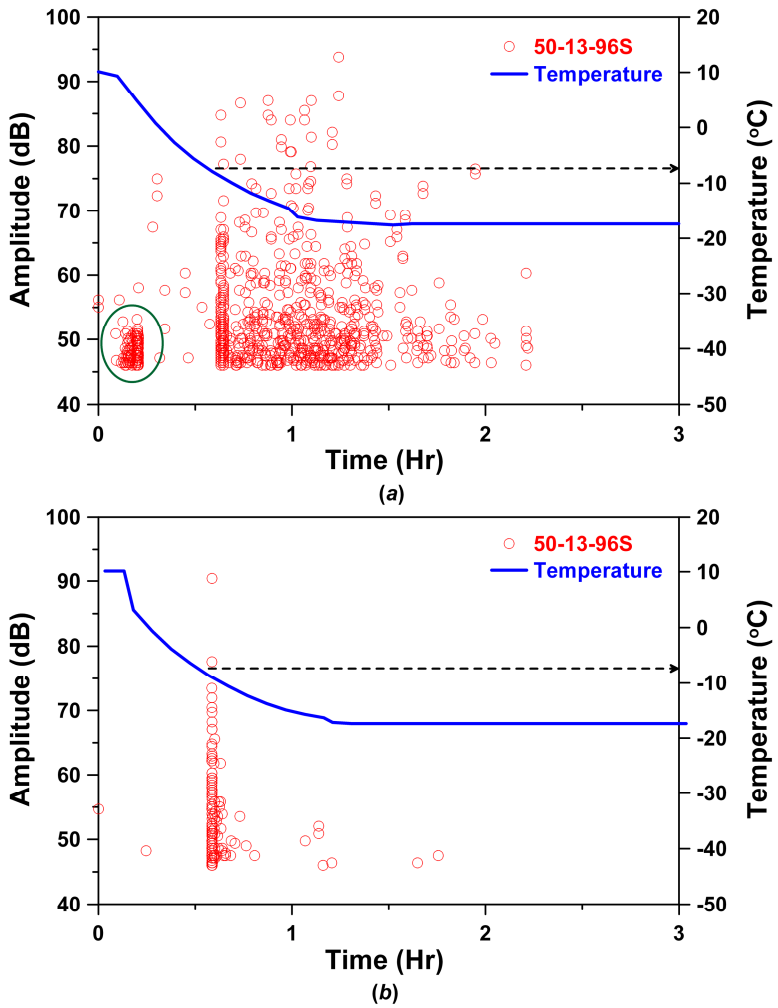

Fig. 11 Amplitude in the transition time of freezing (96*S*): (*a*) first cycle (*b*) second cycle

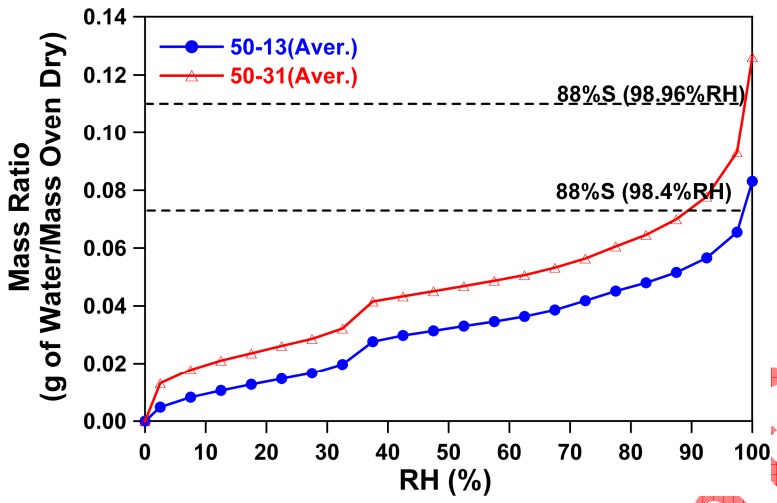

Fig. 12 Mass change at decreasing RH containing de-ionized water

Elsevier Editorial System(tm) for Cement and Concrete Composites
Manuscript Draft

Manuscript Number: CCC-D-10-00479

Title: Effect of sample conditioning on the water absorption of concrete

Article Type: Research Paper

Keywords: Water absorption; Sample conditioning; Moisture effect; Relative humidity

Corresponding Author: Mr. Javier Castro,

Corresponding Author's Institution: Purdue University

First Author: Javier Castro

Order of Authors: Javier Castro; Dale Bentz; Jason Weiss

Abstract: ASTM C1585 is commonly used to determine the absorption and rate of absorption of water in unsaturated hydraulic cement concretes. ASTM C1585 preconditions the samples for a total of 18 days. Unfortunately, the range of relative humidities that can exist in the samples after this relatively short conditioning period may provide a wide enough variation to considerably influence the results of the test. Three main variables were studied in this program to assess the effect of preconditioning. First, the role of water to cement ratio was investigated by testing mortar samples with 55 % aggregate by volume with four different water-to-cement ratios (w/c of 0.35, 0.40, 0.45 and 0.50). Second, the role of paste volume was investigated by considering samples with 55 %, 45 %, and 35 % aggregate by volume with a w/c = 0.50. Finally, the effect of conditioning was assessed by exposing all the samples in three different relative humidities (50 %, 65 % and 80 %) until they reached mass equilibrium (defined as a change of mass less than 0.02 % over 15 days), taking approximately 14 months. Oven dry samples were also prepared and tested for comparison. The results confirm that water absorption testing is considerably influenced by sample preparation. Samples conditioned at 50 % relative humidity can show up to six times greater total absorption than similar samples conditioned at 80 % relative humidity. Samples that were conditioned in the oven at 105 °C do not appear to follow a similar trend when compared with specimens conditioned in chambers for the longer duration. The absorption is also influenced by the volume of paste in the samples. The experiments show that a lack of control on moisture content or lack of consideration of the material composition may lead to a misunderstanding of the actual absorption behavior.

Javier Castro
Purdue University
School of Civil Engineering
550 Stadium Mall
West Lafayette, IN, 47907
765-494-7999
Email: jcastro@purdue.edu

Dear Editor:

Enclosed for your consideration in an original research article, entitled "**Effect of sample conditioning on the water absorption of concrete**". A brief description of this paper is provided below.

Best regards,

Javier Castro

Brief description of the present work:

ASTM C1585 is commonly used to determine the absorption of water in unsaturated hydraulic cement concretes. Unfortunately, the initial moisture content that can exist in the samples after the samples preparation may provide a wide enough variation to considerably influence the results of the test. This paper provides a series of measurements to evaluate the role of the relative humidity of the samples prior the test. The role of the w/c and the cement paste volume were also evaluated. The results of this research confirm that water absorption testing is considerably influenced by sample preparation, the w/c and by the volume of paste in the samples. The experiments show that a lack of control on moisture content or lack of consideration of the material composition may lead to a misunderstanding of the actual absorption behavior.

Effect of sample conditioning on the water absorption of concrete

Javier Castro
Graduate Research Assistant and Ph.D. Candidate
School of Civil Engineering
Purdue University
School of Civil Engineering
550 Stadium Mall, West Lafayette, IN 47907-2051, USA
E-mail: jcastro@purdue.edu
Phone: (765) 494-7999

Dale Bentz
Chemical Engineer
National Institute of Standards and Technology
Materials and Construction Research Division
Building and Fire Research Laboratory
100 Bureau Drive, Stop 8615, Gaithersburg, MD 20899-8615, USA
E-mail: dale.bentz@nist.gov
Phone: (301) 975-5865

Jason Weiss
Professor and Director of Pankow Materials Laboratory
Associate Director of the Center for Advanced Cement Based Materials
School of Civil Engineering
Purdue University
School of Civil Engineering
550 Stadium Mall, West Lafayette, IN 47907-2051, USA
E-mail: wjweiss@purdue.edu
Phone: (765) 494-2215

1. Introduction

The durability of concrete subjected to aggressive environments depends largely on transport properties, which are influenced by the pore system [1-7]. Three main mechanisms can be used to describe transport in cementitious systems: permeability, diffusion and absorption. Permeability is the measure of the flow of water under a pressure gradient, while diffusion is the movement of ions due to a concentration gradient. Absorption can be described as the ability to take in water by means of capillary suction. All three mechanisms are heavily influenced by the volume of pores as well as the connectivity of the pore network. A large fraction of concrete in service is only partly saturated and the initial ingress of water and dissolved salts is influenced, at least in part, by capillary absorption [7]. As such, water absorption has been used as an important factor for quantifying the durability of cementitious systems [4-11]. Water absorption is the primary focus of this study since it is being increasingly used by specifiers and in forensic studies to provide a parameter that can describe an aspect of concrete durability. It is also important that these properties be adequately described for use in service life models [6, 11].

1.1 Water absorption test

ASTM C1585 [1] is commonly used to determine the absorption and rate of absorption (commonly referred to as sorptivity) of water in unsaturated hydraulic cement concretes. This test method, based on work reviewed by Hall [12], consists of preconditioning samples to a known moisture content, then exposing the bottom surface of the sample to liquid water and measuring the increase in mass resulting from water absorption. According to the standard conditioning procedure, samples are conditioned for 18 days. This conditioning period begins by first placing the sample in a 50˚C and 80 % relative humidity (RH) environment for three days. The samples are then removed from this environment and placed in individually sealed containers where they remain for a minimum 15 days at 23 °C, to allow internal moisture to redistribute throughout the specimens before the test begins.

The absorption test involves recording incremental mass change measurements at relatively frequent intervals during the first six hours after the sample comes in contact with water and subsequently taking one measurement every day for the next eight days. The amount of absorbed water is normalized by the cross-section area of the specimen exposed to the fluid using Equation 1:

$$i = \frac{m_t}{(a \cdot \rho)} \qquad (1)$$

where: i is the normalized absorbed fluid volume, m_t is the change in specimen mass at time t; a is the area of the specimen exposed to the fluid (i.e., that of the bottom face), and ρ is the density of the absorbed fluid (taken to be 1000 kg/m^3 at 23 °C for water).

These absorbed fluid volumes are then plotted as a function of the square root of time. The initial sorptivity is determined as the slope of the curve during the first six hours, while secondary sorptivity is determined using the slope of the same measurements between one and eight days, as outlined in ASTM C1585 (1). It should be noted that these times work well for

water though they may not work as well for other fluids with different surface tension and/or viscosity [13].

The initial and secondary sorptivities can be used to evaluate the connectivity of the pore network [9]. Additionally, the secondary sorptivity, combined with exposure conditions, has been used for performing service life predictions [11].

1.2 The role of the relative humidity

Water ingress in unsaturated concrete is dominated by capillary suction upon initial contact with water [7, 12-18]. Capillary absorption can be related to the volume of the pores as well as the size (i.e. radius) of the partially empty capillary pores (Figure 1a). The relation between the equilibrated relative humidity and the radius of the smallest empty pore is given by the Kelvin-Laplace equation (Equation 2).

$$\mathrm{Ln}\,(RH) = \frac{2\,\sigma\,\mathrm{V_m}}{r_m\,R\,T} \qquad (2)$$

where: RH is the relative humidity, σ is the surface tension of water (pore solution), V_m is the molar volume of water, r_m is the average radius of curvature, R is the universal gas constant, and T is the absolute temperature.

It should be noted that this expression is simplified as it does not consider the effect of water that is absorbed on the walls of the pores. Largely the concrete community has considered two sizes of pores as introduced by Powers [19]. The gel pores are considered to be small pores (< 10 nm diameter) that are a part of the hydration products. Capillary pores are larger pores that occur due to excess water. Capillary porosity is particularly of concern in transport, as is the interconnectivity of the capillary pores.

Figure 1b) shows a conceptual illustration based on Powers [19] that uses a desorption isotherm to illustrate the volume of water located in the different size pores at different relative humidities.

The relative humidity used to condition the sample prior to the sorption test can have a significant impact on the results [1]. Previous test results by Parrot [20, 21] indicated that the water absorption rate was very sensitive to the moisture content of the concrete, particularly at relative humidities above 60 % which were common for field exposure. Water leaves the largest accessible pores first. It can be seen from Figure 1b that capillary pores occupy the range of humidity from approximately 80% to 100% RH. As such, initially upon drying water leaves the capillary pores. The lower the relative humidity, the greater the total volume of pores that are empty and available to be filled with water during the sorption test. Further, the lower humidity will empty smaller pores, creating a higher suction force in the materials and resulting in a greater sorption rate and a larger overall total absorption.

According to ASTM C1585, the standardized test conditioning will generally provide an internal relative humidity similar to relative humidities found near the surface in some field concrete

structures [1, 22, 23]. This range of relative humidities can represent what is found in samples in the field; however, it is wide enough to considerably affect the test results.

Castro et al. [24] shows that the relative humidity of samples that were kept in the field under different exposure conditions was in the range of 80 % to 100 % depending on the type of exposure, which is somewhat higher than what is mentioned in ASTM C1585.

1.3 Research objectives

The objectives of this research are threefold. First, this research will examine the influence of conditioning relative humidity (oven dry, 50%, 65% and 80% RH) on the results of sorption tests performed on mortars with different *w/c*, containing a fixed volume of aggregate. Second, this research will examine the influence of the volume of aggregate (or equivalently the paste content) on the results of sorption testing. Third, this research will examine the effect of the conditioning method specified in ASTM C1585-04.

2. Materials

An ASTM C150 Type I ordinary portland cement (OPC) was used in this study, with a Blaine fineness of 370 m^2/kg and an estimated Bogue composition of 56 % C_3S, 16 % C_2S, 12 % C_3A, 7 % C_4AF and a Na_2O equivalent of 0.68 % by mass.

A polycarboxylate-based high-range water-reducing admixture (HRWRA) was added in varying rates as indicated in Table 1, depending on the mixture proportions, to maintain similar consistencies (i.e., workability). The sand used was natural river sand with a fineness modulus of 2.71, an apparent specific gravity of 2.58, and a water absorption of 1.8 % by mass.

2.1 Mixture proportioning

Six different mixtures were prepared in total. Four of the mixtures were mortars with a single volume fraction of fine aggregate (55% of the total volume) and different *w/c* (0.35, 0.40, 0.45, and 0.50). These mixtures were designated as 55/0.35, 55/0.40, 55/0.45 and 55/0.50, with the number on the left representing the volume fraction of fine aggregate and the number on the right representing *w/c*. Additionally, two other mortars were prepared with *w/c* of 0.50, but with different volume fractions of fine aggregate (35 % and 45 % of the total volume). They were designated as 35/0.50, 45/0.50. A list of the mixture proportions can be found in Table 1.

2.2 Mixing procedure

The mixing procedure used for the mortar was in accordance with ASTM C192-06 [25]. The aggregate was oven dried and cooled for 24 h before mixing. The volume of water was corrected by the absorption of the aggregate. The water and cement were conditioned for 24 h at room temperature prior to mixing.

3. Experimental method

Six 100 mm × 200 mm cylinders were cast for each mixture. After one day of curing, the samples were demolded and then sealed in double plastic bags for sealed curing. Bags were stored in a room at 23 ± 1 °C until samples reached an age of 28 d. After that, cylinders were removed from bags and three 50 mm ± 2 mm thick samples were cut from the central portion of each cylinder with a wet saw using water as the cooling fluid.

After cutting, samples were conditioned by placing them in environmental chambers at 23 ± 0.5 °C. Specimens from mixtures 55/0.35, 55/0.40, 55/0.45 and 55/0.50 were placed in environmental chambers at three different relative humidities (50 ± 1 %, 65 ± 1 % and 80 ± 1 %). Specimens from mixtures 35/0.50 and 45/0.50 were placed in an environmental chamber at 50 ± 1 % relative humidity. Samples were kept in the environmental chamber until they reached mass equilibrium, defined as a mass change of less than 0.02 % over a 15 day period. Mixture 55/0.35 placed at 50 ± 1 % relative humidity required the longest period of time (14 months) to reach mass equilibrium. However, all samples were maintained in the chambers for 14 months to test them all at the same age.

Additional specimens from mixtures 55/0.35, 55/0.40, 55/0.45 and 55/0.50 were placed at 50 ± 1 % RH. After the 14 months, these specimens were dried in an oven at 105 ± 2 °C until they reached mass equilibrium.

Once the samples were removed from the chambers or from the oven, the side surface (i.e. outer circumference) was sealed with epoxy and the top surface was covered with plastic to avoid evaporation from the sample during testing. After the samples were prepared, testing occurred in accordance with ASTM C1585-04 [1]. Specimens from mixtures 55/0.35, 55/0.40, 55/0.45 and 55/0.50 were tested over a period of 90 days. Specimens from mixtures 35/0.50 and 45/0.50 were tested over a period of 8 days.

Two additional 100 mm × 200 mm cylinders were cast for each mortar mixture. After one day of curing, the samples were demolded and then sealed in double plastic bags for sealed curing. Bags were stored in a room at 23 ± 1 °C until samples reached an age of 28 d. After that, cylinders were removed from bags and 10 mm ± 2 mm thick samples were cut from the central portion of each cylinder with a wet saw. After cutting, mortar samples were vacuum saturated for 24 h. After that, specimens were placed in environmental chambers at six different relative humidities (93 ± 1 %, 87 ± 1 %, 80 ± 1 %, 75 ± 1 %, 65 ± 1 % and 50 ± 1 %) to determine their desorption isotherms.

4. Experimental results and discussion

4.1 Desorption isotherms

Figure 2 shows the desorption isotherm curves measured using 10 mm thick samples. Mass change was monitored at regular intervals until it reached equilibrium, defined as a mass change

of less than 0.02 % over a 15 day period. At the end, all samples were oven dried to express water absorption in terms of the dry mass of the sample.

It can be noticed that while the values of the moisture content are similar at 50% and lower RH (lower RH results not shown in Figure 2), as it refers to the small gel pore system [19], the capillary pores at high RH are strongly influenced by the *w/c*.

4.2 Effect of initial conditioning on water absorption tests

4.2.1 Effects of relative humidity on sorption test

Figure 3 shows the absorbed water during the 90 days of testing performed on mortars conditioned at different relative humidities (mixtures 55/0.35, 55/0.40, 55/0.45 and 55/0.50). It can be noticed that the water absorption is very sensitive to the relative humidity at which the specimens were pre-conditioned before testing. In each case, as the conditioning relative humidity increases, more water is retained in the pore system and thus the absorption decreases.

These results can be viewed in a slightly different manner if they include the initial amount of water held in the pores before the test. In order to do this, samples were oven dried at the end of the sorption test to calculate the amount of water they held before starting the test. Additional specimens that were kept at 50 ± 1 % RH during the 14 months were oven dried and then saturated by the procedure described in ASTM C642-07 [26] to measure the total amount of interconnected porosity in the systems. Results from Figure 3 were then normalized by the total amount of pores in the system, which can be viewed as the degree of saturation of the sample as a function of time. This is presented in Figure 4. Figure 5 shows the total degree of saturation for the samples after 90 days.

Figures 4 and 5 show that samples prepared at different relative humidities with a low *w/c* (e.g. *w/c* = 0.35) do not reach values near to saturation even after 90 days of being in contact with water. It may be attributed to the refined pore network of this low *w/c* system which makes it difficult for water to move through the sample to fill all the pores. This is commonly referred to as depercolation, which occurs after different hydration times for different *w/c* [27].

In contrast after 90 days, samples prepared with a higher *w/c* (e.g. *w/c* = 0.50) reach much higher levels of saturation. It can be noted from Figure 4 that samples conditioned at 50 % RH reach values near saturation after about 40 days of testing, similar to what is obtained with oven dry samples. Again this may be attributed to the connectivity of the pore network and the size of these pores. In this case, a more interconnected pore network will facilitate the movement of water to the interior of the specimens and the diffusion of water vapor out of the sample. However, when these samples were conditioned at higher relative humilities (65 and 80 % RH), the amount of initially retained water is high enough to reduce the diffusion of vapor out of the sample. As a result, this may explain why the level of saturation of these specimens is lower.

4.2.2 Effects of relative humidity on the amount of absorbed water after 8 days

Figure 6 shows the cumulative water that was absorbed after 8 days of testing performed on mortars conditioned at different relative humidities, expressed as a function of *w/c* (Figure 6a) and as a function of the relative humidity (Figure 6b).

Figure 6a) shows that mixture 55/0.50 can exhibit six times higher absorption when the samples are conditioned at 50 % RH compared with similar samples conditioned at 80 % RH.

Figure 7 shows a normalization of the data presented in Figure 6. In Figure 7a) the normalization is made with respect to the absorption of samples with *w/c* = 0.35 (mixture 55/0.35). In Figure 7b) the normalization is made with respect to the absorption of samples conditioned at 50 % relative humidity. It can be seen that the values follow a consistent trend in each case, except for the oven dry samples. This is in general agreement with the parallel nature of the desorption isotherms for the mortars provided in Figure 2.

4.2.3 Effects of relative humidity on initial sorptivity

Figure 8 shows the initial sorptivity calculated as the slope of the absorption vs. the square root of time during the first six hours of test [1].

Figure 8a) shows that mixture 55/0.50 can exhibit a ten times higher initial sorptivity when the samples are conditioned at 50 % RH compared with similar samples conditioned at 80 % RH.

It needs to be noted that the oven dry samples show a much higher initial sorptivity, due to the fact that the gel's capillary pores are empty and possibly to microcracking. While the increase in sorptivity is observed to be linear for the specimens conditioned at 50%, 65% and 80% relative humidity, this trend appears to break down for the oven dry samples which may be attributed to micro-cracking generated during the sample preparation [28-32].

4.2.4 Effects of relative humidity on secondary sorptivity

Figure 9 shows the secondary sorptivity calculated as the slope of the absorption vs. the square root of time between 1 d and 8 d of testing. Trends are similar to those observed for the initial sorptivity. However, it needs to be noted that samples that were oven dry prior to the test present a considerably lower secondary absorption with respect to the samples conditioned in environmental chambers. This may be explained by the high initial absorption of the oven dry samples shown in Figure 8. During this initial absorption it can be noticed that since a majority of the water was already absorbed in the first hours of the test, the secondary rate of absorption will be much lower. It can also be expected that microcracking enabled a more rapid ingress of water [33].

Figure 9 shows a similar trend to what was noted in the case of total absorption and initial sorptivity, namely that the secondary sorptivity of samples conditioned in chambers exhibits a consistent trend when the results are plotted against the w/c or the relative humidity at which

samples were conditioned. However, samples that are conditioned by drying them in an oven at 105 °C do not follow the same tendency.

4.3 Effects of initial moisture of samples on ASTM C1585 conditioning method

At the age of 24 months, samples from each mixture conditioned at the three different relative humidities were removed from the chambers. The side surface was sealed with epoxy to be then "re-conditioned" using the 18 day procedure described in ASTM C1585. In addition, three other samples from each mixture were saturated following the procedure described in ASTM C642 [26], to then be "re-conditioned" following the same 18 day procedure. While such a resaturation procedure was employed in the initial sorption testing upon which the ASTM C1585 standard was based [34], it was subsequently omitted from the standard. After samples were fully prepared, testing was performed in accordance with ASTM C1585 over a period of 8 days, with results provided in Figure 10. In addition, Figure 11 shows the calculated initial and secondary sorptivities from these tests. Secondary sorptivity values are not reported when the correlation coefficient is lower than 0.98.

Figures 10 and 11 show that the 3 days of controlled drying at 50 ± 2 °C and 80 % RH followed by the 15 days for internal moisture equilibration is not capable of eliminating the effects of the "moisture history". These results suggest that the ASTM C1585 preparation method does not prepare all the samples to the same water content before a water absorption test. As such this accelerated method can make a substantial difference in how the data is interpreted. This may be due to a moisture hysteresis effect [35]. It should be noted that this can be a concern for field samples evaluated using this method, as their as-received relative humidities may easily vary between the extremes examined in this study.

4.4 Effects of volume of aggregate on sorption test

Figure 12 shows the absorbed water during 8 days of testing performed on mortars containing different volumes of aggregate (mixtures 55/0.50, 45/0.50 and 35/0.50) conditioned at 50 % relative humidity. In Figure 12 a) the effect of a higher volume of paste is observed as the mixture containing the lower volume of aggregate has the higher absorption. However, when the results are normalized by the volume of paste (volume of the main absorbent material), a reversal in the order of the samples is observed (Figure 12 b). The samples with the higher volume of aggregates have a higher absorption.

Water absorption is typically reported without considering the effect of the absorption of the aggregate in the samples. To better understand its effect, Figure 13 was calculated assuming five different sand absorptions (0.0 %, 0.6 %, 1.2 %, 1.8 %, and 2.4 %) to then subtract these values from the absorption in Figure 12 b). When the sand absorption is assumed to be 0.0 %, the resulting absorption at 8 days will be the same as the absorption presented in Figure 12 b). From Figure 13, it can be noticed that for the assumed 1.8 % sand absorption, the normalized water absorbed for the sample is the same after 8 days, independent of the amount of aggregate in the sample.

Figure 14 shows a desorption isotherm for the sand used in these mixtures. It can be noted that at 50 % RH (humidity at which the samples were conditioned), the amount of water on the sand is about 0.2%. Considering that the aggregate used in this study has a 24 h absorption of 1.8%, the difference on water absorption of samples containing different amounts of aggregate can be explained mainly by the amount of water absorbed by the aggregates.

5. Conclusions

This paper has described the absorption behavior of mortars conditioned at different relative humidities. As was shown in previous works by Hall [12], Hooton et al. [4, 7] and Martys and Ferraris [16, 34], the water absorption test is considerably affected by the relative humidity of the samples before starting the test, which if not properly accounted for can lead to a misunderstanding of the actual absorption behavior. Samples conditioned at a 50 % relative humidity can show a total absorption that is approximately six times greater than similar samples conditioned at 80 % relative humidity. This is consistent with expectations based on the mortars' desorption curves.

Initial sorptivity, secondary sorptivity and total absorption at 8 days for samples conditioned in chambers show a linear trend related to the *w/c* and the relative humidity at which samples were conditioned. Samples that are conditioned by drying in an oven at 105 °C do not follow the same trend as samples conditioned in other approaches. This is attributed to two factors: 1) emptying of a wider range of pores, and 2) the potential for microcracking. The conditioning procedure described in ASTM C1585-04 is not able to eliminate the "moisture history" of the samples, and thus can lead to a misunderstanding of the water absorption test results, especially in field samples which have obtained a lower relative humidity. It is recommended that field samples be pre-saturated prior to being exposed to the conditioning regimen of ASTM C1585.

Comparing samples containing different volumes of aggregate can also lead to a misunderstanding of the actual absorption behavior. Samples containing higher volumes of cement paste will absorb more water. When the results are normalized by the volume of cement paste, the sample containing lower volumes of cement paste will absorb more water. However, for the materials examined in this study, this difference can be mainly explained by the amount of water absorbed by the aggregates in the sample.

Acknowledgments

This work was supported in part by the Joint Transportation Research Program administered by the Indiana Department of Transportation and Purdue University (Project SPR 3093). The contents of this paper reflect the views of the authors, who are responsible for the facts and the accuracy of the data presented herein, and do not necessarily reflect the official views or policies of the Federal Highway Administration and the Indiana Department of Transportation, nor do the contents constitute a standard, specification, or regulation. The authors gratefully acknowledge support received from the Center for Advanced Cement Based Materials.

References

[1] ASTM International, ASTM C1585. Standard test method for measurement of rate of absorption of water by hydraulic-cement concretes; 2004.

[2] Sabir B, Wild S, O'Farrell M. A water sorptivity test for mortar and concrete. Mater Struct 1998; 31(8): 568-574.

[3] Maltais Y, Samson E, Marchand J. Predicting the durability of Portland cement systems in aggressive environments - laboratory validation. Cement Concrete Res 2004, 34(9); 1579-1589.

[4] Hooton RD, Mesisc T, Beal DL. (1993). Sorptivity testing of concrete as an indicator of concrete durability and curing efficiency. Proceedings of the Third Canadian Symposium on Cement and Concrete, Ottawa, Ontario, 1993; p. 264-275.

[5] Parrot LJ. Water absorption in cover concrete. Mater Struct 1992; 25(5): 284-292.

[6] Fagerlund G. Predicting the service-life of concrete exposed to frost action through a modeling of the water absorption process in the air pore system. The Modeling of Microstructure and its Potential for Studying transport Properties and Durability, Jennings H, Kropp J, Scrivener K, editors. The Netherlands, 1996; p. 503-539.

[7] Hearn N, Hooton D, Mills R. Pore structure and permeability. Significance of Tests and Properties of Concrete and Concrete-Making Materials, ASTM STP 169C. Klieger P, Lamond J, editors; 1994; 240-262.

[8] Henkensiefken R, Castro J, Bentz D, Nantung T, Weiss J. Water Absorption in Internally Cured Mortar Made with Water-Filled Lightweight Aggregate. Cement Concrete Res 2009; 39(10): 883-892.

[9] Neithalath N. Analysis of moisture transport in mortars and concrete using sorption-diffusion approach. ACI Mater J 2006; 103(3): 209-218.

[10] Yang Z. Assessing cumulative damage in concrete and quantifying its influence on life cycle performance modeling. PhD thesis, Purdue University, 2004.

[11] Bentz DP, Ehlen MA, Ferraris CF, Garboczi EJ. Sorptivity-based service life predictions for concrete pavements. Proceedings. 7th international conference on concrete pavements, Orlando FL, 2001; p. 181-193.

[12] Hall C. Water sorptivity of mortars and concretes: a review. Mag Concrete Res 1989; 41(146): 51-61.

[13] Spragg R. Castro J. Li W, Pour-Ghaz M, Huang P, Weiss J. Wetting and drying of concrete in the presence of deicing salt solutions. Submitted to Transportation Research Board 90th annual meeting, 2011.

[14] Yang Z, Weiss J, Olek J. Water absorption in partially saturated fracture concrete. RILEM workshop: transport mechanism in cracked concrete. Ghent, 2007.

[15] Martys NS. Diffusion in partially saturated porous materials. Mater Struct 1999, 32(8): 991-1004.

[16] Martys N. Ferraris CF. Capillary transport in mortar and concrete. Cement Concrete Res 1997; 27(5): 747-760

[17] Lockington D, Parlange JY, Dux P. Sorptivity and the estimation of water penetration into unsaturated concrete. Mater Struct 1999; 32(5): 342-347.

[18] Hall C. Anomalous diffusion in unsaturated flow: fact or fiction?, Cement Concrete Res 2007; 37(3): 378–385.

[19] Powers TC, Brownyard TL. Studies of the physical properties of hardened Portland cement paste. American Concrete Institute Proceedings 1946; 43: 469-482.
[20] Parrott LJ. Moisture conditioning and transport properties of concrete test specimens. Mater Struct 1994; 27(8): 460-468.
[21] Parrott LJ. Factor influencing relative humidity in concrete. Mag Concrete Res 1991; 43(154): 45-52.
[22] DeSouza SJ, Hooton RD, Bickley JA. Evaluation of laboratory drying procedures relevant to field conditions for concrete sorptivity measurements. Cem Concrete Agg 1997; 19(2): 59-63.
[23] DeSouza SJ, Hooton RD, Bickley JA. A field test for evaluating high performance concrete covercrete quality. Can J Civil Eng 1998; 25(3): 551-556.
[24] Castro J, Kompare P, Poursaee P, Nantung T, Weiss J. JTRP Report SPR-3093, Portland cement concrete pavement performance relative to permeability. Indiana Department of Transportation, 2010.
[25] ASTM International, ASTM C305. Standard practice for mechanical mixing of hydraulic cement pastes and mortars of plastic consistency, 2006.
[26] ASTM International ASTM C642. Standard test method for density, absorption, and voids in hardened concrete, 2006.
[27] Powers TC, Copeland LI, Mann HM. Capillary continuity or discontinuity in cement pastes. J. PCA Res. Dev. Lab 1959; 1(2): 38-48.
[28] Hwang C, Young J. Drying shrinkage of portland cement pastes. microcracking during drying. Cement Concrete Res 1984; 14(4): 585-594.
[29] Chatterji S. (1976). “Drying shrinkage of cement paste and concrete: a reappraisal of the measurement technique and its significance. Cement Concrete Res 1976; 6(1): 145-148.
[30] Bisschop J. Van Mier J. How to study drying shrinkage microcracking in cement-based materials using optical and scanning electron microscopy? Cement Concrete Res 2002; 32(2): 279-287.
[31] Samaha H. Hover K. Influence of microcracking on the mass transport properties of concrete. ACI Mater J 1992; 89(4): 416-424.
[32] Yang Z, Weiss J, Olek J. Water transport on concrete damaged by tensile loading and freeze-thaw cycling. J Mater Civil Eng 2006; 18(3): 424-434.
[33] Yang Z. Assessing cumulative damage in concrete and quantifying its influence on life cycle performance modeling. PhD thesis, Purdue University, West Lafayette, Indiana, 2004.
[34] Bentz DP, Ehlen CF, Ferraris CF, Winpigler JA. Service life prediction based on sorptivity for highway concrete exposed to sulfate attack and freeze-thaw conditions, FHWA-RD-01-162, U.S. Department of Transportation, 2002, 62 pp.
[35] Nilsson LO. Hygroscopic moisture in concrete – drying, measurements and related material properties. PhD thesis. Lund University, 1980.

Table

Table 1. Mixture proportions in saturated surface dry (SSD) conditions.

Material	55/0.35	55/0.40	55/0.45	55/0.50	45/0.50	35/0.50
Volume fraction of aggregate	55%	55%	55%	55%	45%	35%
w/c	0.35	0.40	0.45	0.50	0.50	0.50
Cement (kg/m^3)	673	626	585	549	671	793
Water (kg/m^3)	235	250	263	275	336	397
Fine Aggregate (kg/m^3), SSD	1442	1442	1442	1442	1180	918
HRWRA (g/ 100 g cement)	0.60	0.40	0.20	0.00	0.00	0.00

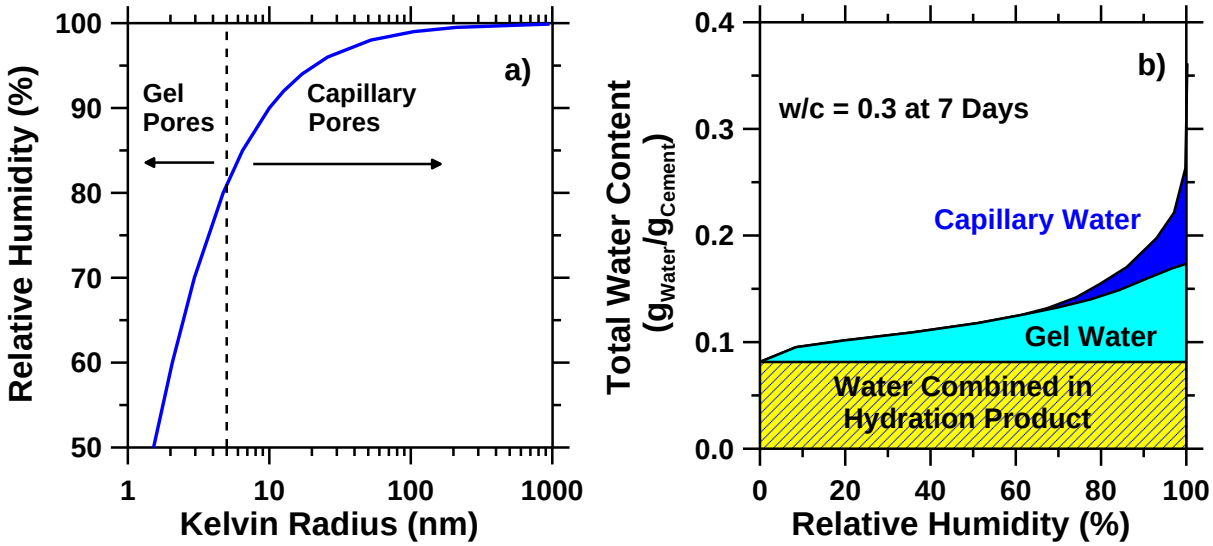

Fig. 1. Relation between relative humidity and partially empty pores in cement paste.

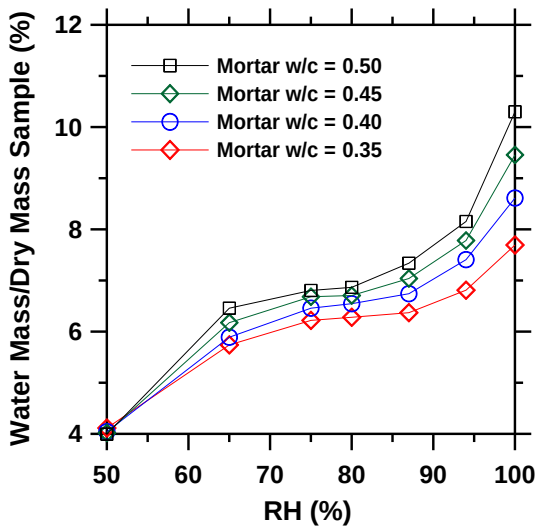

Fig. 2. Desorption curves for 14 m mortar samples (typical standard deviation in the average of 3 samples is lower than 0.2%).

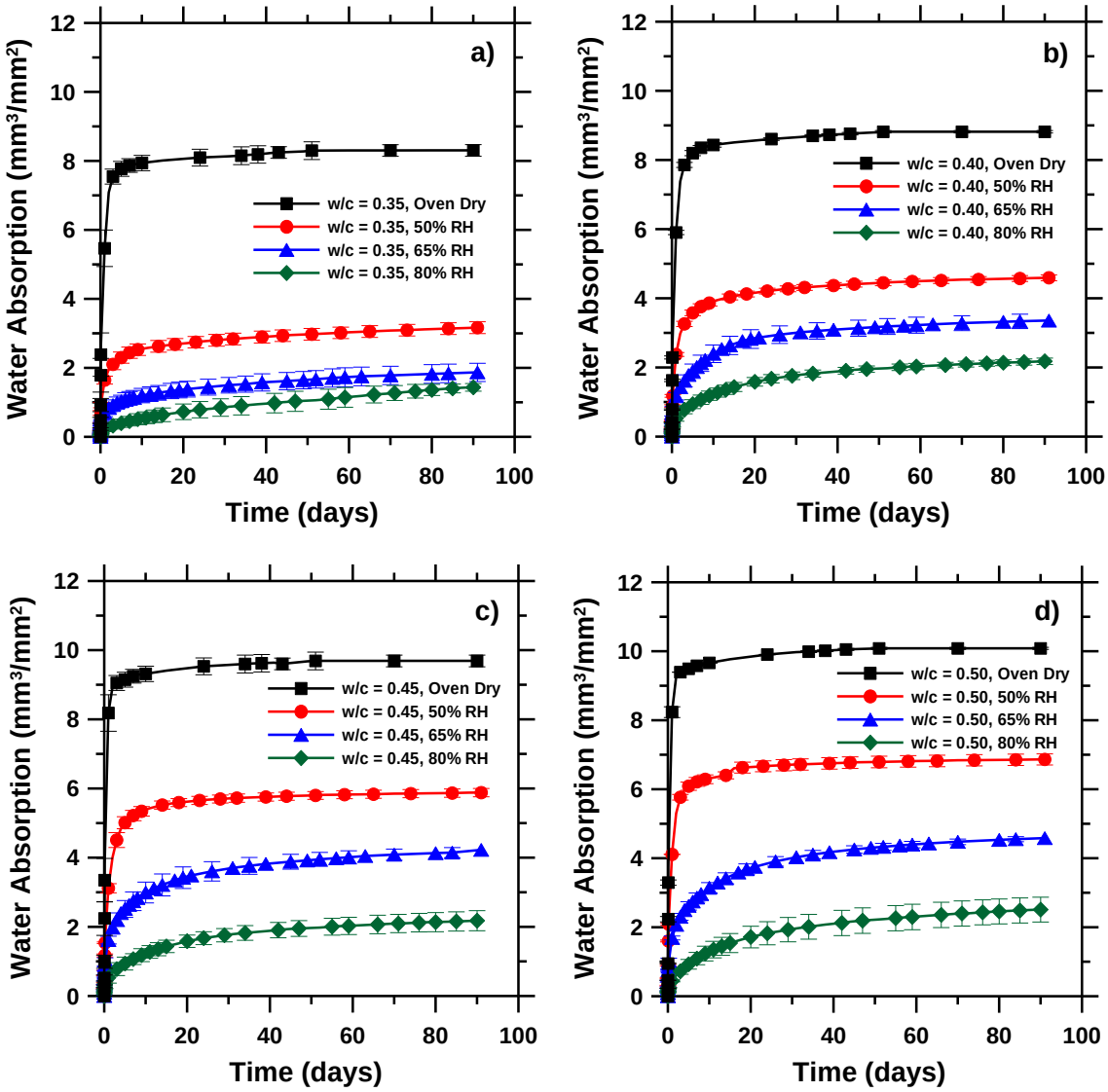

Fig. 3. Absorbed water in mortars as a function of relative humidity a) mixture 55/0.35, b) mixture 55/0.40, c) mixture 55/0.45, d) mixture 55/0.50. Error bars represent the standard deviation for the average of three samples.

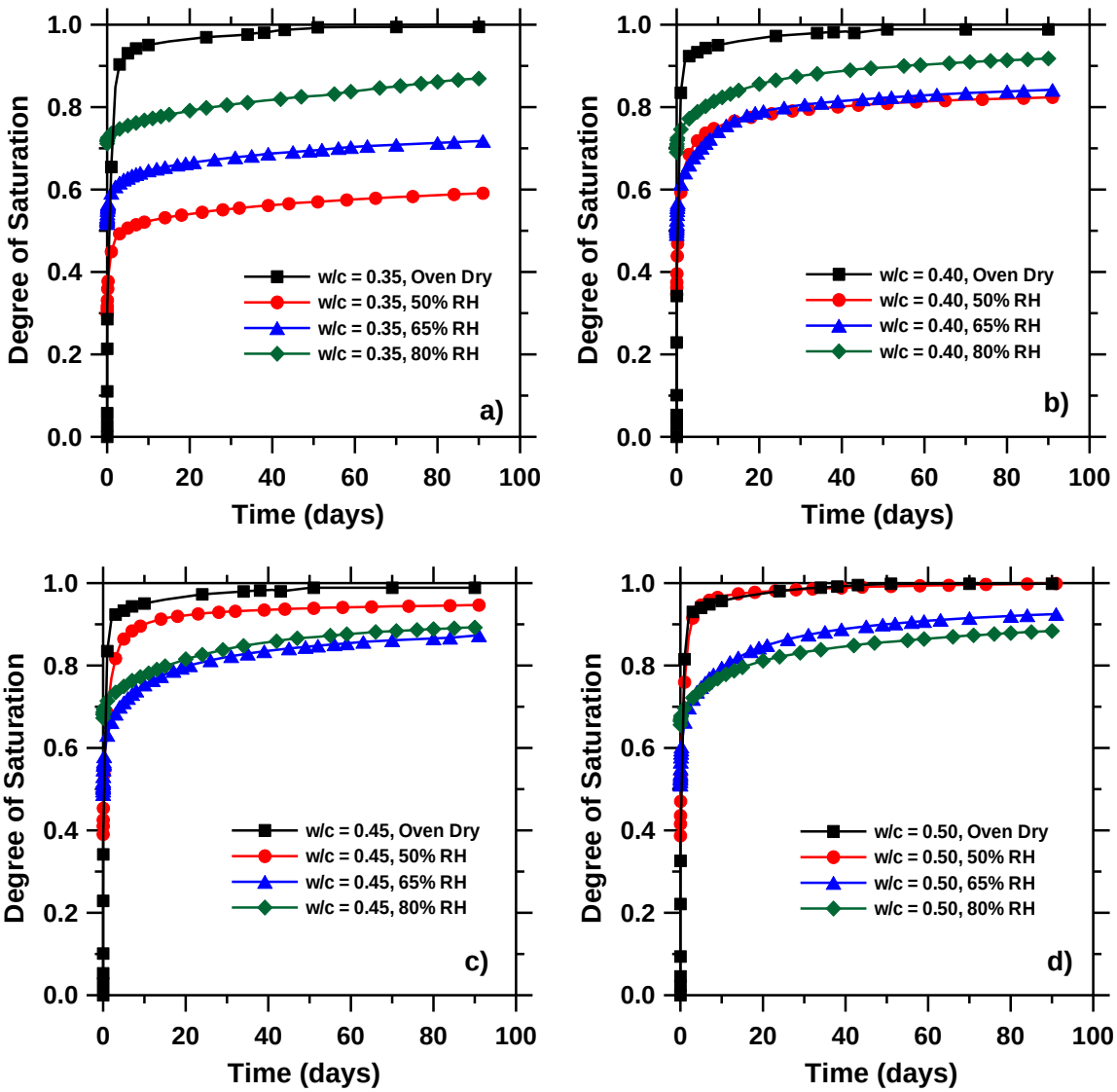

Fig. 4. Degree of saturation as a function of time during the water absorption test: a) mixture 55/0.35, b) mixture 55/0.40, c) mixture 55/0.45, d) mixture 55/0.50. Typical standard deviation of the average of three samples is lower than 0.02 points in the degree of saturation.

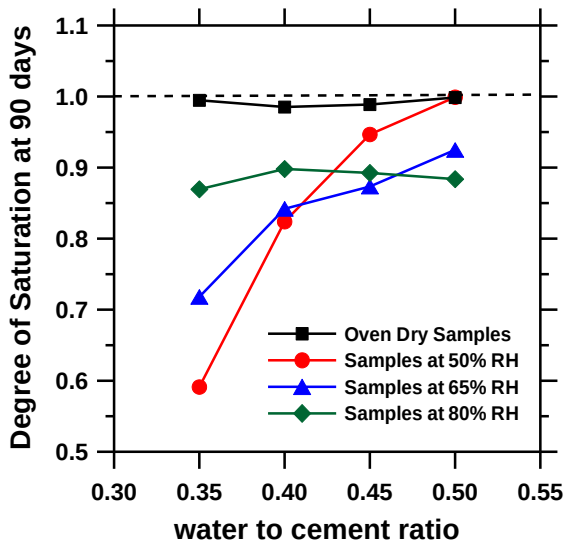

Fig. 5. Degree of saturation after 90 d in contact with water as a function of the *w/c*.

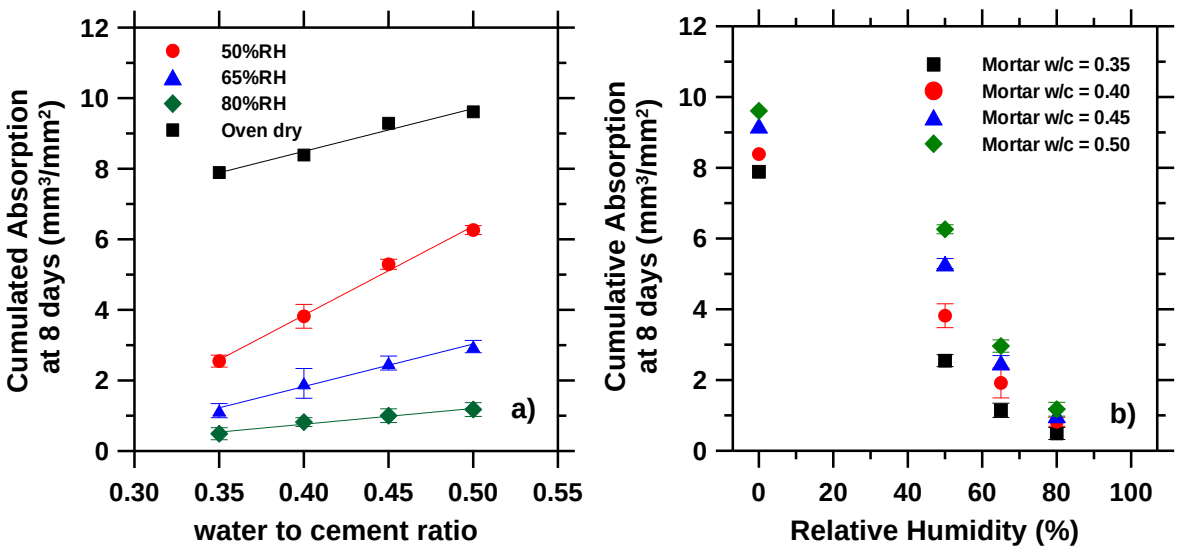

Fig. 6. Cumulative absorption at 8 d for mortars with 55 % aggregates versus: a) *w/c*, b) relative humidity. Solid lines are provided only to show a general tendency in the data. Error bars represent the standard deviation on the average of 3 samples.

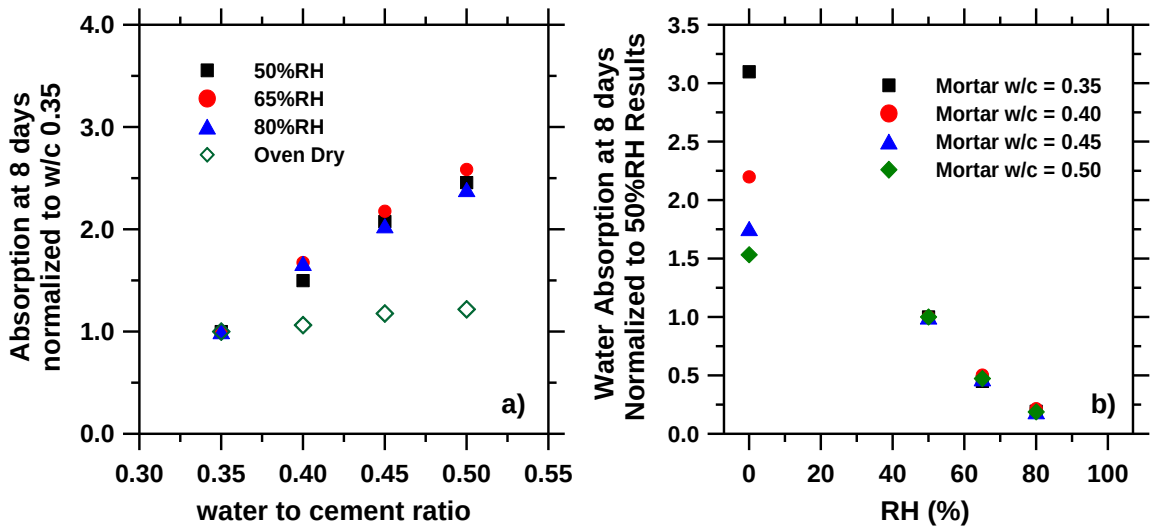

Fig. 7. Cumulative absorption at 8 days versus *w/c* and relative humidity: a) normalized to absorption of mixture 55/0.35, b) normalized to absorption at 50 %RH.

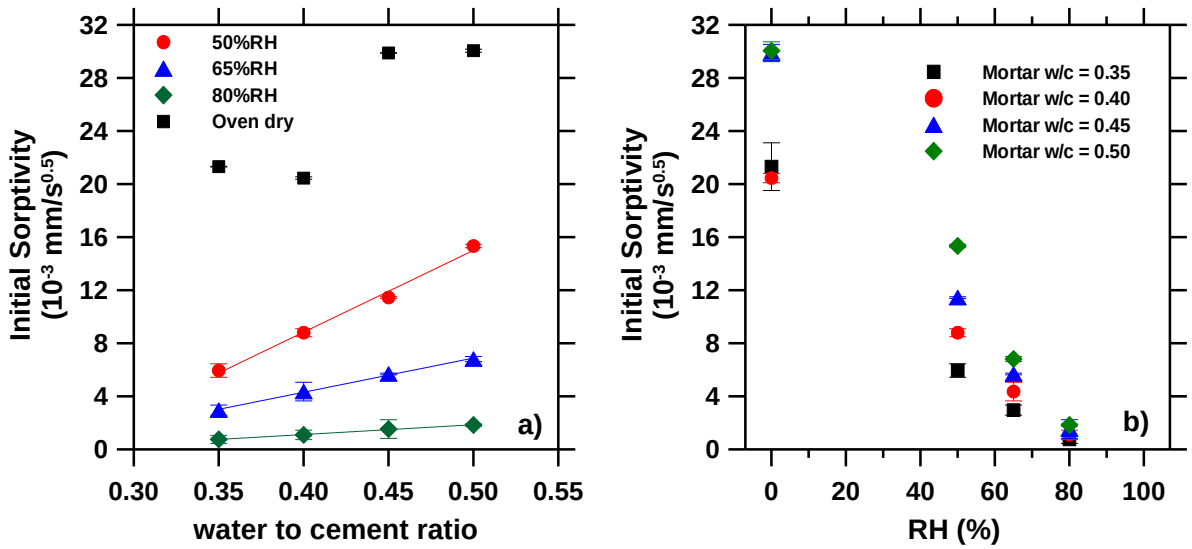

Fig. 8. Initial absorption of the 55 % aggregate mortars conditioned at different RH as a function of: a) *w/c*, b) relative humidity. Solid lines are provided to show a general tendency in the data. Error bars represent the standard deviation on the average of 3 samples.

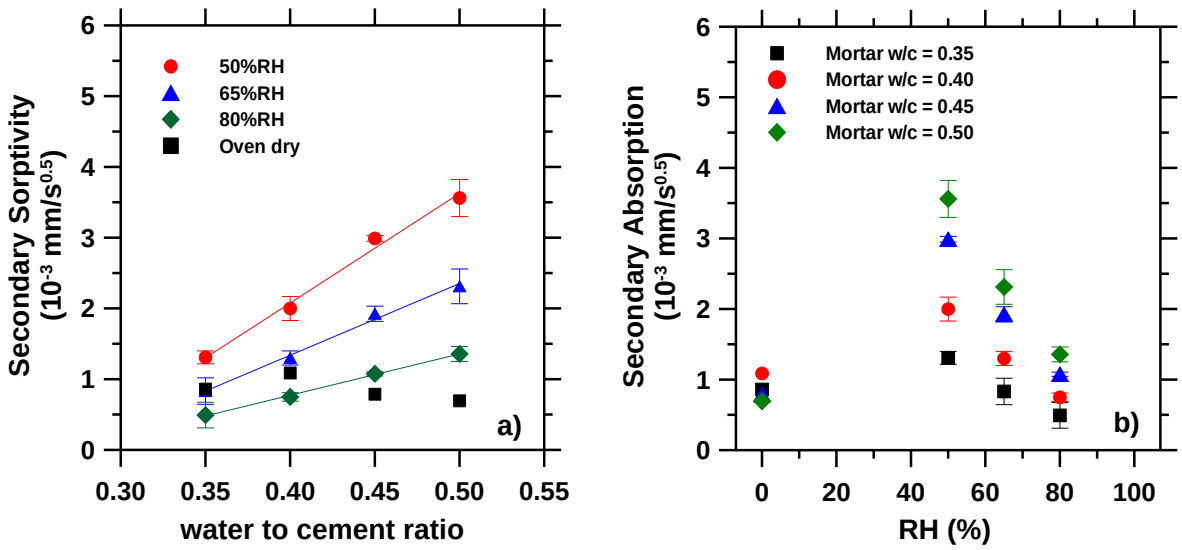

Fig. 9. Secondary absorption on mortars with 55 % aggregates conditioned at different RH as a function of: a) *w/c*, b) relative humidity. Solid lines are provided to show a general tendency in the data. Error bars represent the standard deviation on the average of 3 samples.

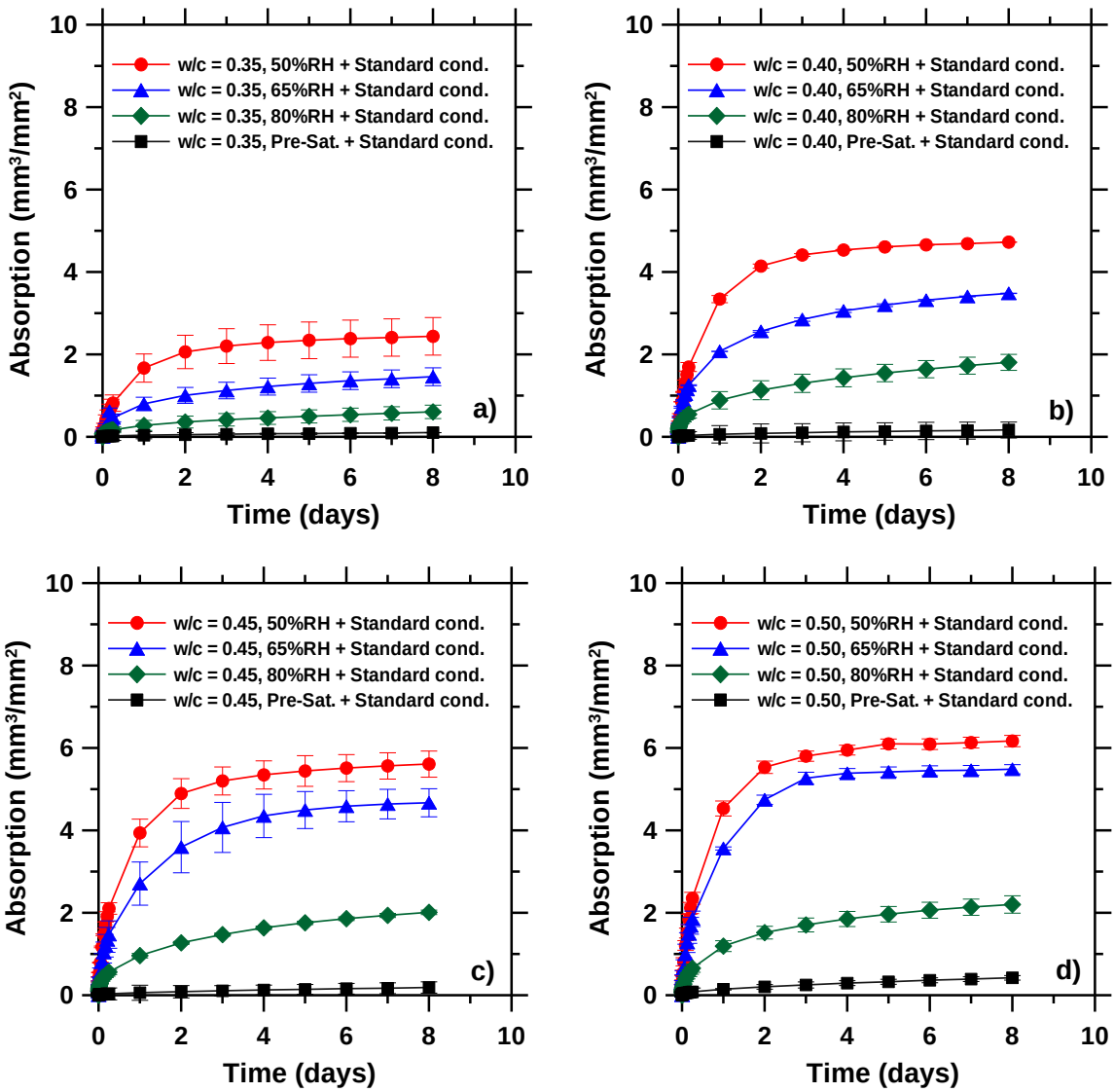

Fig. 10. Effect of initial moisture on the conditioning procedure established in ASTM C1585-04 a) mixture 55/0.35, b) mixture 55/0.40, c) mixture 55/0.45, d) mixture 55/0.50. Error bars represent the standard deviation for the average of three samples.

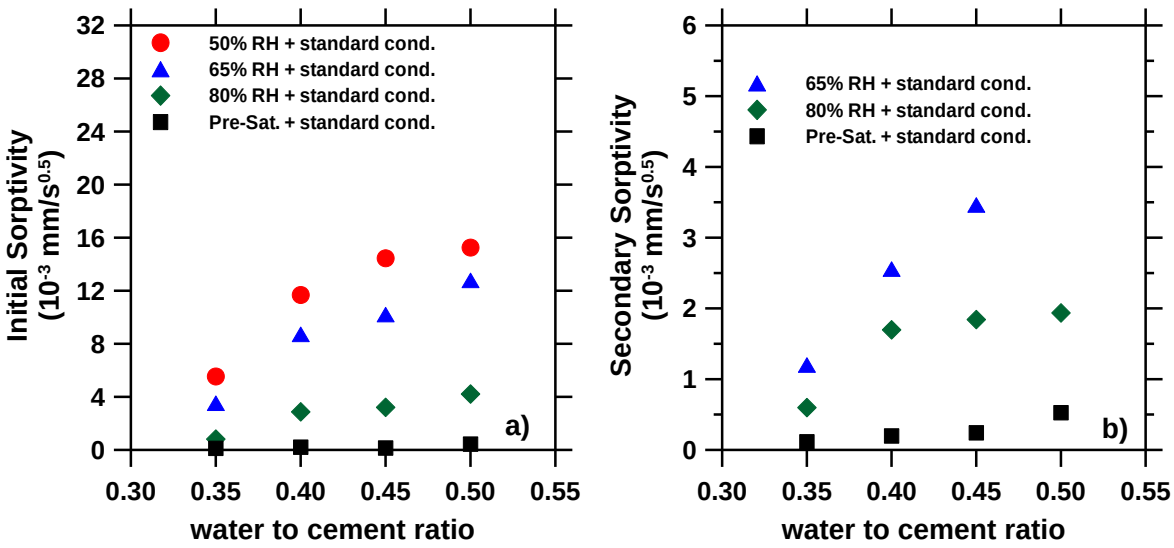

Fig. 11. Initial and secondary sorptivities on mortars with different initial moisture contents, conditioned with the procedure established in ASTM C1585-04.

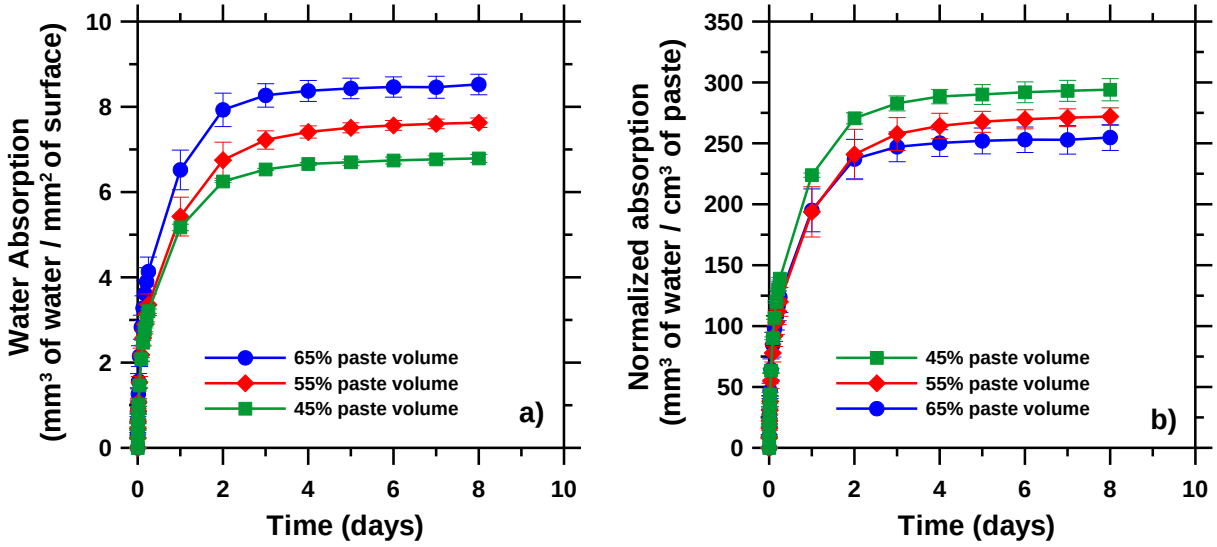

Fig. 12. Water absorption in mortars containing different volume of aggregates: a) normalized by surface in contact with water, (b) normalized by volume of paste.

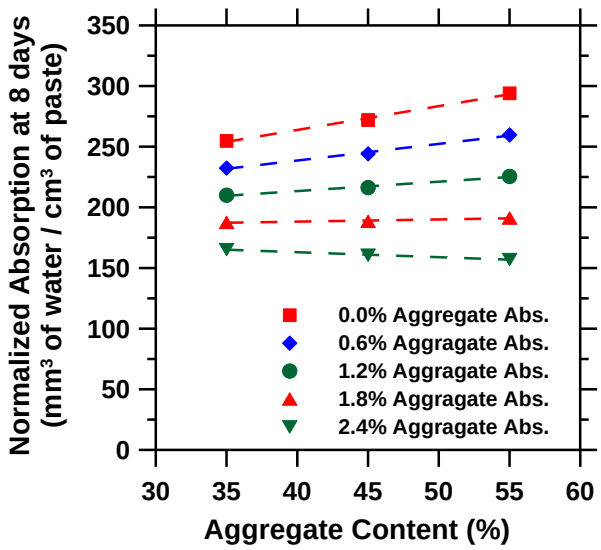

Fig 13. Water absorption at 8 d normalized by volume of paste, corrected by different values of aggregate absorption.

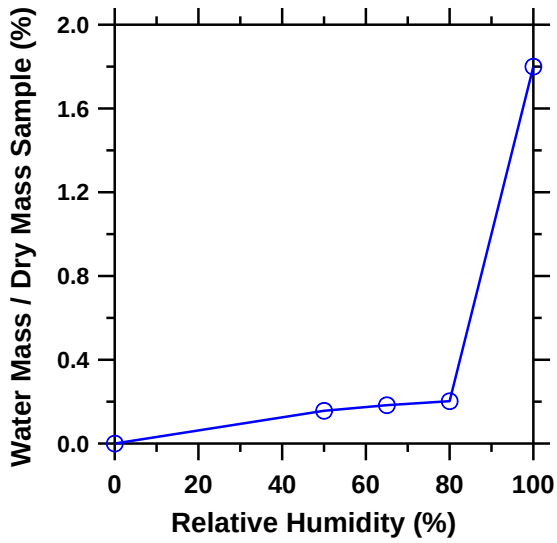

Fig. 14. Desorption isotherm for the sand used in this research.

Automation in Construction 19 (2010) 485–490

Contents lists available at ScienceDirect

Automation in Construction

journal homepage: www.elsevier.com/locate/autcon

An automated electrical monitoring system (AEMS) to assess property development in concrete

A. Poursaee *, W.J. Weiss

School of Civil Engineering, Purdue University, West Lafayette, IN, 47907, United States

ARTICLE INFO

Article history:
Accepted 29 December 2009

Keywords:
Electrical impedance
Automation
Concrete
Electrical properties
Imaging
LabVIEW

ABSTRACT

Electrical impedance measurement techniques are being increasingly used to measure material property development and permeability of concrete and other cement based materials. This paper describes the development of an automated electrical measurement system (AEMS) for measuring the properties of cementitious materials. The components of this system are an electrical impedance spectrometer, a digital multi-meter, a switching unit, and a customized software (AEMS) which communicates between different components of the system to control the testing and to collect data. This system enables electrical properties of multiple specimens to be measured in an automated fashion thereby making this approach very amenable for use in quality control applications. Further, an extension of this system is proposed which would enable its use to detect flaws in concrete using electrical imaging.

1. Introduction

Electrical impedance measurement techniques have been shown to provide useful information that can be used to characterize cementitious systems [1–3]. This technique studies the system response to the application of a small amplitude alternating potential signal at different frequencies. AC electrical impedance measurements have the advantages of being non-invasive and non-destructive, require little in term of preparation of the sample, and offer the possibility of continual measurements to describe the effect of hydration [4,5] drying [6], or permeability [7].

Electrical impedance techniques have been used in different research projects in concrete to study a wide range of concrete properties specifically this included studies on the microstructural development of cementitious materials [8,9], precipitation of calcium hydroxide on the surface of steel after the setting of the mortar [10], long-term effectiveness of concrete inhibitors for steel in concrete [11–15], the chloride diffusivity in concrete [16], chloride permeability of high performance concrete [17], detection of damage during tensile loading of cement composites [18], freezing of water in Portland cement paste [19], water penetration in concrete [20–22], setting time of concrete [23,24], measuring the concrete internal moisture content [25], and assessing the change in microstructure due to rapid chloride permeability test [26,27].

While numerous applications exit, they are frequently limited to the measurement of one sample at a time. It is regularly necessary to conduct experimental measurements at multiple locations in a sample or on multiple specimens. For example, Schmit [28] described the use of multiple sensors and quantified the influence of sensor position and number in uncertainty of the results. The ability to perform multiple measurements is very valuable for monitoring the hydration process, monitoring multiple specimens, or imaging the crack by electrical impedance measurements [29]. In addition, a single measurement cannot properly represent the behavior of a material. To improve measurements accuracy multiple measurements are needed. This paper describes the development of a user friendly Automatic Electrical Monitoring System (AEMS). By using this system, multiple electrical measurements can be performed on specimens and different properties of concrete materials can be monitored. The developed system is discussed and some applications of the AEMS were shown in this paper.

2. Objective

This paper describes the development of an Automated Electrical Monitoring System (AEMS). The data acquisition system consists of a computer, a Keithley digital multi-meter and switching unit [30], and Solartron 1260 impedance spectrometer[1] [31]. The role of the software is to communicate between all components of the system and to control data collection. This paper shows that the system is reliable for both short and long-term monitoring. Further, this paper points out that while in the past the use of electrical impedance

[1] Certain commercial products are identified in this paper to specify the materials used and procedures employed. In no case does such identification imply endorsement by the authors, nor does it indicate that the products are necessarily the best available for the purpose.

* Corresponding author.
E-mail address: poursaee@purdue.edu (A. Poursaee).

0926-5805/$ – see front matter © 2010 Elsevier B.V. All rights reserved.
doi:10.1016/j.autcon.2009.12.016

measurement techniques has been time consuming, automation enables these measurements to be performed efficiently. This enables new applications, like electrical imaging, to be performed effectively and enables EIS to be extended for use in daily quality control processes such as permeability measurements. Since electrical impedance requires less preparation and time, it can be a good replacement for the tests like rapid chloride permeability which is time consuming and can alter the microstructure of the concrete.

3. Component of the measurement system

The system developed for this investigation can be used to measure the AC electrical impedance response of the material. The components in the system consist of an impedance spectrometer, digital multi-meter, and a switching unit.

The electrical impedance spectrometer used in this study is capable of performing only one measurement at a time. There are multi-channel spectrometer units on the commercial market. However, in addition to their high cost most of the units are limited to only a few measurements (up to 16) at a time which also may be a limiting factor.

The digital multi-meter and switching unit chosen for this project included a Keithley model 2750 mainframe which has five slots and a model 2700 which has two slots for inserting the plug-in switch/control modules. Each slot can support a series of multiplexer, matrix, or control modules. For example the Module 7708 which was used in this project has 40 channels. The general features of this module are described in [32]. The role of the mainframe is to communicate between channels. Temperature can also be measured using this system as this is needed for temperature corrections [33].

For each impedance measurement (each sample), 2 channels are required, (i.e., the Keithley model 2750 mainframe with five 7708 modules can be used for 100 impedance measurements). If more than 100 measurements are necessary, several mainframes can be joined together to provide the appropriate number of channels.

To combine the mentioned components, the software (named AEMS) was developed, using LabVIEW. This software selects the sample that will be tested and then runs the impedance spectrometer on that sample. After the measurements are completed, the AEMS, stops the spectrometer, switches the sample and runs the test again. The measurements are performed one by one not simultaneously. In all the graphs shown in the paper, this time is considered. This time for AC measurements is a function of selected frequency and in all examples in this paper it was about 40 s. However, when the concrete is hardened, this time difference is not considerable. If some interval time is necessary between measurements, the AEMS can be programmed to place the necessary time interval between measurements. In addition, the AEMS can communicate with the mainframe to measure voltage, DC resistance and temperature independent from the spectrometer. Fig. 1 schematically shows the component of the system and the actual parts are shown in Fig. 2.

While an RS-232 serial port was used to control the multi-meter and switching system in this study, faster data transfer can be performed using a GPIB[2] [34] card. The role of the AEMS software is to control and switch the channels for each measurement, to control and run the spectrometer and save data to the computer for later analysis.

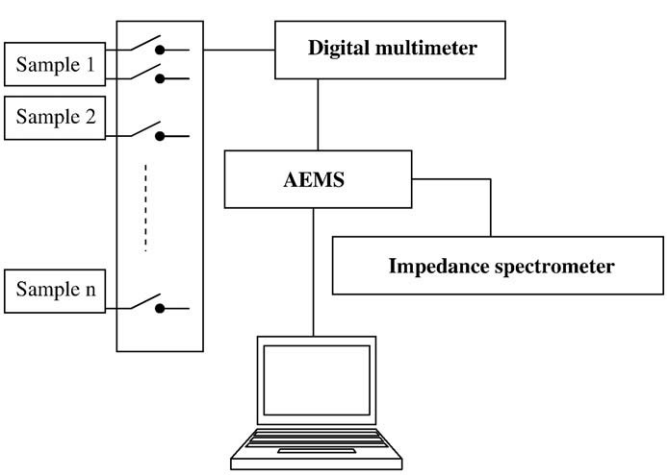

Fig. 1. Schematic relationship between the components of the system.

Fig. 2. Components of the system.

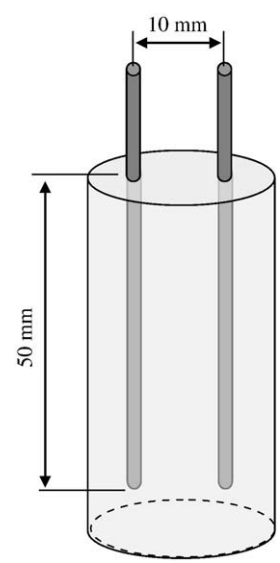

Fig. 3. Schematic view of the cylindrical paste specimens, used to measure variability in cement paste.

[2] The General Purpose Interface Bus (GPIB) is an industry standard published by the Institute of Electrical and Electronic Engineers (IEEE) as ANSI/IEEE Standard 488. GPIB defines the electrical, mechanical, functional, and software specifications of an interfacing system to connect PCs to programmable instrument.

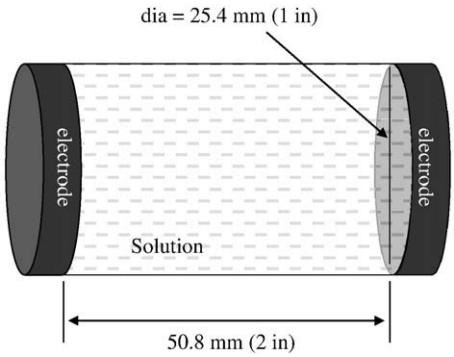

Fig. 4. Schematic view of the container with known geometry, to measure the conductivity of the solutions.

The software contains options which enable the user to set the number of samples, measurement frequency, and the time between each set of measurements. The saved data can be opened and analyzed in Excel®. Based on the number of measurements, one may end up with thousands of data files. Therefore, a macro was developed to automatically analyze individual data and place the summarized results in a worksheet.

4. Experimental results

To verify the performance of the switching units, two simple experiments were conducted. In the first test, a known resistor (10 Ω) was connected to all available channels and the resistance was measured. In the second test, a known potential was measured, using all channels. Results show that there is no significant difference between measured values with each channels and the relative standard deviation was less than 0.005%.

4.1. Electrical conductivity of cement paste sample during hydration

Electrical measurements can provide information about the change in pore structure due to hydration process [23,35]. It is important to use multiple specimens for these measurements due to the inhomogeneity and corresponding variability of cementitious materials. To determine the variation between different samples the electrical conductivity of cement paste samples was measured using cylindrical paste specimens as described in Fig. 3. Type I ordinary Portland cement was used with a Blaine fineness of 360 m^2/kg and a Bogue phase composition of 60% C_3S, 12% C_2S, 12% C_3A, 7% C_4AF and Na_2O equivalent of 0.72%. Fifteen samples were prepared with a *w*/*c* of 0.45 and 5 samples were prepared with a *w*/*c* of 0.50. The measurement frequency range that was used for the tests ranged from 1 MHz to 10 Hz with ten measurements per decade using the 500 mV AC stimulus. To determine the conductivity of the material, the bulk resistance (R_b) obtained from the impedance response normalized for the effects of specimen and electrode geometries, using the following equation:

$$\sigma_t = k / R_b \quad (1)$$

where, σ_t is the conductivity (S/m) of the paste, R_b is the measured bulk resistance (Ω) and *k* is a geometry factor. The geometry factor

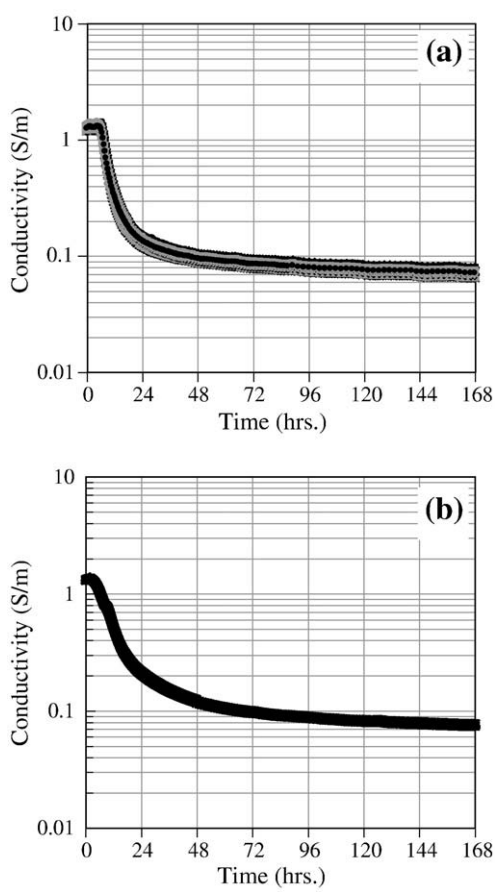

Fig. 5. Development of the conductivity of (a) 15 cement paste samples with *w*/*c* = 0.45 and, (b) 5 cement paste samples with *w*/*c* = 0.5.

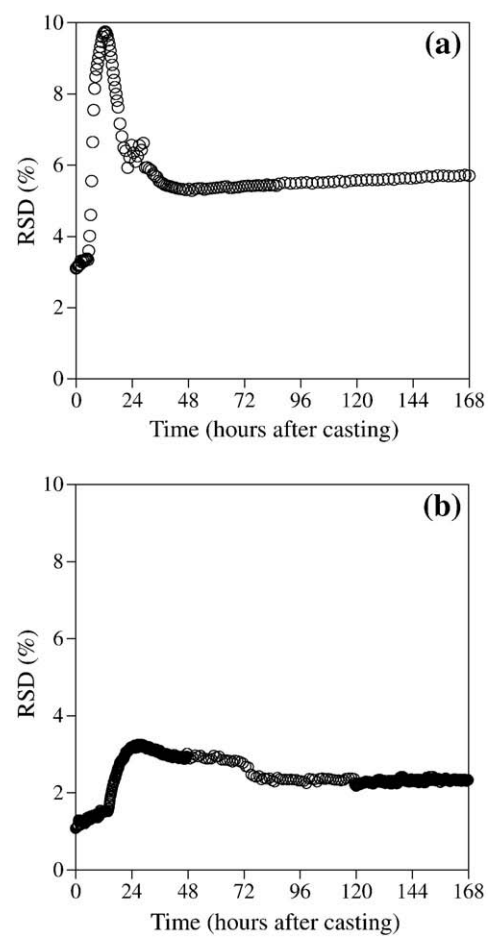

Fig. 6. Relative standard deviation between (a) 15 cement paste samples, with *w*/*c* = 0.45, at different ages and, (b) between 5 cement paste samples, with *w*/*c* = 0.50, at different ages.

was determined by filling the molds with solutions of known conductivity and measuring the bulk resistance between the electrodes. In this experiment two sodium chloride solutions were prepared with two different concentrations (0.1 M and 1 M). The conductivity of the two solutions was measured (7.72 and 1.01 S/m for 1 M and 0.1 M solutions, respectively), using a container with known geometry as shown in Fig. 4. By using this information, the value of the geometry factor, k, was calculated to be 15.5/m for the geometry shown in Fig. 3.

The electrical impedance of the samples was measured for 7 days, starting 30 min after casting. Fig. 5 shows the conductivity of the samples with w/c of 0.45 and 0.50, respectively. At the end of the test, all samples were inspected to ascertain the uniformity of specimen.

It can be seen that the conductivity of all samples follows the same pattern. As expected, the conductivity decreases as the system hydrates [36–38].

To better assess the variation, the relative standard deviation (RSD) can be used. The RSD is useful for comparing the uncertainty between different measurements of varying absolute magnitude. The RSD is the absolute value of the coefficient of variation calculated using Eq. (2):

$$\mathrm{RSD} = \frac{(\text{Standard devation of conductivity})}{\text{Average of conductivity}} \times 100 \tag{2}$$

Fig. 6 shows the RSD of the samples at different ages. Results show that, even when the samples are made from one mixture there is variability in the conductivity of the samples, especially at early ages when the properties change most dramatically. However, the RSD decreases over time as the measurements stabilize. This is shown in Fig. 7, which gives the histograms of conductivities for $w/c = 0.45$ (15 samples) at two different ages. The maximum difference is less than 10% for $w/c = 0.45$ and 3.5% for $w/c = 0.50$ at all ages.

Table 1
Mixture proportions of concrete samples.

Materials	Batch proportion for 100 kg (kg)		
	$w/c = 0.48$, no WR	$w/c = 0.53$, no WR	$w/c = 0.48$ with WR
Cement (Type I)	8.0	8.0	8.0
Water	3.9	4.3	3.9
Coarse aggregate	68.9	68.6	68.7
Fine aggregate	19.1	19.0	19.0
Water reducer (WR)	0.0	0.0	0.3

4.2. Electrical conductivity of concrete sample

To show the capability of the AEMS, the conductivity of concrete cylinders was measured with different mixture proportions (shown in Table 1). For this purpose, 200 mm (diameter) × 400 mm (length) concrete cylinders were prepared with two (1.9 mm diameter) stainless steel rods as the electrodes. The electrodes were spaced 100 mm apart from each other and fixed in the mold. For each mixture, five cylinders were cast and impedance tests were performed every 15 min. The impedance measurements began 30 min after casting and continued for 7 days. Results show that the conductivities of all five samples of each mixture have very similar results with the RSD between 1 and 2.5% as can be seen in Fig. 9. As can be seen in Fig. 8, at about 10 h, the conductivity of concrete samples is similar. It is obvious from the results that impedance spectroscopy technique is capable to evaluate and compare different samples with different mixture proportions.

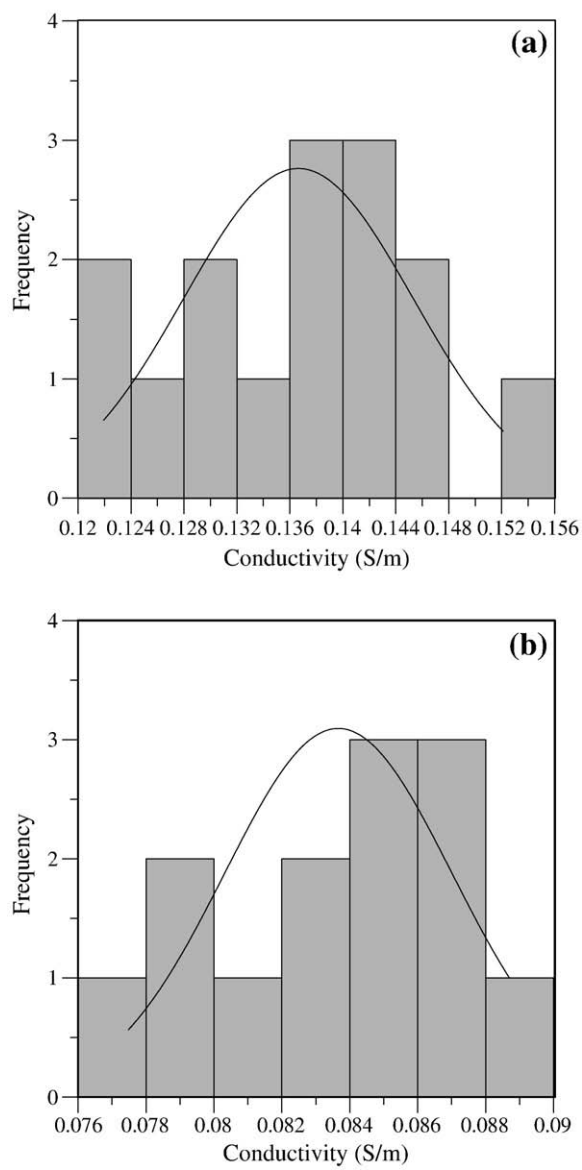

Fig. 7. Histogram of conductivity of paste samples with $w/c = 0.45$ (a) 24 h after casting, (b) 72 h after casting.

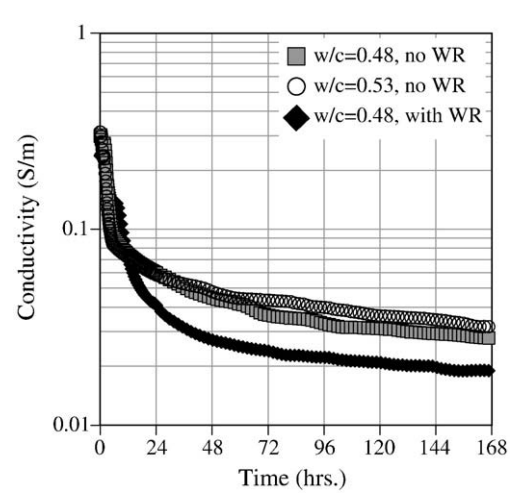

Fig. 8. Conductivity of concrete with three different mixture proportions, shown in Table 1.

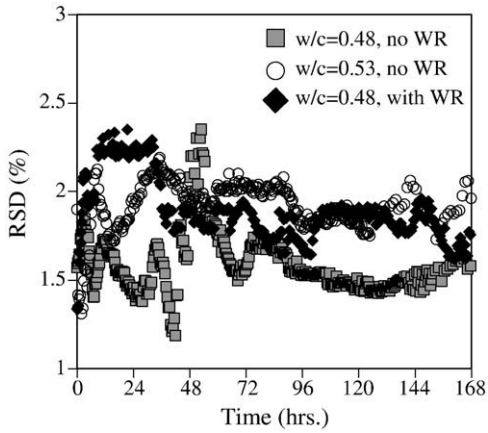

Fig. 9. Relative standard deviation between concrete samples with three different mixture proportions, shown in Table 1, at different ages.

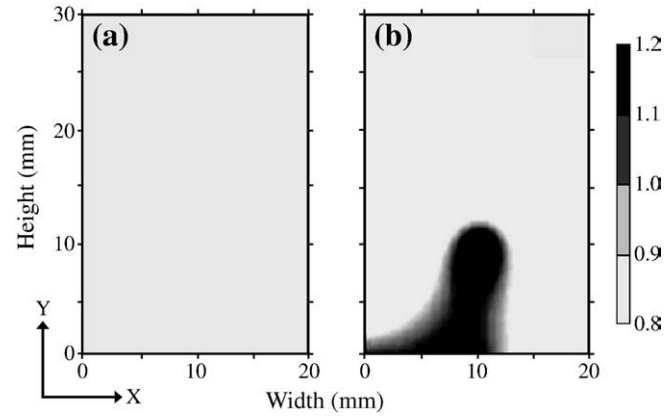

Fig. 11. Image of the concrete sample (a) without and (b) with saw cut, created by electrical impedance measurements.

4.3. Crack imaging in cement paste and concrete, using impedance spectroscopy

Electrical impedance imaging has been used by many researchers in the medical field to monitor various physiological variables [39–41]. Previous studies indicated that this technique can also be used in imaging the defects in cementitious materials [29,42]; however, studies in cement are somewhat limited. The approach consists of measuring the impedance at different locations on the surface of the concrete and constructing electrical conductivity (or resistivity) contour plot from the measured impedances. Since the presence of damage (e.g., a crack) changes the path of electrical flow in the concrete, any damage will appear on the plot. Electrical contour plots can be used to locate visible and invisible damage. In order to investigate this technique a small test unit developed consisting of twenty electrodes, as shown in Fig. 10. The impedance was measured between each pin, in *X* and *Y* directions. Then the measured values were used to construct electrical resistance contour plots. For this experiment, two concrete samples were prepared with water: cement:coarse aggregates:fine aggregates ratio of 0.4:1:3:2.85:2.37. The measurement frequency range was 1 MHz to 10 Hz, with the 500 mV AC stimulus. After performing the measurements, the resistances measured between each pin were normalized based on the maximum measured value in each case and then the normalized values were mapped. Fig. 11 shows the constructed image. The location of the saw cut is clearly visible in this image. A similar setup (with different size and spacing between electrodes) can be used to determine the location of the damaged area beneath the sealed saw cut or joints which is currently under investigation.

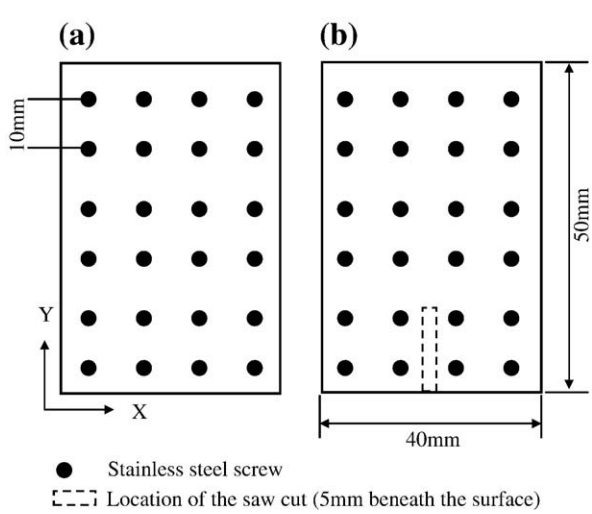

Fig. 10. The dimensions of the concrete samples and the measurement setup, used for imaging: (a) concrete sample with no cut, and (b) concrete sample with the saw cut.

5. Conclusion

This paper described an approach to automate electrical impedance measurements with an automated electrical monitoring system (AEMS) that enable multiple measurements to be made.

This switching system enables measurements to be performed on multiple specimens or where multiple locations are needed. This enables the aging processes be better quantified, allows variability to be qualified for quality control, and enables electrical imaging to be performed.

The system described in this paper was successfully used to investigate the behavior of concrete sample with different mixture proportions by continuously monitoring their conductivity. In addition, variability among different samples was studied and the results show that there is variability between samples even cast from one batch which needs to be considered, specifically in statistical analysis. Constructed electrical image maps can be used to locate the cracked and damaged area, even if it is beneath the surface.

Acknowledgements

This work was supported in part by the Joint Transportation Research Program administered by the Indiana Department of Transportation and Purdue University (study no. TPF-5(179)). The contents of this paper reflect the views of the authors, who are responsible for the facts and the accuracy of the data presented herein, and do not necessarily reflect the official views or policies of the Indiana Department of Transportation, nor do the contents constitute a standard, specification, or regulation.

References

[1] W.J. McCarter, et al., Characterization and monitoring of cement-based systems using intrinsic electrical property measurements, Cement and Concrete Research 33 (2003) 197–206.
[2] B.J. Christensen, et al., Impedance spectroscopy of hydrating cement-based materials: measurement, interpretation, and application, Journal of the American Ceramic Society 77 (1) (1994) 2789–2801.
[3] P. Gu, P. Xie, J.J. Beaudoin, Some applications of AC impedance spectroscopy in cement research, Cement, Concrete and Aggregates 17 (2) (1995) 113–118.
[4] F. Rajabipour, W.J. Weiss, Electrical conductivity of drying cement paste, Materials and Structures 40 (2007) 1143–1160.
[5] W.J. Weiss, J.D. Shane, A. Mieses, T.O. Mason, S.P. Shah. Aspects of monitoring moisture changes using electrical impedance spectroscopy. In 2nd Symposium on Self-Desiccation and Its Importance in Concrete Technology. 1999. Lund, Sweden: Lund Institute of Technology, Division of Building Materials.

[6] A. Schiessl, et al., Assessing the moisture profile of drying concrete using impedance spectroscopy, Concrete Science and Engineering 2 (2) (2000) 106–116.
[7] Z. Liu, J.J. Beaudoin, An assessment of the relative permeability of cement systems using A.C. impedance techniques, Cement and Concrete Research 29 (7) (1999) 1085–1090.
[8] P. Gu, P. Xie, J.J. Beaudoin, Microstructural characterization of the transition zone in cement systems by means of A. C. impedance spectroscopy, Cement and Concrete Research 23 (1993) 581–591.
[9] R.A. Olson, et al., 1995. Microstructure-electrical property relationships in cement-based materials. in Materials Research Society Symposium. Boston, MA, USA: Materials Research Society, Pittsburgh, PA, United States.
[10] L. Lemoine, F. Wenger, J. Galland, Study of the corrosion of concrete reinforcement by electrochemical impedance measurement, Corrosion Rates of Steel in Concrete ASTM STP 1065, American Society for Testing and Materials, 1990.
[11] L. Dhouibi, E. Triki, A. Raharinaivo, The application of electrochemical impedance spectroscopy to determine the long-term effectiveness of corrosion inhibitors for steel in concrete, Cement & Concrete Composites 24 (2002) 35–43.
[12] C. Monticelli, A. Frignani, G. Trabanelli, A study on corrosion inhibitors for concrete application, Cement and Concrete Research 30 (2000) 635–642.
[13] G. Trabanelli, et al., Electrochemical study on inhibitors of rebar corrosion in carbonated concrete, Cement and Concrete Research 35 (2005) 1804–1813.
[14] P. Gu, et al., A study of corrosion inhibitor performance in chloride contaminated concrete by electrochemical impedance spectroscopy, ACI Materials Journal 94 (5) (1997) 385–395.
[15] B.B. Hope, A.K.C. Ip, Corrosion inhibitors for use in concrete, ACI Materials Journal 86 (6) (1989) 602–608.
[16] M. Shi, Z. Chen, J. Sun, Determination of chloride diffusivity in concrete by AC impedance spectroscopy, Cement and Concrete Research 29 (7) (1999) 1111–1115.
[17] M.R. Hansen, et al., 1993. Chloride permeability and AC impedance of high performance concrete. ACI–SP140-06. 140: p. 121–146.
[18] A. Peled, et al., Electrical impedance spectra to monitor damage during tensile loading of cement composites, ACI Materials Journal 98 (4) (2001) 313–322.
[19] S. Perron, J.J. Beaudoin, Freezing of water in Portland cement paste—an AC impedance spectroscopy study, Cement & Concrete Composites 24 (5) (2002).
[20] W.J. McCarter, H. Ezirim, M. Emerson, Properties of concrete in the cover zone: water penetration, sorptivity, and ionic ingress, Magazine of Concrete Research 48 (1996) 149–156.
[21] A. Schieβl, et al., Assessing the moisture profile of drying concrete using impedance spectroscopy, Concrete Science and Engineering 2 (2) (2000) 106–116.
[22] F. Rajabipour, et al., Procedure to interpret electrical conductivity measurements in cover concrete during rewetting, ASCE Journal of Materials in Civil Engineering 17 (5) (2005) 586–594.
[23] Z. Li, L. Xiao, X. Wei, Determination of concrete setting time using electrical resistivity measurement, Journal of Materials Science in Civil Engineering 19 (5) (2007) 423–427.
[24] G. Sant, F. Rajabipour, P. Fishman, P. Lura, W.J. Weiss. Electrical conductivity measurements in cement paste at early ages. in International RILEM Workshop on Advanced Testing of Fresh Cementitious Materials, 2006, Stuttgart, Germany: RILEM.
[25] G.D. Davis, M.J. Rich, L.T. Drzal, Monitoring moisture uptake and delamination in CFRP-reinforced concrete structures with electrochemical impedance sensors, Journal of Nondestructive Evaluation 23 (1) (2004) 1–9.
[26] J.D. Shane, et al., Microstructural and pore solution changes induced by rapid chloride permeability test measured by impedance spectroscopy, Concrete Science and Engineering 1 (2) (1999) 110–119.
[27] C. Shi, Effect of mixing proportions of concrete on its electrical conductivity and the rapid chloride permeability test (ASTM C1202 or ASSHTO T277) results, Cement and Concrete Research 34 (2004) 537–545.
[28] T.J. Schmit, A fundamental investigation on utilizing error propagation, Monte Carlo simulation, and measurement interpretation technique to design efficient in situ covercrete sensing systems MS thesis in Civil Engineering, Purdue University, 2005.
[29] M. Niemuth, Using Impedance Spectroscopy to Detect Flaws in Concrete, Purdue University, MS thesis in Civil Engineering, 2004.
[30] Keithley Instruments Inc., 2700, 2701 and 2750 Multimeter/Data Acquisition/Switch Systems, Keithley Instruments Inc., 2009 http://www.keithley.com/products/dmm/integrasystems/?path=2700/Documents#4.
[31] Solartron Group, 2009. *www.solartronanalytical.com/downloads/datasheets/1260.pdf*.
[32] Keithley Instruments Inc., Integra Series Technical Data Sheet, 2003.
[33] G. Sant, F. Rajabipour, W.J. Weiss, The influence of temperature on electrical conductivity measurements and maturity predictions in cementitious materials during hydration, The Indian Concrete Journal (April 2008) 1–10.
[34] National Instruments, What is NI GPIB?, 2009.
[35] P. Gu, et al., Study of the hydration and setting behavior of OPC-HAC pastes, Cement and Concrete Research 24 (4) (1994) 682–694.
[36] C.A. Scuderi, T.O. Mason, H.M. Jennings, Impedance spectra of hydrating cement pastes, Journal of Materials Science 26 (1991) 349–353.
[37] J.M. Torrents, R. Pallas-Areny, 1997. Measurement of cement setting by impedance monitoring. in IEEE Instrumentation and Measurement, Technology Conference. May 19–21. Ottawa, Canada.
[38] A. Poursaee, C.M. Hansson, Reinforcing steel passivation in mortar and pore solution, Cement and Concrete Research 37 (2007) 1127–1133.
[39] D. Murphy, et al., Impedance imaging in the newborn, Clinical Physics and Physiological Measurement 8 (Suppl. A) (1987) 131–140.
[40] M. Weindling, et al., Electrical impedance to study cerebral haemodynamics in the newborn: which index is best? Biology of the Neonate 45 (1984) 300.
[41] L. Tarassenko, P. Rolfe, Imaging spatial distribution of resistivity—an alternative approach, Electronics letters 20 (1984) 574–576.
[42] T. Hou, J.P. Lynch, Electrical impedance tomographic methods for sensing strain fields and crack damage in cementitious structures, Journal of Intelligent Material Systems and Structures, , 2008, pp. 1–18.

The influence of temperature on electrical conductivity measurements and maturity predictions in cementitious materials during hydration

Gaurav Sant, Farshad Rajabipour and Jason Weiss

Electrical property measurements are being increasingly used to assess the transport properties of building materials. While conductivity measurements have been extensively used, the combined dependence of electrical conductivity on measurement temperature and microstructural development (cement hydration) is often overlooked. In this paper the influence of temperature and microstructural development (i.e. hydration) are separated. Two cement paste mixtures are assessed at 283K, 296K, and 309K, and the conductivity response is analysed to differentiate the contribution of maturity (pore structure refinement due to hydration) and temperature (due to changing ionic mobility). The conductivity measurements are used to determine the activation energy of electrical conduction (i.e. temperature dependence of ion mobility) and hydration (i.e. temperature dependence of reaction rates). This work provides an improved understanding of how temperature influences electrical measurements in cementitious systems at early ages, and can provide for an accurate interpretation of the electrical properties of the system. This information will enable improvements in the use of electrical measurements for quality control and quality assurance (QC/QA) testing.

Keywords: *Electrical conductivity, hydration, maturity, temperature, quality control.*

Electrical measurements are powerful non-destructive testing techniques that are capable of providing information about hydration reactions, microstructural features and the transport properties of cement based materials. However, electrical measurements (e.g., conductivity or resistivity) exhibit temperature dependence due to changing ionic mobility with temperature. In an electrolyte, electrical conduction occurs due to the migration of ions through the solution under an applied potential gradient[1]. Consequently, conduction in aqueous electrolytes is dependent on ionic mobility and the solution's concentration. In cementitious materials, temperature change influences ionic mobility and salt solubility resulting in a change in the electrical conduction response as a function of temperature[2]. These considerations highlight the need to account for the temperature dependent conductivity response of cementitious materials. Further, chemical reactions (such as cement hydration) are influenced by temperature[3]. This topic has received significant treatment in the literature with the objective of determining how temperature influences the rate of material property development[4,5,6,7]. Maturity transformations have been extensively used to correlate material properties to the extent of reaction that occurs in the system[8,9].

Due to the influence of temperature on the rate of hydration and ionic mobility it would be reasonable to consider that the electrical properties (conductivity or

resistivity) of cement systems are a function of maturity and temperature effects as shown in Equation 1.

$$\sigma(t,T) = f(M) \bullet f(T) \qquad .....(1)$$

where, $\sigma(t,T)$ is the time and temperature dependent electrical property (in this case the conductivity (S/m)) of the sample, $f(M)$ is a function which defines the influence of time and temperature on the sample maturity (microstructure development), and $f(T)$ is a function that defines the influence of sample temperature and accounts for effects such as the ionic mobility and solution concentration.

The temperature dependence of electrical properties in cement based systems was studied several decades ago by Hammond and Robson who used the Hinrichson-Rasch law to describe the conductivity of concrete over a range of temperatures (Equation 2).[10,11]

$$ln\left(\frac{\sigma(T)}{\sigma(T_{REF})}\right) = A\left(\frac{1}{T} - \frac{1}{T_{REF}}\right) \qquad .....(2)$$

where, $\sigma(T)$ is the concrete conductivity (S/m) at temperature T (K), $\sigma(T_{REF})$ is the conductivity (S/m) at a reference temperature T_{REF} (296K for this work) and 'A' is an empirical constant (K). Hammond and Robson indicated 'A' to be equal to 5500K based on work by Spencer[10,12]. Later, Elkey and Sellevold extended the scope of this investigation and determined 'A' to vary between 2000 and 5000K depending on the mixture composition[13].

Whittington et al. used a similar approach to investigate concrete using electrical resistivity[14]. Using a slightly different form of relationship (Equation 3) described by Hammond and Robson they determined concrete to have a negative temperature coefficient of resistivity, equal to 0.022/°C.

$$\frac{\rho(T)}{\rho(T_{REF})} = \frac{1}{1 + \alpha(T - T_{REF})} \qquad .....(3)$$

where, $\rho(T) = 1/\sigma(T)$ is the resistivity (ohms.m) at temperature T (K), $\rho(T_{REF})$ is the resistivity (ohms.m) at a reference temperature T_{REF} (K) and α is temperature coefficient of resistivity of the material. The work of Whittington et al translates to an empirical constant 'A' of 2130 K for the concretes tested.

In the 1990s, McCarter determined the temperature coefficient of resistivity of concrete as 0.026/°C.[15] More recently, McCarter proposed a formulation to determine the activation energy of electrical conduction based on the Arrhenius Law (Equation 4)[16,17].

$$\sigma_{Bulk} = A \bullet exp\left[\frac{-E_{aC}}{R \bullet T}\right] \qquad .....(4)$$

where, σ_{Bulk} is the bulk sample conductivity (S/m) at an absolute temperature T (K), R is the universal gas constant (8.314 J/K mol), E_{aC} is the activation energy for the conduction process (J/mol) and A (S/m) is a material constant (theoretically equivalent to the conductivity at infinite temperature; $\sigma(T = \infty)$). The activation energies of electrical conduction were determined to be in the range of 16-30 KJ/mole for the mixtures evaluated in this project.

Research objective

This paper proposes an approach to simultaneously assess the influence of temperature and microstructural changes (i.e. maturity) on the measured electrical conductivity in cementitious systems. The results of this work are aimed at understanding the influence of temperature on early-age conductivity measurements. This understanding would permit the reliable use of electrical measurements in early-age quality control and quality assurance (QC/QA) testing and for specification compliance of cement-based materials.

Materials and mixing procedures

Two different cement paste mixtures were prepared according to the mixture proportions shown in Table 1. Type I ordinary portland cement was used with a Blaine fineness of 360 m^2/kg and a Bogue phase composition of 60% C_3S, 12% C_2S, 12% C_3A, 7% C_4AF and a Na_2O equivalent of 0.72%. To enhance the workability of the mixtures, a high range water reducing admixture was added. A commercially available shrinkage reducing admixture (SRA) was added at a 5% concentration of the initial water content by replacement (by mass) of the initial mixing water. For the measurement of electrical conductivity de-aired, neat cement pastes were prepared using de-ionised water. The water was de-aired by boiling then cooled to room temperature before mixing. The dry constituent materials were placed inside a special mixing chamber[18]. The chamber was then sealed, air was evacuated from the chamber using a vacuum pump, and the solution of water and the chemical admixtures was introduced into the chamber

under the same evacuated condition. The chamber was then placed in a commercial paint shaker and shaken for five minutes to uniformly mix the constituents and obtain a consistent cement paste mixture. After mixing, the chamber was opened and the cement paste slurry was placed in the moulds using external vibration.

Table 1. Mixture proportions (mass)

	W/C = 0.30	W/C = 0.30 + 5% SRA
Water	0.300	0.285
Cement	1.000	1.000
HRWRA	0.005	0.005
SRA	~	0.015

Experimental procedures

Electrical conductivity of fresh and mature cement pastes

The electrical conductivity of cement paste samples was measured using cylindrical paste specimens (22 mm diameter, 50 mm height). The specimens were cast and stored in an airtight plastic vial. Two stainless steel electrodes (2.5 mm diameter rods spaced 10 mm centre to centre) were embedded longitudinally inside each vial (Figure 1b). A impedance gain-phase analyser measured the impedance response of each specimen. The measurements were made over a wide frequency range; i.e. 10 MHz to 1 Hz (10 steps/frequency decade) using a 100 mV AC stimulus. The bulk resistance (R_b) obtained from the impedance response was used to determine the material's conductivity after normalising for the effects of specimen and electrode geometry (Equation 5).

$$\sigma_t = \frac{k}{R_b} \qquad .....(5)$$

where, σt is the paste conductivity (S/m), R_b is the bulk resistance (ohms; Ω) and k is a geometry factor (15.76/m) that was determined experimentally for this specific geometry[19]. During measurements, the specimens remained sealed inside plastic vials. Electrical impedance measurements were performed for a duration of 7 days (at a reference temperature of 296K) after casting on

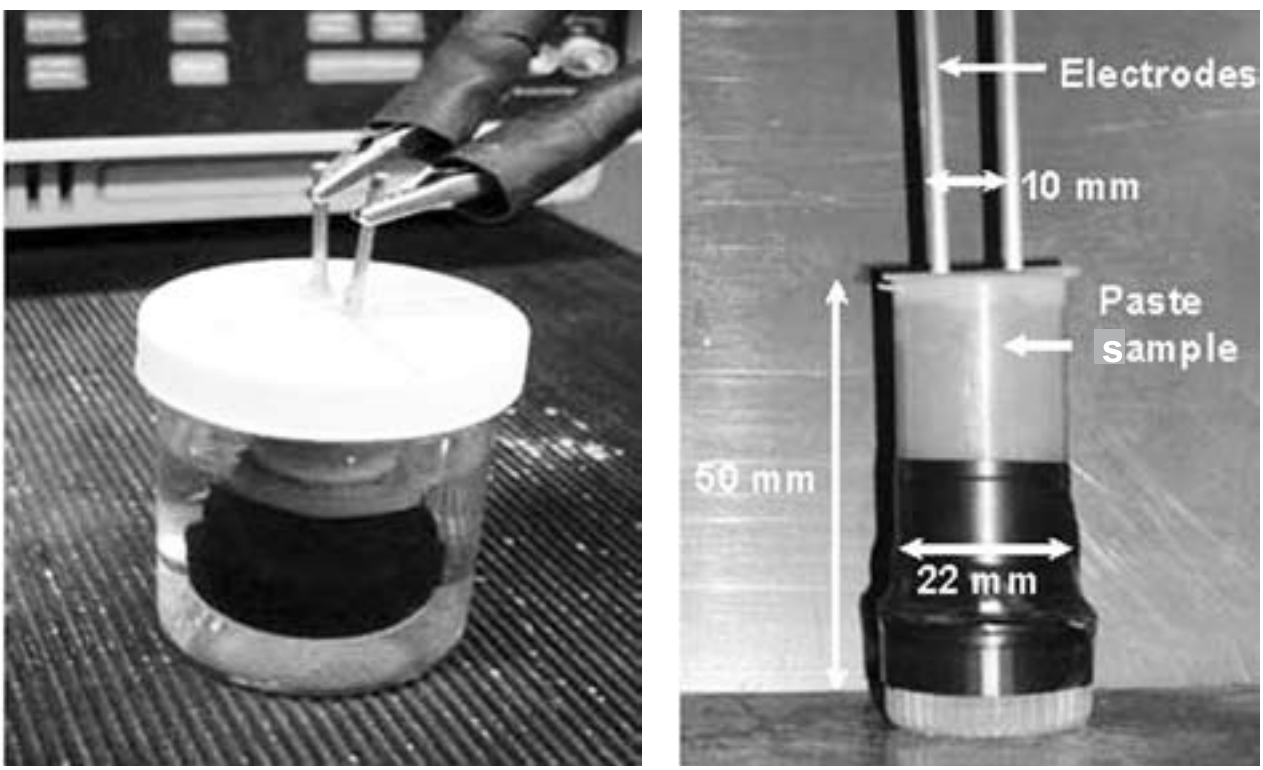

(a) (b)

Figure 1. An illustration of the apparatus used for the measurement of electrical conductivity of cement pastes (a) The conductivity cell for cement pastes immersed in a water bath (b) The vial with embedded electrodes for paste and pore solution conductivity assessment

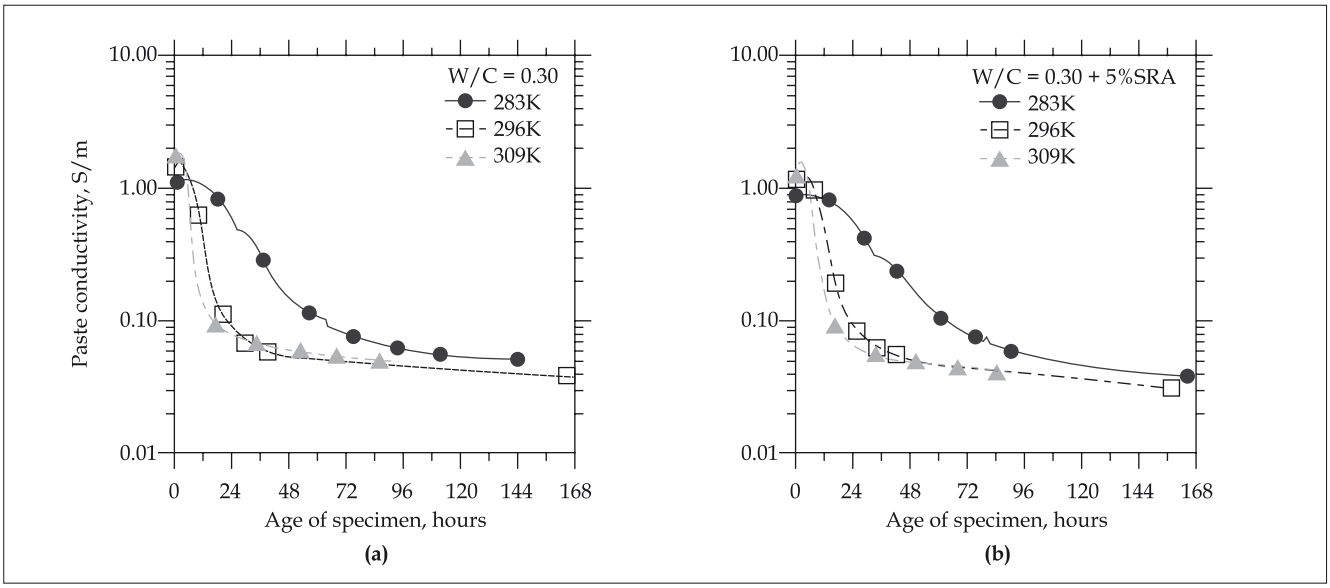

Figure 2. The electrical conductivity of the cement pastes as function of specimen age (a) W/C = 0.30 and (b) W/C = 0.30 + 5% SRA

specimens which were kept in a water bath to minimise temperature variations (Figure 1a). Measurements were performed on samples cured at 283K (14 days), 296K (7 days) and 309K (4 days). Prior to mixing, the raw materials were temperature conditioned to ensure an appropriate mixture temperature (equivalent to the measuring temperature) at the end of the mixing cycle. For consistency, conductivity measurements until an age of 168 hours (real and equivalent age) are presented in this paper. The measurements were used to determine the activation energy of cement hydration, after a correction to account for the influence of temperature (ionic mobility) on electrical conductivity.

To determine the influence of temperature on the conductivity of the pore solution (i.e. activation energy of electrical conduction; E_{aC} (J/mol)) in cement pastes, conductivity measurements were performed on cement paste samples (cured for 7 days at 296K; ~70% hydration – which corresponds to the maximum degree of hydration for the mixture as computed using Powers model[20] that were conditioned to 283K, 296K and 309K (± 0.5K) in an environmental chamber. Further, companion specimens were cast with thermocouples embedded to monitor the temperature profile of the cement paste mixtures.

Electrical conductivity of synthetic pore solutions

To determine the activation energy of electrical conduction in an electrolyte, synthetic pore solutions of varying concentrations were prepared (0.35 KOH + 0.05 NaOH, 0.70 KOH + 0.10 NaOH, 1.40 KOH + 0.20 NaOH). The solutions were then conditioned to 283K, 296K and 309K (± 0.5K) in an environmental chamber. When the solutions had achieved an equilibrium temperature (measured using thermocouples immersed in the solution), the conductivity of the solutions was measured using a conductivity cell (Figure 1b) connected to a impedance gain-phase analyser[20].

Experimental results

Influence of the rate of reaction on the electrical conductivity

Figure 2 shows the electrical conductivity of cement paste mixtures cured at temperatures of 283K, 296K and 309K. An initial increase in the conductivity is noted for ~1.5 hours for all the cement paste mixtures. This may be explained by the rapid initial dissolution of alkalis and sulphates into the mixing water. After this time (1.5 hours), a reduction in conductivity is noted for all mixtures. A significantly different trend is observed in the rate of measured conductivity (Figure 2) for specimens cured at different temperatures. The samples cured at low temperatures show a gradual decrease in the conductivity, while mixtures cured at higher temperatures exhibit a more rapid decrease. This observation may be explained by the temperature dependence of the rate of hydration in these cement paste mixtures (i.e. the rate of pore structure refinement as a function of the reaction temperature).

Influence of temperature on the electrical conductivity of cement pastes

Figure 3 shows the measured electrical conductivity of two cement paste specimens (cured for 7 days), which have been subjected to thermal cycles. After being cured for 7 days at 296K, the samples were placed at temperatures of 283K and 309K (alternate heating and cooling was performed for 12 hours to ensure equivalent maturity). The results are shown in Figure 3(b). As expected, the measured conductivity is lower at lower temperatures. The lower conductivity of the SRA mixture as compared to the plain mixture is attributed to the non-conductive nature of the SRA in cement paste and pore solution[20,21]. The measured value of conductivity was then used to determine the activation energy of the conduction process in cement pastes. This is further discussed later.

Influence of temperature on the electrical conductivity of pore solution

Figure 4 shows the measured electrical conductivity of synthetic pore solutions (0.35 KOH + 0.05 NaOH, 0.70 KOH + 0.10 NaOH, 1.40 KOH + 0.20 NaOH) conditioned to temperatures of 283K, 296K and 309K. The electrical conductivity is observed to increase linearly over the temperature range from 283K to 309K. This is consistent with the increase in ionic mobility and the extent of dissociation of the dissolved ionic species as a function of temperature. The measured value of conductivity was then used to determine the activation energy of the conduction process in the electrolytes. This is further discussed later.

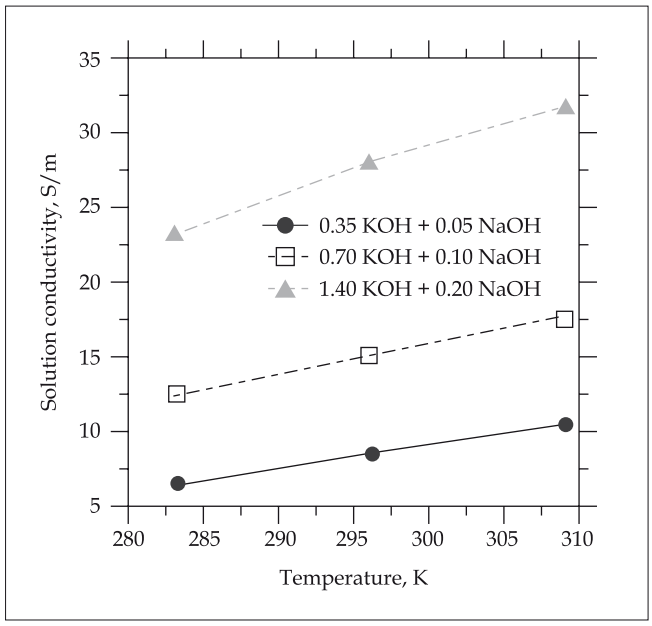

Figure 4. The temperature dependent response of electrical conductivity of synthetic pore solutions investigated in this project

Discussion of experimental results

The electrical conductivity of cementitious materials has been described extensively using a modified parallel

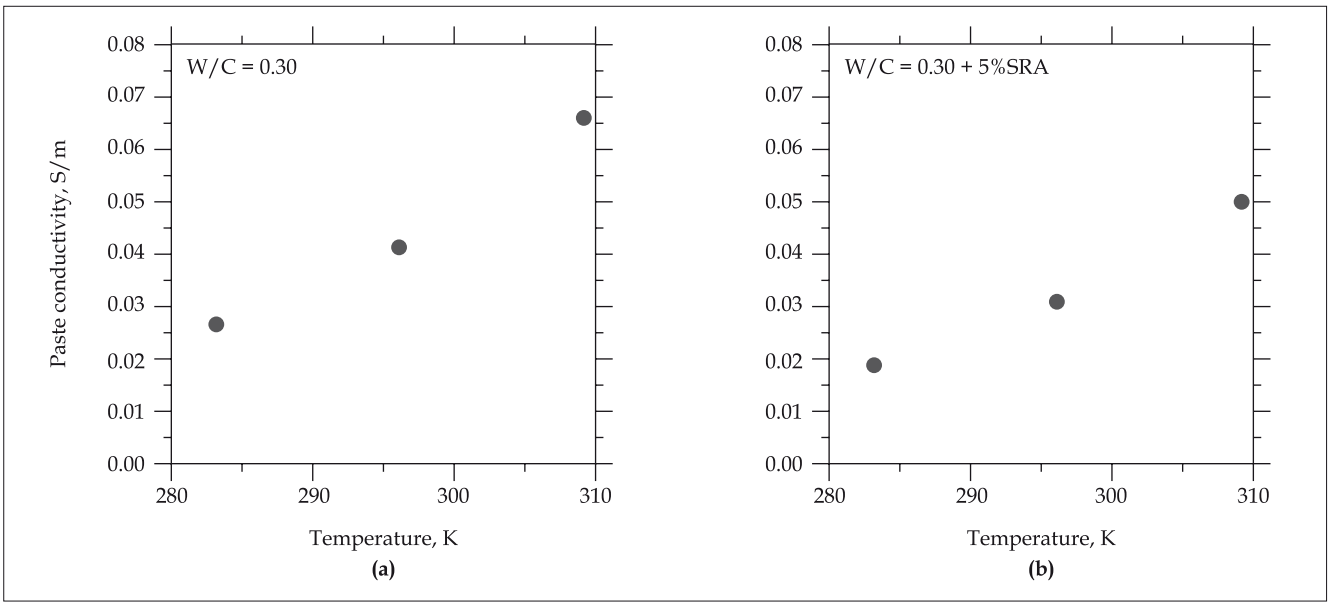

Figure 3. The temperature dependent electrical conductivity of the cement pastes (a) W/C = 0.30 and (b) W/C = 0.30 + 5% SRA

law[22,23,24]. This relationship can be described using Equation 6.

$$\sigma_t = \sigma_0 \phi \beta \qquad .....(6)$$

where, σ_t is the bulk cement paste conductivity (S/m), σ_0 is the pore solution conductivity (S/m), φ is the volume fraction of the solution contained in the pores and β is the pore connectivity. The modified parallel law can be used to determine which parameters are impacted by a change in temperature. The first component which would contribute to the bulk conductivity would be the pore solution conductivity. Considering hydrated products and cement particles to be non-conductive (their conductivity is several orders of magnitude lower than the ionic pore solution), electrical conduction in cementitious materials can be modelled to occur primararily through the ionic pore fluid (in the gel and capillary porosity)[20,23]. This is significant, as temperature influences chemical equilibrium states; impacting ionic mobility (primary effect) and solubility (secondary effect)[25,26]. Ionic mobility (or equivalent conductivity) is noted to increase with increasing temperature due to the decreasing viscosity of the fluid (water), and an increase in the extent of dissociation of the dissolved ionic species, which increases the conductivity of the system[1]. An inverse effect (decreasing conductivity) would be noted with decreasing temperature.

The second component which contributes to the overall conductivity would be the pore fluid volume. For a sealed system, at a given degree of hydration ignoring changes in fluid volume due to changes in density with temperature, the pore fluid volume would be fixed; as solution is not removed from or added to the system. This should however be distinguished from a change in the pore fluid volume due to the consumption of water during hydration.

The third component is the pore fluid connectivity (equivalent to the inverse tortuosity), which decreases due to pore structure refinement with increasing maturity; a function of time and the reaction temperature.

Activation energy of electrical conduction in cement paste and pore solution

Cement paste specimens subjected to thermal cycling were used to determine the influence of temperature on the cement paste conductivity, Figure 3. The results were used to determine the activation energy of electrical conduction (E_{aC}) in cement pastes, Figure 5. The activation energy of conduction was determined to be 25.6 kJ/mol for the plain mixture and 27.6 kJ/mol for the SRA mixture. A higher activation energy of conduction

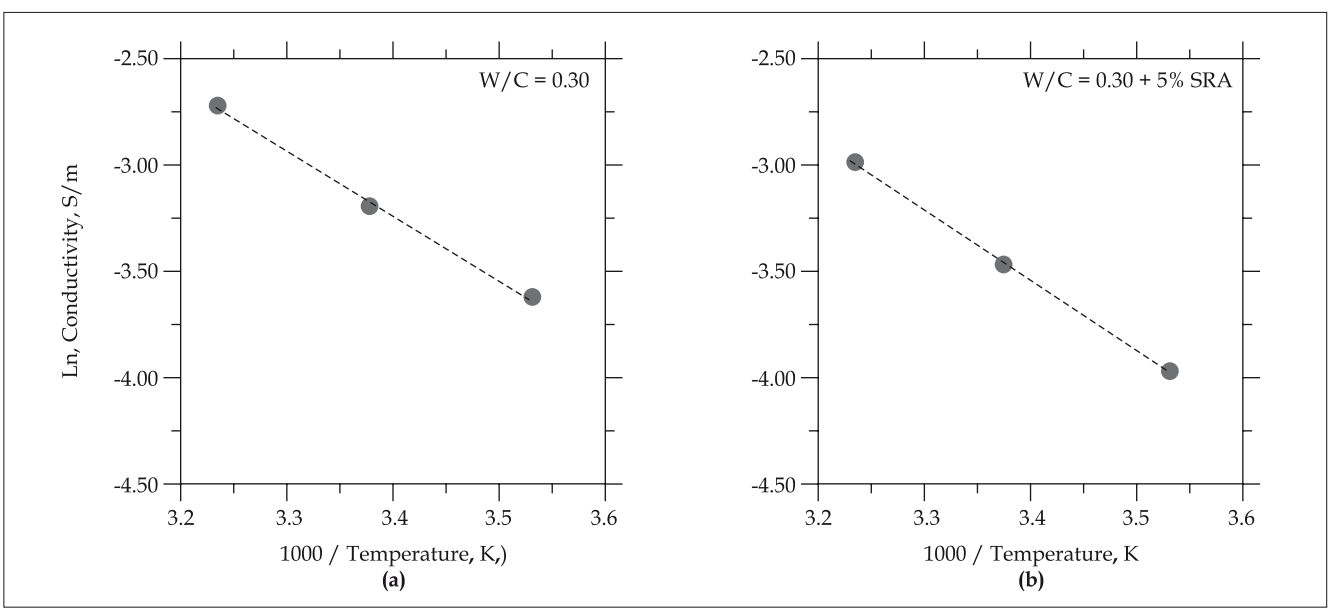

Figure 5. The activation energy of electrical conduction for cement pastes investigate (a) W/C = 0.30 and (b) W/C = 0.30 + 5% SRA

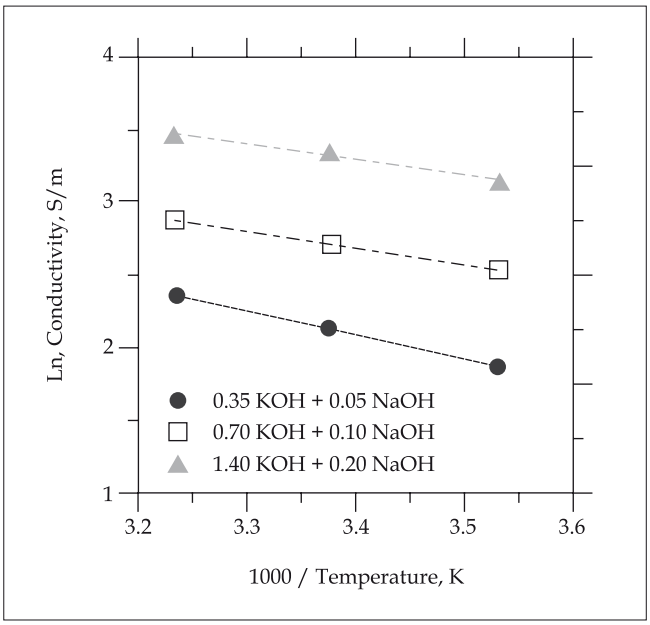

Figure 6. The activation energy of the conduction process for synthetic pore solutions

in mixtures containing a SRA may be explained by the non-conductive nature of the SRA which impedes ion migration in the system. Further, the SRA may bind ions reducing electrical conduction in the system[21].

To fully understand the influence of temperature on the conductivity of an aqueous electrolyte a brief background on electrolytic conductivity is needed. The conductivity of an aqueous electrolyte can be expressed using Equation 7 where, z is the species valence (unitless), c is the molar concentration of the electrolyte (mol/L) and λ is the equivalent conductivity (cm^2 S/mole) of each species at infinite dilution (which is a function of temperature) and is proportional to the ionic mobility[26]. At low concentrations (< 0.01 mol/l), that is, in dilute solutions the equivalent conductivity is a constant for a specific species. However, at high concentrations the equivalent conductivity is observed to decrease inversely (but non-linearly), due to ion-ion interactions in the solution[19,27].

$$\sigma_{Solution} = \sum z_i c_i \lambda_i \qquad .....(7)$$

Conductivity measurements were performed on synthetic pore solutions subjected to thermal cycling. The solutions were selected to correspond to the concentration of the pore fluid of an early-age cement paste (~ 2 hours), a later age cement paste (48 hours), and a pore fluid with a very high molar (ionic) strength. The results of these tests were used to determine the activation energy of the conduction process (E_{aC}) (Figure 6; 13.55 kJ/mole, 9.65 kJ/mole and 8.98 kJ/mole, respectively, in order of increasing solution concentration) in the ionic solutions. It is noticed that the activation energy decreases with increasing concentration, indicating concentrated solutions are less sensitive to temperature change as compared to dilute solutions. This observation can be explained by the large degree of inter-ionic interactions in concentrated solutions, which significantly alter the conductivity behaviour[27].

Temperature correction for electrical conductivity

The activation energy of conduction in an electrolyte can be used to correct the influence of temperature, by transforming the conductivity at any temperature (in this case 283K or 309K) to a reference temperature (in this case 296K) using the expression shown in Equation 8.

$$\sigma(T_{REF}) = \frac{\sigma(T)}{exp\left(-\frac{E_{ac}}{R}\left(\frac{1}{T} - \frac{1}{T_{REF}}\right)\right)} \qquad .....(8)$$

where, $\sigma(T)$ is the sample conductivity (S/m) at any temperature T (K), $\sigma(T_{REF})$ is the conductivity (S/m) at a reference temperature, T_{REF} (296K), E_{aC} is the activation energy of electrical conduction in an electrolyte (or cement paste) (J/mole) and R is the universal gas constant (J/K.mole). The temperature correction is performed using the activation energy of conduction of the pore solution, having the lowest concentration (conductivity). This solution was selected as it is noted to correspond to the pore solution chemistry (conductivity) of a 2 hour old cement paste (0.35 KOH + 0.05 NaOH), which contains a large fluid volume; whose electrical conductivity behaviour is most sensitive to changes in temperature (Figure 6 – highest E_{aC}).

Determination of the activation energy of the hydration reaction

Electrical conductivity can be corrected to account for the influence of temperature on the rate of hydration and, consequently microstructural development (pore structure refinement). This component may be accounted for using a temperature transformation such as an equivalent age (i.e. maturity) function proposed by Hansen and Pedersen[28]; Equation 9. In this paper, the equivalent age function (Equation 9) is used to

determine the activation energy of cement hydration (E_{aR}), after normalising conductivity at any temperature to a reference temperature T(K); using Equation 8.

$$M(t,T) = \int_0^t exp\left(-\frac{E_{aR}}{R}\left(\frac{1}{T} - \frac{1}{T_{REF}}\right)\right) \bullet dt \qquad .....(9)$$

where, M (hours) is the maturity (or equivalent age) of the specimen at a reference temperature T_{REF} (K), E_{aR} (KJ/mol) is the apparent activation energy of the hydration reaction, R (J/(mol · K)) is the gas constant (8.314 J/mol-K), T (K) is the average temperature of the concrete, and dt (hours) is the time interval[28]. The apparent activation energy determined from 10% to 35% hydration; (39.50 kJ/mol) is similar to values determined by other methods (e.g. chemical shrinkage) for the cement systems investigated[20].

Correction for the influence of temperature on hydration and electrical conductivity

As illustrated in Equation 1, the conductivity behaviour of a cementitious material can be expressed as a function of maturity and the measurement temperature. This section will describe a procedure which can be used to simultaneously account for the influence of temperature on cement hydration and electrical conductivity. Due to space considerations, this paper will describe the procedure only for the plain cement mixture (W/C = 0.30).

A function can be fit to describe the experimental conductivity measurement (W/C = 0.30) at the reference temperature (in this case 296K). This function is shown in Equation 10 (R2 = 0.9996).

$$\sigma(t,296K) = \frac{1.38 - 0.82t + 0.19t^2 - 0.01t^3 + 0.0002t^4}{1.00 - 0.66t + 0.19t^2 - 0.02t^3 + 0.001t^4 + 0.00002t^5} \qquad .....(10)$$

where, $\sigma(t,296K)$ is the measured conductivity at time t (hours) at a measurement temperature of 296K (the reference temperature). The type of fit used to describe the conductivity response is not important. To extend the applicability of this function to describe the electrical conductivity behaviour at any temperature requires the incorporation of a reaction rate constant k_R (unitless) which accounts for the influence of temperature on the rate of cement hydration and an electrical conduction constant k_T (unitless) which accounts for the influence of temperature on electrical conductivity. This approach is described in Equations 11, 12 and 13.

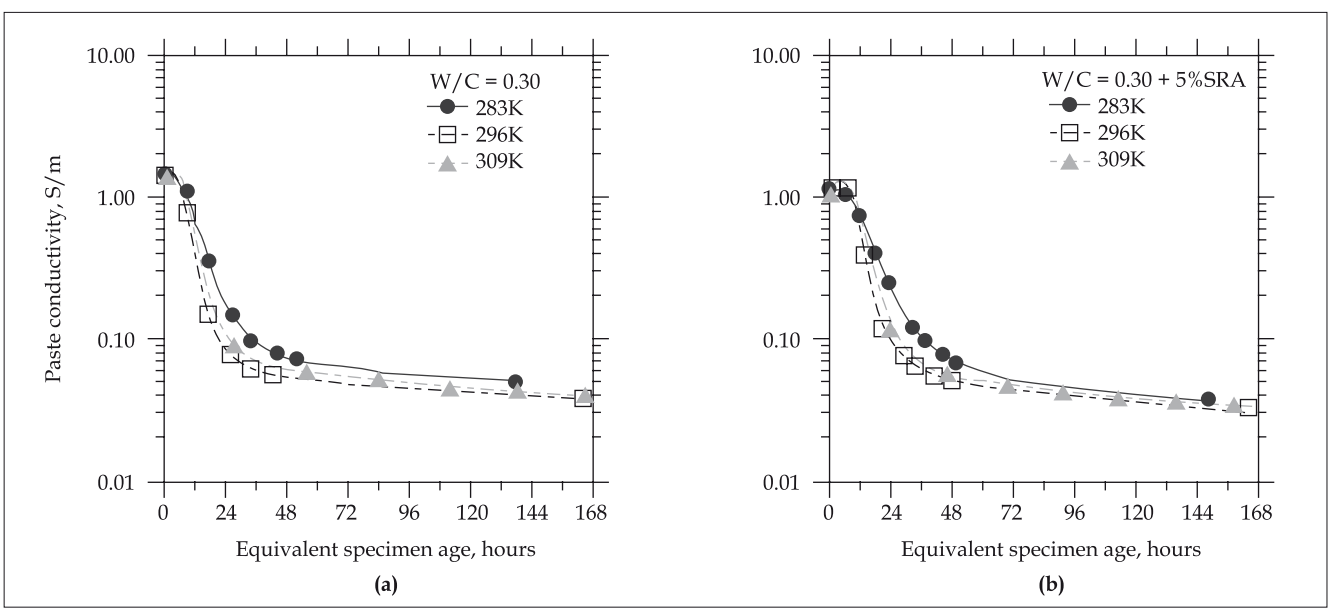

Figure 7. The reaction and solution temperature corrected electrical conductivity of the cement pastes as a function of equivalent specimen age (a) W/C = 0.30 and (b) W/C = 0.30 + 5% SRA

$$\sigma(t,T) = \left(\frac{1.38 - 0.82(t \bullet k_R) + 0.19(t \bullet k_R)^2 - 0.01(t \bullet k_R)^3 + 0.0002(t \bullet k_R)^4}{1.00 - 0.66(t \bullet k_R) + 0.19(t \bullet k_R)^2 - 0.02(t \bullet k_R)^3 + 0.001(t \bullet k_R)^4 + 0.00002(t \bullet k_R)^5} \right) \bullet (k_T) \quad .....(11)$$

where,

$$k_R = exp\left[-\frac{E_{aR}}{R}\left(\frac{1}{T} - \frac{1}{T_{REF}}\right)\right] \quad .....(12)$$

$$k_T = exp\left[-\frac{E_{aC}}{R}\left(\frac{1}{T} - \frac{1}{T_{REF}}\right)\right] \quad .....(13)$$

where, k_R (unitless) is the reaction rate constant which accounts for the influence of temperature on the rate of cement hydration, k_T (unitless) is the electrical conduction constant which accounts for the influence of temperature on electrical conductivity and T (K) is the average temperature of the concrete.

Figure 7 shows the electrical conductivity response of the two cement paste mixtures evaluated using the approach described above, to account for the influence of temperature on cement hydration and electrical conductivity; using the activation energy of cement hydration (E_{aR} = 39.50 kJ/mole) and electrical conduction for the electrical conductivity response of an early pore fluid (0.35 KOH + 0.05 NaOH; EaC = 13.55 kJ/mole). It can be seen that (Figure 7), using the approach described in Equation 11, the influence of temperature on hydration and electrical conductivity can be comprehensively described for mixtures cured at any temperature.

An improved approach is proposed to perform the temperature correction for electrical conductivity if the pore solution chemistry (conductivity) at early-ages is well known. This would involve determining the activation energy of electrical conduction in electrolytes (pore fluids) having an age-dependent concentration (and conductivity). This information can be used to perform a comprehensive temperature correction for electrical conductivity. An example of such an approach is illustrated in Figure 8 which shows the activation energy of electrical conduction as a function of the solution's conductivity at the reference temperature (296K)[20,29].

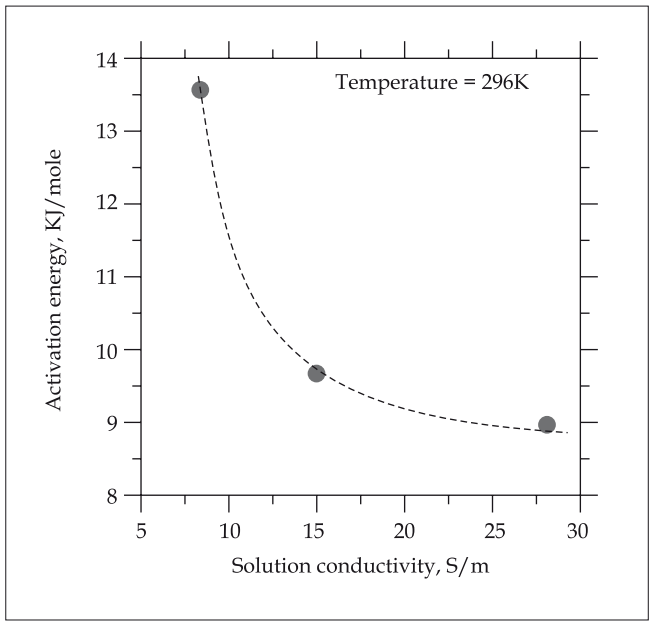

Figure 8. The non-linear relationship between the activation energy of electrical conduction(E_{aC}) and the solution conductivity at 296K

Conclusions

Measurements of electrical conductivity performed on paste, mortar and concrete require a two-part correction to accurately describe early-age behaviour. The first part of this approach accounts for the influence of temperature on cement hydration (pore refinement), and the second part accounts for the influence of temperature on electrical conductivity. This paper demonstrates the successful application of this correction for electrical conductivity measurements using the activation energy of electrical conduction and cement hydration. In this context, the activation energy of electrical conduction has been determined for electrolytes of varying concentrations and for cement pastes. In addition, the activation energy of cement hydration has been determined to be 39.50 kJ/mol (independent of w/c) and is noted to be similar to values determined using other techniques (e.g. chemical shrinkage or heat of hydration). The approach demonstrated in this paper would be crucial for forecasting the long-term durability performance of field concretes, based on the early-age electrical properties of the material using an approach similar to that presented by Lane[30]. An approach of this nature would provide fundamental information needed for quality control and quality assurance (QC/QA) applications and for ensuring the specification compliance of field concretes. This information would have an immense impact in determining how field concrete is specified, evaluated or purchased.

Acknowledgement

The authors gratefully acknowledge the support from the Center for Advanced Cement Based Materials (ACBM) and the National Science Foundation (NSF). This material is based in part on work supported by NSF Grant No. 0134272: a 'CAREER AWARD' granted to the last author. This work was conducted in the Material Characterisation and Sensing Laboratory at Purdue University and as such, the authors gratefully acknowledge the support that has made this laboratory and its operation possible. The contents of this paper reflect the views of the authors, who are responsible for the accuracy of the data presented herein.

References

1. Adamson, A.W., *A Text-book of Physical Chemistry*, Academic Press, USA, 1973.
2. Binder, R.C., *Fluid Mechanics*, Prentice-Hall Inc., Englewood Cliffs, NJ, 1973.
3. Activation Energy, *Encyclopedia Britannica*, 2007.
4. Carino, N.J., The maturity method, *CRC handbook on nondestructive testing of concrete* , Edited by V.M. Malhotra and N.J. Carino, CRC Press, Boca Rotan, Florida, 1991, pp. 101-146.
5. Weiss, W.J., Experimental determination of the 'Time-Zero', *Early age cracking in cementitious systems* – RILEM report TC-EAS, Edited by Arnon Bentur, 2002.
6. Pinto, R.C.A. and Hover, K.C., Application of maturity approach to setting time,' *ACI Materials Journal*, 1999, Vol. 96, No. 6, pp. 686-691.
7. Roy, D.M., Scheetz, B.E., Sabol, S., Brown, P.W., Shi, D., Licastro, P.H., Idorn, G.M., Andersen, P.J., and Johanson, V., Maturity model and curing technology, Strategic Highway Research Program, SHRP-C-625, (1993)
8. Nurse, R.W., Steam curing of concrete, *Magazine of Concrete Research*, 1949, Vol. l, No. 2, pp. 79-88.
9. Saul, A.G.A., Principles underlying the steam curing of concrete at atmospheric pressure, *Magazine of Concrete Research*, 1951, pp. 127-140.
10. Hammond, E., and Robson, T.D., Comparison of Electrical Properties of Various Cements and Concretes, *The Engineer*, 1955, Vol. 199, pp. 78-80.
11. Rasch, E. and Hinrichsen, F.W., Uber eine beziehung zwischen elektrischer leitfahigkeit und Temperatur, *Zeitschrift fur electrochemie*, 1908, Vol. 14, No. 41, pp. 41- 48.
12. Spencer, R.W., Measurement of the Moisture content of concrete, *Journal of the American Concrete Institute*, 1937, Vol. 9, No. 1, pp. 45-61.
13. Elkey, W. and Sellevold, E.J., *Electrical resistivity of concrete, Norwegian Road Research Laboratory*, Publication No. 80, 1995, Oslo.
14. Whittington, H.W., McCarter, W.J. and Forde, M.C., The conduction of electricity through concrete, *Magazine of Concrete Research*, 1981, Vol. 33, No. 114, pp. 48-60.
15. McCarter, W.J., Effects of temperature on conduction and polarization in portland cement mortar, *Journal of the American Ceramic Society*, 1995, Vol. 78, No. 2, pp. 411-415.
16. McCarter, W.J., Starrs, G. and Chrisp, T.M., Electrical conductivity, diffusion, and permeability of portland cement-based mortars, *Cement and Concrete Research*, 2000, Vol. 30, No. 9, pp. 1395-1400.
17. Arrhenius, S., On the reaction velocity of the inversion of cane sugar by acids, Zeitschrift für physikalische Chemie, 4, 226, (1889).
18. Sant, G., Lura, P. and Weiss, W.J., Measurement of volume change in cementitious materials at early ages: Review of testing protocols and interpretation of results, *The Transportation Research Record*, 2006, 1979.
19. Rajabipour, F., Weiss, W.J. and Abraham, D., Insitu electrical conductivity measurements to assess moisture and ionic transport in concrete, Advances in concrete through science and engineering, *Proceedings of the International RILEM Symposium*, Evanston, Illinois, 2004.
20. Sant, G., *Examining volume changes, stress development and cracking in cement-based systems*, MSCE Thesis, Purdue University, West Lafayette, Indiana, USA, 2007.
21. Rajabipour, F., Sant, G. and Weiss, W.J., Interactions between shrinkage reducing admixtures and cement paste's pore solution, *Cement and Concrete Research*, 2008, Vol. 38, pp. 606-615.
22. Garboczi, E.J., Permeability, diffusivity, and microstructural parameters : A critical review, *Cement and Concrete Research*, Vol. 20, No. 4, pp. 591-601.
23. Rajabipour, F., *Insitu electrical sensing and material health monitoring in concrete structures*, PhD Dissertation, Purdue University, West Lafayette, Indiana, USA, 2006.
24. Christensen, B.J., Coverdale, R.T., Olson, R.A., Ford, S.J., Garboczi, E.J., Jennings, H.M. and Mason, T.O., Impedance spectroscopy of hydrating cement-based materials: Measurement, interpretation, and application, The American Ceramic Society, 1994, Vol. 77, No. 11, pp. 2789-2802.
25. Taylor, H.F.W., *Cement Chemistry*, Academic Press, London, (1990)
26. Bockris, J.O.M., and Reddy, A.K.N., *Modern electrochemistry*, Vol. 1, Section 4.4, 1970, Plenum, New York City, NY, USA.
27. Snyder, K.A., Feng, X., Keen, B.D. and Mason, T.O., Estimating the electrical conductivity of cement paste pore solutions from OH-, K+ and Na+ concentrations, *Cement and Concrete Research*, 2003, Vol. 33, No. 6, pp. 793-798.
28. Hansen, F., and Pedersen, E. J., Maturity computer for controlled curing and hardening of concrete, *Nordisk Betong*, 1977, No. 1, pp. 21-25 (in Danish).
29. _____*Standard practice for estimating concrete strength by the maturity method*, ASTM C1074-04, ASTM International, West Conshohocken, Pennsylvania, USA, 2004.
30. Lane, D.S., Supplanting the rapid chloride permeability test with a quick measurement of concrete conductivity, Virginia Transportation Research Council, Charlottesville, Virginia, USA, 2005.

Mr. Gaurav Sant received his bachelor's (BSCE) and master's degrees (MSCE) in civil engineering from Purdue University with an emphasis in construction materials. Currently, he is pursuing his PhD at the School of Civil Engineering at Purdue University. His research interests include early-age shrinkage and cracking, non-destructive testing and moisture transport in cementitious materials.

Dr. Farshad Rajabipour received his BSc from Sharif University of Technology (Tehran) and his MS and PhD from Purdue University. Currently, he is an assistant professor of civil and environmental engineering at the University of Hawaii, Mānoa. His research interests include materials science of concrete, construction sustainability and use of recycled materials, and non-destructive testing and health monitoring.

Prof. Jason Weiss is associate head in the School of Civil Engineering at Purdue University and the associate director of the National Science Foundation, Center for Advanced Cement Based Materials at Northwestern University. His research interests include early-age shrinkage, cracking and its influence on durability, durability of environmentally friendly binders, moisture transport and service-life predictions of civil infrastructure.

Variability Analysis of the Bulk Resistivity Measured Using Cylinders

R.P. Spragg[(1)], J. Castro[(2)], T Nantung[(4)], M. Paredes[(3)], and J. Weiss[(5)]

[(1)] Graduate Research Assistant, Purdue University, School of Civil Engineering, 500 Stadium Mall Dr., West Lafayette, IN, 47907, rspragg@purdue.edu

[(2)] Assistant Professor, Pontificia Universidad Catolica de Chile, School of Civil Engineering, Casilla 306, Correo 22, Santiago, Chile, jecastro@ing.puc.cl

[(3)] Manger for Pavement Materials and Construction Research, Indiana Department of Transportation, Division of Research and Development P.O. Box 2279, West Lafayette, IN, 47906, tnantung@indot.in.gov

[(4)] State Corrosion Engineer, Florida Department of Transportation State Materials Office, Corrosion Research and Durability Laboratory, 6007 NE 39th Avenue, Gainesville, FL, 32609, mario.paredes@dot.state.fl.us

[(5)] Professor of Civil Engineering and Director of Pankow Materials Laboratory, Purdue University, School of Civil Engineering, 500 Stadium Mall Dr., West Lafayette, IN, 47907, wjwweiss@purdue.edu

ABSTRACT

Many agencies are interested in using a rapid test method for measuring the electrical properties of concrete (i.e., the resistivity or conductivity) since they are related to fluid transport (e.g., diffusion). The advantage of the electrical testing is that it is relatively easy to perform and the test method is relatively fast (on the order of 1 minute). Over the last century, many studies have investigated different approaches to measuring electrical properties. This paper describes the variability associated with the method of measuring the bulk resistivity along the longitudinal axis of a cylinder after placing electrodes on either end. A multi-laboratory study of ten participating laboratories provided variability data for twelve concrete mixtures at testing ages of 28, 56, and 91 days. The variability within the same laboratory was evaluated as the operator variability while the variability between laboratories was evaluated as the multi-laboratory variability. Information on the variability is important in the development of precision and bias statements for this test. In addition, this work discusses how the resistivity results obtained from this test can be correlated with surface resistivity measurements made using the Wenner probe. After correcting for geometry using the approach proposed by Morris et. al. (1996), a linear agreement was noticed between the Wenner test and the measurement through the cylinder. Additionally, the effect of the electrode resistance was discussed and for high resistivity concrete such as that used in much of the transportation infrastructure, this effect appears to be negligible, however it can be accounted for numerically.

1.0 INTRODUCTION

For at least a century, tests have been proposed to measure the electrical properties of concrete [1-7]. These methods have an advantage of being relatively fast to perform and the principle behind these tests is relatively straightforward. While concrete is a composite consisting of a vapor phase (vapor filled porosity or "air"), a solid phase (aggregate and cementitious solids) and a fluid phase (the pore solution) the conductivity of each of these individual phases are very different. The conductivity of the solid and vapor phases are extremely low, approximated as 10^{-9} and 10^{-15} S/m respectively, while the conductivity of the liquid phase is several orders of magnitude higher, ranging from 1 to 20 S/m [8, 9].

As such, it can be assumed that the majority of conduction occurs through the pore fluid. A number of composite models have been developed where this concept is used [10-13]. Two of the more popular equations that are used in the cement and concrete literature are Archies expression and the modified parallel expression [11, 14]. While several documents have reviewed these methods previously, the goal of this section is to describe that the overall conduction is dependent on three factors as illustrated with the modified parallel rule in Equation 1:

$$\sigma_c = \frac{\sigma_0 \cdot \phi \cdot \phi}{\tau} \qquad [1]$$

Where σ is the bulk conductivity, σ_0 represents the conductivity of the fluid phase, ϕ is the volume portion of the fluid phase, s is the degree of saturation and , τ is the tortuosity of the pore network. Collectively, the factor , τ/ϕ can be referred to as the formation factor for a given saturation. This implies that electrical testing is sensitive to concrete with a higher fluid volume (higher water content) and a more open pore network that leads to higher connectivity (higher w/c).

One of the more popular electrical test methods is the Rapid Chloride Permeability Test or RCP test [15, 16]. This test method involves placing a saturated concrete specimen, typically four-inch diameter and two inches thick, between electrodes in different solutions and integrating the charge that is passed over a six hour testing period [15]. While this test has gained wide use, there are a few drawbacks that have been pointed out [17-19]. First this test is destructive in nature. As a result each sample can only provide a single measurement at a single age. Second, saturating the specimen can take a relatively long preparation time. Third, the potential for heating effects due to the large voltage and long test period, and possible modification of the microstructure [20, 21]. There has been research regarding temperature correction for the RCP test [22, 23], but for many RCP test setups monitoring of temperature can be difficult or is frequently not done. Proposed changes to this test have been proposed include extrapolating the charge passed after a test duration of 30-minutes and extrapolating to the 6-hour value [24], increasing the size of the reservoirs to reduce the heating effects [25], and using a single resistance reading measured at an early age, often 1-minute or 5-minutes [18, 19].

Alternative testing methods have been proposed that require little to no sample preparation or enable the sample to be tested at different ages. One rapid test for electrical resistivity of concrete is the Wenner probe. As with any test, there are certain considerations that can impact the results. For example, the probe spacing, geometry of the sample, aggregate size and surface moisture conditions can all influence the measured electrical response. Since the moisture conditions at the surface of the test specimens are quite important, care should be taken to protect against drying or using on surface treated concretes [26-28]. Some work has been done to evaluate the effect of differing layer properties [29]. Additionally, some work has suggested the need for an additional non-linear geometry factor for this method that occurs from the constricted geometry, such as that of a standard test cylinder [30]. Further, when this method is used on real structures the location and proximity of the rebar needs to be considered [29, 31].

Several of these concerns can be addressed if a standard testing protocol is adopted. A draft test method has been developed to use a four-probe Wenner configuration on a 102 mm x 205 mm cylinder with probe spacing of 38.1 mm [32]. This surface resistivity (SR) test method places the probes directly on the surface of the test specimen. This test method has been accepted for use by the Florida Department of Transportation as a quality control test [26]. Additional departments of transportation have evaluated

the SR method as a possible quality control method as well [33]. Work has also been done to correlate RCP testing and diffusion testing with SR [26, 34, 35]. This method has a distinct advantage in that it is rapid to perform and easy to perform on the surface of a cylinder.

The resistance of a concrete cylinder can alternatively be evaluated by using plate electrodes that can be placed on the end of the sample [31, 36]. The resistance value obtained can be normalized by specimen geometry, simply the ratio of sample cross-sectional area to length, to obtain the sample resistivity, termed the bulk resistivity or BR. For this test, good electrical contact must be ensured between the plate electrodes and the test specimen [30, 36]. While this can be assisted through the use of a conductive medium, the surface finish of the cylinder ends should be flat. Some work was also done on evaluating the contact pressure between the plate and the specimen [36]. This test has the distinct advantage of rapid testing and a simple geometry factor. To the best of the authors knowledge, a multi-laboratory study of variability has not been performed on this geometry though some studies have reported exchanges of samples between two labs [36].

Three major factors that should be considered in any electrical resistivity testing are the effects of geometry and temperature. While the bulk resistivity of concrete can be considered a material property, the tests that are performed provide a measure of electrical resistance. The resistance measurement should be corrected for the geometry. This correction can be determined empirically or numerically, although some corrections are simpler. Different geometries have been considered where the geometry factor can be determined experimentally [8, 37]. Temperature is another important factor in the testing of concrete resistivity. This occurs as the primary conduction path is through the ionic pore solution; the increase of temperature increases the mobility of the ions decreasing the resistivity. There has been work that has investigated the possibility of a temperature correction for resistivity test s [6, 38-42]. In this work the samples are all performed in laboratory conditions, as such the sample should be 23+/-2C. Lastly, from Equation 1, saturation is a major component of the bulk conductivity of concrete. As such, knowledge of the moisture history and moisture content at testing are important considerations in the evaluation of resistivity data [43].

The main objectives of this study are fourfold:

- First, it provides some background on electrical property measurements for concrete and provides some of the physical principles behind these tests.
- Second, it presents the results of an inter-laboratory test of the electrical bulk resistivity of concrete. This information can be used in the development of precision and bias statements
- Third, it demonstrates the relationship between surface resistance test methods (e.g. wenner) and measurements performed on a cylindrical geometry.
- Fourth, it highlights important considerations in the development of testing standards and development of policies for the use of electrical methods as quality control/quality assurance tests.

2.0 EXPERIMENTAL DETAILS

2.1 Materials

A round robin test testing program was proposed in 2009 to evaluate the repeatability of the Wenner and bulk resistance tests on concrete cylinders. A series of twelve concrete mixtures were prepared at the laboratories who participated in this study. The mixtures are structural/bridge deck concretes used by state departments of transportation from around the country. A final report detailing a parallel series of wenner and bulk resistivity tests conducted by AASTHO TIG group are available [44, 45].

Table 1—Summary of mixture proportions used in this study, SSD masses

Mixture No.	w/cm	Water	Cement	Fly Ash	Micron Fly Ash	Slag	Silica Fume	Meta-Kaolin	Coarse Aggregate 1	Coarse Aggregate 2	Fine Aggregate
		kg/m^3	kg/m^3	kg/m^3	kg/m^3	kg/m^3	kg/m^3	kg/m^3	kg/m^3	kg/m^3	kg/m^3
1	0.34	163	237	119	-	119	-	-	1059	-	717
2	0.40	144	285	71	-	-	-	-	282	854	824
3	0.39	199	392	119	-	-	-	-	785	-	724
4	0.35	158	279	178	-	-	-	-	940	-	793
5	0.40	164	308	103	-	-	-	-	909	-	879
6	0.37	145	390	-	-	-	-	-	1068	-	712
7	0.40	160	297	80	-	-	24	-	532	528	686
8	0.39	131	251	84	-	-	-	-	555	-	1295
9	0.41	151	291	65	-	-	15	-	1032	-	697
10	0.30	151	297	153	44	-	-	-	1009	-	638
11	0.30	157	430	95	-	-	-	-	1033	-	577
12	0.35	156	402	-	-	-	-	44	1009	-	624

2.2 Sample Conditioning

The samples were demolded at an age of 48-hours and placed into a saturated lime-water bath kept at a constant room temperature until the age of testing (23+/- 2C). At an age of 14-days, the respective laboratories removed the samples and wrapped them in paper towels soaked in saturated lime-water. The samples were then double-bagged and prepared to be shipped via two-day shipping to the other participating laboratories. The goal is to ensure the samples remain wet during testing.

After the samples were received by other testing laboratories, they were removed from the bag and place into saturated lime water baths kept at room temperature (23+/- 2C). At ages of 28, 56, and 91-days, the samples were removed from saturated lime bath, the surface was wiped dry, and the samples were tested for SR and DR. After this testing the samples were placed back in the saturated lime water.

3.0 TESTING PROCEDURE

It should be noted that the test described herein (the plates placed on the end of the cylinder) was a part of a larger study conducted by the AASTHO TIG evaluating surface resistivity [44, 45]. Not all of the labs chose to participate in this portion of the study, so those laboratories have been excluded from the following data though to avoid confusion the original laboratory numbers were retained.

3.1 Equipment

The equipment involved in this test consisted of a CNS Farnell Mk II, U95 surface resistivity meter using an alternating current at 13 Hz, a set of 4-inch diameter stainless steel plate electrodes, and 16 gauge, two-conductor wire to connect the probe tips of the surface resistivity meter to the plate electrodes.

The cable was outfitted with alligator clips on one end to allow easy access to the probe tips of the resistivity meter. The other end of the cable was outfitted with a ring terminal to connect to the plate electrode. The plate electrode was drilled and tapped to allow easy and consistent attachment.

An important consideration is to ensure proper electrical contact between the cylinder and the plate electrodes [30, 36]. For this study, this was done using thin, lime-water saturated sponges.

3.2 Testing Procedure

The plate electrodes should be connected to the pins of the surface resistivity meter. The first two pins that generate the current and measure the potential were connected to one of the steel plate electrodes and likewise for the second set of pins, as shown in Figure 1.

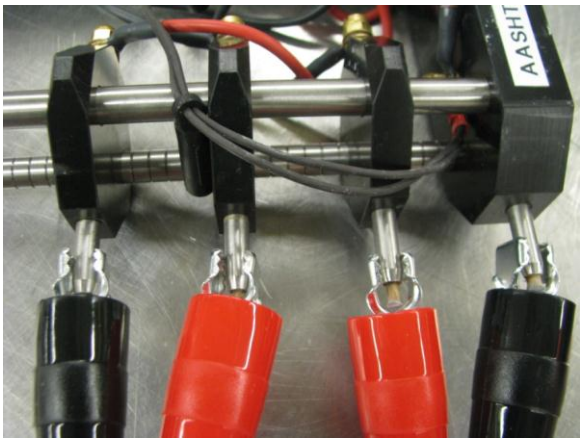

(a)

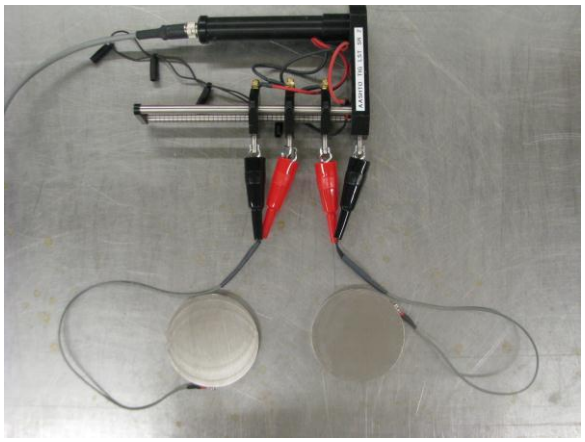

(b)

Figure 1—Attach the alligator clips to the Wenner probe tips. a.) close-up b.) at a distance

The resistances of the top and bottom sponges were then measured, as shown in Figure 2. As resistance of the sponges is largely dependent on moisture content, a test cylinder was used to ensure the pressure on the sponge was consistent for the test of sponge resistance and the measurement of the test cylinder. This was to ensure approximately the same moisture content. The goal of this was to provide a correction for sponge resistance, as discussed below.

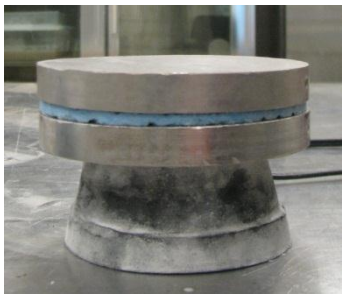

(a)

(b)

Figure 2—Measuring the sponge resistance for a.) the top and b.) the bottom sponges.

The concrete cylinder is then placed between the plate electrodes, with sponges being placed between the plates and the concrete cylinder, as shown in Figure 3.

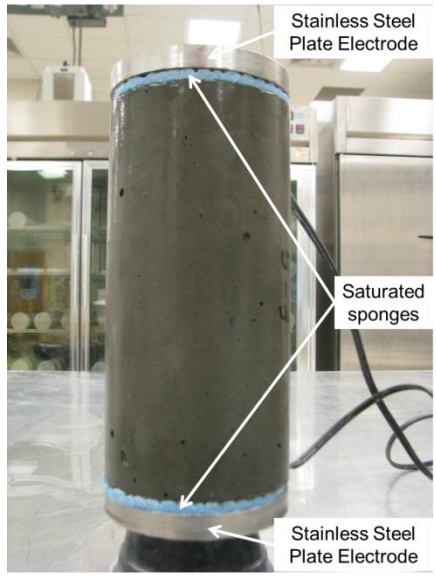

Figure 3—Measuring the resistance of the system.

3.3 Calculations

The resistances of the top and bottom of the top and bottom sponge are termed $R_{\text{top sponge}}$ and $R_{\text{bottom sponge}}$ respectively. The measured resistance of the system, as depicted in Figure 3, was termed R_{measured}. The measured resistance was corrected for the resistance of the sponges by treating the system as resistors in series, as shown in Equation 2. [36]. It was noticed for the sponges used in this study that their resistance values in each lab tended to remain relatively constant. Thus, for sponges that show this constant resistance it is proposed they only be measured periodically and their resistances can be assumed.

$$R_{\text{cylinder}} = R_{\text{measured}} - R_{\text{top sponge}} - R_{\text{bottom sponge}} \quad [2]$$

The bulk resistivity, denoted ρ, can be determined by using Equation 2. Where the geometry factor, K,for current flow through the bulk material is given by Equation 3.

$$\rho = \mathrm{K} \cdot R_{\text{cylinder}} \quad [3]$$

$$\mathrm{K} = \frac{\mathrm{A}}{\mathrm{L}} \quad [4]$$

where R_{cylinder} is the calculated resistance of the concrete test cylinder from Equation 1, A is the cross-sectional area, and L is the length of test specimen.

4.0 RESULTS AND DISCUSSION

4.1 Bulk Resistivity Data

The samples were tested at three ages: 28, 56, and 91-days. The average bulk resistivity (BR) and coefficient of variation (COV) of three test cylinders measured at each testing age is presented below. Cells marked with N/A represent no data reported.

Data measured at ages of 28-days is presented in Table 2. Mixtures 1 through 5 were not tested for 28-day BR as the equipment was in the process of being distributed. Data measured at ages of 56-days is

presented in Table 3. Mixture 1 was not tested for 56-day BR as the equipment had still not been received by one laboratory. Data measured at ages of 91-days is presented in Table 4.

Table 2—Average BR and COV obtained at a testing age of 28-days.

Lab	Test Statistic	Mix 1	Mix 2	Mix 3	Mix 4	Mix 5	Mix 6	Mix 7	Mix 8	Mix 9	Mix 10	Mix 11	Mix 12	Average
1	Average	N/A	N/A	N/A	N/A	N/A	5.29	13.41	14.97	8.84	12.67	6.46	14.89	
	COV	N/A	N/A	N/A	N/A	N/A	0.52	1.15	8.52	1.84	0.47	9.96	5.52	4.00
2	Average	N/A	N/A	N/A	N/A	N/A	5.27	14.12	16.98	8.36	13.49	6.73	18.84	
	COV	N/A	N/A	N/A	N/A	N/A	0.21	1.50	1.07	0.23	2.23	9.56	3.21	2.57
3	Average	N/A	N/A	N/A	N/A	N/A	5.19	13.54	14.03	7.69	11.53	5.43	16.04	
	COV	N/A	N/A	N/A	N/A	N/A	0.58	0.85	1.69	1.79	1.50	0.91	10.67	2.57
5	Average	N/A	N/A	N/A	N/A	N/A	5.65	15.19	16.73	8.31	16.93	7.36	N/A	
	COV	N/A	N/A	N/A	N/A	N/A	0.97	0.63	2.83	1.58	0.97	1.38	N/A	1.39
6	Average	N/A	N/A	N/A	N/A	N/A	5.55	15.24	15.69	9.60	13.72	6.68	20.24	
	COV	N/A	N/A	N/A	N/A	N/A	1.84	1.14	0.57	0.87	3.17	0.77	0.07	1.20
7	Average	N/A	N/A	N/A	N/A	N/A	5.03	13.59	15.01	8.91	12.87	6.88	16.90	
	COV	N/A	N/A	N/A	N/A	N/A	0.89	0.89	1.06	0.08	1.12	1.03	0.39	0.78
8	Average	N/A	N/A	N/A	N/A	N/A	5.84	14.36	16.58	8.63	14.59	6.81	18.21	
	COV	N/A	N/A	N/A	N/A	N/A	0.55	2.54	0.83	1.11	3.07	1.90	0.85	1.55
9	Average	N/A	N/A	N/A	N/A	N/A	5.31	14.39	16.37	8.91	13.15	7.00	16.48	
	COV	N/A	N/A	N/A	N/A	N/A	0.03	0.06	0.68	0.58	3.03	0.58	5.07	1.43
10	Average	N/A	N/A	N/A	N/A	N/A	5.12	14.20	15.60	8.62	14.22	6.77	18.55	
	COV	N/A	N/A	N/A	N/A	N/A	0.01	0.35	0.13	4.51	0.92	0.22	0.63	0.97
12	Average	N/A	N/A	N/A	N/A	N/A	5.68	14.02	15.11	8.30	12.30	6.40	16.76	
	COV	N/A	N/A	N/A	N/A	N/A	0.01	0.20	0.04	0.21	0.26	0.13	0.11	0.14
All Labs	Average	N/A	N/A	N/A	N/A	N/A	5.39	14.21	15.71	8.62	13.55	6.65	17.43	
	COV	N/A	N/A	N/A	N/A	N/A	5.00	4.45	6.03	5.89	11.01	7.62	9.46	

Table 3—Average BR and COV obtained at a testing age of 56-days.

Lab	Test Statistic	Mix 1	Mix 2	Mix 3	Mix 4	Mix 5	Mix 6	Mix 7	Mix 8	Mix 9	Mix 10	Mix 11	Mix 12	Average
1	Average	N/A	6.73	8.76	12.63	8.07	6.56	24.34	29.99	14.78	22.20	11.98	18.14	
	COV	N/A	3.86	3.23	3.35	1.51	2.46	0.87	0.73	2.65	2.62	2.50	1.02	2.25
2	Average	N/A	8.64	9.10	12.05	10.83	7.22	24.52	27.25	13.14	22.53	12.69	20.12	
	COV	N/A	2.68	2.55	2.65	7.47	4.17	4.61	1.20	1.67	3.95	6.31	3.21	3.68
3	Average	N/A	6.18	7.81	12.26	7.71	5.81	23.13	21.61	12.17	17.26	N/A	17.71	
	COV	N/A	7.82	2.81	0.82	0.60	0.79	3.70	2.87	2.68	2.55	N/A	6.87	3.15
5	Average	N/A	7.98	9.26	11.41	7.26	7.08	24.10	29.12	14.92	22.48	10.91	N/A	
	COV	N/A	0.00	7.48	1.52	4.69	2.13	2.58	1.67	7.09	1.65	0.76	N/A	2.96
6	Average	N/A	7.70	9.16	12.89	9.99	6.70	N/A	25.02	N/A	19.62	10.09	21.49	
	COV	N/A	3.24	7.42	1.12	1.01	6.86	N/A	3.74	N/A	4.50	2.77	1.62	3.59
7	Average	N/A	8.38	8.55	12.34	8.33	6.57	24.20	27.18	16.50	21.37	12.16	19.88	
	COV	N/A	9.52	3.50	2.29	2.77	3.06	2.15	4.45	1.48	0.66	8.34	3.96	3.83
8	Average	N/A	7.18	9.27	13.64	9.31	6.72	25.89	31.29	14.38	24.98	12.55	20.85	
	COV	N/A	5.85	3.66	1.75	3.01	2.68	5.07	2.63	3.47	2.42	2.55	3.24	3.30
9	Average	N/A	N/A	9.20	13.50	8.59	6.52	26.09	30.28	15.13	23.23	13.43	20.27	
	COV	N/A	N/A	3.61	6.27	1.17	3.48	1.00	2.98	2.05	4.15	3.52	2.47	3.07
10	Average	N/A	7.98	8.92	14.85	7.94	6.26	26.58	26.03	14.20	22.24	11.22	21.46	
	COV	N/A	0.00	5.33	5.28	4.52	1.91	2.20	1.09	6.33	1.83	1.60	2.32	2.95
12	Average	N/A	6.10	8.34	11.94	7.90	6.52	22.21	23.65	13.06	18.67	9.95	15.99	
	COV	N/A	3.00	1.44	1.35	5.13	2.55	5.98	3.48	5.57	4.57	2.21	5.79	3.73
All Labs	Average	N/A	7.43	8.84	12.75	8.59	6.59	24.56	27.14	14.25	21.46	11.66	19.55	
	COV	N/A	12.51	5.43	7.91	13.01	5.95	5.79	11.50	9.14	10.72	10.27	9.60	

Table 4—Average BR and COV obtained at a testing age of 91-days.

Lab	Test Statistic	Mix 1	Mix 2	Mix 3	Mix 4	Mix 5	Mix 6	Mix 7	Mix 8	Mix 9	Mix 10	Mix 11	Mix 12	Average
1	Average	10.24	8.07	12.14	18.71	11.36	7.58	38.05	42.08	19.44	34.98	17.90	18.80	
	COV	4.31	2.81	3.92	3.35	1.33	3.20	0.26	6.35	3.14	3.16	2.49	4.73	3.25
2	Average	12.16	10.43	15.12	18.83	16.81	8.31	32.40	39.19	17.58	29.78	16.17	24.58	
	COV	5.71	2.68	2.55	4.65	4.68	2.46	5.09	1.27	1.14	3.75	5.82	4.22	3.67
3	Average	10.43	7.85	10.61	16.58	9.46	6.65	28.87	31.78	14.63	22.71	13.10	17.18	
	COV	3.85	8.39	7.77	1.60	4.56	7.64	5.05	5.11	3.86	2.00	6.79	3.49	5.01
5	Average	11.01	8.36	12.12	16.21	10.20	8.48	33.45	37.14	20.19	28.66	15.45	N/A	
	COV	4.08	1.53	5.63	1.44	3.94	1.70	2.12	2.79	8.16	1.82	3.51	N/A	3.34
6	Average	13.91	10.11	14.34	23.58	N/A	7.65	30.97	30.81	15.60	29.92	15.80	20.96	
	COV	0.17	1.78	7.11	1.28	N/A	8.25	3.19	0.76	3.77	3.15	1.58	0.58	2.87
7	Average	10.67	10.05	14.11	19.27	12.58	7.94	35.83	40.06	20.81	29.55	17.18	21.03	
	COV	3.59	6.60	6.45	1.04	2.23	2.30	2.34	3.88	1.12	1.08	0.94	3.29	2.91
8	Average	12.22	8.92	13.25	20.47	13.29	7.67	38.06	45.59	19.19	35.36	18.49	20.29	
	COV	1.05	5.37	3.19	2.36	2.46	2.86	5.27	3.06	3.44	2.89	2.29	3.52	3.15
9	Average	11.16	14.35	14.35	19.54	12.06	8.60	37.74	43.37	N/A	34.48	22.41	19.55	
	COV	0.21	1.58	1.58	8.51	2.65	7.51	0.38	7.26	N/A	5.63	9.89	4.55	4.52
10	Average	12.39	9.75	13.71	22.44	12.65	6.74	37.54	38.41	18.26	30.51	16.50	21.15	
	COV	2.19	9.15	4.24	6.30	9.41	0.59	1.31	0.75	6.02	2.23	2.30	2.26	3.90
12	Average	10.07	7.82	11.12	15.96	10.40	7.26	31.21	33.11	14.93	22.67	12.69	18.01	
	COV	4.73	1.84	0.55	1.32	3.78	2.91	5.62	4.19	4.85	3.89	0.63	0.71	2.92
All Labs	Average	11.43	9.57	13.09	19.16	12.09	7.69	34.41	38.15	17.85	29.86	16.57	20.17	
	COV	10.66	20.39	11.56	13.25	18.07	8.77	10.03	13.06	12.95	15.08	16.71	10.75	

4.2 Operator Variability

The operator variability is described from the average COV from each mixture for each different laboratory. This is shown as the last column in Tables 2-5. The maximum of average within-laboratory COV for each testing age is presented in Table 6. Previous work evaluating the development of an automated resistivity testing system has reported similar within-laboratory variability [46].

Table 6—Maximum within-laboratory COV

Testing Age	Within-laboratory COV
28-days	4.00 %
56-days	3.83 %
91-days	5.01 %

4.3 Multi-laboratory Variability

The multi-laboratory variability can be described from the average COVs from each laboratory for the different mixtures. This is shown as the last row in Tables 2-5, termed All Lab COV. The maximum of average multi-laboratory COV for each testing age is presented in Table 7, and is used to develop the precision statement for multi-laboratory variability. It should be noted that the variation increases over time. It is believed that this may be due to slight variations in curing conditions which may have occurred at each lab which could amplify differences overtime.

Table 7—Maximum multi-laboratory COV

Testing Age	Multi-laboratory COV
28-days	11.01 %
56-days	13.01 %
91-days	20.39 %

4.4 Precision Statements

Precision estimates were calculated [47]. For this experiment, the fundamental statistic was determined to be the COV, represented as 1s% in ASTM C670-10. Therefore, the calculated precision indices will correspond to d2s% described in ASTM C670-10. This index represents the maximum difference between two individual test results, expressed as a percentage of their average. The precision indices for different testing ages are shown in Table 8.

Table 8—Precision indices for direct resistivity

Testing Age	Within-laboratory	Multi-laboratory
28-days	11.30	31.14
56-days	10.84	36.79
91-days	14.17	57.66

The maximum precision index for the within-laboratory and multi-laboratory variability will be used to form the precision statements.

The maximum pooled single-operator coefficient of variation was found to be 5.01 %. Therefore, the results of two properly conducted tests by the same operator on the same concrete material at the same age are not expected to differ by more than 14.2 % of their average. The maximum pooled multi-laboratory coefficient of variation was found to be 20.39. Therefore, the results of two properly conducted tests by different laboratories on the same concrete material at the same age are not expected to differ by more than 57.7 % of their average.

4.5 Correlation with Surface Resistivity Measurements

Surface resistivity measurements were conducted as a part of this study [44]. Figure 4 compares the measured SR and the calculated BR.

A linear correlation was noticed, except that SR measurements tended to be 1.86 times higher than BR. This large data of experimental results support previous work using finite element that showed additional geometry factors must be used to account for test geometry, such as probe spacing, cylinder length, and cylinder diameter [30]. The factor of 1.86 is in good agreement with the geometric correction proposed by Morris et. al. (1995) for a cylinder with a length of 205 mm, diameter of 102 mm, probe spacing of 38.1 mm and a MSA of 19 mm, which was approximately 1.9.

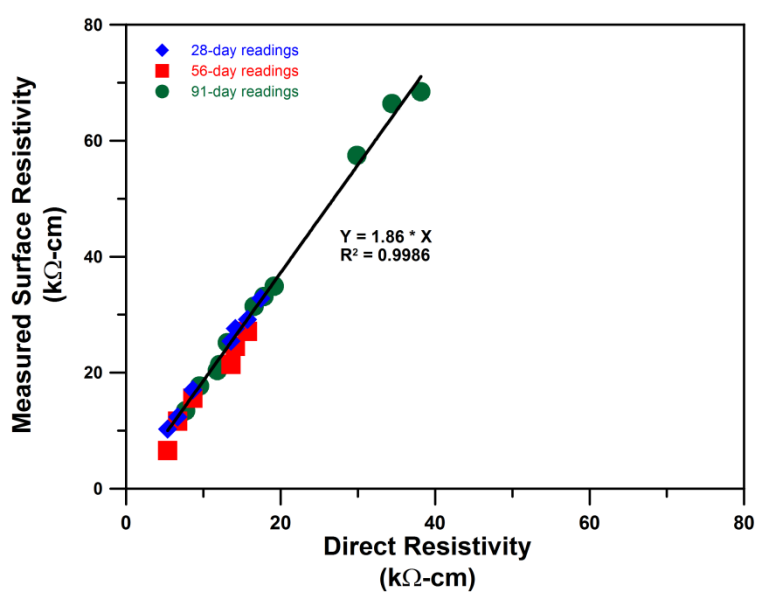

Figure 4—Correlation of measured SR and DR of samples from differing ages, each data point represents the average of three samples.

4.6 Effects of Electrode Resistance

Previous work has shown that electrode resistance (and other factors to insure connectivity between the electrode and sample) may influence the results as discussed in Equation 2.

The major contributor to electrode resistance is bad contact between the plate electrode and the surface of the test cylinder. Some work has suggested the possibility of using flexible electrodes [30]. However, a more practical solution is to use an aid that allows for good electrical contact. In the laboratory, this can be accomplished through the use of an electrically conductive jelly [48, 49]. The alternative is to use another soft, conductive medium. Popular solutions have included the use of saturated sponges, chamois cloth, and paper towels [21, 36].

An important issue becomes the associated resistance of the sponges. Previously, this associated resistance can be treated as a series of resistors in parallel with the test cylinder, which produces the correction shown and described by Equation 2.

The sponge resistance is largely dependent on the moisture content of the sponges and the conductivity of the solution in which they are saturated. For this study, the solution was saturated lime water, which was also used as the storage solution for the test cylinders. Furthermore, to ensure proper moisture content, the contact pressure for the sponge was kept constant between the sponge resistivity test and the cylinder test, as shown in Figures 2 and 3.

While this correction provides the truest value for resistivity, the results of this study show that this correction might not always be very large. For the sponges used in this study, the resistances of the two sponges were much less than the resistance of the cylinder. Figure 5a shows the measured resistance (i.e., sample, sponges and electrodes) as a function of the cylinder resistance (i.e., the sample alone), as defined in Equation 2.The best fit line shows only a small difference between the measured resistance and the cylinder resistance.

Additionally, the ratio of the measured resistance to the cylinder resistance, as defined in the preceding paragraph, can be shown against the concrete resistivity, depicted in Figure 5b. This ratio represents the correction from cylinder resistance. Figure 5b shows that for high resistivity concrete, the resistance correction become almost negligible, while for lower resistivity concrete the sponge resistance might play a larger role.

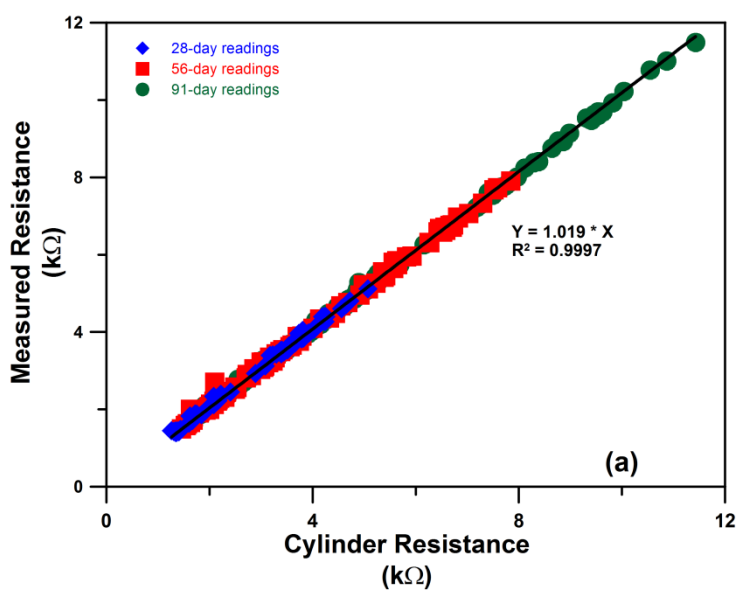

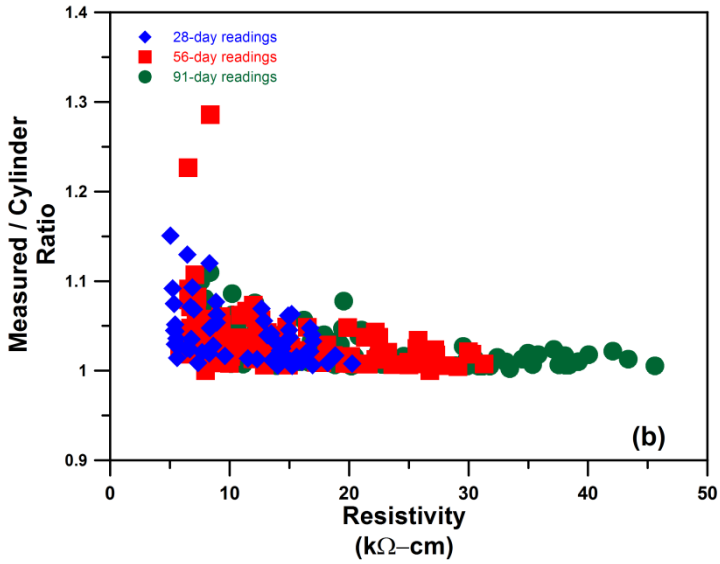

Figure 5—Influence of electrode resistance on a.) the measured resistance (sample and electrodes) as a function of the cylinder (sample) resistance and b.) the ratio of measured resistance (sample and electrodes) and cylinder (sample) resistance as a function of concrete resistivity.

5.0 SUMMARY AND CONCLUSIONS

This paper reports results from a multi-laboratory investigation of the variability associated with testing the electrical bulk resistivity of concrete cylinders by placing plate electrodes on the ends of the cylinder. An analysis of the data is presented. The following observations can be made regarding the variability of the resistivity test method. It should be noted that the samples used in this study were conditioned by storing in lime saturated water between test measurements. First, resistivity testing is a rapid test method that allows for rapid results. This rapid test drastically reduces the amount of time a technician needs to spend conditioning the sample and conducting the test. Therefore, this test is well suited for quality control testing. Second, resistivity testing can be considered a non-destructive test. This means that for each mixture being evaluated using resistivity, only a small number of samples need be prepared. This can be contrasted with other destructive electrical tests that require a larger series of samples for proper mixture evaluation. In fact, this testing can be performed on cylindrical samples before they are tested for compressive or splitting tensile strength. Third, the operator and multi-laboratory precision of this test method have been quantified using data from the maximum COV obtained from an inter-laboratory study consisting of ten laboratories and twelve differing mixtures. Fourth, specimen geometry can greatly influence the results of an electrical test. This often requires the use of a geometry correction factor. For the direct resistivity test, this geometry factor is simply the ratio of sample area to sample length. Finally, the effects of electrode resistance were addressed using a series model. While previous work described corrections for end plate resistance, the variability data from this investigation shows that for the materials used in this study, the correction that is needed is quite small. It is suggested that a resistivity test be developed that could include a variety of sample geometries including 1) the wenner probe geometry, 2) the direct bulk resistance described herein, and 3) alternative geometries provided the geometry factor can be quantified.

6.0 ACKNOWLEDGEMENTS

The experiments reported in this paper were conducted as part of a larger study sponsored by the Pooled Fund Program and the American Association of American Highway and Transportation Officials Technology Implementation Group and organized by the Florida Department of Transportation. This portion of the present study was conducted in conjunction with the Indiana Department of Transportation. The contents of this report reflect the views of the authors, who are responsible for the facts and the accuracy of the data presented herein. The contents do not necessarily reflect the official views or

policies of the Indiana Department of Transportation or the Federal Highway Administration at the time of publication. This report does not constitute a standard, specification, or regulation.

The authors would like to thank the participating laboratories and testing personnel for their time and efforts. This includes, but is not limited to, Rob Reis, Cipriano Manansala, and Joe Shanabrook, California Department of Transportation; Jagan Gudimettla, FHWA Mobile Concrete Laboratory; Celik Ozyildirim and Bill Ordel, Virginia Department of Transportation; Wilfredo Malpica and Javier Molinari, Grupo-Carmelo; Ed McGaffin and Dan Dennis, New York State Department of Transportation; Lieska Halsey, Jeremy Weigel, and Tim Krason, Nebraska Department of Transportation; Eric Prieve and Azis Khan, Colorado Department of Transportation; John Kern and Wayne DeMarco, CEMEX; Thomas Frank and Ronald Simmons, Florida Department of Transportation; Jeremiah Hersey and Professor Mike Jackson, University of North Florida.

Check up to 26

7.0 REFERENCES

[1] E. Hammond, T.D. Robson, Comparison of electrical properties of various cements and concretes. I-II, The Engineer, 199 (1955) 78-80.
[2] Y. Shimizu, An electrical method for measuring the setting time of portland cement, Concrete, 32 (1928) 111-113.
[3] J. Calleja, Effect of current frequency on measurement of electrical resistance of cement pastes, J Am Conc Inst, 24 (1952) 329-332.
[4] W.J. Weiss, J.D. Shane, A. Mieses, T.O. Mason, S.P. Shah, Aspects of monitoring moisture changes using electrical impedance spectroscopy, in: Second symposium on the importance of self desiccation in concrete technology, Lund, Sweden, 1999.
[5] G.E. Monfore, The electrical resistivity of concrete, Portland Cement Association, Research and Development Laboratories, Skokie, IL, 1968.
[6] H.W. Whittington, J. McCarter, M.C. Forde, The conduction of electricity through concrete, Mag Concr Res, 33 (1981) 48-60.
[7] B.J. Christensen, R.T. Coverdale, R.A. Olson, S.J. Ford, E.J. Garboczi, H.M. Jennings, T.O. Mason, Impedance spectroscopy of hydrating cement-based materials: measurement, interpretation, and application, J Am Ceram Soc, 77 (1994) 2789-2804.
[8] F. Rajabipour, Insitu electrical sensing and material health monitoring in concrete structures, Ph.D. Dissertation, Purdue University, West Lafayette, Indiana, 2006.
[9] F. Rajabipour, J. Weiss, Linking health monitoring in concrete structures with durability performance simulations, in: B. Cross, J. Finke (Eds.) ASCE Structures Congress, ASCE, St. Loius, MO, 2006.
[10] S. Torquato, Random heterogeneous materials: microstructure and macroscopic properties, Springer, New York, NY, 2002.
[11] G.E. Archie, The electrical resistivity log as an aid in determining some reservoir characteristics, SPE Reprint Series, (2003) 9-16.
[12] K.L. Aplin, Aspirated capacitor measurements of air conductivity and ion mobility spectra, Rev Sci Instrum, 76 (2005) 104501.
[13] D.S. McLachlan, M. Blaszkiewicz, R.E. Newnham, Electrical resistivity of composites, J Am Ceram Soc, 73 (1990) 2187-2203.
[14] E.J. Garboczi, Permeability, diffusivity, and microstructural parameters: A critical review, Cem Concr Res, 20 (1990) 591-601.
[15] ASTM C1202, 2010, Standard test method for electrical indication of concrete's ability to resist chloride ion penetration, ASTM International, West Conshohocken, PA.
[16] AASTHTO T277, 2007, Standard method of test for electrical indication of concrete's ability to resist chloride ion penetration, American Association of State Highway and Transportation Officials, Washington, D.C.
[17] J.D. Shane, C.D. Aldea, N.F. Bouxsein, T.O. Mason, H.M. Jennings, S.P. Shah, Microstrucutral and pore solution changes induced by the rapid chloride permeability test measured by impedance spectroscopy, Concr Sc Eng, 1 (1999) 110-119.
[18] K.A. Riding, J.L. Poole, A.K. Schindler, M.C.G. Juenger, K.J. Folliard, Simplified concrete resistivity and rapid chloride permeability test method, ACI Mater J, 105 (2008) 390-394.

[19] K.A. Snyder, C. Ferraris, N.S. Martys, E.J. Garboczi, Using impedance spectroscopy to assess the viability of the rapid chloride test for determining concrete conductivity, J NIST, 105 (2000) 497-509.
[20] D. Sohn, T.O. Mason, Electrically induced microstructural changes in portland cement pastes, Adv Cem Based Mater, 7 81-88.
[21] J.D. Shane, Electrical conductivity and transport properties of cement-based materials measured by impedance spectroscopy, Ph.D. Dissertation, Northwestern University, Evanston, IL, 2000.
[22] G.A. Julio-Betancourt, R.D. Hooton, Study of the Joule effect on rapid chloride permeability values and evaluation of related electrical properties of concretes, Cem Concr Res, 34 (2004) 1007-1015.
[23] B. Dale P, A virtual rapid chloride permeability test, Cem Concr Compos, 29 (2007) 723-731.
[24] P.F. McGrath, R.D. Hooton, Re-evaluation of the AASHTO T259 90-day salt ponding test, Cem Concr Res, 29 (1999) 1239-1248.
[25] C.C. Yang, S.W. Cho, R. Huang, The relationship between charge passed and the chloride-ion concentration in concrete using steady-state chloride migration test, Cem Concr Res, 32 (2002) 217-222.
[26] R.J. Kessler, R.G. Powers, M.A. Paredes, Resistivity Measurements of Water Saturated Concrete as an Indicator of Permeability, in, 2005.
[27] S.G. Millard, Reinforced concrete resistivity measurement techniques, Proceedings - Institution of Civil Engineers Part 2 Research and theory, 91 (1991) 71-88.
[28] F. Rajabipour, J. Weiss, J.D. Shane, T.O. Mason, S.P. Shah, Procedure to interpret electrical conductivity measurements in cover concrete during rewetting, J Mater Civ Eng, 17 (2005) 586-594.
[29] F. Presuel-Moreno, Y. Liu, M. Paredes, Concrete resistivity on the apparent surface resistivity measured via the four-point wenner method, in: Corrosion 2009, March 22, 2009 - March 26, 2009, National Assoc. of Corrosion Engineers International, Atlanta, GA, United states, 2009, pp. Carboline; Multi-chem; Corrpo; Champion Technologies; Loresco.
[30] W. Morris, E.I. Moreno, A.A. Sagues, Practical evaluation of resistivity of concrete in test cylinders using a Wenner array probe, Cem Concr Res, 26 (1996) 1779-1787.
[31] R.B. Polder, Test methods for on site measurement of resistivity of concrete — a RILEM TC-154 technical recommendation, Constr Build Mater, 15 125-131.
[32] FM 5-578, 2004, Florida Method of Test for Concrete Resistivity as an Electrical Indicator of its Permeability, Flordia Department of Transportation,
[33] T.D. Rupnow, P. Icenogle, Evaluation of Surface Resistivity Measurements as an Alternative to the Rapid Chloride Permeability Test for Quality Assurance and Acceptance, in, Louisiana Department of Transportation, Baton Rouge, LA, 2011, pp. 68.
[34] N.S. Berke, M.C. Hicks, Estimating the Life Cycle of Reinforced Concrete Decks and Marine Piles Using Laboratory Diffusion and Corrosion Data, in, 1992.
[35] E. Vivas, H.R.I. Hamilton, A.J. Boyd, Permeability of Concrete - Comparison of Conductivity and Diffusion Methods, in, Department of Civil and Coastal Engineering, University of Florida, Gainsville, FL, 2007, pp. 238.
[36] M.D. Newlands, M.R. Jones, S. Kandasami, T.A. Harrison, Sensitivity of electrode contact solutions and contact pressure in assessing electrical resistivity of concrete, Mater Struct, 41 (2008) 621-621-632.
[37] J. Castro, R. Spragg, P. Kompare, W.J. Weiss, Portland Cement Concrete Pavement Permeability Performance, in, Joint Transportation Research Program, Indiana Department of Transportation and Purdue University, West Lafayette, Indiana, 2010.
[38] M. Nokken, A. Boddy, X. Wu, R.D. Hooton, Effects of temperature, chemical, and mineral admixtures on the electrical conductivity of concrete, J ASTM Int, 5 (2008).
[39] M. Castellote, C. Andrade, C. Alonso, Temperature correction, from 3 to 25C of the electrical resistivity of mortars and concretes, Industria Italiana del Cemento, 71 (2001) 916-923+850-851.
[40] G. Sant, F. Rajabipour, J. Weiss, The influence of temperature on electrical conductivity measurements and maturity predictions in cementitious materials during hydration, Indian Concr J, 82 (2008) 7-16.
[41] Y.A. Villagran Zaccardi, J. Fullea Garcia, P. Huelamo, A.A. Di Maio, Influence of temperature and humidity on Portland cement mortar resistivity monitored with inner sensors, Mater Corros, 60 (2009) 294-299.
[42] W.J. McCarter, M.C. Forde, H.W. Whittington, RESISTIVITY CHARACTERISTICS OF CONCRETE, Proceedings of the Institution of Civil Engineers (London) Part 1 - Design & Construction, 71 (1981) 107-117.

[43] J. Castro, R. Spragg, J. Weiss, Water Absorption and Electrical Conductivity for Internally Cured Mortars with a W/C between 0.30 and 0.45, J Mater Civ Eng, In press (2011).
[44] N.M. Jackson, Results of Round-Robin Testing for the Development of Precision Statements for the Surface Resistivity of Water Saturated Concrete, in, Ponte Vedra Beach, Florida, 2011.
[45] Draft standard method of test for surface resistivity indication of concrete's ability to resist chloride ion penetration, American Association of State Highway and Transportation Officials, Washington, D.C.
[46] A. Poursaee, W.J. Weiss, An automated electrical monitoring system (AEMS) to assess property development in concrete, Autom Constr, 19 (2010) 485-490.
[47] ASTM C670, 2010, Standard practice for preparing precision and bias statements for test methods for construction materials, ASTM International, West Conshohocken, PA.
[48] R. Henkensiefken, J. Castro, D. Bentz, T. Nantung, J. Weiss, Water absorption in internally cured mortar made with water-filled lightweight aggregate, Cem Concr Res, 39 (2009) 883-892.
[49] M.D.A. Thomas, The use of conductive gel, personal communication, W.J. Weiss, 2008.

Wetting and Drying of Concrete Using Aqueous Solutions Containing Deicing Salts

Robert P. Spragg
Undergraduate Research Assistant
School of Civil Engineering
Purdue University
West Lafayette, IN 47907-2051
E-mail: rspragg@purdue.edu
Phone: 765.494.0358

Javier Castro
Graduate Research Assistant and Ph.D. Candidate
School of Civil Engineering
Purdue University
West Lafayette, IN 47907-2051
E-mail: jcastro@purdue.edu
Phone: 765.494.0358

Wenting Li
Graduate Research Assistant
School of Civil Engineering
Purdue University and Southeast University
West Lafayette, IN 47907-2051
Nanjing, China 211189
E-mail: li448@purdue.edu
Phone: 765.494.0358

Mohammad Pour-Ghaz
Graduate Research Assistant
School of Civil Engineering
Purdue University
West Lafayette, IN 47907-2051
E-mail: mpourghaz@purdue.edu
Phone: 765.494.0358

Pao-Tsung Huang
Graduate Research Assistant
School of Civil Engineering
Purdue University
West Lafayette, IN 47907-2051
E-mail: huang69@purdue.edu
Phone: 765.494.6242

Jason Weiss (Corresponding Author)
Professor and Director of Pankow Materials Laboratory
Associate Director of the Center for Advanced Cement Based Materials
School of Civil Engineering
Purdue University
West Lafayette, IN 47907-2051
E-mail: wjweiss@purdue.edu
Phone: 765.494.2215

Abstract

A series of wetting and drying tests were performed on concrete using different aqueous solutions containing deicing salts. The rate of fluid absorption was generally lower for aqueous solutions containing deicing salts than it was for water. In addition, less fluid was absorbed for samples exposed to aqueous solutions containing deicing salts than for samples exposed to water. The change in the rate of aqueous fluid absorption was proportional to the square root of the ratio of surface tension and viscosity of the absorbed fluid. Concrete that has been exposed to solutions containing deicing salts showed less mass loss during drying. Measures of equilibrium relative humidity over the salt solutions are used to interpret drying behavior. Experimental data indicates that concretes that had previously been exposed to deicing solutions can also exhibit reduced rate of absorption, even if water is the fluid being absorbed.

1. Research Need and Significance

Some jointed plain portland cement concrete pavements in freezing prone climates have shown premature deterioration at the longitudinal and transverse joints. While some have attributed this damage to a chemical attack, inadequate air entrainment, poor mixture design, inadequate constituent materials, or poor construction practices; it is the hypothesis of the authors of this paper that this joint deterioration may be attributed, at least in part, to preferential absorption of fluid at joints. This hypothesis was developed based on observations from the field that show these deteriorated locations frequently occurred at low spots in the pavement, where joint sealers were damaged, where water has collected, or where the joint does not appear to have opened thereby trapping water [1]. Preferential fluid ingress at joints could increase a variety of damage mechanisms including deleterious chemical reactions, crystallization pressure, or freeze thaw damage that may degrade the concrete. To fully evaluate fluid ingress at the joints it is essential that the wetting and drying behavior of concrete is evaluated using aqueous solutions containing deicing salts.

This work is limited in scope as it considers only the ingress of aqueous solutions over short time periods and does not explicitly consider any chemical reaction that occurs between the aqueous solution and the concrete. This information is intended to provide reference for those developing tests to evaluate potential deicer-concrete interactions [2], for developing tests on fluid absorption, for evaluating fluid absorption in concrete [3], for input parameters in computer simulation of fluid ingress at joints [4], and for potential approaches to limit joint deterioration like penetrating sealers for possible use in concrete pavements [5].

2. Fluid Absorption in Porous Materials

Fluid absorption is a frequently used test to provide an indication of the durability of concrete systems since it is simple to perform. Several standard tests exist for measuring water absorption including ASTM C 1585-04 [6], BS 1881-99 [7], and ASTM D6489-99 [8]. While the concept behind these tests is very similar, there are differences in how the samples are conditioned, treated, and tested. In each of these tests water is typically used as the fluid that is being absorbed. Hall [9] discusses that water can interact with the cement matrix adding complexity to the interpretation of results. To overcome some of these limitations or to indicate how absorption can be reduced by fluid composition other solutions have been tested [9-13].

MacInnis and Nathawad [14] assessed the absorption of an aqueous solution consisting of a NaCl deicing salt and reported a decrease in absorption. Sutter et al. [15] reported that sorptivity decreased from highest to lowest in the order of water, NaCl, $CaCl_2$ and $MgCl_2$. Similar data has recently been observed by Janusz [16]. As a result, it can be observed that concrete exposed to deicing salt solutions absorb fluid at a slower rate than they would absorb water; however the previous work has not related this behavior to the fluid properties or described the influence of salt concentration or properties of the aqueous solution.

The results of one-dimensional fluid absorption tests (assuming negligible gravitational effects) are typically reported as the cumulative water absorbed per surface area (surface from which water is absorbed) versus the square root of wetting time. Equation 1 is frequently used to

describe the water absorption (total volume of fluid absorbed) and the sorptivity (related to the rate of absorption) [17].

$$i = S\tau^{1/2} \qquad \text{Eq. 1}$$

where i [mm^3/mm^2] is the cumulative water absorption, S [mm/s$^{1/2}$] is the sorptivity, and τ [s] is the elapsed time. It should be noted that additional equation have been proposed to account for time dependent properties [18].

Hall [9] proposed that the diffusion would scale proportionately with the ratio of surface tension (γ) and viscosity (η) of the fluid. Hall further related this to sorptivity since sorptivity is related to the square root of diffusion. Kelham [19] derived an expression for fluid absorption (Equation 2) that shows the relationship between depth of penetration and the square root of the ratio of surface tension and viscosity.

$$x(\tau) = \sqrt{\frac{4k\gamma\cos(\theta)\tau}{p\eta r}} \qquad \text{Eq. 2}$$

where $x(\tau)$ [mm] is the penetration depth, γ [N/mm] is the surface tension, θ [rad] is the liquid-solid contact angle, p [Dimensionless] dis the porosity of the medium, r [mm] is the pore radius, k [mm^2] is the intrinsic permeability of the material, and η [Pa.s] is the viscosity of fluid. An expression similar to equation 2 was derived by Scherer and Wheeler [20] for stone consolidates.

Previous research using organic fluids has shown an absorption rate that scales proportionally with the square root of the ratio of surface tension and viscosity of the fluid ($(\gamma/\eta)^{1/2}$). This work will use this approach to attempt to interpret results from absorption tests that used aqueous solutions containing deicing salts.

3. Properties of Deicing Salt Solutions

Physical properties of pure solutions were gathered from literature and compared with measured values for the industrially available deicing solutions tested in this research, and they are provided here for convenience in one location. The properties of the deicing solutions will be used in interpreting the wetting and drying results, discussed later in this paper. This section is divided into four sections. The first three sections describe the influence of the deicing solutions in terms of surface tension, viscosity, and equilibrium relative humidity over the aqueous solution. The fourth section describes the specific gravity of the solution as a function of concentration as this is used to determine the volume of solution absorbed during the absorption test.

3.1 Surface Tension of Deicing Salt Solutions

Figure 1 (a) shows surface tension measurements at different concentrations for the three solutions used in this research: NaCl, $CaCl_2$, $MgCl_2$. The surface tension for NaCl was obtained from [10], $CaCl_2$ from [21] and $MgCl_2$ from [22]. A Du Noüy Ring Tensiometer KRÜSS was used with a resolution of 0.1 mN/m for the industrial deicers tested in this study. The tensiometer was cleaned between measurements following ASTM D971-04 [24]. The tensiometer was first calibrated using de-ionized water, which provided a value of 71.0 x 10^{-6} N/mm. A series of three measurements were performed for each solution, with the average reported.

The closed points in Figure 1 (a) are the values measured for the industrially available solutions. The lines represent values taken from literature for pure salt solutions at different mass concentrations. While the general trends are consistent, differences between the solutions containing industrial deicing salts and literature values may be due to impurities or other additves however further work is needed to examine this in greater detail.

3.2 Viscosity of Deicing Salt Solutions

Figure 1 (b) shows a comparison of the viscosities for the solutions used in this research between pure solutions taken from literature and measurements of the deicing solutions. Viscosity measurements for the industrial deicers were performed on the salt solutions using an Anton-Parr rheometer, model Physica MCR 301. The rheometer kept the solution being tested at 23.0 ± 0.02 ºC and from the torque applied to the fluid that causes a shear from which the viscosity can be found. Calibration of the device was performed using a reference standard.

The dashed lines presented are viscosities at different concentrations and are taken from literature [10, 21-23], while the points represent measured viscosities of the industrially available solutions. Again, differences between literature values and those of the solutions measured can be explained by differences in possible additions or chemistries of the industrial deicers.

3.3 Relative Humidity of Deicing Salt Solutions

Relative humidity measurements were performed on the salt solutions using Rotronic HygrClip2S sensors (± 0.8 % RH at 23 ± 0.1 °C). The relative humidity probes were mounted in a 75 mm x 68 mm stainless steel cylinder that was placed over a water jacketed sample cup holder. The water jacket was connected with a water bath at a constant temperature of 23.0 ± 0.1 ºC.

Figure 1 (c) shows the relative humidity measured over salt solutions for a wide range of solution concentrations. As the concentration increased the relative humidity over the solution decreased. The measured relative humidities of these unsaturated salt solutions are higher than that of the saturated solution of these salts which are 75.4 % RH for NaCl [25], 33.0 % RH for $MgCl_2$ [25] and 22 % for $CaCl_2$ [21].

3.4 Specific Gravity of Deicing Salt Solutions

Figure 1 (d) shows the specific gravity of different deicing solutions as a function of concentration. The specific gravity of the solution increases with concentration. The $CaCl_2$ and $MgCl_2$ increase at very similar rates with an increase in concentration, while the NaCl increases slightly less than the $CaCl_2$ and $MgCl_2$ (i.e., 25 % less increase with concentration). This may be attributed to the colligative properties of solutions.

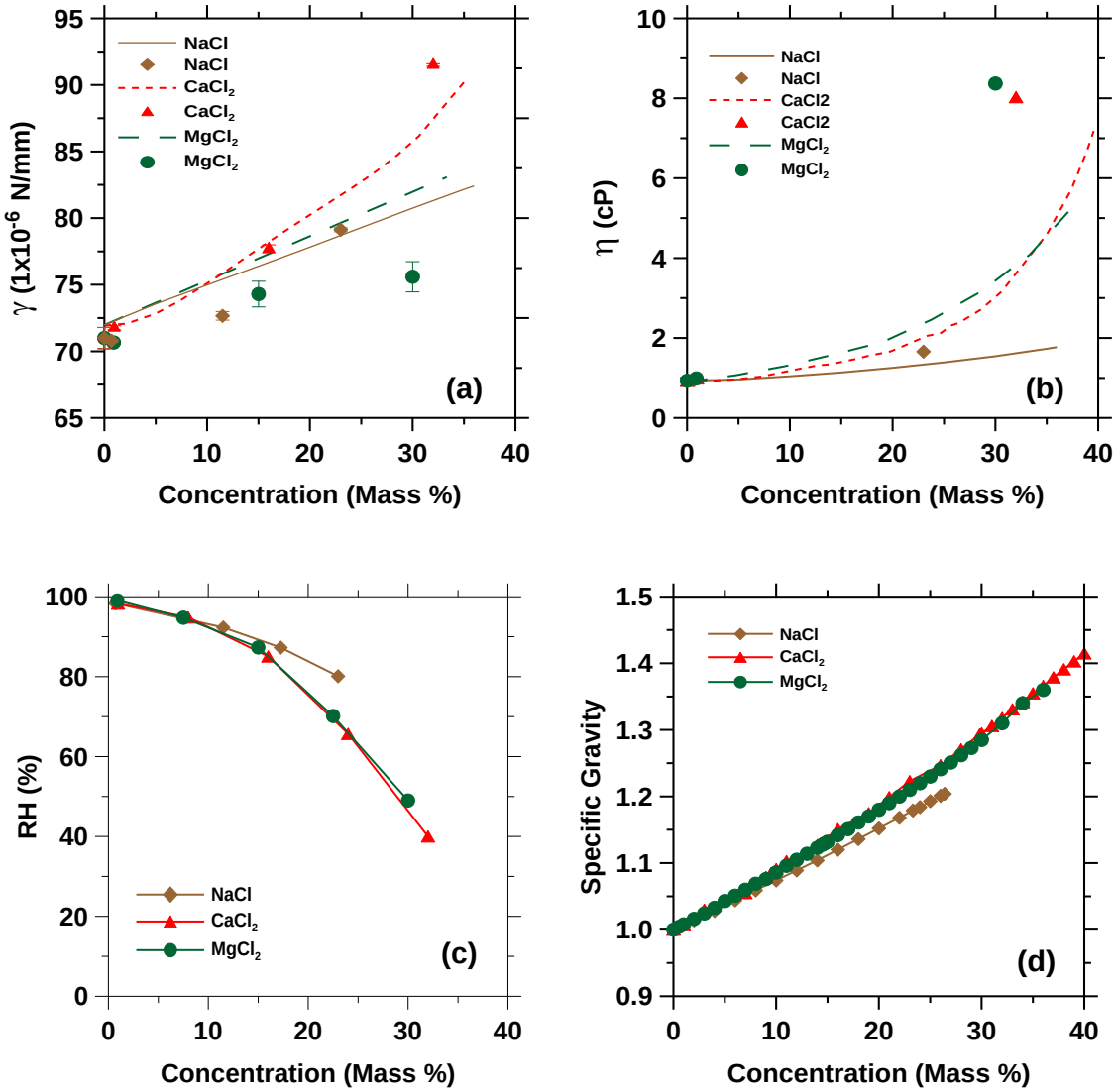

Fig .1. Properties of Deicing Salts at 23-25 ºC: (a) Surface Tension (b) Viscosity (c) Relative Humidty (d) Specific Gravity (Rosenburgh 2010, unpublished data)

4. Wetting and Drying for Concrete with Deicing Solutions

4.1 Experimental Program of Wetting and Drying of Concrete with Deicing Solutions

The concrete mixture that was used for these tests was a typical INDOT class C bridge deck concrete. The mixture proportions of this concrete are shown in Table 1. The fresh air content was 5.7 %, which was measured according to ASTM C231-09 [26]. The hardened air content of the concrete was 4.4 % as assessed using an automated optical scanning approach [18] based on the method proposed by Peterson et al. [28].

Table 1. Mixture Proportions of Concrete Assuming Saturated Surface Dry (SSD) Conditions

Material	Mass
Cement (kg/m^3)	316
Class C Fly Ash (kg/m^3)	60
Water (kg/m^3)	150
Fine Aggregate (kg/m^3)	736
Coarse Aggregate (kg/m^3)	1049
Air Entraining Admix. (ml/100 kg of cem. materials)	20
High Range Water Reducer Admix. (ml/100 kg of cem. materials)	456
Retarder Admixture (ml/100 kg of cem. materials)	98

The concrete was produced in a central mix plant and discharged from a ready mix concrete truck. A series of 100 mm × 200 mm cylinders were cast. After one day of curing, the cylinders were demolded and sealed in double plastic bags at 23 ± 0.5 °C until the samples reached an age of 28 d. After 28 days of curing the cylinders were removed from bags and three 50 mm ± 2 mm thick samples were cut from the central portion of each cylinder using a wet saw.

Two different sets of samples were used in this study. The first set of samples were used to evaluate the effect of sample conditioning on water absorption. In each condition, three samples were used. A total of five conditions were considered: ASTM C1585-04, oven-dry, 50 % RH, 65 % RH and 80 % RH. To ensure that these samples that were conditioned at 50 %, 65 %, and 80 % RH, reached equilibrium, a 12-month conditioning was period was considered. The second set of

samples that were used for aqueous salt solution absorption, drying, and de-ionized water re-absorption were conditioned at 50 ± 2 % RH, 23 ± 0.5 °C for 36 months and two samples were tested for each salt solution.

To prepare the specimens for fluid absorption testing, the sides of the samples were sealed with epoxy. After the epoxy had hardened, the top surface was covered with plastic to avoid evaporation from the sample during testing.

The absorption test involves recording incremental mass change measurements during the first six hours after the sample comes in contact with the fluid and subsequently taking one measurement every day for the next eight days. The amount of absorbed fluid is normalized by the cross-section area of the specimen exposed to the fluid using Equation 3.

$$i = \frac{m_t}{(a \cdot \rho)} \qquad \text{Eq. 3}$$

where: i (mm^3/mm^2) is the normalized absorbed fluid, m_t (g) is the change in specimen mass at time t; a (mm^2) is the area of the specimen exposed to the fluid (i.e., that of the bottom face), and ρ (g/mm^3) is the density of the absorbed fluid (this is provided in greater detail in 3.1). These absorption measurements are then plotted as a function of the square root of time, as provided by Equation 1. The sorptivity is the slope of this graph.

The second series of samples were tested using seven different fluids. Their composition was primarily based on one of three different industrially available deicing products, either NaCl, $MgCl_2$ or $CaCl_2$. A low concentration was used for each salt solution as well as a higher concentration that was selected to be near the eutectic composition for each salt. De-ionized water was also used as a reference fluid.

4.2 Experimental Results from Wetting with Water for Different Conditioning Methods

Figure 2 shows the results from water absorption tests performed on the first series of samples that were conditioned with different environmental conditions as mentioned earlier (ASTM C1585-04 accelerated conditioning, 80 % RH, 65 % RH, 50 % RH and oven drying). It should be remembered that these samples were conditioned for 12 months while the remainder of the samples discussed in this paper were conditioned at 50 % RH for a much longer time. Sample preparation has an enormous impact on the water absorption results as more severe drying enables a greater volume of water to be absorbed during the test.

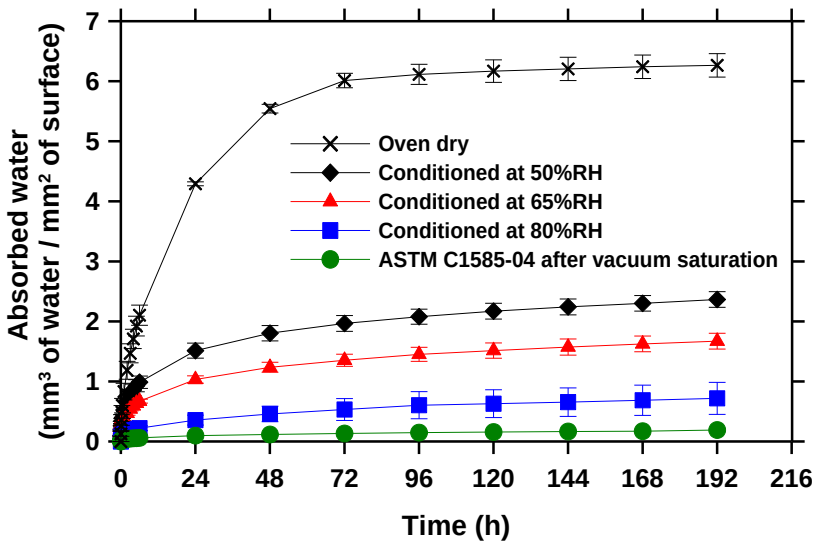

Fig. 2. Water absorption on samples subjected to different conditioning procedures.

4.3 Experimental Results from Wetting and Drying with Deicing Solutions

Figure 3 illustrates the results of the fluid absorption test as a function of time (for concrete at 50 % RH for a longer conditioning time than the samples in Figure 2). It can be seen that even though the concrete that is used for all the tests in Figure 3 has the same conditioning and exposure conditions, the volume of solution absorbed by each material is dependent on the deicing salt solution and the concentration of the deicing salt solution that was absorbed. The sample with the low concentration of NaCl showed a slight increase in the rate of absorption (as compared with water) as well as the amount of fluid absorbed. This is consistent with the data reported by

MacInnis and Nathawad [14]. The absorption of all the other fluids was reduced when compared with water. As a result, it can be concluded that in general as the salt concentration increased the rate of absorption reduced and and the total absorption was reduced. Further work is needed to examine lower concentrations for NaCl to ascertain why a slight increase is typically reported.

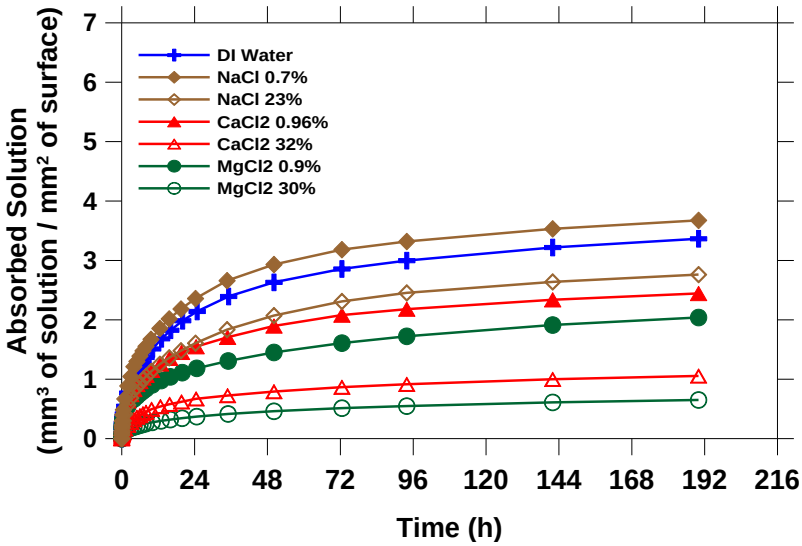

Fig. 3. Volume of deicing solutions absorbed by concrete as a function of time (typical standard deviation less than 0.1 mm^3/mm^2).

After the fluid absorption test was performed for 8 days the samples were dried at 50 ± 2 % RH, 23 ± 0.5 °C for seven days. The samples were kept in the same one-faced exposed condition for the drying test; however, the exposed surface that was facing down in the absorption testing was placed facing up to simulate drying from the top. During the drying test the mass of the samples was recorded at regular intervals.

Figure 4 shows the volume of water loss during the drying period. It is important to note that the drying test will result in only the water portion of the solution being evaporated from the system leaving the salt to become more concentrated in the solution before it eventually precipitates out. It can be noticed that as the concentration of deicing solution was increased the mass loss during drying decreased. This was particularly evident in the high concentration solutions, which showed nearly no mass loss or even a slight gain during drying.

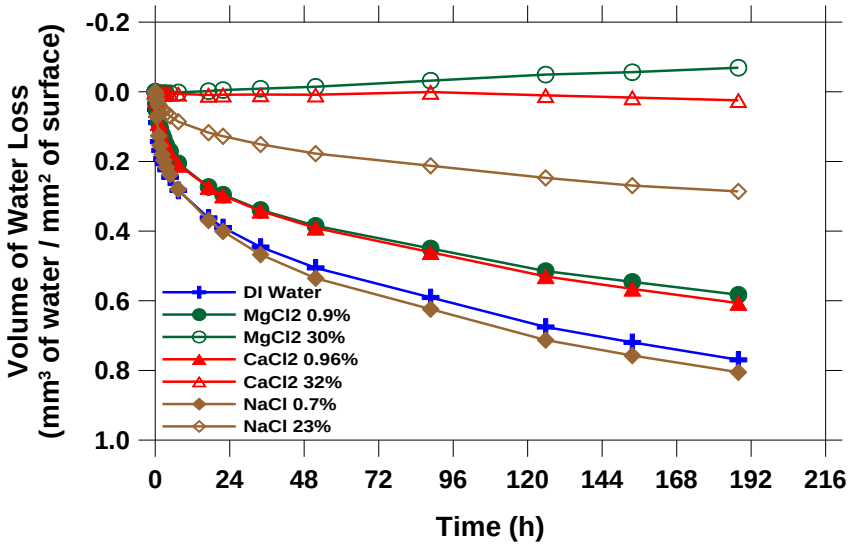

Fig. 4. Drying of concrete prewetted with different salt solutions as a function of time (typical standard deviation less than 0.03 mm^3 water/mm^2).

4.4 Experimental Results from Wetting Previously Exposed to Deicing Solutions

The same set of samples that were previously tested for absorption and drying were oven dried to be tested for second absorption test using de-ionized water. This was done to investigate the effects of previously absorbed salts on re-absorption of de-ionized water. However, in the case of the oven-dried samples, higher water absorption is expected. This can be due to the empty capillary pores and possibly to microcracking generated during oven drying [29-33].

To prepare the samples for the de-ionized water re-absorption test, the samples were placed in an oven at 105 ± 2 °C until they reached to equilibrium. The equilibrium condition was defined as a difference less than 0.5 % between two successive mass measurements (24 hours apart). It is important to note that this drying process will evaporate only the water portion of the solution pre-absorbed, leaving salt in the pores. Since these samples were oven dried, their absorption rates and absorbed water are not comparable with any previous tests.

Figure 5 shows the results for this second absorption test. It can be seen by comparing the results to the results in Figure 3 that the behavior of the samples was dependent on the deicing solutions and the concentrations of deicing solutions used in the first wetting test. These results are a clear indication that the history of the samples affects the results of fluid absorption. This suggests when sorption testing is preformed on field concretes, some understanding of the admixtures or salts that remain in the pore system is needed to fully interpret the results.

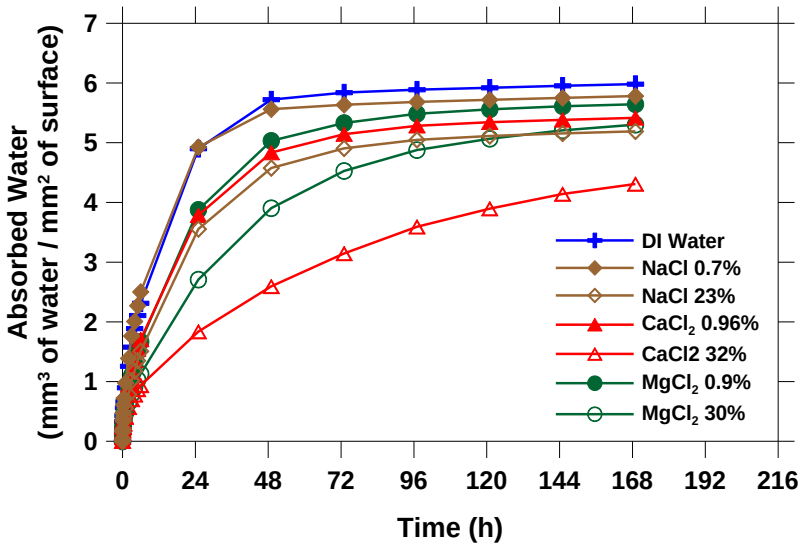

Fig 5. Volume of de-ionized water absorbed by concrete as a function of time in the second fluid absorption test (Fluid from the original test is shown in the caption).

4.5 Drying of Mortars Saturated with Different Deicing Salts

Moisture desorption is an established technique for evaluating the effect of moisture loss at a given humidity for a material. A TA Q5000 SA moisture sorption analyzer was used to carefully control temperature and humidity. Mortar samples were prepared (*w/c* = 0.42 and 55 % aggregate by volume) and cast in a cylindrical mold with a 34 mm diameter and 50 mm height. At an age of 28 days the specimens were demolded and 34 mm diameter 0.8 ± 0.05 mm thick slices were taken from the middle of the samples. The samples were dried under controlled conditions (at 23 ± 0.1 °C and 50 ± 1 % RH) in a CO_2 free chamber until they reach mass

equilibrium. Then, samples were submerged for a minimum of 5 days in aqueous solutions with 23 % NaCl, 32 % $CaCl_2$, and 30 % $MgCl_2$ by mass.

For the samples submerged in NaCl, $CaCl_2$, and $MgCl_2$ solutions a 50 mg to 70 mg piece of sample was placed in a tared quartz pan after a minimum of 5 days of submersion. The pan containing the sample was then suspended from the balance (± 0.001 mg accuracy) and placed in the relative humidity chamber to equilibrate at 23.0 ± 0.1 °C and 97.5 ± 0.1 % RH for up to 96 h or until the sample had achieved a stable mass (less than an 0.001 % mass change/15 minutes). Then, the relative humidity was reduced to reach 95 %. After the sample mass equilibrated, the relative humidity in the chamber was changed in 10 % RH steps to 55 % RH, allowing the sample to attempt to equilibrate (12 h or 0.01% change in mass over 15 minutes) at each new humidity. After equilibrating at 55 % RH the samples were dried to 0 % RH. For the sample submerged in de-ionized water the procedure was similar, but the relative humidity was reduced in 5 % steps from 97.5 % to 2.5 %, and then reduced to 0 % RH.

Figure 6 shows the plot of mass change as a function of time for the mortar saturated in de-ionized water. The sample soaked in water can be seen to lose mass with the decrease of RH. For this system, when the environment is below 100 % RH, water will move from the pores to outside of the sample and classical drying behavior is observed. The maximum mass of the sample is 8.5 % higher than the mass of the oven dry sample.

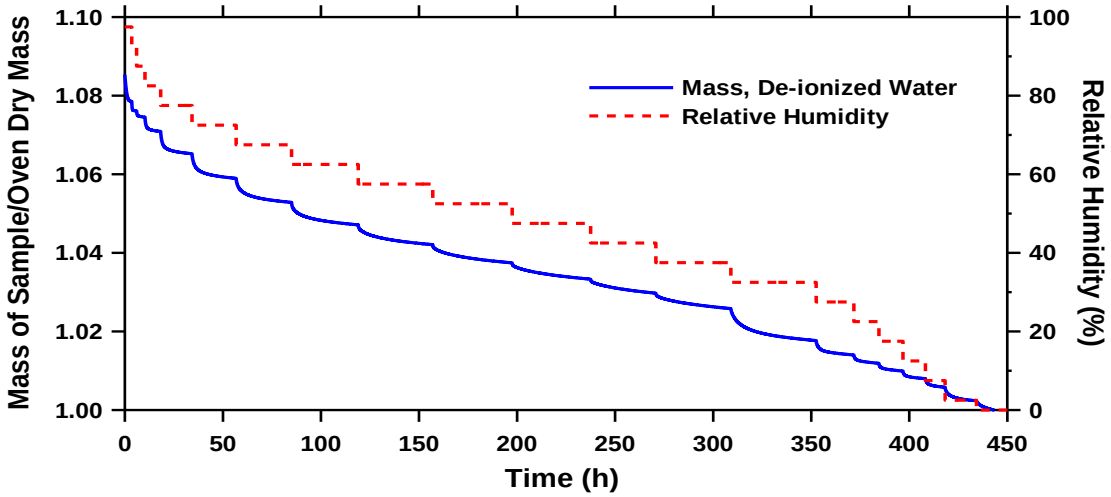

Fig. 6. Mass change at decreasing RH for samples containing de-ionized water

Figure 7 shows a plot of mass change for the mortar samples submerged in aqueous solutions of 23 % NaCl, 32 % $CaCl_2$, and 30 % $MgCl_2$. It can be observed that initially upon placement in the testing chamber at 97.5 % relative humidity the mass of the sample increases for the first 96 h until the relative humidity of the chamber is changed. The samples absorb water during this time of preconditioning, with values much higher than the 8.5 % increase in mass of the sample with de-ionized water as compared with the oven dry sample.

The sample loses weight as the relative humidity is decreased however it should be noted that the sample mass does not decrease to below the initial mass obtained from soaking the sample in the deicing solution until relative humidity was decreased below 85 %, 55 % and 55 % for NaCl, $CaCl_2$ and $MgCl_2$ respectively. This will be compared with the equilibrium relative humidity of the salt solution later in the paper.

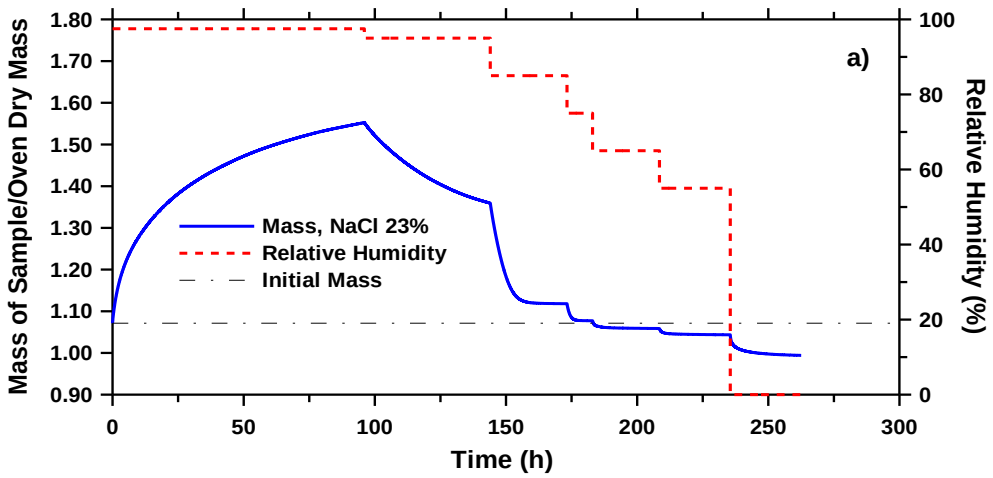
a)
Mass, NaCl 23%
Relative Humidity
Initial Mass
Mass of Sample/Oven Dry Mass
Relative Humidity (%)
Time (h)

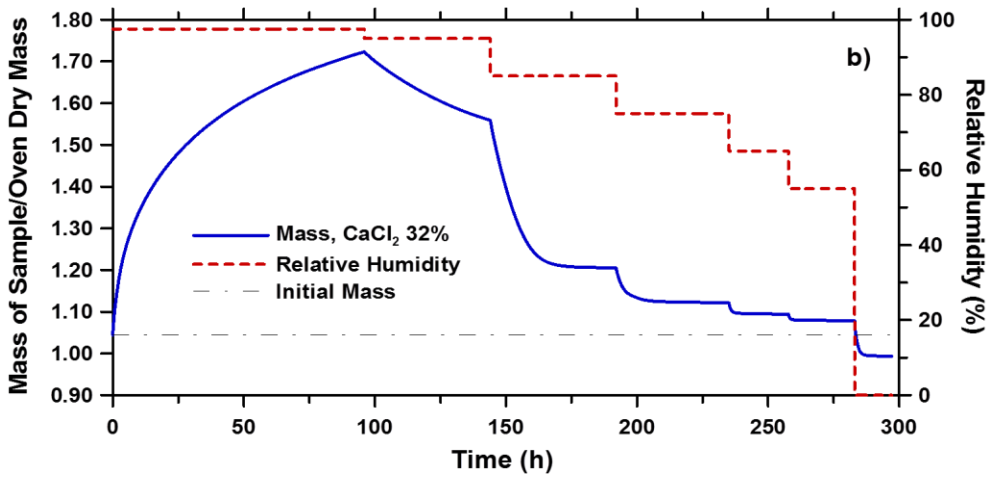
b)
Mass, CaCl2 32%
Relative Humidity
Initial Mass
Mass of Sample/Oven Dry Mass
Relative Humidity (%)
Time (h)

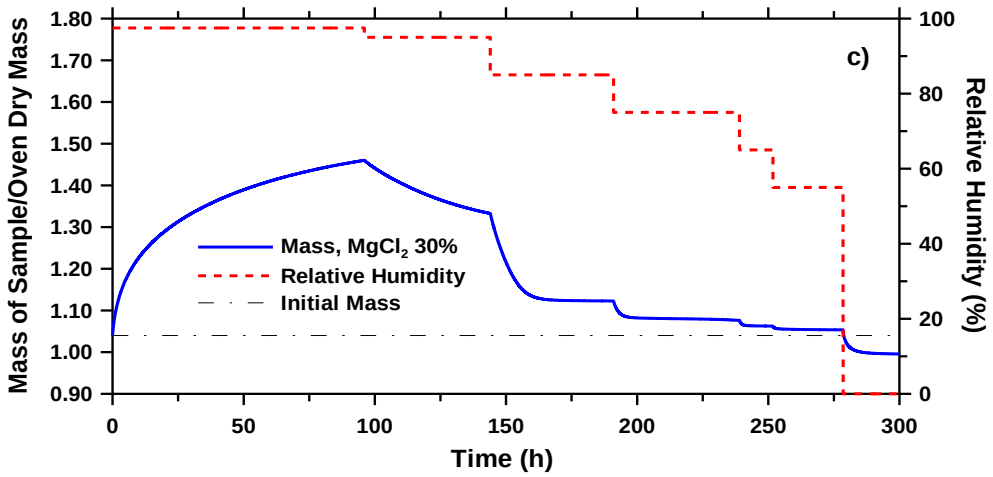
c)
Mass, MgCl2 30%
Relative Humidity
Initial Mass
Mass of Sample/Oven Dry Mass
Relative Humidity (%)
Time (h)

Fig. 7. Mass change for samples submerged in aqueous solutions containing deicing salts: (a) NaCl 23% (b) $CaCl_2$ 32 % and (c) $MgCl_2$ 30%.

5. Discussion of Results

5.1 Aqueous Solution Absorption Behavior as a Function of Surface Tension and Viscosity

Equation 3 showed that the rate of absorption was related to the square root of surface tension and viscosity. Figure 8 plots the square root of the ratio of surface tension and viscosity versus mass concentration of salt. Pure salt solutions are shown as lines while industrial deicing solutions are presented as solid points, and the open points represent the measured sorption response of concrete (i.e., salt sorptivity/water sorptivity) from Figure 3. Figure 8 confirms that as the solution concentration increases, the rate of fluid absorption (i.e., sorptivity) decreases. Further, while the properties of pure solutions may not exactly represent the response of industrially available deicing solutions they do provide a comparable trend. Reasonable agreement is seen between the measured sorption and square root of the ratio of surface tension and viscosity the measured properties. Additional work is currently being performed to extend these results to a wide range of temperatures.

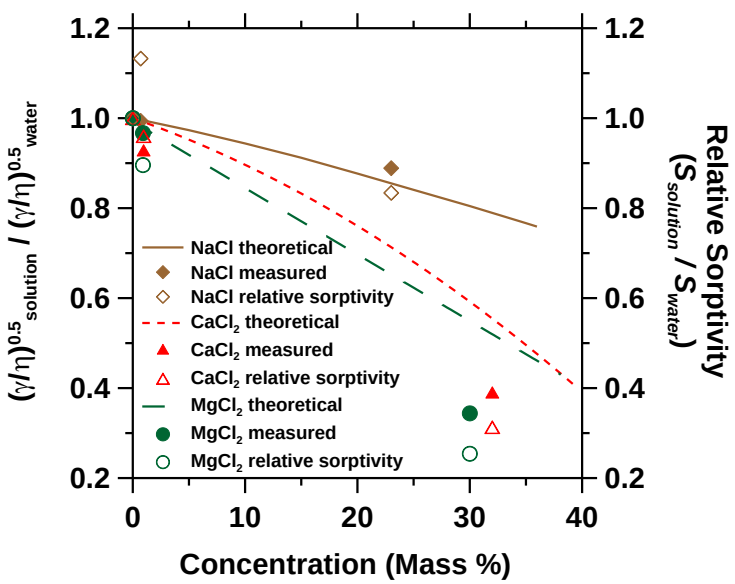

Fig 8. Relative sorptivity for deicing solutions.

5.2 Drying Time Versus Wetting Time

Comparing Figures 3 and 4 indicates that wetting happens much faster than drying. When de-ionized water was used as the absorbed fluid, the amount of fluid that was evaporated from the sample after eight days was 0.8 mm^3/mm^2. In contrast, it took just two hours for samples to absorb the same amount of fluid. These differences are even larger when salt solutions were used as the absorbed fluid. When $MgCl_2$ solution was used as the absorbed fluid, the amount of fluid that was evaporated from the sample after eight days was 0.07 mm^3/mm^2, but it took just ten minutes for the samples to absorb the same amount of fluid.

This is important as it suggests that field concrete may be more susceptible to increasing its level of saturation over time rather than drying out. Further, it shows that laboratory tests that use equal times for drying and wetting increase the saturation level of the concrete over time. Researchers [34] observed an increase in sample mass during wetting and drying cycling with deicers which was attributed to microcracking; however an increase in mass would be consistent with the wetting and behavior observed in this paper.

5.3 Reduced Drying with Salt Solutions – The Role of Solution Equilibrium Humidity

The relative humidity of different salt solutions presented in Figure 1 (b) help to understand the results from the drying tests. The equilibrium relative humidity for the 23% NaCl, 32% $CaCl_2$ and 30% $MgCl_2$ solutions are 80 %, 40 % and 50 % respectively. When the samples are placed in an environment with a relative humidity that is greater than or equivalent to the approximate equilibrium relative humidity over the aqueous solution in the pores water will not be lost to then environment. (Figure 4) and the sample can actually gain mass (Figure 4 and 7), most likely due to the water absorption on the surface of the sample. This can be seen by the thinner (dashed lines in Figure 7), which show the initial mass of the sample after it has been submerged in a

aqueous solution for over 5 days. At relative humidity higher than the equilibrium of the aqueous salt solution the samples will increase in mass. At relative humidities where the environment is less than the equilibrium humidity over the salt solution, the samples will be expected to decrease in mass. The drying behavior of systems containing concentrated aqueous solutions of deicing salts is complex and requires additional research.

5.4 Effect of Solution on Rewetting

When samples of concrete that were previously exposed to deicing solutions were rewet with water they had an absorption and rate of absorption that depended on the history of the specimens (Figure 5). The absorption of water can be 30 % to 50 % less in specimens that were exposed to deicing solutions at some point in their lives. This is an important, yet subtle, factor to understand. This is important since absorption tests of field concrete may be mistakenly interpreted by relating the reduction in sorption to pore filling or delayed sorption. Both of these observations (lower sorptivity and delayed sorption) are consistent with data here for samples that did not have reduced porosity or differences in sample damage.

6. Summary and Conclusions

This paper has reported experimental results of fluid absorption measurements and drying of concrete in the presence of deicing solutions. The following observations can be made. First, the absorption of fluid in concrete depends on the drying environment used to condition the samples. Samples stored at a lower RH absorbed a greater volume of fluid. Second, it was observed that the deicing solutions reduce the rate of fluid absorption. This reduction can be related to the square root of the ratio of surface tension and viscosity [10]. Third, the time scale between drying and wetting is different and concrete is more likely to become preferentially increasingly wet over time. Fourth, the drying of concrete containing aqueous solutions with deicers differs from that of water. The equilibrium relative humidity of the aqueous solution plays an important role on limiting drying. Finally, the presence of deicing salts in field samples

impacts the absorption when field samples are tested in the lab using water. This suggests that care must be taken in analyzing field concrete exposed to deicing salt solutions.

7. Acknowledgments

The experiments reported in this paper were conducted in the Pankow Materials Laboratories at Purdue University. This work was supported in part by the Joint Transportation Research Program administered by the Indiana Department of Transportation and Purdue University (SPR 3093 and 3200). The contents of this paper reflect the views of the authors, who are responsible for the facts and the accuracy of the data presented herein, and do not necessarily reflect the official views or policies of the Indiana Department of Transportation, nor do the contents constitute a standard, specification, or regulation.

8. References

1. Weiss J, Nantung T. INDOT Proposal on the Permeability of Concrete Pavement Performance Relative to Permeability, 2006.
2. Shi X, Fay L, Peterson MM, Yang Z. Freeze-Thaw damage and chemical change of a Portland cement concrete in the presence of diluted deicers. Mater Struct, 2010; 43(7): 933-946.
3. Hong K, Hooton RD. Effect of cyclic chloride exposure on penetration of concrete cover. Cement Concrete Res 1999, 29(9): 1379-1386.
4. Pour-Ghaz M, Rajabipour F, Couch J, Weiss J. Numerical and experimental assessment of unsaturated fluid transport in saw-cut (notched) concrete elements. SP-266 American Concrete Institute: Modeling as a solution to concrete problems, 2009.
5. Coates K, Mohtar S, Tao B, Weiss J. Can soy methyl esters reduce fluid transport and improve the durability of concrete? Transport Res Rec, 2009; 2113:.22-30.
6. ASTM International, ASTM C1585. Standard test method for measurement of rate of absorption of water by hydraulic cement concretes; 2004.

7. British Standard Institution, BS 1881. Methods of testing concrete part 5: Methods of testing hardened concrete for other than strength; 1990.
8. ASTM International, ASTM D6489. Standard test method for determining the water absorption of hardened concreted treated with a water repellent coating; 2006.
9. Hall C, Marchand J, Gerard G, Sosoro M. Chapter 2: Transport of fluids in homogenous isotropic cementitous composites. In: Reinhardt HW, editor. Penetration and permeability of concrete, RILEM report 16, 1997; pp. 5-79.
10. Hall C, Hoff WD. Water-transport in brick, stone and concrete. London: Spon Press, 2002.
11. Weiss WJ. Prediction of early-age shrinkage cracking in concrete. Ph.D. thesis. Evanston, IL Northwestern University, 1999.
12. Bentz DP, Peltz MA, Snyder KA, Davis JM. VERDiCT: Viscosity enhancers reducing diffusion in concrete technology. Concrete International, 2009; 31(1): 31-36.
13. Sant G, Eberhardt A, Bentz DP, Weiss J. Influence of shrinkage-reducing admixtures on moisture absorption in cementitious materials at early ages. J Mater Civil Eng, 2010; 22(3): 277-286.
14. MacInnis C, Nathawad YR. The effects of a deicing agent on the absorption and permeability of various concretes. In: Litvan GG, Sereda PJ, editors. Proceedings of the first international conference on durabaility of building materials and components, ASTM Special Technical Publication STP-691, 1980. pp 485-496.
15. Sutter L, Peterson K, Julio-Betancourt G, Hooton D, Van Dam T, Smith K. The deleterious chemical effects of concentrated deicing solutions on Portland cement concrete. South Dakota Department of Transportation, Final Report, 2008.
16. Janusz A. Investigation of Deicing Chemicals and Their Interactions with Concrete Materials. Master Thesis. West Lafayette, IN Purdue University, 2010.
17. Martys, NS. (1995). Survey of concrete transport properties and their measurments. NISTIR 5592, U.S. Departament of Commerce
18. Martys N, Ferraris CF. Capillary transport in mortar and concrete. Cement Concrete Res 1997; 27(5): 747-760
19. Kelham M. A Water absorption test for concrete. Mag Concrete Res, 1988; 40(143): 106-110.

20. Scherer G, Wheeler GS. Silicate consolidants for stone. Key Engineering Materials, 2009; 391: 1-25.
21. Conde M. Aqueous solutions of lithium and calcium chlorides: Property formulations for use in air conditioning equipment design. International Journal of Material Sciences, 2004; 43(4): 367-382.
22. Phang S, Stokes RH. Density, Viscosity, Conductance and transference numbers of concentrated aqueous magnesium chloride at 25C. J Solution Chem, 1980; 9(7): 497-505.
23. Afzai M, Saleem M, Mahmood MT. Temperature and concentration dependence of viscosity of aqueous electrolytes from 20 to 50C. Chlorides of Na+, K+, MG2+, Ca2+, Ba2+, SR2+ Co2+, Ni2+, Cu2+, and Cr3+. Journal of Chemical Engineering Data, 1989; 34(3): 339-346.
24. ASTM International, ASTM D971. Standard test method for interfacial of oil against water by the ring method; 2004.
25. Greenspan L. Humidity fixed points of binary saturated aqueous solutions. Journal of Research of the National Bureau of Standards – A, Physics and Chemistry, 1977; 81A(1): 89-96.
26. ASTM International, ASTM C231. Standard test method for air content of freshly mixed concrete by the pressure method; 2009.
27. Castro J, Kompare P, Poursaee A, Nantung T, Weiss J. JTRP Report SPR-3093, Portland cement concrete pavement performance relative to permeability. Indiana Department of Transportation, 2010.
28. Peterson KW, Swartz RA, Sutter LL, Van Dam TJ. Hardened concrete air void analysis with a flatbed scanner. Transport Res Rec 2001; 1775: 36-43.
29. Hwang C, Young J. Drying shrinkage of portland cement pastes. microcracking during drying. Cement Concrete Res 1984; 14(4): 585-594.
30. Chatterji S. (1976). Drying shrinkage of cement paste and concrete: a reappraisal of the measurement technique and its significance. Cement Concrete Res 1976; 6(1): 145-148.
31. Bisschop J, Van Mier J. How to study drying shrinkage microcracking in cement-based materials using optical and scanning electron microscopy? Cement Concrete Res 2002; 32(2): 279-287.
32. Samaha H, Hover K. Influence of microcracking on the mass transport properties of concrete. ACI Mater J 1992; 89(4): 416-424.

33. Yang Z, Weiss J, Olek J. Water transport on concrete damaged by tensile loading and freeze-thaw cycling. J Mater Civil Eng 2006; 18(3): 424-434.
34. Wang K, Nelsen D, Nixon W. Damaging effects of deicing chemicals on concrete materials. Cement and Concrete Composite, 2006; 28(2): 173-188.

International RILEM Conference on Use of Superabsorbent Polymers and Other New Additives in Concrete
15-18 August 2010, Technical University of Denmark, Lyngby, Denmark

MOISTURE PROFILES AND DIFFUSION COEFFICIENTS IN MORTARS CONTAINING SHRINKAGE REDUCING ADMIXTURES

Mohammad Pour-Ghaz[(1)], Robert Spragg [(1)] and Jason Weiss [(1)]

(1) Purdue University, School of Civil Engineering, West Lafayette, Indiana, USA

Abstract
Shrinkage reducing admixtures (SRAs) have been used over the last three decades to reduce the volume change (i.e., shrinkage) that occurs in cement paste, mortar, and concrete during drying. The goal of reducing shrinkage is to reduce the risk of shrinkage cracking in concrete elements. SRAs alter the properties of the pore solution, such as surface tension and viscosity, which result in a reduction in the magnitude of drying shrinkage, especially at humidities below 80-85%. In addition to altering the magnitude of shrinkage, SRAs appear to alter the rate of drying and diffusivity coefficient. This paper examines the role of SRAs in two ways. First, desorption spectra are measured to obtain the moisture diffusivity of plain mortar and mortar containing SRA. Second, the paper measures relative humidity in slabs to obtain moisture profiles. The relative humidity profile predicted from the non-linear diffusion coefficient is compared with the measured humidity profile.

1. Background

Shrinkage Reducing Admixtures (SRAs) were introduced to the concrete industry in the 1980's [1, 2]. Recent reviews have summarized three decades of research on SRA on concrete properties [3-6]. SRA's are generally observed to reduce shrinkage which can substantially reduce the propensity for restrained shrinkage cracking.

The majority of shrinkage measurements on concrete containing SRA are performed on concrete samples with a relatively large cross section, like those that one may use in standard shrinkage tests like ASTM C-157 [7]. While this type of test can provide information on the benefits of SRA, it has two primary limitations. First, it generally only describes the shrinkage of the concrete at one relative humidity (50% for example for ASTM C-157 [7]). Second, it measures the average length change of the prism and does not explicitly account for moisture gradients.

To overcome the limitation of measuring shrinkage at one relative humidity, a series of tests were performed measuring small paste and mortar samples with and without SRA at different relative humidities [8]. This response can be used to describe the shrinkage that may be expected over a wide range of relative humidities [9-11]. This does however indicate, not surprisingly, that shrinkage is not linearly related to relative humidity [8]. The shrinkage of the paste can be extended to mortar or concrete using the Pickett [12] or Hobbs [13] approaches.

Previous work has been performed to measure relative humidity profiles in concrete. This includes the work of Monfore [14] and Grasley et al. [15] who used resistance based gages to measure humidity in vapor filled cavities in concrete, the work of Molina [16] who measured relative humidity using chilled mirror technology, and work of Schieβl et al. [17] using electrical resistance measurements of concrete to assess the moisture distribution.

Relative humidity measurements in slabs can be complicated by the size of the probe that is used to measure the humidity. Measurements in small cavities with limited vapor volume can make it difficult to use techniques that require a substantial air flow rate like chilled mirrors. Previous measures of electrical resistance of concrete require two assumptions. First, that there are no hysteretic effects [18, 19] and second, that the resistance is measured at the depth of the electrodes. It can be noted that the first assumption is required since electrical measurements measure water content and not relative humidity directly and hysteretic effects due to drying and wetting can complicate the interpretation [19]. The second assumption is more nebulous as the shape of the electrical field that develops between the two electrodes is not symmetric at the plane of the electrodes since more charge will pass through the side containing more liquid [19]. As such it may be beneficial to measure the moisture diffusion coefficient directly rather than measuring relative humidity profiles and back calculating the diffusion coefficient.

One advantage of using desorption measurements to obtain a non-linear diffusion coefficient is the fact that the testing can be performed over a much shorter duration than drying of thick concrete slabs. For example, the non-linear diffusion coefficient measured in this paper took approximately 5 days to measure after casting and curing which is substantially shorter than allowing a concrete slab to dry and back-fitting the diffusion coefficient (which can take many many months). Second, this approach is not subjected so some of the issues that arise in attempting to ascertain the correct depth of the relative humidity measurement or the influence of a relatively large size cavity on the measured value.

2. Research Objective

This paper describes research that is attempting to measure a non-linear moisture diffusion coefficient in a mortar. Mortar was preferred to cement paste to minimize the potential impact of different pore size distributions that may occur between pastes and mortars. In addition the mortar was preferred to minimize potential issues that may occur with inconsistent mixing action that can be encountered in paste samples. This paper has three main objectives:

- First, the paper describes tests on mortar that is dried in a controlled fashion to evaluate the non-linear diffusion coefficient following the approach used by Anderberg and Wadso [20] and Garbalinska [21],
- Second, the paper provides data that illustrates the influence of shrinkage reducing admixture on the non-linear diffusion coefficient, and
- Third, the paper will provide a comparison of the relative humidity profile predicted using the non-linear diffusion coefficient with a measured relative humidity profile in a slab.

3. Relative Humidity Gradient and Cracking Potential

Previous work [9, 10, 22-24] has suggested that the humidity gradient in a slab can be used to predict the free shrinkage, stress development, slab cracking, and curling in a thick concrete element. The background for this type of approach can be found in [10, 25]. Figure 1 schematically illustrates the approach can be taken to utilize the relative humidity profile to compute the stress distribution and gradient. Strong dependence of diffusion coefficient on the shape and magnitude of the relative humidity profile can result in higher stress gradient and increase in cracking potential.

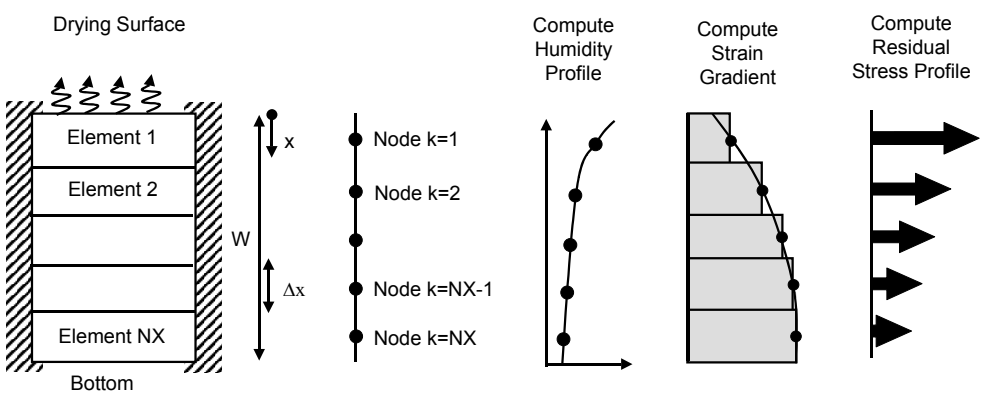

Figure 1: Schematically illustrates the approach can be taken to utilize the relative humidity and moisture content (W) profile to compute the stress distribution [10].

4. Materials and Methods

Three mortar mixtures were prepared for this study. The plain mortar had a water to cement ratio (w/c) of 0.50 and consisted of 55% aggregate by volume. The mortars containing shrinkage reducing admixture (SRA) had 1% and 5% of the mix water replaced with a SRA (denoted as 1% SRA and 5% SRA respectively). ASTM C150 [7] Type I ordinary portland cement (OPC) was used with a Blaine fineness of 370 m^2/kg and an estimated Bogue phase composition of 56 % C_3S, 16 % C_2S, 12 % C_3A, 7 % C_4AF and a Na_2O equivalent of 0.68 % by mass. The normal weight aggregate (NWA) was natural river sand with a fineness modulus of 2.71, an apparent specific gravity of 2.58, and an absorption of 1.8 % by mass.

The SRA was commercially available Tetragaurd AS20. All of the NWA was oven-dried and air-cooled for 24 hr before mixing. The mixing procedure used for the mortar was in accordance with ASTM C192-06 [7]. The samples were all tested in a sealed condition unless otherwise noted.

The experiments that were performed consist primarily of two specimen geometries. The first sample geometry was used for the diffusivity tests. This sample consisted of a 0.8 mm thick by 6 mm diameter mortar disk that was taken from a larger cylinder that was sealed from the time of casting before being exposed to progressive drying at an age of 7 days for determination of the moisture diffusivity. The second sample geometry consisted of slab specimens (177.8 mm x 254.0 mm x 508.0 mm) with relative humidity sensors embedded at four depths (12.7, 25.4, 38.1 and 92 mm) measured from the drying surface. The slabs were exposed to drying at 50 ± 1% at an age of 7 days. The slab geometry is shown in Figure 2.

Figure 2: Slab geometry with one-sided drying

5. Measurements of a Non-Linear Diffusion Coefficient

The samples used for determining the diffusion coefficient were cut from a small cylinder of mortar using a high precision wet saw. The test started approximately 5 minutes after cutting the sample. The samples were kept in water. At the start of the test the sample was removed from the water and was placed in a clean towel for a few seconds to remove the surface water. The sample was then placed in the desorption analyzer. The diffusivity test was performed in an automated absorption/desorption analyzer [26, 27] at 23°C in which samples were subjected to isothermal desorption at different relative humidities. The first step in the isothermal desorption was isothermal conditioning at 97.5 % relative humidity. The samples were allowed to equilibrate to 97.5%. After isothermal conditioning at 97.5% the relative humidity was decreased in 5% relative humidity increments. Samples at each step of the desorption were considered to be at equilibrium when the mass change was smaller than 0.001 mg for 15 minutes [26].

For a slab geometry with double-sided drying (where the contribution of mass transfer from the edges of the sample is negligible compared to mass transfer from the surface of the slab [20, 21, 28]) the mass change due to drying (M_t), at any time (t), can be related to the moisture diffusivity, (D), using Equation 1 [20, 21, 28]

$$\frac{M_t}{M_\infty} = \frac{4}{\pi}\left(\frac{Dt}{L^2}\right)^{1/2} \quad (1)$$

where M_∞ is the mass change at equilibrium and L is the thickness of the sample.

The diffusivity over each relative humidity step can be obtained from the linear portion of a plot of $(M_t / M_\infty)^2$ against $(16t/\pi^2 L^2)$. Generally the mortar samples tested exhibited the linear portion of their curve between 20 and 80% of the equilibrium mass. For materials for which the diffusivity is a function of relative humidity, Equation 1 can be used provided that the diffusivity can be assumed constant during each isothermal desorption step. In the present work since the samples were subjected to 5% change of relative humidity, the diffusivity can be assumed constant during each step of desorption. Better results can be obtained by decreasing the size of the steps, however the duration of the testing would increase but a sensitivity analysis would need to be determined.

Figure 3 illustrates the calculated diffusivity of the 0.8 mm thick specimens (exposed to 2 sided drying) of plain mortar, and mortar samples with 1 and 5% SRA. Note that the diffusivity at each step is expressed as diffusivity at average relative humidity of that step (e.g., the diffusivity of the samples that is equilibrated at 97.5% relative humidity and exposed to 92.5% relative humidity is reported as diffusivity at 95%). The samples with SRA demonstrate a lower diffusivity than the plain system at higher relative humidity. This lower relative humidity in the SRA system corresponds with a reduced rate of drying (at high relative humidity). This would suggest that plain mortar has a more non-linear moisture diffusivity while samples with SRA are more linear with respect to the diffusivity over a large range of moisture contents. This can have substantial implications on the moisture profile, shrinkage profile, reduction in curling, drying rate, and microcracking at the surface of the slab [29].

6. Relative Humidity Measurements in Slabs

The internal relative humidity and temperature of the slab was measured at four depths (12.7, 25.4, 38.1 and 92 mm) in a series of 250 mm hollow shafts (parallel to the surface) that contain I-button sensors [30] that measure temperature and relative humidity. The depth of the hollow shaft reported is measured from the exposed surface of the slab to the center of the shaft. Slabs were exposed to drying from the top surface.

The I-button data loggers measure the relative humidity with $\pm$1.0% and temperature $\pm$0.1^{o}C accuracy respectively. The advantage of this type of relative humidity sensor is the fact that it measures the relative humidity of the air inside the hollow shaft directly which is in equilibrium with surrounding materials. To ensure accuracy of the measurements all the sensors were compared to two salt solutions with 87 and 78% relative humidities. The sensors were within $\pm$1.0% of the expected relative humidity. In addition to calibration, data were corrected for saturation drift [30].

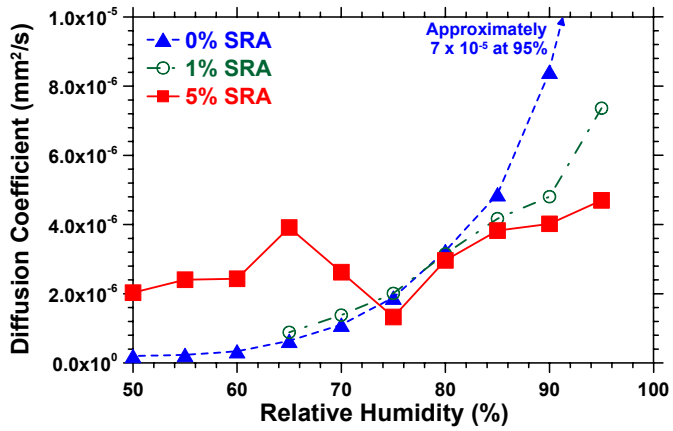

Figure 3: Moisture diffusivity of mortar samples with different loadings of shrinkage reducing admixture (SRA)

At the time of casting the slabs, cylindrical samples (with 2.54 cm diameter and 5.1 cm height) were cast from the same materials used to make the slabs and was kept sealed. These samples were used to measure the internal relative humidity at 7, 28 and 63 days (two samples at each age). The measurements were performed by crushing the samples and placing them in an air-tight container against a temperature and relative humidity sensor [26]. These measurements were performed to account for the self-desiccation effect which is needed in Equation 2.

Figure 4 illustrates the relative humidity of the slabs that have been exposed to drying at an age of 7 days (results are based on the average independent measurement in two slabs). It can be noticed that the relative humidity appears to remain higher in the samples containing SRA. The depth of the sensors is the distance to the center of the hollow shaft (in which sensor in placed in) from the surface of the slab. It is expected that the measured relative humidity with sensor may be more representative of the top of the hollow shaft.

7. Comparing Slab Measurements with Predictions Using the Diffusion Coefficient

Equation 2 describes the relative humidity as a function of time and position [31-35]

$$\frac{\partial H}{\partial t} = div\left(D_H \; grad \; H\right) - \frac{\partial H_s}{\partial t} \qquad (2)$$

where H is the relative humidity, D_H is the moisture diffusivity as a function of relative humidity and H_s is the variation of relative humidity due to self-desiccation.

Equation 2 assumes that the contribution of thermal gradients and aging are negligible [33]. The second term on the right-hand-side of Equation 2 is the contribution of self-desiccation [33]. The self-desiccation term in the present work is measured independently from crushed samples as described above. The boundary conditions at the sealed (bottom) surface of the

slab and top (exposed to drying) surface of the slab can be expressed by $\partial H / \partial x = 0$ and $H = 0.50$ respectively. The initial condition of the slab at drying (i.e., humidity at 7 days) is obtained by measuring the internal relative humidity of the crushed samples.

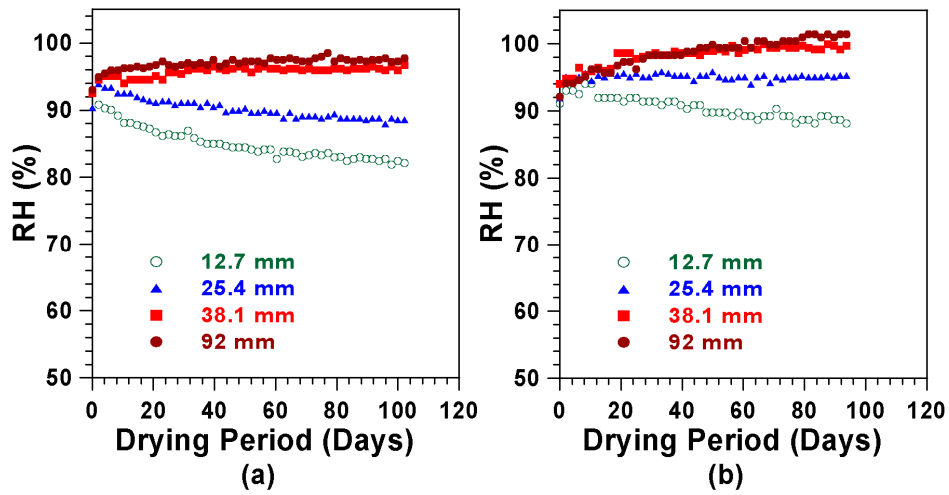

Figure 4: Change of internal relative humidity of slabs at different depth measured from exposed surface of the slab, (a) plain mortar, (b) mortar containing 5% shrinkage reducing admixture (SRA)

A non-linear finite difference scheme [33, 36, 37] was used. To effectively capture the non-linearity caused by the diffusivity, Crank-Nicolson (central difference) scheme was used. Crank-Nicolson scheme is stable [33, 36, 37] and effective in capturing non-linearities caused by strong dependence of diffusivity on relative humidity. In using this scheme any oscillations around the exact solution can be avoided by decreasing the time increments. In each time step the first solution was obtained by time lagging the diffusivity one time step and then improving the solution by subsequent iterations. In subsequent iterations, a weighted average diffusivity of the last two iterations was used. This method of averaging is known as modified Picard iterations [38] and requires less number of iterations in each time step.

Figure 5 illustrates the comparison of the experimentally obtained relative humidity at different locations and the numerically obtained profiles using the non-linear diffusivity coefficients.

8. Implications of Differences in Relative Humidity Profiles

Results of the non-linear diffusion coefficient can be used to describe moisture distribution at early ages and its potential impact on microcracking, curling and through cracking. The SRA's, especially at 5% show a reduced rate of drying. This is confirmed with less mass loss. This work may also provide insight on microcracking and damage localization that ultimately leads to through cracking in restrained elements. Acoustic emission has shown that the inclusion of SRA substantially reduces the acoustic activity due to microcracking in the specimens that contain 5% SRA as compared with the plain mixture.

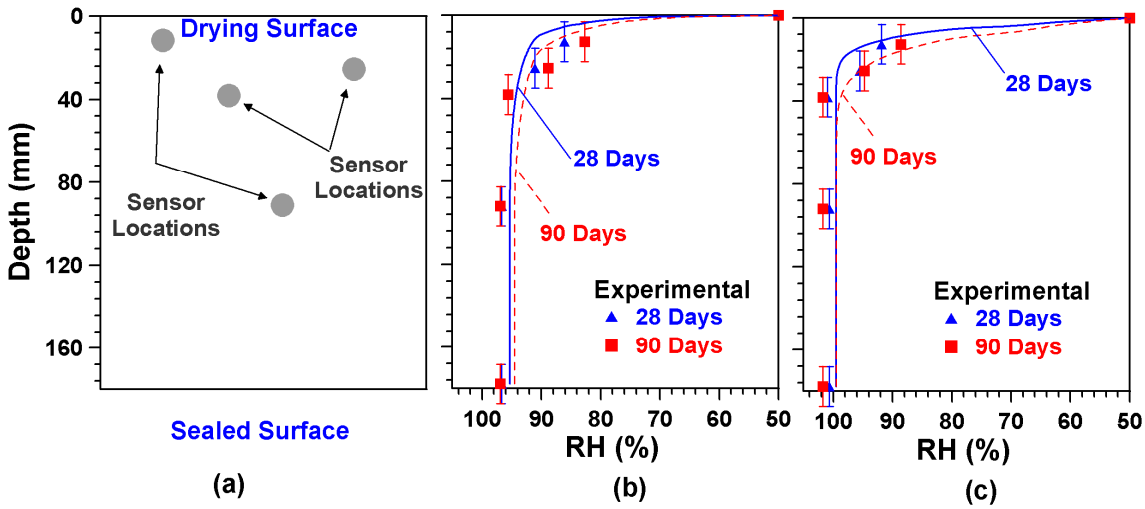

Figure 5: Comparison of the experimentally measured relative humidity and numerically obtained relative humidity profile, (a) illustration of location of the sensors and boundary conditions of the slab, (b) plain mortar, (c) mortar with 5% shrinkage reducing admixture (SRA)

9. Conclusions

This paper examined the role of SRAs on the relative humidity profile that develops in a drying mortar. The paper begins by describing the measurement of desorption spectra to obtain the moisture diffusivity of plain mortar and mortar containing SRA. The paper uses these non-linear diffusion coefficients to predict the moisture profiles that would be expected to occur in drying slabs. The results indicate that SRA dries more slowly at high relative humidities (liquid diffusion) however this trend may be reduced for lower relative humidities when the vapor diffusion prevails. The relative humidity profiles computed using the non-linear diffusion coefficient were directly compared with independently measured relative humidity in slabs. A reasonable comparison was observed given the issues associated with errors in relative humidity depth location and the shortcomings of using a non-aging coefficient. The implications of this approach could be more rapid indications of relative humidity profiles in concrete as well as explanations of shrinkage, stress and cracking distributions throughout the sample cross section.

10. Acknowledgements

The authors gratefully acknowledge the support of BASF, the Construction Chemical Company. This work was conducted in the Charles Pankow Concrete Materials Laboratory at Purdue University. As such, the authors gratefully acknowledge the support which has made this laboratory and its operation possible.

8. References

[1] Sato, T., Goto, T., and Sakai, K., 'Mechanism for Reducing Drying Shrinkage of Hardened Cement by Organic Additives,' *CAJ Review,* (1983) 52-54.

[2] Tomita, R., Simoyama, Y., and Inoue, K., 'Properties of hardened concrete impregnated with cement shrinkage reducing agent,' *CAJ Review,* (1986) 314-317.

[3] ACI.Committee.231, 'Report on Early-Age Cracking: Causes, Measurement, and Mitigation,' American Concrete Institute ACI 231R-10, 2010.

[4] Nmai, C., Tomita, R., Hondo, F., and Buffenbarger, J., 'Shrinkage reducing admixtures,' *Concr. Int.,* **20** (4)(1998) 31-37.

[5] Shah, S.P., Weiss, W.J., and Yang, W., 'Shrinkage cracking – can it be prevented?,' *Concr. Int.,* **20** (4)(1998) 51-55.

[6] Weiss, J. and Berke, N.S., 'Shrinkage reducing admixtures,' in *Early age cracking in cementitious systems, RILEM state-of-the-art report—Report 25*, A. Bentur, Ed., ed Bagneux, France: RILEM, 2002.

[7] *Annual Book of ASTM Standards*. West Conshohocken, PA: American Society for Testing and Materials, ASTM International, 2009.

[8] Weiss, J., Lura, P., Rajabipour, F., and Sant, G., 'Performance of shrinkage-reducing admixtures at different humidities and at early ages,' *ACI Mater. J.,* **105** (5) Sep-Oct (2008) 478-486.

[9] Bazant, Z.P., Ed., *Fourth RILEM International symposium on Creep and Shrinkage of Concrete: Mathematical Modeling* Northwestern University, 1986.

[10] Weiss, W.J., 'Prediction of early-age shrinkage cracking in concrete,' Ph.D., Civil Engineering, Northwestern University, Evanston, IL, 1999.

[11] Moon, J.H., 'Shrinkage, Residual Stress, and Cracking in Heterogeneous Materials,' Ph.D., Civil Engineering, Purdue University, West Lafayette, IN, 2006.

[12] Pickett, G., 'Shrinkage stresses in concrete,' *Mater. Struct.,* **42** (8)(1946) 165-204.

[13] Hobbs, D.W., 'Influence of aggregate restraint on the shrinkage of conrete,' *ACI Journal,* **71-30** (1974) 445-450.

[14] Monfore, G.E., 'A small probe-type gauge for measuring relative humidity,' *Journal of the PCA Research and Development Laboratories,* **5** (2)(1962).

[15] Grasley, Z.C., Lange, D.A., and D'Ambrosia, M.D., 'Internal relative humidity and drying stress gradients in concrete,' *Mater. Struct.,* **39** (9) Nov (2006) 901-909.

[16] Molina, L., 'Measurement of high humidity in cementitious material at an early age,' Swedish Cement and Concrete Research Institute, Stockholm, Sweden1990.

[17] Schielβl, A., Weiss, W.J., Shane, J.D., Berke, N.S., Mason, T.O., and Shah, S.P., 'Assessing the moisture profile of drying concrete using impedance spectroscopy,' *Concr. Sci. Eng.,* **2** (2000) 106-116.

[18] Elkey, W. and Sellevold, E.J., 'Electrical resistivity of concrete,' Norwegian Road Research Laboratory1995.

[19] Rajabipour, F., 'Insitu electrical sensing and materials health monitoring in conrete structures,' Ph.D., Civil Engineering, Purdue University, West Lafayette, IN, 2006.

[20] Anderberg, A. and Wadso, L., 'Method for simultaneous determination of sorption isotherms and diffusivity of cement-based materials,' *Cem. Concr. Res.,* **38** (1) Jan (2008) 89-94.

[21] Garbalinska, H., 'Application of root t-type, logarithmic and half-time methods in desorptive measurements of diffusivity in narrow humidity ranges,' *Cem. Concr. Res.,* **36** (7) Jul (2006) 1294-1303.

[22] Moon, J.H. and Weiss, J., 'Estimating residual stress in the restrained ring test under circumferential drying,' *Cem. Concr. Compos.,* **28** (5) May (2006) 486-496.

[23] Weiss, W.J., Yang, W., and Shah, S.P., 'Shrinkage cracking of restrained concrete slabs,' *J. Eng. Mech.,* **124** (7) Jul (1998) 765-774.

[24] Weiss, W.J., Yang, W., and Shah, S.P., 'Influence of specimen size/geometry on shrinkage cracking of rings,' *J. Eng. Mech.,* **126** (1) Jan (2000) 93-101.

[25] Bazant, Z.P., 'Material Models for Structural Creep Analysis,' in *Mathematical Modeling of Creep and Shrinkage of Concrete*, Z. P. Bazant, Ed., ed New York: John Wiley and Son Ltd, 1988.

[26] Castro, J., Lura, P., Rajabipour, F., and Weiss, J., 'Internal curing: discussion on the role of pore solution on relative humidity measurements and desorption of lightweight aggregate (LWA) ' in *Advances in the Material Science of Concrete*. vol. SP-270, J. H. Ideker and A. Radlinska, Eds., ed Chicago, IL: American Concrete Institute, 2010.

[27] Instruments, T., 'Dynamic Vapor Sorption Analysis: Q5000 SA,' http://www.tainstruments.com2010.

[28] Crank, J., *The Mathematics of Diffusion*, 2nd ed. New York: Oxford University Press, 1980.

[29] Neithalath, N., Pease, B.J., Moon, J.H., Rajabipour, F., Weiss, J., and Attiogbe, E., 'Considering moisture gradients and time-dependent crack growth in restrained concrete elements subjected to drying,' in *High Performance Cement Based Concrete Composites*, J. J. Bernacki*, et al.*, Eds., ed Chennnai, India: American Ceramics Society, 2005, pp. 279-290.

[30] Maxim, 'Data Logger, Temperature/Humidity Loggers, and Sensors,' Sunnyvale, CA, 2010.

[31] Bazant, Z.P. and Kim, J.K., 'Consequences of Diffusion-Theory for Shrinkage of Concrete,' *Mater. Struct.,* **24** (143) Sep (1991) 323-326.

[32] Bazant, Z.P., Kim, J.K., and Panula, L., 'Improved Prediction Model for Time-Dependent Deformations of Concrete .1. Shrinkage,' *Mater. Struct.,* **24** (143) Sep (1991) 327-345.

[33] Bazant, Z.P. and Najjar, L.J., 'Nonlinear water diffusion in nonsaturated concrete,' *Mater. Struct.,* **5** (25)(1972) 3-20.

[34] Xi, Y.P., Bazant, Z.P., and Jennings, H.M., 'Moisture Diffusion in Cementitious Materials - Adsorption-Isotherms,' *Adv. Cem. Based Mater,* **1** (6) Nov (1994) 248-257.

[35] Xi, Y.P., Bazant, Z.P., Molina, L., and Jennings, H.M., 'Moisture Diffusion in Cementitious Materials - Moisture Capacity and Diffusivity,' *Adv. Cem. Based Mater,* **1** (6) Nov (1994) 258-266.

[36] Crank, J. and Nicolson, P., 'A Practical Method for Numerical Evaluation of Solutions of Partial Differential Equations of the Heat-Conduction Type,' *Proceedings of the Cambridge Philosophical Society,* **43** (1)(1947) 50-67.

[37] Ozisik, M.N., *Finite Difference in Heat Transfer*. London: CRC Press, 1994.

[38] Pour-Ghaz, M., 'A novel approach for practical modelling of steel corrosion in concrete,' M.A.Sc, Civil Engineering, Carleton University, Ottawa, Canada, 2007.